Improving Camber Predictions for Precast, Prestressed Concrete Bridge Girders

by

David M. Mante

A dissertation submitted to the Graduate Faculty of
Auburn University
in partial fulfillment of the
requirements for the Degree of
Doctor of Philosophy

Auburn, Alabama
May 8, 2016

Keywords: deflection, overstrength, elastic modulus, time-dependent, creep and shrinkage, thermal effects

Approved by

Robert W. Barnes, Chair, Associate Professor of Civil Engineering
Anton K. Schindler, Professor and Director of Highway Research Center
J. Michael Stallings, Professor of Civil Engineering
Mary L. Hughes, Lecturer in Civil Engineering

Abstract

In precast, prestressed concrete construction, the eccentricity of the prestressing force typically results in a net upward girder deflection known as camber. Camber is first observed at the time of prestress transfer and tends to increase thereafter as a function of time-dependent material properties. While accurately predicted levels of camber are desirable to concrete bridge construction, inaccuracies in design camber estimates can result in construction difficulties and the need to modify bridge designs to ensure proper girder fit. In order to mitigate such troublesome issues, the Alabama Department of Transportation (ALDOT) sponsored this investigation to develop a suggested procedure for use during girder design to more accurately predict pre-erection camber in precast, prestressed concrete bridge girders. In support of this objective, various laboratory and field studies were conducted exploring relevant regionally-variable concrete material properties (e.g. concrete compressive strength, concrete unit stiffness, and creep and shrinkage behavior) as well as the effect of transient environmental conditions on girder camber. Relying on the conclusions of these laboratory and field studies, a revised camber prediction procedure was developed, implemented in a user-friendly computer software, and validated by comparison to multiple design and production cycles of ALDOT precast, prestressed concrete bridge girders.

Dedicated to Mom and Dad.

Nothing in this world can take the place of persistence.

Talent will not: nothing is more common than unsuccessful men with talent.

Genius will not; unrewarded genius is almost a proverb.

Education will not: the world is full of educated derelicts.

Persistence and determination alone are omnipotent.

-Calvin Coolidge

Acknowledgments

Special thanks are extended to Dr. Barnes and Dr. Schindler, without whom, the research performed in this dissertation would not have been possible. I'm especially grateful for the faith and trust Dr. Barnes has shown in my abilities throughout our work together and for the contagious enthusiasm with which Dr. Schindler has inspired many students, including myself, to share his love of all things concrete. Additionally, the support of committee members Dr. Hughes and Dr. Stallings is greatly appreciated, along with the support and encouragement of the rest of the faculty and support staff within the Auburn University Civil Engineering Department. Particular thanks are extended to Dr. Ramey and Dr. Abbas for their respective roles in my academic and personal development and to Mr. Billy Wilson and Mrs. Sherry Smith for providing assistance, friendship, and council throughout the previous six years.

The work of this dissertation would not have been possible without a cast of supporting research assistants. The pivotal contributions of Andric Hofrichter and Levent Isbiliroglu are gratefully acknowledged–along with additional assistance provided by Dr. Taylor Rawlinson, Dr. Sam Keske, Jamieson Matthews, Rebecca Nylen, Eric Gross, Aaron Grubbs, Adam Carroll, Will Childs, Jon Browne, and U.S. Air Force Second Lieutenants Daniel Cartin and Phillip Warden. To these assistants–It has been a pleasure to work alongside each of you and I remain convinced that hiring help smarter than one's self is among the soundest of practices.

In addition to the contributions of the Auburn family noted above, this project would not have been possible without funding and assistance from multiple outside agencies. The work detailed in this dissertation was primarily funded by the Alabama Department of Transportation (ALDOT)–with special thanks extended to Mr. Buddy Black, Mr. Tim Colquette, Mr. Drew Waldrop, Mr. Keith Hegler, and the ALDOT field inspection team for their contributions to this work. Additional support provided by the American Concrete Institute (ACI) Fellowship program is also gratefully acknowledged. The support of the Highway Research Center (HRC), particularly in regards to the funding of multiple laboratory upgrades in support of this experimental effort, is also gratefully acknowledged. Furthermore, the assistance and cooperation of various field producers including Hanson Building Products, Gulf Coast Prestress, and Standard Concrete were instrumental to the success of this research program. Particular thanks are extended to Mr. Nathan Emmerich, Mr. Frankie Smith, Mr. Dwayne Hamby, and Mr. Don Theobald for their patience and assistance. Donations in support of the laboratory portion of this program from BASF Corporation, Holcim Inc., Elkem Materials Inc., and CEMEX are also gratefully acknowledged. Finally, the ongoing support of the Abbvie PAF is also gratefully acknowledged for its role in ensuring the timely completion of this research work.

My time in Auburn has been graced by many special friendships–collectively forming the support network necessary to endure the sometimes trying life of PhD study. While it's not possible to acknowledge all by name, particular thanks are extended to Dr. Sam Keske, Dr. Taylor Rawlinson, Dr. Hughes and Carl Hollopeter, Dr. Wesley Zech and family, the soon-to-be Dr. George Kantrales and family, the soon-to-be Dr. Ross

Stanley and family, Ruddy Thompson, and Mike Perez. I am forever grateful to Dr. Keske for serving as my mentor and friend, to Dr. Rawlinson for being one of my closest friends and for his eagerness to help whenever needed, and to the soon-to-be Dr. Kantrales for his enduring friendship, support, and inspiration. The kindness and generosity of Dr. Hughes and Carl Hollopeter through the past six years have been awe-inspiring. Particular thanks to Carl for the many hours of shop therapy provided while working on my beloved Jeep. Similarly, Dr. Wesley Zech, April, Watson, and Winter are gratefully acknowledged for their role in filling the past six years with laughter and joy. The kindness and love provided by Dr. Peter, Sophia, George, Peter, and Angelo Kantrales on weekend visits to Florida are also gratefully acknowledged. Finally, the generosity, love, and encouragement provided by Ross, Mary, and Knox Stanley kept me motivated and well-fed throughout the previous four years. Studying roughly 908 miles removed from my immediate family would not have been possible without the love provided by these aforementioned adoptive families.

I'm most of all grateful to my immediate family for their unconditional love and support of my decision to pursue my PhD. The countless letters, cards, and care packages received kept me motivated when the outlook seemed bleak or the obstacles overwhelming. I'm continually grateful for the sense of hard work and persistence instilled in me by my parents and for their unbounded belief in my abilities. I'm grateful to my late grandfather, Dr. Arthur A. Witkin, for his role in funding my early education and for stressing the importance of higher education. I'm thankful for my older brother Russell and his role in encouraging me throughout my studies and also for his demonstration of courage and positivity in the face of unexpected adversity. I'm grateful

to my older sister Meredith for her continual encouragement and her stubborn faith in my abilities. Without the love and continual support of my family, the pursuit of my PhD would not have been possible. It is to them that I truly owe this accomplishment.

Lastly, I thank God for the bounty of undeserved blessings in my life. With Him, all things are possible.

Table of Contents

List of Tables

List of Figures

Chapter 1: Introduction

1.1 Background on Camber in Precast, Prestressed Concrete Girders

Camber can be defined as a deflection intentionally built into a structural element or form to improve appearance or to compensate for the deflection of the element under the effects of loads, shrinkage, and creep (ACI 2013). Within the precast, prestressed concrete community, camber is more precisely regarded as the net *upward* deflection due to the eccentricity of the prestressing force (Buettner and Libby 1979), as shown in Figure 1-1.

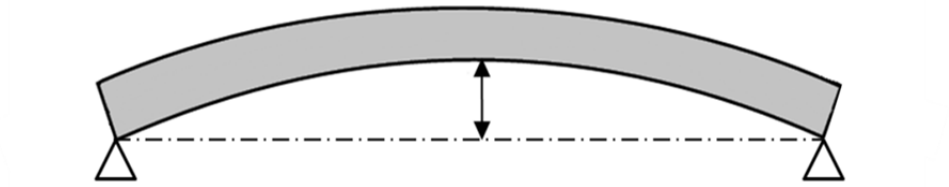

Figure 1-1: Exaggerated Girder Deformation and Midspan Camber

When properly predicted during the design phase, an appropriate amount of camber is desirable to avoid the perception of sagging under applied loads and to ensure proper alignment of adjacent bridge components.

Initial camber, or elastic camber, is the camber induced upon transfer of the prestressing force during fabrication of a bridge girder and is heavily dependent on the geometric properties of the girder, the stiffness of the constitutive materials, and the magnitude of the prestressing force (PCI 2011). The term camber growth refers to the tendency of the initial camber to experience a net time-dependent increase as a result of various interrelated factors including maturing concrete properties, time-dependent

deformations of concrete (creep and shrinkage), relaxation of the prestressing steel, and varying girder curing and storage conditions. Midspan camber in precast, prestressed bridge girders is widely regarded as the beam deformation of greatest interest to bridge designers (PCI 2011) and thus, is the deflection most essential to accurately predict during the girder design phase.

1.2 Justification for Research

During the design of a bridge which relies on precast, prestressed concrete girders as the primary flexural elements, it is essential for engineers to accurately predict the midspan camber to ensure proper fit of girders during installation. Predictions of camber during the design phase are based heavily on assumptions—namely, those of future material properties used in constructing the element, and therefore are regarded as estimates at best (ACI Committee 435 2003). Design engineers are frequently cautioned against placing a high degree of confidence in the accuracy of predicted camber values to avoid constructability problems and related litigation exposure (Tadros, Fawzy, and Hanna 2011; Buettner and Libby 1979).

With the recent widespread implementation of high-strength concrete and self-consolidating concrete (SCC) for use in producing prestressed bridge girders, the accuracy of traditional camber prediction methods has been called into question by researchers and industry alike. Specifically, PCI bulb-tee shaped girders seem to exhibit some of the greatest disparities between predicted and observed camber, with design camber estimates most commonly tending to over-predict the actual observed field camber (Stallings, Barnes, and Eskildsen 2003; Rosa, Stanton and Eberhard 2007; PCI Committee on Bridges 2012). That is, the camber magnitude observed in the field is

significantly less than that predicted during the girder design phase. Overestimation of camber can lead to construction difficulties and the need for placement of more deck concrete than originally estimated, as well as the unforeseen dead load that accompanies this additional concrete. In extreme cases, overestimations of camber during the design phase can even result in a bridge that ultimately sags under superimposed dead loads. Consequences of inaccurate camber predictions negatively affect multiple parties involved in the bridge construction industry, and thus, there has been a rising industry research effort to address this problem.

In recent years, the Alabama Department of Transportation (ALDOT) has experienced many cases where less-than-expected field camber values have resulted in construction difficulties and contentious relations between contractor, girder producers, and ALDOT. Although each involved entity has hypothesized various reasons for the disparity between the predicted and observed values, little has been done to date to alleviate the problem. Accordingly, this research study aims to explore the primary causes of inaccurate camber predictions in precast, prestressed concrete girders in the study region and provide recommendations to those parties involved in the design and production of bridge girders to mitigate this troublesome issue in the future.

1.3 Research Objectives

The primary objective of this work is to advance the understanding of various factors that collectively influence the accuracy with which the magnitude of the observed camber can be predicted during the girder design phase. The scope of this investigation includes those factors influencing both the initial elastic camber, as well as the camber growth occurring prior to deck placement. A primary goal of this study is to develop and

recommend a procedure resulting in more accurate predictions of camber in precast, prestressed girders during the design phase. Areas of particular focus include the following key topics:

- The disparity between the concrete compressive strength as specified by the design engineer and the strength achieved during girder production (hereafter termed overstrength);
- The relationships between modulus of elasticity and concrete compressive strength for regionally specific concrete mixtures utilizing varying constitutive materials;
- The time-dependent behavior (creep and shrinkage) of regionally specific concrete mixtures composed of varying constitutive materials;
- The effects of transient temperature gradients on the deformations of precast, prestressed girders; and
- The extent that camber predictions can be improved by implementing the cumulative recommendations resulting from the aforementioned focus areas.

1.4 Research Approach

A variety of research approaches are employed in this study to ensure that solutions practical, relevant, agreeable, and useful to all interested parties can be reached. This research represents a close collaborative effort among Auburn University Highway Research Center (AUHRC) researchers, ALDOT design and construction personnel, and various regional precast, prestressed concrete producers. The results of three major research approaches are documented in this report: (1) a historical review of available field production records, (2) a laboratory investigation aimed at characterizing various

concrete material properties relevant to camber prediction, and (3) a series of field-monitoring studies during and after the production of ALDOT prestressed bridge girders.

The historical review of available girder production records was primarily aimed at exploring the standard practices of the precast, prestressed concrete industry in the region and quantifying the difference between the concrete compressive strength as specified by the design engineer and the strength observed in the field during girder production. This effort included visits to four regional precast, prestressed concrete producers and the compilation of available production records for various ALDOT bridge girder projects produced in the preceding seven-year period. From these historical data, various valuable trends were captured regarding the practices of the precast, prestressed concrete industry in the region, and recommendations were derived to help design engineers estimate the overstrength expected in a bridge girder.

The laboratory phase of this project was designed to explore the effect of varying regional prestressed concrete compositions on those concrete material properties most relevant to camber predictions. Most importantly, the laboratory effort sought to capture the effect of varying coarse aggregate sources and supplementary cementing materials (SCMs) on concrete modulus of elasticity as well as creep and shrinkage behavior. By systematically varying the composition of the concrete mixtures included in this study, valuable information regarding the material properties of concretes used in the precast, prestressed industry was discovered.

The field monitoring phase of this project was performed to validate and expand the findings of the previous phases, while also capturing the in-place structural and deformational behavior of ALDOT bridge girders during construction. In an attempt to

provide a view of various in-situ camber-relevant factors uninfluenced by research efforts, a deliberate effort was made by researchers to minimize disruptions to the girder production process. The field monitoring phase included (1) on-site concrete testing, (2) measurement of beam deformations and temperatures during production, (3) extended field monitoring covering the early life of selected girders, and (4) targeted field studies to quantify the influence of temperature on girder camber behavior. Using this approach, researchers were able to document the observed field camber and camber growth of various production girders in order to compare to the results of analytic camber prediction techniques.

1.5 Dissertation Organization and Outline

This dissertation is divided into eleven chapters representing three distinct sections. Chapters 1-4 acquaint the reader with the research topic, provide a general background of previous work in the area, and document the current design and girder production practices in the region. The literature review of Chapter 3 serves as an introduction to, and a general summary of, previous camber studies. Chapters 5-8 each address a specific research objective and incorporate a synthesized literature review of each topic. Then, the experimental efforts, analytical work, and conclusions are presented for each topic. Chapters 9-10 detail (1) the implementation of the cumulative recommendations proposed in Chapters 5-8 to generate predictions of camber for the projects observed during field monitoring studies and (2) comparisons between the predicted cambers and the observed field cambers as used to evaluate the adequacy of the recommendations to improve camber predictions in precast, prestressed concrete girders. Finally, the various

appendices contain raw data and extended data analysis procedures not included elsewhere in this dissertation.

Chapter 2: Background

2.1 Introduction

This chapter is intended as a brief background discussion of deflections in one-way prestressed flexural elements and various intrinsically related topics. Explicit design code provisions or specific recommendations by previous researchers are withheld until later chapters, where presented by topic. A brief discussion on the variability and expected degree of accuracy of deflection calculations is first offered, followed by a general introduction to deflections of one-way prestressed flexural elements and a review of the primary factors affecting these deflections. Finally, various common methods for computing both short-term deflections (e.g. instantaneous elastic camber) and long-term deflections (e.g. camber growth) are reviewed.

2.2 Variability and Limitations of Deflection Predictions

A logical first question in a study aimed at improving predictions of deflections is how accurately can an engineer expect to predict deflections during the design phase? This section aims to provide a discussion of this topic, as well as to address other related questions including (1) when are deflection predictions accurate enough, and (2) to what extent is effort spent attempting to improve the accuracy of deflection predictions justified in the precast, prestressed concrete industry?

Control of Deflection in Concrete Structures (ACI Committee 435 2003), representing the consensus of ACI Committee 435, is a logical starting point for those

seeking clarification on the anticipated accuracy of deflection calculations. ACI Committee 435 (2003) notes that deflection calculations are based on various randomly distributed variables (e.g. concrete strength, concrete stiffness, and creep and shrinkage behavior) and that the distributions of these constitutive variables cannot be established with great precision. An example showing the random variability (as represented by the mean, μ, and standard deviation, σ) in a simple parameter such as a measured length (or quantity derived thereof) is shown in Figure 2-1.

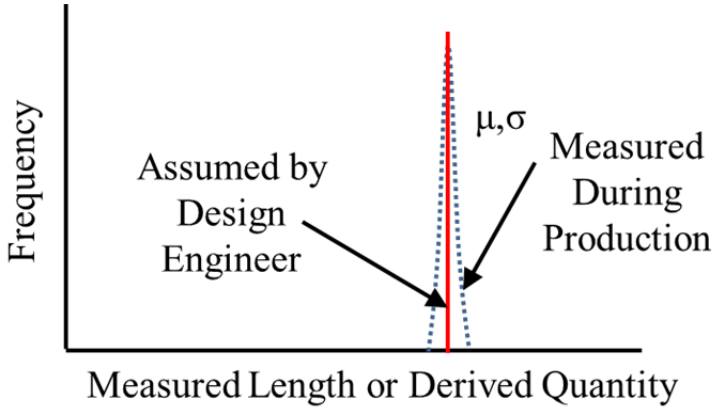

Figure 2-1: Random Variability of a Measured Length

The vertical solid line might represent an exact value for the specified length of a girder (i.e. 1,000 in.). Here, it is assumed that the contractor producing beams targets the specified length as precisely as possible given available measurement techniques (i.e. a length measurement tool with precision of 1/16 in.). The dashed curve represents a sampling of the random variable girder length for all similar girders produced. This dashed curve is normally distributed by virtue of it being derived from a manufacturing process with discrete limits to the precision of available tools. In this case, the mean, μ, of the sampled distribution coincides with the targeted value and the sampling distribution indicates excellent agreement between the girder length specified by design engineer and the average girder length observed during construction. While the

distribution for the variable girder length is rather narrow (as evidenced by a small standard deviation, σ), the distribution of other random variables necessary for design computations (i.e. concrete strength, concrete stiffness, and internal force effects) exhibit much greater variability. By virtue of the compounded effect of those random variables used in deflection calculations, an intrinsic level of variability is unavoidable in these computations. Accordingly, deflection calculations should be regarded only as reasonable estimates of the anticipated deflection response of a structure. Buettner and Libby (1979); Tadros, Fawzy, and Hanna (2011); and the PCI Bridge Design Manual (2011) share this cautionary sentiment, advising design engineers against heavy reliance on the accuracy of design deflection predictions.

Another logical question is how accurate is accurate enough when predicting deflections during the girder design phase? At first thought, the answer appears to be simple—when deflections are predicted accurately enough, constructability issues do not ensue during production or erection of the element. While partially true, it is important to note that the avoidance of constructability issues may not be wholly due to an overly accurate *estimate* of deflections, but instead due to a forgiving level of tolerance in design or construction. In fact, various parties have suggested that the solution to camber prediction inaccuracies lies not in improving camber prediction methods, but instead in increasing design and construction tolerances to avert constructability issues (PCI 2012; Tadros et al. 2011). A complex relationship exists between these parameters and is perhaps best stated as follows: for a given level of design and construction tolerance, a deflection prediction is accurate enough when constructability problems (of the nature capable of being avoided by progressively more accuate predictions) do not ensue during

production or erection of the element. More simply put, the degree of accuracy in camber predictions needed to avert constructability problems in a bridge detailed with relatively low levels of design tolerance (i.e. minimal thickness girder haunch[1]) is much higher than the degree of accuracy needed to avert constructability problems in a bridge detailed increased levels of design tolerance (i.e. more substantial haunch).

An additional factor also further complicates the issue of pinpointing an acceptable level of accuracy for deflection predictions for girders designed with varying cambers. Suppose a certain procedure used by a design engineer for computing deflections yields up to a 25 percent error when compared to the constructed element. Those girders with a relatively small camber may still fall within prescribed tolerance allowances, while girders with larger cambers may exceed tolerance allowances and experience constructability problems. For instance, a 50 percent error on a predicted camber of 1 in. is unlikely to be significant, but a 50 percent error on a girder with a more extreme design camber of 5 in. may well cause constructability problems. The relevance of the concept (relative error versus absolute error) was first discussed by Buettner and Libby (1979) in the context of camber prediction accuracy, but remains equally relevant today.

A final discussion is now offered exploring (1) the extent to which effort spent attempting to improve deflection *estimates* is justified and (2) the most logical and practical approaches to improve deflection *estimates*. As noted by ACI Committee 435 (2003), the accuracy of deflection *estimates* typically does not significantly improve with advanced analytical or mathematical modeling techniques. Even these advanced

[1] The term haunch refers to the concrete build-up used to fill the distance from the top of the girder to the bottom elevation of the bridge deck along the girder length.

estimates are still based on variables with random variability and, therefore, may not yield significantly more accurate estimations than simple calculations. In fact, in an effort to be seemingly *more accurate*, some advanced analytical approaches rely on the introduction of additional random variables and can therefore actually yield *less accurate* results (ACI Committee 435 2003). The pertinent question then becomes—with no easily identifiable single metric of camber accuracy to target in all cases, what is the most logical approach to attempt to improve the accuracy of deflection *estimates*?

Tadros et al. (2011) noted that the inherent variability in deflection calculations is often incorrectly used as a catch-all to justify the usage of theoretically-questionable analytic procedures and less than accurate assumptions of future material properties. It is important that the presence of random variability in deflection computations not be confused with that of systematic error introduced by incorrect assumptions of future material properties during the girder design phase. The differences between these two concepts is illustrated in Figure 2-2 for concrete modulus of elasticity.

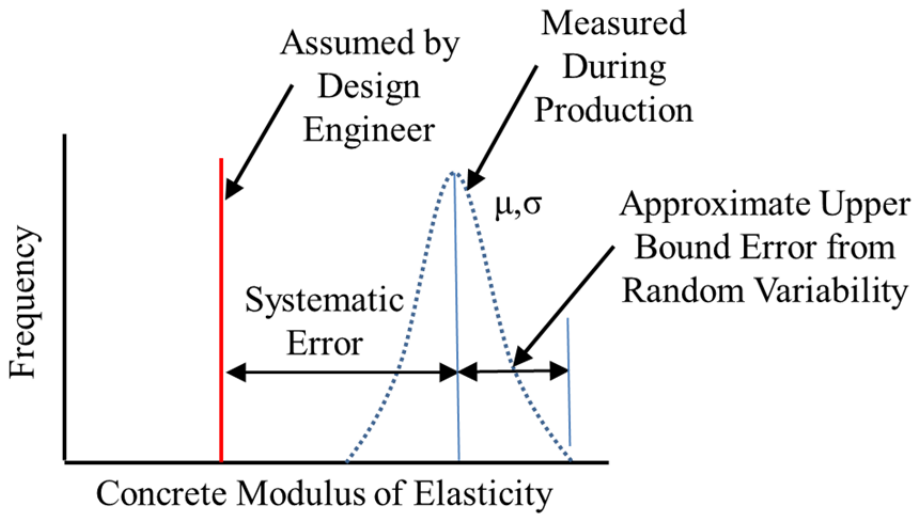

Figure 2-2: Systematic Error of a Random Variable

Similar to the previous example, the solid vertical line indicates the assumed modulus of elasticity used in deflection calculations, while the dashed curve denotes the sampling distribution of the random variable during production. A relatively widely dispersed normal distribution is indicated due to the large number of construction activities affecting this variable (compounding of random error) and the relatively large bias present in performing concrete material testing. For example, Tadros et al. (2011) note that the field measurements of the modulus of elasticity for identical concretes can vary by ± 22 percent at the time of prestress transfer. In this case, the assumed value for modulus of elasticity does not coincide with the mean of the sampled distribution, indicating that the assumption of future material properties was inaccurate and fell well below the actual sampled value. This disparity represents a systematic error, independent from the random variability of the parameter. This concept of systematic error is also discussed by Buettner and Libby (1979).

With an understanding of the difference between systematic error and random variability, it becomes clear that the most logical and greatest potential for increases in the accuracy of camber predictions may be achieved by improving the assumptions of future material properties during the design phase, thereby minimizing certain sources of systematic error. The issue of improving camber predictions, as explored in this dissertation, is not then one of a particularly advanced analytical nature, but instead predominately an issue of making more educated design phase assumptions regarding the material properties of the girder concrete expected to be used in girder production.

2.3 Deflections in One-Way Prestressed Flexural Members

Deflections in one-way prestressed flexural members can be divided into two primary categories: short-term deflections and long-term deflections. Each of these categories is defined and discussed in this section. For the purposes of this section and in accordance with regional design practices, the focus remains on computing deflections in uncracked prestressed concrete flexural members, that is, Class U (uncracked) sections as classified in ACI 318-14 (ACI Committee 318 2014).

The initial net camber (a short-term deflection) of a prestressed concrete girder is first observed during production upon transfer of the prestressing force to the bulk concrete section. This initial camber represents a superposition of two simultaneous effects: the tendency of the eccentric prestressing to induce negative bending and that of the girder self-weight to induce positive bending, as shown in Figure 2-3.

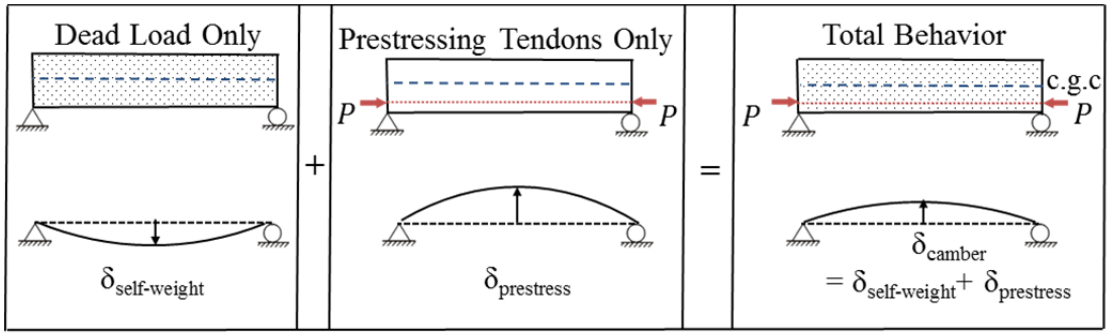

Figure 2-3: Net Instantaneous Deflections at Prestress Transfer in Prestressed Girders (adapted from Isbiliroglu 2014)

Immediately upon transfer of the prestressing force during girder production, the process of camber growth begins. The term camber growth refers to the tendency of the initial camber magnitude to experience a *net increase* with time as a result of various interrelated factors including the maturing of concrete properties, time-dependent deformations of concrete (creep and shrinkage), and relaxation of the prestressing steel

(ACI 435 2003). Concrete creep is the factor primarily responsible for the camber growth tendency, while the simultaneous gradual loss of prestressing force (caused by a combination of creep, shrinkage, and strand relaxation) tends to have a mitigating effect, slightly reducing the initial rate of camber growth as time progresses (PCI 2011).

2.4 **Primary Factors Influencing Flexural Deflection Predictions**

This section includes a description of the primary factors influencing both short-term and long-term deflections in one-way prestressed flexural members. In the following sections, an effort is made to clearly differentiate between those quantities relevant to short-term deflections, long-term deflections, and both short- and long-term deflections, with a summary shown in Figure 2-4. For those topics that are of a primary focus of this investigation (i.e. concrete strength, concrete stiffness, concrete creep and shrinkage behavior), only a brief background is presented in this section in lieu of comprehensive treatment of these topics in standalone chapters later in this dissertation.

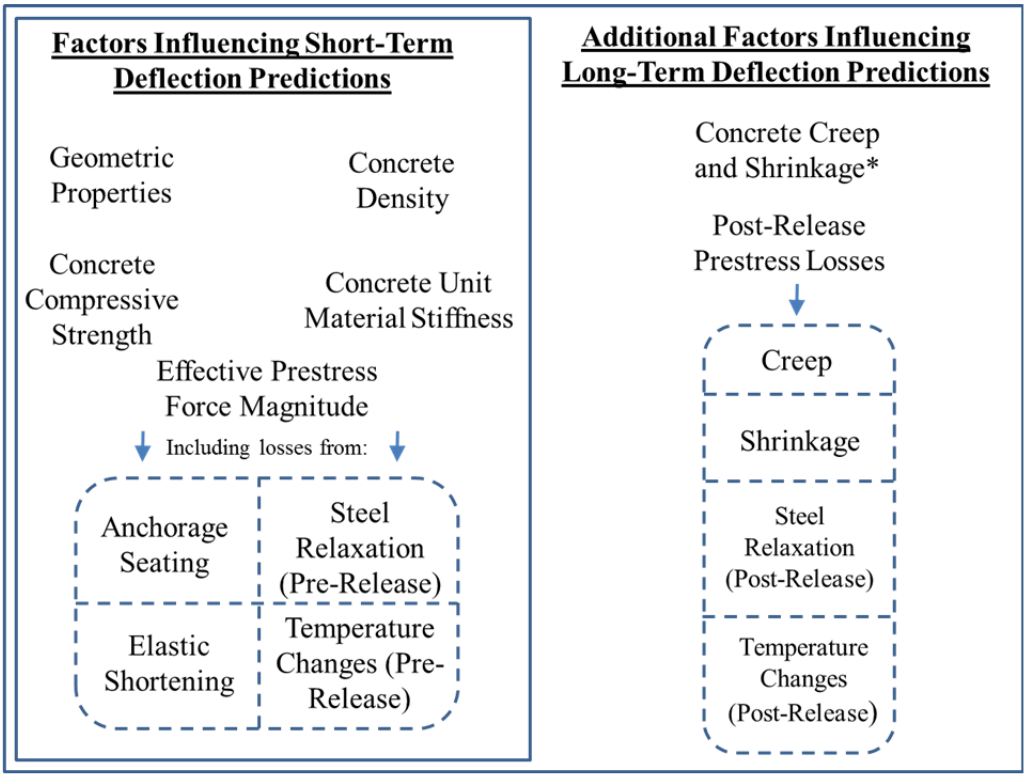

Note: * = Concrete creep and shrinkage behavior are indicated separately from their contribution to post-release prestress losses due to their tendency to induce changes in time-dependent deformations independent of the presence of prestressing steel (i.e. in conventionally-reinforced concrete beams).

Figure 2-4: Primary Factors Influencing Deflections in Prestressed Concrete Girders

2.4.1 Geometric Properties

Precast, prestressed concrete girders are an economical choice for bridge construction due, in large part, to the use of standardized cross sections enabling efficient mass production (PCI 2011). Among the most commonly used cross sections are PCI bulb-tee shapes (most commonly used in three primary depths: 54, 63, and 72 in.) and AASHTO standard sections (Types I-VI). PCI bulb-tee shapes are of primary relevance to this dissertation due to their widespread use in Alabama. Selected cross-sectional dimensions of various standard PCI bulb-tee shapes are shown in Figure 2-5. Also shown in this figure are standardized potential strand locations located in a 2 in. by 2 in. grid pattern.

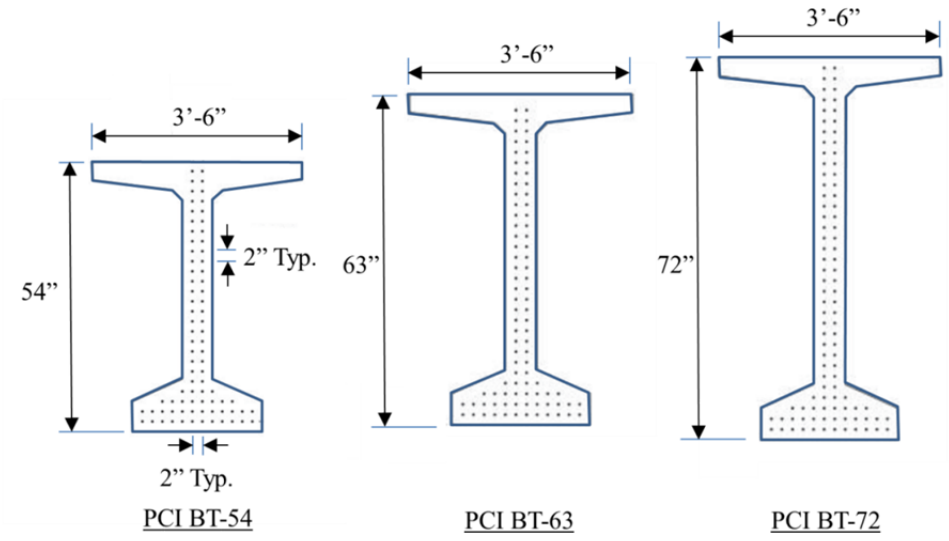

Figure 2-5: Standard Dimensions of PCI Bulb-Tee Cross-Sections (Adapted from PCI 2011)

More detailed dimensions, as well as various section properties of these standard sections, are shown in Figure 2-6.

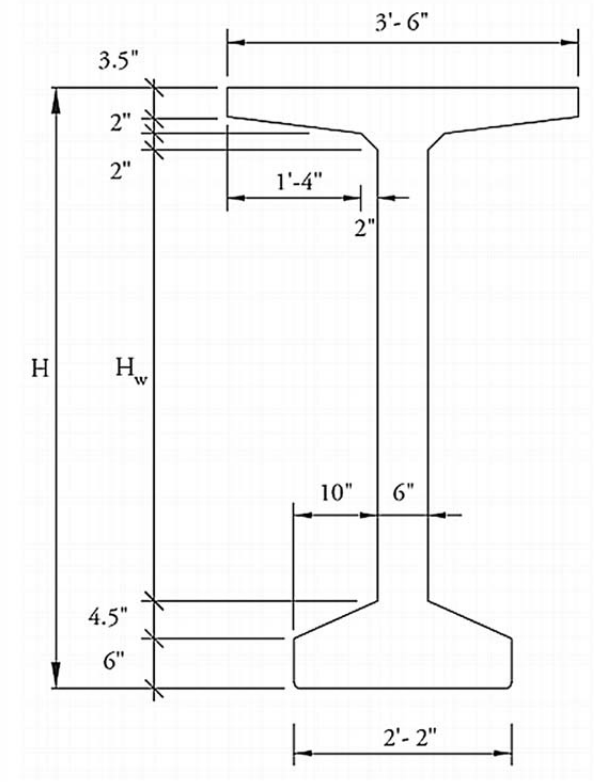

	BT-54	BT-63	BT-72
H (in.)	54	63	72
H_w (in.)	36	45	54
Area ($in.^2$)	659	713	767
Inertia ($in.^4$)	268,077	392,638	545,894
y_{bottom} (in.)	27.63	32.12	36.6
Weight (kips/ft.)	0.686	0.743	0.799

Figure 2-6: Detailed Section Properties of PCI Bulb-Tee Shapes (Adapted from PCI 2011)

Maximum design span length for each bulb-tee shape is primarily a function of the transverse lateral spacing of girders, due in large part to standardized bridge loadings and the maximum prestress force magnitude and orientation being somewhat prescribed by virtue of a limited number of strand locations and orientations. BT-72 shapes are capable of the longest clear spans, approaching 160 ft in bridges with 6 ft transverse girder spacing. BT-63 girders typically span up to approximately 140 ft, while BT-54 girders are capable of spanning up to approximately 125 ft (PCI 2011). Generally speaking, increased span lengths correspond to increases in the magnitude of required prestressing forces, which in turn lead to higher design cambers in long-span bridge girders, as noted by Stallings et al. (2003).

2.4.2 Concrete Density

Concrete density influences the magnitude of initial and long-term girder deformations both directly and indirectly. The density of the concrete used in girder fabrication is relied on to compute the self-weight component of deflection at the time of prestress release and, therefore, directly affects the magnitude of net camber at both the time of prestress transfer and all subsequent girder ages. Concrete density is also indirectly related to concrete unit stiffness, which is a critical parameter in any deflection computation.

2.4.3 Concrete Compressive Strength

The compressive strength of concrete is the property most valued to design and quality control engineers and is generally defined as the ability of the concrete to resist compressive stress without failure (Mehta and Monteiro 2014). Not only essential for structural design and quality-assurance purposes, concrete strength also provides perhaps the most complete overall picture of the quality of a given concrete (Neville 2013). Concrete compressive strength is indirectly relevant to both short-term and long-term deflection predictions because it serves as a basis for estimating concrete stiffness. A full discussion of this topic, including a synthesized literature review and the experimental program on this topic, is included in Chapter 5 of this dissertation.

2.4.4 Concrete Stiffness

Concrete unit material stiffness, as represented by the modulus of elasticity, is a parameter fundamental to the computation of both short-term and long-term deflections in prestressed concrete elements. Generally speaking, the modulus of elasticity of a given material is defined as the ratio between the applied uniaxial stress and

instantaneous strain within an assumed proportional limit (Mehta and Monteiro 2014). It is this relationship that governs elastic material behavior and serves as the basis for deflection computations in structural elements. A full discussion of this topic, including a synthesized literature review and an experimental program, is included in Chapter 6 of this dissertation.

2.4.5 Concrete Creep

Naaman (2004) defines creep as "the time-dependent strain in excess of elastic strain induced in concrete subjected to a sustained stress." While creep does not influence short-term deflections in prestressed concrete, it is the primary factor contributing to the tendency for camber growth to occur. If concrete did not exhibit creep under sustained compressive loading, camber growth would simply not occur. Instead, short-term camber would actually tend to decrease with time as a function of concrete shrinkage and steel relaxation. Full treatment of this topic is detailed in Chapter 7 of this dissertation.

2.4.6 Concrete Shrinkage

The term shrinkage of concrete refers to the total time-dependent volume reduction experienced by concrete due to changes in the moisture content. In general, concrete shrinkage is assumed to not significantly influence short-term deflections, but is a factor that influences long-term deflections. The primary effect of shrinkage on deflections stems from its restraint by eccentric reinforcement, which accompanies a prestress loss in that reinforcement. In general, concrete shrinkage acts a mitigating factor, not directly contributing to the growth of long-term deflections, but actually reducing the rate of continued time-dependent camber growth. Full treatment of this topic is detailed in Chapter 7 of this dissertation.

2.4.7 Steel Relaxation

The steel strands used to prestress concrete girders are prone to relaxation due to the relatively high levels of stress sustained over an extended time period. While steel relaxation can affect both short-term and long-term deflections, the effect of steel relaxation prior to prestress transfer is largely negligible when compared to post-transfer losses due to the relatively short time-period elapsed between strand stressing and transfer of the prestressing force (PCI 2011). Thereby, steel relaxation primarily affects long-term deflection computations by its contribution to the total magnitude of prestress losses, as discussed in the following section.

2.4.8 Prestress Losses

A discussion of the factors influencing deflection computations in prestressed concrete members is not complete without mention of prestress losses. The partial loss of the prestressing force occurs beginning at the time of prestress transfer and continues, theoretically, through the life of the girder. In order to compute anticipated member deflections, it is necessary to calculate the effective prestress force (that is, the jacking force minus losses) in a member as a function of time. Prestress losses affect both short-term and long-term deflection computations and can accordingly be divided into two primary groups: short-term prestress losses[2] and long-term prestress losses.

Short-term prestress losses include losses caused by anchorage seating, steel relaxation, temperature effects, and elastic shortening (Tadros, Al-Omaishi, Seguirant, and Gallt 2003). These short-term losses are graphically depicted in Figure 2-7 by letters

[2] As an alternate to the term "short-term prestress losses", a forthcoming publication from ACI Committee 423 will suggest the consensus term "immediate losses". In this dissertation, the term "short-term prestress losses" is preferable due to the inclusion of pre-release steel relaxation and temperature losses—neither of which are immediate or instantaneous sources of prestress losses.

A through D. While the contribution of anchorage seating losses, steel relaxation, and temperature effects are relatively minimal (often due to contractors actively compensating for these effects during production), elastic shortening is the primary contributor to short-term prestress losses (Tadros et al. 2003).

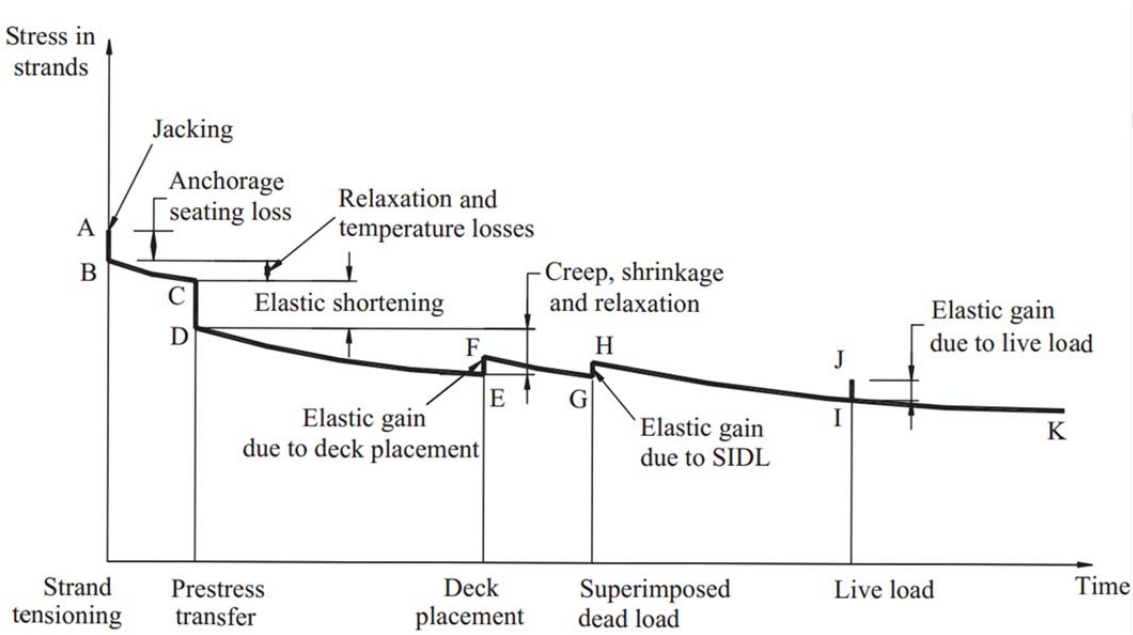

Figure 2-7: Graphical Representation of Prestress Loss Contributions (Adapted from Tadros et al. 2003)

In the context of this dissertation, the term "long-term losses" is used to identify those losses occurring after the transfer of the prestressing force and prior to the time of deck placement. These long-term losses are caused by the complex interaction of creep and shrinkage behavior of concrete, steel relaxation, and temperature changes. Long-term losses are signified in Figure 2-7 by letters D through E. While many different techniques exist to estimate or compute long-term prestress losses, each of these techniques fundamentally relies on selecting accurate material models for concrete stiffness, steel relaxation, and creep and shrinkage behavior. Steel relaxation is fairly well-documented by others (i.e. Magura, Sozen, and Seiss 1964 and AASHTO 2014) and

is generally not viewed as a major contributor to variability in estimating the effective prestressing force in concrete elements due to the relatively small magnitude of relaxation losses as compared to other prestress loss sources (PCI 2011). Conversely, concrete stiffness, and creep and shrinkage behavior are major contributors to variability in estimating the effective prestress force, and therefore have a large potential impact on the accuracy of deflection computations. More detail on the specific methods used to predict concrete material behavior and prestress losses in this research project, implemented as part of incremental time-steps analysis, is included in Chapter 9 of this dissertation.

2.5 Techniques For Computing Short-Term Deflections

This section reviews three common techniques for computing short-term deflections in uncracked one-way prestressed flexural elements. The first two techniques, the moment-area method and tabulated equation method, are the techniques most commonly used. The third method detailed herein, an energy method, represents an effort to evaluate the feasibility of computing camber using a method not typically applied to deflection computations in prestressed concrete flexural elements. Each of the three techniques summarized here represent either a direct or in direct application of engineering beam theory.

2.5.1 Elastic Camber Computation by Moment-Area Theorem

One of the most commonly used analytical methods to compute design deflections in simple flexural elements is the moment-area theorems as originally developed by Otto Mohr and later refined by Charles E. Greene in 1873 (Hibbeler 2006). These theorems provide a semi-graphical technique for determining the slope of the elastic curve and corresponding beam deflections due to bending. Due to their importance and widespread

use in predicting initial elastic camber, a summary of the application of the moment-area theorems follows. While these methods can equally be applied to member self-weight to compute the simultaneous downward deflection component, this discussion focuses on the computation of the upward camber component for some of the most common prestressing strand patterns.

In accordance with engineering beam theory, for a beam with a length much greater than its depth, the internal moment in a beam can be related to the displacement and slope of the elastic curve resulting from that moment by Equation 2-1 as follows:

$$\frac{1}{\rho} = \frac{M}{EI} \tag{2-1}$$

where

ρ = the radius of curvature at a specific point on the elastic curve;

M = the internal moment in the beam at the point where ρ is determined; and

EI = the flexural rigidity (the product of the elastic modulus of the material, E, and the moment of inertia of the beam computed about the neutral axis, I).

Using the geometry of the deformed beam and the arc-length relationship illustrated in Figure 2-8, the radius of curvature, ρ, can be approximated as $\frac{dx}{d\theta}$, where dx represents the infinitesimal portion of the elastic curve along the neutral axis for each cross section and $d\theta$ represents the change in angle between cross sections due to the internal moment, M.

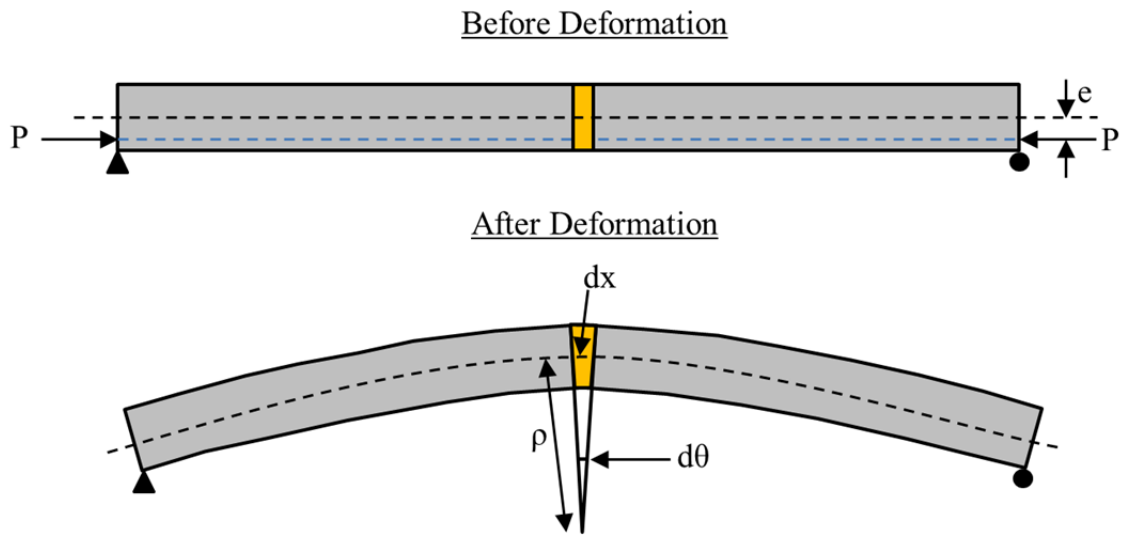

Figure 2-8: Engineering Beam Theory in a Flat-Strand Prestressed Girder (Adapted from Hibbeler 2006)

Substitution of this relationship into Equation 2-1 and simplification yields the following:

$$d\theta = \frac{M}{EI} dx \tag{2-2}$$

Equation 2-2 serves as the direct basis for development of the first moment-area theorem. By integrating Equation 2-2 along a length of beam, the first moment area theorem is derived, stating that the change in slope between any two points on the elastic curve equals the area of the *M/EI* diagram between these two points (Hibbeler 2006).

The second moment-area theorom expands on the first theorom and provides a method to determine the deviation between two tangents on a beam's elastic curve. The second moment-area theorem is stated by Hibbeler (2006) as follows:

> "The vertical deviation of the tangent at [one point] on the elastic curve with respect to the tangent extended from another point… equals the moment of the area under the *M/EI* diagram between these two points… [taken about the first point]."

The primary factors making this theorem possible are the assumption of small deformation angles and the use of the arc-length formula. Generally, the second moment-area theorom does not yield a direct solution for the desired deflection within a beam. However, in the specialized case of a simple-span prismatic beam with symmetric loading (i.e. midspan camber in a precast, prestressed concrete element), the vertical deviation between a point at the girder end and midspan does indeed give the magnitude of the midspan deflection. This concept is graphically explained in subsequent sections detailing the application of the second moment-area theorom to computation of the upward component of camber at the midspan section.

A prestressed concrete beam with a uniform-eccentricity profile is shown in Figure 2-9 (top). In this simplified idealization, the net prestressing force (after losses), P, is assumed to be known and applied as a concentrated load at the end of the beam, thus the effects of debonding and end-region transfer length are neglected at present. A resulting curvature diagram is also shown in the figure, derived from constant internal moment along the length of the girder of magnitude Pe, where e is the eccentricity from the elastic centroid of the cross section.

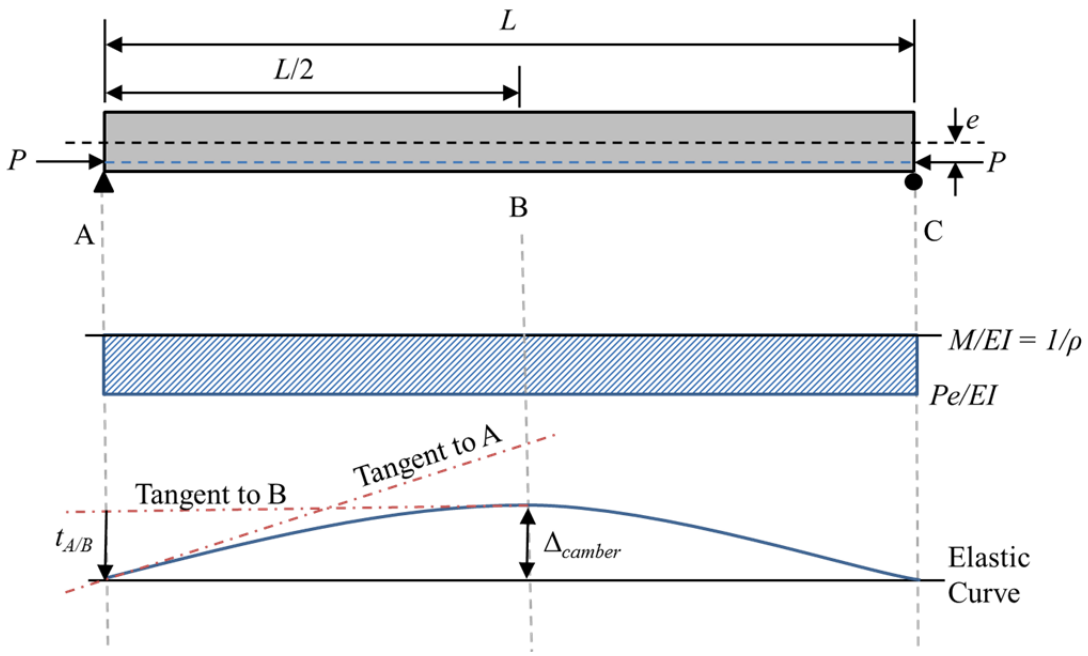

Figure 2-9: Application of Moment-Area Theorem to Calculate Elastic Camber in Flat-Strand Prestressed Girder

In the bottom of Figure 2-9, an exaggeration of the elastic curve is shown and tangent lines are shown intersecting the elastic curve at point A (left-support) and point B (midspan). By virtue of the symmetric deflected shape, the vertical deviation of the two tangents at A, denoted $t_{A/B}$, is the same vertical distance as the upward midspan camber tendency, Δ_{camber}. The upward camber tendency in flat-strand prestressed girders can be calculated as:

$$\Delta_{camber} = t_{A/B} = \left[\left(\frac{L}{2}\right)\left(\frac{Pe}{EI}\right)\right]\left(\frac{L}{4}\right) = \frac{Pe}{EI}\left(\frac{L^2}{8}\right) = \frac{M}{EI}\left(\frac{L^2}{8}\right) \qquad (2\text{-}3)$$

Another frequently used pattern of prestressing strands in prestressed concrete girders is that of a harped (draped) strand configuration. Harped strands can be present at any elevation within the cross section, but are typically positioned highest at the girder ends and lowest towards the girder center to counteract gravity-induced force effects (PCI 2011). A harped-strand profile is shown in Figure 2-10 (top), with the strands

intersecting the elastic centroid at beam ends and exhibiting a known eccentricity, *e*, at the girder midspan. In this example, the strands follow a straight line harp pattern through a distance *bL* from the girder end.

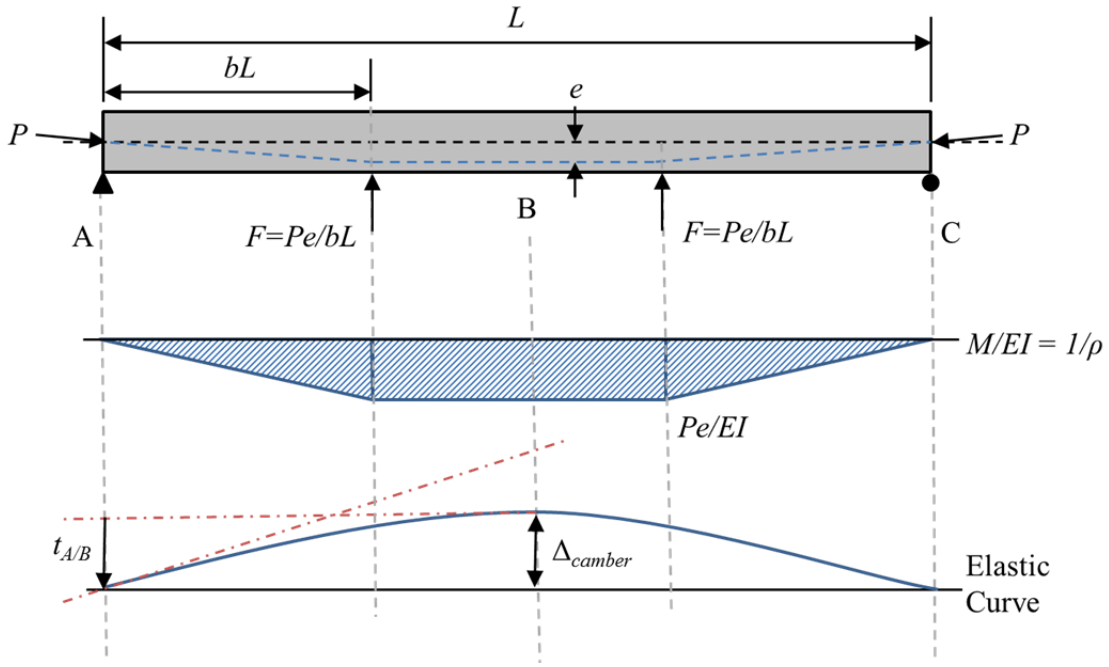

Figure 2-10: Application of Moment-Area Theorem to Calculate Elastic Camber in Simple Harped-Strand Prestressed Girder

A corresponding curvature diagram is also shown in Figure 2-10 (middle). In similar fashion to the previous example, the upward midspan camber tendency for this harped-strand girder can be then calculated as:

$$\Delta_{camber} = t_{A/B} = \left[\left(\frac{Pe}{EI}\frac{bL}{2}\right)\left(\frac{2}{3}bL\right)\right] + \left[\left(\frac{Pe}{EI}\right)\left(\frac{L}{2} - bL\right)\right]\left(bL + \frac{\left(\frac{L}{2} - bL\right)}{2}\right) \qquad (2\text{-}3)$$

Due to the straight line nature of the curvature diagrams in the two preceding examples, it is possible to compute the desired midspan deflection relatively simply by discretizing the curvature diagram into three distinct sections. If a deflection at a location other than midspan (i.e. one-sixth span) is desired, the linear nature of the curvature diagrams

discussed above again allow for simple computation of the required area under the curvature diagram. In other strand profiles representing higher-order curvature diagrams (e.g. parabolic draped strands), the solution for deflections at locations other than girder midspan (i.e. one-sixth span) can become more complex due to the higher-order nature of the curvature diagrams and the associated complexities in computing the required area of interest under the curvature diagram.

The moment-area method provides a robust, easily-programmable method, with the inherent flexibility to accommodate varying cross-sectional properties along the length of the girder. Among the most frequent refinements to the simplified procedures detailed above are the inclusion of debonding of prestressing strands and inclusion of the effect of transfer length at girder ends. The moment-area method is the primary technique for computing short-term deflections in two of the most popular prestressed concrete girder design software packages, *LEAP Conspan* by Bentley Systems, Inc. (Bentley Systems, Inc. 2012) and *PSBEAM* by Eriksson Technologies[3].

2.5.2 Elastic Camber Computation by Tabulated Equation

In today's design environment, deflection computations for prestressed concrete members are seldom calculated by hand, but instead, are computed in advanced software packages. For those design engineers needing to verify the outputs of their computer analyses, the somewhat tedious direct application of engineering beam theory (either by the moment-area technique or other implementation of beam theory) is hardly a practical choice. Instead, the PCI Bridge Design Manual (PCI 2011) offers tabulated expressions of the upward camber tendency for seven of the most common prestressing patterns as shown in

[3] As verified through author correspondence with Eriksson Technologies.

Figure 2-11. It is worthwhile to note that Cases 3 and 5 in the following table correspond to the two cases previously derived in this report by the moment-area method. Another convenience of the use of tabulated expressions is the simplicity with which the method of superposition may be applied to quickly solve for midspan camber magnitude for nearly any possible prestressing pattern and self-weight loading pattern. For instance, a design engineer attempting to compute the net design deflection due to a harped-strand prestress arrangement, not centered around the elastic centroid, including the effect of self-weight, might use a superposition of Cases 3, 5, and 6 (although the sign on Case 6 would become negative.)

Prestress Pattern	Equivalent Moment or Load	Equivalent Loading	Camber	End Rotation	
(1)	M=Pe		$+\frac{M\ell^2}{16EI}$	$+\frac{M\ell}{3EI}$	$-\frac{M\ell}{6EI}$
(2)	M=Pe		$+\frac{M\ell^2}{16EI}$	$+\frac{M\ell}{6EI}$	$-\frac{M\ell}{3EI}$
(3)	M=pe		$+\frac{M\ell^2}{8EI}$	$+\frac{M\ell}{2EI}$	$-\frac{M\ell}{2EI}$
(4)	$N=\frac{4Pe'}{\ell}$		$+\frac{N\ell^3}{48EI}$	$+\frac{N\ell^2}{16EI}$	$-\frac{N\ell^2}{16EI}$
(5)	$N=\frac{Pe'}{b\,\ell}$		$+\frac{b(3-4b^2)N\ell^3}{24EI}$	$+\frac{b(1-b)N\ell^2}{2EI}$	$-\frac{b(1-b)N\ell^2}{2EI}$
(6)	$N=\frac{8Pe'}{\ell^2}$		$+\frac{5w\ell^4}{384EI}$	$+\frac{w\ell^4}{24EI}$	$-\frac{w\ell^4}{24EI}$
(7) Debond length	M=Pe		$+\frac{M\ell^2}{8EI}(1-2b_1^2-2b_2^2)$	$+\frac{M\ell^2}{2EI}[(1-2b_1)^2-b_2^2]$	$-\frac{M\ell^2}{2EI}[(1-2b_1)^2-b_2^2]$

* The tabulated values apply to the effects of prestressing. By adjusting the directional rotation, they may also be used for the effects of loads. For patterns 4 to 7, superimpose on 1, 2 or 3 for other C.G. locations

Figure 2-11: Camber and Rotational Coefficients for Prestress Force and Loads (Precast/Prestressed Concrete Institute 2011)

2.5.3 Elastic Camber Computation by Energy Method

Energy methods are commonly used for computing elastic deflections in the field of structural mechanics. In fact, as structural members and assemblages become more complex, the application of energy methods and their scalar nature make them an attractive choice for deflection computations in these complex systems (Boresi and Schmidt 2003). Through a comprehensive review of available literature on deflections and more specifically, camber in prestressed concrete girders, no evidence was found of any past attempt to compute camber by the use of an energy method. As such, an independent effort was undertaken to investigate the feasibility of employing energy methods to compute elastic design deflections in prestressed concrete girders. A full discussion of this effort is outside the scope of this document, but a description is included in Appendix A for the interested reader. While it did prove possible to calculate deflections in prestressed concrete members by the direct application of the conservation of energy principle, this approach was extremely complex and likely not practical for use by design engineers. It is interesting to note, however, when using energy principles to compute short-term camber, there may be unique opportunities afforded to account for second-order deformations typically neglected by other types of analyses.

2.6 Techniques to Compute Long-Term Deflections

The computation of long-term deflections is substantially more complex than that of short-term deflections due to the number of parameters involved and the time-dependent and interrelated nature of these parameters. ACI 435R-95 (2003) provides guidance on five methods appropriate for computing long-term deflections in one-way prestressed concrete flexural members. Of these five methods, the following four methods are

applicable to computing deflections in uncracked flexural members: (1) PCI multiplier method, (2) incremental time-steps method, (3) approximate time-steps method, and (4) the prestress loss method. A brief review of each method is offered in this section. Readers may consult Chapter 9 for more advanced theory and implementation of the incremental time-step method as used in this study.

2.6.1 PCI Multiplier Method

Multiplier methods are the simplest available methods for predicting time-dependent deformations in precast, prestressed elements. The basic premise is that a multiplier is applied to amplify a computed short-term deflection value to approximate the long-term deflection. Early published multiplier methods were arbitrarily assigned by design engineers based on experience and served primarily as rules of thumb. Then, a more logically-grounded multiplier method was proposed by Martin (1977) that is still widely used today and forms the basis for design guidance offered in the PCI Bridge Design Manual (PCI 2011).

The multiplier method, as proposed by Martin, was intended to reflect design equations available at the time for estimating additional long-term deflection of nonprestressed reinforced concrete members. ACI Committee 318 (1971) suggested the following expression for computing the factor representing the *additional* long-term deflections in doubly-reinforced non-prestressed sections:

$$\left[2 - 1.2\left(\frac{A'_s}{A_s}\right)\right] \geq 0.6 \tag{2-4}$$

where

A'_s = the area of compressive steel reinforcement and

A_s = the area of tension steel reinforcement.

It is interesting to note that in present day, ACI Committee 318 (2014) recommends the use of a similar expression to that of Equation 2-4 as developed by Branson (1977). This current-day equivalent, shown below, includes an added factor, ξ, that allows for predictions of additional long-term deflections at various key ages of interest.

$$\lambda_\Delta = \frac{\xi}{1+50\rho'} \tag{2-5}$$

where

ξ = a time-dependent factor for sustained loads, with the recommended range from 1.0 to 2.0, and

ρ' = a ratio of the area of the compressive reinforcing steel, A'_s, to the gross area of the concrete section.

Both equations 2-4 and 2-5 suggest an ultimate multiplier of 2.0 be used for estimating long-term deflections in nonprestressed concrete members without compression steel.

Equations 2-4 and 2-5 are intended to operate on the design elastic deflection magnitude, typically calculated at a concrete age of 28 days. For these equations to be most useful to the precast, prestressed concrete industry, it is desirable for these equations to instead operate on the release elastic deflection magnitude, typically occurring approximately 18 hours after concrete placement. To accomplish this, Martin (1977) modified Equation 2-4 by the ratio of concrete stiffness at prestress release to concrete stiffness at 28 days. By assuming (1) the release strength of precast, prestressed concrete

members is usually about 70 percent of the 28-day strength and (2) that concrete stiffness is proportional to the square root of concrete strength, Martin computed the following stiffness adjustment factor:

$$\sqrt{\left(\frac{f_{ci}}{f_c}\right)} = \sqrt{0.70} \approx 0.85 \tag{2-6}$$

Finally, combining Equations 2-4 and 2-6, while further modifying to transition from a factor for calculating *additional* long-term deflections to a convenient all-inclusive multiplier, Martin (1977) proposed the following multiplier to estimate long-term deflection due to member weight from the initial elastic deflection at the release of prestress:

$$1 + \left[0.85(2.0)\right] = 2.7 \tag{2-7}$$

Next, Martin computed a multiplier intended to estimate the long-term change in the initial upward camber component due to the prestress force. By assuming that an average of 15 percent of the prestressing force is lost after prestress transfer (85 percent remaining), Martin proposed the following multiplier to determine the upward camber component of the final camber:

$$1 + \left[0.85(2.0)(0.85)\right] = 2.45 \tag{2-8}$$

Similar expressions are derived by Martin (1977) for estimation of the time-dependent changes in both the self-weight component and the upward camber component occurring by the time of erection, assumed to be 30 to 60 days after production. Intrinsic in Martin's proposed multipliers is the assumption that approximately 50% of the ultimate creep and shrinkage behavior, and, therefore, the net camber, will have occurred by the time of erection. A summary of the multipliers as originally proposed by Martin (1977)

and currently published in the PCI Bridge Design Manual (PCI 2011) is shown in Table 2-1.

Table 2-1: Long-Term Deflection Multipliers (Adapted from Martin 1977)

	Without Composite Topping	With Composite Topping
At Erection:		
(1) Deflection (downward) component – apply to the elastic deflection due to the member weight at release of prestress.	**1.85**	1.85
(2) Camber (upward) component – apply to the elastic camber due to prestress at the time of release of prestress.	**1.80**	1.80
Final:		
(3) Deflection (downward) component – apply to deflection calculated in (1) above.	**2.70**	2.40
(4) Camber (upward) component – apply to camber calculated in (2) above.	**2.45**	2.20
(5) Deflection (downward) – apply to elastic deflection due to super-imposed dead loads only.	3.00	3.00
(6) Deflection (downward) – apply to elastic deflection caused by the composite topping.	--	2.30

Although Martin (1977) also derived multipliers for composite topping assemblages and for the effect of superimposed dead loads, those multipliers of primary relevance to this dissertation are the four multipliers emphasized in Table 2-1.

2.6.2 Incremental Time-Steps Method

The incremental time-steps method is a method of analysis based on combining the computation of deflections with those of prestress losses due to time-dependent creep, shrinkage, and relaxation (ACI Committee 435 2003). By dividing the life of the flexural element into discrete time intervals and dividing the girder length into discrete cross-

sections, incremental changes in shrinkage, creep, and relaxation can be computed for each time interval and girder cross-section. Then, these incremental changes can be summed to yield strain distributions, curvatures, and prestressing forces for a particular time interval of interest, and ultimately used to compute girder deflection parameters of interest (ACI Committee 435 2003). The incremental time-steps method is particularly well-suited for computer solution (Stallings, Barnes, and Eskildsen 2003). Further discussion of the theoretical derivation, assumptions involved, and implementation of the incremental time-steps method as used in this research effort is included in Chapter 9 of this dissertation.

2.6.3 Approximate Time-Steps Method

The approximate time-steps method, as originally proposed by Branson and Ozell (1961) and refined shortly thereafter by the newly renamed ACI Committee 435[4] (1963), is based on a simplified form of the summation of constituent deflections due to various time-dependent parameters (ACI Committee 435 2003). The summation of factors is completed twice, once at prestress release and at the final condition. Serving as a compromise between complexity and efficiency of calculation, the approximate time-steps method yields results comparable to the PCI multiplier method (Stallings and Eskildsen 2001).

2.6.4 Prestress Loss Method

The prestress loss method is a computation method for use in uncracked prestressed concrete sections that uses stress loss coefficients (to approximate the effect of creep and

[4] Prior to 1963, the ACI Committee "Control of Deflection in Concrete Structures" was identified as ACI Committee 335, instead of the present-day designation of ACI Committee 435.

shrinkage losses) and a series of multipliers (similar to the PCI multiplier method) to compute the total deflection after prestress loss and before live-load application (ACI Committee 435 2003). While comparably simpler than the incremental time-steps method, the prestress loss method is heavily based on time-dependent multipliers and as such, may not yield substantially more accurate results than the PCI multiplier method.

Chapter 3: Previous Camber Studies

3.1 Introduction

The intent of this chapter is to provide a concise introduction to various previous studies relating to camber and camber prediction in precast, prestressed one-way flexural elements. By the nature of the many interrelated variables involved in deflection predictions (i.e. geometric properties, concrete compressive strength, concrete stiffness, concrete creep and shrinkage behavior, steel relaxation, and prestress losses) and the varying extent to which different researchers explore each variable, it is extremely difficult to synthesize a single literature review organized by topic without first introducing each study. Accordingly, a concise introduction and summary of each past study is presented in chronological order in this chapter. Specific previous researcher findings relevant to the major scope areas of this dissertation are presented by topic in synthesized literature reviews in later chapters as follows: concrete compressive strength (Chapter 5), concrete stiffness (Chapter 6), creep and shrinkage behavior (Chapter 7), and thermal effects (Chapter 8). Literature on the above topics, not conducted as part of a larger camber study effort, is also referenced in the synthesized literature reviews of future chapters.

3.2 Previous Camber Literature

Early literature (pre-1979) largely represents the development and refinement of various techniques for computing deflections in one-way prestressed flexural elements.

Literature of this period is frequented by the names of early prestressed concrete pioneers including Branson, Ozell, Sozen, Corley, Martin, Seiss, Burns, Nawy, and Naaman who jointly laid much of the fundamental groundwork still reflected in present-day code provisions. Much of this historic work was referenced in Chapter 2, and thus, is not repeated here.

3.2.1 Buettner and Libby (1979)

As a result of discussions within ACI Committee 435 meetings, Buettner and Libby (1979) published a paper acknowledging the growing problem of inaccurate camber predictions in prestressed concrete girders and documented the various serviceability problems often resulting from these inaccurate predictions. This paper included a survey of 37 bridge girders produced in Fairfax County, VA to determine the percent variation between predicted and measured camber at various unspecified ages. It is important to note that by present-day standards, the girders included in this study had relatively short spans averaging approximately 50 ft. It was concluded that while there was consistent variability in the surveyed girders, there appeared to be a systematic error in the calculation procedures (a similar concept to that reflected in Figure 2-2) that tended to result in over-predictions of camber. Buettner and Libby suspected the systematic error was related to (1) an inaccurate prediction of concrete stiffness, (2) an incorrect assumption of uncracked behavior when the section may actually have been cracked, (3) inaccurate calculation of the prestress force and related parameters, (4) inconsistent or inaccurate time-estimates of shipping and erection events, and (5) the effects of temperature gradients. This paper suggested the development of code provisions as follow: (1) initial prestress deflection should be measured and recorded for all projects,

(2) shop drawings should show anticipated deflections including some measure of required consistency between similar girders, and (3) the difference between the anticipated deflection and the actual deflection shall not exceed L/1200. Buettner and Libby's paper constituted the first documentation of widespread camber prediction issues in the precast, prestressed concrete industry and also correctly hypothesized many of the probable causes of these inaccuracies.

3.2.2 Tadros, Ghali, and Meyer (1985)

Tadros, Ghali, and Meyer (1985) conducted research work aimed at more precisely computing prestress losses and time-dependent deflections of prestressed concrete members. One of the main focuses of this work was to update the PCI multiplier method (originally proposed by Martin [1977]) to reflect assumptions more characteristic of high-strength concrete. In doing so, additional factors were introduced to represent the effect of relative humidity on creep and shrinkage, the effect of nonprestressed steel, and the effect of concrete cracking. The method proposed by Tadros et al. (1985), often called the revised PCI multiplier method, is substantially more complex than that proposed by Martin (1977) and yields similar results for average environmental conditions in typical girders. Despite the recommendation of Tadros et al. (1985), the multipliers contained in the PCI Bridge Design Manual (Precast/Prestressed Concrete Institute 2011) remained unchanged and still reflects the original work by Martin (1977).

3.2.3 Kelly, Bradberry, and Breen (1987)

Kelly, Bradberry, and Breen (1987) documented the instrumentation and field monitoring of eight long-span (127 ft) pretensioned AASHTO Type IV bridge girders made with high-strength concrete and low-relaxation prestressing steel. This effort was part of a

larger study aimed at evaluating the feasibility of utilizing high-strength concrete and low-relaxation steel in pretensioned bridge girders. Measurements of deformations and internal beam temperatures were recorded periodically beginning during girder production and ending one year after the bridge entered service. Deformation measurements included concrete surface strains, prestressing strand strains, and quarter- and mid-span deflections. The average camber of the eight girders included in this study was 3.3 in. The measured time-dependent camber was compared to the results of various period-specific analytical techniques for computing deflections. Most notable conclusions include: (1) the primary factors affecting time-dependent camber are concrete age-strength development, concrete creep, relative humidity, the age of concrete at release, and the construction schedule, (2) support conditions for girders in storage can dramatically affect camber and should be considered when calculating beam responses, (3) the camber of girders is very sensitive to the age and strength of concrete at prestress release, and (4) by adjusting the PCI multiplier method to reflect regional practices, increased accuracy of time-dependent camber predictions was achieved.

3.2.4 Brown (1998)

Brown (1998) examined the validity of camber growth computation methods used by the Idaho Department of Transportation (IDOT) for prestressed concrete girders. Camber measurement data was gathered from four different prestressed concrete girder manufacturers and compared to camber predictions computed by then-current IDOT design procedures. It was found that the standard IDOT prediction method tended to underestimate camber at the time of prestress release. Primary conclusions of this study included the following: (1) the primary contributor to prestress losses at release is elastic

shortening, while losses due to steel relaxation are minimal and can be neglected, (2) the incremental time-steps method provided an accurate prediction of camber after calibration of creep and shrinkage coefficients, (3) a modified PCI multiplier method was developed to include local concrete material properties and a regionally appropriate construction timeline, and (4) no clear correlation was observed between camber growth and relative humidity. Brown (1998) stressed that the camber prediction methods recommended in this study are based on estimates of the modulus of elasticity, ultimate creep coefficient, and ultimate shrinkage strain and should be validated by a future material testing program. Also noteworthy from Brown's work is the first historical discussion of various methods for camber control—that is, manually inducing a change in camber after production to meet a specified camber magnitude.

3.2.5 Wyffels, French, and Shield (2000)

Conducting a study for the Minnesota Department of Transportation (MnDOT), Wyffels, French, and Shield (2000) investigated the effect of pre-release cracking in precast, prestressed concrete bridge girders. Often observed during the fabrication process upon removal of formwork, pre-release cracking is typically assumed to have a negligible effect on prestressed girders due to the closing of cracks upon prestress release and the corresponding autogenous healing which may occur thereafter (Wyffels et al. 2000). The findings of various analytical techniques employed in this study suggested the following: (1) if discrete pre-release cracking occurs predominately above the girder neutral axis, it is possible that upon prestress release, the closing of these cracks may cause a reduced compressive stress at the bottom of a section, and thereby cause (2) a reduced camber effect in bridge girders exhibiting widespread pre-release cracking. This concept is

illustrated in Figure 3-1. Despite evidence from various analytical models, this hypothesis by Wyffels et al. (2000) has not yet been verified by experimental work. Accordingly, some researchers are skeptical and contend that the effect of pre-release cracking is indeed negligible for precast, prestressed concrete bridge girders.

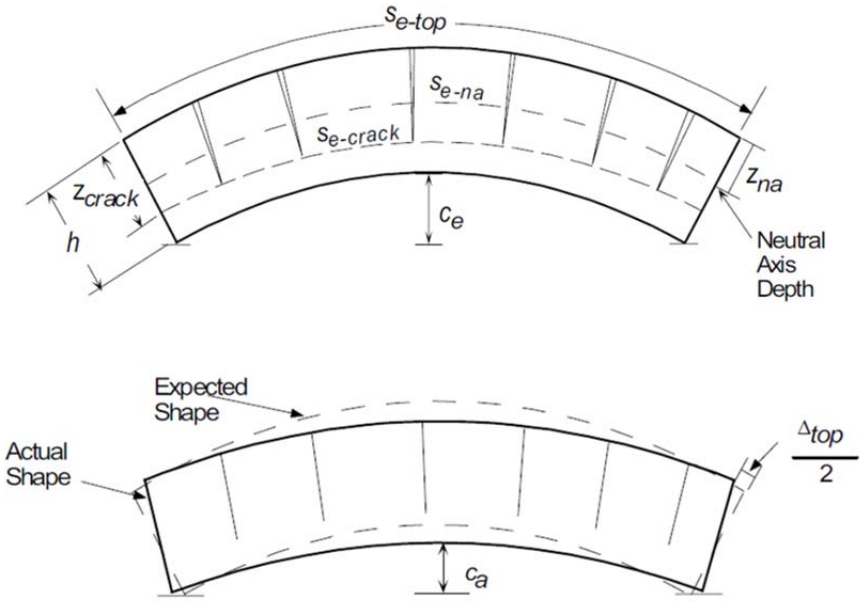

Figure 3-1: Effect of Pre-Release Cracking on Elastic Camber Magnitude (Adapted from Wyffels et al. 2000)

3.2.6 Stallings, Barnes, and Eskildsen (2003)

As part of a study conducted for the Alabama Department of Transportation (ALDOT), Stallings, Barnes, and Eskildsen (2003) investigated the accuracy of available camber and prestress loss prediction methods for bridge girders produced with high-performance concrete (HPC). This effort included a field instrumentation study of five BT-54 bridge girders used in Alabama's HPC Showcase Bridge. Field measurements included concrete strain, internal temperature, and midspan camber at various times throughout the early life of the girder. A complementary laboratory phase of this study was conducted to

determine the creep, shrinkage, and elastic properties of the HPC concrete used in the field project. Primary conclusions of Stallings et al. (2003) included: (1) accurate predictions of camber can be achieved using the incremental time-steps method and approximate time-step method so long as material parameters representative of the actual concrete used in girder production are used, (2) measured camber values at erection were significantly less than those predicted by the PCI multiplier method (attributed to the tendency of HPC to exhibit reduced creep and shrinkage behavior), (3) concrete strains at the level of prestressing strands showed good agreement (within 20 percent) of predicted values for times up to 300 days, and (4) time-dependent prestress loss predictions using the HPC material parameters were sufficiently accurate.

3.2.7 Cook and Bloomquist (2005)

Cook and Bloomquist (2005), funded by the Florida Department of Transportation (FDOT), conducted a study to verify the accuracy of camber estimates in prestressed concrete bridge girders in the state of Florida. As part of this effort, time-dependent deformations and concrete surface temperatures were monitored for 13 precast, prestressed concrete bridge girders and compared to camber values predicted by the software package *PSBEAM* developed by Erikkson Technologies. Cook and Bloomquist developed a curvature-based analytical procedure to compensate for the effect of varying temperature gradients on field-measured camber values, thereby providing more consistent comparisons between measurements regardless of varying ambient conditions. The following primary conclusions were developed by Cook and Bloomquist (2005): (1) the observed camber increase with time for the field-monitored girders was significantly less than predicted by design software, (2) future work is needed to experimentally

determine the creep and shrinkage properties of typical FDOT concretes, (3) the influence of thermal gradients on camber must be accounted for in field measurements, (4) storage conditions (namely, the height between the bottom of the girder and the ground) seem to affect the development of time-dependent concrete properties and, therefore, can affect the time-dependent development of camber, and (5) consistent differences were documented between camber measurements taken at prestress release and measurements taken shortly thereafter when girders were relocated to storage. A follow-up study (also sponsored by FDOT) was conducted by Tia, Liu, and Brown (2005) that focused on determining time-dependent properties (i.e. modulus of elasticity and creep and shrinkage behavior) for various FDOT concretes. This follow-up study is reviewed in the synthesized literature reviews of Chapter 6 (Concrete Stiffness) and Chapter 7 (Creep and Shrinkage Behavior).

3.2.8 Barr, Stanton, and Eberhard (2005)

Concurrent with the work of Cook and Bloomquist (2005), Barr, Stanton, and Eberhard (2005) also independently examined the effect of temperature variations on precast, prestressed concrete girders in a project funded by the Washington Department of Transportation (WSDOT). By monitoring five precast, prestressed concrete girders during fabrication and service, Barr et al. (2005) were able to determine the effect of elevated curing temperatures on prestress losses and also validated a curvature-based temperature correction procedure. Primary findings of this work include the following: (1) a curvature-based approach for computing thermally-induced deformations and stresses was developed and verified to accurately predict observed girder thermal responses and (2) the elevated curing temperatures typical of precast, prestressed concrete

can cause a significant reduction in the magnitude of the prestressing force (up to approximately 12 ksi), which corresponds to a significant decrease in observed midspan camber.

3.2.9 Hinkle (2006)

Hinkle (2006) conducted a study to identify the most accurate time-dependent material models for use in predicting time-dependent deflections of 27 high-strength prestressed concrete bridge girders in South Carolina. Girder deflections were periodically measured to determine camber growth and limited concrete materials testing (strength and stiffness) was conducted during girder production. An incremental time-steps method was implemented for predicting camber growth and allowed trial iterations to determine best-suited time-dependent material parameters for the analysis. Notable conclusions of Hinkle (2006) include the following: (1) same-day measured cambers tended to vary by up to ½ in. due to thermal exposures, (2) the PCI multiplier method (proposed by Martin 1977) tended to overestimate camber by 48 percent at an age of 60 days, (3) and the revised PCI multiplier method (proposed by Tadros et al. 1985) tended to overestimate camber by 21 percent at an age of 60 days. Specific recommendations relevant to key focus areas of this dissertation are reviewed in later chapters.

3.2.10 Rosa, Stanton, and Eberhard (2007)

Sponsored by the Washington State Department of Transportation (WSDOT), Rosa, Stanton, and Eberhard (2007) conducted a research investigation to develop improved methods for predicting camber in prestressed concrete girders. As part of this project, prestressed girders were monitored from four WSDOT bridge projects (146 girders for short-term monitoring and 91 girders for long-term monitoring.) Typical measured data

included deflections at various ages and selected concrete material properties (compressive strength, modulus of elasticity, and creep and shrinkage behavior). Using a time-steps method for camber-growth analysis, Rosa et al. (2007) calibrated various constitutive models to reflect the field-observed deflections of girders and achieved much-improved predictions of camber. In addition, the effect of friction (between the girder and the prestressing bed) on the magnitude of initial elastic camber was investigated using a roller assembly placed under a girder end immediately after prestress release. Most notable conclusions by Rosa et al. (2007) included the following: (1) various noteworthy recommendations regarding concrete strength, stiffness, and creep and shrinkage behavior (which are included in the synthesized literature reviews of later chapters), (2) the effect of lifting and re-seating a girder tended to increase the measured camber by 0.15 in., and (3) girders stored on oak blocks tended to behave as if they were approximately 50 percent stiffer than those seated on elastomeric bearings (attributed to the partial restraint provided by oak blocks).

3.2.11 Jayaseelan and Russell (2007)

In a study funded by the Oklahoma Department of Transportation (OKDOT), Jayaseelan and Russell (2007) implemented a time-steps method to compute prestress losses of precast, prestressed concrete girders at varying ages. While this study was primarily a study of prestress losses, the effect of changes in prestressing forces were frequently extrapolated to the camber-growth behavior of the girder. For instance, for an AASHTO Type IV girder with a 105 ft span and a prestressing arrangement typical of an OKDOT girder, Jayaseelan and Russell (2007) concluded the following: (1) the addition of two top prestressing strands reduced the expected camber magnitude by 35 percent, while the

addition of four top prestressing strands reduced the camber by 70 percent, (2) the addition of five #9 longitudinal mild steel reinforcement bars did not appreciably alter the values of long-term losses, but decreased the long-term camber by approximately 17 percent, (3) a 20 percent decrease in creep coefficient corresponded to a 6.8 percent decrease in long-term camber, and (4) a 20 percent increase in elastic modulus reduced the long-term prestress losses by 6 percent and the long-term camber by 12 percent.

3.2.12 Omar, Pui Lai, Poh Huat, and Omar (2008)

A study conducted in Malaysia by Omar, Pui Lai, Poh Huat, and Omar (2007) gives an international perspective on camber prediction in prestressed concrete girders. It is interesting to note that the beam deflection domestically referred to as "camber" is referred to as "pre-camber" in Malaysia. Omar et al. identify the fundamental disparity between assumed and observed properties for concrete strength and stiffness and recommend the use of local concrete properties in pre-camber computations. Furthermore, a simplified expression is proposed (somewhat similar in principle to the PCI multiplier method) in order to approximate the time-dependent change in pre-camber occurring after girder production. This proposed expression relies on assumptions of an average prestressing force magnitude (and therefore an assumed prestress loss) and a creep coefficient parameter. Omar et al. found that by accounting for the time-dependent nature of concrete through the use of a creep coefficient and assumed prestress loss magnitude, improved accuracy of pre-camber predictions was achieved for early-life girder ages (up to 15 days).

3.2.13 Barr and Angomas (2010)

As a follow-up to the efforts of Barr, Stanton and Eberhard (2005), Barr and Angomas (2010) revisited the previous research work, revised certain portions of the analytical procedure, and more thoroughly compared the predicted behaviors to field-observed behaviors. Key findings by Barr and Angomas (2010) included the following: (1) high curing temperatures caused a corresponding reduction in computed camber of 33 percent, not 40 percent as previously reported, (2) changes in camber due to elevated curing temperature are a result of both a reduction in strand stress and a non-uniform temperature profile at the estimated time of bonding, (3) the time-steps method implemented using the material properties recommended in NCHRP Report 496 (Tadros et al. 2003) resulted in camber predictions within 10 percent of the measured long-term cambers, and (4) the PCI multiplier method (Martin 1977) yielded predicted cambers 22 percent lower than observed, while the modified multiplier method (Tadros et al. 1985) yielded predicted cambers 27 percent higher than observed.

3.2.14 Lee (2010)

Lee (2010) conducted an experimental and analytical study on a BT-63 concrete girder segment to investigate thermal effects on the girder. Using a two-dimensional finite element heat-transfer analysis model and a three-dimensional solid finite element analysis, vertical and lateral displacements due to measured environmental conditions were computed. After validation of the model, extremes in thermal effects were used to predict the maximum thermal vertical and lateral movements in terms of span length for four PCI girder shapes. Finally, additional work focused on evaluating the effect that varying assumptions of thermal concrete properties had on the computed maximum

deflections of the four PCI girder shapes. Conclusions and recommendations by Lee (2010) are presented in the synthesized literature review of Chapter 8 of this dissertation.

3.2.15 Tadros, Fawzy, and Hanna (2011)

A study conducted by Tadros, Fawzy, and Hanna (2011) served largely as a review of the state-of-the-art on camber prediction in precast, prestressed concrete girders, but also included a valuable discussion on the anticipated variability in camber and best practices for accommodating this variability in design detailing efforts. Tadros et al. (2011) suggested the following: (1) designers should accommodate camber variation of up to 50 percent from the predicted value in detailing of bridges, (2) all bridges should be designed with a minimum girder haunch of 2.5 in., (3) shear reinforcement should be detailed to accommodate camber variability by keeping protruding bars vertical prior to erection and bending on-site to final elevations, (4) girder seats should be finalized near the time of girder installation to accommodate variable elevations, (5) contractor pay items based on concrete volume should be avoided and instead, the contractor should account for girder variability in their initial bid, and (6) designers should accommodate local material properties and storage and construction practices during design, if practical.

3.2.16 French and O'Neill (2012)

Sponsored by the MnDOT, French and O'Neill conducted a field study to validate beam deflections and camber estimates of prestressed concrete I-beams. Historical data gathered as part of this project representing 1,067 bridge girders showed that camber at release and erection was typically overpredicted by 74 percent and 83.5 percent, respectively. These inaccuracies in camber prediction were attributed primarily to under-

predictions of the concrete compressive strength and corresponding modulus of elasticity of the concrete. This project included limited field concrete material testing (concrete strength and stiffness) and field monitoring of the time-dependent deflections in 14 girders of varying lengths and cross-sections through the time of shipping. An analytical model was developed to evaluate the influence of various time-dependent effects on long-term camber and used to develop a multiplier-based prediction model for use by MnDOT. Primary conclusions from French and O'Neill (2012) relevant to the work of this dissertation include the following: (1) various recommendations regarding predicting concrete compressive strength and modulus of elasticity during the design phase (as summarized in Chapters 5 and 6 of this dissertation), (2) ambient relative humidity was found to be a primary contributor to camber variability (a change in relative humidity of 30 percent caused a corresponding change in long-term camber of 10 percent), (3) various changes to standard construction timing and practices were proposed to decrease the girder-to-girder variability, and (4) varying sets of revised multipliers were proposed to predict time-dependent changes in deflections more accurately.

3.2.17 Schrantz (2012)

Schrantz (2012) developed a visual-basic (VB) computer program that implemented an incremental time-steps method for computing initial and time-dependent camber in prestressed concrete girders. Various models for concrete modulus of elasticity and creep and shrinkage behavior were included in the software development allowing users to easily compute camber and camber-growth using these varying parameters. Schrantz (2012) validated the accuracy of the software program using measured strain and camber results from three previous research programs (Boehm 2008, Levy 2007, Stallings et al.

2003) and provided preliminary recommendations of the material models best suited for camber predictions in Alabama. Chapter 9 details the fundamental theory and development of the incremental time-steps method implemented in this dissertation, largely based on the initial work by Schrantz (2012), later refined by Johnson (2012), and finally expanded and finalized by Isbiliroglu (2014).

3.2.18 Johnson (2012)

As part of a comprehensive project evaluating the suitability of self-consolidating concrete (SCC) for precast, prestressed concrete applications, Johnson (2012) conducted comparisons of predicted and actual measured time-dependent deformations in 28 bulb-tee girders for an Alabama Department of Transportation (ALDOT) bridge replacement project. Data gathering efforts relevant to Johnson's work included the measurement of internal concrete strains and internal girder temperatures and the testing of selected time-dependent concrete material properties. The development of a curvature-based temperature correction procedure (similar to that of Barr et al. [2005]) was developed as part of Johnson's work to remove the effect of varying temperature gradients on field camber measurements. By comparing measured field data to the predicted structural behavior, Johnson (2012) reached the following conclusions: (1) time-dependent strain predictions in the bottom-flange of girders were reasonably accurate for all creep and shrinkage models evaluated in this study, (2) there was a systematic over-estimation of concrete strains occurring at later girder ages, (3) the effective prestressing force was overpredicted in the first months after prestress transfer and underpredicted at later ages, (4) measured midspan camber magnitudes were generally less than predicted for ages up to 200 days, and (5) none of the creep and shrinkage models investigated as part of this

study tended to predict time-dependent camber growth particularly well. Work by Johnson (2012) demonstrated the need for improved methods to predict time-dependent camber growth in ALDOT prestressed concrete girders and thus, partly spurred the research efforts contained in this dissertation.

3.2.19 Precast/Prestressed Concrete Institute Committee on Bridges (2012)

In order to evaluate the appropriateness of the current PCI construction tolerance limits for camber of prestressed concrete bridge girders, the PCI Committee on Bridges (2012) gathered data representing the measured and predicted release camber values for 1,835 girders from eight states across the United States. Using these data, the PCI Committee on Bridges (2012) recommended changes to the permissible camber tolerance at release to more accurately represent the variability of the historical data set as shown in Figure 3-2. The blue-shaded areas represent those areas within the current camber tolerance limits, while the red-shaded areas show the expanded area proposed to be considered within tolerance. By increasing the tolerance limits as shown, the number of girders in the historical sample falling within tolerance increased from 66 percent to nearly 90 percent.

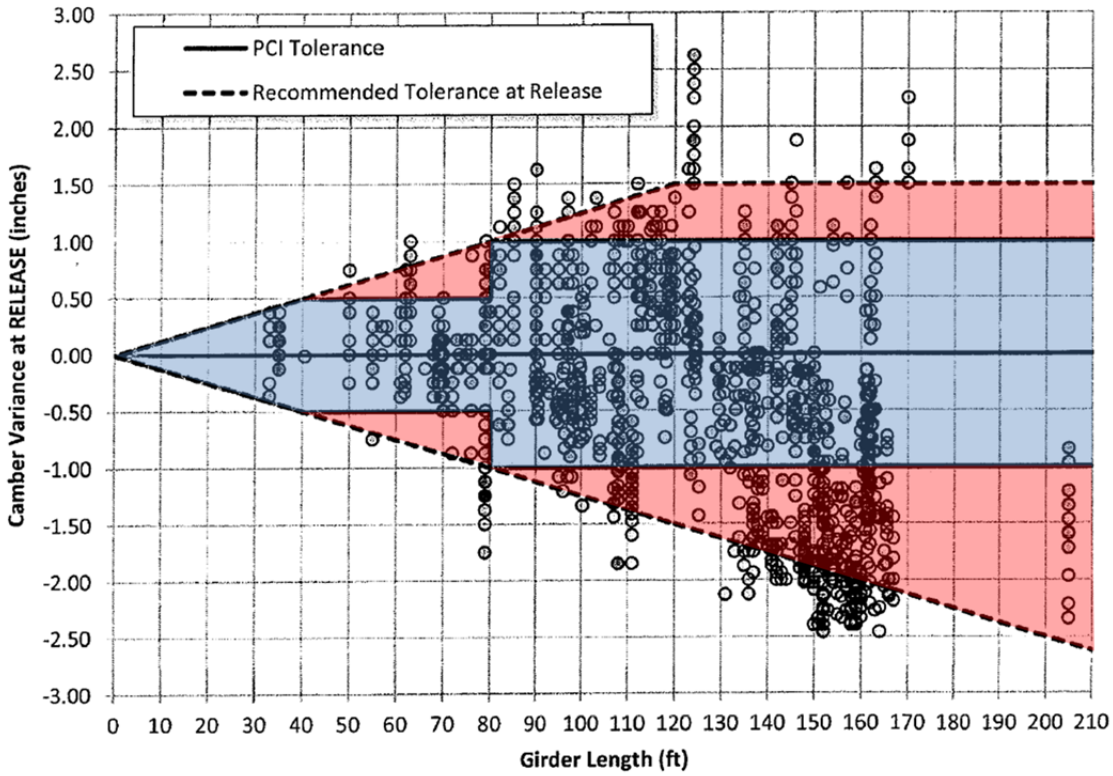

Figure 3-2: Proposed PCI Camber Tolerance Limit Revisions (Adapted from PCI Committee on Bridges 2012)

It is interesting to note that the revised camber tolerance upper limit is capped at a value of +1.5 in., reflecting the more severe consequence for a girder with underestimated camber as opposed to a girder with over-estimated camber. The efforts of the Committee on Bridges (2012) do not examine the procedures or assumptions used for computing camber and thus, may not address the root causes of inaccurate camber predictions in precast, prestressed concrete girders.

3.2.20 Storm, Rizkalla, and Zia (2013)

Storm, Rizkalla, and Zia (2013) conducted a field and laboratory study to examine the various parameters affecting camber predictions, with particular attention to factors related to girder production. As part of this study, camber measurements at the time of

prestress transfer were collected for 382 pretensioned concrete girders from nine states and supplemental concrete material testing was conducted to determined compressive strength, elastic modulus, and unit weight at various concrete ages. Camber was measured immediately after prestress transfer, at the beginning of storage, prior to shipment, and after erection. Primary findings of Storm et al. (2013) relevant to this research effort included the following: (1) recommendations are proposed to more accurately predict concrete strength and stiffness during the design phase (as referenced in Chapters 5 and 6 of this dissertation), (2) neglecting the effect of debonding and transfer length at girder ends caused errors as high as 13 percent in camber computations, (3) the effect of thermal effects on the loss of prestressing prior to prestress transfer may be as high as 7 percent, and (4) both an approximate method (based on the PCI multiplier method) and an incremental time-steps method provided reasonably accurate camber predictions within 10-15 percent of measured values.

3.2.21 Mahmood (2013)

Mahmood studied the theoretical feasibility of using post-tensioned strands as a means of camber control in simply-supported prestressed concrete bridge girders and also explored the corresponding reduction in girder load capacity. Mahmood (2013) concluded that camber control by the use of post-tensioned strands was a viable method and resulted in minimal reductions to the load-carrying capacity of corrected members (the load-carrying capacity of an AASHTO Type IV member was reduced by 2.9 percent per 100,000 lb. of post-tensioning jacking force). Future work was recommended to investigate the effect of camber control on other girder types and to evaluate the practical feasibility of this proposed method.

3.2.22 He (2013)

To improve the accuracy of long-term camber predictions in prestressed concrete girders for the Iowa Department of Transportation (IDOT), He (2013) conducted a laboratory study to investigate selected time-dependent properties (modulus of elasticity and creep and shrinkage behavior) of seven regional concrete mixtures and later compared the results of various camber prediction techniques to the observed time-dependent camber behavior of 26 prestressed high-performance concrete bridge girders. He (2013) concluded the following: (1) the errors between the predicted and measured modulus of elasticity values were up to 20 percent, (2) sealed concrete specimens tended to represent the creep and shrinkage behavior of the full scale prestressed girder better than unsealed specimens, (3) when calculated by gross section properties instead of transformed section properties, girder camber was on average 13 percent higher, (4) the time-steps method implemented in this study predicted camber within 25 percent accuracy, (5) roughly 50 percent of ultimate camber growth had occurred one year after girder production. More specific recommendations and findings are reviewed in Chapter 7 of this dissertation.

3.2.23 Nervig (2014)

Also funded by IDOT, Nervig (2014) focused on improving the predictions of instantaneous camber for prestressed concrete bridge girders through comparisons of measured and predicted release cambers for 105 prestressed concrete beams. Nervig concluded that a combination of inconsistent field measurement techniques and inaccurate estimates of material properties were the primary factors resulting in inaccurate camber predictions and accordingly, provided guidance to producers and designers in an attempt to improve the accuracy of camber predictions. Various specific

recommendations by Nervig (2014) are referenced in Chapters 5 and 6 of this dissertation.

3.2.24 Keske (2014)

Keske (2014) expanded on the previous efforts of Johnson (2012), exploring the time-dependent behavior of full-scale precast, prestressed girders. Specifically, Keske included the influence of measured concrete material properties (coefficient of thermal expansion and creep and shrinkage and behavior) on the accuracy of deflection predictions. While Keske's efforts were aimed predominately at evaluating the difference between conventionally-vibrated concrete (CVC) and self-consolidating concrete (SCC), the accuracy of various time-dependent property prediction models was evaluated. Specific recommendations of Keske (2014) are included in Chapters 6, 7, and 8 of this dissertation.

3.2.25 Hofrichter (2014)

As part of the work of this dissertation, Hofrichter (2014) completed an analysis of historical records representing more than 1,900 precast, prestressed girder pours to examine the common practices of the prestressed industry in Alabama and to recommend relationships for predicting concrete compressive strength and modulus of elasticity at the time of girder design. Hofrichter's efforts reflect earlier iterations of a portion of the work detailed in Chapters 5 and 6 of this dissertation.

3.2.26 Isbiliroglu (2014)

Further refining the work of Schrantz (2012) and Johnson (2012), Isbiliroglu (2014) compiled a near-finalized version of the time-steps camber prediction software used in

this dissertation and validated this software using the results from previous experimental research including those of Johnson (2012), Schrantz (2012), Boehm (2008), Stallings et al. (2003), and Levy (2007). Improvements to the camber prediction software made by Isbiliroglu (2014) included: (1) development of a more user-friendly interface capable of importing and exporting project files and results, (2) implementation of new versions of design code parameters and material prediction models; and (3) implementation of various recommendations of Hofrichter (2014) and Keske (2014).

3.2.27 Davison (2014)

Davison (2014) developed a camber prediction algorithm that attempted to link time-dependent constitutive material models while also explicitly considering various discrete fabrication events in a computationally efficient manner. Advantages of the proposed method include: (1) the time-dependent concrete behavior, as well as its interdependence with strand relaxation and environmental loading in the form of shrinkage and thermal affects is analyzed explicitly at every step, (2) the analysis begins with the stressing of the strand and includes all pre-release activities relevant to camber, and (3) the developed algorithm is flexible and allows the exploration of alternative constitutive models for the material behavior. Preliminary comparisons of predicted behaviors from this algorithm and measured data show promising agreement, but additional work is needed to validate this algorithm and more accurately calibrate the various constitutive models.

3.3 Comments on Previous Camber Studies

From the brief review offered of the aforementioned camber studies, it is evident that a great deal of research effort has been devoted to improving the accuracy of short-term

and long-term deflection predictions in prestressed concrete elements within the last 35 years. The following comments are offered as a general impression of these past efforts:

- Available methods for computing short-term and long-term deflections are capable of providing fairly accurate estimations of deflections in precast, prestressed concrete girders assuming that accurate values of material properties are known and utilized in computations;
- The constitutive materials in concrete are regionally-variable and thus, studies in various geographical areas are necessary to accurately capture local concrete material parameters;
- Design and production practices can greatly affect the accuracy of deflection computations in precast, prestressed concrete members and, therefore, designers should make educated assumptions of future material properties that reflect regional practice whenever possible;
- It is relatively rare for a single camber study to conduct thorough supplemental concrete materials research to thoroughly explore concrete strength, stiffness, creep and shrinkage behavior, and thermal properties;
- The majority of studies rely on measured camber as a metric of prediction accuracy and do not consider the accuracy of internal concrete strain predictions that are prerequisite computations in any curvature-based camber prediction procedure; and
- Despite the development and implementation of multiple incremental time-steps procedures for computing long-term camber in precast, prestressed concrete girders, software packages are rarely published or freely distributed for use by others.

Chapter 4: Current Design and Construction Practices for ALDOT Precast, Prestressed Concrete Bridge Girders

4.1 Introduction

A logical starting point for a study aimed at improving camber predictions in precast, prestressed concrete girders is to explore and document the existing procedures used for design and construction of precast, prestressed concrete bridge girders within the study region. Without intimate knowledge of these production practices and the often complex relationships among designers, material suppliers, producers, and erectors, it is difficult to propose viable and efficient solutions to real-world problems that are both convenient and agreeable to all vested parties. Accordingly, this dissertation chapter documents the current state-of-the-art of the precast, prestressed concrete girder industry as applicable to ALDOT bridge projects. Included in this chapter is a general background of the prestressed concrete industry in Alabama, a review of typical girder design roles and procedures, a discussion of concrete mixture proportioning for regional prestressed applications, a brief review of girder production practices relevant to camber and camber-prediction, and a summary of the documentation required to be recorded during girder production. The majority of the information presented herein is derived from field visits to various prestressed concrete plants within the study region, a review of available historical plant records, and correspondence with ALDOT Bridge Bureau design personnel.

4.2 Background

The precast, prestressed concrete industry in Alabama and surrounding states actively manufactures concrete bridge girders and prestressed concrete piles for use in Alabama Department of Transportation (ALDOT) bridge construction projects. The work reflected in this study deals exclusively with precast, prestressed concrete bridge girders and focuses primarily on PCI bulb-tee standard shapes.

4.2.1 Prevalence of Precast, Prestressed Concrete Bridges in Alabama

The use of precast, prestressed concrete girders is fairly widespread in bridges throughout the State of Alabama. As of 2012, there were 1,113 prestressed concrete stringer/multi-beam bridges in service throughout the state, as compared to 2,104 steel stringer/multi-beam bridges (Svirsky 2015). Available data representing the frequency of prestressed concrete bridge girder usage in the five Alabama counties with more than 500 bridges is shown below in Table 4-1. This data is compiled by the Federal Highway Department (FHWA) as part of the National Bridge Inventory (NBI) program.

Table 4-1: Prevalence of Prestressed Concrete Bridges in Alabama (Baughn 2014)

Alabama County Name	Number of Prestressed Concrete Bridges In Service	Total Number of Bridges In Service	Prestressed Concrete Bridges as Percent of Total (%)
Montgomery	61	592	10.3
Mobile	83	576	14.4
Tuscaloosa	46	458	10.0
Jefferson	136	1,022	13.3
Madison	75	639	11.7
Total	401	3,287	12.2

Note: Data last compiled in 2013 from FHWA National Bridge Inventory.

As seen in Table 4-1, on average, 12.2 percent of the bridges in the five most bridge-populous counties in Alabama utilize precast, prestressed concrete girders as primary

flexural elements. While this percentage may seem relatively low, it is important to note that the total number of bridges in service includes a disproportionately high number of short-span concrete culverts and concrete slab bridges. Without more detailed data available, the author estimates that roughly one-half of all bridges with span lengths exceeding 100 ft in Alabama are constructed using prestressed concrete elements.

4.2.2 Regional Precast, Prestressed Concrete Producers

Throughout the course of this research study, the precast, prestressed concrete industry proved to be rather dynamic with multiple production facilities closing, changing ownership, or ceasing to produce ALDOT bridge girder products altogether. In order to be eligible to produce ALDOT precast, prestressed bridge girders, a production facility must be certified by the Precast/Prestressed Concrete Institute (PCI) to a level of at least Category B4 (deflected strand bridge members) and also maintain pre-qualification from ALDOT. The PCI plant certification program ensures that each certified plant develops and maintains an in-depth, in-house quality system based on time-tested national industry standards and requires two unannounced audits per calendar year (PCI 2011). Qualification by ALDOT is independent of PCI-certification and is based on a producer's ability to satisfy the requirements of all applicable ALDOT specifications and standards (ALDOT 2012). At the commencement of this study in 2012, there existed eleven PCI-qualified prestressed concrete plants in Alabama and the states directly adjacent as shown in Figure 4-1.

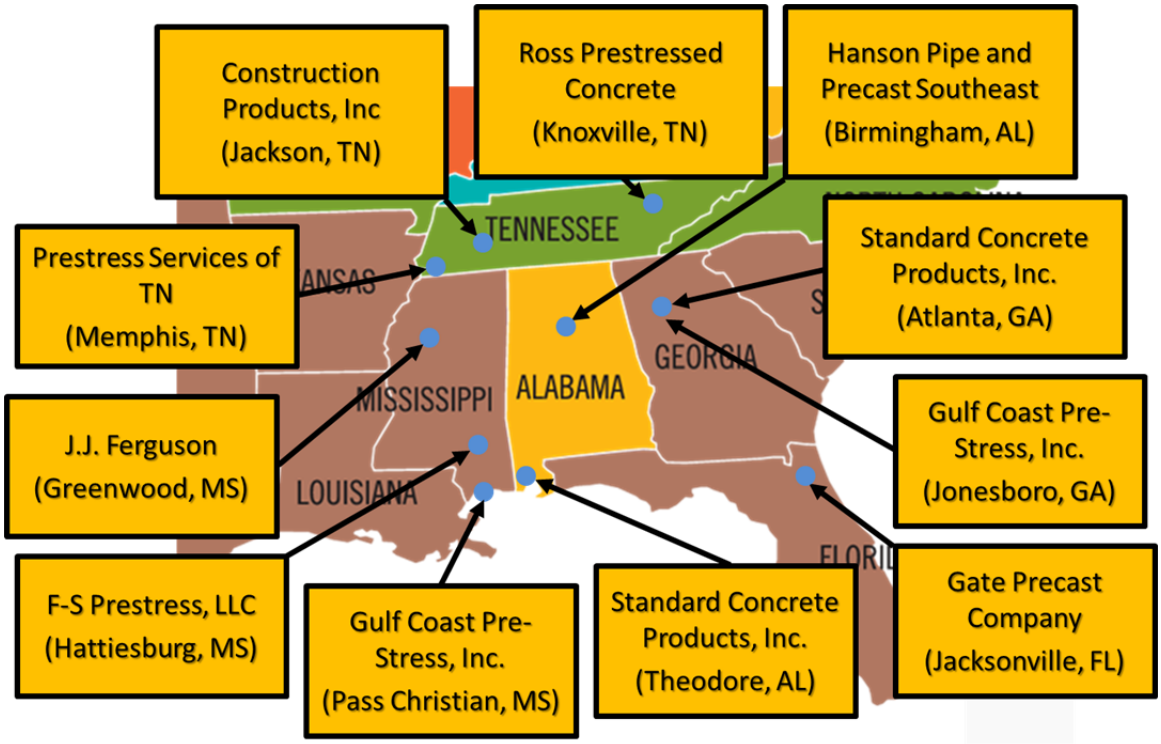

Figure 4-1: PCI-Qualified Prestressed Concrete Plants in Alabama and Neighboring States

Early discussions with ALDOT personnel identified five of the eleven precast, prestressed plants that maintained active ALDOT qualifications to bid precast, prestressed concrete bridge girder work. These five producers were the subject of plant visits by researchers early in this project and included two plants within Alabama, two in Georgia, and one in Mississippi, as shown in Figure 4-2.

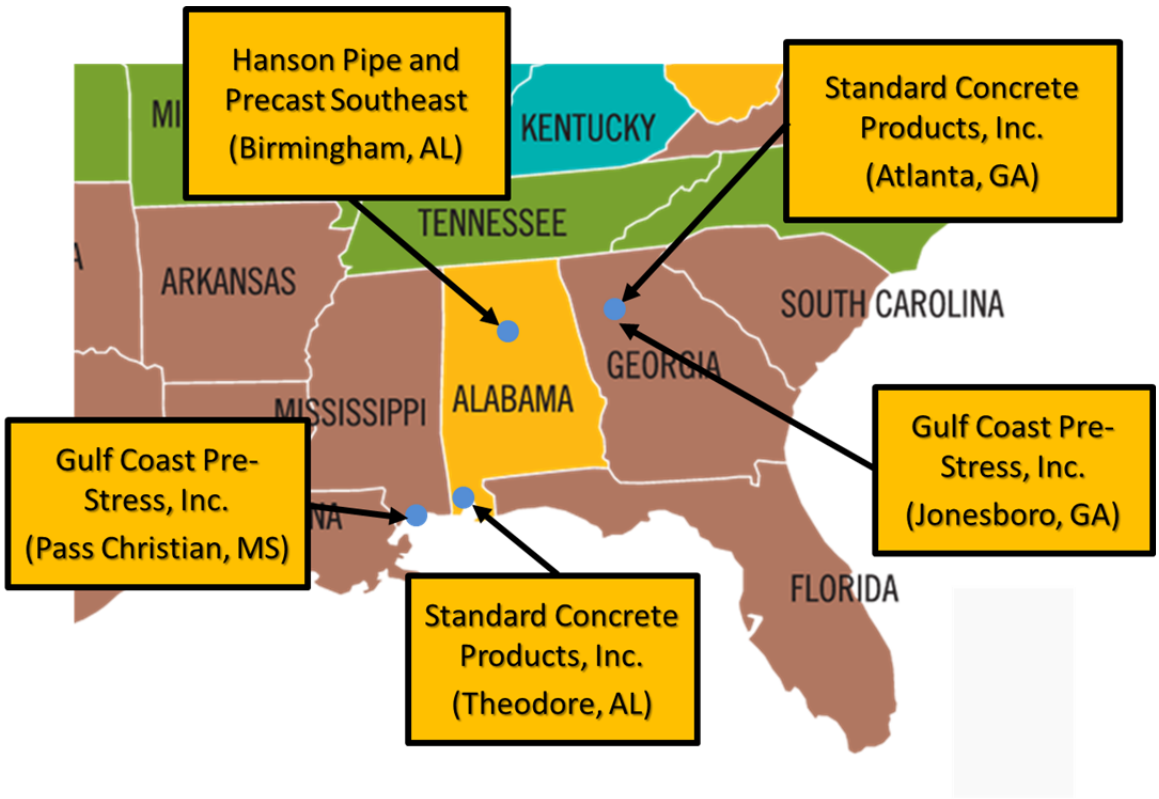

Figure 4-2: ALDOT Qualified Precast, Prestressed Concrete Producers in 2012

Throughout the course of this study, two of the five ALDOT-qualified plants would change ownership and ultimately close, while an additional plant would cease producing ALDOT bridge girders. At the conclusion of the data-gathering phase of this study in 2015, only two plants remained eligible to produce ALDOT precast, prestressed bridge girders: Hanson Pipe and Precast Southeast in Birmingham, Alabama and Gulf-Coast Pre-Stress, Inc. in Pass Christian, Mississippi. The dynamic nature of the prestressing industry in the study region would prove to hamper field-data gathering efforts to some extent and necessitate changes to the data-gathering methodology of the research effort.

4.2.3 Distribution of ALDOT Girder Types

As part of this research effort, historical data representing nearly 5,000 ALDOT precast, prestressed girders was collected from over 1,900 girder concrete placement events[5] throughout the six-year period spanning from 2007 to 2013. The frequency of usage for various standard girder shapes during this time period is shown in Figure 4-3.

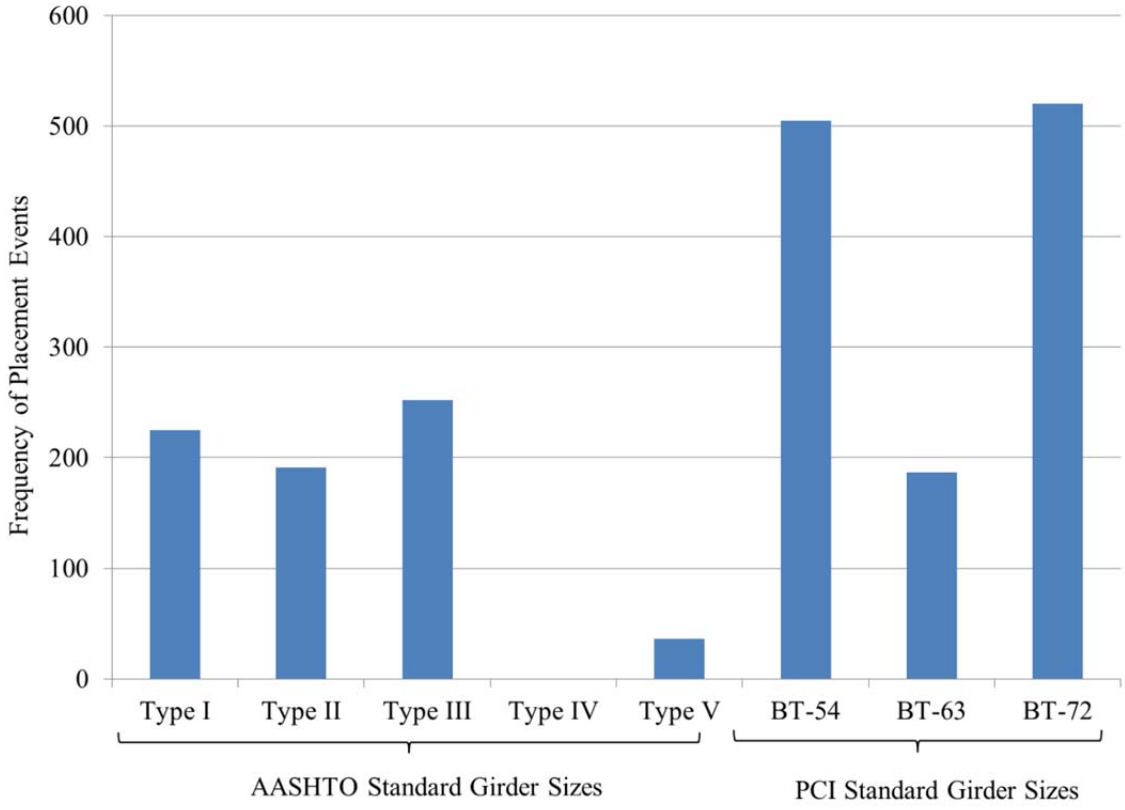

Figure 4-3: Frequency of ALDOT Girder Types from 2007-2013

The most common shapes for ALDOT prestressed concrete bridge projects are the PCI BT-54 and BT-72 shapes, with a lesser proportion of girders utilizing PCI BT-63 and standard AASHTO shapes. The increased incidence of BT-54 and BT-72 girders is likely attributed to the tendency of designers to use BT-72 sections for main spans and then

[5] The term "girder placement event" refers to the practice of producing multiple precast, prestressed concrete girders on a single production line. Typically, between 2 and 3 girders are produced in a single girder placement event.

default to the smallest bulb-tee shape, the BT-54, for shorter approach spans on bridge ends.

4.3 Design of Precast, Prestressed Concrete Bridge Girders in Alabama

The design and pre-construction planning of precast, prestressed concrete bridge girders in the state of Alabama is an interactive process typically involving both ALDOT in-house bridge designers and design staff at prestressing plants. First, a comprehensive prestressed concrete bridge design is completed in accordance with the ALDOT Structural Design Manual (ALDOT 2014) and other applicable design codes. Approximately 85 percent of the time[6], this comprehensive design is completed fully in-house by ALDOT bridge designers without the assistance of outside bridge consultants. After completion of the design and preparation of the contract documents, the project is let for competitive bidding by bridge erection contractors. Each bridge erector must include the cost of fabrication of the precast, prestressed concrete girders from an ALDOT-qualified prestressing plant. After award of the project, the engineering team at the awarded prestressing plant conducts independent design checks of the girders at varying stages of production and prepares shop drawings for ALDOT approval. The purpose of these shop drawings is to confirm the design intent of the project and expand the information on contract drawings as necessary for production of a component. The following sections summarize the requirements of structural design and detailing for ALDOT precast, prestressed concrete bridge girders and also discuss the role of shop drawings and the independent design review conducted by prestressing plant design engineers. The subsequent sections also attempt to highlight specific factors relevant to

[6] Per discussions with ALDOT Bridge Bureau Bridge Design Personnel (February 2015)

camber and camber-prediction within the following two phases of design: (1) preliminary design and (2) the design-review phase.

4.3.1 Preliminary Girder Design by ALDOT

This section aims to discuss (1) the requirements and code provisions applicable to the design of ALDOT prestressed concrete girders, (2) various design software typically used by ALDOT and procedures implicit to these software, and (3) the preparation of contract drawings, specifically with regards to noting camber magnitude and top-flange build-up (interchangeably referred to as "haunch") requirements.

The requirements for the design of precast, prestressed concrete bridge girders for Alabama are set forth in the ALDOT Structural Design Manual (ALDOT Bridge Bureau 2014), most recently published in June 2014. This manual contains specific design criteria policies for the ALDOT Bridge Bureau and applies equally to ALDOT as well as to consultants completing structural designs on behalf of ALDOT. Noted in this manual is the adoption of the AASHTO LRFD Design Specifications, Sixth Edition (AASHTO 2012) as the code governing all bridge design within the state of Alabama. The following are specific design requirements of ALDOT prestressed concrete bridge girder projects—exceptions to which require the approval of the State Bridge Engineer:

- For prestressed concrete girders, specified design 28-day compressive strength of concrete shall be between 5.0 and 8.0 ksi;
- Standard shapes of AASHTO Type I, II, and III and PCI BT-54, BT-63, and BT-72 shall be used;
- Girder design shall be for simple span for all dead and live loads;

- The transformed area of bonded reinforcement shall not be included in the calculations of section properties;
- Standard pretensioning strand sizes shall be used;
- Members shall be designed such that no tension occurs (after losses) for the Service III load limit state;
- Girder shear reinforcing shall be at least #5 bars, spaced no greater than 18 in. on center, with 4 in. spacing in the girder ends for a distance equal to the girder depth;
- Confining steel shall be #3 bars spaced at 4 in. for a distance equal to the girder depth at each girder end;
- Calculation of camber at erection shall be based on a 60-day interval between release of the strand and erection of the girder;
- Debonding shall be permitted per AASHTO LRFD Section 5.11.4.3 (AASHTO 2012);
- For calculating losses, the AASHTO LRFD Approximate Method (neglecting gains) shall be used with the following parameters:
    - Time at release: 0.75 days
    - Age of deck placement: 60 days
    - Final age: 27,500 days (75 years)
    - Relative humidity: 75 percent;
- While the use of edge beams/end walls shall be a required typical detail, intermediate diaphragms shall only be used as required by calculation;

- A minimum 1 in. haunch shall be provided at girder midspan (as calculated at the critical edge of the girder flange);
- A prestress camber diagram shall be pictographically represented on bridge plans showing girder depth, haunch thickness, deck thickness, total deck plus haunch thickness, theoretical camber, and dead load deflection.

While the above design requirements have historically proven to yield safe and serviceable prestressed concrete bridges, constructability issues stemming from inaccurate camber predictions have been observed in bridges designed to the requirements summarized above.

Bridge designs complying with the above-summarized requirements are typically completed by ALDOT bridge designers with the assistance of various software packages including *LEAP CONSPAN* by Bentley Systems and *PSBEAM* by Erikkson Technologies. In general, ALDOT maintains subscriptions to both of these software to ensure compliance with current AASHTO code provisions and allows designers to choose a preferred software package for design and analysis. In order to ensure the research team could thoroughly understand the design procedures currently used by ALDOT design personnel and make recommendations compatible with these software, saved design files for previous ALDOT prestressed concrete bridge projects (in both *LEAP CONSPAN* and *PSBEAM* format) were acquired from ALDOT and reviewed thoroughly by the research team.

Both *CONSPAN* and *PSBEAM* have similar graphical user interfaces (GUI's) that allow bridge designers to input relevant material properties as shown in Figures 4-4 and 4-5, respectively. The value used by ALDOT design engineers for the unit weight of

concrete in all reviewed project design files is 150 pcf. While a full discussion of various code provisions for computing the concrete modulus of elasticity is withheld until Chapter 6 of this dissertation, it is interesting to note that both *LEAP CONSPAN* and *PSBEAM* allow the user to adjust the computed modulus of elasticity value to reflect regional calibration studies.

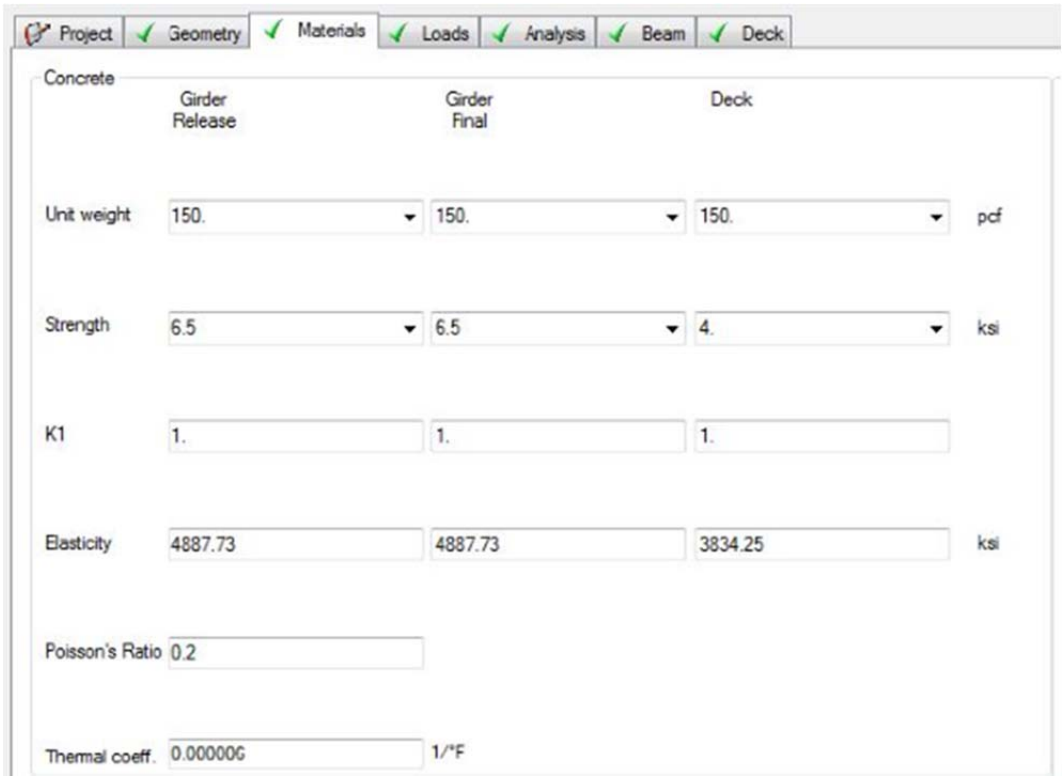

Figure 4-4: LEAP CONSPAN Material Input GUI

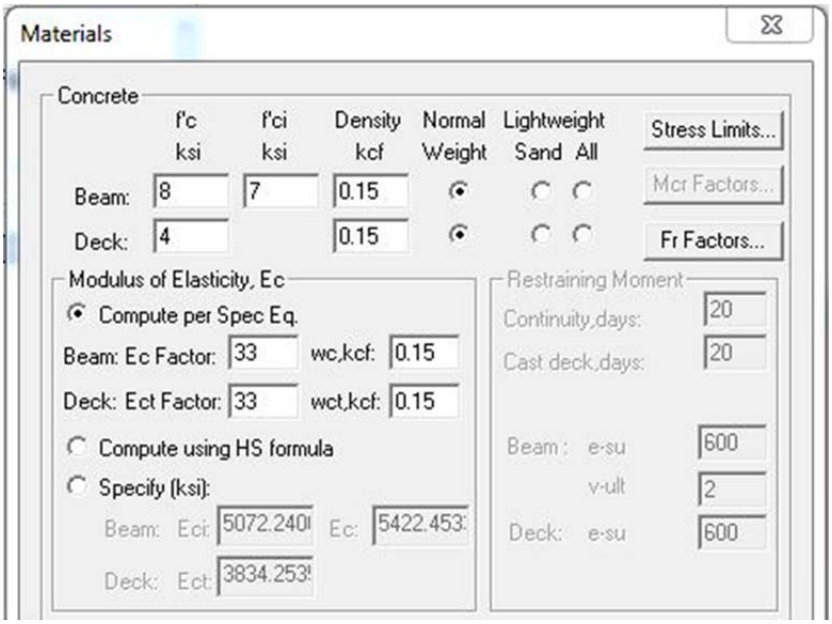

Figure 4-5: *PSBEAM* Material Input GUI

LEAP CONSPAN accepts direct user input for a *K1* parameter (a regionally calibrated factor used to represent the effect of aggregate stiffness) and *PSBEAM* allows users to modify the overall factor used to compute the modulus of elasticity.

Another key topic of interest in these software packages is the method used for computing long-term deflections for precast, prestressed concrete girders. Both programs default to the PCI multiplier method (as discussed in Chapter 2 of this dissertation) and use the coefficients as originally proposed by Martin (1977). Within the GUI of each software program, it is possible to display the default long-term multipliers (as shown in Figure 4-6) and to change them as needed.

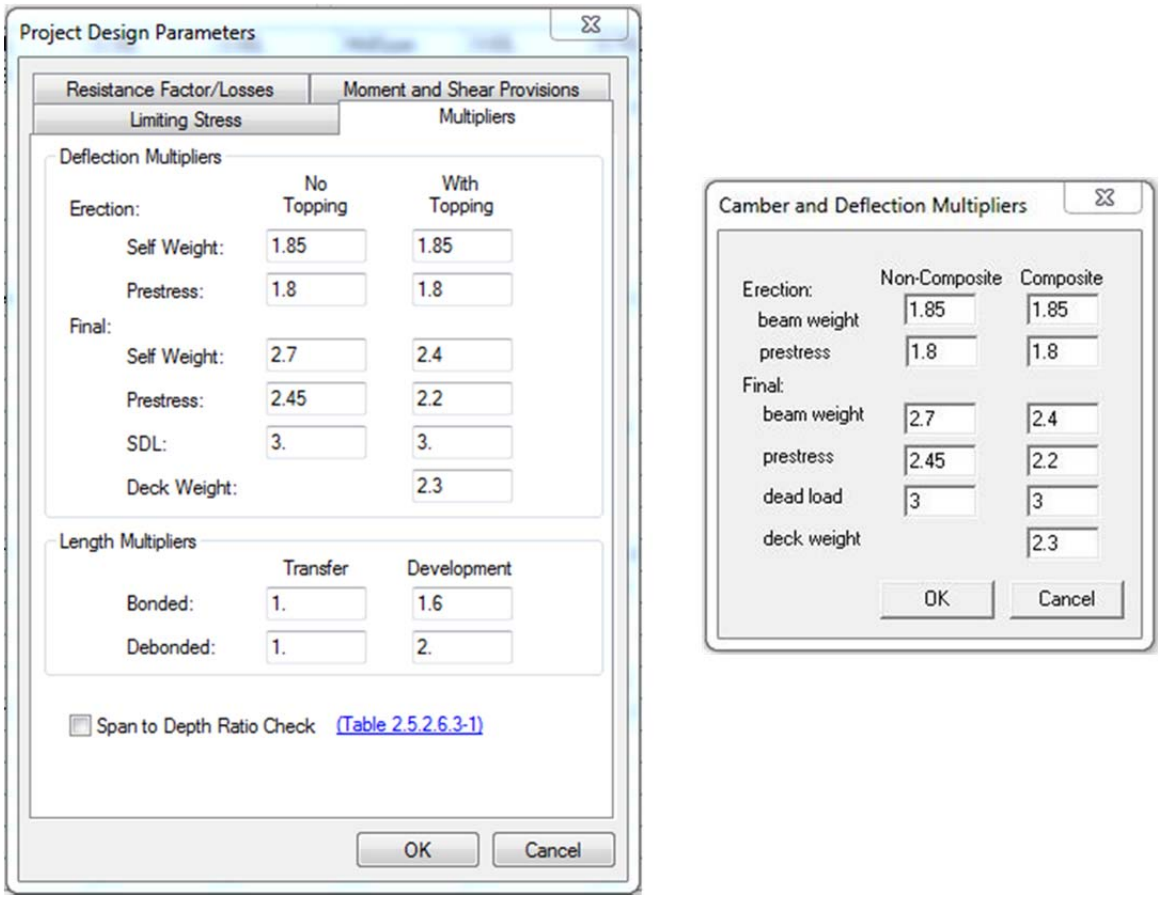

Figure 4-6: Long-term Deflection Multipliers in *CONSPAN* (left) and *PSBEAM* (right).

After the preliminary structural design is completed, a complete set of contract drawings is prepared in accordance with the ALDOT Bridge Plans Detailing Manual (ALDOT 2014) prior to the project proceeding to public bid. Included in this set of contract drawings is the following: plan view and elevations of the bridge, sections at bridge bents, typical cross sections and webwall details, and girder reinforcing details. As previously mentioned, the ALDOT Structural Design Manual (ALDOT 2014) also requires specific information regarding the build-up over top of prestressed concrete girders to be noted and visually displayed on contract drawings. A typical representation of the camber in a precast, prestressed concrete bridge is shown in Figure 4-7.

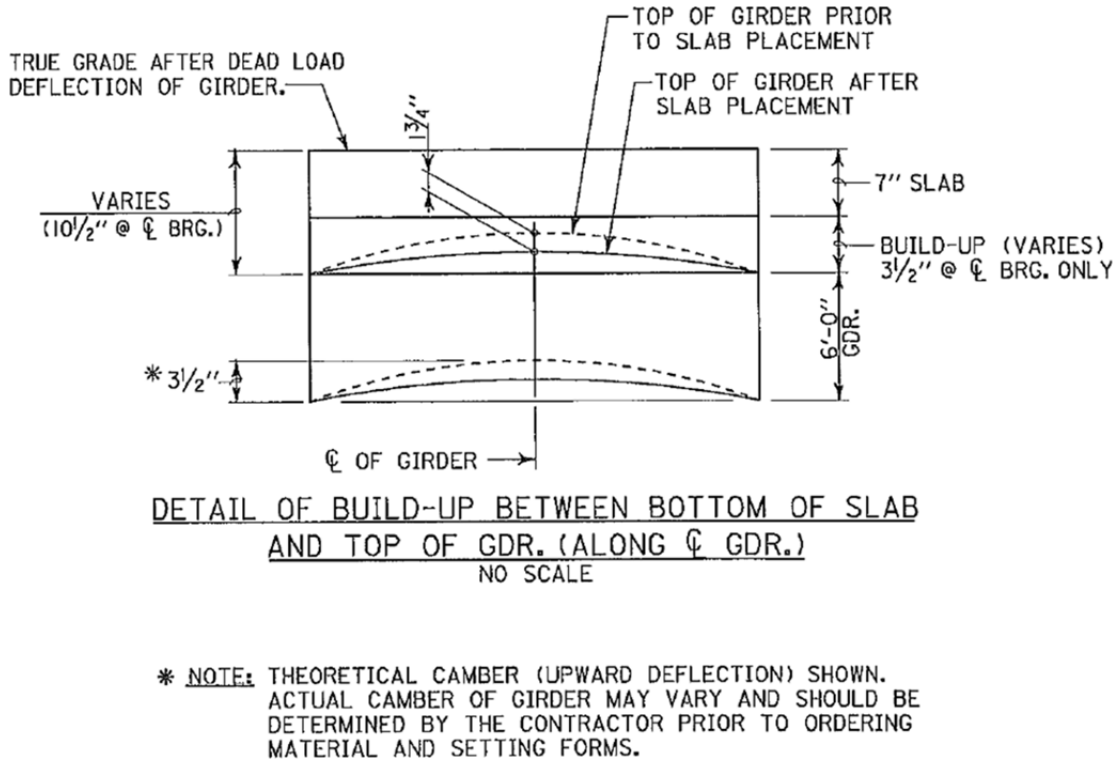

Figure 4-7: Typical Camber Diagram on ALDOT Contract Drawings

In this case, the anticipated theoretical midspan girder camber at the instant before deck placement is +3 ½ in., where positive denotes upward. While placing a 7 in. thick concrete bridge deck, the girder is anticipated to deflect -1 ¾ in. (downward) to a new net midspan camber of +1 ¾ in. Accounting for the 1 in. minimum haunch thickness specified by the ALDOT Structural Design Manual (ALDOT Bridge Bureau 2014), the absolute minimum bridge build-up at the centerline of bearing is 2 ¾ in. The actual buildup specified on the drawing is 3 ½ in., or ¾ in. greater than the minimum required for a level and flat deck. Hypothetically speaking, if the theoretical midspan girder camber was underpredicted and the true value exceeded 5 ¼ in. at the instant preceding deck placement, the specified 3 ½ in. build-up in this scenario would be insufficient and the girder would impede on the bottom deck elevation. More common in Alabama, however, is that the theoretical midspan camber is overpredicted. In extreme cases, the

true value of pre-deck placement camber may be less than 1 ¾ in, resulting in a situation where the downward dead load component from deck placement tends to reverse the net camber and cause a sagging under sustained dead loads. The preceding thought-exercise regarding the potential error that may be accommodated in camber prediction serves to demonstrate that the minimum 1 in. midspan haunch requirement by ALDOT is technically a tolerance allowance, which safeguards against conflicts stemming from inaccurate camber predictions.

4.3.2 Design Review and Shop Drawing Submittal by Producer

Upon receipt of contract drawings for a precast, prestressed concrete project within Alabama, the prestressing plant engineering team begins the process of reviewing the design, proposing any necessary changes, and preparing shop drawings for submittal to ALDOT. Shop drawings typically contain an erection plan including a production sequence, precise dimensions and quantities necessary for girder fabrication, and a fabrication plan showing bed layout, elongation calculations, and detensioning sequences. In the experience of the research team, it is not uncommon for shop drawing submittals to also propose minor changes to contract drawings for ease of construction or to substitute more readily available components. Most typically, the design engineer at the prestress plant producing the girders also conducts a thorough structural analysis in order to verify the adequacy of the girder for design service loads and ultimate capacity and to confirm the deflection computations shown on contract drawings.

At the time of shop drawing preparation, the producer's design engineer likely knows substantially more about the probable material properties of girder concrete than the initial ALDOT bridge designer knew at the time of preliminary design. In addition,

as a result of computing required quality-assurance calculations (i.e. anticipated girder shortening), the producer's engineer can also likely better estimate the prestress losses at different stages of production. For these reasons, it is common for girder producers to compute the expected initial camber at prestress transfer based on these refined parameters. Currently, ALDOT contract drawings typically do not publish expected camber at prestress transfer, and thus, girder producers are unable to either confirm or refute the anticipated prestress release camber as computed by the ALDOT bridge designer. In some cases, girder producers may even incorrectly compare their own refined estimation of camber at prestress transfer with the camber value published on ALDOT contract drawings, which is intended at a girder age of 60 days. Through discussions with girder producers, the research team learned that current industry practice dictates that the camber magnitude shown on producer shop drawings should reflect the same value as shown on ALDOT contract drawings. This practice makes it difficult to identify inaccuracies in camber prediction soon after girder production and instead, encourages a delay in the evaluation of camber until an age of at least 60 days.

This research effort strives to make recommendations that allow ALDOT bridge designers and girder producers to improve the accuracy of both their initial camber calculations at prestress transfer (currently unpublished) and the camber-growth as the girder ages (published for 60 day value). By increasing the accuracy of these predictions in a transparent fashion, it is hoped that the girder producer's design staff will also participate in further refining the accuracy of camber predictions during the design review phase of a precast, prestressed concrete bridge project.

4.4 Concrete Mixtures for Precast, Prestressed Bridge Girders in Alabama

The intent of this section is to review ALDOT mixture design and approval provisions, summarize ALDOT requirements for concretes used in precast, prestressed bridge girders, review sample approved concrete mixtures typical within the study region, and discuss various fresh concrete properties as measured in the study region by girder producers.

4.4.1 ALDOT Mixture Design and Approval Procedures

ALDOT 170-82 (Method of Controlling Concrete Operations for Structural Portland Cement Concrete) (ALDOT 2009) is the primary specification governing approval of all concrete mixtures used within the state of Alabama including those used for precast, prestressed concrete applications. Outlined in this document are the following requirements for mixture design and approval:

- All concrete mixtures shall undergo a verification mixture design test at a laboratory certified by ALDOT with specific requirements as follow:
    - Mixture proportions shall be selected based on trial batches of at least three different water-cementitious materials ratios;
    - Trial mixtures shall use the exact materials intended to be used during actual production;
    - Target 28-day compressive strengths shall exceed specified requirements by 1,000 psi for compressive strengths less than 3,000 psi, by 1,200 psi for compressive strengths greater than 3,000 psi but less than 5,000 psi, and by 1,400 psi for compressive strengths greater than 5,000 psi;

    - Concrete cylinders shall be tested at the age of 7 days and 28 days in accordance with applicable ASTM and AASHTO testing standards;
- The formal submittal of the concrete mixture design shall contain all information related to the source and type of materials used, the aggregate material properties and geometric distributions, proportions for one cubic yard of concrete, freshly mixed concrete properties (including slump, air content, and temperature), and the results of the laboratory verification test summarized above; and
- Approved concrete mixtures are valid for a four-year period after which, they are subject to re-approval by ALDOT.

The mixture approval process as summarized above encourages producers to maintain a minimal inventory of approved concrete mixtures capable of satisfying a wide range of potential project requirements.

4.4.2 ALDOT Requirements for Concrete in Precast, Prestressed Bridge Girders

Specific requirements for concrete mixtures to be used in the construction of prestressed concrete bridge members are published within the *ALDOT Standard Specification* (ALDOT 2012) Section 513. Key requirements include the following:

- All constitutive materials shall meet ALDOT specifications and be from approved ALDOT source lists;
- Minimum 28-day strength of 5,000 psi (or as noted on plans);
- Minimum cementitious factor = 550 pcy;
- Maximum *w/cm* = 0.45;
- Air content between 2.5 percent and 6.0 percent by volume;

- Maximum slump (prior to admixture) = 4.0 in.;
- Maximum slump total (with admixture) for conventionally vibrated concrete = 9 in.; and
- Slump flow range for self-consoldating concrete = 25–29 in.

Supplementing the provisions of the *ALDOT Standard Specification*, ALDOT-367 (2015) (Production and Inspection of Precast Non-Prestressed and Prestressed Concrete) outlines requirements for the production and inspection of precast, prestressed concrete members and addresses some additional intricacies of girder fabrication. Included in this document are ALDOT requirements for the following: strand tensioning procedures, formwork, prestressing steel, reinforcing steel, concrete testing and acceptance, curing, strand detensioning, final approval of members, tolerances, and documentation procedures. While the provisions of the *ALDOT Standard Specification* are mainly relevant to pre-construction planning and approval, the requirements of ALDOT-367 are routinely referenced and enforced by on-site ALDOT field inspectors during girder production.

4.4.3 ALDOT-Approved Concrete Mixture Proportions

Concrete mixtures typically used in the precast, prestressed industry are characterized by low water-to-cementitious materials ratios (*w/cm*), relatively high total paste content, the use of Type III cement and supplementary cementing materials (SCMs), and medium- to high-dosages of chemical admixtures (PCI 2011). Producers attempt to optimize mixture designs to minimize raw material cost, concrete placement labor, and chronological time to prestress release, while simultaneously maximizing finish quality.

In the geographical study area, each ALDOT-approved prestressed girder producer tends to maintain between one and three approved mixtures at any given time.

A comparison of typical mixture proportions representing four prestress producers included in this study is shown in Table 4-2.

Table 4-2: Typical Mixture Proportions for Alabama Precast, Prestressed Concrete

	Plant A		**Plant B**		**Plant C**		**Plant D**	
Label	#1	#2	#1	#2	#1	#2	#1	#2
Cement (lbs/yd^3)	639	751	788	765	788	600	697	765
SCM #1 Type	Slag Cement	Slag Cement	Class F Fly Ash	Class F Fly Ash	Class F Fly Ash	Class F Fly Ash	Class F Fly Ash	Class F Fly Ash
SCM #1 (lbs/yd^3)	113	133	173	100	150	170	123	135
SCM #2 Type	None	None	None	Silica Fume	None	Silica Fume	None	None
SCM #2 (lbs/yd^3)	0	0	0	75	0	85	0	0
Water (lbs/yd^3)	277	282	292	275	253	248	258	283
w/cm	*0.37*	*0.32*	*0.30*	*0.29*	*0.27*	*0.29*	*0.32*	*0.32*
Coarse Aggregate Type	#57/#67 Limestone (Dolomitic)	#57/#67 Limestone (Dolomitic)	#67 Granite	#67 Granite	#78 Limestone (Regular)	#67 Gravel	#67 Granite	#67 Granite
Coarse Aggregate (lbs/yd^3)	1860	1861	1345	1426	1720	1675	1655	1576
Source of Coarse Aggregate	Helena, AL	Helena, AL	Forest Park, GA	Forest Park, GA	Calera, AL	Pearl River, LA	Mulgrave, Canada	Mulgrave, Canada
Fine Aggregate	#100 Sand	#100 Sand	#100 Sand	#100 Sand	#100 Sand	#100 Sand	#100 Sand	#100 Sand
Fine Aggregate (lbs/yd^3)	1172	1048	1301	1278	1091	1048	1249	1189
Source of Fine Aggregate	Prattville, AL	Prattville, AL	Butler, GA	Butler, GA	Pearl River, LA	Pearl River, LA	Atmore, AL	Atmore, AL
Sand/total aggregate (by weight)	*0.39*	*0.36*	*0.49*	*0.47*	*0.39*	*0.39*	*0.43*	*0.43*
Max. AEA Dosage (oz/cwt)	0.13	0.11	0.21	0.21	0.42	0.47	0.40	0.40
Max. HSA Dosage (oz/cwt)	1.0	1.0	3.5	4.5	1.3	1.1	2.0	2.0
Max. HRWRA Dosage (oz/cwt)	10.0	10.0	5.9	7.0	5.1	5.0	6.5	5.5

Notes:

1. Admixture abbreviations: Air-Entraining Admixture (AEA), Hydration Stabilizing Admixture (HSA), and High-Range Water Reducing Admixture (HRWRA).
2. All aggregates in saturated-surface dry state.

From the mixture proportions shown in Table 4-2, the typical concrete mixtures used in the Alabama precast, prestressed industry can be characterized as follows:

- Average *w/cm* = 0.31;
- High cementitious materials content (on average = 881 pcy);
- Average water content = 270 pcy
- Average sand/total aggregate ratio = 0.42;
- Replacement of Type III cement with slag cement, fly ash, or a combination of fly ash and silica fume in varying percentages is common;
- The majority of producers use a #67 limestone or granite coarse aggregate;
- All producers use a #100 natural sand;
- Relatively low dosages of air-entraining admixtures (AEA) and hydration stabilizing admixtures (HSA); and
- Medium to high dosages of high-range water-reducing admixtures (HRWRA).

A more thorough discussion of mixture proportions as developed and used in the laboratory portion of this research study is included in Chapter 6 of this dissertation.

4.4.4 Prestressed Concrete Fresh Properties

To further characterize the precast, prestressed concrete industry in Alabama, historical values were compiled for selected fresh concrete properties for the six-year period from 2007 through 2013. Frequency histograms for slump and percent air content (by volume) are shown in Fig. 4-8.

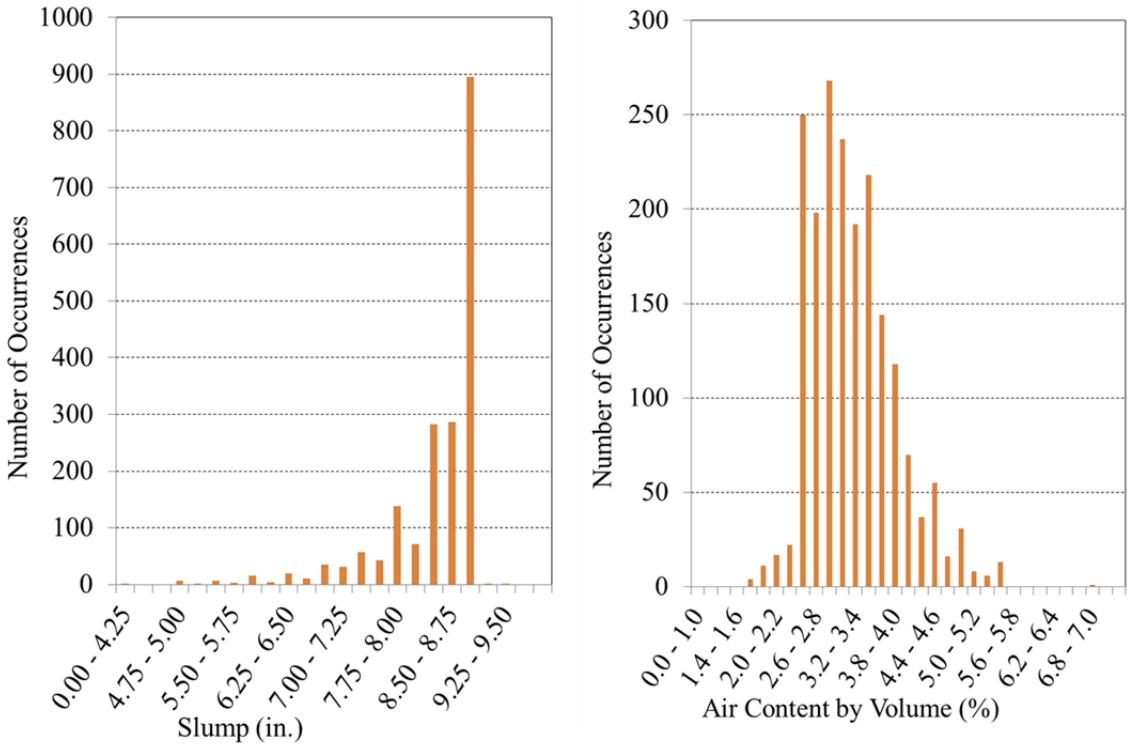

Figure 4-8: Historical Data for Select Fresh Concrete Properties: Slump (left) and Air Content (right).

It is not surprising that producers prefer to target the maximum allowable slump of 9 in. to maximize the workability of concrete. The mean slump value for all historical records considered was 8.5 in., with a most common measurement of 9 in. With regards to air content, it is most common for producers to target minimum requirements for air content (2.5 percent) given the relatively mild climate of the region. This minimal air content can typically be achieved without the need for air-entraining admixtures (AEA). The mean air content for the historical data was 3.3 percent, with a most frequent measurement of 3.0 percent.

4.5 Construction Practices Relevant to Camber

The construction procedures and practices used to produce ALDOT prestressed concrete girders at various girder producers have been thoroughly documented by others in recent

years. These practices are fairly standardized and were found to be in accordance with the requirements of ALDOT specifications. Most recently, as part of this research effort, Hofrichter (2014) provided a detailed portrayal of typical construction procedures at four regional prestressed concrete producers. Previously, Dunham (2011) also documented the production of prestressed concrete girders within the study region. Rather than providing a repetitive account of production procedures, the focus of this section remains on those construction factors most relevant to camber and camber prediction in precast, prestressed concrete bridge girders.

4.5.1 Production Camber Measurements and Permissible Tolerances

Pursuant to the requirements of ALDOT-367 (ALDOT 2015), girder camber is typically measured within 24 hours after strand detensioning for at least half of all members cast. These measurements of camber are intended to verify consistency among members of the same project and are not intended to confirm theoretical shop drawing camber. However, ALDOT-367 does require that significant variations from the camber shown on shop drawings be reported to the ALDOT for evaluation. In the experience of the research team (and in agreement with previous researchers' work summarized in Chapter 3), production camber measurement practices are quite inconsistent among girder producers and of little practical use from a research perspective.

Also included in ALDOT-367 (ALDOT 2015) are permissible tolerances for camber in precast, prestressed bulb-tee girders as shown in Figure 4-9. As noted, the variation from design camber is +/- 1/8 in. per 10 ft of girder length and the differential camber between adjacent members of the same design is ¼ in. per 10 ft of girder length.

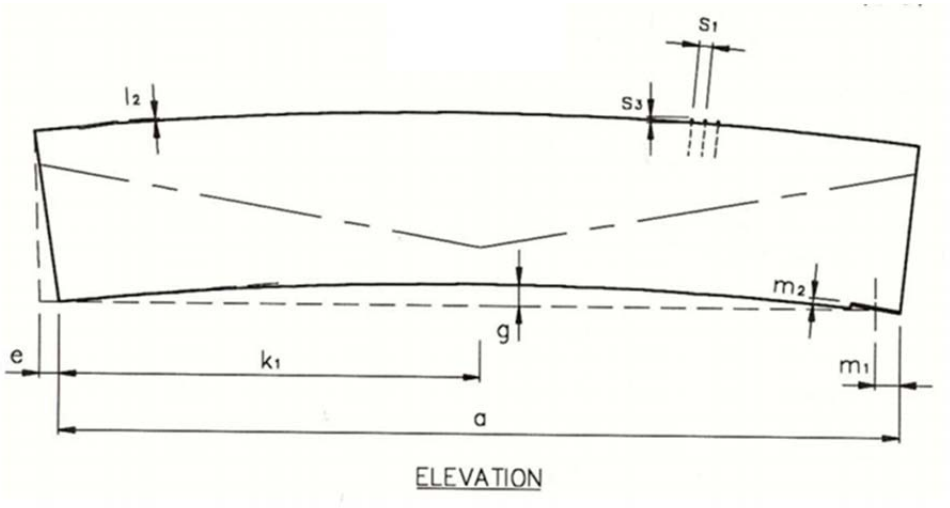

g = Camber variation from design camber* ..... ± ⅛ in. per 10 ft.
g1 = Differential Camber Between Adjacent Members of the Same Design* ..... ¼ in. per 10 ft.

Figure 4-9: Permissible Camber Production Tolerances (Adapted from ALDOT 367 2015)

The first requirement, camber variation from design camber, is difficult to evaluate because a specific age of measurement is not specified. While ALDOT contract drawings typically specify an anticipated theoretical camber at an age of 60 days after production (in accordance with the assumptions of Martin [1977]), the magnitude of camber is most commonly measured either directly after prestress release (0.75 days) or directly prior to shipping (frequently in excess of 60 days). The second requirement, differential camber between similar members, is a more useful and quantifiable metric because no specific age is necessary for evaluation. Most typically, differential camber is evaluated directly after prestress release, but also applies equally at any girder age.

4.5.2 Chronological Time to Prestress Release

The chronological time to prestress release is one of the most influential variables in determining concrete compressive strength at prestress release, and, therefore, is of the utmost relevance to this research effort. While the entirety of Chapter 5 is devoted to

concrete strength considerations, this section discusses the average chronological time to prestress release in the context of field construction practices.

It is desirable for girder producers to maintain an average chronological time to prestress release of approximately 18 hours in order to maximize production efficiency and allow reuse of production beds within 24 hours. As part of this research effort, Hofrichter (2014) compiled data for the chronological time to prestress release for 1,917 girder concrete placement events during the six-year period preceding 2013. A histogram of chronological ages at the time of prestress release for the full data set is shown in Figure 4-10. Two significant peaks occur in this histogram, demonstrating the two most common scenarios in which girder production and prestress release take place.

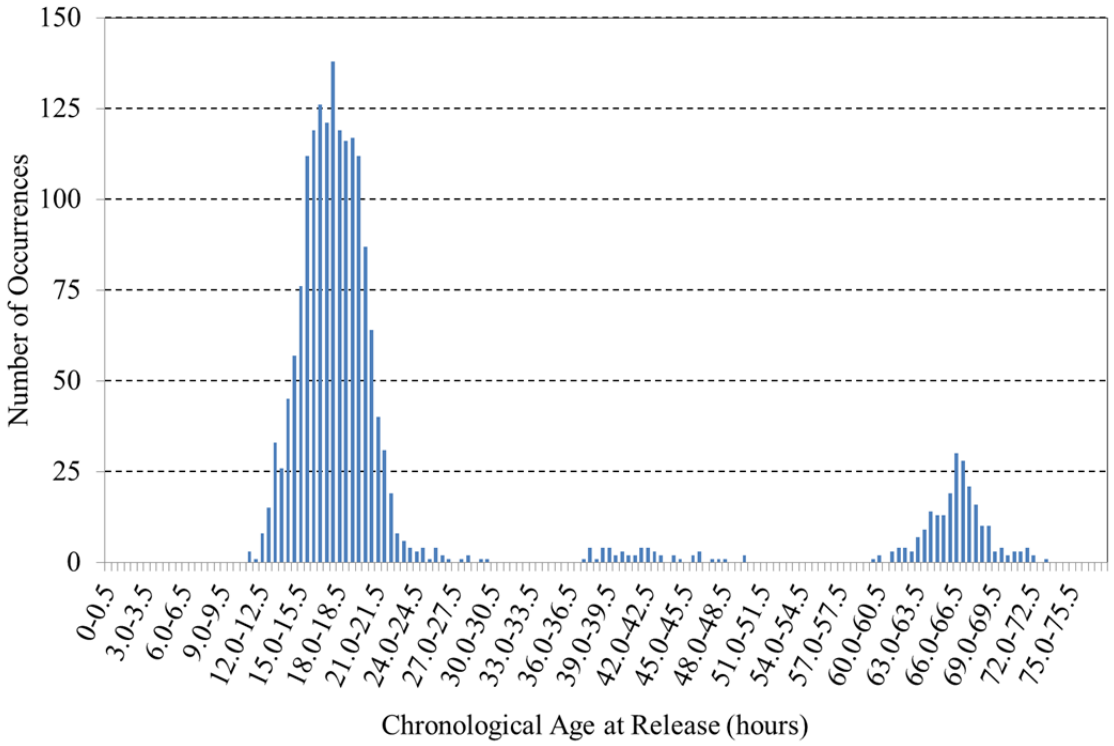

Figure 4-10: Frequency Histogram for Chronological Age at Release.

The first and primary peak occurs at the age of approximately 18 hours, which is representative of standard plant practices. Concrete is most often placed during the late

morning or early afternoon, with the intent to transfer the prestressing force to the girders very early the next morning to facilitate the re-use of formwork on a 24-hour cycle. A second peak in the histogram is observed around 66 hours and represents non-standard pours typically taking place on Fridays and subjected to extended curing over the weekend prior to a Monday prestress release event. A cumulative percent occurrence plot of the same data set is shown in Figure 4-11. It can be seen that chronological ages at release of less than 24 hours represent roughly 84% of the full data set.

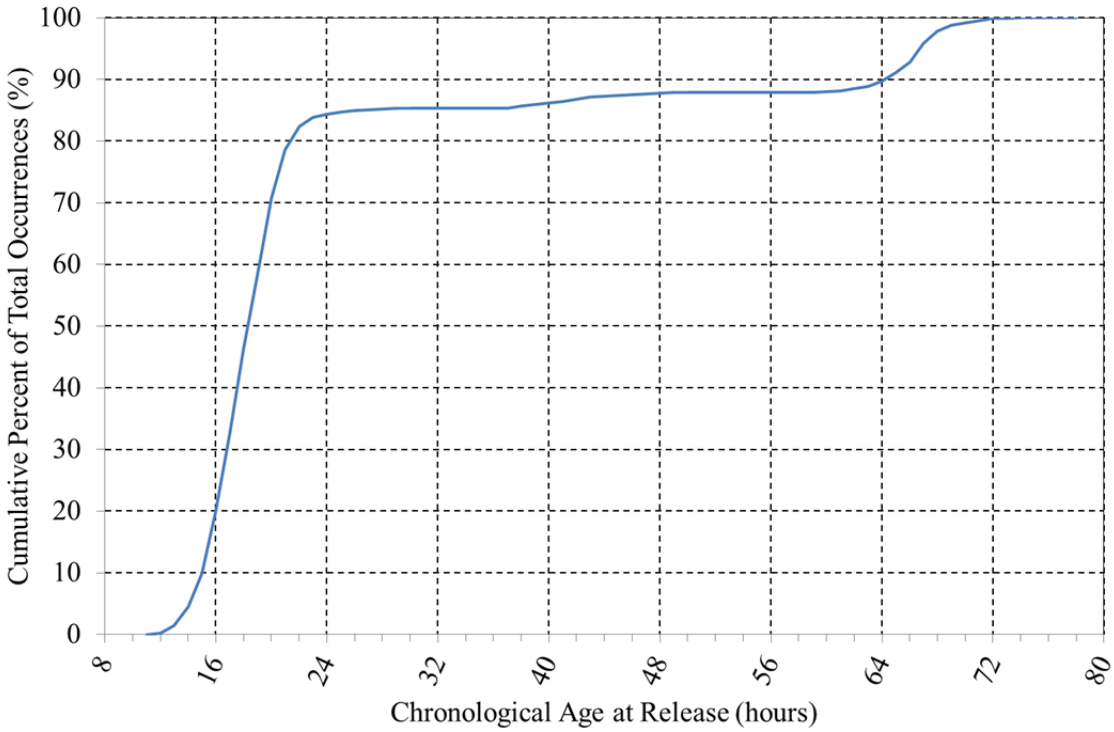

Figure 4-11: Cumulative Percent Occurrence for Chronological Age at Release.

The mean chronological age of release for the full data set is 25.1 hours, with a most frequently observed value of 17 hours. This disparity between the mean chronological age to release and the mode of the sampled data suggest that the sampled data represents two distinct populations, namely, standard plant practices and extended release practices. The sampled data was divided into two subgroups, those with release times less than or

equal to 24 hours (identified as standard plant practices) and those with release times exceeding 24 hours (identified as extended release practices.) Statistical summaries for the reduced data sets are shown in Table 4-3**.**

Table 4-3: Statistical Summary of Chronological Age to Release by Subgroup

	Standard Plant Practices (≤24 hrs.)	Extended Release Practices (>24 hrs.)
Number of Values	1602	226
Sample Mean, $\bar{x}$ (hrs.)	17.7	66.2
Sample Mode, $\boldsymbol{Mo}$. (hrs.)	17	66
Sample Standard Deviation, $\boldsymbol{s}$ (hrs.)	2.2	2.2

For standard plant practices, the mean chronological age at prestress release is 17.7 hours, with a sample mode of 17 hours, and a sample standard deviation of 2.2 hours. The summary statistics in Table 4-3 are offered as useful parameters for future designers of experimental research programs, in lieu of relying on anecdotal reports claiming a chronological time to release of 18 hours.

4.5.3 Maturity at Prestress Release

While the chronological time to release may be the most readily available parameter for timing in the precast, prestressed concrete industry, the widespread use of accelerated curing methods (i.e. steam curing) make it desirable to express average time to prestress release in terms of a concrete maturity or equivalent age. Steam curing protocols vary by region, but most often limit maximum exposure temperatures to approximately 150°F and specify the maximum rate at which the concrete temperature may change (typically 36-40°F/hour) (PCI 2011). Local ALDOT guidelines permit up to a maximum temperature of 160°F with a maximum rate of temperature change of 40°F/hour. For the purposes of this analysis, a reduced data set of 435 concrete placement events was randomly sampled from the full data set. To be eligible for selection for this reduced data

set, a concrete placement event needed to have clear reliable temperature data recorded throughout fabrication, full fabrication records available, and belong to the standard plant practices (≤ 24 hour chronological age to release) data set.

Calculation of the equivalent age at release for each placement event was conducted based on ASTM C1074 (2011). For the analysis, a value of 45,000 J/mol was used for activation energy in accordance with the recommendations of Carino and Tank (1992) and a reference temperature of 22.5°C. A frequency histogram of the reduced data set for equivalent age is shown in Figure 4-12.

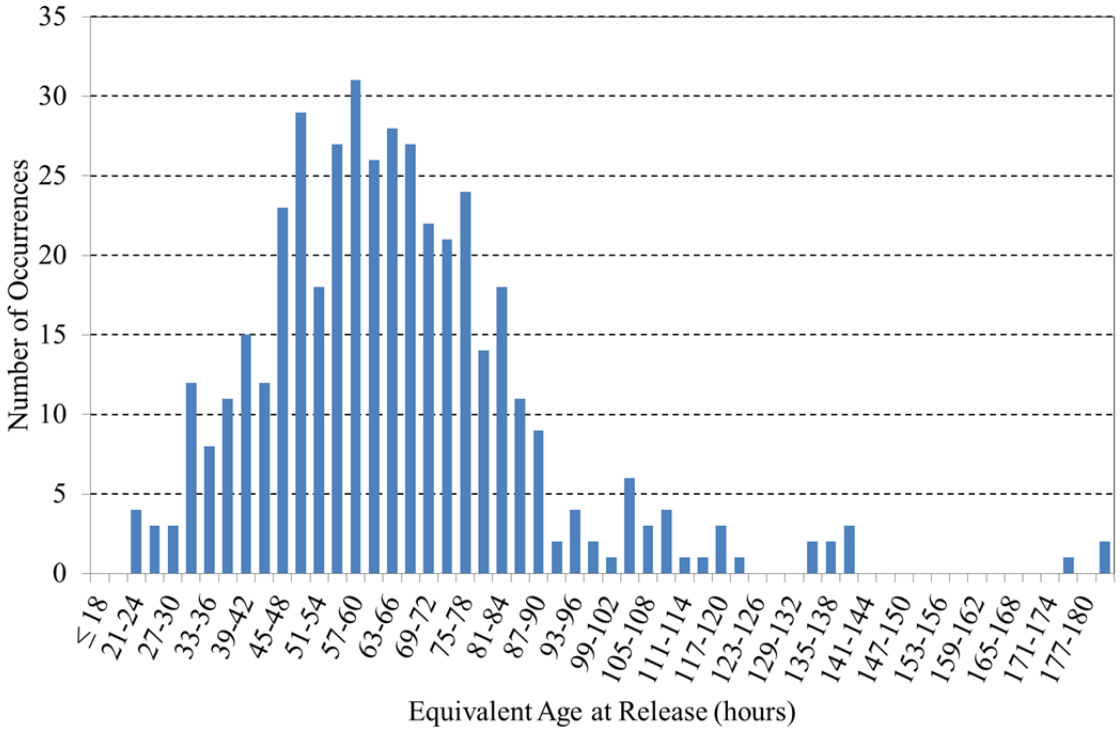

Figure 4-12: Frequency Histogram for Equivalent Age at Prestress Release.

The mean equivalent age at prestress transfer from the considered data set was 65.0 hours with a sample mode of 50 hours, and a sample standard deviation of 24.4 hours. A relatively large variance, as compared to the chronological age to release data set, was noted for the equivalent age distribution and may (1) question the reliability and

consistency of in-plant temperature recording efforts or (2) suggest that the chronological time to transfer is intrinsically a more constrained parameter than the maturity at transfer.

4.5.4 Girder Handling and Storage Conditions

After production is complete, precast, prestressed concrete girders are typically stored at the girder production facility until transported to the bridge site for erection. As documented by Hofrichter (2014), a wide variety of storage conditions were observed in the four prestressed concrete plants included in this study. Most frequent was the use of timber dunnage or waste concrete piles (with a plywood bearing surface) located directly under the lifting points, approximately 5 ft from each girder end as required by ALDOT-367. With regards to camber and camber growth, ALDOT-367 (ALDOT 2015) specifies that all precast, prestressed concrete bridge members remaining in storage for a period in excess of 120 days shall be repositioned every 120 days to ensure that deformations due to creep, shrinkage, loads, and uneven support conditions are kept to a minimum.

4.6 Required Girder Production Documentation and Data Reporting Formats

This section summarizes the documentation required by ALDOT during girder production and the most common recording formats. Of the information discussed in this section, historical concrete strength testing records proved to be the most useful and are thoroughly discussed and analyzed in Chapter 5 of this dissertation.

In accordance with the requirements of ALDOT-367 (ALDOT 2015), the following field data are typically recorded during the production of precast, prestressed concrete bridge girders:

- Fresh concrete properties for each concrete placement and sampling location, including slump, air content, ambient air temperature, and fresh concrete temperature;
- Measured cylinder compressive strengths at the time of prestress release and at an age of 28 days;
- Prestressing strand force and/or elongation predictions and measurements; and
- Curing temperature records for the girder or cylinders produced.

Record keeping is a joint effort between ALDOT inspectors and girder producers, with each party maintaining independent copies of all records. In general, ALDOT on-site records tended to be thorough and consistent between all production facilities, while girder producer records tended to vary more in format and completeness.

4.7 Summary

In order to provide viable and efficient solutions to assist ALDOT to more accurately predict camber in precast, prestressed concrete girders, it was first necessary to explore and document the existing procedures used for the design and construction of precast, prestressed concrete bridge girders within the study region. In the context of girder camber, this chapter summarized the current state-of-the-art of the precast, prestressed girder industry in Alabama and included a general background, a review of typical girder design roles and procedures, a discussion of concrete mixture proportioning for regional prestressed applications, a brief review of pertinent girder production practices, and a summary of typical record-keeping practices.

4.8 Recommendations

In order to assist with improving the accuracy of camber predictions, the following modification to current design and construction practices is proposed: ALDOT contract drawings should show the estimated *release* camber based on the bridge designer's calculations in addition to the 60-day erection camber currently included. By including this parameter on contract drawings, prestress plant engineers and quality-control personnel may be able to more readily confirm the accuracy of initial camber and identify troublesome discrepancies up to 60 days earlier than current practice allows. In addition, it may be advantageous to also show a 120-day estimate of camber to provide a metric of camber growth potential.

Chapter 5: Accurately Predicting Expected Concrete Compressive Strength

5.1 Introduction

Compressive strength is the concrete material property of paramount importance in structural design. Compressive strength is directly related to the structure of the hydrated cement paste and, therefore, provides an overall picture of the quality of concrete (Neville 2013). In typical structural design, the design engineer is primarily concerned with satisfying strength limit states (i.e. life-safety considerations) and places significantly less emphasis on the accuracy of serviceability calculations (i.e. deflections). Common practice for typical U.S. design engineers is to use specified concrete properties for both strength and serviceability limit state computations.

In reality, the specified concrete strength is a lower-bound value not intended to represent the average in-place concrete strength (alternately termed the "expected" strength) of a completed structural member. Instead, the expected concrete strength must always exceed the specified concrete strength by a statistically determined margin in order to ensure that the vast majority of the concrete strengths in the structure exceed the specified strength. The disparity between specified and expected concrete compressive strength is not presently accounted for in serviceability structural design computations.

For design engineers in certain practice areas, the accuracy of serviceability computations is of the utmost importance in order to avoid potential costly effects. Examples of engineers with an increased emphasis on serviceability may include the following: (1) engineers designing precast, prestressed concrete girders that must satisfy a

minimum camber requirement, (2) design engineers for tall buildings estimating elastic shortening of columns and specifying corresponding tolerances/details, (3) designers of floor systems for owners with stringent deflection or floor flatness requirements. For these design engineers, it is essential that *expected* values for concrete material properties are used in serviceability computations in lieu of the common practice of using specified, lower-bound parameters. It is important to note that the *choice* to use expected parameters in serviceability computations is completely independent of the *requirement* to use specified parameters for strength limit state designs. Specified parameters must always be used in strength limit state designs in order to ensure a sufficiently small code-intended probability of failure to safeguard life safety.

This chapter provides analyses and guidance to allow design engineers to more accurately predict the expected concrete compressive strength at various ages for the purposes of serviceability computations. By more accurately predicting the expected concrete strength, the accuracy of serviceability computations can be greatly improved. It is important to reiterate that the mean expected concrete compressive strength as predicted using the provisions of this chapter should not be used in strength limit state computations.

5.1.1 Chapter Objectives

The primary objective of this chapter is to improve the accuracy of design serviceability predictions by identifying relationships between specified concrete compressive strength and expected concrete compressive strength. Major tasks include the following:

- Review current code-provisions related to predicting expected concrete compressive strength in general and discuss the appropriateness of their usage in serviceability computations;
- Discuss recent research efforts within the precast, prestressed concrete industry aimed at predicting expected concrete compressive strength at the time of prestress release and 28 days after the start of production;
- Identify and discuss the primary causes of overstrength in the precast, prestressed concrete industry;
- Provide recommendations to more accurately predict expected concrete compressive strength at the time of prestress release in the precast, prestressed concrete industry; and
- Provide recommendations to more accurately predict expected concrete compressive strength 28 days after the start of production in the precast, prestressed concrete industry.

5.1.2 Chapter Outline

This chapter begins with a brief background section (Section 5.2) discussing concrete compressive strength. Next, Section 5.3 contains a discussion of current code provisions related to expected in-place concrete compressive strength and an examination of the appropriateness of their usage in serviceability computations. Section 5.4 contains a synthesized literature review of previous efforts in the precast, prestressed industry to predict expected concrete compressive strength at the time of prestress release and 28 days after production. Next, Section 5.5 details a historical data set compiled as part of this effort and any subsequent post-processing. Section 5.6 contains details and

recommendations of an analysis conducted to identify relationships between specified and expected concrete compressive strength at the time of prestress transfer. Section 5.7 contains the results of a similar analysis for 28-day strength. Finally, Section 5.8 provides a summary and conclusions of the research effort contained in Chapter 5 and highlights specific recommendations that address the study objectives listed in Section 5.1.1.

5.2 Background

5.2.1 Concrete Compressive Strength

Concrete compressive strength is defined as "the measured maximum resistance of a concrete specimen to axial compressive loading, expressed as force per unit cross sectional area" (ACI 2013). Compressive strength is commonly tested by applying a standard loading protocol to cylindrical concrete specimens as outlined in *ASTM C39: Standard Test Method for Compressive Strength of Cylindrical Concrete Specimens* (ASTM C39 2010). A tested specimen is judged to have reached failure when it is no longer capable of carrying increased load due to an advanced state of internal cracking and/or external fracture (Mehta and Monteiro 2014). Although non-standard testing ages may be specified to meet unique project requirements, the most common specified ages of testing are 24 hours, 3 days, 7 days, 28 days, and 90 days (ASTM C39 2010).

A large number of factors affect concrete compressive strength, but can be classified into two major groups: (1) characteristics and proportions of materials and (2) curing conditions. The first grouping, characteristics and proportions of materials, primarily affects concrete compressive strength by influencing the porosity of the hardened concrete. As porosity increases, the concrete compressive strength tends to

decrease (Mehta and Monteiro 2014). The second grouping, curing conditions, tends to influence concrete compressive strength by governing the extent and rate of cement hydration. The following two paragraphs discuss the general effect of each of these groupings on concrete compressive strength.

Without doubt, the material parameter most influential to concrete compressive strength is the water-to-cement ratio, *w/c*. As documented by Duff Abrams in 1927 and shown in Figure 5-1, as the water to cement ratio decreases, the compressive strength of the concrete tends to increase exponentially. Perhaps next most important is the effect of air-entrainment on concrete compressive strength. As the volume of entrained air in the hydrated cement paste increases, the porosity of the concrete mixture as a whole also increases, tending to cause a decrease in concrete compressive strength. An approximate rule of thumb for the effect of air content on compressive strength is as follows: a one percent decrease in the air content of a given mixture corresponds to approximately a five percent increase in compressive strength. Additional material factors tending to affect concrete compressive strength, although to lesser extent than those outline above, are cement type, aggregate type and gradation, mixing water quality, and chemical admixture usage (Mehta and Monteiro 2014).

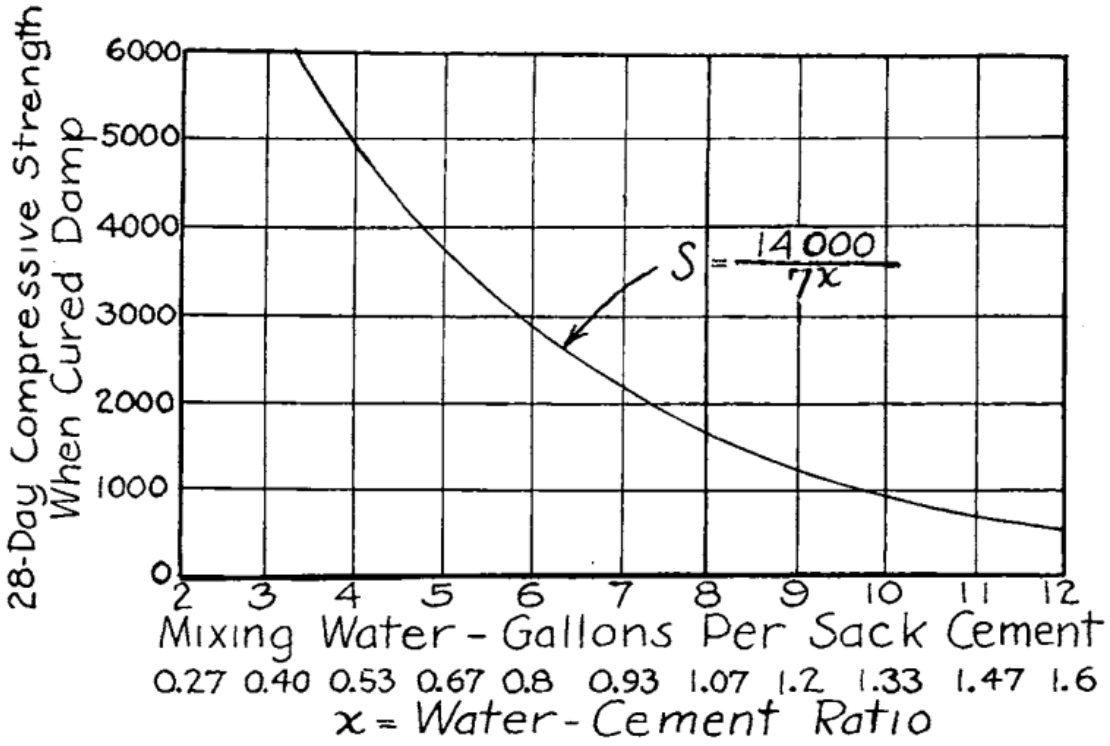

Figure 5-1: Relationship between water to cement ratio, *w/c*, and compressive strength as expressed by D. Abrams (1927)

Curing conditions, namely time, temperature, and humidity, are directly related to determining the total extent of cement hydration and the rate at which cement hydration occurs, thereby influencing concrete compressive strength. Time is a primary factor influencing concrete strength, as the hydration process of cement is a time-dependent chemical reaction that essentially terminates at either the complete consumption of hydration reactants or in the global (or local) absence of available water. Owing to the importance of this topic with regards to this research effort, Section 5.2.3 includes a thorough discussion of the influence of time on concrete strength. With regards to temperature, increased temperature is generally correlated with more rapid hydration of cement, thereby causing an increased rate of strength development at early ages (Mehta and Monteiro 2014). Finally, the availability of moisture during early-age hydration (as measured by relative humidity) can also affect concrete strength by increasing the total

degree of hydration achievable for a given concrete. In general, hydration slows or ceases when the vapor pressure in capillaries falls below 80 percent of the saturation humidity (Mehta and Monteiro 2014). By artificially maintaining a high external humidity, the hydration reaction is encouraged to continue for longer, thereby increasing the degree of hydration achieved.

5.2.2 Concrete Compressive Strength Nomenclature and Definitions

This section defines necessary nomenclature relating to concrete compressive strength and strength prediction models developed later in this chapter. In general, this section is heavily based on the definitions offered by Hofrichter (2014), although expanded to include additional quantifications of overstrength.

There are four "types" of strength at any given age that are discussed or used in the rest of this dissertation. The system used for differentiating among these four types is as follows:

1. The strength level that is measured by cylinder testing at any given age is simply called the "measured strength" at that age. The variables used to describe this are the simplest of the four types, and are shown here:

   f_{ci} = measured compressive strength of concrete at prestress release (psi)

   f_c = measured compressive strength of concrete at 28 days (psi)

2. The strength level specified by the design engineer at a given time is called the "specified" strength at that age. The variables used to describe this type are shown here:

   f'_{ci} = specified compressive strength of concrete at prestress release (psi)

f'_c = specified compressive strength of concrete at 28 days (psi)

The prime in the f' variable denotes it as a specified value.

3. The strength level that is expected or predicted based on the provisions recommended as part of this chapter and is called the "expected" strength at a given age. The variables used to describe this type are shown here:

   f^*_{ci} = expected compressive strength of concrete at prestress release (psi)

   f^*_c = expected compressive strength of concrete at 28-days (psi)

   The asterisk in the f^* variable denotes it as an expected value.

4. The strength level that concrete producers target during mixture approval testing (discussed further in Section 5.3) and is called the "target" strength or "required strength" at a given age. The variables used to describe this type are shown here:

   f'_{cir} = target compressive strength at prestress release (psi)

   f'_{cr} = target compressive strength at 28 day (psi)

For the purposes of the analyses conducted in this chapter, the following derived nomenclature is also used to provide comparisons between some of the above strength parameters:

1. The ratio of the strength level that is measured by cylinder testing to the strength level specified by the design engineer at any given time. This is called the "actual overstrength factor" at any given age. The variables used to describe this type are shown here:

   $OS_i = f_{ci} / f'_{ci}$ = actual overstrength factor at prestress release

$OS_{28} = f_c / f'_c$ = actual overstrength factor at 28 days

2. The ratio of the strength level that is expected or predicted to the strength level specified by the design engineer at any given time. This is called the "expected overstrength factor" at any given age. The variable form used to describe this type are shown here:

   $OS_i^* = f_{ci}^* / f'_{ci}$ = expected overstrength factor at prestress release

   $OS_{28}^* = f_c^* / f'_c$ = expected overstrength factor at 28 days

   In general, the "actual overstrength factor", (OS_i or OS_{28}) is a parameter based on the random variable "measured strength" (f_{ci} or f_c). Conversely, the "expected overstrength factor", (OS_i^* or OS_{28}^*) is based on the result of an expected strength prediction computation, f_{ci}^* or f_c^*. In the case of a perfectly accurate prediction model, the "expected overstrength factor" would be equal to "actual overstrength factor".

3. The difference between the strength measured by cylinder testing and the strength level specified by the design engineer at any given time is called the "difference statistic" ($dstat$). The variables used to describe this type are shown here:

   $dstat_i = f_{ci} - f'_{ci}$ = difference statistic at prestress release (psi)

   $dstat_{28} = f_c - f'_c$ = difference statistic at 28 days (psi)

   The "difference statistic" parameter serves an important role in the analysis procedure of Section 5.7.

5.2.3 Concrete Compressive Strength Growth Provisions

As discussed in Section 5.2.1, the nature of concrete is such that its mechanical properties change substantially over time. This section reviews two of the most common models for describing compressive strength development as a function of time—the ACI 209 method and the Model Code 2010 (MC 2010) method. Then, a summary of the research findings by Hofrichter (2014) conducted as part of this research effort is provided. These findings are later utilized in the analysis of Section 5.7, as well as the software implementation detailed in Chapter 9 of this dissertation.

The nature of the two concrete strength growth provisions described herein is such that the strength development curve can be defined completely with knowledge of concrete strength at any two ages (chronological age or concrete maturity). If strength at only one age is known, published values of growth-rate coefficients may be used to apply the strength growth provisions to estimate strength at other ages of interest. The most typical application of strength growth provisions is for the estimation of concrete strength at any age other than 28 days given a known strength at 28 days. The standard form of the equations in ACI 209R-92 (2008) and MC 2010 (fib 2010) are published with this intended use in mind.

Based on the independent work of six research groups, ACI 209 (2008) proposed an equation of the following form for modeling concrete strength growth as a function of time:

$$f_c(t) = f_{c28}\left(\frac{t}{\alpha + \beta \cdot t}\right) \tag{5-1}$$

where

$f_c(t)$ = concrete strength at any concrete age t (psi);

f_{c28} = concrete strength at a concrete age of 28 days (psi);

t = concrete age (days);

α = constant (days); and

β = constant (unitless).

Rearranging Equation 5-1 as follows, the strength growth term can be isolated on the right-hand side of the equation:

$$\frac{f_c(t)}{f_{c28}} = \left(\frac{t}{\alpha + \beta \cdot t} \right) \tag{5-2}$$

Setting the left-hand side of the equation equal to 1.0 at t = 28 days (synonymous to constraining the strength growth term to equal 1.0 at 28-days) gives the following:

$$1 = \left(\frac{28}{\alpha + \beta \cdot 28} \right) \tag{5-3}$$

Solving for the constant α yields:

$$\alpha = (1 - \beta)28 \text{ days} \tag{5-4}$$

Equation 5-4 denotes that α is dependent on β to ensure the strength growth factor equals 1.0 at t = 28 days. A plot of Equation 5-2 with varying combinations of α and β satisfying Equation 5-4 is shown in Figure 5-2. The series corresponding to α = 0.70 and β = 0.98 reflects the ACI 209R-92 recommendation for steam-cured concrete containing Type III cement.

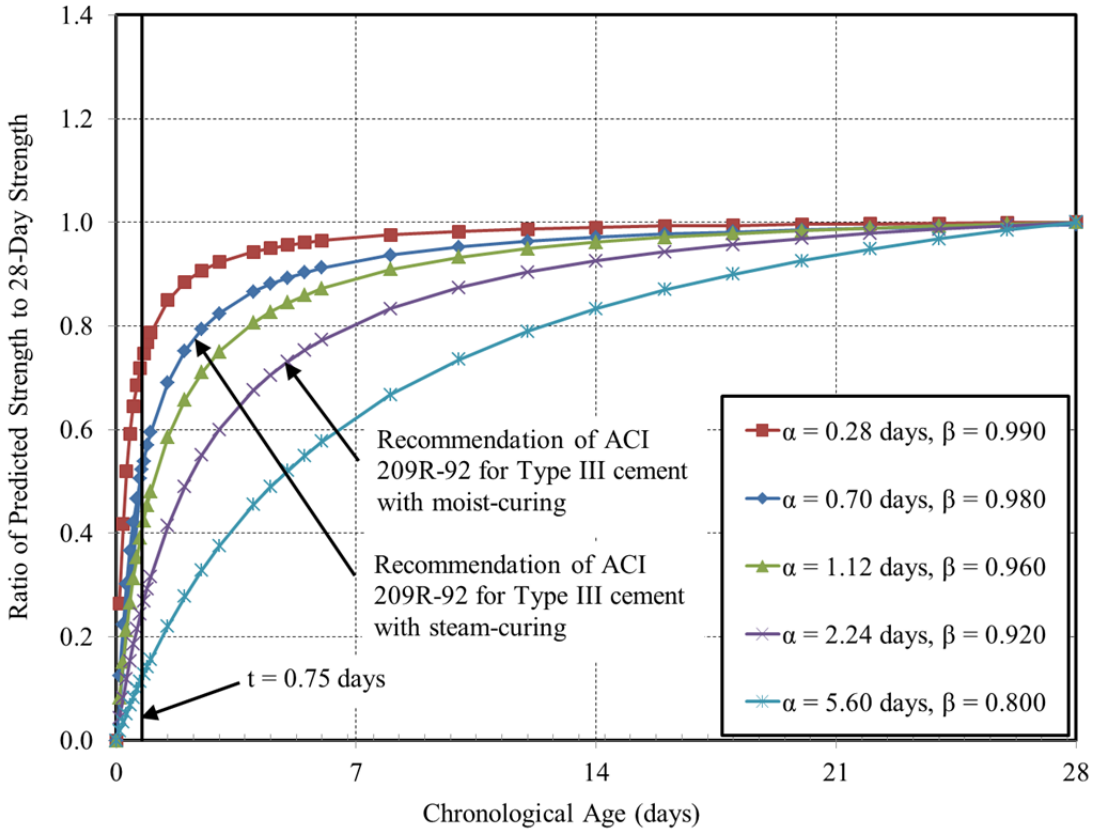

Figure 5-2: ACI 209R-92 Strength Growth Equation with Various Constants

As shown in Figure 5-2, the ACI 209R-92 recommendation implicitly assumes that at the typical chronological time of prestress release (t = 0.75 days), approximately 50 percent of the 28-day concrete strength has developed in steam-cured concrete.

The other primary strength growth equation, as proposed by MC 2010 (fib 2010), is given as:

$$f_{cm}(t) = \beta_{cc}(t) \cdot f_{cm} \tag{5-5a}$$

with

$$\beta_{cc}(t) = \exp\left\{ s \cdot \left[1 - \left(\frac{28}{t} \right)^{0.5} \right] \right\} \tag{5-5b}$$

where

$f_{cm}(t)$ = the mean compressive strength at temperature-adjusted age t (MPa);

$\beta_{cc}(t)$ = a function to describe strength development with time;

f_{cm} = the mean compressive strength at an age of 28 days (MPa);

s = coefficient that depends on the strength class of given cement; and

t = temperature-adjusted concrete age relative to 20°C. (days).

In Equation 5-5, the parameter $\beta_{cc}(t)$ is similar to the strength growth term of Equation 5-2, except unlike the ACI 209 method, it reflects the maturity of the concrete. Equation 5-5b is plotted in Figure 5-3 for varying values of the coefficient s. As shown, the growth curve is generally similar to the ACI 209 expression, with the exception of the horizontal-axis reflecting temperature-adjusted age instead of chronological age. The series corresponding to s= 0.20 reflects the recommendation of MC 2010 for the concrete type most similar to that used in the U.S. precast, prestressed industry.

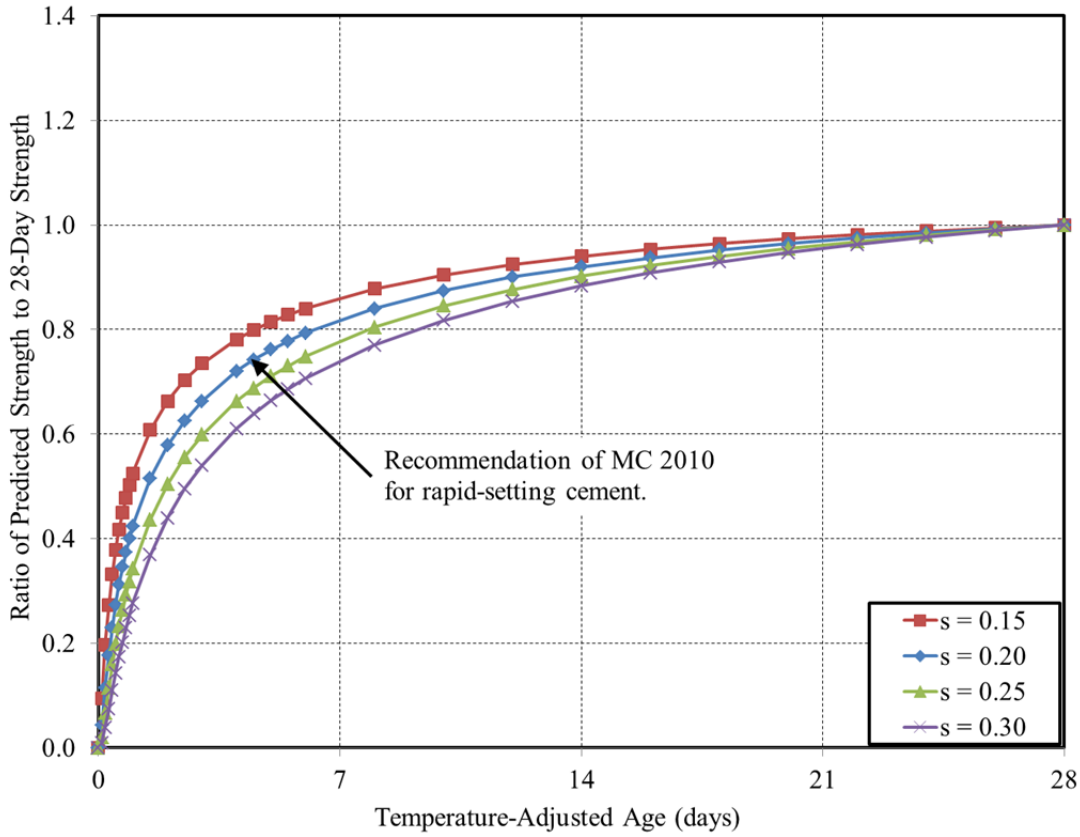

Figure 5-3: MC 2010 Concrete Strength Growth Provisions with Varying Constants

As part of this research effort, Hofrichter (2014) examined the applicability of the above strength growth provisions to concretes typical of the Alabama precast, prestressed concrete industry. By examining historical strength testing records of 435 concrete placement events for the production of ALDOT precast, prestressed girders, Hofrichter (2014) proposed revised calibrations of the above strength growth as appropriate for the regional precast, prestress industry:

- A recommended form of the ACI 209-R92 strength growth equation appropriate for use in the precast, prestressed industry is as follows:

$$f_c = f_c(t) \cdot \left(\frac{\alpha + \beta \cdot t}{t} \right) \tag{5-6}$$

where

$f_c(t)$ = concrete strength at any concrete age t (psi)

f_c = concrete strength at 28 days (psi)

t = concrete age (days)

α = constant (days)

β = constant (unitless);

- A recommended form of the MC 2010 strength growth equation appropriate for use in the precast, prestressed industry is as follows:

$$f_{cm} = \frac{f_{cm}(t)}{\beta_{cc}(t)} \tag{5-7a}$$

with

$$\beta_{cc}(t) = \exp\left\{ s \cdot \left[1 - \left(\frac{28}{t} \right)^{0.5} \right] \right\} \tag{5-7b}$$

where

f_{cm} = the mean compressive strength at a temperature-adjusted time of 28 days (psi)

$f_{cm}(t)$ = the mean compressive strength at temperature-adjusted time t (psi)

$\beta_{cc}(t)$ = a function to describe strength development with time

s = coefficient which depends on the strength class of given cement

t = temperature-adjusted concrete age relative to 20°C. (days);

- Hofrichter recommended the use of Equation 5-6 in the absence of knowledge of curing temperatures and the use of Equations 5-7a and 5-7b when curing temperature information is known; and

- To accompany the above recommended strength prediction equations, Hofrichter (2014) provided updated values for the constants of Equations 5-6 and 5-7a and 5-7b for Type III accelerated-cured concretes as shown in Table 5-1.

Table 5-1: Recalibrated Constants for Strength Prediction Equations (Hofrichter 2014)

			Chronological Age	Equivalent Age
MC2010	Suggested based on Plant Data	s	NA	0.15
	Suggested by MC2010	s	NA	0.20
ACI 209	Suggested based on Plant Data	α (days)	0.34	NA
		β	0.99	NA
	Suggested by ACI 209	α (days)	0.70	NA
		β	0.98	NA

The findings of Hofrichter (2014) as summarized here are brief and aim only to provide the reader with the information necessary for understanding of subsequent sections of this dissertation. Readers are encouraged to consult the complete work of Hofrichter (2014) for a comprehensive accounting of the strength growth analysis summarized here.

5.3 Current Overstrength Provisions in the Concrete Industry

The intent of this section is to review and explore existing available relationships to relate specified concrete compressive strength, f'_c, to expected concrete compressive strength, f_c^* for a given age. This section is applicable to the concrete industry as a whole and as such, any recommendations related to this section are not limited exclusively to the precast, prestressed concrete industry. Sections 5.7 and 5.8 discuss the applicability of these provisions to the precast, prestressed concrete industry in particular.

5.3.1 General Concept

By virtue of concrete production being a combination of tools, materials, methods, and people engaged in producing a measureable output, inherent statistical variability is expected and will always be present. ACI 214 (2011) attributes the variability observed in measured concrete compressive strength to the following nine parameters: (1) variations in characteristics and proportions of ingredients, (2) changes in *w/cm*, (3) variations in concrete mixing, transporting, and sampling, (4) variations in placing and consolidation, (5) variations in concrete temperature and curing, (6) improper sampling procedures, (7) variations due to fabrication techniques, (8) differences in curing between sampled and in-place concrete, and (9) variations in sample testing procedures. These primary contributors to variability are defined more explicitly in Table 5-2.

Table 5-2: Principal Sources of Strength Variation Adapted from ACI 224R-11 (ACI Committee 214 2011)

Batch-to-batch variations	Within-batch variations
Variations in characteristics and proportions of ingredients: • Aggregates; • Cementitious materials, including pozzolans; and • Admixtures *Changes in w/cm caused by:* • Poor control of water; • Variation of aggregate stockpile moisture conditions; • Variable aggregate moisture measurements; and • Retempering. *Variations in mixing, transportation, and sampling:* • Mixing time and speed; • Distance between plant and placement; • Road conditions; and • Failure to obtain a representative sample from the batch *Variations in placing and consolidation:** • Chute, pump, or buggy; • Internal or external vibration; and • Different operators *Variations in concrete temperature and curing:** • Season; • Ambient humidity; • Wind speed	*Improper sampling from the batch sample.* *Variations due to fabrication techniques:* • Substandard conditions; • Incorrect tools; • Poor quality, damaged or distorted molds; • Nonstandard molding and consolidation; and • Incorrect handling of fresh test samples. *Differences in curing:* • Delays in beginning initial curing; • Temperature variation; • Variable moisture control; • Nonstandard initial curing; • Delays in bringing cylinders to the laboratory; • Rough handling of cylinder in transport; and • Improper final curing. *Variations in sample testing* • Uncertified tester; • Specimen surface preparation; • Inadequate or uncalibrated testing equipment; • Nonstandard loading rate; and • Poor record keeping.

*Applies to in-place strength of the structure.

For a sufficiently large sample of tests for concrete compressive strength ($n \geq 30$), the sampling distribution (shown as a shaded histogram) approaches a Gaussian (normal)

distribution as illustrated by Figure 5-4 (ACI Committee 214 2011). Cook (1982) contends that the assumption of a normal distribution may not be correct for concrete compressive strengths exceeding 10,000 psi. However, Neville (2013) notes that the assumption of normality is conservative for high-strength concrete. This topic is explored further in Section 5.8 of this dissertation.

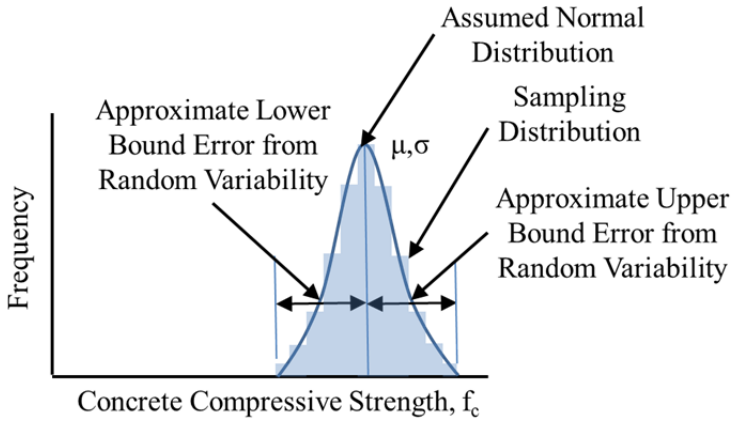

Figure 5-4: Gaussian Distribution of Sampled Concrete Compressive Strength

Any normal distribution can be described completely by a mean, μ, and a standard deviation, σ. For a normal distribution, approximately 68 percent of results fall within +/- one standard deviation of the mean and approximately 95 percent of the results fall within +/- two standard deviations of the mean, as illustrated in Figure 5-5 (ACI Committee 214 2011).

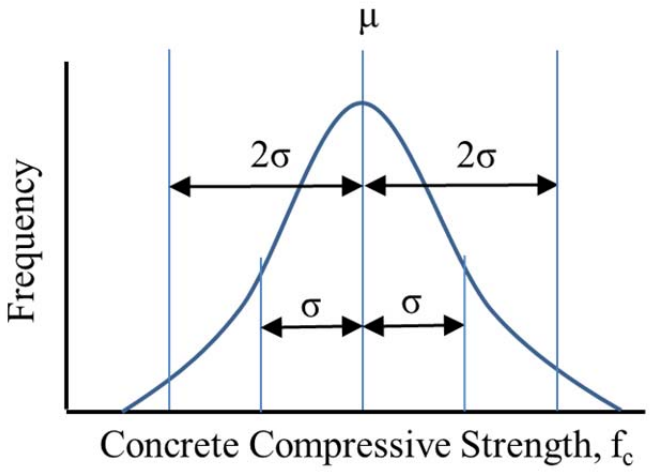

Figure 5-5: Relationship between Standard Deviation and Expected Data Spread

For this discussion, let us assume that given an engineer's specified concrete strength, f'_c, a concrete producer can proportion a mixture with a mean measured concrete strength, f_c, precisely matching the specified value. This case is illustrated graphically in Figure 5-6 (top). If this situation occurred in a structure, it would be expected that approximately 50 percent of the concrete in the structure would have a strength falling below the specified strength, f'_c. A less extreme case is shown next in Figure 5-6 (middle). Here, the concrete producer arbitrarily targets a compressive strength 1.2 times the specified value. As evidenced by the reduced shaded area under the curve, the resulting structure would likely be safer than the first case (top) with a smaller proportion of concrete exhibiting insufficient strength. In the final case shown in Figure 5-6 (bottom), the concrete producer decides to target a compressive strength 1.7 times larger than the specified value hoping to ensure that all concrete within the final structure exceeds the specified concrete strength. While the probability of failure for the final case is indeed very low, it is still non-zero as a result of the probabilistic nature of

random variables. In reality, the arbitrary proportions targeted above are code-dictated to promote a uniform level of minimum safety as is discussed further in Section 5.3.2.

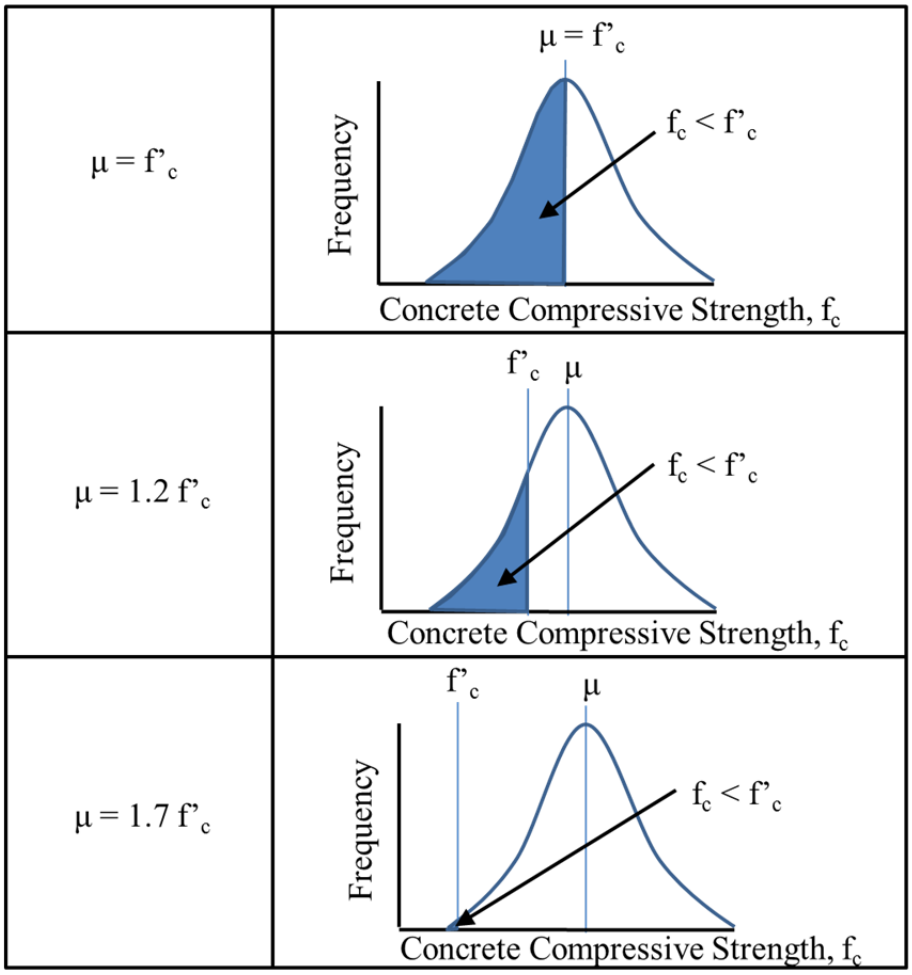

Figure 5-6: Concept of Probability of Failure

5.3.2 Measures of Variability

There are two main parameters suggested by ACI 214R-92 (ACI Committee 214 2011) to quantify the degree of dispersion of a normal distribution of sampled concrete strengths—the standard deviation and the coefficient of variation. The sample standard deviation for a series of concrete strength tests can be computed as follows:

$$s = \sqrt{\frac{\sum_{i=1}^{n}\left(X_i - \bar{X}\right)^2}{n-1}} \tag{5-8}$$

where

n = the number of strength test results;

$\overline{X}$ = the sample mean; and

X_i = the ith test result.

The coefficient of variation, also an indicator of the relative dispersion of a sampled distribution, is expressed as a percentage of the mean strength as follows:

$$V = \frac{s}{\overline{X}} \cdot 100 \tag{5-9}$$

where

s = the sample standard deviation; and

$\overline{X}$ = the sample mean.

An obvious question regarding the above two metrics of variability is if one metric is more preferable than the other for use in the concrete community. This topic has been spiritedly debated in the literature for the last 35 years without clear consensus. ACI 214R-11 (ACI Committee 214 2011) allows the use of both standard deviation and coefficient of variation somewhat interchangeably, although Committee 214 supports the use of the coefficient of variation for comparisons of spread over a wide range of compressive strengths (in excess of 1,000 psi) and for overall variation of concrete strengths exceeding 5,000 psi. The recommendations of ACI Committee 214 are partly based on the work of Cook (1989) who concluded that the standard deviation approach may not be "a fair evaluation for higher strength concretes" and instead preferred the unitless coefficient of variation owing to the fact that it is less affected by the magnitude of the compressive strengths considered. Cook also concluded that for high-strength concretes, the coefficient of variation for varying concrete strengths tended to remain

constant, while the standard deviation varied. In contrast, Neville (2013) points out that various laboratory studies have failed to consistently show that either the standard deviation or coefficient of variation remain constant for concretes of varying strength produced by the same facility and quality control practices. The common assumption, however, is that either standard deviation or the coefficient of variation remains constant for a given producer (regardless of strength level) as a product of control standards for concrete production. For varying mean target strength levels and varying constant standard deviations, the corresponding coefficient of variation is computed as shown in Figure 5-7.

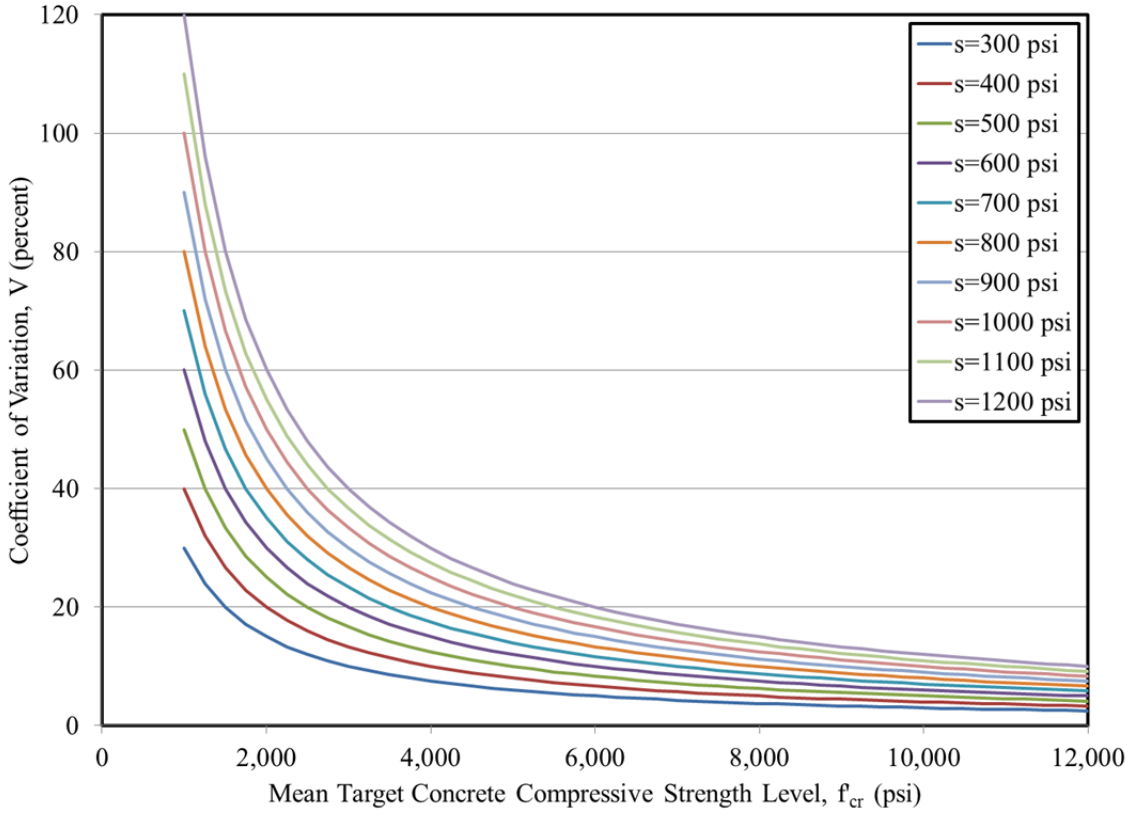

Figure 5-7: Relationship between Standard Deviation and Coefficient of Variation for Various Target Strength Levels

It can be seen that for concrete target strength levels exceeding approximately 6,000 psi, the computed coefficients of variation for various constant standard deviations tends to approach a horizontal line with a relatively small amount of vertical spread between curves. Therefore, for strength levels exceeding 6,000 psi, the choice to assume a constant variance (as promoted by Cook) or a constant standard deviation (as promoted by Neville) yields approximately identical results.

The use of a standard deviation approach offers a distinct advantage for the statistical analyses performed later in this chapter. If we recall the definition of the difference statistic, $dstat$, from Section 5.2.2, this quantity represents the difference between the measured concrete strength, f_c, and the specified concrete strength, f'_c, at a particular age. As previously discussed, for a concrete strength distribution of sufficient size, the probability distribution is expected to be approximately normal. This concept is reiterated in Figure 5-8 (top) for the hypothetical situation of the mean measured concrete strength precisely equaling the specified strength. In this example, a given concrete is prepared and sampled 30 times, resulting in an assumed normal distribution with μ = 8,000 psi and σ = 400 psi. Next, the difference statistic is computed and the distribution shown in Figure 5-8 (top right). As intuitively expected, computation of the difference statistic preserves the standard deviation of the initial distribution while shifting the mean. Next, the results of similar concrete trials are shown for two different strength mixtures in Figure 5-8 bottom. Here, each mixture is prepared and sampled 15 times for a total of 30 tests. In this example, it is assumed that the standard deviation is identical to that of the first example and remains 400 psi for each mixture. Notice that the height of each frequency curve is precisely half the height of the

previous example, but the spread remains identical. By calculating the difference statistic for each of the two concrete mixtures and combining on the same plot by summing (Figure 5-8 bottom right), it is observed that the distribution of the difference statistic is again preserved at 400 psi.

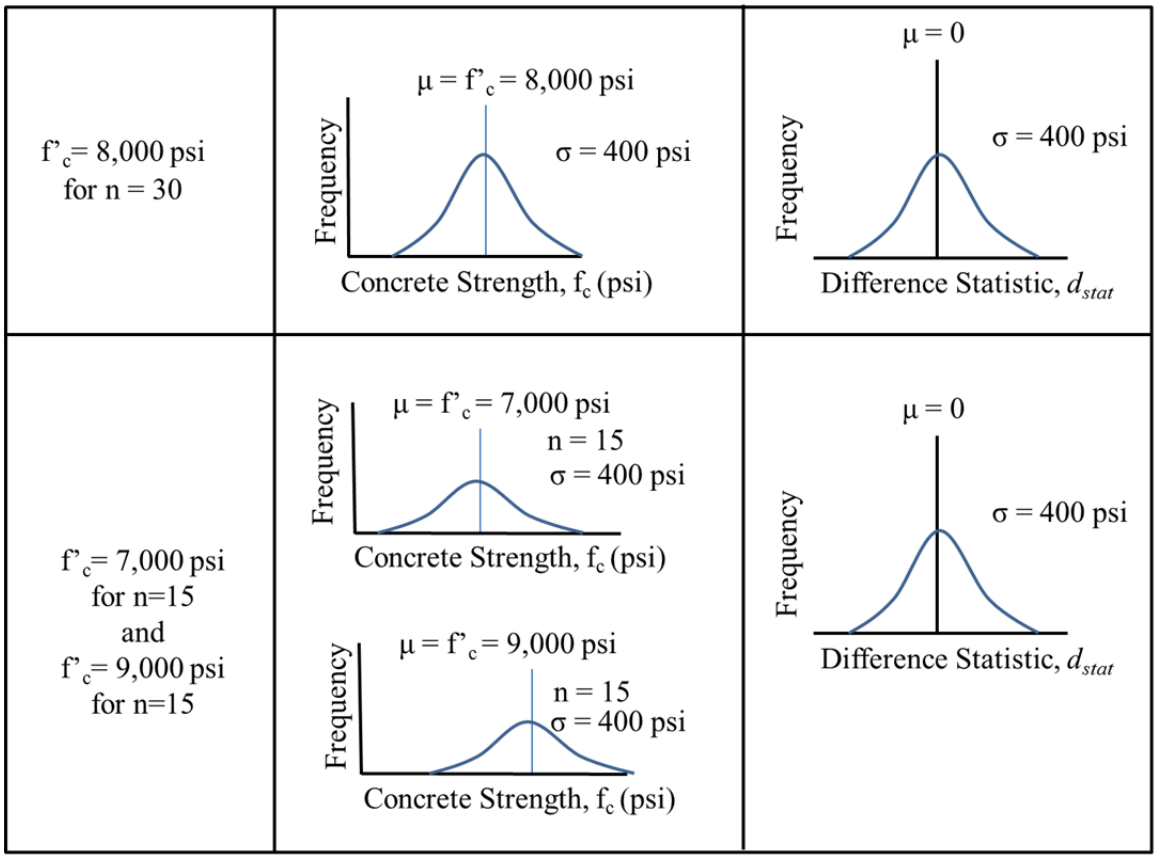

Figure 5-8: Concept of Preservation of Standard Deviation

The concept illustrated in Figure 5-8 was verified by performing statistical simulations with varying sample sizes, a varying number of constitutive mixtures, and varying distribution means. The concept can perhaps best be stated as follows:

> *For an assumed (or approximated) constant standard deviation value at all considered strength levels, the distribution of the difference statistic is identical regardless of the number of constitutive mixtures or the relative mean strength levels of each mixture.*

The concept of preservation of standard deviation as summarized above does not equally apply to the coefficient of variance, V, due to the inclusion of the sample mean in the computation of this parameter. Statistical evidence of this concept is included in Appendix B of this dissertation. The concept of preservation of standard deviation of the difference statistic is a convenient analysis tool used throughout the remainder of this chapter and is used to obtain a representative standard deviation from historical testing results (similar to Figure 5-8 bottom) that represents the standard deviation parameter (Figure 5-8 top) intended for use in existing published overstrength prediction equations.

ACI 363-R-11 *Report on High-Strength Concrete* (ACI Commitee 363 2010), ACI 211.4-08 *Guide for Selecting Proportions for High-Strength Concretes Using Portland Cement and Other Cementitious Materials* (ACI Commitee 211 2008), and ACI 301-10 *Specifications for Structural Concrete* (ACI Commitee 301 2010) default to the use of a standard deviation to describe the spread of concrete compressive strength tests. Due to the (1) previously discussed similarities between standard deviation and coefficient of variation for concretes with compressive strength exceeding 6,000 psi, (2) the distinct analytical advantages offered by its use, and (3) the default of ACI guidance to its use, standard deviation is used as the preferred metric for describing dispersion in concrete strength testing results for the remainder of this dissertation.

5.3.3 Relevant Design Code Provisions

As previously discussed, the relationship between the design engineer's specified concrete strength and the concrete producer's target strength is intrinsically related to the reliability and safety of a given building or structure. Accordingly, it is expected that design and building codes should dictate this relationship (based on an acceptable

probability of failure) in order to ensure a minimum level of safety is preserved in all structures. This section reviews current design code provisions applicable to quantifying the relationship between specified design strength and expected strength or in-place mean strength. This discussion focuses on the provisions of ACI 318-14 (ACI Committee 318 2014) and the *fib* Model Code 2010 (fib 2010).

ACI 318-14 Section 26.4.3.1 summarizes the requirements for the proportioning of concrete mixtures for structural applications. In this section, it is required that a concrete mixture shall be proportioned either by the provisions of the *Specification for Structural Concrete* (ACI Commitee 301 2010) or by some other method approved by the design engineer that preserves the minimum probability associated with the methods set forth in ACI 301[1]. ACI 318-14 also references the *Guide to Evaluation of Strength Test Results of Concrete* (ACI 214R-11) for further guidance on the probabilistic nature of this topic. The requirements for the ACI provisions regarding overstrength as outlined in ACI 301 are

1. For all concrete strengths ranges, the average of any three consecutive strength tests shall exceed the specified concrete strength, f'_c, 99% of the time. That is, failure to meet this criteria should not be anticipated more than 1 in 100 times;
2. For concrete strengths ≤ 5,000 psi, on average no more than one percent of individual strength test results shall be permitted to fall below the specified strength, f'_c, by more than 500 psi; and

[1] The omission of the specific target strength provisions in ACI 318-14 is a departure from the previous ACI 318 building codes, which contained some of the information currently maintained in ACI 301.

3. For concrete strengths > 5,000 psi, on average, no more than one percent of individual strength test results shall be permitted to fall below 90 percent of the specified strength, f'_c.

ACI 214R-11 offers two approaches to ensure that the above probabilistic requirements are satisfied. First, with sufficient knowledge of the variability typical for a specific concrete producer (based on historical test records), probabilistic equations may be used to compute the f'_{cr} as a function of f'_c. Equations for this purpose are summarized in Table 5-3 below, adapted from ACI 301-10. Equations 5-10a and 5-10c correspond to requirement one in the list above, Equation 5-10b corresponds to requirement two, and Equation 5-10d corresponds to requirement three.

Table 5-3: Required Average Compressive Strength, f'$_{cr}$, with Historical Data (Adapted from ACI 301-10)

f'_c (psi)	f'_{cr} (psi)	
	Use the larger of	
5,000 or less	$f'_{cr} = f'_c + 1.34s$	**(Equation 5-10a)**
	$f'_{cr} = f'_c + 2.33s - 500$	**(Equation 5-10b)**
Over 5,000	$f'_{cr} = f'_c + 1.34s$	**(Equation 5-10c)**
	$f'_{cr} = 0.9f'_c + 2.33s$	**(Equation 5-10d)**

The standard deviation, *s*, intended to be used in Equations 5-10 a through d is defined in ACI 214R-11 Section 5.2 as the sample standard deviation as computed by Equation 5-8 for a data set satisfying the following requirements:

- Historical strength testing records must reflect at least 30 tests (most commonly interpreted to mean at least 30 consecutive batches[2] of concrete produced to meet

[2] ACI 214R-11 allows for the computation of a sample standard deviation with fewer than 30 samples, but requires the use of a modification factor to account for increased uncertainty. This procedure was suggested by Philleo (1981).

a specified strength within 1,000 psi of the specified strength for the project at hand); and

- Historical concrete batches shall be similar in composition and production as those intended to be used for the project at hand;

ACI 214-R11 offers guidance on the interpretation of the standard deviation as computed according to the above requirements. In general, the standard deviation is regarded as a metric of the standard of control for a given concrete producer and represents the consistency of a producer's production and testing practices. A smaller standard deviation of strength testing results means there is less dispersion in the strength testing results and is generally correlated to better quality control during concrete production, placement, and testing. Various categories representing the standard of concrete control for general construction concrete applications are shown in Table 5-4.

Table 5-4: Standards of Concrete Control for General Construction (Adapted from ACI 214-R11)

Concrete Compressive Strength	**Excellent**	**Very good**	**Good**	**Fair**	**Poor**
$f'_c < 5{,}000$ psi	*Standard deviation for different control standards (psi)*				
	Below 400	400 to 500	500 to 600	600 to 700	Above 700
$f'_c \geq 5{,}000$ psi	*Coefficient of variation for different control standards (%)*				
	Below 7.0	7.0 to 9.0	9.0 to 11.0	11.0 to 14.0	Above 14.0
Strength level that above requirements are approximately equal (psi)	5,710	5,630	5,500	5,200	5,000

As shown and previously discussed, ACI 214-R11 prescribes the use of a standard deviation approach for compressive strengths below 5,000 psi and the use of a coefficient of variation for strengths exceeding 5,000 psi. For comparison between the two

standards of concrete control, the strength level at which the provisions are equal is also shown in Table 5-4 (bottom). For example, at a concrete compressive strength of 5,710 psi, a coefficient of variation of 7.0 is approximately equal to a standard deviation of 400. In the absence of historical strength testing data, ACI 301-10 provides equations to directly compute the required concrete strength, f'_{cr} as summarized in Table 5-5.

Table 5-5: Required Average Compressive Strength, f'$_{cr}$, without Historical Data (Adapted from ACI 301-10)

f'_c (psi)	f'_{cr} (psi)
Less than 3,000	$f'_c + 1{,}000$ **(Equation 5-11a)**
3,000 to 5,000	$f'_c + 1{,}200$ **(Equation 5-11b)**
Over 5,000	$1.1f'_c + 700$ **(Equation 5-11c)**

It would appear that there must be an assumed level of variability implicit to the development of Equations 5-11. By systematically setting Equations 5-11a-c equal to Equations 5-10 a-d and solving for the implicit standard deviation at various strength levels, the results of Figure 5-9 can be computed. It is observed that for specified concrete compressive strengths less than 5,000 psi, an implicit value of s = 730 psi is assumed (corresponding to poor concrete control for general construction). For specified strength values exceeding 5,000 psi, s follows a linear trend with lower bound of s = 730 psi for f'_c = 5,000 psi and upper bound approaching s = 1,330 psi for f'_c = 12,000 psi. Accordingly, it can be concluded that when examining standard deviation as a metric of the dispersion of strength testing results, current ACI provisions include the implicit

hypothesis that higher concrete strengths correlate to increased dispersion about the mean of strength testing results[3].

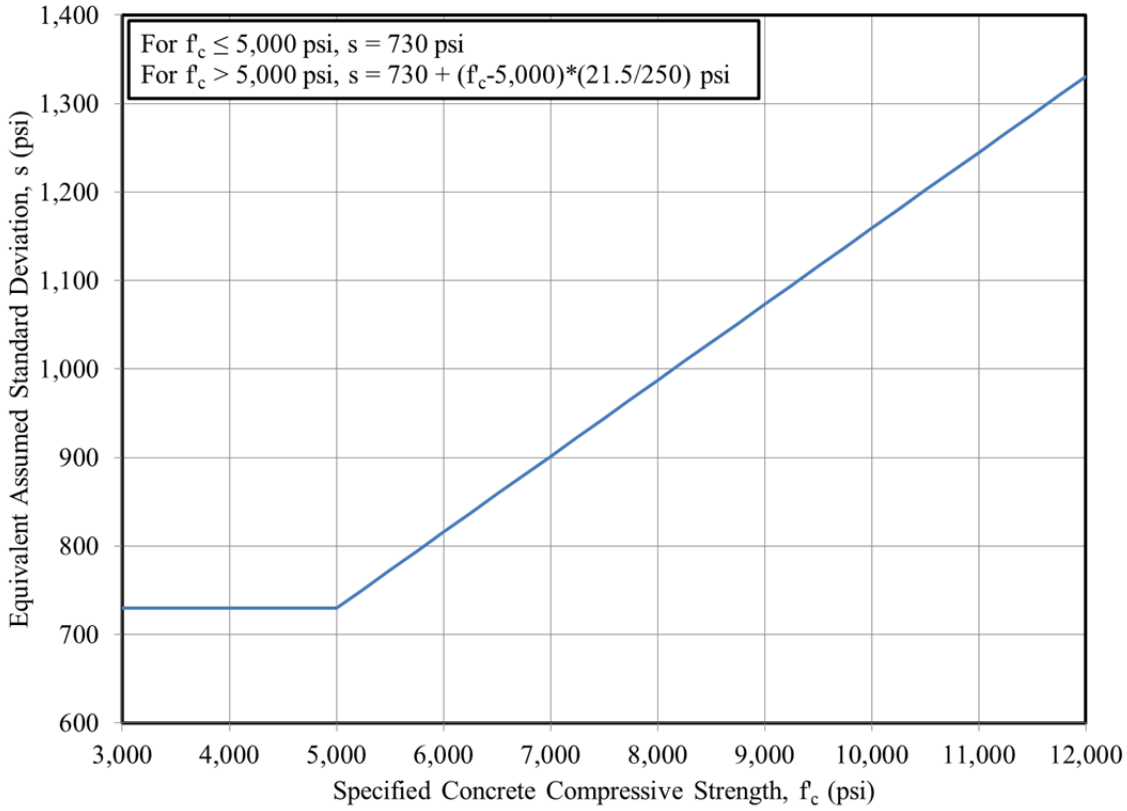

Figure 5-9: Implicit Standard Deviations for No Historical Data ACI Overstrength Provisions

The linear portion of Figure 5-9 affirms that current ACI provisions default to a coefficient of variation approach for specified concrete strengths exceeding 5,000 psi. A relative comparison of the provisions of Equations 5-10 a-d and 5-11 a-c is shown in Figure 5-10. As expected, Equations 5-11 a-c (denoted by "No Historical Data Available") are verified to be conservative as compared to the lines of Equations 5-10 a-d (denoted by *s* = XXX psi), particularly for higher values of f'_c and the slope of the "No

[3] The preference in this dissertation is to examine dispersion of strength testing results independent of magnitude of the compressive strength and, thus, standard deviation is chosen as a metric of dispersion. If the coefficient of variation were instead considered as the metric of interest, the conclusions reached in this section may be different.

Historical Data Available" series exhibits a slight jog due to the use of coefficient of variation for strengths exceeding 5,000 psi as compared to the use of a constant standard deviation approach for all strength levels as discussed earlier in this section.

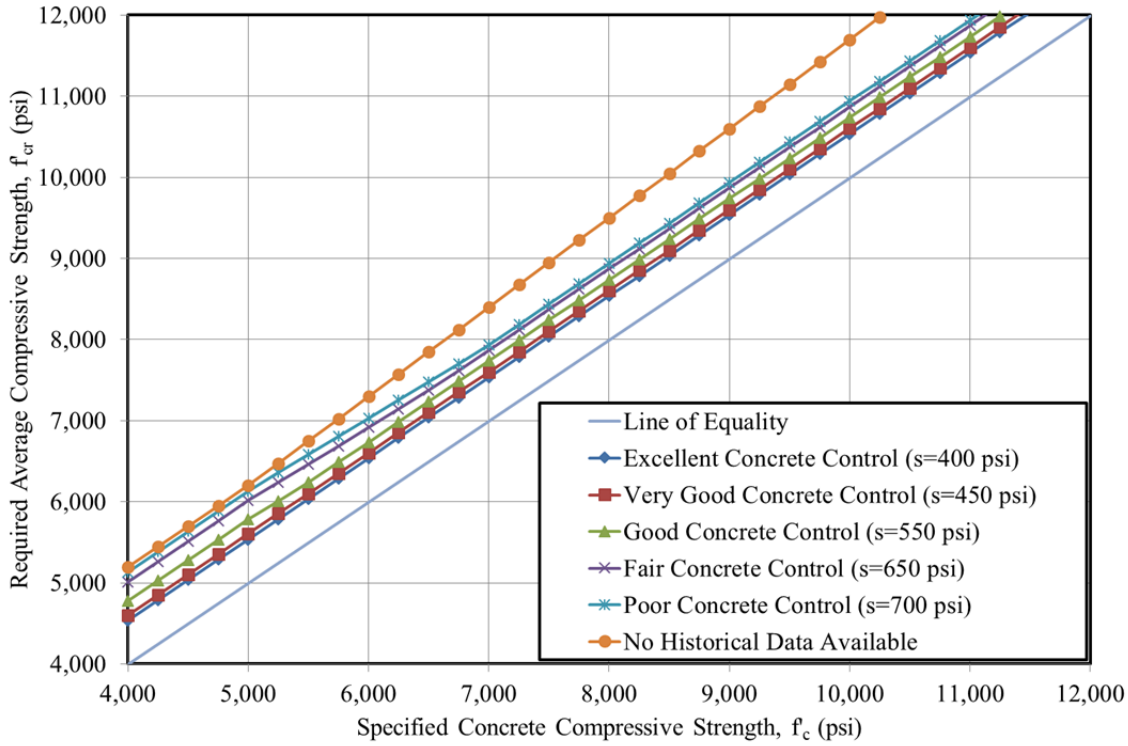

Figure 5-10: Comparison of Current ACI Overstrength Parameters

The *Model Code for Concrete Structures* 2010 (fib 2010) contains provisions somewhat similar to those of the American Concrete Institute as reviewed above with a few marked differences. First, MC 2010 uses the term *characteristic compressive strength*, f_{ck}, in lieu of the ACI convention of specified concrete strength, f'_c. Both of these parameters are similar in that they represent a lower bound value of concrete strength, but represent different probabilities of failure for each code. In the Model Code, the characteristic strength, f_{ck}, is defined as the value below which 5 percent of all possible strength measurements are expected to fall (Muller et al. 2013) instead of the one percent probability of failure for three consecutive cylinders used in ACI 301-10

provisions. MC 2010 also includes an additional parameter, the mean compressive strength, f_{cm}, which represents the mean value of a sampled distribution of compressive strength tests. (This value is most similar to f'_{cr} in ACI terminology.) Muller et al. (2013) suggest the following relation between the characteristic strength, f_{ck}, and the mean compressive strength, f_{cm}:

$$f_{cm} = f_{ck} + 1.645 \cdot \sigma_s \tag{5-12}$$

where

σ_s = the standard deviation of the sample.

The 1.645 factor in Equation 5-12 is analogous to the 2.33 factor in the ACI equivalent equations of 5-10 b and d and is again derived from a Gaussian strength distribution. The MC 2010 code assumes a constant standard deviation of approximately 5 MPa (equal to 725 psi) regardless of strength level as is common practice in the European concrete industry (Muller et al. 2013). Substituting the assumed standard deviation value of 5 MPa into Equation 5-12 and rounding for simplicity gives the fib Model Code 2010 expression:

$$f_{cm} = f_{ck} + 8 \text{ MPa} \tag{5-13}$$

The predominant use of the overstrength provisions summarized above is for the proportioning of concrete mixtures to ensure that the code-prescribed level of life safety is achieved for strength limit states. For this life-safety application, it is essential that the standard deviation value used in specification equations must either accurately or else conservatively describe the distribution of strength tests of the produced concrete. The

provisions above have been time-tested and repeatedly proven to provide satisfactory levels of safety for strength limit state design.

5.3.4 Regional Use of Overstrength in Serviceability Computation

Up to this point, the discussion on overstrength provisions has focused on relating the specified compressive strength, f'_c, to a target or required compressive strength, f'_{cr} in order to satisfy the probabilistic nature of the random variable concrete compressive strength. In order to extend this discussion further and to the main topic of this dissertation, it is useful to recognize that the target or required compressive strength, f'_{cr}, at a given age is also equal to the best prediction of the expected compressive strength, f_c^*, at that age. Simply put, if a concrete mixture is proportioned to achieve a certain mean strength, f'_{cr}, at a given age, this mean strength is the value most reasonable to "expect" from a series of concrete strength tests performed at that age.

In general, serviceability computations are intended to provide the most accurate estimate or prediction of deflections and, therefore, do not use safety-related factors in computations. These serviceability computations rely almost universally on a concrete modulus of elasticity value that is obtained from a correlation to the concrete compressive strength (as is explored in Chapter 6). Therefore, Model Code 2010 provisions suggest that the mean concrete strength, f_{cm}, be used in the computation of deflections instead of the characteristic strength, f_{ck}. The corollary to this Model Code provision in American design would be to recommend the use f'_{cr} or f_c^* in deflection computations for concrete structures in lieu of f'_c.

At the time of design, the f'_{cr} value cannot be precisely computed because the concrete producer and mixture proportions are not yet determined. However, even an imprecise estimate of the expected concrete strength, f_c^*, will yield a substantially more accurate serviceability computation than the use of the specified concrete strength, f'_c. An important distinction is necessary here—for strength or life-safety computations, the standard deviation must accurately or conservatively reflect the actual distribution of concrete strength tests for the given producer. However, for the purpose of serviceability computations, the accuracy of the standard deviation used to compute an expected value f_c^* is not as critical. Statistically speaking, even a relatively poor estimate of the expected value, f_c^* (incorrect by up to approximately 1.34 times the standard deviation) will still yield a more accurate estimation of the expected concrete strength than the incorrect usage of the specified strength, f'_c. Using the specified concrete strength in serviceability computations—as is currently done in U.S. practice, provides one of the *worst* possible estimations of expected mean concrete strength that is systematically and statistically an incorrect approximation.

A next logical discussion is the extent to which deflection computations might be improved if an expected concrete strength value, f_c^*, is used in lieu of the specified value, f'_c, in design computations. Although this topic is intrinsically related to multiple analyses and findings of this dissertation, a brief discussion is offered here. The modulus of elasticity of concrete is typically correlated to the square root of the concrete compressive strength (ACI Committee 318 2014). Therefore, it seems logical to compare percent differences between the square root of the specified concrete strength and the

square root of the expected concrete strength computed according to ACI 301 provisions. This analysis is shown in Figure 5-11. It is evident that (1) the percent difference is greater for lower specified concrete strengths than for higher strengths, and (2) for the strength range considered, the percent difference ranges from 18 percent to 2 percent.

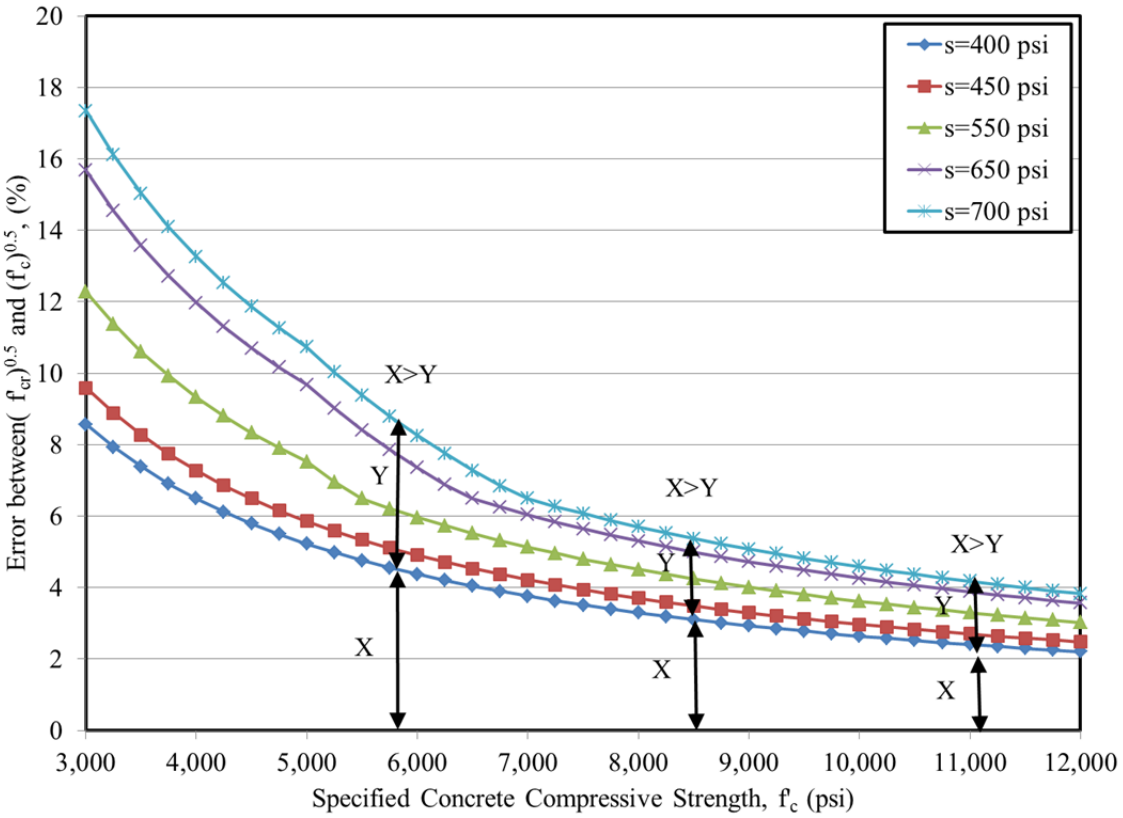

Figure 5-11: Percent Error in Square Root of Compressive Strengths

Notice in Figure 5-11 that two distances are denoted at various points along the plotted curves. The distance X represents the minimum percent difference for a given strength, while the distance Y represents the range of the percent differences at a given strength for a variety of practical standard deviation values. For strengths above approximately 6,000 psi, it is evident that X > Y, meaning that regardless of the accuracy of the standard deviation used to predict the mean strength (within a logical range), f'_{cr}, the percent error will be less than if the specified concrete strength were used in serviceability

computations. Simply stated, any reasonable estimate of the standard deviation will cause a corresponding improvement in the accuracy of deflection computations for concrete strengths exceeding 6,000 psi.

Further discussion is contained in subsequent chapters of this dissertation, but it is clear that the practice of using specified concrete strengths for serviceability computations is fundamentally flawed. While it is tempting to propose that all serviceability computations in American design should immediately adopt the practice of using an expected concrete strength, f_c^*, in design computations, this topic must be explored further in order to evaluate the effect of this potential recommendation on the concrete industry as a whole, specifically with regard to any previously empirically calibrated constants acting to modify either concrete compressive strength or concrete stiffness in existing design equations.

5.4 Overstrength in the Precast, Prestressed Concrete Industry

In contrast to the previous discussion that applied to the concrete industry as a whole, this section focuses solely on overstrength in the precast, prestressed industry. Included is a general discussion of the factors contributing to overstrength in the precast, prestress industry, a summary of previous work by others, and a discussion that examines the suitability of applying the overstrength provisions of Section 5.3 to the field of precast, prestressed concrete. It is important to note that while efforts to quantify overstrength at the time of prestress release are more relevant to the major objectives of this dissertation, a limited discussion is also offered of efforts to quantify overstrength at the age of 28 days.

5.4.1 Overstrength at Prestress Release

At the time of the release of the prestressing force during girder fabrication, the concrete strength is required to have reached a specified concrete release strength, f'_{ci}. It is important to recognize that this requirement is primarily a serviceability requirement, owing to the fact that it is not directly tied to the life safety of the in-service structure. Accordingly, ACI 318-14 (ACI Committee 318 2014) includes specified values for maximum permissible stresses in prestressed members in Chapter 24: Serviceability Requirements. Here, the primary concern is ensuring that the concrete is strong enough, on average, to resist the internal stresses induced during prestress transfer without compromising the gross concrete section. A localized area with concrete strength falling slightly below f'_{ci} is not cause for concern because a failure of the concrete gross section remains unlikely. That being said, however, if the prestressing force was released at the precise moment when the girder concrete strength, f_{ci}, were equal to the specified strength, f'_{ci}, one would expect the concrete at approximately half of the critical locations within the girder to be of insufficient strength.

The primary causes of overstrength at prestress release include both those general factors contributing to variability previously discussed in Section 5.2 as well as a few additional factors unique to the precast, prestressed industry. Of the factors summarized in Section 5.2, it may be expected that certain factors will contribute to higher overall variation in the distribution of girder strength due to the large size and scale of precast, prestressed concrete plants. For example, one may expect more variability in concrete age, temperature, and curing conditions for a 150 ft long prestressed concrete girder placed over a three-hour period than would be expected for a smaller concrete placement

taking place in a shorter time period with more consistent temperature control in place. In addition, there are two main factors unique to the precast, prestressed industry that are primary contributors to overstrength at prestress release—(1) the practice of using preapproved concrete mixtures and (2) the additional construction events required in the precast, prestressed industry as compared to cast-in-place concrete. As concluded in Section 4.4.1, the rigorous approval process for precast, prestress mixture designs encourages prestress producers to maintain a limited inventory of concrete mixtures suitable for a wide variety of projects. By making use of only a limited inventory of concrete mixtures, the expected concrete strength at prestress release, f_{ci}^{*} is not especially well matched to the specified release strength, f'_{ci}, but instead, errs on the conservative side and tends to provide a strength well in excess of f'_{ci} for many structures. Savvy prestress producers realize this and tend to either (1) capitalize on the reduced chronological time necessary to reach the specified release strength for lower strength designs or (2) subjectively adjust curing conditions (i.e. steam temperature or use of moist curing) as necessary to ensure the required release strength is met in a convenient chronological time period (most often 18 hours). A final cause of increased overstrength in the precast, prestressed industry is the increased variability in the distribution of concrete strengths caused by additional construction events contributing to a single final parameter. For instance, the standard deviations representing varying degrees of control for concrete previously discussed in Section 5.3.2 and shown in Table 5-4 (i.e. s = 450 psi for "very good") are intended for concrete strength tests at a single chronological age (i.e. all test results for concretes tested at 28 days). In the precast, prestressed industry, the testing of compressive strength at the time of release of the

prestressing force does not adhere to a strict chronological time requirement. Instead, as shown in Figure 4-10, the distribution of the chronological age for concrete strength testing exhibits an approximately normal shape centered on an approximate age of 17.9 hours. This distinction is especially important due the rapid strength gain occurring at prestress transfer as compared to 28 days after production. By adding in this additional source of variation, it is expected that the overall dispersion of strength testing results about the mean may increase for prestressed concrete as compared to a strictly single-age data set. Given the above discussion, it is reasonable to expect that a greater spread of strength testing results will likely be present at the time of prestress release in the precast, prestressed industry than may be expected in the general concrete industry[4], and thus, higher amounts of *overstrength* may be observed in the precast, prestressed industry at prestress release.

Various previous researchers have conducted studies aimed at improving camber predictions in precast, prestressed concrete bridge girders and have similarly identified the importance of accurately predicting the expected concrete compressive strength at the time of prestress release during the girder design phase. Most typically, researchers perform a historical review of regionally available strength testing records and recommend a relationship between the specified concrete strength at release, f'_{ci}, and the expected concrete strength at release, f^*_{ci}. Conducting a study for MnDOT, French and O'Neill (2012) found that concrete cylinders exhibited an average strength 15.5 percent higher than the design release strength for that pour. Somewhat similarly, Storm

[4] This trend is counter to the opinion that the increased quality-control practices in precast concrete production generally result in less variability in concrete as placed. While these practices likely do result in more consistent concrete delivered to the site (than in typical cast-in-place construction), the additional sources of variability discussed above likely outweight any advantage gained by increased quality-control of concrete mixtures.

et al. (2013) found that the average ratio of measured compressive strength to the specified strength at the time of prestress release was approximately 1.24 for girders produced for NCDOT. Rosa et al. (2007) suggested similar findings for WSDOT girders, finding that on average, the measured compressive strength at release was 10-11 percent higher than the specified release strength. Most recently, Nervig (2014) concluded that for IDOT bridge girders with specified release strengths between 4,500 and 5,500 psi, the measured value of compressive strength tended to exceed the specified value by approximately 39.5 percent; the specified value was exceeded by 11.5 percent for specified concrete release strengths between 6,000 and 7,000 psi. The relatively large variability exhibited in the study results above seems to suggest that the research approach of conducting a historical review to determine a single indiscriminant overstrength multiplier may not be an ideal approach for quantifying overstrength due to its sensitivity to variations in regional practice or strength level.

The approach of this dissertation research with respect to quantifying overstrength at the time of prestress release differs somewhat from previous efforts. While similar regressions of historical data to those detailed above are completed for the sake of comparison to previous work, the dominant approach employed in this dissertation for predicting expected concrete strength at prestress release is a logical approach consistent with the concepts currently contained in by ACI 214R-11.

5.4.2 Overstrength at 28 Days

At the chronological age of 28 days after girder fabrication, the concrete compressive strength of a structural member is required to have reached a specified concrete strength, f'_c, prior to entering service. Unlike the concrete strength requirement at prestress

release, this 28-day requirement is a strength limit state requirement. This section discusses the primary causes of overstrength at the chronological age of 28 days, previous research on this topic, and the research approach taken in this research study.

During the initial design of a precast, prestressed concrete girder, the design engineer must perform designs for both strength and serviceability limit states. While the primary serviceability limit state (allowable concrete stresses at prestress release) is evaluated using material properties from the time of prestress release, ultimate strength computations are performed using material properties at a chronological age of 28 days. In almost all cases, the serviceability limit state (strength at release) controls the proportioning of concrete for a given project (PCI 2011). More simply put, any concrete mixture that has the strength development characteristics capable of achieving the specified release strength, f'_{ci} , at 18 hours will typically hardily surpass the specified 28-day specified strength, f'_c (or more correctly any required 28-day strength, f'_{cr}), by the age of 28 days. This concept is primarily due to the fact that prestressed concrete producers aim to maximize productivity by minimizing the time required to meet the specified concrete release strength. In doing so, producers can make maximum usage of a limited number of fabrication lines and steel formwork modules.

Given that the concrete strength at release is typically the controlling factor in mixture selection for precast, prestressed concrete products, it is most logical to "expect" the 28-day concrete strength to be that predicted in accordance with Equation 5-6.

$$f_c = f_c(t) \cdot \left(\frac{\alpha + \beta \cdot t}{t} \right) \tag{5-6}$$

Substituting a mean time to release of 0.75 days (18 hours) and using the recommendations of Hofrichter (2014) for constants α and β, Equation 5-6 simplifies to

$$f_c = f_{ci} \cdot 1.44 \tag{5-14}$$

The constant of Equation 5-14 can be interpreted to mean that for the precast, prestressed concretes typical of Hofrichter's work, the 28-day strength is expected to be 1.44 times the release strength. In this way, the expected 28-day strength is dictated by a known controlling release strength and calibrated values of strength growth parameters (α and β).

Given the above discussion, it becomes evident that the magnitude of overstrength at 28 days is a function of two primary parameters—(1) the "expected" 28-day strength (which is a function of a known or expected release strength, f_{ci}, and calibrated growth parameters α and β), and (2) the choice by the design engineer of a specified 28-day strength, f'_c. This concept is shown more clearly in Figure 5-12 with the two primary parameters noted above shown in red. Notice that at the time of prestress release (0.75 days) there are two concrete strengths indicated—the specified release strength, f'_{ci}, and the measured release strength, f_{ci}. As expected, the measured value exceeds the specified value. The difference between these two values is shown on the plot (also called the difference statistic). Next, each of the two release values are extrapolated to 28 days, with the likely measured value denoted as f_c and the expected value based on the controlling specified release strength is denoted as f^*_c. Also pictured are the choices of the specified 28-day strength by the design engineer, f'_c, and slightly amplified required value to satisfy the mixture design specification, f'_{cr}.

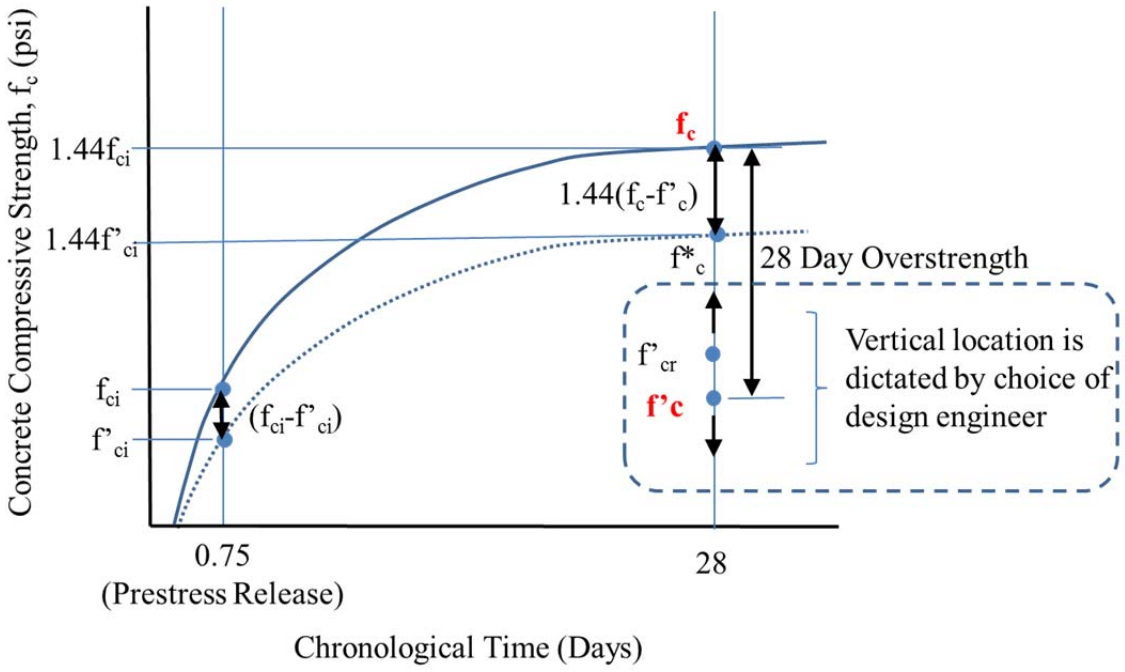

Figure 5-12: Concept of 28-Day Overstrength Derivation

The following conclusions can be drawn from the figure for the case of prestress release controlling concrete mixture proportioning (that is, $1.44\,f_{ci} \geq f'_{cr}$):

- In the case that the design engineer specifies values precisely satisfying the ratio $f'_c / f'_{ci} = 1.44$, the magnitude of the overstrength (the difference statistic) at 28 days is expected to be approximately 1.44 times the difference statistic at prestress release;
- In the case that the design engineer specifies values resulting in the ratio $f'_c / f'_{ci} \leq 1.44$, the 28-day overstrength magnitude is expected to be substantially greater than 1.44 times the difference statistic at release; and

- In the case that the design engineer specifies values resulting in the ratio $f'_c / f'_{ci} > 1.44$, the 28-day overstrength is expected to be substantially smaller than 1.44 times the difference statistic at release.

The above general summary is expanded in later sections of this dissertation, but is presented here to confirm that the magnitude of the 28-day overstrength present is not an independent parameter, but instead, is related to select parameters from the time of prestress release.

Given the above discussion, it is not surprising that the efforts of previous researchers to quantify overstrength at the age of 28 days have resulted in inconsistent conclusions. For instance, while Storm et al. (2013) found that the average ratio of measured compressive strength to the specified design strength at 28 days to be approximately 1.45, Rosa et al (2007) suggested that on average, the measured compressive strength at 28 days was 25 percent higher than the specified strength. This variability is likely due to the preference of design engineers in different regions to choose varying values of f'_c / f'_{ci}, thereby determining the degree of overstrength at 28 days.

5.4.3 Applicability of Existing Overstrength Provisions to Precast, Prestressed Industry

A final logical topic of the discussion regarding overstrength in the precast, prestressed concrete industry is to examine if the existing overstrength provisions of Section 5.3.2 are appropriate to apply to this industry. Without doubt, the concept of statistically adjusting the specified strength to some mean strength is a valuable tool presented by ACI 214-11.

However, certain difficulties arise when one considers applying this concept to the precast, prestressed industry. Two of these key difficulties are summarized below.

1. Because release strength is a serviceability computation and not a strength limit state computation, it is not strictly *required* to apply the provisions of ACI 214-11 to concrete strength at prestress release. However, as discussed in Section 5.4.1, it seems proper to maintain some level of conservatism so that the likelihood of delay of prestress transfer is minimized and thus, the provisions of ACI 214-11 are an attractive option for consideration; and
2. The standards of control presented in ACI 214-11 (i.e. s = 450 psi for "very good") are intended to describe the variability of strength testing results (and therefore also of concrete batch consistency) at a single age and do not account for the increased variability in strength testing results resulting from the varying chronological times to prestress release. Even if intentional trial batching is completed by a precast, prestressed producer, it will be difficult to capture the intrinsic variation in release timing, as this is often dictated by construction considerations, manpower availability, weather, etc.

Based on the above justification, the effectiveness of the provisions of ACI 214-11 for predicting overstrength in the precast, prestressed industry is evaluated in the remainder of this chapter. One should note that in order for this to be a feasible option, some alternative representation of the standard deviation, s, will need to be developed and recommended for use in the precast, prestressed industry.

5.5 Historical Data Set

As noted in Section 5.4, one of the most common approaches to explore the topic of overstrength in the precast, prestressed industry is to conduct a review of historical regional concrete strength testing records. During the course of this research effort, historical strength records representing nearly 5,000 precast, prestressed bridge girders were collected from 1,917 girder concrete placement events performed by four producers during the six-year period preceding 2013. While the work of Hofrichter (2014) thoroughly details the data gathering process, this dissertation section provides a brief summary of the data set as applicable to subsequent analyses.

5.5.1 Historical Strength Data Set Description

The data set compiled by Hofrichter (2014) included a large number of parameters describing both the fresh and hardened properties of girder concretes and the timing of various construction activities. The findings of Hofrichter (2014) with regards to fresh concrete properties and average timing to prestress release were previously summarized in Chapter 4 of this dissertation. For the purposes of the overstrength analyses contained in this chapter, Hofrichter's complete data set is condensed to include only those parameters relevant to concrete strength. The format of the condensed database is shown in Table 5-6, with the complete data set provided in Appendix C.

Table 5-6: Format of Condensed Raw Strength Data Set

Producer (A-D)	Specified Release Strength, f'_{ci} (psi)	Specified 28-Day Strength, f'_c (psi)	Measured Air Content (%)	Chronological Time to Prestress Release (days)	Average Measured Release Strength, f_{ci} (psi)	Average Measured 28-Day Strength, f_c (psi)
#	#	#	#	#	#	#

A logical first visualization of the raw data is a plot comparing the specified release strength, f'_{ci} to the measured release strength, f_{ci} as shown in Figure 5-13. It can be observed that the measured release strength exceeds the specified release strength in all cases as evidenced by all values being located above the line of equality. A similar comparison plot for the age of 28 days is shown in Figure 5-14.

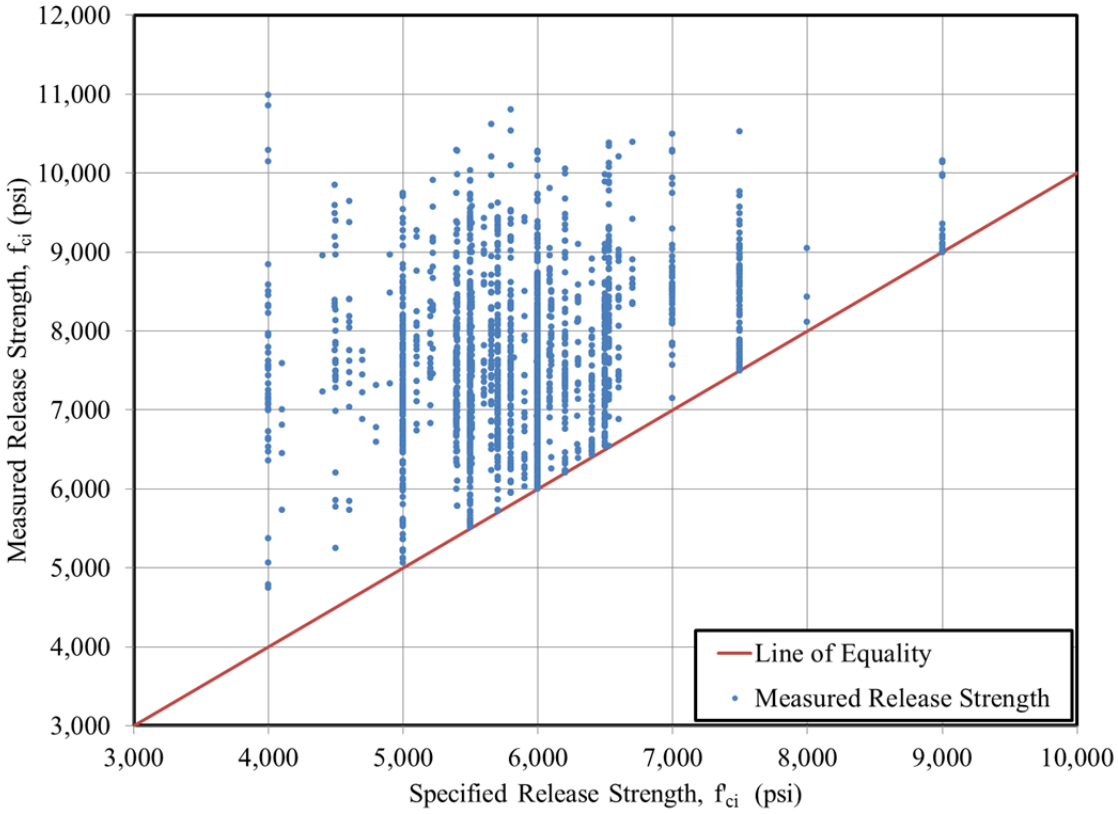

Figure 5-13: Comparison of Specified vs. Measured Release Strength for Historical Data Set

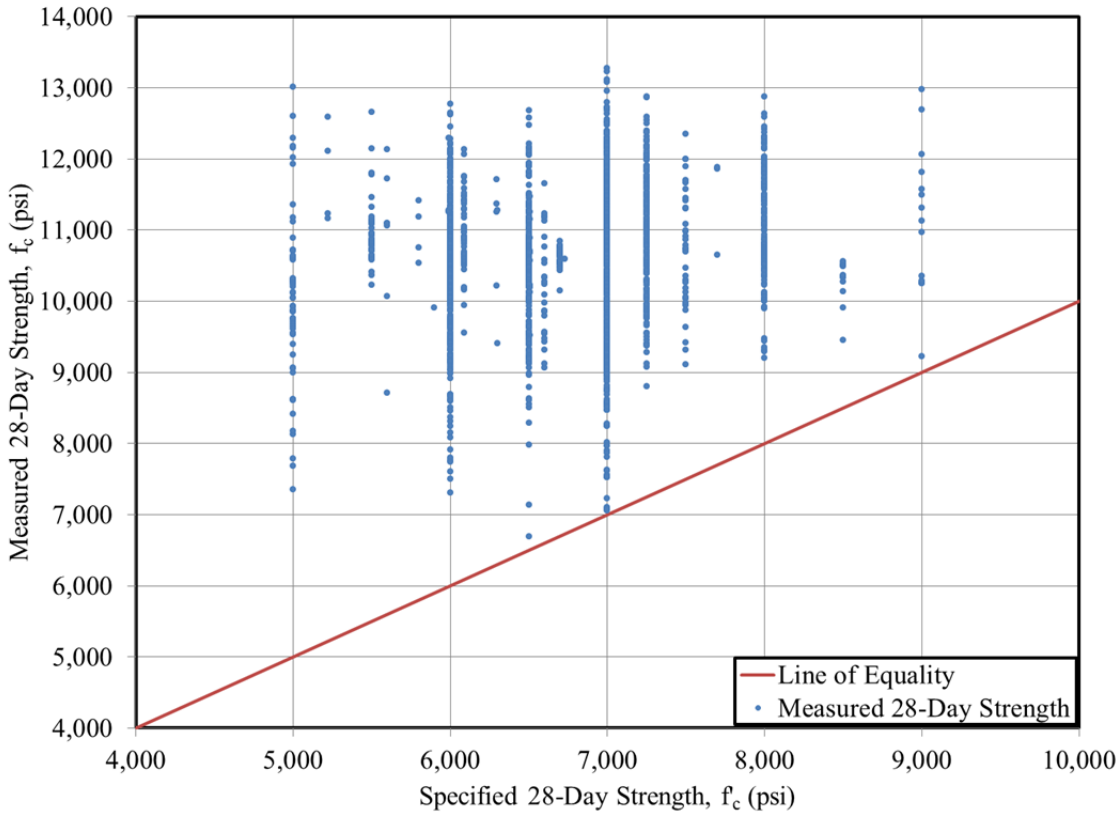

Figure 5-14: Comparison of Specified vs. Measured 28-Day Strength for Historical Data Set.

As demonstrated by the closer proximity of the data points to the line of equality in Figure 5-13 as compared to Figure 5-14, release strength requirements tend to control the selection of concrete mixture proportions in the precast, prestressed concrete industry. Figure 5-14 confirms this concept because the majority of data points fall well above the line of equality at 28 days.

Another logical visualization of the data set is to display the calculated value of overstrength in accordance with the nomenclature introduced in Section 5.2.2. Recall, overstrength at a given age is defined as the ratio of the measured strength to the specified strength and is denoted as OS_i, with the subscript denoting age. Computed

overstrength ratios for the time of release and 28 days are shown in Figures 5-15 and 5-16, respectively.

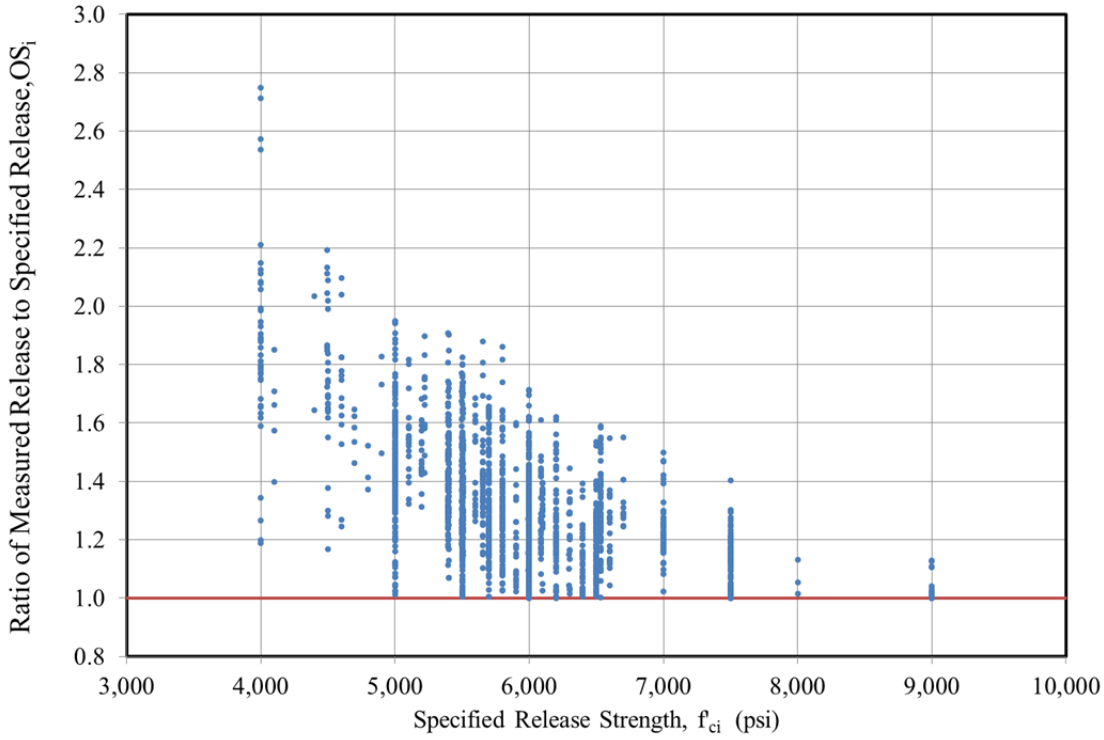

Figure 5-15: Overstrength Values at Prestress Release for the Historical Data Set

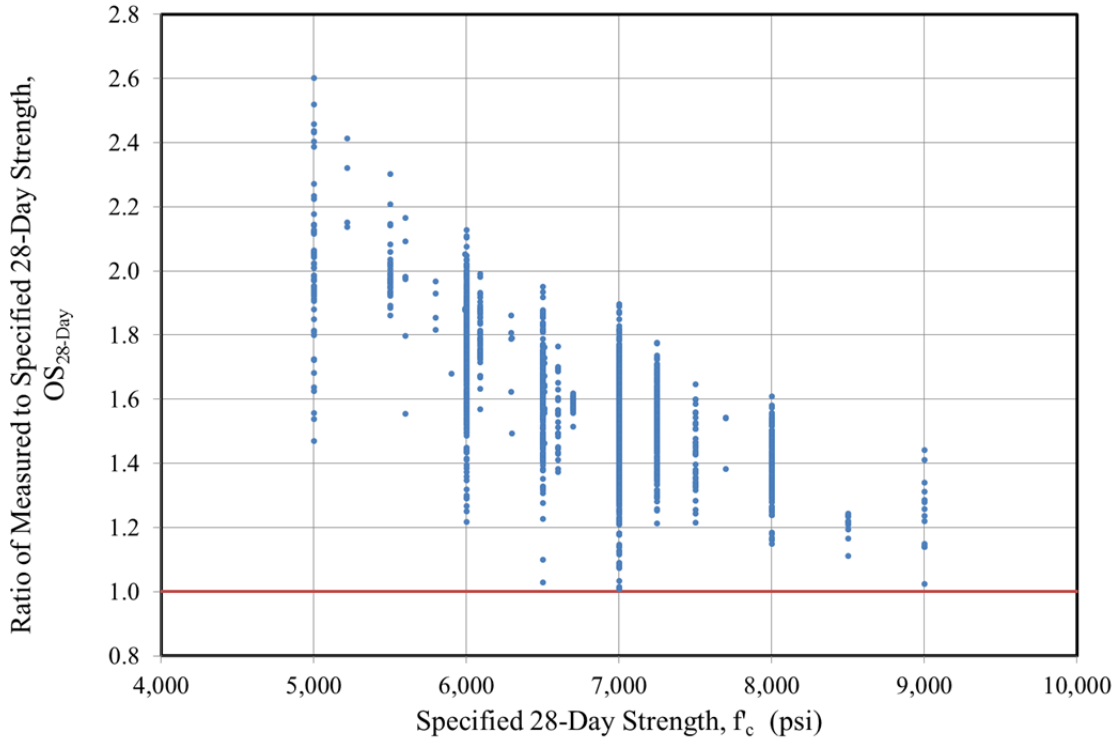

Figure 5-16: Overstrength Values at 28 Days for the Historical Data Set

As expected, all overstrength ratios exceed 1.0, meaning that the minimum strength requirements at both ages for all concrete placement events have been achieved. It is also interesting to note that the ratio of overstrength for a given age tends to decrease with increasing specified strength requirements. Further visualizations and comprehensive analyses of the condensed data sets are presented in Sections 5.6 and 5.7 of this chapter.

5.5.2 Normalizing for Air Content

In the preliminary work of Hofrichter (2014), an effort was made to adjust the measured concrete strengths of the data set in accordance with the measured air content for each concrete placement event. Using the rule of thumb discussed in Section 5.2.1 (A one percent decrease in the air content of a given mixture corresponds to approximately a five percent increase in compressive strength), Hofrichter adjusted the values of measured compressive strengths to reflect those of a uniform target air content of 4.5 percent. This

value was selected because it reflected the target air content from the ALDOT *Standard Specifications* (ALDOT 2012). In doing so, Hofrichter noted that the measured concrete strengths were generally adjusted downward because the mean air content of the full data set is 3.3 percent. The approach used by Hofrichter (2014), while successfully standardizing the air content of the data set, has the undesired consequence of artificially shifting the average air-content of the data set from 3.3 to 4.5 (and therefore, artificially shifting the mean compressive strength of the data set). The use of a target air content of 4.5 percent is undesirable in this case because it fails to account for the preference of the majority of concrete producers to target the bare minimum 2.5 percent air content by neglecting to use air-entraining admixtures (as discussed in Section 4.4.4). A more logical approach (as contained in this dissertation) is to instead adjust measured strength values to a uniform target air content of the data set mean, 3.3 percent. In doing so, the artificial offsets of the data set mean air content and mean compressive strength noted by Hofrichter are avoided. The raw data set, as adjusted to a uniform target air content of 3.3 percent, is shown in Figures 5-17 and 5-18.

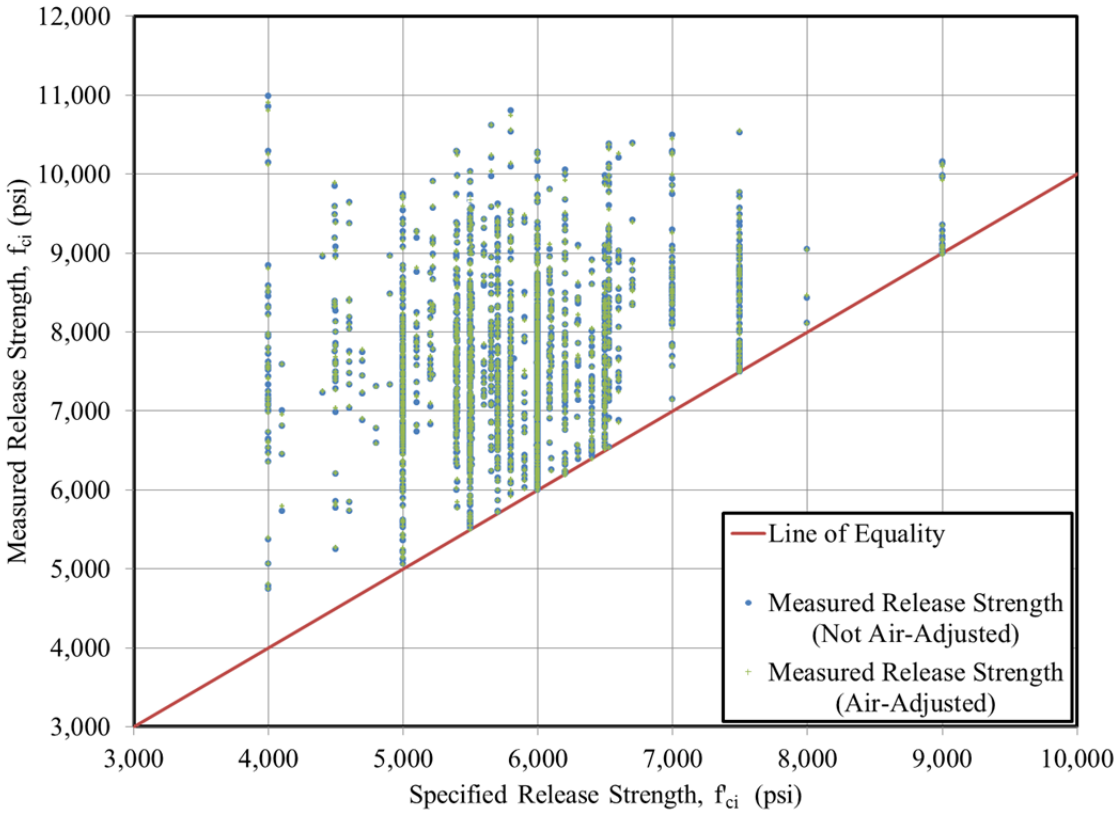

Figure 5-17: Comparison of Specified vs. Air Content Adjusted Measured Release Strength for Historical Data Set.

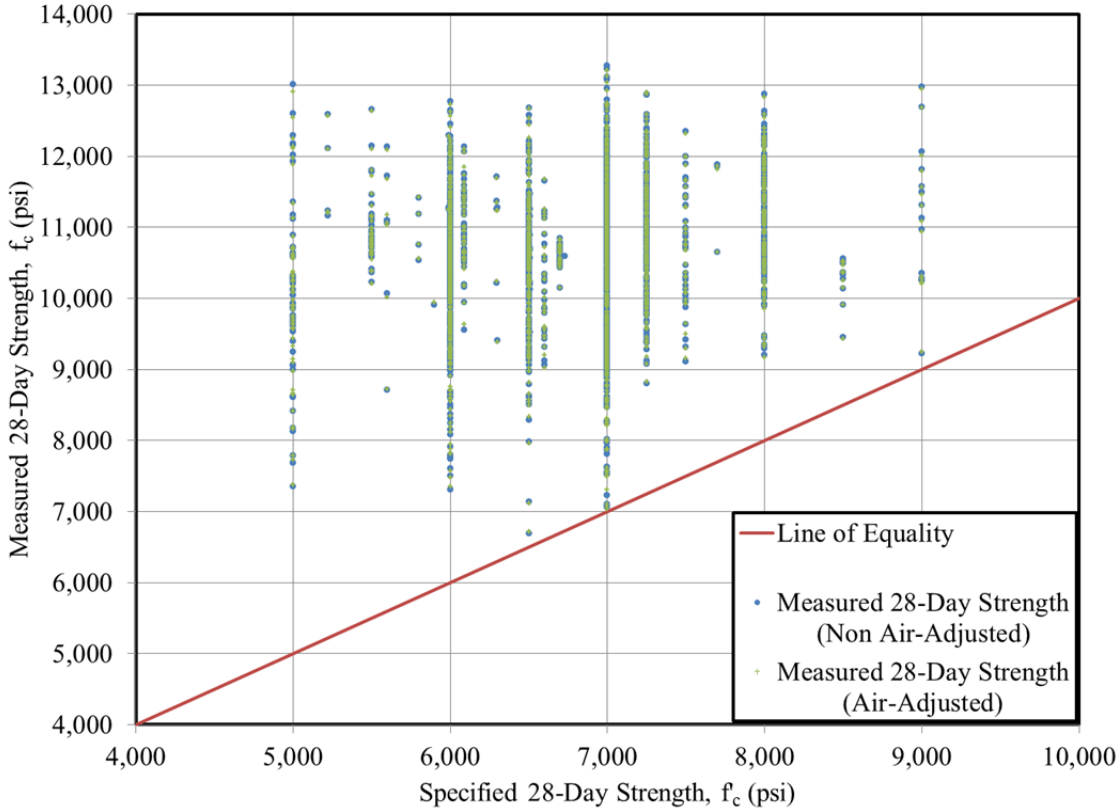

Figure 5-18: Comparison of Specified vs. Air Content Adjusted Measured 28-Day Strength for Historical Data Set.

Inclusion of the normalization for air content, performed in the manner discussed above, results in insignificant changes to the data set. The overall mean measured strengths of the nearly 1,900 data points remains unchanged and no significant changes in the dispersion of the data set (as evidenced by standard deviation) are evident[5]. Accordingly, the data set used in the remainder of the analyses in this chapter is the raw data set without normalization for air content. This decision has the added benefit that the recommendations derived from the analyses of this data set intrinsically capture the

[5] For the uncorrected data set, mean concrete compressive strengths of 7,660 psi and 10,600 psi and standard deviations of 980 psi and 986 were documented for release and 28 days, respectively. For air content corrected to 4.5 percent (Hofrichter's method), means of 7,200 psi and 9,950 psi and standard deviations of 910 psi and 910 were documented for release and 28 days, respectively. For air content corrected to 3.3 percent, means of 7,660 psi and 10,590 psi and standard deviations of 976 psi and 977 were documented for release and 28 days, respectively.

anticipated small variations in air content likely to be observed in regional precast, prestressed plants.

5.6 Predicting Expected Concrete Compressive Strength at Prestress Release

The primary goal of this section is to recommend a relationship that may be used at the time of girder design to more accurately predict the expected concrete compressive strength at prestress release, f_{ci}^{*}. This dissertation section begins by summarizing the analytical approach and criteria used to evaluate the goodness of fit for the various explored prediction models. Next, a logical mechanistic concept is hypothesized prior to its inclusion in subsequent prediction models. Finally, five major groupings of prediction models are explored and evaluated for their accuracy. Of these five groups of models, the first is purely empirical in nature, while the remaining four incorporate varying degrees of mechanistic concepts and existing design code provisions.

5.6.1 Analytical Approach

The general format of the analysis for predicting release strength as contained in this dissertation is that various candidate prediction models are developed and evaluated against the measured concrete strength results of the condensed data set. The analytical approach is presented in an organizational chart as detailed in Figure 5-19.

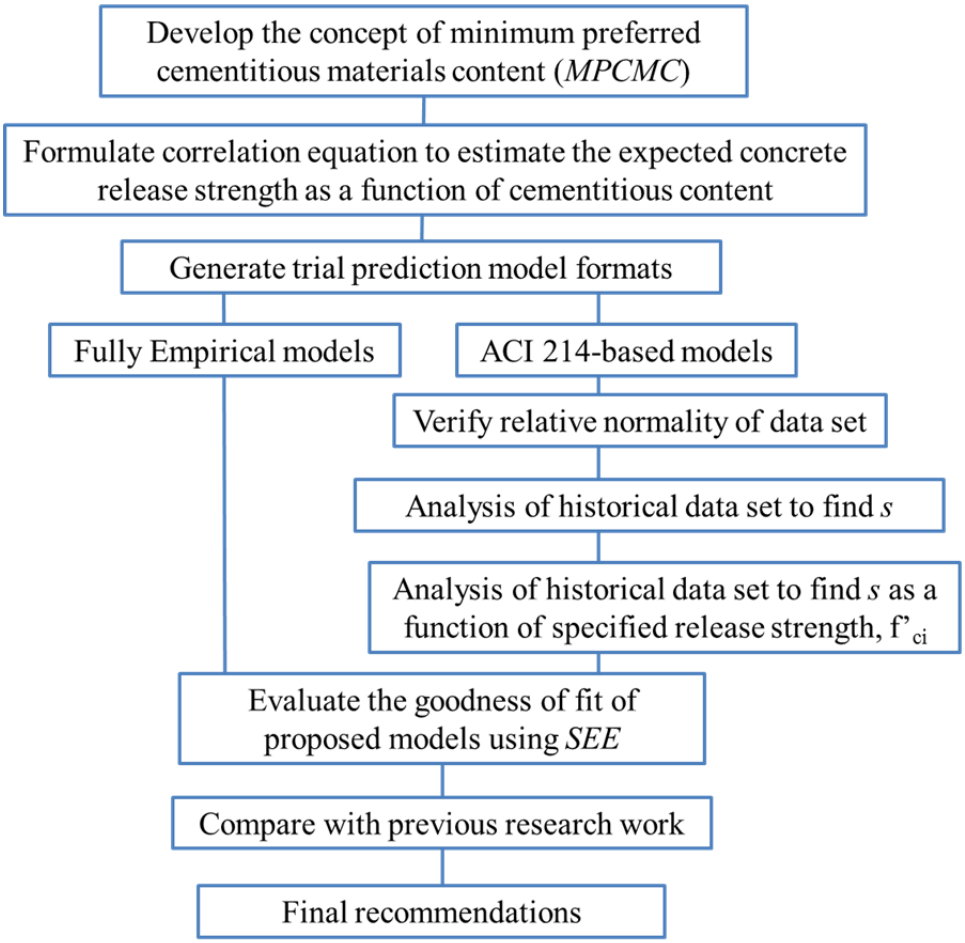

Figure 5-19: Analytical Approach of Release Strength Prediction Equation Development

First, the concept of a minimum preferred cementitious materials content (MPCMC) is developed and a correlated prediction equation is formulated. Next, the forms of various fully empirical models and semi-empirical models (those including the MPCMC concept) are selected by a combination of engineering judgment and the desire to maintain simplicity in recommended relationships. Next, using a GRG nonlinear solver, empirical and semi-empirical models are calibrated against the condensed data set by minimizing the standard error of the estimate, the *SEE*, denoted as follows (Vardeman and Jobe 2001):

$$SEE = \sqrt{\frac{\sum\left(f_c^* - f_c\right)^2}{N}} \tag{5-15}$$

where

f_c^* = the expected concrete compressive strength as predicted by a given model at a given age;

f_c = the measured concrete compressive strength at the corresponding age; and

N = the total number of data points the prediction model is being evaluated for.

For the code-based prediction models, the overstrength concepts of ACI 214-R11 (ACI Committee 214 2011) are used in conjunction with various sub-analyses aimed at quantifying typical measures of variability (in the form of a standard deviation) within the precast, prestressed industry. Finally, by comparing trial prediction models to each other and to previous work by others, a final relationship is recommended for use at the time of girder design to more accurately predict the expected concrete compressive strength at prestress release, f_{ci}^*

5.6.2 Concept of Minimum Preferred Cementitious Materials Content (MPMPC)

The PCI Bridge Design Manual (PCI 2011) notes that for concrete compressive strengths between 4.0 and 10.0 ksi, the total cementitious materials content typically varies between 600 and 1,000 pcy. Early in this research effort, it became evident that there existed a preference for precast, prestressed producers to use concrete mixtures with a high total cementitious materials content, often in excess of the content required to meet the governing specified strength for a given volume of mixing water. In discussions with girder producers, the research team learned that producers preferred targeting some minimum paste content in order to ensure a "creamy" mixture with sufficient workability

and improved surface finish characteristics, as first documented by Hofrichter (2014). By maximizing workability and surface finish quality, labor costs associated with concrete placement and surface finishing are markedly reduced. The term, *minimum preferred cementitious materials content* (MPCMC) refers to the minimum content of cementitious materials that a producer tends to use, even if the strength provided by this cementitious content and the selected mixing water volume far exceeds the required specified strength. Although producers also rely on relatively high dosages of chemical admixtures to achieve sufficient workability, the preference to use a minimum cementitious materials content helps ensures that the paste volume is such that surface finish is improved (e.g. the potential for honeycombing is reduced) and the chemical admixtures are most effective in achieving the desired workability.

For the duration of the experimental portion of this project, the concept of a minimum preferred cementitious content remained a somewhat troublesome metric. While the MPCMC itself could be readily identified by either 1) asking a regional concrete producer or 2) conducting a statistical averaging of an inventory of approved mixture designs, there did not exist a reliable method to correlate the MPCMC to a corresponding minimum expected concrete release strength, hereafter denoted $f^*_{c,\min}$ due to potential variations in the *w/cm* of different mixtures. Recognizing the need for this correlation, a conservative prediction equation was developed based on various ACI mixture proportioning guidance and the strength growth provisions of Hofrichter (2014).

Beginning with the ACI 211.4R-08: *Guide for Selecting Proportions of High-Strength Concrete Using Portland Cement and Other Cementitious Materials* (ACI Commitee 211 2008), the expected mean concrete compressive strength at 28 days, f^*_c,

can be predicted for typical plain cement mixtures with specific *w/cm* as shown in Table 5-7.

Table 5-7: Approximate Correlation between *w/cm*, Cementitious Materials Content, and Expected 28-Day Strength for Typical Concrete Mixtures (Adapted from ACI 211.4R-08 Table 6.5)

w/cm	Approximate cementitious materials content (pcy) for 285 pcy mixing water volume	Expected 28-day mean concrete compressive strength, f_c^* (psi)
0.45	633	7,000
0.40	713	8,000
0.35	814	9,000
0.31	919	10,000
0.27	1,056	11,000
0.25	1,140	12,000

Note: Values are for maximum-size coarse aggregate of ¾ *in.*

Using a first estimate of the mixing water volume of 285 pcy (in accordance with ACI 211.4R-08 for ¾ *in.* maximum-size aggregate [No. 67]), the approximate cementitious content can be computed as shown in the second column of Table 5-7. Next, the recommendations of Hofrichter (2014) may be used to relate the 28-day strength to the strength at the time of release using Equation 5-7 and corresponding calibrated coefficients. A finalized correlation between minimum preferred cementitious materials content (MPCMC) and an estimate of the minimum expected concrete release strength (also called the minimum mean concrete strength), $f_{ci,\min}^*$, are shown in Figure 5-20 with tabulated values superimposed at the lower right.

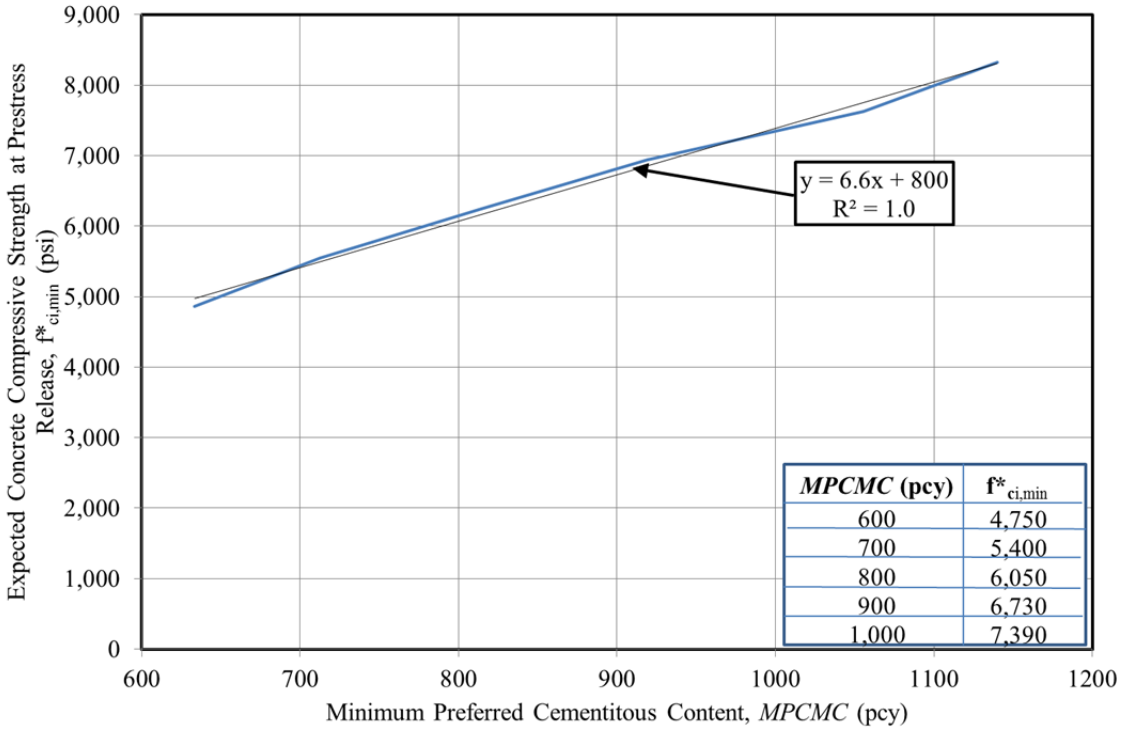

Figure 5-20: Correlation between MPCMC and Expected Concrete Compressive Strength at Prestress Release

For the state of Alabama, the average cementitious content for the sample approved mixtures in Section 4.4.3 is 881 pcy. Using the expression of Figure 5-20 that includes the implicit assumption of 285 pcy mixing water, this corresponds to an minimum expected concrete compressive strength at prestress release, $f^*_{ci,\min}$, of approximately 6,600 psi.

The concept of a minimum preferred cementitious content, MPCMC, seems appropriate for the precast, prestressed industry and, therefore is incorporated into various trial models evaluated in subsequent sections of this dissertation. In some cases, the value of $f^*_{ci,\min}$ is determined by linear regression of experimental data (in the case of semi-empirical models), whereas in other trial cases, the ACI 211-based relationship of Figure 5-20 is used to systematically estimate the value of $f^*_{ci,\min}$.

5.6.3 Simple Fully Empirical Models

The fit of purely empirical models to the condensed historical data set is completed primarily to allow valid comparisons to the work of previous researchers. Three primary prediction model formats were employed as shown below in Table 5-8.

Table 5-8: Simple Fully Empirical Model Description

Fully Empirical Model Designation	Format of Model (psi)	Description of Model	Calibration Constants
FE-1	$f_{ci}^{*} = a \cdot f'_{ci}$	Factor	a = 1.30
FE-2	$f_{ci}^{*} = b + f'_{ci}$	Offset	b = 1,840 psi
FE-3	$f_{ci}^{*} = a \cdot f'_{ci} + b$	Factor and Offset	a = 0.34 b = 5,662 psi

The format of FE-1 is deliberately similar to that used by French and O'Neil (2012), Storm et al. (2013), Rosa et al. (2007), and Nervig (2013). Each of these three models was calibrated by minimizing the *SEE* using a GRG nonlinear solver. The calibrated models for FE-1 through FE-3 are plotted in Figure 5-21, accompanied by the condensed data set.

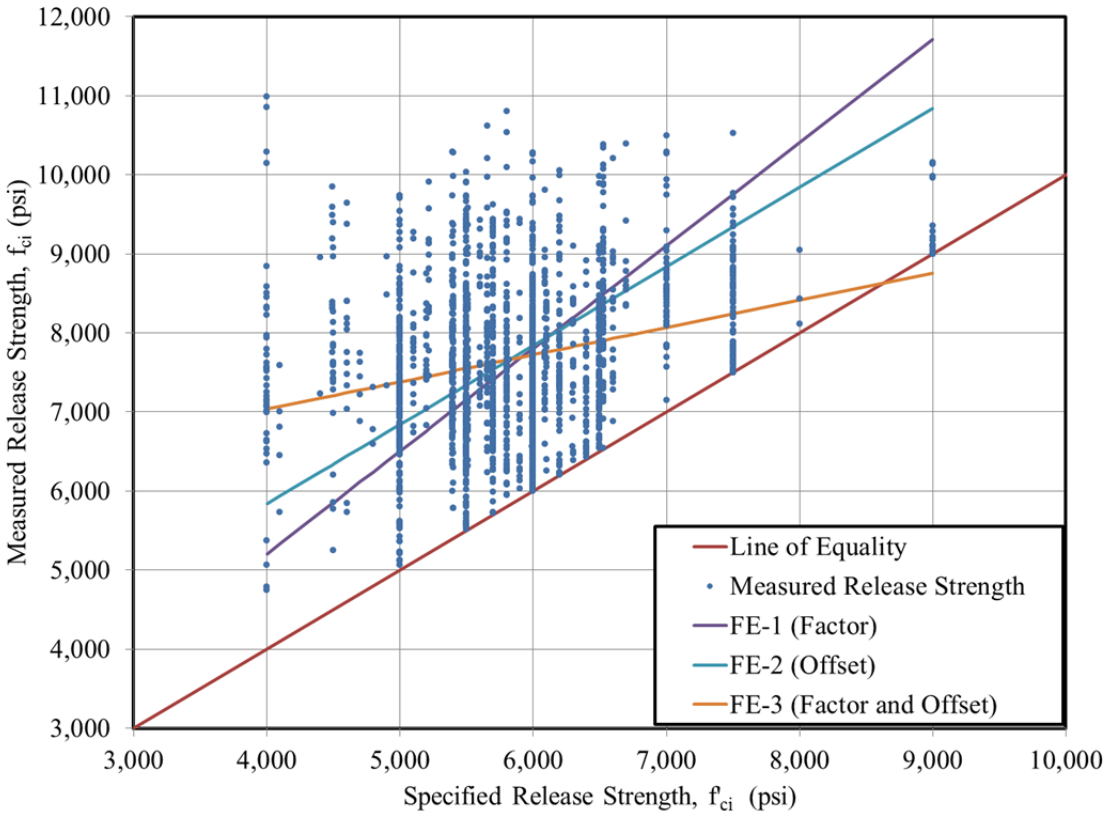

Figure 5-21: Calibrated Simple Fully Empirical Release Strength Prediction Models

The FE-1 and FE-2 model appear somewhat similar, although the FE-2 model tends to predict increased overstrength for higher specified release strengths. The fit of FE-3 is conceptually not desirable as it predicts insufficient strength for specified release strengths exceeding approximately 8,500 psi. For this reason, FE-3 is omitted from future comparisons between models. The single factor coefficient of 1.30 of model FE-1 generally agrees with the range suggested by previous researchers of 1.15–1.40. Evaluation of the relative goodness-of-fit of each model to the historical data set is withheld until after development of all considered models in the following sections.

5.6.4 Piecewise Fully Empirical Models

The piecewise fully empirical fits were similar to the fully empirical simple models described above, except they also included the hypothesized concept of a minimum

concrete strength fit to the historical data set. In order to completely define a model, the calibration of three constants was required as shown in Table 5-9. A GRG nonlinear solver was again used to calibrate the three constants against the historical data set. In this case, the algorithm minimized the error of the estimate by systematically varying combinations of the three variables until a minimum *SEE* value was obtained.

Table 5-9: Piecewise Fully Empirical Model Description

Fully Empirical Model Designation	Format of Model	Description of Model	Calibration Constants
FE-4	$f_{ci}^{*} = c$ when $f_{ci} \le d$ $f_{ci}^{*} = b + f'_{ci}$ otherwise	Piecewise Constant and Offset	c = 7,500 psi d = 6,100 psi b = 1,400 psi
FE-5	$f_{ci}^{*} = c$ when $f_{ci} \le d$ $f_{ci}^{*} = a \cdot f'_{ci}$ otherwise	Piecewise Constant and Factor	c = 7,500 psi d = 6,300 psi a = 1.18

The results of the calibration yielded piecewise continuous functions as plotted in Figure 5-22. Models FE-4 and FE-5 tended to predict similar results with an approximate minimum mean release strength of 7,500 psi (in contrast to the 6,600 psi estimate provided by the expression of Section 5.6.2).

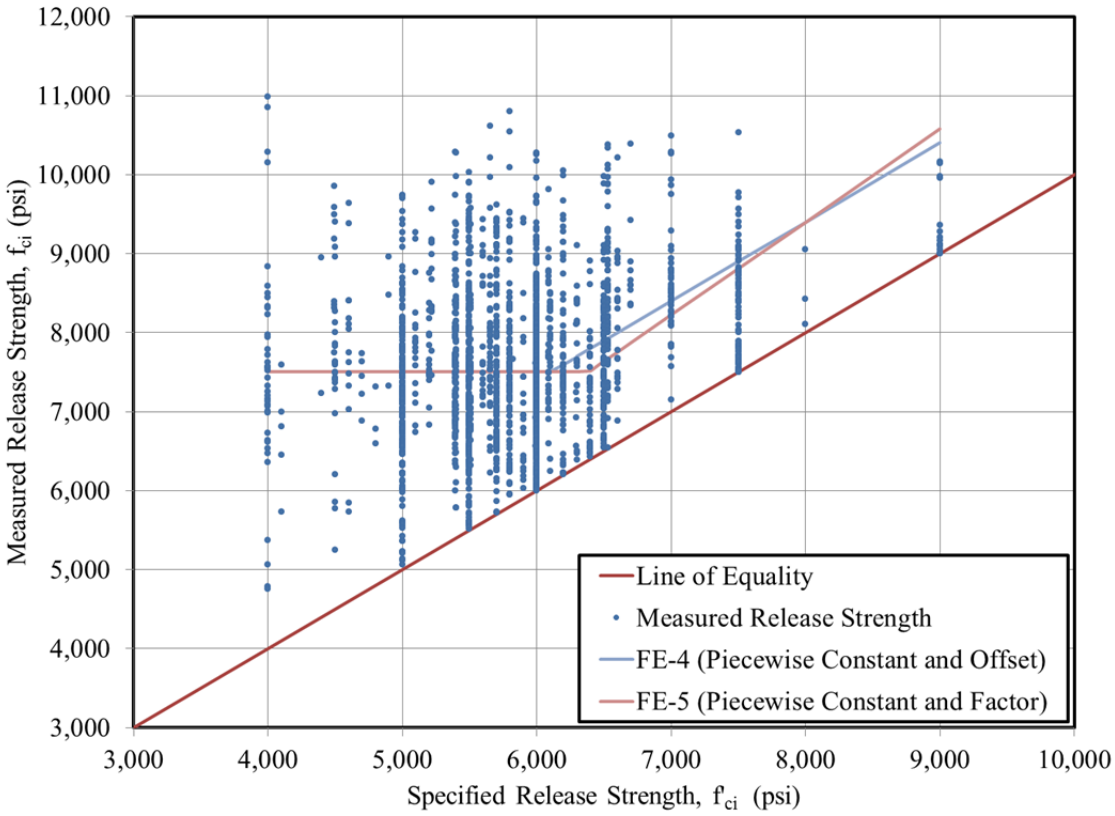

Figure 5-22: Calibrated Piecewise Fully Empirical Release Strength Prediction Models

5.6.5 Semi-Empirical Piecewise Data Fit with MPCMC Concept

In contrast to the fully empirical model development above, the use of a semi-empirical function to fit the data set was also explored. These semi-empirical models were similar to those of Section 5.6.4 in the linear empirical fit for higher strengths, but used the MPCMC prediction equation detailed in Section 5.6.2 to establish the minimum average strength, $f^{*}_{ci,\min}$. The form of the two semi-empirical models, SE-1 and SE-2, and calibration constants are shown in Table 5-10 and plotted in Figure 5-23.

Table 5-10: Semi-Empirical Piecewise Model Description

Semi-Empirical Model Designation	Format of Model (psi)	Description of Model	Calibration Constants
SE-1	$\max(b + f'_{ci}, 6.6(MPCMC) + 800)$	Piecewise Constant and Offset	b = 1,750 psi *MPCMC* = 881 pcy (Alabama)
SE-2	$\max(a \cdot f'_{ci}, 6.6(MPCMC) + 800)$	Piecewise Constant and Factor	a = 1.27 *MPCMC* = 881 pcy (Alabama)

By forcing the SE model fits through a calculated *MPCMC* value (that is lower than the fully empirical mean minimum average), the tendency of the solver is to minimize the portion of the fit described by the horizontal line as shown in Figure 5-23.

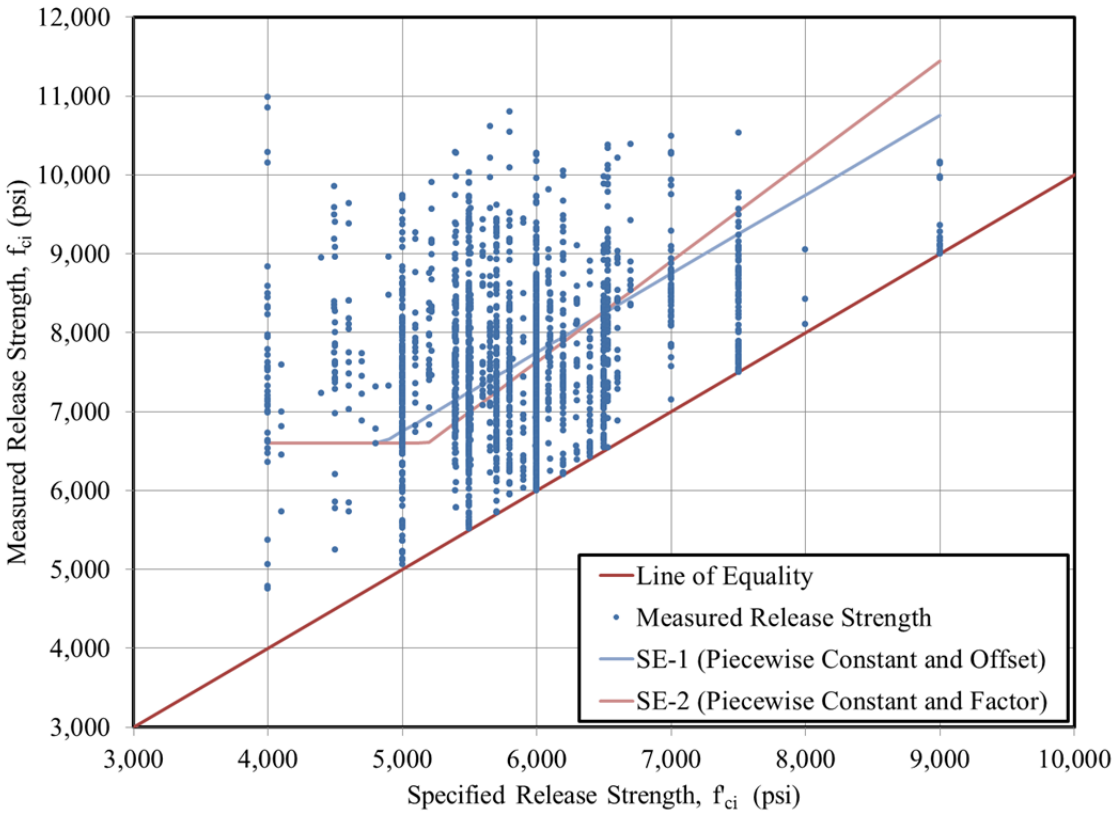

Figure 5-23: Calibrated Piecewise Semi-Empirical Release Strength Prediction Models

Overall, both models SE-1 and SE-2 yield similar results in the considered strength range, with the SE-2 model tending to predict higher strengths than the SE-1 model for specified concrete strength greater than approximately 6,500 psi.

5.6.6 ACI 214-Based Model (Constant *s)*

A more logical and universally applicable prediction model was desired than the fully empirical and semi-empirical fits previously developed. To achieve this goal, a prediction method based on the overstrength provisions of ACI 301 and ACI 224-R11 (detailed in Section 5.3.2) was explored. For the purposes of this discussion, ACI 301 overstrength provisions with historical data available are reproduced here in Table 5-11.

Table 5-11: Required Average Compressive Strength, f'$_{cr}$, with Historical Data (Adapted from ACI 301-10)

f'_c (psi)	f'_{cr} (psi)
	Use the larger of:
5,000 or less	$f'_{cr} = f'_c + 1.34s$
	$f'_{cr} = f'_c + 2.33s - 500$
Over 5,000	$f'_{cr} = f'_c + 1.34s$
	$f'_{cr} = 0.9f'_c + 2.33s$

Assuming that the target strength value, f'_{cr} is also the most likely concrete strength to expect, f_c^*, the use of the above provisions can be adapted to predict the expected strength as a function of specified strength. However, the issue remains of selecting or assuming an appropriate value of the standard deviation, *s*, for the precast, prestressed industry.

Recall, within the context of the ACI 301 and ACI 214 overstrength provisions, the standard deviation, *s*, is intended to be a function of the standard of control of a given concrete producer. A better standard of control by a producer corresponds to a narrower distribution of strength testing results about some target level, and, therefore, a smaller

standard deviation, *s*. In the context of mixture proportioning, *s* is typically determined by considering a sample of at least 30 consecutive historical strength testing results all targeting a single concrete strength level. For the purposes of this dissertation, it is advantageous to compute *s* using the large historical database generated as part of this research effort. For this purpose, a histogram was generated showing the frequency of occurrence for various ranges of measured release strengths, f_{ci}, in the historic data set as shown in Figure 5-24. The frequency distribution shown is relatively normal with a mean of 7,622 psi and a standard deviation of 967 psi.

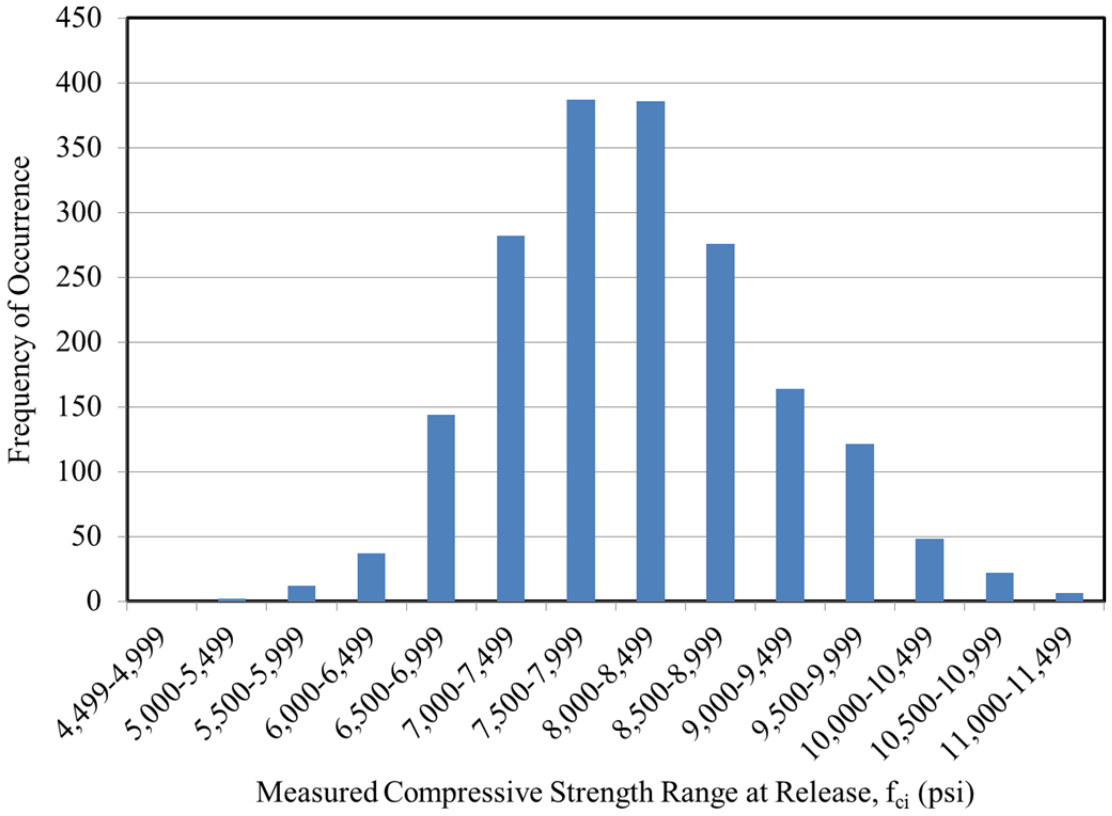

Figure 5-24: Frequency Histogram of Measured Release Strengths in Historical Data Set

While the standard deviation computed from the distribution pictured in Figure 5-24 does describe the general variability evidenced in *measured* concrete release strengths typical in Alabama for the previous 5 years, it is important to note that the historical strength

testing results used to generate this distribution are not all for a single specified strength level. As such, it is difficult to differentiate between the portion of the variability attributed to a given typical producer's standard of control and the portion of the variability due to differing target strengths of the historical data set. Accordingly, it is not appropriate to use the standard deviation representing the distribution of Figure 5-24 in an ACI 214-based models and instead, an alternate metric is required.

In order to determine an appropriate standard deviation, *s*, for use in an ACI 214-based model, the concept of the difference statistic, d_{stat}, is instead applied to the historical data set and a standard deviation of the difference statistic distribution computed accordingly. Recall, the difference statistic is a measure of the difference between the measured concrete strength and the strength level specified by the design engineer at a given time. Implicit to the use of this approach is the assumption that a single typical standard deviation, *s*, is applicable regardless of varying concrete strength levels. The distribution of the difference statistic at prestress release for the combined historical data set representing four independent producers is shown in Figure 5-25.

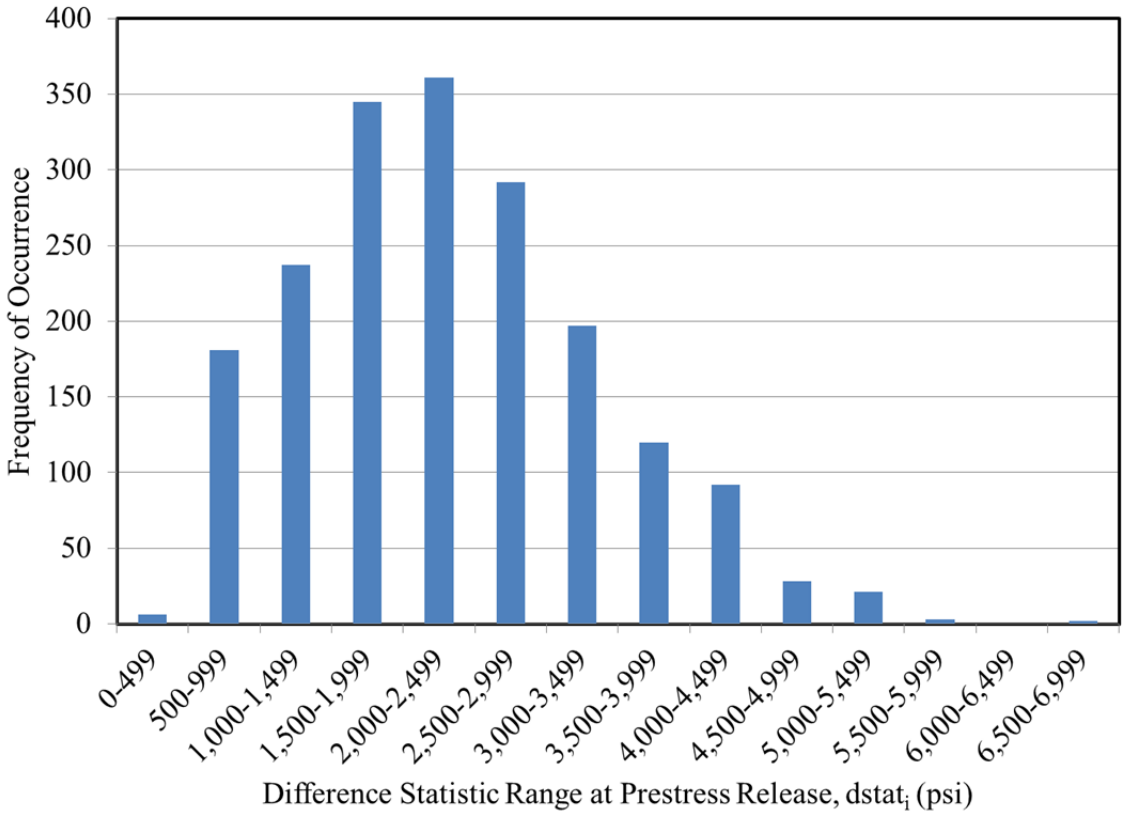

Figure 5-25: Frequency Histogram of Difference Statistic at Prestress Release in Historical Data Set

The standard deviation of the distribution of the difference statistic shown in Figure 5-25 is 1,063 psi. Relying on the concept of the preservation of standard deviation (as detailed in Section 5.3.1), it is evident that the standard deviation of 1,063 psi is a more appropriate metric to be used in conjunction with the ACI overstrength provisions than the previously discussed standard deviation of 967 psi.

To further validate and generalize the results of this section, it is desirable to examine the standard deviations of the difference statistic distributions independently for each of the four producers included in this research effort. If similar results are obtained independently from each plant, it may be possible to suggest a typical value of *s* appropriate for use by the precast, prestressed industry. The standard deviations of the difference statistic distribution for each plant are shown in Table 5-12.

Table 5-12: Standard Deviation of the Difference Statistic Distribution by Producer

Producer	Standard Deviation of the Difference Statistic Distribution, *s* (psi)		F-Test for Equal Variances Between Ages (α =0.05)	Curing Method
	Prestress Release	28 Days		
A	1,003	992	0.68 (True)	Steam
B	955	1,045	0.06 (True)	Steam
C	887	1,019	0.13 (True)	Steam
D	1,258	1,268	0.90 (True)	Moist
Full Data Set	1,063	1,132		

As shown, the standard deviations of the difference statistics appear quite similar for each of the four producers at the time of prestress release and at 28 days. Using an F-test to test for equivalent variances (α =0.05), it is shown that the distribution of the difference statistic for a given plant is not substantially different regardless of the age of consideration (as evidenced by F-test results greater than α =0.05). Next, a series of F-tests are used to evaluate the similarity of the variances among the four plants, with results shown in Table 5-13.

Table 5-13: Results of Statistical Analysis of Variances of the Difference Statistic among Plants

Combination	F-Test for Equal Variances At Prestress Release (α =0.05)	F-Test for Equal Variances At 28 Days (α =0.05)
A+B	0.23 (True)	0.18 (True)
A+C	0.09 (True)	0.61 (True)
A+D	<0.01 (False)	<0.01 (False)
B+C	0.35 (True)	0.76 (True)
B+D	<0.01 (False)	<0.01 (False)
C+D	<0.01 (False)	0.01 (False)

As shown, the variance of the difference statistic appears to be significantly different for Plant D, but similar for plants A, B, and C. A possible reason for this difference is that Plant D (which has since ceased operation) was the only plant included in the study without steam-curing capabilities. If the standard deviation of the difference statistic is

computed for Plants A, B, and C only, values of s = 1,039 psi for prestress release and s = 1,126 psi for 28 days are obtained.

In accordance with the above analysis, the standard deviation value, s, used in the preliminary development of the ACI 214-based model (constant s) is rounded to the value of 1,050 psi. While this value does greatly exceed the typical range of standards of quality control recommended by ACI 214-R11 (between 400 and 700 psi) for conventional concrete work, it is not entirely unexpected based on the previous discussion of the unique causes of variability of concrete strength at the time of prestress transfer in the precast, prestressed concrete industry (Section 5.4.1). Substituting the value of s = 1,050 psi into the equations of Table 5-11 and recognizing the controlling equation for each strength interval, the preliminary ACI 214-based model equations of Table 5-14 are derived and plotted in Figure 5-26.

Table 5-14: Preliminary ACI 214-Based Model (Constant s = 1,050 psi)

f'_{ci} (psi)	f^*_{ci} (psi)
5,000 or less	$f^*_{ci} = f'_{ci} + 1{,}950$
Over 5,000	$f^*_{ci} = 0.9 f'_{ci} + 2{,}450$

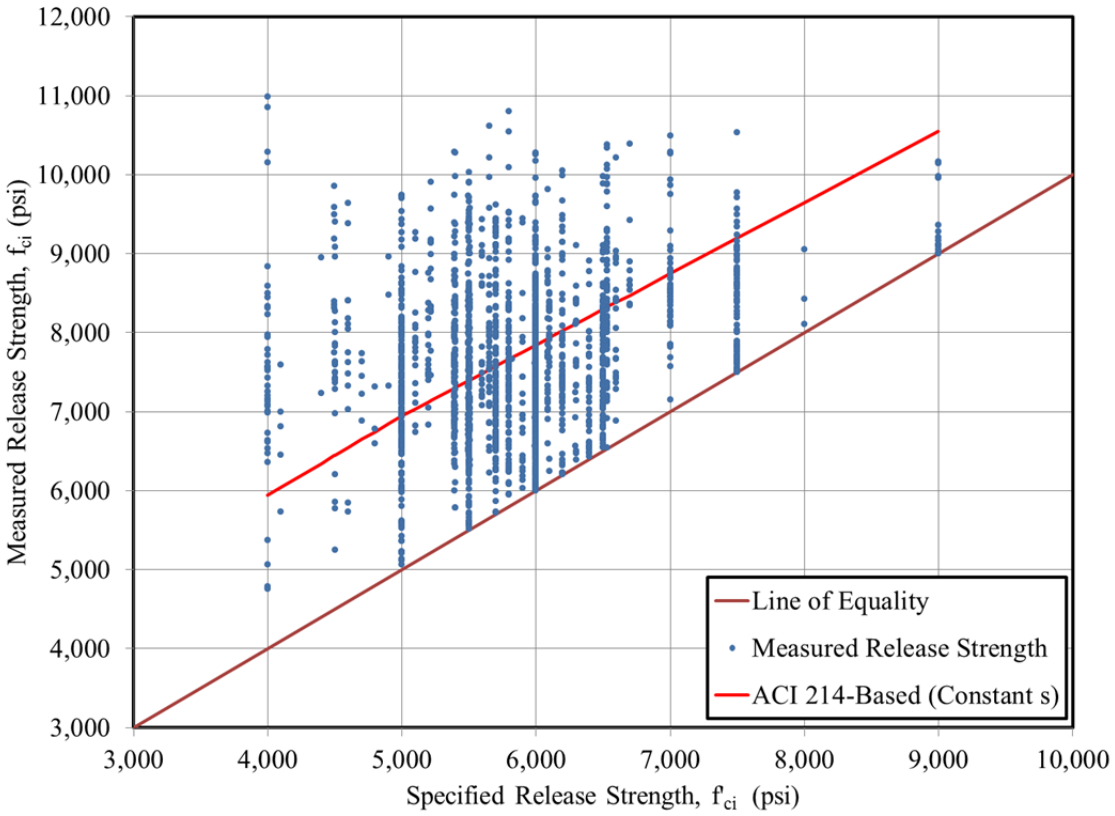

Figure 5-26: Preliminary ACI 214-Based Prediction Model (Constant *s* = 1,050 psi)

For an input value of f'_{ci} = 5,000 psi, both equations from Table 5-13 yield f^*_{ci} = 6,950 psi as shown in Figure 5-26.

5.6.7 ACI 214-Based Model (Constant *s* and MPCMC Concept)

In an attempt to improve the accuracy of the previous prediction model for lower specified concrete strengths, the MPCMC concept was incorporated into the previous model resulting in an ACI 214-based model with constant *s* and the MPCMC concept. The MPCMC prediction equation of Section 5.6.2 was used to predict the minimum mean concrete strength, which was then extended to the point of intersection with the ACI 214-Based Model (Constant *s*) as shown in Figure 5-27.

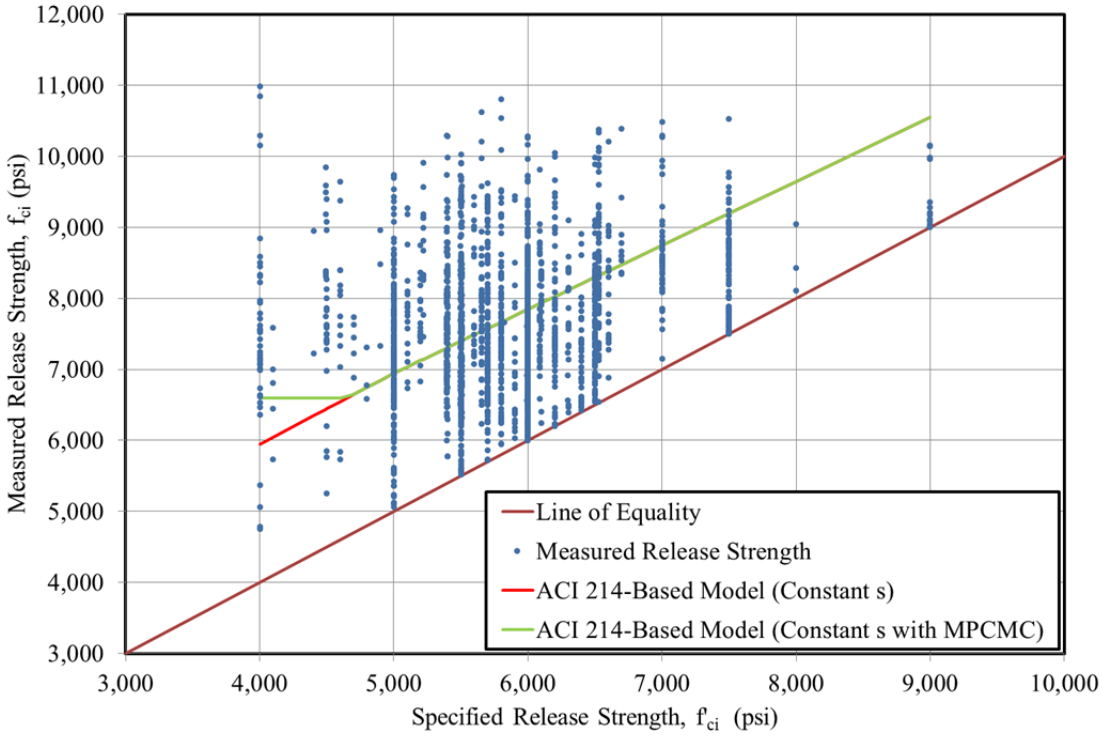

Figure 5-27: ACI 214-Based Prediction Model with MPCMC (Constant *s* = 1,050 psi)

5.6.8 ACI 214-Based Model (Variable *s* and MPCMC Concept)

In the previous ACI 214-based model, the implicit assumption was included that a single standard deviation representative of a typical producer standard of concrete control was appropriate for use at all specified strength levels. In the final model developed in this section, this assumption is further explored by allowing the standard deviation, *s*, to vary for different ranges of specified release strengths, f'_{ci}. The d_{stat} is still used in this analysis, but on a more limited level than in previous analyses. Previously, the d_{stat} was used to normalize the difference between specified and actual strength into a single distribution representing the full range of specified strengths. In this analysis, the difference statistic is used on individual subsets of historical data corresponding to a range of specified strengths within 500 psi of each other.

For this analysis, the historical strength data was divided by specified release strength, f'_{ci}, into eight data subsets each representing a range of specified release strengths of 500 psi. The difference statistic was then computed for each data point within each subset at the time of prestress release and at 28 days. For each subset, statistical descriptive parameters including means and standard deviations were computed as shown in Table 5-15.

Table 5-15: Analysis of Standard Deviation by Specified Release Strength Subsets

		Prestress Release		28 Days		F-Test for Equal Variances at both ages (α =0.05)	Pooled Standard Deviation (psi)
f'_c Range (psi)	n	Mean of the Difference Statistic Distribution (psi)	Standard Deviation of Difference Statistic Distribution (psi)	Mean of the Difference Statistic Distribution (psi)	Standard Deviation of Difference Statistic Distribution (psi)		
4,000-4,499	55	3,585	1,312	5,050	1,452	0.23 (True)	1,384
4,500-4,999	49	2,984	953	4,555	1,123	0.13 (True)	1,042
5,000-5,499	402	2,313	920	4,504	915	0.45 (True)	918
5,500-5,999	509	1,888	1,014	3,840	1,047	0.23 (True)	1,031
6,000-6,499	553	1,482	856	3,514	1,077	<0.01 (False)	972
6,500-6,999	179	1,522	887	3,772	884	0.48 (True)	886
7,000-7,499	43	1,643	723	3,365	679	0.34 (True)	702
7,500-7,999	79	869	667	2,795	695	0.36 (True)	681

It is interesting to note that there appears to be a decreasing mean value of the difference statistic distribution for increasing specified strengths at both prestress release and at 28 days. Furthermore, F-tests (α=0.05) confirm that with the exception of one subset, the subset variances at prestress release and at 28 days are not substantially different. Accordingly, it is appropriate to compute a pooled standard deviation, a single parameter representing the distribution of the difference statistic for a given subset. Much of the data from Table 5-15 is shown graphically in Figure 5-28.

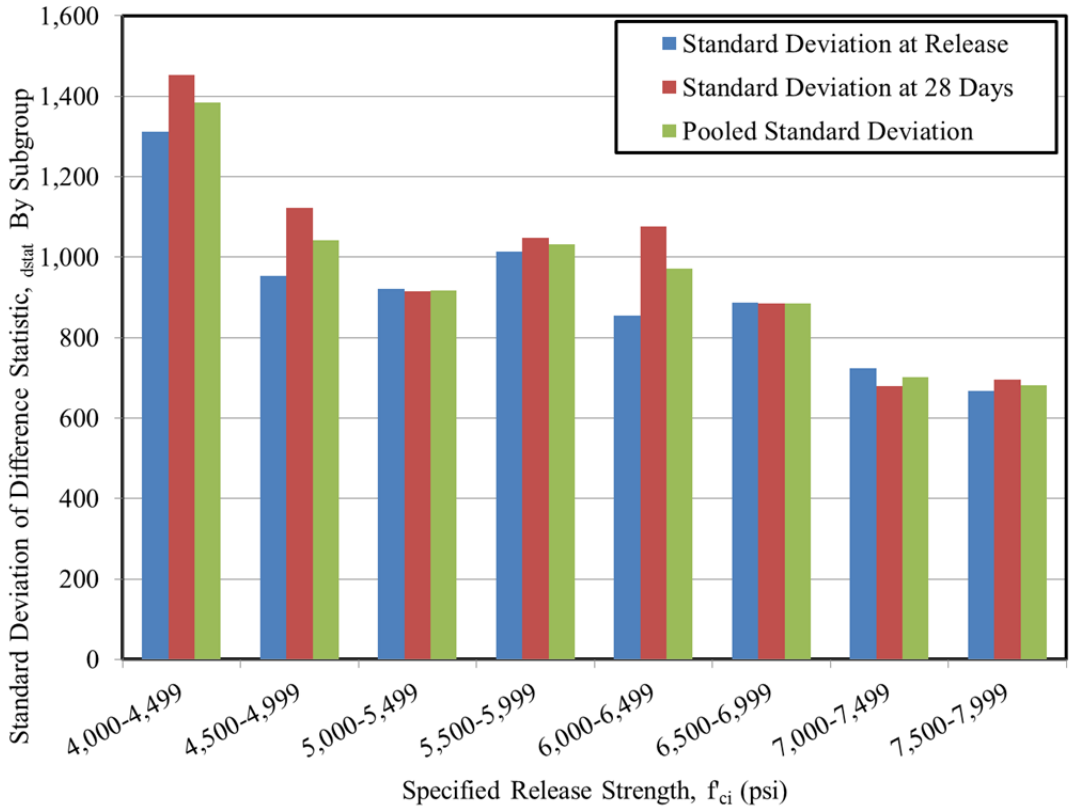

Figure 5-28: Standard Deviation of Difference Statistic by Subgroup

As shown in Figure 5-29, the pooled standard deviation tends to decrease with increasing specified release strengths, f'_{ci}. This decreasing tendency[6] is in contrast to the trend of the implicit assumed standard deviation included in the ACI 224 overstrength provisions for use without historical data as plotted in Figure 5-9. In order to facilitate the use of the pooled standard deviation trend with respect to specified release strength, a linear regression of the pooled standard deviation values was completed with results shown in Figure 5-29. Also shown on the plot is the line representing the simplified constant *s* used in the two ACI 214-based models discussed in Sections 5.6.6 and 5.6.7.

[6] This offered conclusion may be different if the coefficient of variation approach is relied on instead of the standard deviation. In this case, the primary interest is in the dispersion of the data set around the mean—independent of the magnitude of the mean.

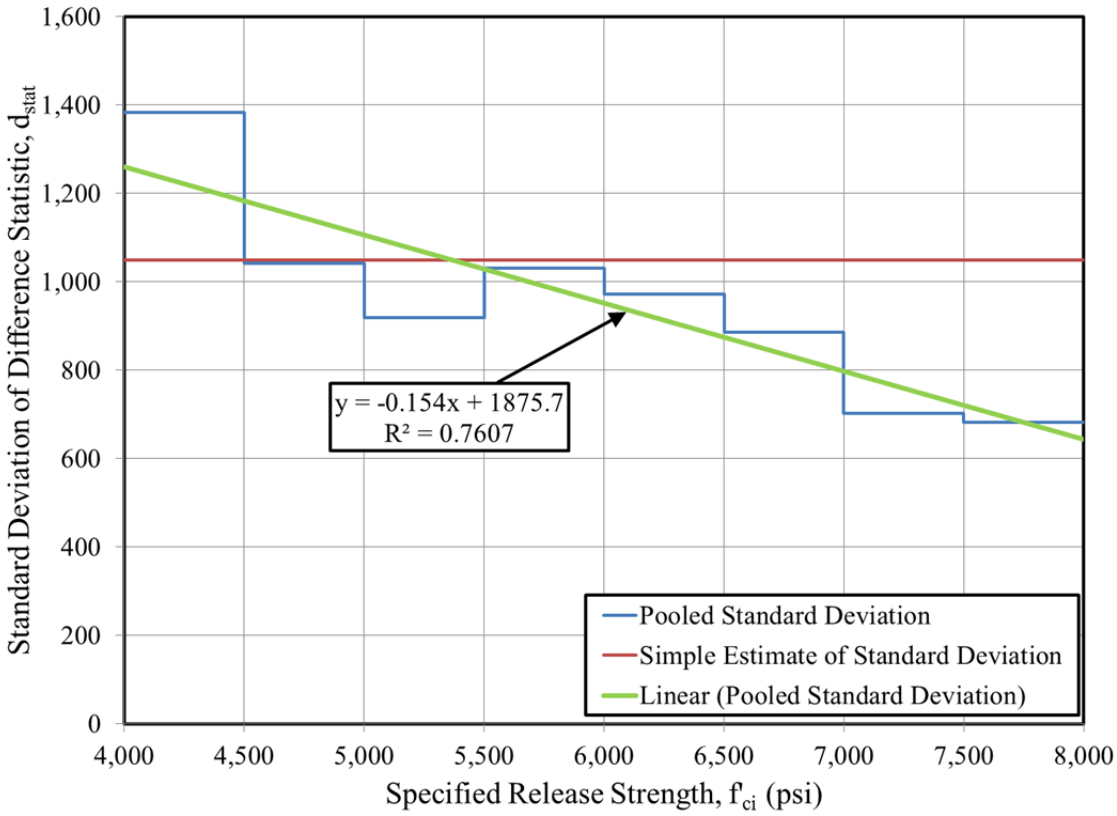

Figure 5-29: Linear Regression of Standard Deviation of Difference Statistic

While the explicit form of the model is withheld until Table 5-16, the completed model is defined by use of the following:

- the MPCMC prediction equation of Section 5.6.2;
- the overstrength provisions of ACI 301 as discussed in Section 5.3; and
- the linear regression equation for *s* as a function of f'_{ci} as shown in Figure 5-29.

The completed ACI 214-based model (variable *s* and MPCMC concept) is shown in Figure 5-30, alongside the previous ACI-based models for comparison.

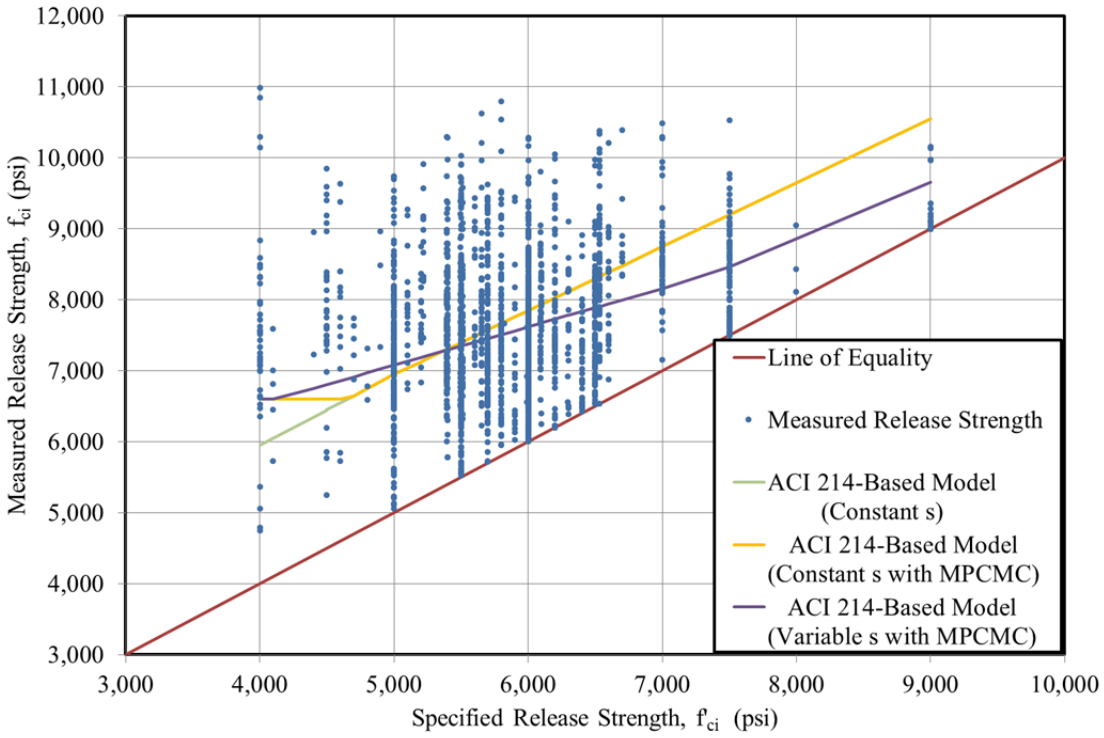

Figure 5-30: ACI 214-Based Model (Variable *s* with MPCMC)

5.6.9 Comparison of Trial Models

The standard error of the estimate (SEE) was used to evaluate and compare the goodness-of-fit of the trial models developed in this chapter. This section compares and contrasts the trial prediction models and provide final recommendations to be used during the design phase for predicting the expected concrete compressive strength at the time of prestress release, f_{ci}^{*} as a function of the specified compressive strength, f'_{ci}.

For reference, each of the trial models, with the exception of FE-3 (previously dismissed in Section 5.6.3), is tabulated in Table 16 and shown in Figure 5-31. The corresponding SEE for each model is shown in Table 5-17. For comparison, the recommendation of Hofrichter (2014) is also included.

Table 5-16: Trial Prediction Equations for Prestress Transfer

Model Designation	Model Definition	Calibration Constants
FE-1	$f_{ci}^{*} = a \cdot f'_{ci}$	a = 1.30
FE-2	$f_{ci}^{*} = b + f'_{ci}$	b = 1,840 psi
FE-3	$f_{ci}^{*} = a \cdot f'_{ci} + b$	a = 0.34 b = 5,662 psi
FE-4	$f_{ci}^{*} = c$ when $f'_{ci} \le d$ $f_{ci}^{*} = b + f'_{ci}$ otherwise	c = 7,500 psi d = 6,100 psi b = 1,400 psi
FE-5	$f_{ci}^{*} = c$ when $f'_{ci} \le d$ $f_{ci}^{*} = a \cdot f'_{ci}$ otherwise	c = 7,500 psi d = 6,300 psi a = 1.18
SE-1	$\max(b + f'_{ci}, 6.6(MPCMC) + 800)$	b = 1,750 psi *MPCMC* = 881 pcy (Alabama)
SE-2	$\max(a \cdot f'_{ci}, 6.6(MPCMC) + 800)$	a = 1.27 *MPCMC* = 881 pcy (Alabama)
ACI 214-Based (Constant s)	$f_{ci}^{*} = f'_{ci} + 1{,}950$ psi when $f'_{ci} \le d$ $f_{ci}^{*} = 0.9 f'_{ci} + 2{,}450$ psi otherwise	d = 5,000 psi (Implicit assumptions s = 1,050 psi)
ACI 214-Based (Constant s and MPCMC)	$\max(f'_{ci} + 1{,}950 \text{ psi}, 6.6(MPCMC) + 800)$ when $f'_{ci} \le d$ $\max(0.9 f'_{ci} + 2{,}450 \text{ psi}, 6.6(MPCMC) + 800)$ otherwise	d = 5,000 psi (Implicit assumptions s = 1,050 psi) *MPCMC* = 881 pcy (Alabama)
ACI 214-Based (Variable s and MPCMC)	$\max(f'_c + 1.34s, f'_c + 2.33s - 500, 6.6(MPCMC) + 800)$ when $f'_{ci} \le d$ $\max(f'_c + 1.34s, 0.9 f'_c + 2.33s, 6.6(MPCMC) + 800)$ otherwise	d = 5,000 psi $s = -0.154 f'_{ci} + 1876$ psi *MPCMC* = 881 pcy (Alabama)
Recommendation of Hofrichter (2014)	$f_{ci}^{*} = c$ when $d \le f'_{ci} \le e$ $f_{ci}^{*} = b + f'_{ci}$ otherwise	c = 7,500 psi d = 4,000 psi e = 7,000 psi b = 500 psi

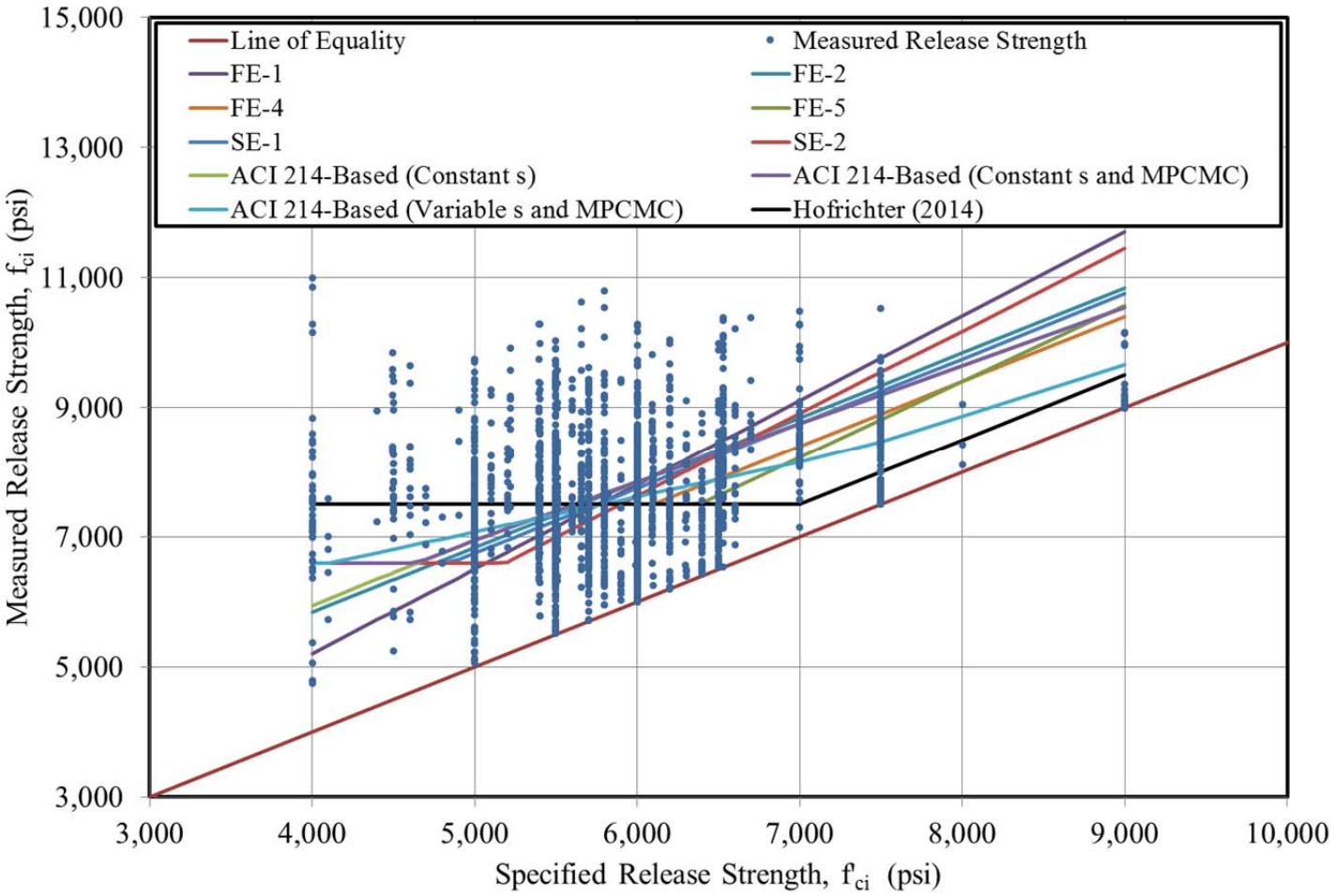

Figure 5-31: Trial Prediction Models for Expected Concrete Release Strength at Prestress Release

Table 5-17: Goodness-of-Fit for Trial Prediction Equations at Prestress Release

Prediction Model Label	Standard Error of Estimate (SEE) (psi)
Current Practice ($f_{ci}^{*} = f'_{ci}$)	2,126
FE-1	1,185
FE-2	1,064
FE-3	947
FE-4	945
FE-5	950
SE-1	1,032
SE-2	1,097
ACI 214-Based (Constant *s*)	1,038
ACI 214-Based (Constant *s* and MPCMC)	1,016
ACI 214-Based (Variable *s* and MPCMC)	968
Hofrichter (2014)	966

As a metric for comparison, the SEE corresponding to the current design practice of assuming $f_{ci}^{*} = f'_{ci}$ is shown prior to the SEE for the nine trial models. In general, all trial models represent a large improvement over current design practice. For the simple fully empirical models (FE-1 to FE-3), it is evident that the combination multiplier and constant offset formulation of FE-3 tends to be most accurate form to fit the historical data set. This is not surprising, as the ACI 301 recommendations for concrete strengths exceeding 5,000 psi follow the same multiplier and constant offset formulation as shown in Equation 5-11d. The introduction of the piecewise formulation in the fully empirical models of FE-4 and FE-5 does not significantly increase the accuracy of the prediction models when compared to the historical data set. In general, the fully empirical fits represent the most accurate prediction equations of the nine trial expressions. However, due the empirical nature of these equations, their usefulness is rather narrow, likely confined only to the geographic region from which the historical strength data set was compiled.

The semi-empirical models of SE-1 and SE-2 utilize the MPCMC concept and thus, are somewhat more logically based prediction models than the fully empirical model set. However, it appears that the use of the MPCMC prediction equation included in these models offers a conservative estimate of the minimum mean concrete strength at release for the region represented by the historical data set and, therefore, results in larger SEE values. While the fully empirical models suggest a minimum mean concrete strength of approximately 7,500 psi, the MPCMC prediction equation estimates the minimum mean concrete strength at 6,600 psi. Recall that the MPCMC concept included certain implicit assumptions of a fixed volume of mixing water (285 pcy), a fixed *w/cm* (0.32), and the absence of any supplementary cementing materials. Accordingly, use of the MPCMC prediction equation should be used as an approximation of the minimum mean concrete strength only as a last resort, in the absence of designer knowledge of local concrete mixture properties and corresponding minimum mean concrete strengths. Put more simply, if a designer considers estimating the paste content of a likely to be used concrete mixture, he or she is likely better served to estimate the minimum mean concrete strength directly based on region-specific plant practices.

If capable of accurately estimating the expected concrete release strength, f_{ci}^{*}, the ACI 214-based prediction models may be the most preferable of all the trial models considered in this dissertation due to their potential for more widespread implementation than the fully empirical models. Because these models are largely based on the existing overstrength concepts of ACI 214-R11 and ACI 301, they require little or no calibration from a historical strength data set. For the constant standard deviation models, the rounded value of s = 1,050 psi was confirmed as an appropriate value for precast,

prestressed construction in historical data subsets from three independent producers at two varying ages. Both of the ACI 214-based constant *s* models (with and without the MPCMC concept) tend to provide predictions on the same approximate accuracy level as the semi-empirical models and many of the fully empirical models. The slightly lower SEE of the ACI 214-based constant *s* model with MPCMC suggests that for most accurate results with a constant *s* model, it is may be appropriate to include the concept of a minimum preferred compressive strength. Finally, for most accurate results of the ACI 214-based trial models, the variable *s* and MPCMC concept model offers prediction accuracy on par with some of the most accurate fully empirical models. This is not surprising, as the equation for determining *s* as a function of specified concrete strength, f'_{ci}, (variable *s*) is somewhat more tailored to the historical data set than the constant *s* prediction equations. Overall, due to the historical data set in this study containing a relatively few data for comparison at the upper extremes of the strength range (strengths in excess of f'_{ci} = 7,500 psi), the increased complexity of the variable *s* equation does not seem justified for most typical applications.

Prior to determining a final prediction recommendation, it was desirable to compare a leading candidate prediction model from this research (ACI 214-based [constant *s* with MPCMC]) to previous work by others. As detailed in Section 5.4.1, the predominant research efforts conducted to date tend to rely on the use of a single amplification factor method. Findings of previous researchers are shown in Table 5-18 and Figure 5-32, accompanied by the ACI 214-based (constant *s* with MPCMC) prediction equation of Section 5.6.7. Where explicit bounds of applicability were not available for previous researcher's recommendations, a range of 4,000 psi to 9,000 psi

was assumed. In addition, it is important to note that recommendations of Nervig (2014) are undefined between the specified strength range of 5,500 psi and 6,000 psi.

Table 5-18: Findings of Previous Researchers for Overstrength at Prestress Transfer

Model Reference	Model Definition[1]	Calibration Constants
French and O'Neill (2012)	$f_{ci}^{*} = a \cdot f'_{ci}$	$a = 1.16$
Storm et al. (2013)	$f_{ci}^{*} = a \cdot f'_{ci}$	$a = 1.24$
Rosa et al. (2007)	$f_{ci}^{*} = a \cdot f'_{ci}$	$a = 1.11$
Nervig (2014)	$f_{ci}^{*} = a_1 \cdot f'_{ci}$ for $4{,}500 \le f'_{ci} \le 5{,}500$ $f_{ci}^{*} = a_2 \cdot f'_{ci}$ for $6{,}000 \le f'_{ci} \le 8{,}000$	$a_1 = 1.40$ $a_2 = 1.12$

Note: [1] = Where explicit bounds of applicability were not available for previous researcher's recommendations, a range of 4,000 psi to 9,000 psi was assumed.

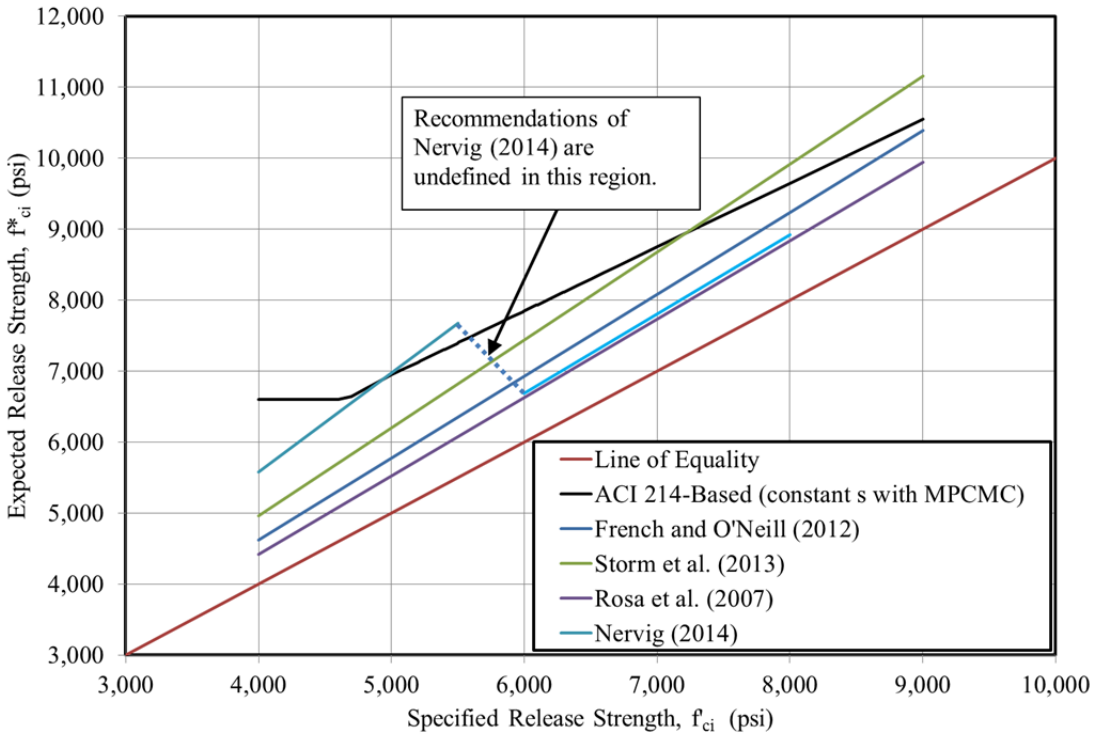

Figure 5-32: Comparison of ACI 214-Based Prediction Equation with Previous Findings by Others

For specified strengths in the lower range, the work of Nervig (2014) provides similar expected release strengths. For higher specified strengths, the ACI 214-based prediction

equation yields similar results to those of Storm et al. (2013) and Nervig (2014). A quantitative comparison of the goodness-of-fit of each equation is shown in Table 5-19.

Table 5-19: Comparison of Trial Prediction Equations at Prestress Release Suggested by Previous Researchers to Experimental Data

Prediction Model Label	Standard Error of Estimate (SEE) (psi)
Current Practice ($f_{ci}^{*} = f'_{ci}$)	2,126
ACI 214-Based (Constant *s* and MPCMC)	1,016
French and O'Neill (2012)	1,445
Storm et al. (2013)	1,238
Rosa et al. (2007)	1,630
Nervig (2014)	See Note 1.
Hofricher (2014)	966

Note 1: In the historic strength data set, 323 f'_{ci} values were contained in the undefined interval of Nervig's recommendation (i.e. between 5,500 psi and 6,000 psi) making computation of an *SEE* not possible.

As demonstrated in Table 5-19, the fully empirical recommendations of previous researchers calibrated for regions outside of Alabama (i.e. all noted models with the exception of Hofrichter [2014]) generate less accurate predictions of release compressive strength than the recommendation of Hofrichter (2014) or the ACI 214-based model recommended as a result of this research effort. This affirms the prior discussion that fully empirical recommendations are limited in application and may not represent the most efficient means of predicting overstrength factors.

5.6.10 Final Recommendations

As a result of the analyses contained in this dissertation section, the design relationship of Section 5.6.6 (ACI 214-based model [constant *s*]) as displayed in Table 5-16 is proposed for predicting the concrete compressive strength at the time of prestress release, f_c^*. This recommendation is consistent with the discussion of Section 5.3.3 that indicates existing overstrength provisions should logically be applied to all design deflection

computations (predictions) in order to avoid a major source of systematic error and to improve the accuracy of these computations. Major conclusions of Section 5.6 are as follow:

1. For the purposes of predicting the expected concrete compressive strength at the time of prestress release, f_c^*, the overstrength provisions of ACI 301 and ACI 214 should be applied with a standard deviation as determined by the distribution of the difference statistic for historical records from production cycles of precast, prestressed products within the region. In the absence of historical data, the standard deviation, *s*, may be assumed to be 1,050 psi, resulting in the following expressions for predicting compressive strength at the time of prestress release:

   For 4,000 psi $\leq f_{ci} \leq$ 5,000 psi $\quad f_{ci}^* = f'_{ci} + 1{,}950$ psi

   For 5,000 psi $< f_{ci} \leq$ 9,000 psi $\quad f_{ci}^* = 0.9 f'_{ci} + 2{,}450$ psi

2. The overstrength factor at release, OS_i, for concrete strengths exceeding 5,000 psi (without inclusion of the MPCMC concept) can be expressed as:

$$OS_i = \frac{f_{ci}^*}{f'_{ci}} = 0.9 + \frac{2{,}450}{f'_{ci}}$$

   where

   OS_i^* = expected overstrength ratio at prestress release;

   f_{ci}^* = the expected concrete strength at prestress release (psi); and

   f'_{ci} = the specified concrete strength at prestress release (psi).

5.7 Predicting Expected Concrete Compressive Strength at 28 Days

Accurately predicting overstrength at the time of 28 days after girder production is of somewhat less importance to design engineers in the precast, prestressed industry than the accuracy of overstrength predictions at the time of prestress release due to the critical role of the initial modulus of elasticity in determining deformations (camber) and prestress losses over the life of the girder. The primary goal of this section is to recommend a relationship for use at the time of girder design to more accurately predict the expected concrete compressive strength 28 days after girder fabrication, f_c^*. This section is structured similarly to that of Section 5.6 as shown below in Figure 5-33.

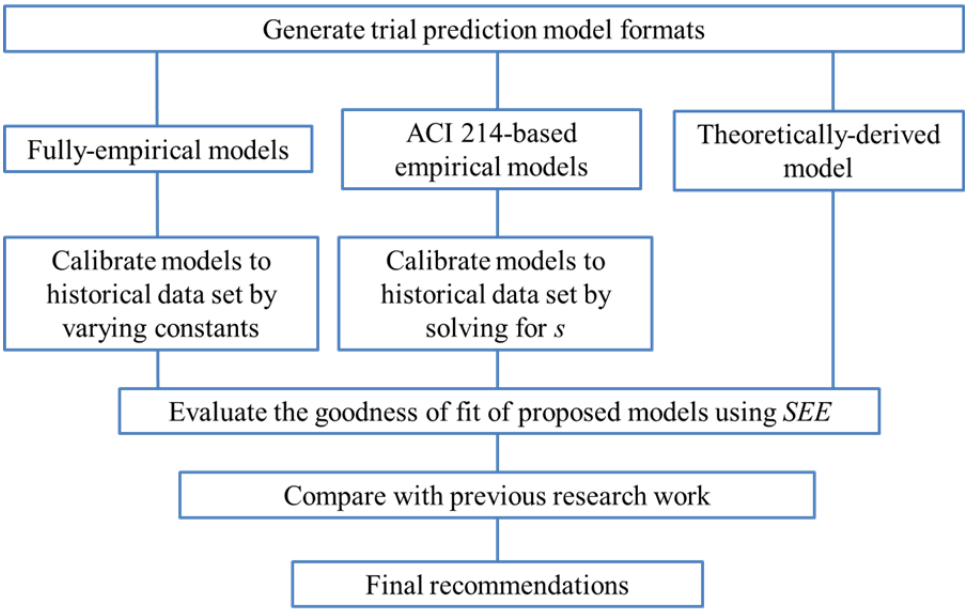

Figure 5-33: Analytical Approach of 28-Day Prediction Equation Development

First, various fully empirical and ACI 214-based trial models are developed and calibrated using the historical data set. While these calibrated trial models do offer relatively good agreement with the 28 day expected strengths of the historical data set, it is important to note that these trial models omit the effect of two important regional variables: (1) the level of overstrength at prestress release and (2) the ratio of the

specified release strength, f'_c, to the specified 28-day strength, f'_c. By including the effect of these parameters in a final prediction model (based on the concepts depicted in Figure 5-12), a more theoretically-correct and logical model capable of capturing regional variations in design practices is investigated and found to be a preferable prediction method.

5.7.1 Fully Empirical Models

The format and calibration constants for each of the five fully empirical models are shown in Table 5-20. The format of these equations is similar to those prestress release models discussed in Section 5.6.3. Each of the five models is plotted, alongside the historical data set, in Figure 5-34.

Table 5-20: Fully Empirical Model Description

Fully Empirical Model Designation	Format of Model (psi)	Description of Model	Calibration Constants
FE-1	$f_c^* = a \cdot f'_c$	Factor	a = 1.56
FE-2	$f_c^* = b + f'_c$	Offset	b = 3,862 psi
FE-3	$f_c^* = a \cdot f'_c + b$	Factor and Offset	a = 0.21 b = 9,172 psi
FE-4	$f_c^* = c$ when $f'_c \le d$ $f_c^* = b + f'_c$ otherwise	Piecewise Constant and Offset	c = 10,500 psi d = 7,300 psi b = 3,330 psi
FE-5	$f_c^* = c$ when $f'_c \le d$ $f_c^* = a \cdot f'_c$ otherwise	Piecewise Constant and Factor	c = 10,500 psi d = 7,450 psi a = 1.43

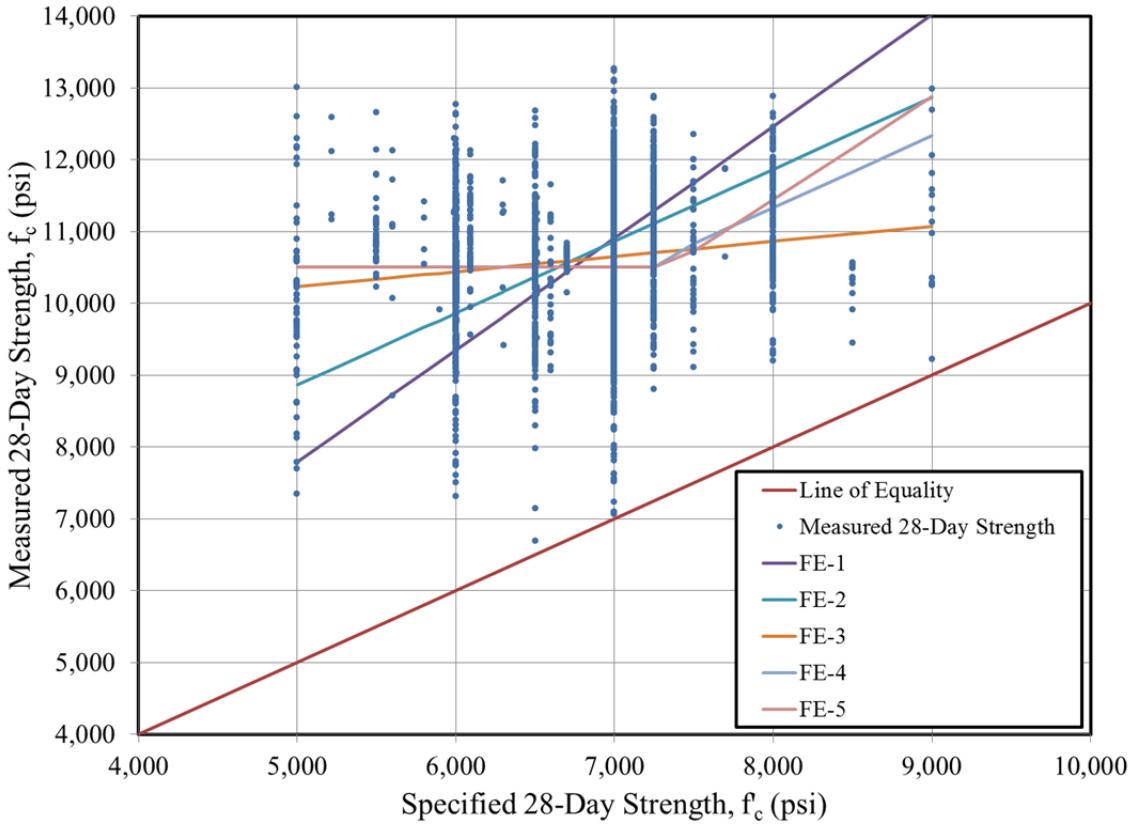

Figure 5-34: Calibrated Fully Empirical 28-Day Strength Prediction Models

Although there is a large variety in the best-fit equations, certain trends are evident. Examining Figure 5-34, it seems that a minimum mean concrete strength, $f^*_{ci,\min}$, of approximately 10,500 psi is suggested by Models FE-3, FE-4, and FE-5. In addition, all models yield similar results for specified strengths of approximately 6,700 psi, which corresponds to the mean specified 28-day strength of the historical database.

5.7.2 ACI 214-Based Empirical Models

Two trial models of the ACI 214-based format were investigated for predicting expected 28-day concrete strength. The first model, the ACI 214-based with constant *s*, was calibrated to the historical data set by varying the standard deviation, *s*, and minimizing the *SEE*. The second model, the ACI 214-based with constant *s* and MPCMC, was calibrated similarly, although an additional parameter, the minimum mean concrete

strength, $f^*_{c,\min}$, was also fit to the historical data set. The form and calibration constants for these trial models are shown in Table 5-21 and plotted in Figure 5-35.

Table 5-21: ACI 214-Based Empirical Model Description

	f'_c (psi)	f^*_c (psi) Use the larger of:	Calibration Constants
ACI 214-Based (Constant *s*)	**5,000 or less**	$f^*_c = f'_c + 1.34s$	**s = 1,950 psi**
		$f^*_c = f'_c + 2.33s - 500$	
	Over 5,000	$f^*_c = f'_c + 1.34s$	
		$f^*_c = 0.9f'_c + 2.33s$	
ACI 214 (Constant *s* and MPCMC)	**5,000 or less**	$f^*_{c,\min} = a$	**a = 10,500 psi**
		$f^*_c = f'_c + 1.34s$	**s = 1,050 psi**
		$f^*_c = f'_c + 2.33s - 500$	
	Over 5,000	$f^*_{c,\min} = a$	**a = 10,500 psi**
		$f^*_c = f'_c + 1.34s$	**s = 1,050 psi**
		$f^*_c = 0.9f'_c + 2.33s$	

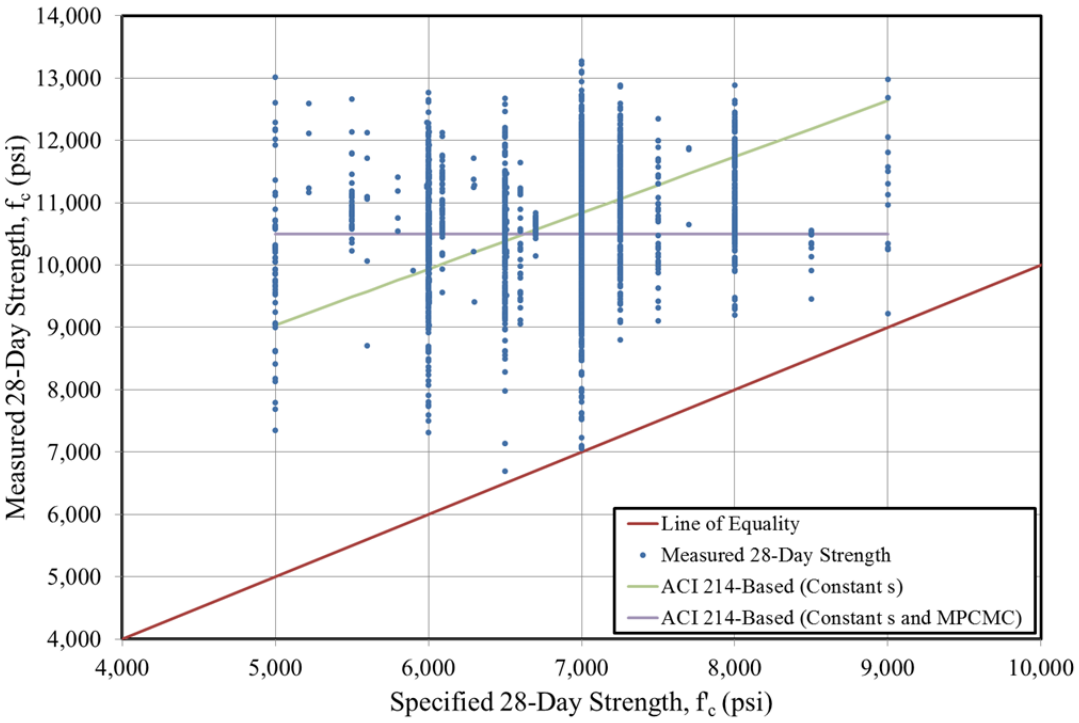

Figure 5-35: ACI 214-Based Empirical Models for 28-Day Concrete Strength

Upon introduction of the MPCMC concept in the second considered model, the model simplifies to a single horizontal line at the value of 10,500 psi, suggesting a constant expected value may be appropriate for all concrete mixtures. This finding is in agreement with the recommendation of Hofrichter (2014) derived in a similar manner. The calibrated standard deviation, *s*, therefore, has no effect on the second model (with MPCMC), but does play a role in defining the first model. The calibrated value of *s* for the first model (ACI 214-based [Constant s]) does not agree with the computed value representing the historical data set for the age of 28 days (*s* = 1,132 psi from Table 5-12). For these reasons, the ACI 214-based empirical models may not be preferable for computing the expected 28-day concrete strength, f_c^*.

5.7.3 Theoretically-Derived Strength Growth Model

Given the previous discussion on the probable causes of 28-day overstrength (Section 5.4.2), it seems appropriate to develop a prediction model incorporating certain logically-relevant parameters. Recall, it was discussed that two key parameters are required to fully define the overstrength ratio present at 28 days: (1) the "expected" 28-day strength computed as a function of the expected release strength, f_{ci}^*, and various strength growth parameters and (2) the selection of a specified 28-day strength, f'_c, by the design engineer to ensure adequate service and strength limit state performance. It would seem that a series of prediction equations for both release and 28 days omitting these parameters would tend to be (1) overly restrictive by definition (i.e. implicitly assuming a strength growth model) and (2) not suitable for widespread usage due to regionally

varying ratios of f'_{ci}/f'_c by design engineers[7]. The theoretically-derived model explored herein includes the relevant parameters discussed above, and thus, is more suited to widespread usage than a fully empirical.

The basic hypothesis explored here is that the actual 28-day compressive strength for typical precast, prestressed girders has very little to do with the magnitude of the specified 28-day concrete strength, f'_c, but instead, is solely a result of the expected release strength, f^*_{ci}, and the strength growth parameters relating the two ages (α and β). A logical first step to evaluate this hypothesis is to validate the applicability of the strength growth provisions suggested by Hofrichter (2014) on the measured concrete strengths of the historical data set. As shown in Figure 5-36, there is close agreement between the values of (1) the expected 28-day strength, f^*_c, computed by applying Hofrichter's strength growth recommendations (i.e. $f_c = f_{ci} \cdot 1.44$) to measured values of release strength, f_{ci}, and (2) the measured value of 28-day strength, f_c.

[7] The ratio of specified concrete release strength to specified 28-day strength is expected to vary regionally in accordance with state-specific allowable design stresses (i.e. Alabama girders are designed as zero-tension members at service—likely requiring higher specified strengths than a state that permits in-service tensile stresses.)

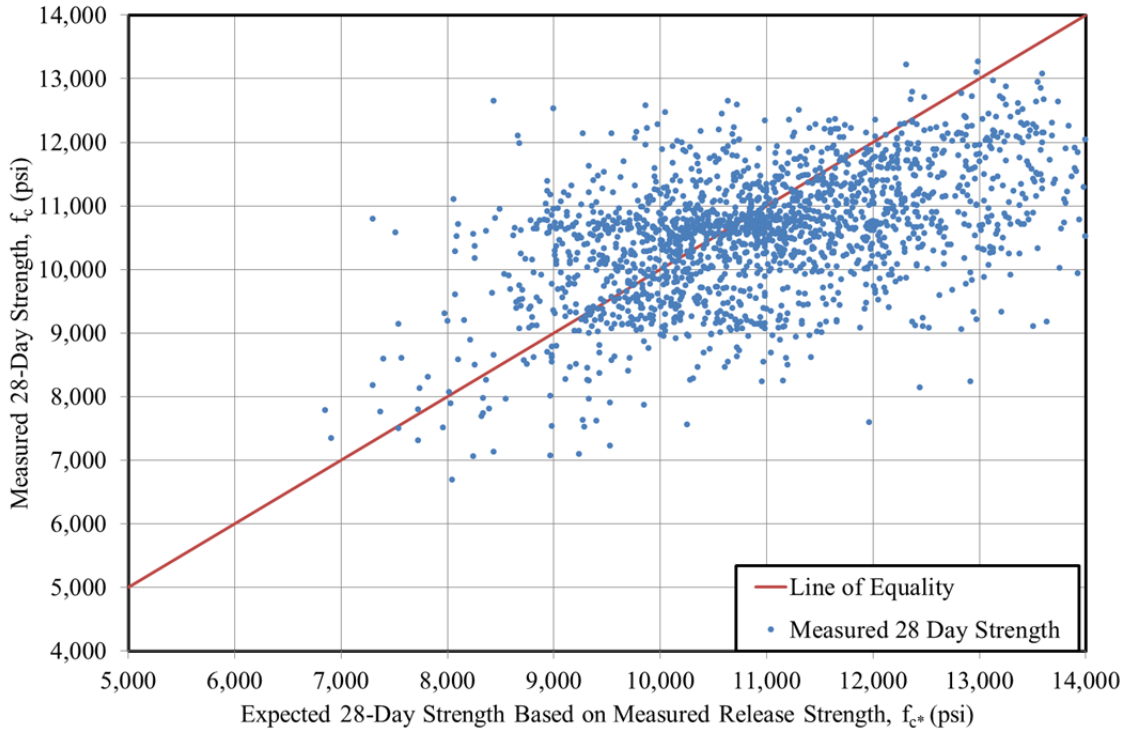

Figure 5-36: Comparison of Expected 28-Day Strength Based on Measured Release Strength and Measured 28-Day Strength.

The measured 28-day strengths tend to be clustered around the line of equality somewhat symmetrically indicating that a relationship may exist between these parameters. The next logical comparison to explore is the relationship between (1) measured 28-day strength, f_c, and (2) expected 28-day strength, f_c^*, based on the combination of the previously proposed equations for computing the expected concrete strength at prestress release, f_{ci}^* (as a function of f'_{ci}), as modified by the strength growth provision by Hofrichter (2014). The results of this analysis are plotted in Figure 5-37.

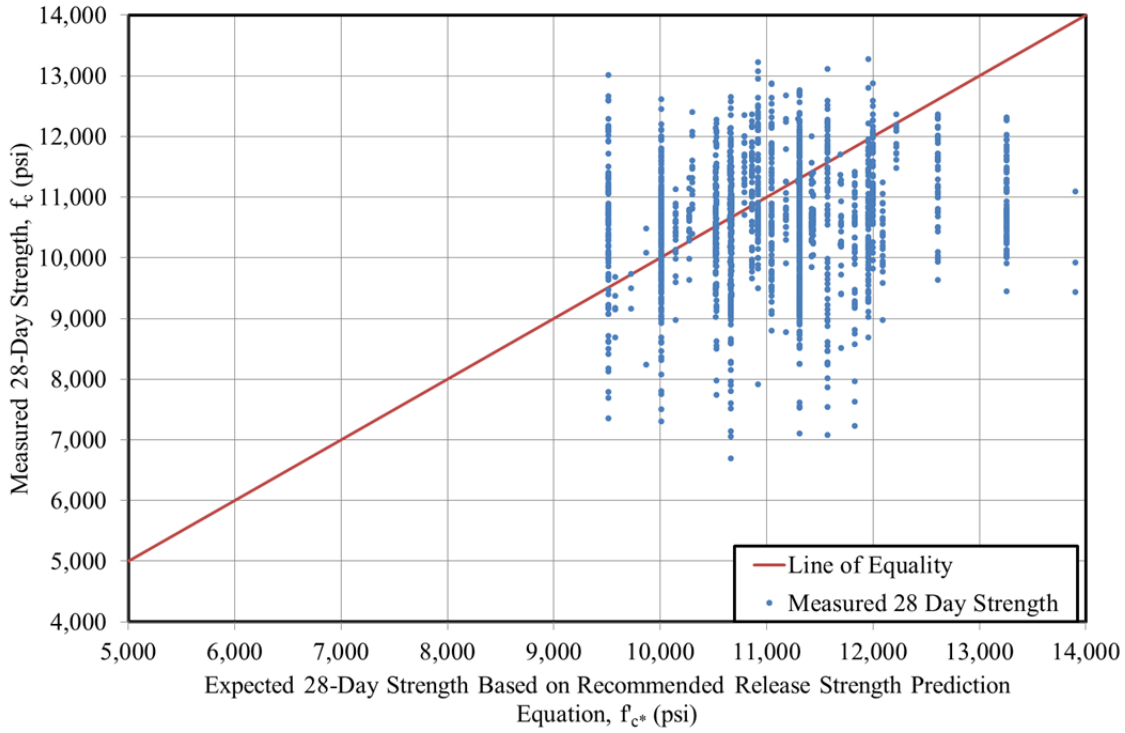

Figure 5-37: Comparison of Expected 28-Day Strength Based on Expected Release Strength and Measured 28-Day Strength.

Again, relatively good agreement is shown between the compared parameters as evidenced by the close proximity of the measured data points to the line of equality. Finally, the measured 28-day strength, f_c , (for the historical 28-day data set) and the expected 28-day strength, f_c^*, (for the release data set adjusted by the strength growth model explored in this section) is plotted versus the specified 28-day strength, f'_c in Figure 5-38. On the plot, it is evident that the values predicted by the theoretically-derived model do not form a continuous line, but instead, are represented by a discrete value for each data point of the historical data set. As shown, there is relatively good agreement between the values predicted by the theoretically-derived model and the measured values of historical data set.

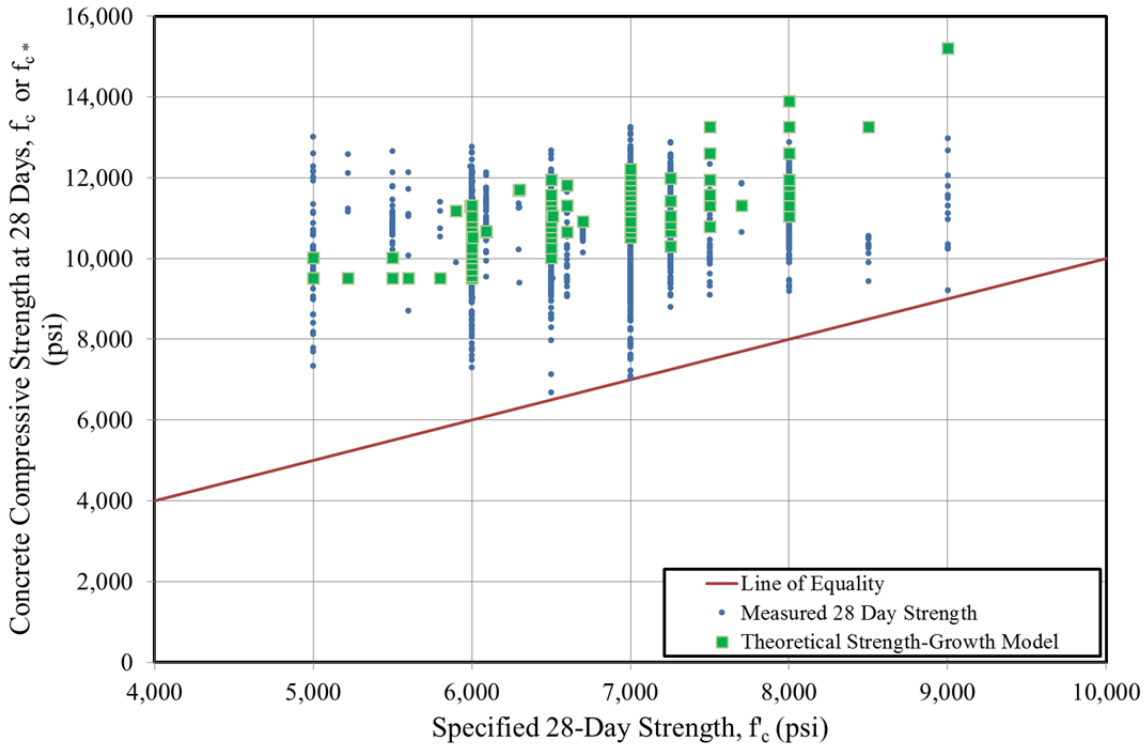

Figure 5-38: Theoretical Strength Growth Model Predictions for 28-Day Concrete Strength Compared with Measured Values of Historical Data Set.

As presented in this section, the theoretically-derived strength growth model is a relatively simple concept in application, but is likely too cumbersome for use by a design engineer. In order to simplify the above procedure, a simple expression for the expected overstrength ratio at 28 days, OS_{28}^{*}, can be derived. As previously defined, OS_{28}^{*} can be expressed as:

$$OS_{28}^{*} = \frac{f_c^{*}}{f'_c} \tag{5-16}$$

where

f_c^{*} = the expected concrete strength at 28 days (psi) and

f'_c = the specified concrete strength at 28 days (psi).

Combining with Equation 5-14 (derived from Hofrichter [2014]) yields:

$$OS_{28}^{*} = \frac{f_c^{*}}{f'_c} = \frac{1.44\, f_{ci}^{*}}{f'_c} \tag{5-17}$$

Substituting in Equation 5-18b (limiting solution to 5,000 psi $< f_{ci} \leq$ 9,000 psi):

$$OS_{28}^{*} = \frac{1.44\, f_{ci}^{*}}{f'_c} = \frac{1.44\left(0.9\, f'_{ci} + 2{,}450\right)}{f'_c} \tag{5-18}$$

Simplifying and grouping terms yields:

$$OS_{28}^{*} = 1.3\left(\frac{f'_{ci}}{f'_c}\right) + \frac{3{,}500}{f'_c} \tag{5-19}$$

where

$\left(\frac{f'_{ci}}{f'_c}\right)$ = the ratio of specified strength at prestress release to 28 days as selected by design engineer.

Examination of Equation 5-19 shows that the expected overstrength 28 days after production is then theoretically a function of only the ratio of specified strengths (as chosen by design engineer) and the specified 28-day strength, f'_c. Equation 5-19 is a multi-variate expression and can be perhaps best visualized in tabulated form as shown in Table 5-22. For ease of the use, values that are not realistic (i.e. specified release strength exceeding 28-day strength or overstrength values less than 1.0) are omitted, values prohibited by ALDOT design specifications are marked in yellow, and possible combinations to be specified by ALDOT are marked in green. Implicit in the table are both (1) the overstrength predictions for prestress release and (2) the strength growth provisions for precast, prestressed concrete as proposed by Hofrichter (2014).

Table 5-22: Expected Overstrength Factor at 28 Days as a Function of Specified Release Strength and Specified 28-Day Strength

Specified Release Concrete Strength, f_{ci} (psi)	Specified 28-Day Concrete Strength, f'_c (psi)																
	4,000	4,500	5,000	5,500	6,000	6,500	7,000	7,500	8,000	8,500	9,000	9,500	10,000	10,500	11,000	11,500	12,000
4,000	2.19	1.94	1.75	1.59	1.46	1.34	1.25	1.17	1.09								
4,500		2.09	1.88	1.71	1.56	1.44	1.34	1.25	1.17	1.10	1.04						
5,000			2.01	1.82	1.67	1.54	1.43	1.34	1.25	1.18	1.12	1.06					
5,500				1.94	1.78	1.64	1.53	1.42	1.34	1.26	1.19	1.12	1.07	1.02			
6,000					1.89	1.74	1.62	1.51	1.42	1.33	1.26	1.19	1.13	1.08	1.03		
6,500						1.84	1.71	1.60	1.50	1.41	1.33	1.26	1.20	1.14	1.09	1.04	
7,000							1.80	1.68	1.58	1.49	1.40	1.33	1.26	1.20	1.15	1.10	1.05
7,500								1.77	1.66	1.56	1.48	1.40	1.33	1.26	1.21	1.15	1.11
8,000									1.74	1.64	1.55	1.47	1.39	1.33	1.27	1.21	1.16
8,500										1.71	1.62	1.53	1.46	1.39	1.32	1.27	1.21
9,000											1.69	1.60	1.52	1.45	1.38	1.32	1.27

Not Realistic Values or Invalid by Assumption

Prohibited by ALDOT Specifications

Predictions for ALDOT Possible Combinations

Table 5-22 is a useful design aid for the precast, prestressed concrete industry, allowing an engineer to first complete strength-limit state design according to current practice and then use Table 5-22 to estimate the magnitude of the expected 28-day overstrength factor, thereby allowing more accurate 28-day deflection computations. For instance, consider the case when a given initial structural design (satisfying allowable stress requirements) warrants a specified release strength, f'_{ci}, of 5,000 psi and a specified 28-day strength, f'_c, of 6,000 psi. Using Table 5-22, a design engineer can determine that an overstrength factor of 1.67 should be applied to the specified 28-day strength, f'_c, for use in computing 28-day deflections of interest.

5.7.4 Comparison of Proposed Models

The standard error of the estimate (*SEE*) for each of the trial models discussed in this section is shown in Table 5-23. Recall, the *SEE* is a measure of the relative goodness-of-fit of a prediction model to measured data from the historical data set.

Table 5-23: Goodness-of-Fit for Trial Prediction Equations at 28 Days

Prediction Model Label	Standard Error of Estimate (*SEE*) (psi)
Current Practice ($f_c^* = f'_c$)	4,026
FE-1	1,391
FE-2	1,133
FE-3	974
FE-4	988
FE-5	1,001
ACI 214-Based (Constant *s*)	1,097
ACI 214-Based (Constant *s* and MPCMC) / Hofrichter (2014)	991
Theoretically-Derived Strength Growth	1,349

As shown, each of the trial models represents a significant improvement in accuracy when compared to current design practice. The fully empirical models, when calibrated

to the historical data set, yield relatively good fits of the historical data with Model FE-3 being the most preferable due to its simplicity. While these fully empirical models are appropriate for use in the study region, they may not be suited for use in other areas due to differing design and production practices. The ACI 214-based methods were not preferable due to the lack of agreement between the standard deviation of the historical data set calibrated empirically and the standard deviation previously computed directly from the historical data set—likely suggesting that form of the ACI 214 overstrength equations are not suit for application at 28 days. Despite being somewhat less accurate for the historical data set, the theoretically-derived strength growth model is the most mechanistic model for predicting concrete overstrength at 28 days in steam-cured concrete and thus, is most well suited for widespread applicability.

5.7.5 Final Recommendations

As a result of the analyses of the preceding dissertation sections, the theoretically-derived strength growth model is selected as the most appropriate model for design estimates of the 28-day concrete compressive strength, f_c^*. While fully empirical models may be useful on a somewhat limited regional basis, the nature of the theoretically-derived strength growth model is conducive to capturing variations in regional design practices (the effect of varying specified strength ratio) by using strength growth provisions appropriate for the curing application. For accelerated-cured concretes (containing Type III cement) typical of the precast, prestressed concrete industry, the strength growth provisions of Hofrichter (2014) are recommended for use (as summarized in Section 5.2.3) and implicitly included in the overstrength prediction expression of Equation 5-23 as represented in Table 5-22.

5.8 Summary and Conclusions

5.8.1 Summary

The primary objective of this dissertation chapter is to identify design relationships between specified concrete compressive strength and expected concrete compressive strength in order to allow engineers to improve the accuracy of design phase serviceability predictions. After a brief background discussion, current relevant code provisions of ACI 301 and *fib* Model Code 2010 are reviewed, compared, and recommended for general usage in structural concrete design serviceability computations. Next, overstrength in the precast, prestressed industry is discussed—including probable causes of overstrength at two key ages of interest and an evaluation of the suitability of applying the provisions of ACI 301 for estimating overstrength in the precast, prestressed industry. Subsequently, the details of a historical concrete strength data set compiled as part of this research effort are presented and discussed prior to its usage in various analyses. The first major analysis is aimed at evaluating various fully empirical, semi-empirical, and ACI 214-based prediction equations for estimating the expected concrete compressive strength at the time of prestress release. Finally, a similar set of analyses is conducted to yield a recommended design relationship for estimating expected concrete strength at 28 days.

5.8.2 Conclusions and Recommendations

Several key conclusions of the work presented in this dissertation chapter are applicable to the concrete industry as a whole:

1. For the purposes of design deflection computations, it is appropriate to use an estimate of the "expected" concrete compressive strength rather than the current practice of using the specified strength.;
2. The existing provisions of ACI 301 and ACI 214R-11 are an appropriate and convenient method for estimating the expected concrete compressive strength as a function of the specified strength;
3. The "difference statistic" and the concept of preservation of standard deviation as summarized below offer a convenient method to compute a standard deviation from a historical data set with varying specified concrete strengths that is appropriate to be used with the provisions of ACI 301 and ACI 214R-11:
    a. *For an assumed (or approximated) constant standard deviation value at all considered strength levels, the distribution of the difference statistic is identical regardless of the number of constitutive mixtures or the relative mean strength levels of each mixture.*

Several key conclusions of the work presented in this dissertation chapter are applicable specifically to the precast, prestressed concrete industry:

1. For the purposes of predicting the expected concrete compressive strength at the time of prestress release, f_c^*, the overstrength provisions of ACI 301 and ACI 214 should be applied with a standard deviation as determined by the distribution of the difference statistic for historical records from production cycles of precast, prestressed products within the region. In the absence of historical data, the standard deviation, *s*, may be assumed to be 1,050 psi based on the results of this study. The overstrength provisions of ACI 301 and ACI 214 are recommended

for predicting compressive strength at the time of prestress release, simplified as follows for the value of s = 1,050 psi:

For 4,000 psi $\leq f_{ci} \leq$ 5,000 psi $\quad f_{ci}^{*} = f'_{ci} + 1{,}950$ psi

For 5,000 psi $< f_{ci} \leq$ 9,000 psi $\quad f_{ci}^{*} = 0.9 f'_{ci} + 2{,}450$ psi

2. Based on Equation 5-18, the overstrength factor at release, OS_i, for concrete strengths exceeding 5,000 psi (without inclusion of the MPCMC concept) can be expressed as:

$$OS_i = \frac{f_{ci}^{*}}{f'_{ci}} = 0.9 + \frac{2{,}450}{f'_{ci}}$$

where

OS_i^{*} = expected overstrength factor at prestress release;

f_{ci}^{*} = the expected concrete strength at prestress release (psi); and

f'_{ci} = the specified concrete strength at prestress release (psi).

3. For the purposes of predicting the expected concrete strength at the age of 28 days after production, the theoretically-derived strength growth model of Section 5.7.3 is recommended. This method consists of using the above recommendations to estimate the expected concrete strength at release and then applying appropriate strength growth provisions to compute expected 28-day strength. For accelerated cured concretes typical of precast, prestressed industry, the expected overstrength at 28 days, OS_{28}^{*}, can be approximated

$$OS_{28}^{*} = 1.3\left(\frac{f'_{ci}}{f'_{c}}\right) + \frac{3{,}500}{f'_{c}}$$

where

$\left(\frac{f'_{ci}}{f'_c}\right)$ = the ratio of specified strength at prestress release to 28 days as selected by design engineer.

Rearranging, the expected 28-day compressive strength, f_c^*, can be computed directly as a function of specified release strength, f'_{ci}

$$f_c^* = 1.3 f'_{ci} + 3{,}500 \text{ psi}$$

where

f'_{ci} = the specified concrete strength at prestress release (psi).

Chapter 6: Concrete Modulus of Elasticity Relationships

6.1 Introduction

Concrete material stiffness, as represented by modulus of elasticity, is a parameter intrinsically related to the computation of both short-term and long-term deflections in prestressed concrete elements. Generally speaking, the modulus of elasticity (also called the elastic modulus) of a given material is defined as the ratio of the applied stress to the instantaneous strain within an assumed proportional limit (Mehta and Monteiro 2014). It is this relationship that governs elastic material behavior and serves as the basis for deformation computations in structural elements.

This dissertation chapter focuses on correlating a known (or expected) concrete cylinder compressive strength to a corresponding modulus of elasticity for typical precast, prestressed concrete. Using a robust regional data set compiled from a laboratory and concurrent field data collection effort, various available elastic modulus prediction equations were first calibrated and then evaluated for potential use by bridge designers. It is assumed that the compressive strength values used in modulus of elasticity prediction models represent either a known (measured) value or a best-estimate of the concrete compressive strength at a given time. While based on a relatively robust regional data set, the concretes considered in this study are all for similar precast, prestressed application and represent a relatively narrow range of compressive strengths and constitutive materials. Therefore, the focus of this chapter remains on fitting those

prediction models with built-in constants to the compiled data set in an effort to appropriately capture regional concrete behavior.

6.1.1 Chapter Objectives

The primary objective of this chapter is to establish the most appropriate relationships for use by design engineers to accurately characterize the elastic modulus of concrete as a function of compressive strength and other relevant variables likely to be known during the preliminary design phase. Tasks completed in pursuit of this primary objective include the following:

- Review relevant background regarding concrete modulus of elasticity and the primary mixture-dependent factors hypothesized to affect elastic modulus;
- Review and discuss various available concrete stiffness prediction equations, their application at various ages, and the results of similar previous research studies;
- Summarize an experimental program consisting of a laboratory and concurrent field data collection effort to compile a robust regional data set;
- Calibrate various available prediction equations to experimental results for two primary ages of interest (prestress release and 28 days after production) and evaluate the effectiveness of various candidate models; and
- Explore and discuss the time-dependent nature of the effect of aggregate stiffness on concrete modulus through consideration of a reduced data set.

6.1.2 Chapter Outline

This chapter begins with a brief background detailing the definition of the modulus of elasticity of concrete and the primary factors affecting concrete material stiffness. Next, various available prediction equations are introduced and discussed. The work of

previous researchers is also discussed in an effort to identify those prediction equations most universally recommended and utilized in design. Then, an experimental program consisting of a laboratory and field data collection effort is presented, which culminated in the compilation of a data set including many variables hypothesized to affect elasticity modulus. By calibrating available prediction models and comparing the accuracy of these prediction equations to measured data, recommendations are then made for use of the most appropriate prediction equations. Finally, a discussion of a potential source of uncontrolled variability in the experimental data is included.

6.2 Background

6.2.1 Modulus of Elasticity Definition

As previously defined, the elastic modulus of a given concrete is the ratio of the applied stress to the instantaneous strain when the concrete is subjected to uniaxial compression up to an assumed proportionality limit (Mehta and Monteiro 2014). For the purposes of this dissertation, the term modulus of elasticity (or elastic modulus) refers exclusively to the static modulus of elasticity (as opposed to the dynamic modulus.) Most commonly, concrete is assumed to exhibit relatively linear-elastic behavior through roughly 40 percent of its ultimate compressive strength. Thereafter, the development of microcracking at interfaces between hydrated cement paste and aggregate particles tend to cause a curved stress-strain relation (Neville 2013) as shown below in Figure 6-1.

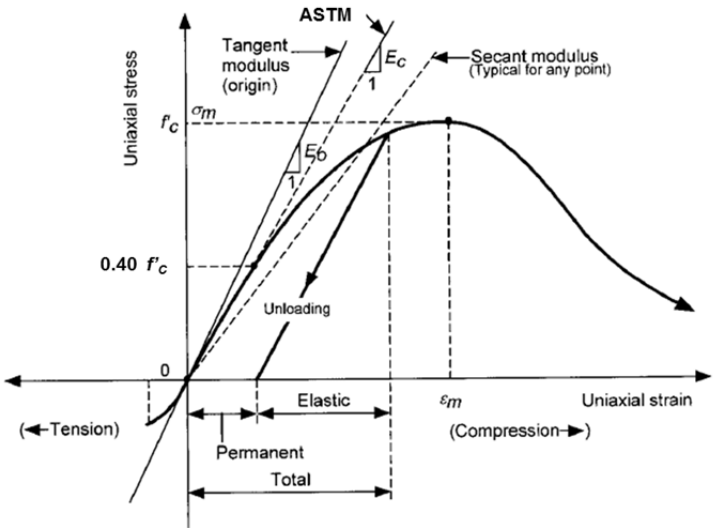

Figure 6-1: Stress-Strain Curve and Elastic Modulus Depictions (Adapted from Naaman 2004)

As expected, the stress-strain response of concrete specimens exhibits no permanent deformation upon unloading in the range of linear-elastic behavior. Also shown in Figure 6-1 are three common representations of elastic modulus including (1) initial tangent modulus, (2) chord modulus, and (3) secant modulus. A tangent modulus is defined for any given point on the stress-strain curve and represents a localized portion of the response. In this case, the initial tangent modulus is depicted, representing the initial stiffness response of the concrete. However, as noted by Neville (2013), the tangent modulus may not accurately describe the overall stiffness response and therefore is of little practical importance. The secant modulus (shown for a stress range of approximately 90 percent of f'_c) offers an improved characterization of stress-strain behavior, but is prone to being skewed by initial response nonlinearities commonly observed at lower stress ranges. The third metric, the chord modulus, is the preferable metric for elastic modulus testing in concrete and the method designated by the standardized testing method ASTM C-469 (2010). This metric, represented by the slope

of a line joining two pre-defined points within the elastic portion of a stress-strain curve, is able to avoid the previously mentioned effect of initial nonlinearities, while also characterizing the elastic response range relatively accurately. In accordance with the requirements of ASTM C-469, the chord modulus of elasticity, E_c, can be computed from test parameters as follows:

$$E_c = (S_2 - S_1)/(\varepsilon_2 - 0.000050) \quad (6\text{-}1)$$

where

S_2 = stress corresponding to 40 percent of ultimate load (psi);

S_1 = stress corresponding to a longitudinal strain, ε_1, of 50 millionths (psi); and

ε_2 = longitudinal strain produced by stress S_2 (in/in).

6.2.2 Primary Factors Affecting Concrete Modulus of Elasticity

This section provides a general discussion of four of the mixture-dependent factors most commonly correlated to concrete elasticity including (1) concrete compressive strength, (2) concrete unit weight, (3) aggregate stiffness, and (4) the use of supplementary cementing materials (SCMs). This discussion is intended to remain general in nature and leads into Section 6.2.3, which introduces candidate prediction equations for E_c.

6.2.2.1 Concrete Compressive Strength

In contrast to other construction materials that tend to exhibit a relatively uniform elasticity regardless of proportional limit (i.e. most structural metals), it was recognized quite early that the stiffness of a given concrete correlates well with the compressive strength. In fact, it is clear that available prediction equations used prior to 1960 relied

on a direct correlation between elastic modulus and compressive strength (Pauw 1960). Prediction equations of this time period were typically were of the following forms:

$$E_c = a \cdot f'_c \tag{6-2a}$$

$$E_c = a \cdot f'_c + b \tag{6-2b}$$

where

f'_c = concrete compressive strength; and

a , b = empirically calibrated constants.

Pauw (1960) observed that each E_c prediction equation of the period tended to apply only to a specific narrow range of concretes (i.e. lightweight aggregate only or compressive strengths not exceeding 3,000 psi), and each equation consistently overpredicted concrete stiffness for higher values of compressive strengths. Citing a previously unpublished study, Pauw (1960) suggested that it may be more accurate to correlate concrete stiffness to the square root of concrete compressive strength—recognizing that this approach might help to curtail over-estimates of E_c for higher strength concretes. By empirically calibrating an E_c prediction equation to a compiled data set, Pauw demonstrated that an equation of the following form more accurately correlated concrete compressive strength to stiffness:

$$E_c = a\sqrt{f'_c} \tag{6-3}$$

where

a = empirically calibrated constant.

While the format of Equation 6-3 and the work of Pauw is still largely in use today in U.S. concrete design, European concrete practice has historically tended to

correlate the modulus of elasticity of concrete to $\sqrt[3]{f'_c}$. Recently, Noguchi et al. (2009) examined the possibility of modifying the exponent of Equation 6-3 to increase the accuracy of modulus correlations. Results of the analysis of a large historical data set are shown in Figure 6-2.

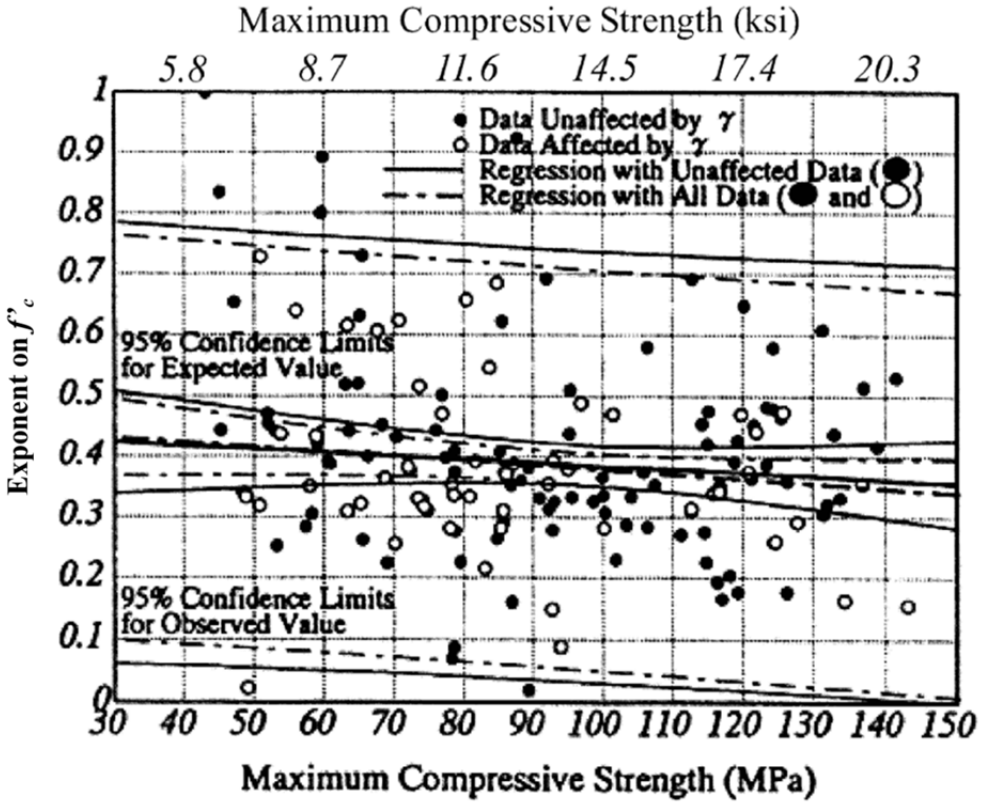

Figure 6-2: Experimental Results of Noguchi et al. (2009)

Noguchi et al. (2009) concluded that the ideal exponent on concrete compressive strength tends to decrease linearly from approximately 0.5 to approximately 0.3–0.4 for higher than typical concrete compressive strengths. Accordingly, Noguchi et al. proposed a revised prediction equation for U.S. practice that correlated concrete stiffness to $\sqrt[3]{f'_c}$, effectively mirroring European practice. Despite the motivation for the proposed change being very similar to that of Pauw in 1960 (correcting over-estimation of E_c for high-

strength concretes), the work of Noguchi et al. has attracted little attention from the American concrete design community.

6.2.2.2 Unit Weight

In addition to suggesting the relationship to $\sqrt{f'_c}$, Pauw (1960) also postulated that concrete modulus of elasticity appeared to be a function of concrete weight. He reasoned that differences in concrete weights were primarily the result of voids within the concrete (either purposely entrained air or vessicules in lightweight aggregate), which would logically also affect concrete stiffness. By empirically exploring correlations among concrete stiffness, unit weight, and compressive strength, Pauw (1960) proposed that concrete stiffness also correlated well to $w^{1.5}$, that is, the equilibrium unit weight of the hardened concrete at the time of testing (w) raised to the exponent of 1.5. The majority of Pauw's work examined structural lightweight aggregate, and as such, Pauw insisted that the unit weight in the above correlation be the equilibrium unit weight, otherwise known as the air-dry unit weight. While the difference between fresh unit weight and air-dry unit weight is negligible for normal-weight concrete, the air-dry unit weight can be up to 12 pcf less than the fresh unit weight for concrete made with lightweight aggregates (Neville 2013). Users of Pauw's prediction equations should be aware of the requirement[1] to use the air-dry density in stiffness computations to provide more accurate estimates of elastic modulus for concrete with lightweight aggregate. Although other researchers since Pauw have proposed that the elastic modulus of concrete may better correlate to the square (exponent of 2.0) of the unit weight (Noguchi et al. 2009), data

[1] ACI 318-14 (2014) does require the use of equilibrium unit weight in the computation of modulus of elasticity for lightweight concretes, as noted in the notation definitions of ACI 318-14.

sets used in these revised analyses do not cover the range of unit weights represented by Pauw's compiled data set.

For the purposes of this dissertation, a discussion of the unit weight of concrete mixtures typical of the precast, prestressed industry is warranted. Historically, the unit weight of plain concrete (excluding steel reinforcing) is most typically assumed to be 145 pcf for cast-in-place concrete applications and 150 pcf for precast concrete (Al-Omaishi et al. 2009). As an alternative, for cases when the 28-day strength of a concrete is known, Al-Omaishi et et al. (2009) recommend the following expression for predicting unit weight, w, as a function of concrete compressive strength:

$$w = 0.140 + \frac{f'_c}{1000} \leq 0.155 \tag{6-4}$$

where

w = concrete unit weight (kcf); and

f'_c = concrete compressive strength (ksi).

Work by Keske (2014) and Storm et al. (2013) both independently confirmed the recommendation of Al-Omaishi et et al. (2009) that designers of precast, prestressed concrete assume a unit weight of 150 pcf in the absence of other information to account for the generally increased paste content of precast, prestressed concrete mixtures. Somewhat similarly, Hofrichter (2014) concluded that an assumed value of 152 pcf may be more appropriate based a review of historic precast, prestressed concrete mixture designs.

6.2.2.3 Aggregate Stiffness

Early research results published by Thoman and Raeder (1934) suggested that the modulus of elasticity of concrete varied with the coarse aggregate used. Work by Alexander and Milne (1995) also demonstrated the effect of aggregate type on the E_c of various concretes. Alexander and Milne (1995) concluded that stiffer concretes are likely to be produced using dolomite or andesite aggregates, while granite and quartzite aggregates tend to produce less stiff concretes. Later, Wu et al. (2001) concluded somewhat contradictory results, finding that quartzite aggregates tend to produce concretes with much greater stiffness than those of granite, limestone, or marble. The major conclusions of these early studies were qualitative in nature.

In 2003, as part of an effort to more accurately estimate prestress losses in pretensioned high-strength concrete bridge girders, Tadros et al. (2003) recognized that despite existing prediction equations for modulus of elasticity accounting for concrete compressive strength and unit weight, there still existed a rather large range of error in experimental data sets. Tadros et al. (2003) concluded that the remaining variation observed between predicted and measured E_c was primarily due to the regional effect of aggregate stiffness. Although this view is widely supported qualitatively in traditional literature (Neville 2013 and Mehta and Monteiro 2014), Tadros et al. (2003) appears to be the first to propose a multiplier, K_1, used to modify elastic modulus predictions in high-strength concrete to account for the difference between national average and local average aggregate stiffness. In the related work of Tadros et al. (2003) and Al-Omaishi et al. (2009), the K_1 factor is referred to as an aggregate stiffness factor—without differentiating between the effect of coarse and fine aggregate. While some believe the

effect of aggregate stiffness is primarily seen in coarse aggregate stiffness variations (Noguchi et al. 2009), others acknowledge the importance of the effect of variations in fine aggregate stiffness (Donza, Cabrera and Irassar 2002; Limeria, Etxeberria and Molina 2011; Shi-Cong and Chi-Sun 2009). Aggregate stiffness factors have been widely studied and most typically range between 0.7–1.2. A full discussion of specific recent work on this topic is included in Section 6.2.3 of this dissertation.

6.2.2.4 Use of Supplementary Cementing Materials

Alexander and Milne (1995) and Noguchi et al. (2009) also explored the effect of the use of varying supplementary cementitious materials (SCMs) on concrete elastic stiffness. Both researchers concluded that the effect of SCMs on E_c also varies according to aggregate type. Although Noguchi et al. (2009) did not track the relative SCM substitution percentages in their data set, they concluded that on average, mixtures containing fly ash tend to be approximately 10 percent stiffer than control mixtures and those mixtures containing silica fume and/or slag cement tended to be roughly 5 percent less stiff than control mixtures. Conversely, Alexander and Milne (1995) concluded that for mixtures with identical aggregates, substitution of silica fume tended to produce stiffer mixtures when compared to control mixtures while substitution of fly ash tended to produce less stiff mixtures. He (2013) provides an extensive discussion of this topic, ultimately citing previous research results tending to agree with those of Alexander and Milne (1995). The experimental efforts of the research program detailed in later sections of this chapter shed further light on this topic.

6.2.3 Available Prediction Equations

In this section, various available prediction equations for concrete modulus of elasticity are presented and discussed. These equations represent the most common relationships used by design engineers to correlate concrete stiffness to concrete compressive strength and other parameters. This section focuses primarily on those relationships most suited for use at the time of preliminary design and contains only a limited discussion of more detailed prediction equations. Many of the expressions reviewed herein contain calibration constants that can be used to tailor expressions to capture regional material variations relevant to E_c.

6.2.3.1 Pauw (1960) / ACI 318-14 / ACI 209 Method

As previously discussed, Pauw (1960) proposed an empirical relationship that correlated the modulus of elasticity of concrete to the square root of compressive strength and unit weight to the 1.5 power. The data set compiled by Pauw, shown in Figure 6-3, comprised mostly structural lightweight concretes with only 52 data points representing normal-weight concrete. The prediction equation recommended by Pauw, approximately represented by the linear regression displayed in Figure 6-3, is as follows:

$$E_c = 33 w^{1.5} \sqrt{f'_c} \tag{6-5}$$

where

E_c = static elastic modulus of concrete (psi);

w = equilibrium unit weight of concrete (pcf); and

f'_c = concrete compressive strength (psi).

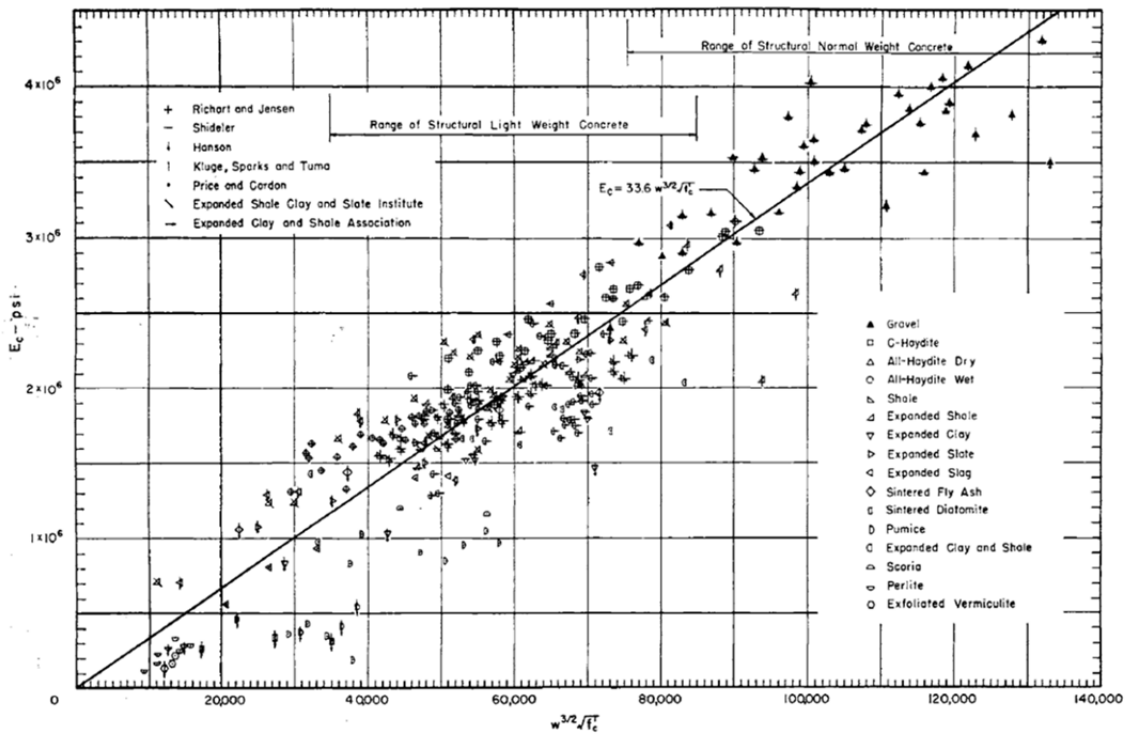

Figure 6-3: Historic Data Set Compiled by Pauw (1960)

Equation 6-5 in its original form is still specified in the building code requirements of ACI 318-14 (ACI Committee 318 2014) as well as in the guidance of ACI 209R-92 (ACI Committee 209 2008). While the original work of Pauw did not explicitly specify the appropriateness of the proposed equation for different concrete ages, ACI 209R-92 clarifies that Equation 6-4 may be applied to concrete strengths at any given age (either known or estimated by the time-development expressions previously discussed in Section 5.2.3). Equation 6-5 can be further simplified to the form of Equation 6-3 by including an assumption of concrete unit weight, as is explored later in this chapter. Hinkle (2006), Brown (1998), and French and O'Neill (2012) recommended the use of Equation 6-5 for precast, prestressed concrete as a result of independent experimental work.

6.2.3.2 AASHTO LRFD (2014) / NCHRP Report 496 Method

As a result of work conducted by Tadros et al. (2003) as part of NCHRP research project 18-07, the following prediction equation for elastic modulus was adopted in the 2005 edition of the AASHTO LRFD Bridge Design Specifications:

$$E_c = 33{,}000 \cdot K_1 \cdot w^{1.5} \sqrt{f'_c} \tag{6-6}$$

where

E_c = static elastic modulus of concrete (ksi);

K_1 = correction factor for source of aggregate;

w = unit weight of concrete (kcf); and

f'_c = concrete compressive strength (ksi).

Equation 6-6 remains in its original form in the 2014 edition of the AASHTO LRFD Bridge Design Specifications (AASHTO 2014). With the exception of the inclusion of a K_1 factor to account for aggregate stiffness variations, Equation 6-6 is functionally identical to Equation 6-5, and therefore may be used with the same time-dependent strength growth provisions previously reviewed.

As part of the work of NCHRP Report 496, Tadros et al. (2003) also proposed an additional modifier, K_2, intended to provide either an upper or lower-bound statistically-based value depending on the purpose of the computation. While an upper bound value corresponding to a 90th percentile would yield conservative results for a crack control analysis, a lower bound 10th percentile value may be more appropriate for prestress loss or deflection computations. Tadros et al. (2003) recommended various empirically calibrated values for K_2—although the lack of continuity among K_2 values calibrated

for four geographic regions instills little confidence in the usefulness of this concept to designers. Recent research by Nervig (2014) and Storm et al. (2013) supported the use of Equation 6-6 for precast, prestressed concrete as a result of independent experimental work.

6.2.3.3 Carrasquillo et al. (1981) / ACI 363 Method

Noting that existing prediction methods of the time period tended to overestimate the stiffness of high-strength concrete by as much as 15 percent, Carrasquillo et al. (1981) proposed the following expression:

$$E_c = \left(40{,}000\sqrt{f'_c} + 10^6\right)\left(w_c/145\right)^{1.5} \tag{6-7}$$

Despite literature frequently claiming that Equation 6-7 is the preferred method of ACI 363R-10 (ACI Commitee 363 2010), it is important to note that ACI 363R-10 presents eight differing prediction methods without showing clear preference for any particular one. However, to provide continuity with the work of previous researchers, Equation 6-7 is hereafter referred to as the ACI 363 method. Experimental work conducted by He (2013) has supported the use of Equation 6-7 for designers of precast, prestressed concrete.

6.2.3.4 *fib* Model Code 2010 Method

The provisions of the *fib* Model Code 2010 (fib 2010) are somewhat fundamentally different from the three previously reviewed prediction equations in two primary ways: (1) E_c is correlated to the cube root of concrete compressive strength instead of the square root and (2) the code includes a prediction equation intended only for use with 28-day concrete compressive strength values. While the first dissimilarity is of little

consequence to this effort, the second makes it somewhat difficult to accurately predict the elastic modulus of a given concrete at the time of prestress release. To explicitly follow the requirements of the *fib* Model Code to compute E_c at prestress release as a function of expected concrete release strength[2], it would seem that a designer must do the following:

1. Estimate the expected concrete release strength for a given project (based perhaps on the recommendations of Chapter 5) or code-prescribed guidance;
2. Utilize a code prescribed strength growth method to project an expected 28-day compressive strength;
3. Compute the elastic modulus using a code-prescribed equation based off the result of Step 2; and
4. Utilize a code prescribed elastic modulus-growth method to estimate the E_c at the time of prestress release.

To further complicate matters, the strength- and modulus-growth parameters contained in the *fib* Model Code (used in Steps 2 and 4) rely on a metric of equivalent age-making it impractical to use the above procedure at the time of design without accurate knowledge of a future curing temperature profile of the concrete. While earlier iterations of this analysis conducted by Hofrichter (2014) on a limited data set attempted to accommodate the above requirements, the results proved no more accurate than the approximation of the above procedure discussed next. For these reasons, the above procedure is judged

[2] An alternate approach is to rely on the prescribed 28-day overstrength by the *fib* Model Code in lieu of first estimating the expected concrete release strength and using the prescribed strength growth provisions. However, the later approach is included in the discussion above due to its similarly in form to the other prediction equations summarized in this section.

impractical for design purposes and, therefore, excluded from the remainder of the analysis effort in this chapter.

As an alternative to the above procedure, Rosa et al. (2007) suggested that the Model Code 2010 modulus prediction equation—although intended for use only with 28-day compressive strengths—be used to compute E_c at any age. This approach is analogous to U.S. practice, where Equations 6-5, 6-6, and 6-7 may be used for any given value of concrete compressive strength. After modifying accordingly and converting to U.S. Customary units, the Model Code 2010 prediction equation for elastic modulus is as follows:

$$E_c = 276{,}000 \cdot \alpha_E \cdot \sqrt[3]{f'_c} \tag{6-8}$$

where

E_c = static elastic modulus of concrete (psi);

α_E = aggregate correction factor (analogous to K_1); and

f'_c = concrete compressive strength (psi).

Recent research by Rosa et al. (2007) has supported the use of Equation 6-8 for precast, prestressed concrete as a result of experimental work.

6.2.3.5 Noguchi et al. (2009) Method

As a result of an examination of more than 3,000 relevant data points, Noguchi et al. (2009) proposed the following prediction equation for elastic modulus:

$$E_c = k_1 \cdot k_2 \cdot 4{,}860 \cdot \left(\frac{w_c}{150}\right)^2 \sqrt[3]{\frac{f'_c}{8.7}} \tag{6-9}$$

where

k_1 = correction factor for aggregate stiffness, and

k_2 = correction factor for supplementary cementing materials.

Simplifying Equation 6-9, assuming a unit weight of 150 pcf, and converting to equivalent units of Equation 6-8 gives:

$$E_c = k_1 \cdot k_2 \cdot 236{,}000 \cdot \sqrt[3]{f'_c} \tag{6-10}$$

where

E_c = static elastic modulus of concrete (psi);

k_1 = correction factor for aggregate stiffness;

k_2 = correction factor for supplementary cementing materials; and

f'_c = concrete compressive strength (psi).

It is interesting to note that the form of Equation 6-10 is similar to that of Equation 6-8 with a different coefficient.

6.3 Experimental Program

An experimental program was undertaken to compile a regionally robust data set of hardened concrete property data for use in evaluating existing E_c prediction equations and recommending the most suitable equation for regional use in precast, prestressed applications. This effort consisted of both an in-plant[3] testing effort and a companion laboratory phase, each of which are described separately in subsequent sections. While the concrete mixtures evaluated in the in-plant monitoring effort represented those mixtures used in commercial production of ALDOT bulb-tee products, the mixtures

[3] Here the term in-plant is used to mean testing conducted by researchers on-site at a regional precast, prestressed concrete producer.

examined in the laboratory study, although similar, were intentionally proportioned to isolate the effect of certain key variables of interest. For the purposes of this work, no distinction is made between test data obtained from self-consolidating concrete (SCC) versus data obtained from vibrated concrete (VC). This is because (1) a designer is unlikely to know whether a product will be fabricated with SCC or CVC and (2) previous researchers established only a small difference in elastic modulus between SCC and VC (Keske 2014) independent of unit weight and compressive strength.

6.3.1 Laboratory Study

This dissertation section details the efforts of a companion laboratory study completed as part of this research effort. While this laboratory effort was designed to yield data useful for both the analyses of this chapter (Chapter 6: Concrete Stiffness-Strength Relationships) as well as Chapter 7 (Creep and Shrinkage Behavior), only those parameters relevant to elastic modulus prediction are reported herein.

6.3.1.1 Summary of Work

In this laboratory study, six concrete mixtures were proportioned to represent typical mixtures currently used in Alabama precast, prestressed work. These six mixtures included three regional coarse aggregates and three varying combinations of supplementary cementing materials (SCMs) in typical substitution percentages. By maintaining a uniform target 18-hour compressive strength, uniform paste content, and uniform sand-to-total aggregate ratio (by volume) for all mixtures, it was possible to isolate certain key variables of interest in this study. Sampled specimens were exposed to either accelerated curing practices mimicking those of steam-curing methods used in precast, prestressed work or a standard curing protocol. Fresh concrete properties and

hardened properties at various key ages of interest (18 hour, 24 hour, and 28 days) were tested in accordance with ASTM C39 (2010) and ASTM C469 (2010) for each mixture.

6.3.1.2 Concrete Mixtures and Raw Materials

Upon making the decision to supplement the in-plant testing work with a concurrent laboratory phase, the question arose as to whether ALDOT-approved mixtures should be prepared strictly from approved proportions of if there may be potential advantages to further tailoring approved mixtures in order to isolate certain key variables. Recognizing that it was unlikely the much smaller mixer of the laboratory (8 cubic foot volume) could impart similar mixing energy to the larger mixing equipment of field producers, it was decided that further tailoring of approved mixtures would be required regardless to yield similar concretes to those observed in the field. For this reason, it was decided that six concrete mixtures would be proportioned according to the following criteria:

- Laboratory mixtures should be similar to typical ALDOT-approved mixtures (as discussed in Section 4.4.3) while also satisfying the requirements of ALDOT 170-82 (ALDOT 2009);
- Laboratory mixtures should use constituent materials identical to those most frequently used (or anticipated to be used in the future) by field producers including:
    - Three regional coarse aggregates;
    - Three combinations of supplementary cementing materials (SCMs) along with a full Type III cement control mixture;
- Mixtures should achieve a uniform compressive strength at the time of prestress release (using accelerated curing practices typical of the local

precast, prestressed industry) of approximately 6,700 psi as reported as the regional average by Hofrichter (2014); and

- Because these mixtures would later also be used for creep and shrinkage testing, all mixtures should have a uniform paste content and sand-to-total aggregate ratio (by volume).

As a consequence of the above criteria, the compressive strengths, while nearly identical at 18 hours, may vary differentially at other times of measurement. In addition, the water-cementitious materials ratio, w/cm, may vary between mixtures to account for different strength-development properties of various SCMs and the requirement to preserve a uniform paste content. As a result of extensive trial batching, the six mixtures shown in Table 6-1 were successfully proportioned to meet the above criteria.

Table 6-1: Laboratory Phase Concrete Mixture Proportions

Mixture ID	Type III Cement (pcy)	Grade 120 Slag Cement (pcy)	Class F Fly Ash (pcy)	Silica Fume (pcy)	Water (pcy)	*w/cm*	Coarse Agg. (pcy)	Fine Agg. (pcy)	*sand/total agg. (volume)*	*total agg. vol. (%)*	*paste vol.* (ft^3/cy)	HRWRA (oz/cwt)	HSA (oz/cwt)
DL-III	878	0	0	0	281	0.32	1,860	1,048	0.37	64	9.0	7.50	1
CL-III	878	0	0	0	281	0.32	1,860	1,048	0.37	64	9.0	7.75	1
GG-III	878	0	0	0	281	0.32	1,823	1,038	0.37	64	9.0	7.50	1
DL-SL	746	130 (15%)	0	0	278	0.32	1,860	1,048	0.37	64	9.0	6.75	1
DL-FA	754	0	132 (15%)	0	262	0.30	1,860	1,048	0.37	64	9.0	7.50	1
DL-FA/SF	606	0	142 (18%)	63 (8%)	276	0.34	1,860	1,048	0.37	64	9.0	7.75	1

Notes:

1. Percent substitutions noted for supplementary cementing materials (SCMS) are by weight of total cementitious materials.
2. High-range water reducer admixture (HRWRA) = Glenium 7700 and hydration-stabilizing admixture (HSA) = Masterset Delvo.
3. All aggregate weights in saturated-surface dry state.

The target 18-hour strength (accelerated cure), paste volume, and sand-to-aggregate ratio for the laboratory mixtures were determined by first preparing the DL-SL mixture. This mixture was closely based on an ALDOT-approved mixture used in a large percentage of precast, prestressed work within Alabama in recent years and seemed a logical choice to determine these target parameters. The DL-SL mixture contains a #67 dolomitic limestone, a #100 river sand, and a 15% (by weight) cement replacement with grade 120 slag cement. Next, the DL-III mixture was proportioned by (1) eliminating the slag cement substitution to arrive at a full cement mixture, and (2) modifying mixture proportions to meet the target 18-hour strength (while preserving uniform paste content and sand-to-aggregate ratio). The DL-III mixture uses the same #67 dolomitic limestone and #100 river sand as the DL-SL. Next, the proportions of the CL-III mixture were determined by trial batching. The CL-III mixture is essentially identical to the DL-III mixture, except the coarse aggregate is a different #67 dolomitic limestone. The proportions of GG-III were then determined in a similar manner—except the coarse aggregate included was a #67 crushed granite. Next, the proportions of the DL-FA and DL-FA/SF mixtures were determined by trial batching, both using the same #67 dolomitic limestone and #100 river sand as the DL-SL and DL-III mixtures. The DL-FA mixtures used a 15% by weight cement replacement with a Class F fly ash and the DL-FA/SF uses a ternary blend of 18% by weight cement replacement by Class F fly ash and 8% by weight silica fume.

The intent of the six mixtures described above (and shown in Table 6-1) was to isolate the effect of coarse aggregate types and SCM substitution on various hardened concrete properties. While it was judged impractical to include a fully expanded

experimental matrix (3 x 4 = 12 mixtures) as shown in Table 6-1, those combinations designated by a check mark were included in the experimental design. By comparing the relative effect of SCM variants on the DL-III control mixture, it was hoped that the effect of SCM substitution, if any, on the CL-III and GG-III mixtures could be estimated from experimental results.

Table 6-2: Experimental Matrix of Laboratory Mixtures

		Cement Replacement Variants			
		Type III Cement	**15% Slag Cement Replacement**	**15% Class F Fly Ash Replacement**	**18% Class F Fly Ash and 8% Silica Fume Replacement**
Coarse Aggregate Variant	**DL**	√	√	√	√
	CL	√			
	GG	√			

6.3.1.3 Mixture Preparation

Laboratory concrete mixing activities conducted as part of this research project were completed in accordance with the general requirements of ASTM C-192: *Standard Practice for Making and Curing Concrete Test Specimens in the Laboratory* (ASTM 2014). The specific mixing procedure employed for all mixtures was as follows:

1. Butter mixer
2. Add rock and sand
3. Start mixer on high speed
4. Add headwater (80%)
5. Mix for 2 minutes, stop mixer
6. Add cementitious materials, start mixer

7. Add tailwater (20%)
8. Add Hydration-stabilizing admixture (HSA)
9. Mix for 1 minute
10. Add high-range water reducer admixture (HRWRA) initial dose
11. Mix for 2 minutes
12. Rest for 3 minutes
13. Mix for 2 minutes
14. Sample fresh properties, if acceptable – done.
15. Re-dose HRWRA
16. Mix for 1 minute
17. Rest for 1 minute
18. Mix for 1 minute
19. Sample fresh properties, if acceptable – done.
20. Repeat 15-19 as necessary.

An important consideration in the laboratory mixing program was whether the above mixing procedure would generate sufficient mixing energy to break down the agglomerations of the bulk-densified silica fume typically used in field-batching of precast, prestressed concretes. While Holland (2005) notes that a modification to the mixing time noted in ASTM C192 can be used to ensure sufficient dispersion of bulk-densified silica fume for laboratory operations, changes to the above mixing durations for silica fume mixtures may be undesirable due to their potential alter mixture air content (and therefore potentially shift compressive strengths). To avoid this potential source of uncontrolled error, a density-controlled silica fume (a less dense form of silica fume) was

selected for use for mixing operations to preserve the above mixing durations for all mixtures.

6.3.1.4 Sampling and Curing Procedures

For each mixing cycle, thirteen 6" x 12" cylinder specimens were sampled in accordance with ASTM C192. After initial set (approximately 4 hours after concrete production), ten of these cylinders were exposed to an elevated curing temperature profile by the use of a *SURECURE* control system, as shown in Figure 6-4. In accordance with the requirements of ALDOT 367 (ALDOT 2010) and typical practice observed plant production, specimens were exposed to a linearly increasing temperature profile (increasing at a rate of 20.5°F hourly) up to a maximum temperature of approximately 150°F.

Figure 6-4: *SURECURE* Jacket for Accelerated Curing

After the maximum temperature was reached (approximately 8 hours after sampling), this temperature was maintained through the time of cylinder testing—either 18 or 24 hours after mixing. Chapter 7 (Early-Age Creep and Shrinkage Behavior) includes computed maturities for each loading event. The three remaining 6" x 12" cylinder specimens were exposed to standard curing conditions in accordance with ASTM C192 (2014) until the time of testing at 28 days after production.

6.3.1.5 Fresh and Hardened Concrete Properties Testing Plan

As noted in the mixing procedure of Section 6.3.1.3, fresh properties including temperature, slump, air content, and unit weight were sampled for each mixing iteration performed in the laboratory. While fresh properties were mainly documented for quality-control purposes, the unit weight recorded for each mixture is instrumental to the analysis efforts of this chapter. Where unit weights were not recorded (due primarily to equipment malfunction), estimates of unit weight were computed from mixture proportions and adjusted for measured air content.

The laboratory portion of this research effort was intended to simulate plant operations as closely as possible. Accordingly, two ages of simulated prestress release were selected based on the historical data set compiled by Hofrichter (2014) documenting the chronological time to prestress release for 1,917 girder concrete placement events. These two chronological ages were 18.0 hours (the approximate average of the primary peak of Figure 4-10) and 24.0 hours (an upper-bound value capturing 99.5 percent of the data of the same primary peak). At both of these ages, concrete compressive strength and modulus of elasticity were measured (in accordance with ASTM C39 and ASTM C469, respectively) for the accelerated-cured specimens. In addition, these same hardened properties were tested at 28 days for the cylinders receiving subjected to standard curing conditions. A concrete cylinder prepared for modulus of elasticity testing is shown in Figure 6-5.

Figure 6-5: Cylinder Prepared for Elastic Modulus Testing

6.3.1.6 Ungrouped Laboratory Data Set

The ungrouped data set compiled as a result of experimental effort described above is shown below in Figures 6-6 and 6-7. For the purposes of this section, both the 18-hour and 24-hour release measurements are combined. The measured relationship between modulus of elasticity and concrete compressive strength (independent of unit weight) is shown in Figure 6-6. Also shown for reference is the prediction equation proposed by Pauw (1960) assuming a unit weight of 150 pcf.

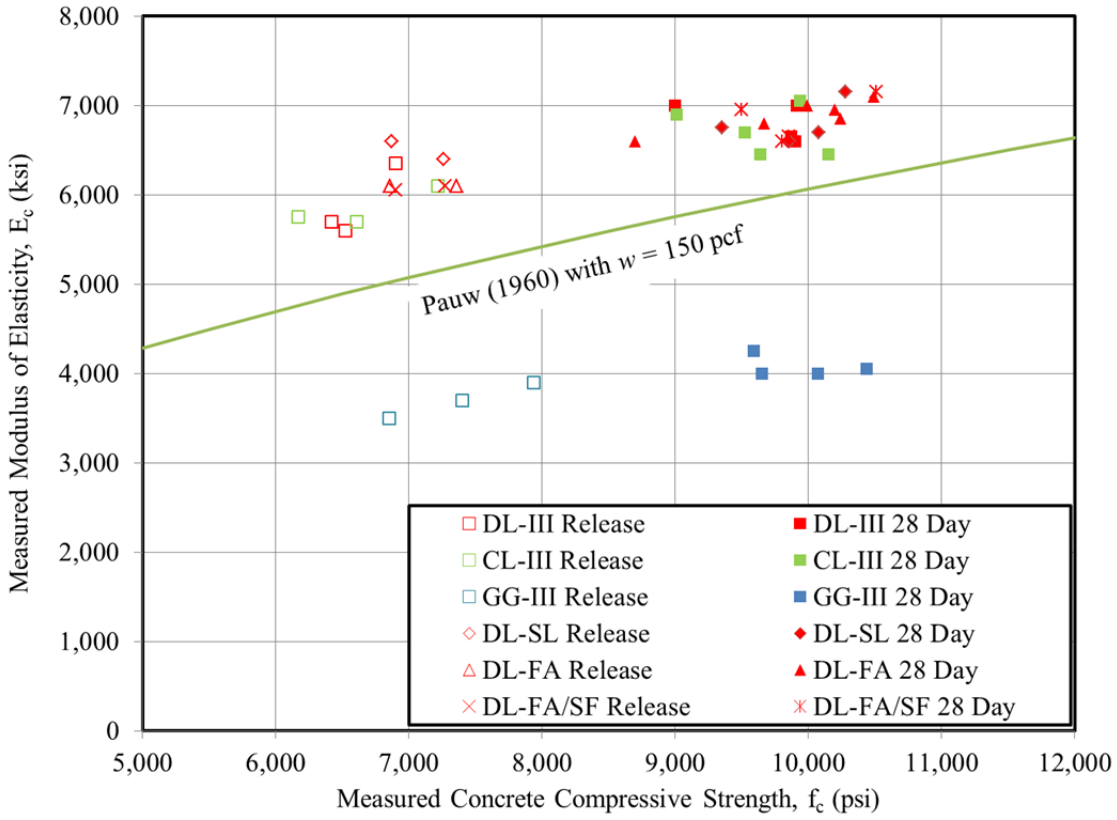

Figure 6-6: Ungrouped Stiffness-Strength Data from Laboratory Study Neglecting Effect of Unit Weight

The same data shown above is displayed in a somewhat different form in Figure 6-7. While the vertical axis remains the measured modulus of elasticity, E_c, the horizontal axis is now the quantity $\left(w^{1.5} f_c^{\,0.5}\right)/10^3$. Recall, this is the method Pauw used (Figure 6-3) in order to perform a simple linear regression to determine the long-used coefficient of 33.0.

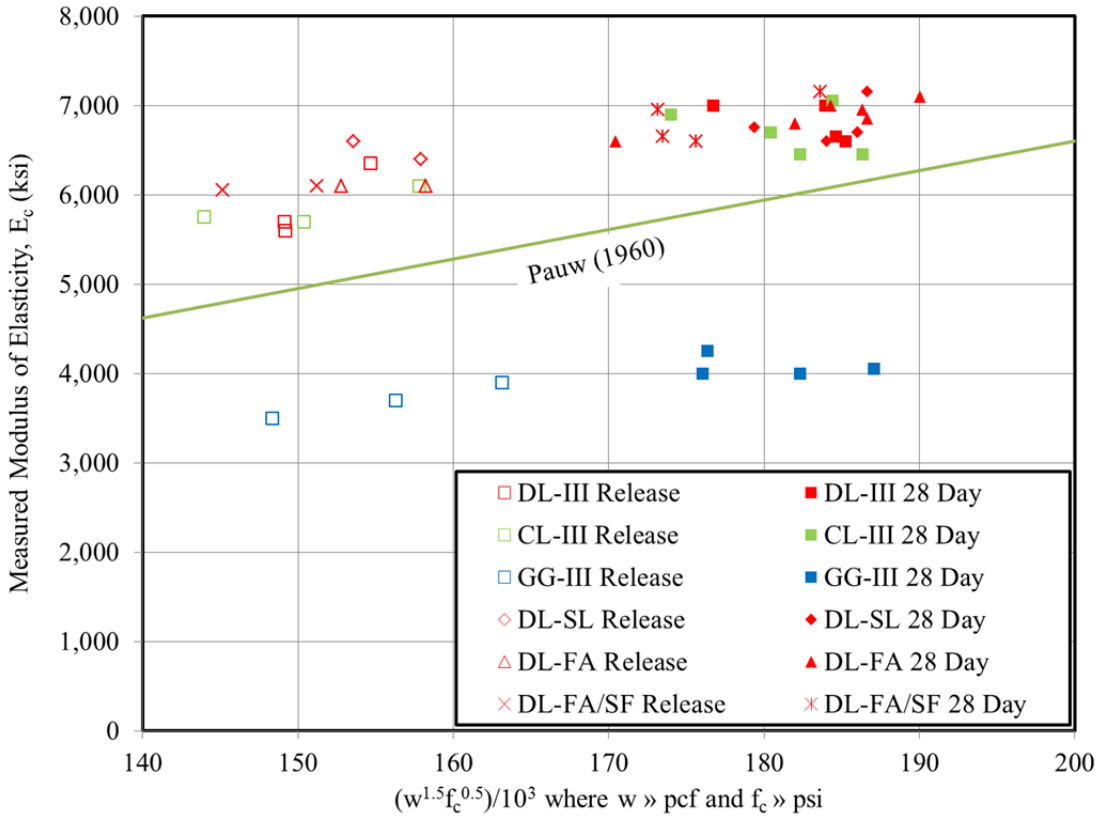

Figure 6-7: Raw Stiffness-Strength Data from Laboratory Study Including Effect of Unit Weight

6.3.2 Field Data Collection

The field data collection effort of this investigation consisted of in-plant monitoring of nine production cycles of ALDOT bulb-tee precast, prestressed concrete bridge girders occurring with the three year period spanning from 2012 to 2015. These in-plant efforts consisted of sampling fresh and hardened properties, the installation and monitoring of sensors in bridge girders both during and after fabrication, and measurement of girder cambers by surveying at various ages of interest. While select fresh and hardened properties of sampled girder concretes are discussed in this section, the remainder of the field-monitoring work is discussed in its entirety and used as a basis for comparison against girder behavior predictions in Chapter 10 of this dissertation.

6.3.2.1 Summary of Work

In this field data collection effort, nine production cycles of ALDOT bulb-tee precast, prestressed bridge girders occurring at two different producers were monitored by researchers. For each production cycle, girder concretes were randomly sampled twice—at least once for every 50 cubic yard of production in accordance with the requirements of ALDOT-367 (ALDOT 2015). Sampled specimens were then subjected to a variety of curing treatments (including steam field curing, standard lime-bath curing, field lime-bath curing, and selected combinations thereof) until the time of hardened property testing. Testing for compressive strength and modulus of elasticity (in accordance with ASTM C39 and ASTM C469, respectively) was conducted at (1) the time of field girder release, (2) 24 hours after girder production, and (3) 28 days after girder production. Research procedures were designed to minimize impact on the typical girder production cycle.

6.3.2.2 Mixtures and Raw Materials

Girder concretes for the field-monitored projects were produced by precast, prestressed producers using typical production practices and mixtures with no influence from the research team. Mixture proportions for the field-monitored projects are summarized in Table 6-3. The mixture used by Plant C in field production most closely resembled the DL-FA/SF mixture of the laboratory portion of this study. Both mixtures contained a crushed dolomitic limestone coarse aggregate, a #100 natural sand, and preserved similar ratios of sand-to-total aggregate (by volume), total aggregate volume (percent), and paste volume. However, the mixture used by Plant C in field production had a lower *w/cm* than the laboratory mixture (0.27 versus the 0.34) and used a #78 dolomitic limestone instead of the #67 used in the DL-FA/SF laboratory mixture. The mixtures used by Plant A in

production cycles 2-6 and 7-9, respectively, most closely resembled the laboratory mixture DL-SL. In fact, by virtue of the DL-SL being based off earlier iterations of the field mixtures used by Plant A, these three mixtures were essentially identical—containing equal proportions of Type III cement, Grade 120 slag cement, #67 dolomitic limestone, #100 natural sand, and water.

While the field monitoring effort of this study allows for comparisons between only the two types of mixtures shown in Table 6-3 (essentially the DL-SL and DL-FA/SF mixtures), the laboratory study allows for comparisons to be among a range of mixtures (DL-FA, DL-III, CL-III, and GG-III) that either have historically been used or could be used in the future for precast, prestressed concrete production within Alabama.

Table 6-3: Mixture Proportions for On-site Production Cycles

Mixture ID	Type III Cement (pcy)	Grade 120 Slag Cement (pcy)	Class F Fly Ash (pcy)	Silica Fume (pcy)	Water (pcy)	*w/cm*	Coarse Agg. SSD (pcy)	Fine Agg. SSD (pcy)	*sand/total agg. (volume)*	*total agg. vol. (%)*	*paste vol.* (ft^3/cy)	HRWRA #1 (oz/cwt)	HRWRA #2 (oz/cwt)	HSA (oz/cwt)
Plant C (Field Production Cycle 1)	745	0	135 (14%)	75 (8%)	258	0.27	1,665 (#78 Dolomitic Limestone)	1,085 (#100 River Sand)	0.40	61	9.4	5.25	N/A	1.25
Plant A (Field Production Cycles 2-6)	751	133 (15%)	0	0	282	0.32	1,861 (#67 Dolomitic Limestone)	1,048 (#100 Natural Sand)	0.37	62	9.1	6.0	4.50	1.0
Plant A (Field Production Cycles 7-9)	751	133 (15%)	0	0	277	0.31	1,861 (#67 Dolomitic Limestone)	1,048 (#100 Natural Sand)	0.38	63	9.0	9.0	N/A	1.0

Notes:

1. Percent substitutions noted for supplementary cementing materials (SCMS) are by weight of total cementitious materials.
2. Plant C (All Cycles): HRWRA #1 = Glenium 7700 and HSA = Pozzolith 100-XR.
3. Plant A (Cycles 2-6): HRWRA #1 = ADVA Cast 575, HRWRA #2 = ADVA Cast 555, HSA = Recover
4. Plant A (Cycles 7-9): HRWRA #1 = Glenium 7700, HSA = Delvo

6.3.2.3 Sampling and Curing Procedures

The sampling effort detailed herein is independent and in addition to that completed by the producer and ALDOT quality control personnel. For each on-site production cycle, the research team randomly sampled two sets of thirteen 6" x 12" cylinders (26 cylinders total) in accordance with ASTM C31 (ASTM 2009). Twenty of the sampled cylinders were stored within the girder formwork and exposed to the field steam curing of the girder product. The other six cylinders were immediately transported to the on-site testing laboratory after completion of sampling and exposed to standard curing conditions by immersion in a lime-saturated water bath regulated to 73.5°F. At the time of form removal, the 20 field-cured cylinders were transferred into a preheated lime-saturated water bath[4] to allow for a gradual transition to ambient temperature until the time of testing.

6.3.2.4 Fresh and Hardened Concrete Properties Testing Plan

Upon delivery of the concrete from the on-site mixing facility, fresh properties (including temperature, slump, and air content) were tested by plant quality control and ALDOT personnel to determine the acceptability of the concrete batch in accordance with the requirements of ALDOT 367 (ALDOT 2010). Due to the large number of concurrent activities required to be completed by researchers, it was not possible to measure the unit weights of the girder concretes during production and thus, unit weights used in the analyses of this chapter are computed based on ALDOT-approved mixture designs and adjusted for measured air content.

[4] The method used for preheating the field lime-saturated water bath was to store the bath adjacent to the girder product under the tarp during steam curing. This practice resulted in varying temperatures of the lime-saturated water bath, but resulted in temperatures approaching those of the gross girder concrete for a given placement event.

The timing of prestress release was determined by plant and ALDOT personnel. At the approximate time of prestress release, concrete compressive strength and modulus of elasticity were tested by the researchers for the first set of sampled cylinders (3 cylinders per sampling location = 6 cylinders total). Approximately 6 hours thereafter (at a time of 24 hours after girder production), compressive strength and modulus of elasticity were again tested for a second set of sampled cylinders (3 cylinders per sampling location = 6 cylinders total). The two remaining cylinder sets (6 field cure + 6 standard cure = 12 cylinders total) were transported back to the laboratory for compressive strength and modulus of elasticity testing at the age of 28 days. Once transported back to the laboratory, field-cured cylinders were stored in a covered outdoor lime-saturated bath (to capture relative ambient temperature variations similar to those experienced by the actual girders) while standard-cure cylinders were stored in a moist room until the time of testing.

6.3.2.5 Field Data Set

The data set compiled as a result of the experimental effort described above is shown in Figures 6-8 and 6-9. As shown, there is significantly more variation in the strengths observed for the plant-produced concrete than for the laboratory concrete. The E_c prediction equation recommended by Pauw (1960) is also shown for reference.

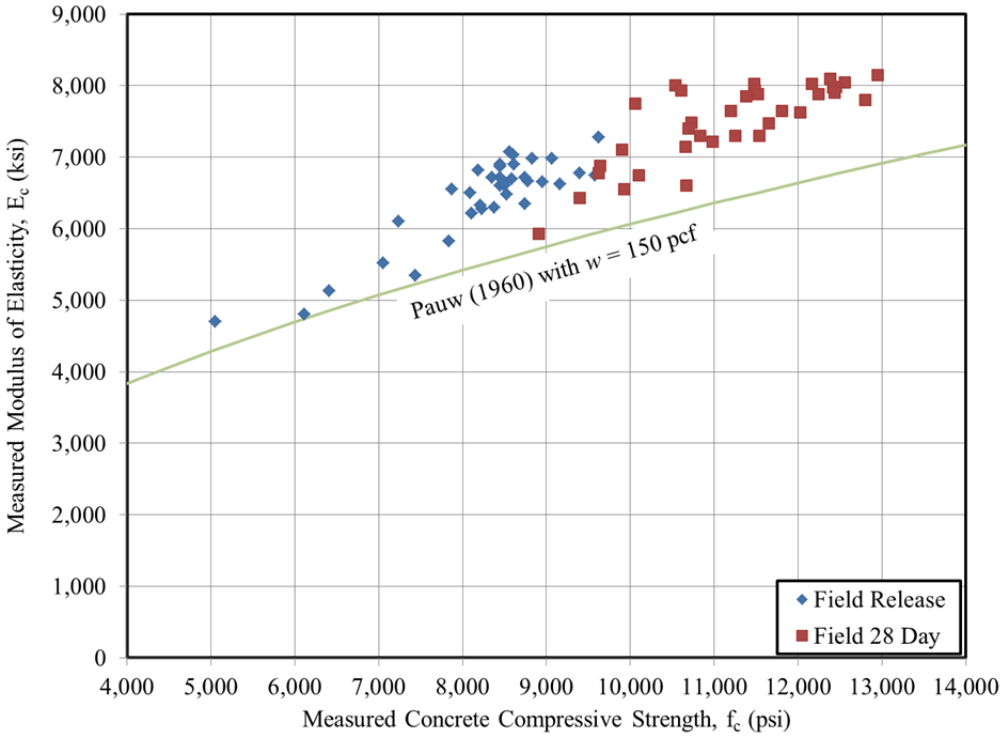

Figure 6-8: Stiffness-Strength Data from Field Study Neglecting Effect of Unit Weight

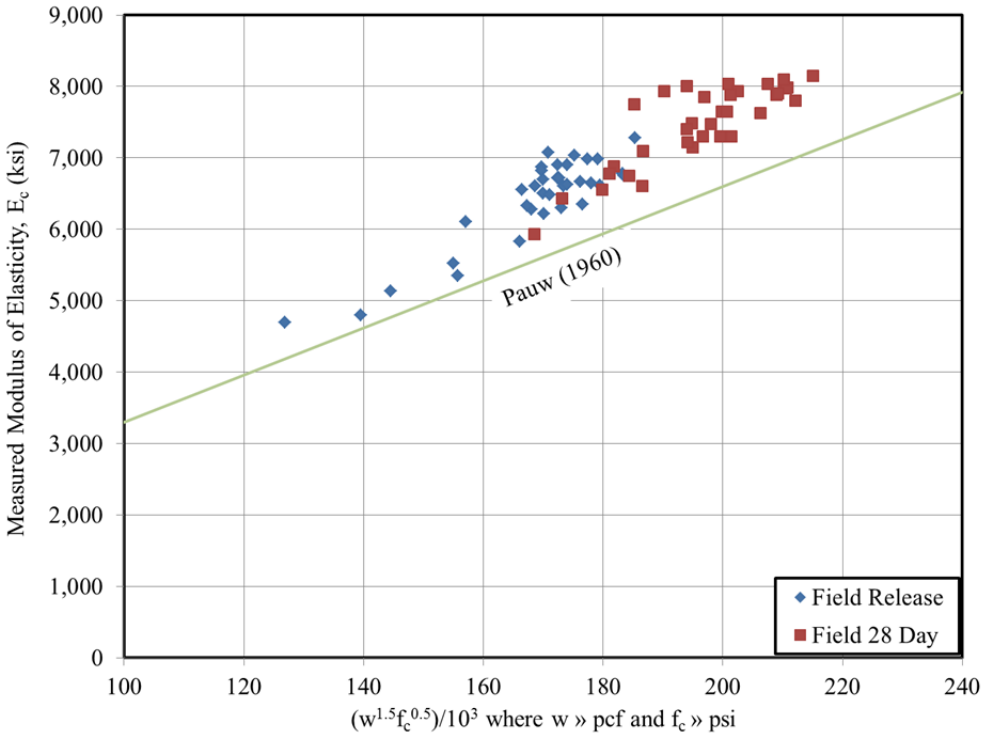

Figure 6-9: Stiffness-Strength Data from Field Study Including Effect of Unit Weight

6.3.3 Additional Data Sources

As a result of the experimental efforts detailed in the laboratory phase of this project and the in-plant testing phase, 110 elastic modulus data points were compiled. While this sample represents a relatively robust data set, two researchers (Keske 2014] and Boehm et al. [2010]) previously gathered similar field data as part of independent experimental efforts. This section provides a brief summary of the experimental efforts and data collection techniques employed by Keske (2014) and Boehm et al. (2010) to compile their respective data sets.

6.3.3.1 Keske (2014)

As part of the experimental effort to investigate the differences between SCC and VC in precast, prestressed bridge girders, Keske (2014) monitored 13 girder placement events at Plant A—conducting hardened material property testing (both compressive strength and E_c) at the time of prestress release and 28 days after casting. Sampled cylinder specimens were field cured (within the girder formwork) until the time of prestress release. Specimens were then exposed directly to ambient conditions until the time of 28-day testing. In this project, two sampling locations were selected for each placement event—yielding a total of 26 additional data points useful to the stiffness-strength analysis performed later in this chapter.

6.3.3.2 Boehm et al. (2010)

Prior to the work of Keske (2014), Boehm et al. (2010) monitored a girder production effort at Plant A as part of a study aimed at evaluating the structural performance of SCC in precast, prestressed bridge girders. Cylinder sampling and curing methods were

identical to those used by Keske (2014), resulting in a total of 12 data points useful to supplement the data set used in this chapter.

6.3.4 Complete Compiled Data Set For Stiffness-Strength Analysis

The full data set compiled as a result of the work described in Sections 6.3.1 through 6.3.3 consists of 148 total data points as shown in Figures 6-10 and 6-11. This complete data set is also included in Appendix D for reference.

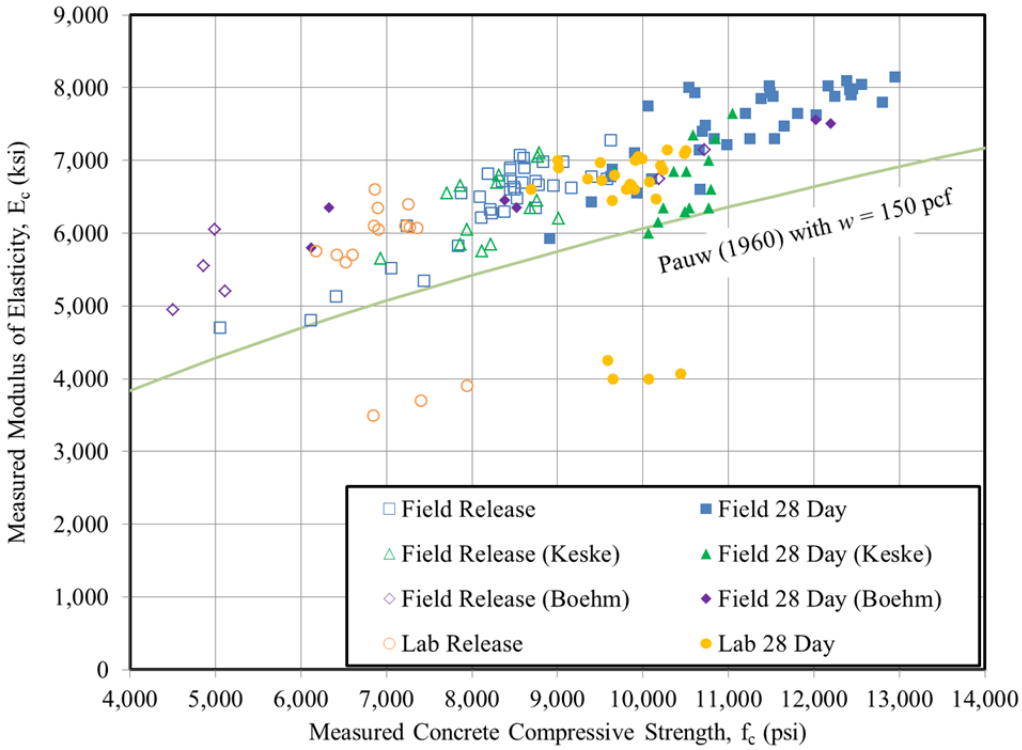

Figure 6-10: Stiffness-Strength Data Neglecting Effect of Unit Weight

The data set shown in Figures 6-10 and 6-11 represents a wide range of compressive strengths and appears to be a relatively robust regional data set.

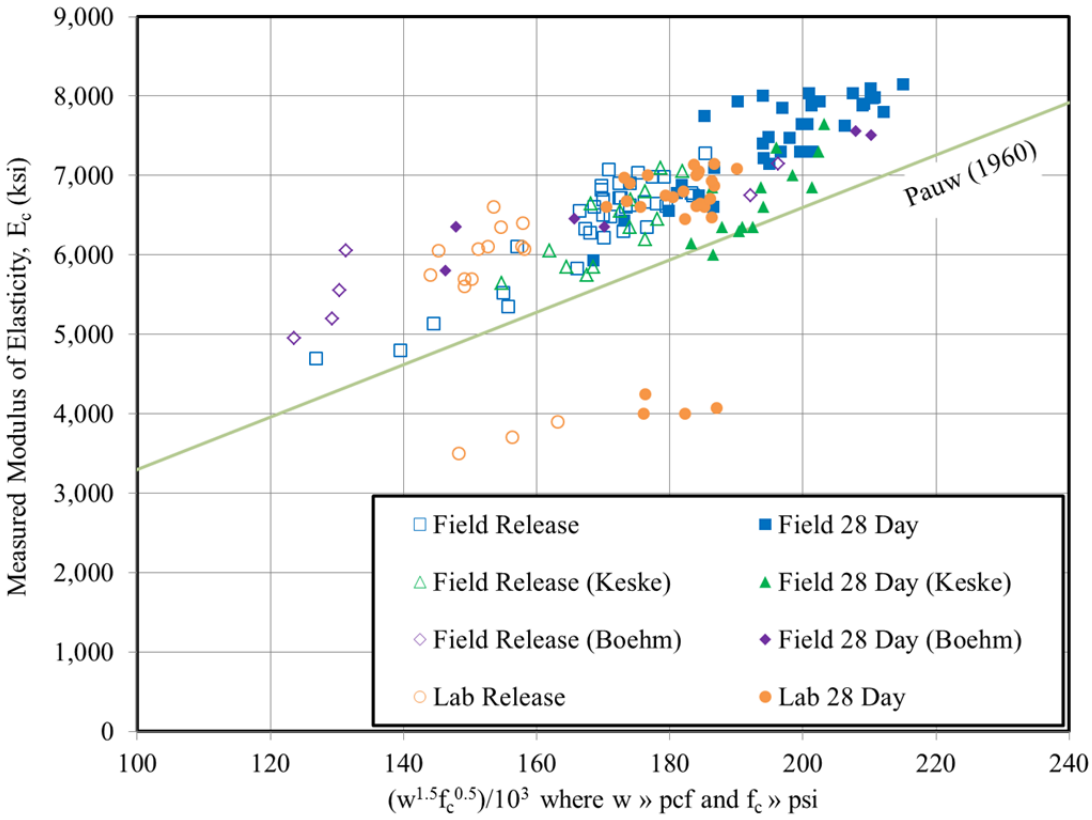

Figure 6-11: Stiffness-Strength Data Including Effect of Unit Weight

6.4 Presentation and Analysis of Results

This section details the methodology used to analyze the compiled stiffness-strength data set. First, a preliminary statistical analysis is performed on selected variables of the raw data set to establish logical groupings for use in the remainder of the analysis of this chapter. Then, for each grouping, the experimental data set is used to appropriately calibrate any of the four previously discussed prediction models capable of calibration. Finally, the results of the prediction equations for E_c are compared to the measured data in an effort to identify the most accurate prediction equations for use by designers. A brief discussion follows the analysis, identifying an uncontrolled variable in the project that may be responsible for an unexpected trend observed in both this research project and previous work by others.

A brief discussion on the analysis approach selected in this study is warranted. Recall, the goal of this work is to identify the E_c prediction equation most appropriate for use in predicting the stiffness of concrete typical of precast, prestressed concrete elements. A common approach by previous researchers (in the absence of a standardized test method) is to (1) generate or compile a data set similar to that of this study, (2) select an E_c prediction equation—most commonly the AASHTO LRFD Equation in American practice, and (3) calibrate the candidate equation by selecting a value of K_1 providing the best agreement between predicted and measured modulus values. While this is a convenient approach, this methodology does little to explore the correctness of the mathematical form of the prediction equation and also tends to incorrectly attribute all prediction error to the aggregate stiffness correction factor, K_1. This practice may be partially unavoidable, it is a troublesome flaw of not having a standardized test method to calibrate K_1 factors. Other researchers (e.g. Hofrichter 2014) have attempted to calibrate the AASHTO LFRD Equation to specified strength levels, f'_c, instead of measured strength levels, f_c. This practice results in a "calibrated" K_1 aggregate stiffness factor that incorrectly includes the effect of strength amplification (as discussed in Chapter 5 of this dissertation). The inconsistencies discussed above make it difficult and unreliable to compare K_1 factors as calibrated by previous studies.

In an effort to avoid the complications discussed above, the following precautions have been taken in this research effort: (1) the effect of overstrength (as explored in Chapter 5) is wholly decoupled from the Chapter 6 efforts of calibrating stiffness prediction equations, and (2) a variety of prediction models are first calibrated to

the experimental data (by linear regression) and then evaluated for relative accuracy by a comparison of the standard error of the estimate (SEE). Using this approach not only facilitates accurate calibrations of existing prediction equations to the experimental data set, but also allows for comment on the relative correctness of the mathematical form of the four candidate prediction equations explored herein.

6.4.1 Preliminary Analysis and Data Groupings

Prior to calibrating the candidate prediction equations, it was first necessary to perform an analysis of the raw data set to identify statistically significant variables for grouping. The final data set (as shown in its final form in Appendix D) consisted of 148 data points each including time of measurement, coarse aggregate type, curing method, unit weight, measured compressive strength, and measured modulus of elasticity. While convenient to have so many variables in the data set, it made it difficult to perform a statistical analysis involving the variables suspected to be significant. It was decided that a single coefficient would be computed to represent a hypothesized relationship between unit weight, compressive strength, and E_c for each data point. Rearranging a portion of Pauw's expression (Equation 6-5), the following coefficient, c, was computed for each data point:

$$c = \frac{E_{c,measured}}{\left(\frac{w_{measured}^{1.5} \sqrt{f_{c,measured}}}{1000} \right)} \tag{6-11}$$

Where

$E_{c,measured}$ = measured modulus of elasticity for a given data point (ksi);

$w_{measured}$ = measured unit weight for a given data point (pcf); and

$f_{c,measured}$ = measured compressive strength for a given data point (psi).

The c value of Equation 6-11 represents the calibrated coefficient of Pauw's equation, equal to a value of 33 from his analysis. The use of Pauw's empirical relationship here is an analytical technique to allow simplification of this statistical analysis. By comparing the relative values of the coefficient c for varying experimental treatments, standard statistical tests (i.e. two-sample two-sided t-tests and ANOVA-tests) may be used to identify statistically significant groupings of the data set.

The first hypothesis explored using this technique was that the type of coarse is a statistically significant predictor of elastic modulus. Using the three hypotheses shown in Table 6-4 (1a to 1c) and the corresponding statistical tests of the compiled data set, there was strong evidence (at a significance level of $\alpha = 0.05$) that the mean of the coefficient c for concrete mixtures with dolomitic limestone was different than for those mixtures with crushed granite.

Table 6-4: Effect of Coarse Aggregate Type on Elastic Modulus

Null Hypothesis:	Result ($\alpha = 0.05$)
1a. The difference in means of the coefficient c between concrete mixtures produced using dolomitic limestone and crushed granite is zero for the entire data set.	***Reject*** ($p \leq 0.001$) (paired t-test assuming unequal variances)
1b. The difference in means of the coefficient c between concrete mixtures produced using dolomitic limestone and crushed granite is zero for the release data set.	***Reject*** ($p \leq 0.001$) (paired t-test assuming unequal variances)
1c. The difference in means of the coefficient c between concrete mixtures produced using dolomitic limestone and crushed granite is zero for the 28-day data set.	***Reject*** ($p \leq 0.001$) (paired t-test assuming unequal variances)

The above hypothesis testing suggested that the compiled data set should be divided by coarse aggregate type for the remainder of analysis efforts.

The next question was whether the time of measurement of a data point (either at prestress release or 28 days) was a significant variable in predicting E_c of a given concrete. For this purpose, the statistical procedure outlined in Table 6-5 was used– essentially comparing the likelihood that the mean value of the coefficient *c* was identical for the two ages of testing.

Table 6-5: Effect of Time of Measurement on Elastic Modulus

Null Hypothesis:	**Result (α = 0.05)**
2a. The difference in means of the coefficient *c* between the time of release and 28 days is zero for concrete mixtures using dolomitic limestone.	***Reject*** ($p = 0.005$) (paired t-test assuming unequal variances)
2b. The difference in means of the coefficient *c* between the time of release and 28 days is zero for concrete mixtures produced using crushed granite.	***Fail to Reject*** ($p = 0.13$) (paired t-test assuming unequal variances)

Note: For hypothesis 2b, n=3 and 4, respectively, making the results questionable due to small sample size.

The analysis of hypothesis 2a affirmed strong statistical evidence that the coefficient *c* differed between the two measurement ages considered for concretes produced using dolomitic limestone. A similar analysis conducted for the crushed granite aggregate (hypothesis 2b) however, failed to detect a significant difference in means between testing ages. Due to the extremely small sample sizes available for use in hypothesis 2b (n=3 and n=4), the validity of this analysis is questionable. To be conservative, it was assumed that the failure to detect a difference in analysis 2b may be a Type II statistical error caused by the small sample size. As a result of the work summarized in Table 6-5, the stiffness-strength data set is grouped by time of measurement for the analysis efforts of the remainder of this chapter.

Another logical question to explore prior to combining the data compiled from four independent efforts was if curing method was a significant factor in predicting concrete stiffness. Because different curing regimes were only used for the 28-day time of testing, the analysis summarized in Table 6-6 focuses only on this measurement time.

Table 6-6: Effect of Curing Conditions on Elastic Modulus

Null Hypothesis:	**Result (α = 0.05)**
3a. The difference in means of the coefficient *c* at 28 days among the four curing conditions is zero for concrete mixtures using dolomitic limestone.	***Reject*** ($p \leq 0.001$) (ANOVA single factor)
3b. The difference in means of the coefficient *c* at 28 days among the three curing conditions (omitting that used by Keske [2014] and Boehm et al., [2010]) is zero for concrete mixtures using dolomitic limestone.	***Fail to Reject*** ($p = 0.37$) (ANOVA single factor)

Using two ANOVA single factor tests with varying input groupings, it was affirmed that, for concretes containing dolomitic limestone aggregate, there existed strong statistical evidence that the means of the coefficient *c* differed between (1) the work of Keske (2014) and Boehm et al. (2010) and (2) the experimental work conducted in this research study. However, it is also important to note that the work of Keske (2014) and Boehm et al. (2010) included SCC in addition to VC, while the experimental work conducted in this research effort included only VC. The work reflected in Table 6-6 suggests that either (1) curing method (specifically, the difference between air-dried specimens versus all other moist curing methods used in this work) is likely a statistically significant predictor of concrete stiffness, (2) the difference detected above is due to differences between the elastic modulus of SCC and VC, or (3) a combination thereof. For the purposes of this project, the above difference was disregarded in order to provide a data set including both

VC and SCC mixtures—as is likely most representative of the precast, prestressed industry in Alabama in future years.

A final consideration for grouping of data was to investigate if the presence of varying supplementary cementing materials (SCMs) was a significant predictor of the variability in E_c. For this purpose, the subset of the stiffness-strength data set generated by the controlled laboratory portion of this study was examined as shown in Table 6-7.

Table 6-7: Effect of Supplementary Cementing Material (SCM) on Elastic Modulus

Null Hypothesis:	**Result (α = 0.05)**
4a. The difference in means of the coefficient *c* at the time of release for the four variants of supplementary cementing materials (SCMs) is zero for concrete mixtures produced in the laboratory using dolomitic limestone.	***Fail to Reject*** ($p = 0.27$) (ANOVA single factor)
4b. The difference in means of the coefficient *c* at 28 days for the four variants of supplementary cementing materials (SCMs) is zero for concrete mixtures produced in the laboratory using dolomitic limestone.	***Fail to Reject*** ($p = 0.51$) (ANOVA single factor)

Note: For hypothesis 4a/b, results are questionable due to small sample size.

At both times of measurement, differences in the means of the coefficient *c* were unable to be detected as a result of the use of varying supplementary cementing materials. Due to the small sample sizes available for these analysis (n=3 and n=4 typically), the failure to detect a statistical difference by varying SCM shown in Table 6-7 is regarded as inconclusive—as opposed to a clear conclusion that varying SCM does not influence concrete stiffness. A study by Brooks (1999) similarly concluded that SCM usage in modest replacement percentages failed to cause an appreciable effect on E_c.

In summary, preliminary statistical manipulation of the stiffness-strength data set confirmed that it is logical to group the compiled data set by both aggregate type and time of testing for analysis purposes. This grouping approach is used in the analysis of

Section 6.4.2 (Concrete Stiffness at Prestress Release) and the analysis of Section 6.4.3 (Concrete Stiffness at 28 Days).

6.4.2 Concrete Stiffness at Prestress Release

This section details the analysis conducted in order to provide a recommendation of the most appropriate modulus of elasticity prediction equation for use during preliminary design to estimate the elastic stiffness at the time of prestress release. The analysis procedure used is this Section is outlined in Figure 6-12.

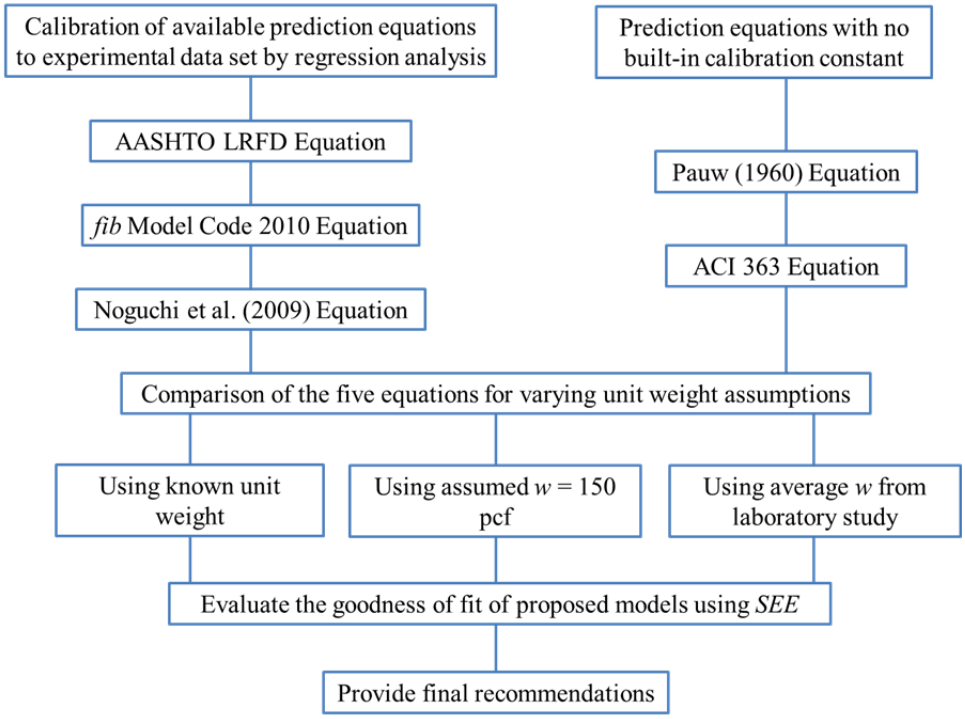

Figure 6-12: Analytical Procedure for Stiffness-Strength Data Set

As noted, first the three prediction equations that include potential calibration constants (AASHTO LRFD, *fib* Model Code 2010, and Noguchi et al. [2009]) are calibrated to the experimental data set. Next, the accuracy of the five available prediction equations is evaluated using the standard error of the estimate (SEE) for differing assumptions of unit weight.

6.4.2.1 Calibration of AASHTO LRFD Equation

The AASHTO LRFD prediction equation, as used in this dissertation, is calibrated in practically the same way Pauw (1960) empirically calibrated his equation. The experimental data for E_c at the time of prestress release, grouped by aggregate type, is shown below in Figure 6-13.

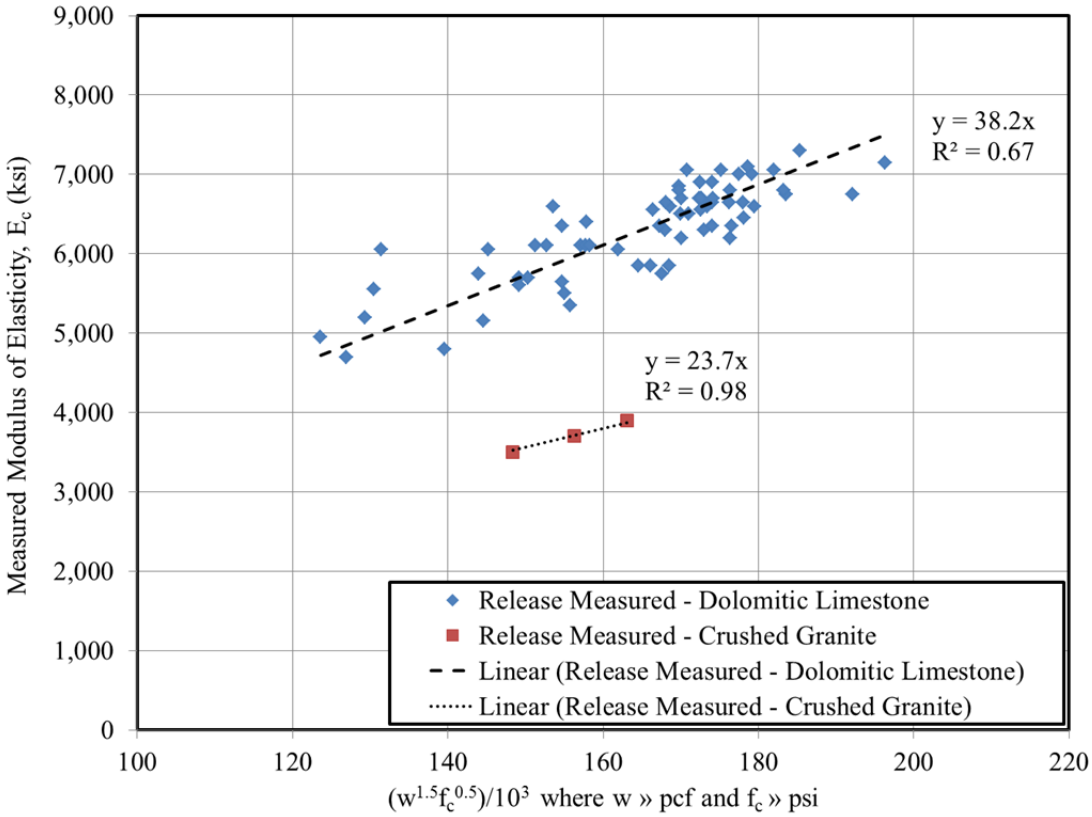

Figure 6-13: Calibration of AASHTO LRFD Equation for Prestress Release

Presenting the data on these axes allow for the use of a simple linear regression to calibrate the prediction equation. As shown, the appropriate coefficient for dolomitic limestone and crushed granite at the time of prestress release are 38.2 and 23.7, respectively. To determine the appropriate K_1 factor for each aggregate type, the previously noted coefficients need simply be divided by 33.0, yielding $K_1 = 1.16$ for dolomitic limestone and $K_1 = 0.72$ for crushed granite at the time of prestress release.

While the value for dolomitic limestone ($K_1 = 1.16$) agrees with typical ranges referenced by Mehta and Monteiro (2014) and the Model Code 2010 (fib 2010) for dense limestone aggregates, the calibrated value for crushed granite ($K_1 = 0.72$) is less than the $K_1 = 1.0$ typically expected for quartzitic aggregates (Mehta and Monteiro 2014). The topic of the crushed granite aggregate exhibiting less than expected stiffness is addressed in Section 6.4.5.

6.4.2.2 Calibration of *fib* Model Code 2010 Equation

In similar fashion to above, the *fib* Model Code 2010 prediction equation was also calibrated by a simple linear regression analysis as shown in Figure 6-14. By dividing the slope of the regression lines for each aggregate type by the leading coefficient of Equation 6-7, α_E values of 1.15 and 0.69 are computed for dolomitic limestone and crushed granite, respectively.

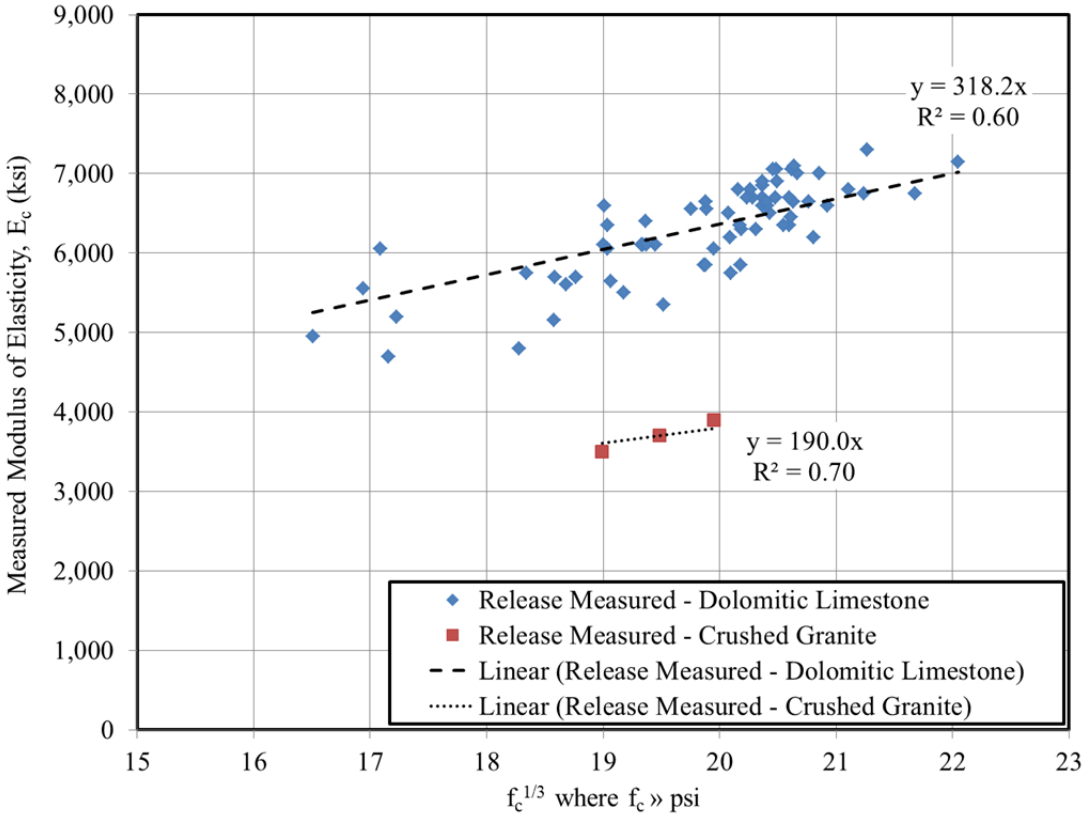

Figure 6-14: Calibration of *fib* Model Code 2010 for Prestress Release

6.4.2.3 Calibration of Noguchi et al. (2009) Equation

Finally, the Noguchi et al. (2009) prediction equation is calibrated in a similar manner. Recall, this prediction equation has two calibration factors—k_1 that accounts for the effect of aggregate stiffness variations and k_2 that accounts for the effect of supplementary cementing materials (SCMs). The factor k_2 is taken as 1.0 as a result of the statistical analysis of the laboratory data set reviewed in Section 6.4.1, that failed to detect a significant difference among SCM type. The factor k_1 is calibrated similarly to that of the *fib* Model Code 2010 as shown in Figure 6-15. Again, by dividing the slope of the regression line for each aggregate type by the leading coefficient of Equation 6-8, k_1 values for the dolomitic limestone and crushed granite were determined as 1.32 and 0.82, respectively.

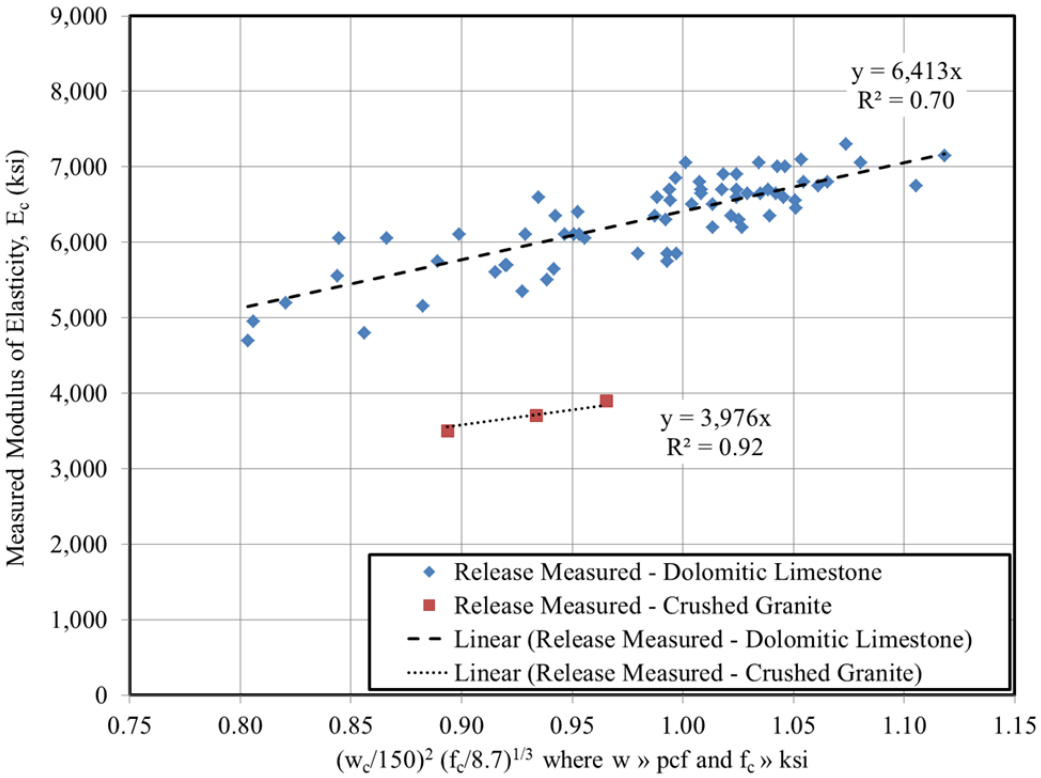

Figure 6-15: Calibration of Noguchi et al. (2009) for Prestress Release

6.4.2.4 Comparison of Available Prediction Equations

The final form of each of the five candidate prediction equations included in this study, as calibrated for use at the time of prestress release, is summarized in Table 6-8. The standard error of the estimate, *SEE*, is used to evaluate the relative goodness-of-fit of each prediction model to the stiffness-strength data set for varying assumptions of unit weight, *w*. An independent analysis is conducted for each aggregate type.

While the stiffness-strength data set compiled in this effort includes a known unit weight for each data point, this information is not available at the time of preliminary design. Therefore, the design engineer must estimate the unit weight of the concrete likely to be used in constructing the structural element. Possible assumptions for this purpose include (1) assume a unit weight of 150 pcf for precast concrete as recommended by Tadros et al. (2003), (2) assume a unit weight based on knowledge of typical regional mixtures, or (3) attempt to correlate the expected concrete strength, f_c^*, to unit weight using Equation 6-4, reproduced below, as developed by Al-Omaishi et al. (2009) and included in the 2014 AASHTO LRFD Bridge Design Specifications (AASHTO 2014).

$$w = 0.140 + \frac{f'_c}{1000} \leq 0.155 \tag{6-4}$$

Conveniently, alternative (1) and (2) are essentially identical, as the average of the mixtures included in the laboratory study is 149.9 pcf. Therefore, the following three assumptions for unit weight are used for the analyses of this section: (1) use known unit weight from data set, (2) assume unit weight of 150 pcf, and (3) use Equation 6-4 to estimate unit weight from expected (or measured in this case) compressive strength.

Table 6-8: Candidate Modulus Prediction Equations Calibrated for Prestress Release

Source	Prediction Equation	Nomenclature
Pauw (1960) / ACI 318-14 / ACI 209	$E_c = 33w^{1.5}\sqrt{f'_c}$	E_c = static elastic modulus of concrete (psi) w = equilibrium unit weight of concrete (pcf) f'_c = concrete compressive strength (psi)
AASHTO LRFD (2014)	$E_c = 33{,}000 \cdot K_1 \cdot w^{1.5}\sqrt{f'_c}$	E_c = static elastic modulus of concrete (ksi) K_1 = correction factor for source of aggregate = 1.16 for dolomitic limestone = 0.72 for crushed granite w = unit weight of concrete (kcf) f'_c = concrete compressive strength (ksi)
ACI 363 Method	$E_c = \left(40{,}000\sqrt{f'_c} + 10^6\right)\left(w_c/145\right)^{1.5}$	E_c = static elastic modulus of concrete (psi) w_c = unit weight of concrete (pcf) f'_c = concrete compressive strength (psi)
fib Model Code 2010	$E_c = 276{,}000 \cdot \alpha_E \cdot \sqrt[3]{f'_c}$	E_c = static elastic modulus of concrete (psi) α_E = aggregate correction factor = 1.15 for dolomitic limestone = 0.69 for crushed granite f'_c = concrete compressive strength (psi)
Noguchi et al. (2009)	$E_c = k_1 \cdot k_2 \cdot 4{,}860 \cdot \left(\frac{w_c}{150}\right)^2 \sqrt[3]{\frac{f'_c}{8.7}}$	E_c = static elastic modulus of concrete (ksi) k_1 = correction factor for aggregate stiffness = 1.32 for dolomitic limestone = 0.82 for crushed granite k_2 = correction factor for supplementary cementing materials = 1.0 w_c = unit weight (pcf) f'_c = concrete compressive strength (ksi)

The results of the *SEE* analysis to evaluate the relative goodness-of-fit for the five prediction equations for two varying aggregates with three assumptions of unit weight are displayed in Table 6-9. For each varying assumption of unit weight, the most accurate prediction model is shaded for reference. Of these shaded models, the standard errors of the estimates represent less than 10 percent of typical values for elastic modulus. Caution is warranted when evaluating the results for crushed granite due to the small sample size. The calibrated AASHTO LRFD, *fib* Model Code 2010, and Noguchi et al. (2009) methods each represent a significant improvement when compared to current practice (represented by Pauw [1960]). For the dolomitic limestone data grouping evaluated with measured unit weights, the Noguchi et al. (2009) method provides a more accurate prediction of modulus (*SEE* = 323 ksi) when compared to the AASHTO LRFD Method (*SEE* = 341 ksi) suggesting that the form of the Noguchi et al. (2009) equation may be slightly theoretically better suited for prediction of elastic modulus at the time of prestress release. When considering the dolomitic limestone grouping for unit weight computed according to Equation 6-4, the *fib* Model Code 2010 prediction equation is identified as most preferable despite this equation not varying as a function of unit weight. For a unit weight assumption of 150 pcf, the AASHTO LRFD equation yields the most accurate predictions (*SEE* = 364 ksi as compared to the next closest of 372 ksi). Another interesting trend is identified by comparing the assumed unit weight of 150 pcf subgroup and the unit weight computed by Equation 6-4 subgroup for dolomitic limestone. The use of Equation 6-4 generates significantly less accurate predictions than does a simple assumption of a unit weight of 150 pcf for the precast, prestressed concretes considered in this study.

Table 6-9: Standard Error of the Estimate, *SEE* for Calibrated Modulus Prediction Equations at Prestress Release

	Dolomitic Limestone			Crushed Granite		
Prediction Model	***SEE* Using Assumed w = 150 pcf (ksi)**	***SEE* Using Measured w (ksi)**	***SEE* Using w Predicted from f_c (Al-Omaishi 2009) (ksi)**	***SEE* assuming w = 150 pcf (ksi)**	***SEE* Using Measured w (ksi)**	***SEE* Using w Predicted from f_c (Al-Omaishi 2009) (ksi)**
Pauw (1960) / ACI 318-14 / ACI 209 / Uncalibrated AASHTO LRFD (2014)	1,008	923	1,109	1,512	1,446	1,377
Calibrated AASHTO LRFD (2014)	**364**	341	422	**73**	**22**	**58**
ACI 363	1,579	1,500	1,670	972	911	850
***fib* Model Code 2010**	372	372	**372**	89	89	89
Noguchi et al. (2009)	392	**323**	455	114	48	88

For the crushed granite data set, similar trends are found, except in this case, the relative level of prediction accuracy agrees with that logically expected (most accurate corresponds to measured unit weights and least accurate corresponds to assumption of 150 pcf).

While the above analysis of *SEE* serves as an objective way to evaluate the relative fit of equations, it does not lend itself to developing a full understanding of the prediction model fits and flaws. For this purpose, the five calibrated prediction equations (for assumed unit weight of 150 pcf) and the experimental data of the stiffness-strength data set (excluding crushed granite) are shown in Figure 6-16.

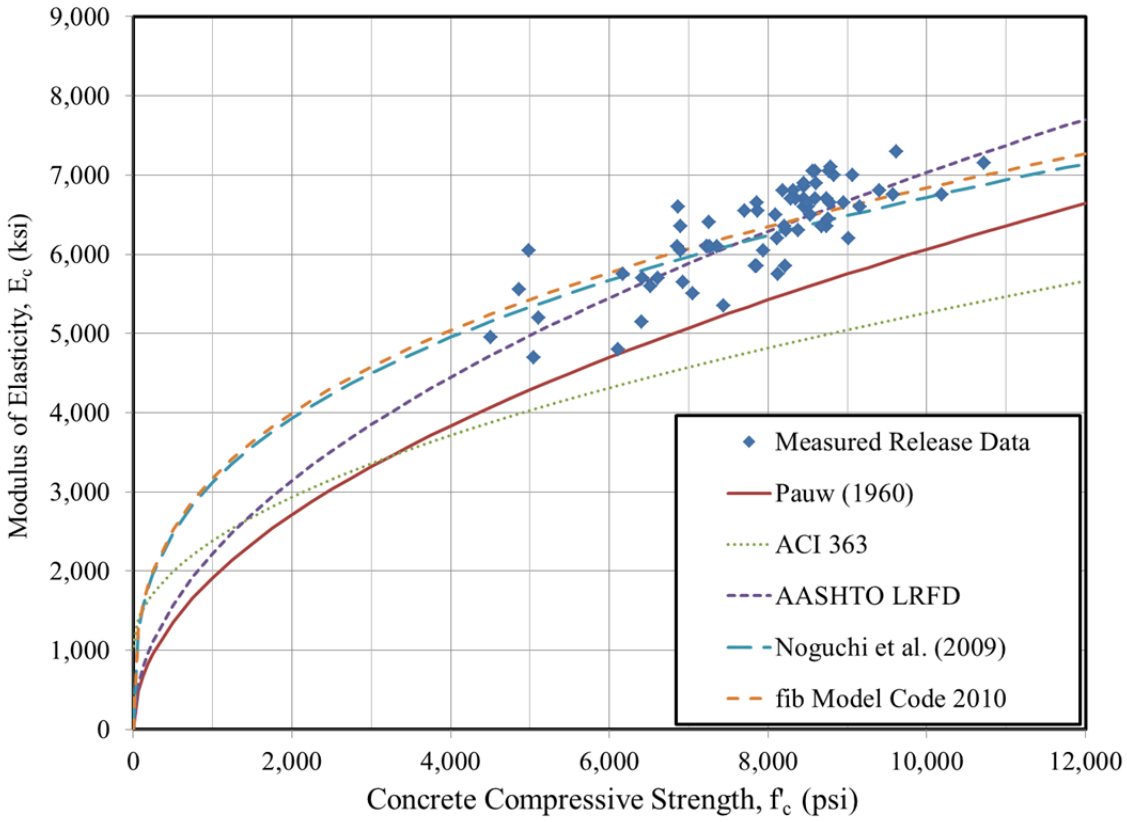

Figure 6-16: Relative Fit of Calibrated Modulus Prediction Equations for Prestress Release Data for Dolomitic Limestones with Assumed Unit Weight of 150 pcf

It can be seen that the recommendation of ACI 363 tends to most significantly under-predict stiffness at the time of prestress release, followed next by the prediction equation

of Pauw (1960). The three calibrated equations appear relatively similar through the strength range of experimental data in this project.

6.4.2.5 Preliminary Recommendations for Designers

As a result of the analysis detailed in Section 6.4.2.5 of this dissertation, the following preliminary recommendation is made for designers of precast, prestressed concrete members within the study region:

- The AASHTO LRFD Bridge Design Specifications (AASHTO 2014) prediction equation, with the assumptions and calibrations noted below, is most appropriate for design predictions of the elastic modulus of precast, prestressed concrete at the time of prestress release.

$$E_c = 33{,}000 \cdot K_1 \cdot w^{1.5} \sqrt{f'_c}$$

where

E_c = static elastic modulus of concrete (ksi);

K_1 = correction factor for source of aggregate;

= 1.16 for dolomitic limestone;

w = unit weight of concrete (kcf);

= assumed equation to 0.150 kcf for design purposes; and

f'_c = concrete compressive strength (ksi).

The K_1 factor referenced above is appropriate for dolomitic limestone most typical of Alabama geologic formations. At the conclusion of this study, only two precast, prestressed producers (Plants A and C) remained active within the study region and both used dolomitic limestone coarse aggregates.

6.4.3 Concrete Stiffness at 28 Days

Accurate prediction of E_c at the time of 28 days after production is not as critical to designers of precast, prestressed elements as the prediction of elastic modulus at prestress release. As previously discussed in Chapter 2, deflections are typically computed for the time of prestress release and modified thereafter by a time-dependent multiplier. Nonetheless, for the purposes of determining appropriate time-dependent multipliers and for completeness of this dissertation, an analysis identical to that of Section 6.4.2 was completed for predicting concrete stiffness at the time of 28 days after production. The analytical procedure (shown in Figure 6-12) was again used in the analysis of this section.

6.4.3.1 Calibration of AASHTO LRFD Equation

Calibration of the AASHTO LRFD Equation for each aggregate type was completed in similar fashion to that discussed in Section 6.4.2.1. The results of the linear regression performed on the compiled data set are shown in Figure 6-17.

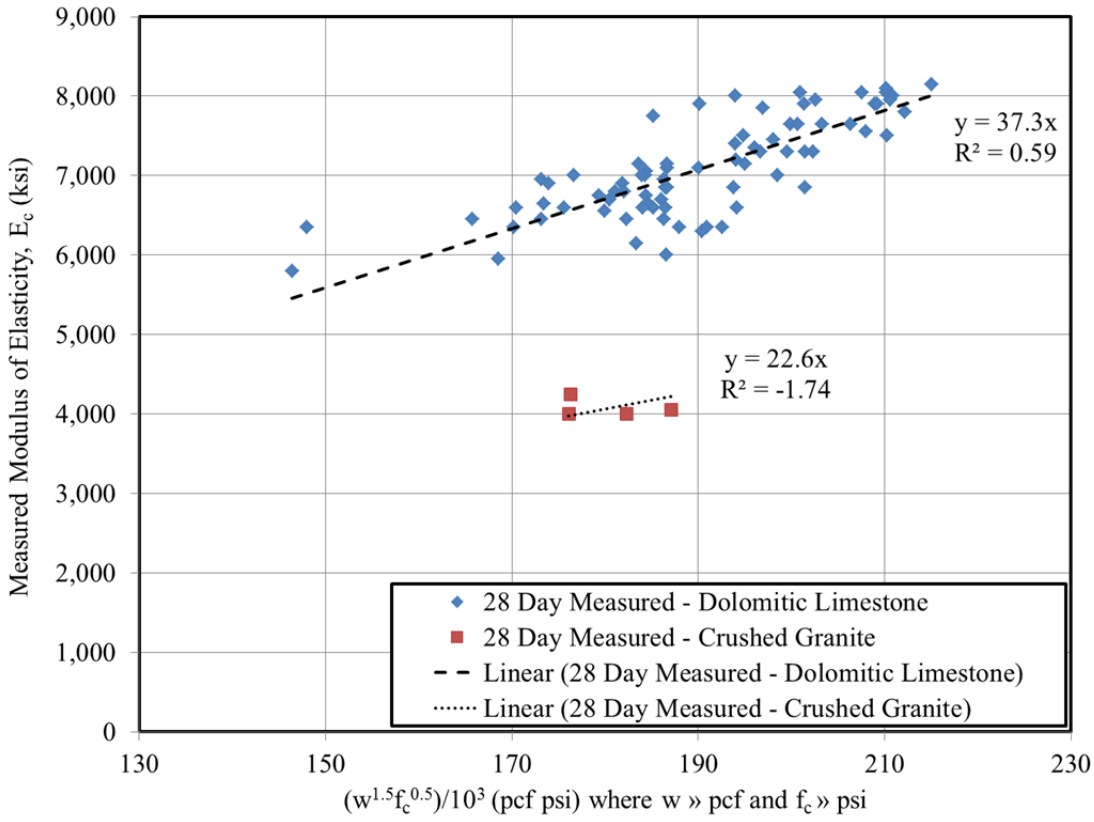

Figure 6-17: Calibration of AASHTO LRFD Equation for 28 Days

The regression coefficients noted in Figure 6-17, when divided by 33.0, yield K_1 factors of 1.13 and 0.68 for dolomitic limestone and crushed granite, respectively. Each of these values is less than the corresponding K_1 factors computed from the release data set (1.16 and 0.72 respectively). A potential reason for this disparity between K_1 values at different times of measurement is discussed in Section 6.4.4.

6.4.3.2 Calibration of *fib* Model Code 2010 Equation

In similar fashion, the *fib* Model Code 2010 prediction equation was calibrated for each aggregate type as shown in Figure 6-18. The values of α_E resulting from the calibration to the stiffness-strength data set are 1.18 and 0.69, respectively (as compared to those values computed for prestress release of 1.15 and 0.69, respectively).

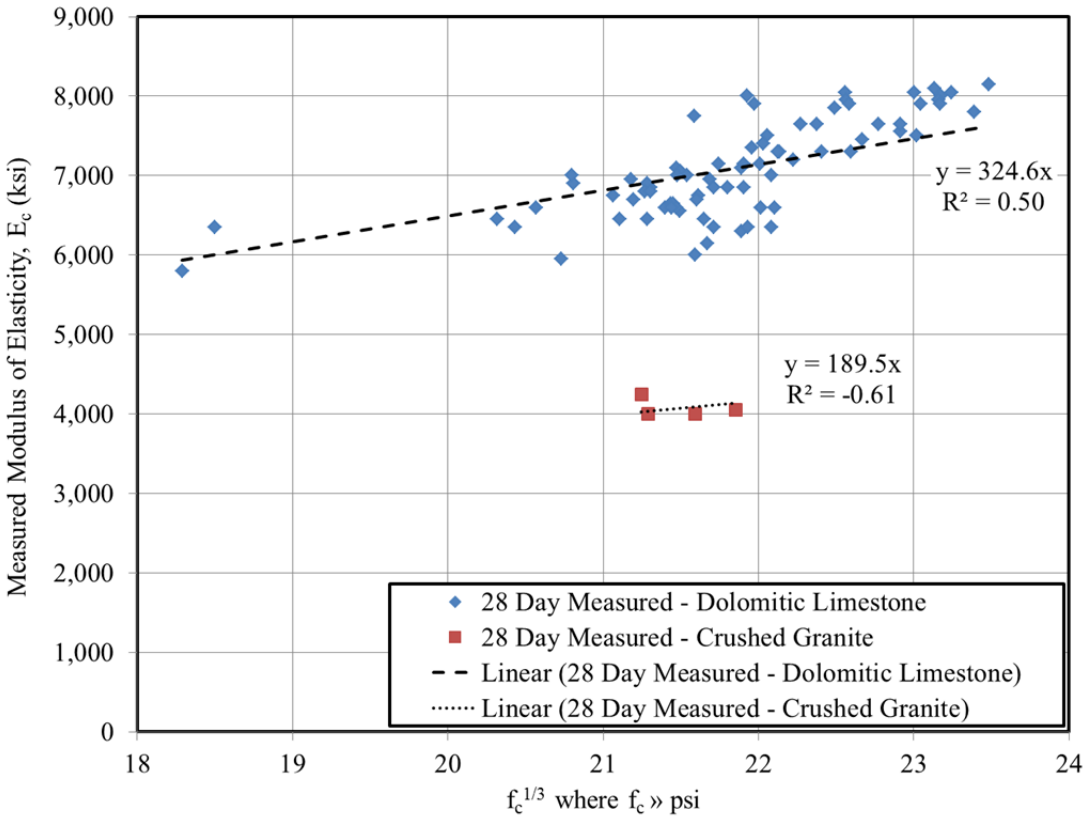

Figure 6-18: Calibration of *fib* Model Code 2010 for 28 Days

6.4.3.3 Calibration of Noguchi et al. (2009) Equation

Finally, the Noguchi et al. (2009) prediction equation is calibrated in a similar manner as previously. The factor k_2 is again taken as 1.0, while the k_1 factor is calibrated to the stiffness-strength data set as shown in Figure 6-19. Again, by dividing the slope of the regression line for each aggregate type by the leading coefficient of Equation 6-8, k_1 for the dolomitic limestone and crushed granite were determined as 1.35 and 0.82, respectively. In this case, the k_1 factor for dolomitic limestone at the time of 28 days exceeds the k_1 for release (previously computed as 1.32), while the k_1 for crushed granite again remains consistent between measurement ages.

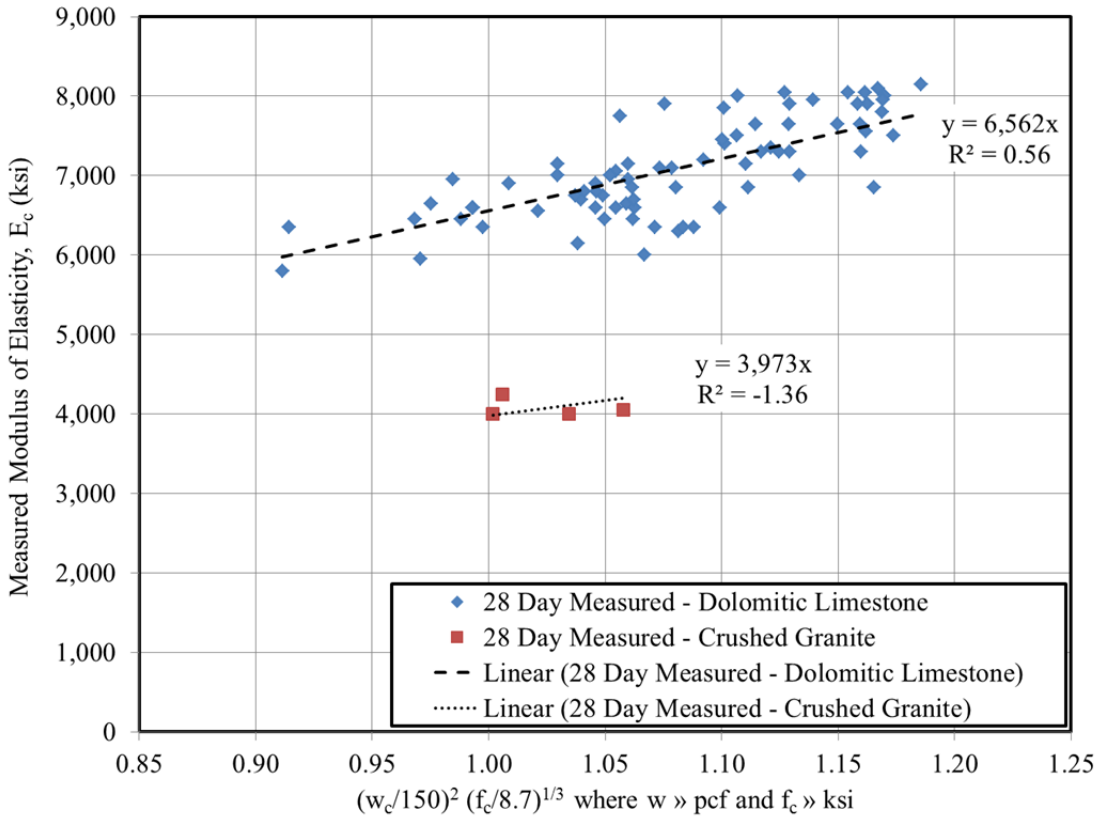

Figure 6-19: Calibration of Noguchi et al. (2009) for 28 Days

6.4.3.4 Comparison of Available Prediction Equations

The final form of each of the five candidate prediction equations included in this study, as calibrated for use at the time of 28 days, is summarized in Table 6-10. This section briefly compares the accuracy of these calibrated prediction equations with the stiffness-strength data set for the varying assumptions of unit weight, *w,* previously noted. The standard error of the estimate (*SEE*) for each combination of prediction model, aggregate type, and unit weight assumption is shown in Table 6-11. In general, for all calibrated models, the magnitude of the SEE is less than 10 percent of E_c. The AASHTO LRFD equation yields the most accurate prediction of E_c for the dolomitic limestone subgroup for all varying assumptions of unit weight. In addition, increasingly more refined

Table 6-10: Candidate Modulus Prediction Equations Calibrated for 28 Days

Source	Prediction Equation	Nomenclature
Pauw (1960) / ACI 318-14 / ACI 209	$E_c = 33w^{1.5}\sqrt{f'_c}$	E_c = static elastic modulus of concrete (psi) w = equilibrium unit weight of concrete (pcf) f'_c = concrete compressive strength (psi)
AASHTO LRFD (2014)	$E_c = 33{,}000 \cdot K_1 \cdot w^{1.5}\sqrt{f'_c}$	E_c = static elastic modulus of concrete (ksi) K_1 = correction factor for source of aggregate = 1.13 for dolomitic limestone = 0.68 for crushed granite w = unit weight of concrete (kcf) f'_c = concrete compressive strength (ksi)
ACI 363 Method	$E_c = \left(40{,}000\sqrt{f'_c} + 10^6\right)\left(w_c/145\right)^{1.5}$	E_c = static elastic modulus of concrete (psi) w_c = unit weight of concrete (pcf) f'_c = concrete compressive strength (psi)
fib Model Code 2010	$E_c = 276{,}000 \cdot \alpha_E \cdot \sqrt[3]{f'_c}$	E_c = static elastic modulus of concrete (psi) α_E = aggregate correction factor = 1.18 for dolomitic limestone = 0.69 for crushed granite f'_c = concrete compressive strength (psi)
Noguchi et al. (2009)	$E_c = k_1 \cdot k_2 \cdot 4{,}860 \cdot \left(\frac{w_c}{150}\right)^2 \sqrt[3]{\frac{f'_c}{8.7}}$	E_c = static elastic modulus of concrete (ksi) k_1 = correction factor for aggregate stiffness = 1.35 for dolomitic limestone = 0.82 for crushed granite k_2 = correction factor for supplementary cementing materials = 1.0 w_c = unit weight (pcf) f'_c = concrete compressive strength (ksi)

Table 6-11: Standard Error of the Estimate, *SEE*, for Calibrated Modulus Prediction Equations at 28 Days

	Dolomitic Limestone			Crushed Granite		
Prediction Model	***SEE* Using Assumed *w* = 150 pcf (ksi)**	***SEE* Using Measured *w* (ksi)**	***SEE* Using *w* Predicted from f_c (Al-Omaishi 2009) (ksi)**	***SEE* assuming *w* = 150 pcf (ksi)**	***SEE* Using Measured *w* (ksi)**	***SEE* Using *w* Predicted from f_c (Al-Omaishi 2009) (ksi)**
Pauw (1960) / ACI 318-14 / ACI 209	975	895	939	1,975	1,892	1,974
AASHTO LRFD (2014)	**399**	**379**	**392**	152	172	163
ACI 363	1,786	1,713	1,751	1,182	1,110	1,180
***fib* Model Code 2010**	423	423	423	**132**	**132**	**132**
Noguchi et al. (2009)	439	394	394	159	159	170

estimates of the unit weight yield increasing more accurate predictions of modulus—with the most accurate predictions observed for measured unit weight. With regards to the crushed granite group, the *fib* Model Code 2010 equation, which does not include a term for unit weight, is the most accurate of all considered prediction models. For the assumed unit weight of 150 pcf, the AASHTO LRFD equation yields the second most accurate predictions for E_c. However, for the AASHTO LRFD equation, the most accurate estimate of unit weight yields the least accurate prediction of modulus. This counterintuitive trend suggests that the crushed granite data set may not be robust enough (n=4) to generate meaningful conclusions.

The five candidate modulus prediction equations, calibrated for dolomitic limestone at 28 days, are shown in Figure 6-20 for an assumed unit weight of 150 pcf. In agreement with the results of Table 6-11, the ACI 363 method is the least accurate method, while the equation proposed by Pauw (1960) is the next most accurate. Of the three calibrated equations (AASHTO LRFD, Noguchi et al. (2009) and *fib* Model Code 2010), the shape of the AASHTO LRFD equation appears to fit the experimental data much more closely than the other two expressions. Looking closely at Figure 6-20, it can be seen that the Noguchi et al. (2009) and *fib* Model Code 2010 equations tend to underestimate experimental results for concrete compressive strengths exceeding approximately 11,000 psi, while overestimating experimental results for strengths less than 9,000 psi. The underestimation of results for higher compressive strengths when using the Noguchi et al. (2009) model is unexpected, as Noguchi et al. (2009) calibrated this model with using a compiled data set including compressive strengths exceeding 20.0 ksi.

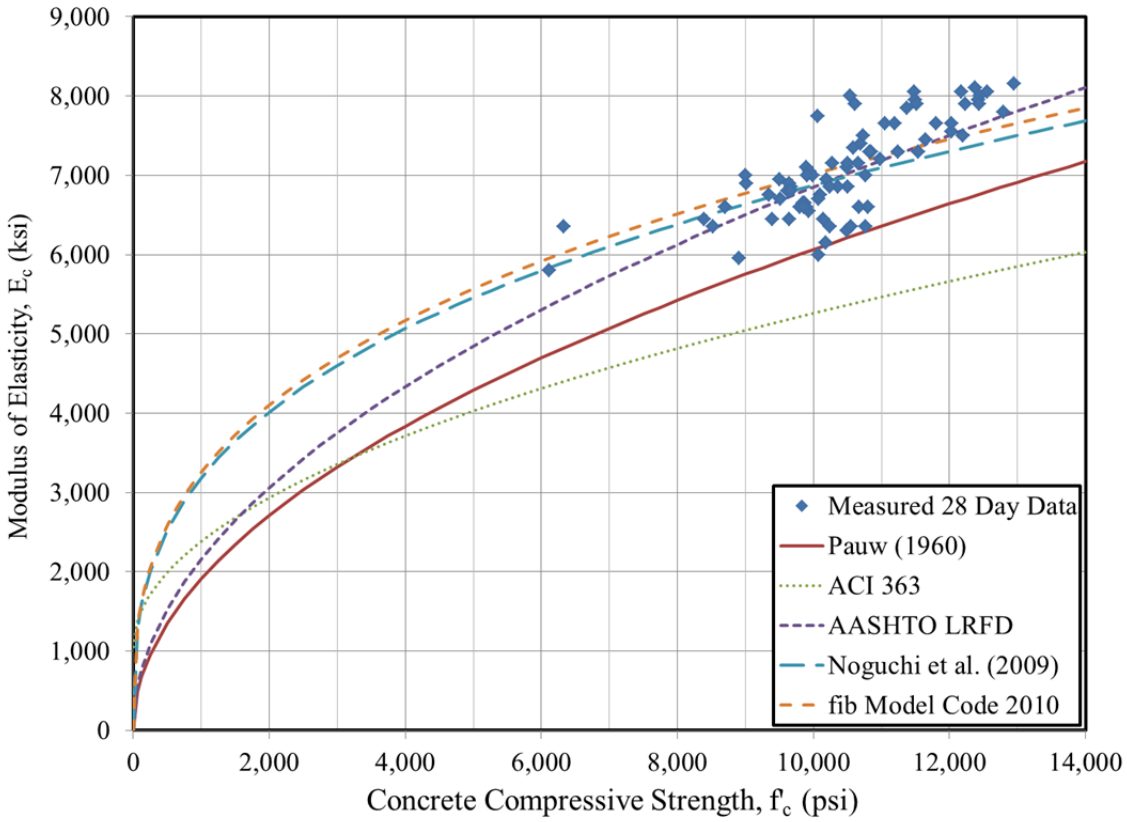

Figure 6-20: Relative Fit of Calibrated Modulus Prediction Equations for 28-Day Data for Dolomitic Limestones with Assumed Unit Weight of 150 pcf

6.4.3.5 Preliminary Recommendations for Designers

Based on the analysis of Section 6.4.3 with regards to evaluating the accuracy of the five calibrated prediction equations for predicting elastic stiffness at 28 days, the following preliminary recommendation is made for designers of precast, prestressed concrete members within the study region:

- The AASHTO LRFD Bridge Design Specifications (AASHTO 2014) prediction equation, with the assumptions and calibrations noted below, is most appropriate for design predictions of the elastic modulus of precast, prestressed concrete at the time of 28 days after production.

$$E_c = 33{,}000 \cdot K_1 \cdot w^{1.5} \sqrt{f'_c}$$

where

E_c = static elastic modulus of concrete (ksi);

K_1 = correction factor for source of aggregate;

= 1.13 for dolomitic limestone;

w = unit weight of concrete (kcf);

= assumed equation to 0.150 kcf for design purposes; and

f'_c = concrete compressive strength (ksi).

The K_1 factor referenced above is appropriate for dolomitic limestone most typical of Alabama geologic formations for the reasons outlined in previous preliminary recommendations for prestress release outlined in Section 6.4.2.5.

6.4.4 Time-Dependence of Aggregate Stiffness Effect

A phenomenon observed both in the experimental work of this dissertation and the previous work of Keske (2014) and Hofrichter (2014) is the seemingly time-dependent nature of the aggregate stiffness effect on the modulus of elasticity of concrete. Keske (2014) reported that computed aggregate stiffness factors, K_1, for the time of prestress release consistently were consistently greater than the K_1 computed for the time of 28 days. This trend is also evident in the earlier analysis work of Hofrichter (2014) and the work of this dissertation. Despite the frequency of this phenomenon in regional research work, this trend has not been referenced previously in published literature. This section provides a hypothesized reason for this difference.

The analysis detailed in Section 6.4.1 of this dissertation affirmed that there existed a statistically significant difference between K_1 factors computed at the time of

prestress release and at 28 days after concrete production for dolomitic limestones. In an attempt to propose a reason for this disparity, key variables (or factors affecting key variables) correlated to E_c were investigated as potential causes.

First, it was noted that the unit weight intended for use in the equation by Pauw (1960) was the equilibrium or air-dry unit weight of concrete. It was hypothesized that perhaps, concrete specimens tested at the time of prestress release contained more free water (than companion specimens tested at 28 days) and thus, may exhibit a higher unit weight. Because Pauw's expression intended the air-dry unit weight as an input, it would be appropriate to reduce the fresh unit weight to a lesser value. Failure to do so may result in over-predictions of the E_c, therefore causing higher K_1 values. While perhaps logically sound, this approach is highly unlikely due to the negligible change in unit weight of normal-weight concrete for varying exposure conditions (Neville 2013). Although not likely not the cause of the disparity observed in this research effort, it is interesting to note that for the computation of elastic modulus for lightweight aggregate concrete, the distinction between using the fresh unit weight or air-dry unit weight (up to a 9 pcf difference) may significantly affect the accuracy of predictions.

Another possible reason for the disparity that was explored was the varying moisture conditions of cylinders at the time of testing. Previously, French and O'Neill (2012) noted a disproportionality between the early-age concrete strength and stiffness as part of their on-site material testing effort at a precast, prestressed producer as shown in their published plots reproduced in Figure 6-21.

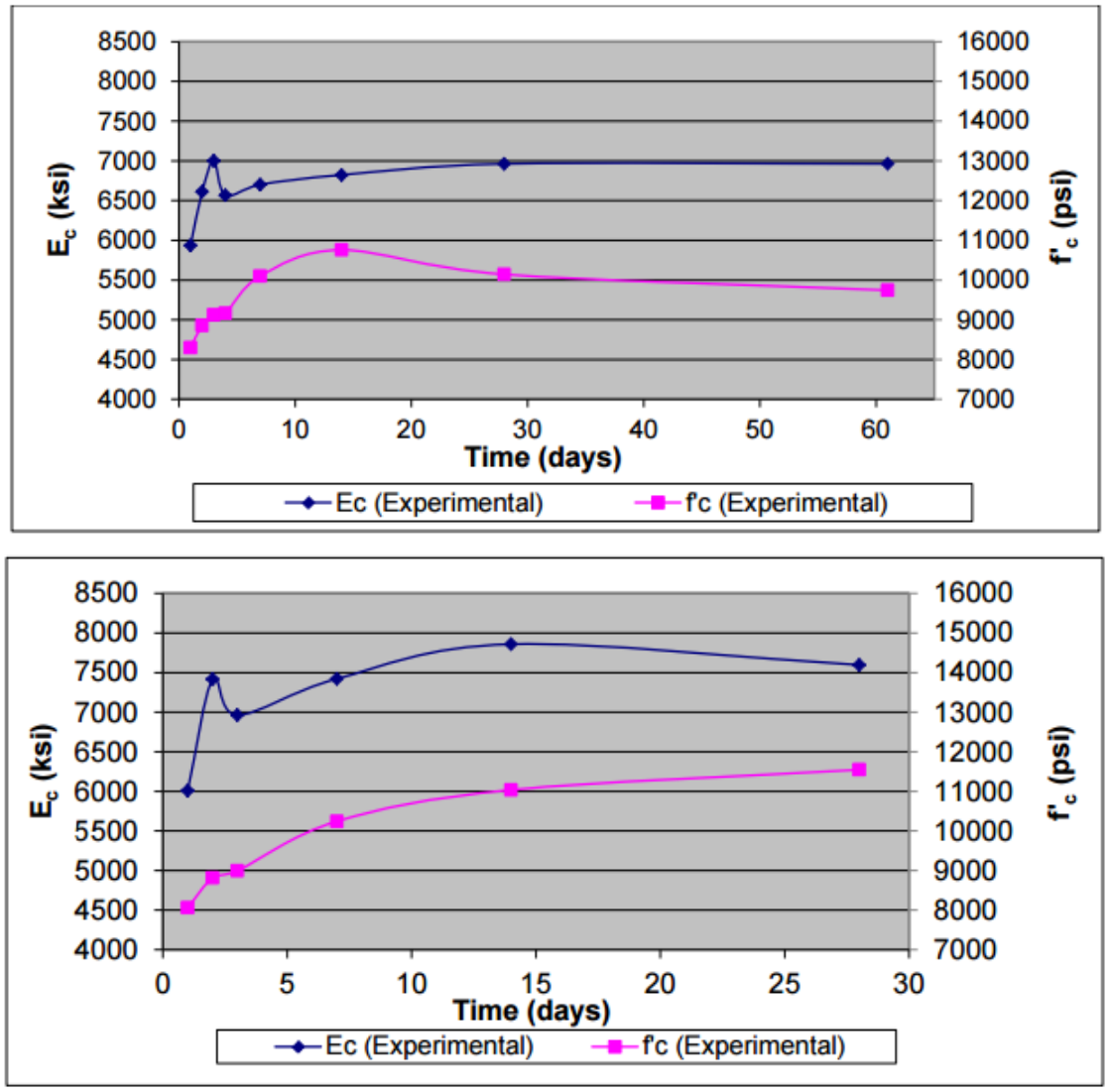

Figure 6-21: Early-Age Disproportionality of Concrete Compressive Strength and Elastic Modulus at Two Producers (French and O'Neill 2012)

French and O'Neill (2012) suggested that the cause of the early-age disproportionality may be due to an increased amount of water inside cylinders at early ages and proposed a separate multiplier of 1.15, not to be confused with K_1, to account for the difference in E_c observed between the time of prestress release and 28 days. However, due to the relatively consistent curing procedures used in the experimental work of this dissertation, it is not possible to extensively evaluate the hypothesis of French and O'Neill (2012) for the experimental data compiled as part of this effort. However, it is interesting to note

that the statistical analysis of Section 6.4.1 did detect a difference in 28-day K_1 factors that is attributable to either 1) varying curing procedures (e.g. varying temperature or moisture exposures) or 2) the inclusion of SCC in the data set, although definitive assignment of the observed variation is not possible.

After considering the hypothesis of French and O'Neill (2012) and noting that the phenomenon of varying K_1 factors has only been noted in precast, prestressed concrete, an alternative hypothesis capable of explaining the observed disparity of K_1 factors was developed and is presented here. Qualitatively reflecting on the field and laboratory efforts of this study, it was noted that the temperature of cylinders at the time of testing varied greatly throughout the study. While release cylinders tested in the field were typically tested approximately 2 hours after the completion of steam-curing (due largely to on-site coordination issues), cylinders tested at the AU Structural Research Lab were tested within minutes of the completion of simulated steam curing. In fact, specimens tested at the AU laboratory were typically hot to the touch and sometimes even uncomfortable to handle at the time of testing. A statistical analysis of the experimental data set was completed to explore if the K_1 factors at release for the laboratory portion of this work tended to be significantly different than those obtained from in-plant testing. It was confirmed that there was strong statistical evidence (p=0.01, t-Test) at significance level $\alpha = 0.05$ that the mean K_1 value determined from laboratory testing exceeded that of the field data.

While not conclusive by any means, the above discussion affirms the plausibility that the temperature at the time of specimen testing may have an effect on the resulting K_1 value. A preliminary literature review on the effect of elevated testing temperature on

the compressive strength and E_c of concrete cylinders highlighted several relevant factors. Freskakis, Burrow, and Debbas (1979) concluded

a. There is a well-documented reduction in the compressive strength of concrete when exposed to elevated temperatures and, particularly when tested at elevated temperatures;
b. There is a well-documented reduction in the E_c of concrete when exposed to elevated temperatures and, particularly when tested at elevated temperatures;
c. The decrease in modulus of elasticity due to elevated temperature exposure is more pronounced than the decrease in compressive strength, but varies with mixture proportions;
d. Specimens heated and then allowed to cool before testing show more strength loss than those tested hot; and
e. Small specimens usually incur greater strength losses than larger specimens.

Design relationships suggested by Freskakis et al. (1979) suggest that for a change in temperature from ambient to approximately 150°F at the time of testing, approximately a 2–12 percent decrease in the compressive strength is expected. Similarly, a corresponding reduction in the elastic modulus of between 0–20 percent is expected. For design purposes, the *Code Requirement for Determining the Fire Resistance of Concrete and Masonry Construction Assemblies* (ACI 2014) affirms the expected reduction in compressive strength as proposed by Freskakis et al. (1979), but offers no comment on the corresponding reduction in stiffness. The design relationships of the *fib* Model Code 2010 assume that the percent loss in compressive strength is the same as the percent loss

of E_c, approximately 18 percent for the temperature range typical of accelerated cured precast, prestressed concrete (fib 2010).

The majority of the literature referenced above documents the observed reductions in compressive strength and E_c for hardened concrete exposed to increasing temperatures (either sustained through the time of testing, called "hot testing" or tested after cooling, called "residual testing"). The situation in steam curing of precast, prestressed elements is somewhat the opposite. The temperature change of interest for hardened precast, prestressed concrete begins at the elevated temperatures present at the conclusion of accelerated curing and ends after cooling to ambient temperature. If similar trends hold for this temperature shift typical of precast, prestressed concrete as those noted in the preceding paragraph for hardened concrete, the following possible hypotheses (or more likely, a combination thereof) are proposed to explain the observed differences in stiffness at the time of prestress release and 28 days:

- The initial reduction in stiffness and strength (as observed by French and O'Neill [2012]) may correspond to the cooling of the concrete from the initial accelerated curing temperatures. Specimens tested at higher temperature will tend to show a smaller reduction in concrete strength than those tested when cold. This may explain the "dip" in the observed strength and stiffness, which then is eclipsed by the continually developing time-dependent hardened properties, and
- The relationship between strength loss and stiffness loss for a given temperature change is a critical factor influencing the K_1 factor for a given concrete. Consider the simple assumption contained in the *fib* Model Code that claims the percent change for a given temperature range of strength and stiffness is equal. For a set

of cylinders tested for strength and E_c when cold yields the following results: $f_c = 5{,}000$ psi and $E_c = 4{,}000$ ksi. Using Equation 6-5 for an assumed unit weight of 0.150 kcf, K_1 is computed as 0.93. Now, if the corresponding cylinders were simultaneously was heated to 150°F and tested again, suppose they exhibit a uniform 10 percent reduction in both strength and stiffness: $f_c = 4{,}500$ psi and $E_c = 3{,}600$ ksi, respectively. Again, using Equation 6-5 to compute K_1, a value of 0.89 is obtained. This simple example affirms the viability of this hypothesis.

It is clear that future research is justified to further examine the effect of cylinder temperature at the time of testing to determine its effect on concrete compressive strength and elastic modulus. This future work will likely be of significant interest to the precast, prestressed concrete industry. Despite identifying a potential cause and mechanism for the observed time-dependent nature of the aggregate stiffness effect, it is not possible at this time to propose a method for combining the stiffness-strength data sets to yield a single K_1 factor for each aggregate type. Accordingly, the recommendations section of this chapter presents two K_1 values for each aggregate type, one for use at prestress release and one at 28 days.

6.4.5 Reduced Stiffness of Crushed Granite Concrete Laboratory Mixtures

The most unexpected result of this study was the comparatively low stiffness exhibited by the crushed granite aggregate mixtures used in the laboratory portion of this research effort. The aggregate in question, currently maintained on ALDOT approved source lists, was previously used by a producer of ALDOT bridge girders (prior to the producer closing in 2013), and, therefore, was selected as a viable aggregate choice for use by a

future producer forecasted to begin girder production operations in the same general vicinity of the closed producer. Typically, crushed granites from this region are regarded as excellent aggregates exhibiting relatively high absorption values when compared to other local aggregates (0.7 percent compared to 0.3 for dolomitic limestone). A study by Haranki (2009) studied the effect of aggregate type on the stiffness of concretes used by the Florida Department of Transportation (FDOT), recommending a K_1 factor of approximately 1.05 for concretes made with similar *w/cm* and crushed granite aggregate. The K_1 factor proposed by Haranki (2009) greatly exceeds the K_1 factors computed as a result of the experimental effort detailed in this dissertation (0.68–0.72.) Although the use of the crushed granite was not a major portion of this study, the comparatively-low stiffness of the crushed granite concrete mixture, GG-III, was briefly investigated to identify a possible reason for this disparity.

Prior to their use in this research project, it was confirmed that all three coarse aggregates and the single source of fine aggregate met the gradation requirements outlined in the *ALDOT Standard Specification for Highway Construction* (ALDOT 2012). For reference, a random sampling of the crushed granite used in the GG-III mixture is shown in Figure 6-22

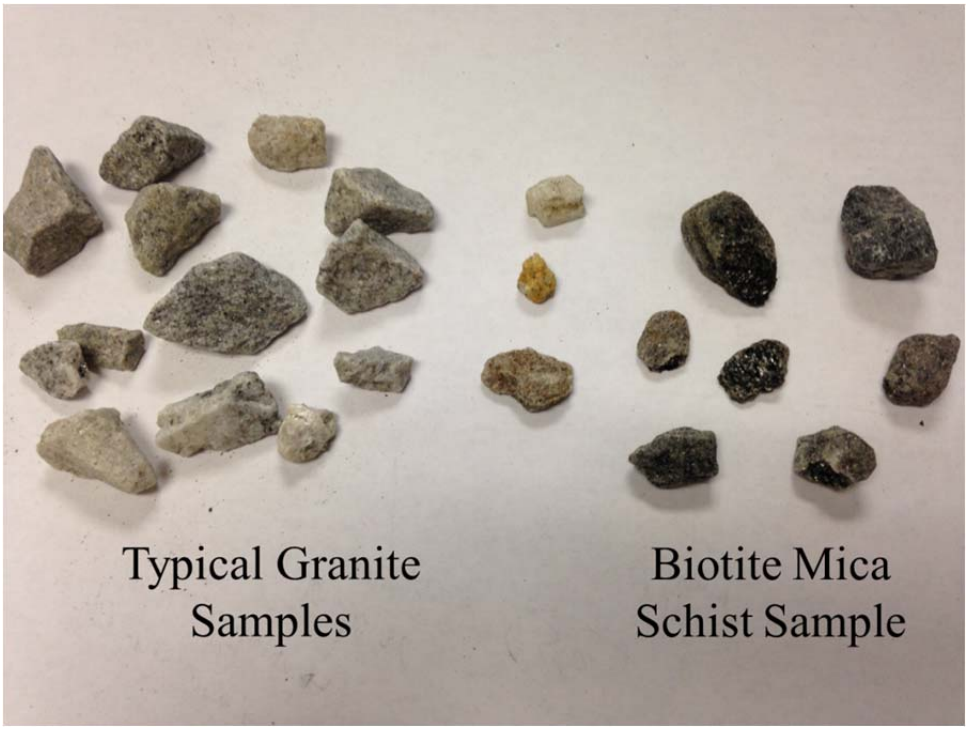

Figure 6-22: Crushed Granite (#67) Aggregate Sample

The particles shown on the left side (white with black striping) and center (white with brown coloring throughout) of Figure 6-22 represent typical granite samples that are dense sound particles and comprise approximately 85 percent (by weight) of the #67 aggregate. Conversely, the particles on the right (black, flakey, and shiny) show samples comprising approximately 15 percent by weight of the #67 crushed granite aggregate. Correspondence with the aggregate supplier confirmed that this dark material is biotite mica schist—a naturally occurring formation found within veins of granite. By inspection, these mica-rich aggregates are relatively soft and unsound particles, easily broken when squeezed between one's fingers. The *ALDOT Standard Specification for Highway Construction* (ALDOT 2012) mandates that all candidate aggregates suspected of containing local deleterious materials (defined in the specification explicitly as shale, mica, marcasite, etc.) be examined by the state laboratory and not exceed two percent of the overall weight (mass) of aggregate for structural concrete applications. In this case,

the crushed granite sample obtained and used for the GG-III mixtures in this project is suspected of exceeding this requirement—containing up to 15 percent (by weight) of mica schist. A study by Aitcin and Mehta (1990) observed the presence of unsound aggregate particles in a crushed granite sample in similar amounts result in less than expected concrete compressive strengths and stiffnesses. Aitcin and Mehta (1990) hypothesized that the inherently weak granite particles caused a weak transition zone, prone to debonding and premature failure. Inspection of the compressive failure of a GG-III specimen included in the work of this dissertation, as shown in Figure 6-23, suggests similar behavior with cracking most often protruding from the vicinity of the soft mica schist aggregate particles.

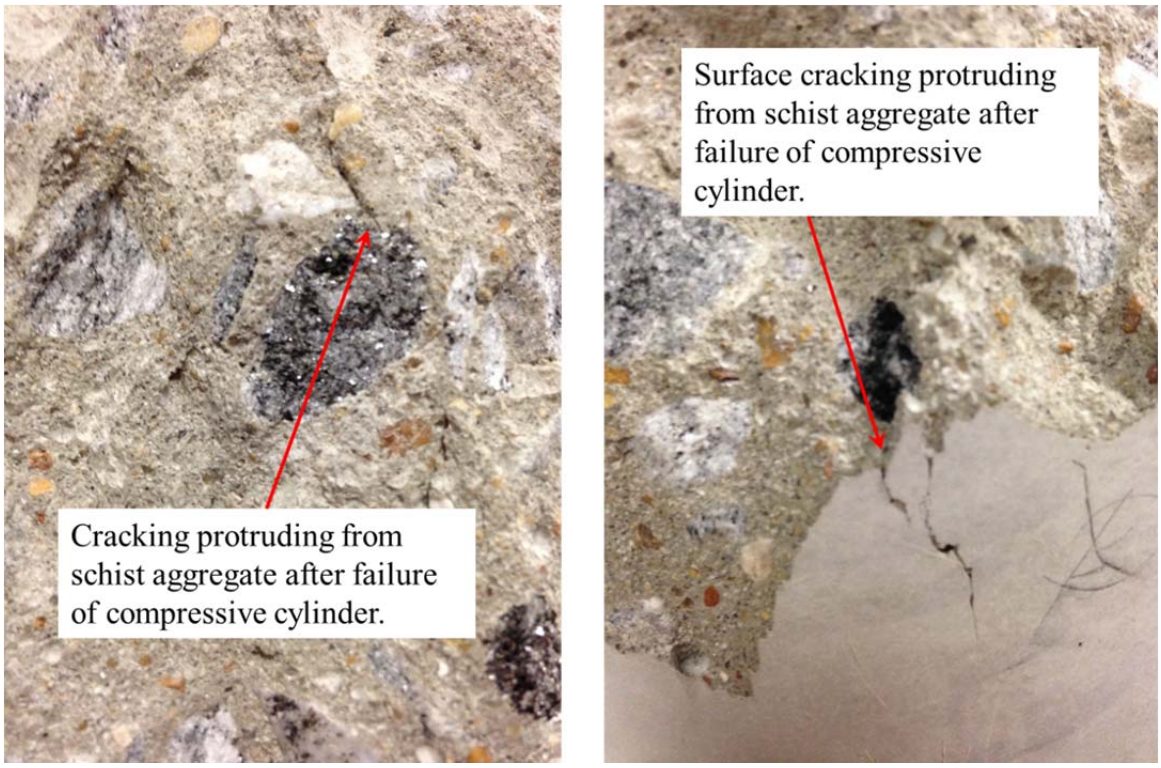

Figure 6-23: Cracking in the Vicinity of Schist Aggregate Particles at Failure

In retrospect, the sample of crushed granite obtained for use in this project is suspected of not meeting the deleterious substance limits of the *ALDOT Standard Specification for Highway Construction* (ALDOT 2012). Approval by the state lab of this aggregate for use in precast, prestressed concrete elements, if tested specifically for suspected high amounts of deleterious substances, would be questionable and likely at the discretion of ALDOT. Accordingly, the major recommendation with regards to the use of regional crushed granite aggregates in precast, prestressed concrete is to ensure that the deleterious substance limits of existing ALDOT specifications (ALDOT 2012) are enforced. That being said, the recommendations for predicting elastic modulus of the crushed granite mixtures contained in the earlier analysis in this chapter are not recommended for implementation by regional designers of precast, prestressed concrete elements due to these results possibly not representing those that may be obtained from sound crushed granite aggregate samples.

6.5 Summary and Conclusions

6.5.1 Summary

The main objective of this chapter was to establish the most appropriate design relationships for use by engineers to accurately characterize the E_c of concrete as a function of compressive strength and other relevant variables likely to be known during the preliminary design phase. By ensuring accurate predictions of concrete stiffness are made at the time of design, the most accurate estimations of short- and long-term deflections can be computed for precast, prestressed concrete members. In this study, a laboratory and field experimental material testing program was relied on to generate a stiffness-strength data set for regional precast, prestressed concretes. Next, a statistical

analysis was performed to identify significant variables and groupings for further analysis. For the ages of prestress release and 28 days, four candidate elastic modulus prediction equations were calibrated to the experimental data set and then compared and contrasted using the standard error of the estimate, *SEE*. Finally, design recommendations were offered and various hypotheses presented as potential explanations of unexpected observed behavior.

6.5.2 Conclusions and Recommendations

Key conclusions of the work presented in this chapter include the following:

- No statistical difference in elastic modulus was detectable among the three laboratory mixtures containing varying supplementary cementing materials (SCMs) in typical percent replacements used in Alabama;
- The AASHTO LRFD Bridge Design Specifications (AASHTO 2014) prediction equation, with the assumptions and calibrations noted below, is most appropriate for design predictions of the elastic modulus of precast, prestressed concrete.

$$E_c = 33{,}000 \cdot K_1 \cdot w^{1.5} \sqrt{f'_c}$$

where

E_c = static elastic modulus of concrete (ksi);

K_1 = correction factor for source of aggregate;

= 1.16 for dolomitic limestone at release;

= 1.13 for dolomitic limestone at 28 days;

w = unit weight of concrete (kcf);

= assumed equation to 0.150 kcf for design purposes; and

f'_c = concrete compressive strength (ksi).

The K_1 factors referenced above are appropriate for dolomitic limestone typical of Alabama geologic formations. At the conclusion of this study, only two precast, prestressed producers (Plants A and C) remained active within the study region and both used dolomitic limestone coarse aggregates. For convenience in design computations not completed in software programs (i.e. manual or approximate computations), the above K_1 factors can be approximated as $K_1 = 1.15$;

- The use of a regional crushed granite aggregate acquired from an ALDOT-approved source resulted in concretes with less than expected E_c values (K_1 values between 0.68–0.72). However, the acceptability of the crushed granite aggregate (specifically with regards to the permitted percentage of deleterious substances) is questionable;
- It is important that the requirements of the *ALDOT Standard Specification for Highway Construction* (ALDOT 2012) with regards to the permissible levels of deleterious substances are enforced, as failure to do so may result in concretes with stiffnesses significantly less than expected; and
- The effect of the testing temperature of the cylinders at the time of prestress release is a potential source of variability observed in K_1 factors at different ages. More study is needed in this area.

Chapter 7: Creep and Shrinkage Behavior of Alabama Precast, Prestressed Concretes

7.1 Introduction

Creep and shrinkage are major contributing factors to the time-dependent growth of initial elastic camber in precast, prestressed concrete girders. The magnitude of long-term deformations due to creep and shrinkage can be several times the elastic deformations in concrete structures (Bazant and Panula 1980). Concrete creep is the primary factor responsible for camber growth over time, while concrete shrinkage plays a secondary role in reducing the effective prestress force over time, thereby acting to mitigate the effect of creep.

The focus of this research investigation is limited to accurately predicting the camber behavior of precast, prestressed concrete girders up until the time of deck placement. For structural design purposes, ALDOT assumes girders will be installed approximately 60 days following production (ALDOT 2014), while the ALDOT construction specifications suggests that an appropriate upper-bound estimate is 120 days (ALDOT 2010). The 60-day design assumption of ALDOT is in agreement with the assumption of Martin (1977) used in developing the PCI multiplier method. For the laboratory phase of this research study, the measurement of time-dependent material properties was extended to 250 days (approximately 8 months), roughly double the upper-bound assumption provided by ALDOT for girder installation time. For a duration

of loading of 250 days, it is estimated that roughly 70–75 percent of the ultimate time-dependent deformations will have occurred (Troxell, Raphael, and Davis 1958).

The research effort detailed herein is intended to provide useful results for designers of precast, prestressed concrete bridge girders by focusing on design-friendly relationships. Available prediction models for creep and shrinkage require varying degrees of detailed input variables. Therefore, when selecting the creep and shrinkage prediction models considered in this study, an effort was made to examine only those models appropriate for use by designer engineers at the time of preliminary girder design—before detailed information is known regarding concrete mixture proportions or constituent materials. In the event that a model requires inputs not likely to be precisely known at the time of design (e.g. air content, slump, cement content, etc.), an average value, as reflected in Chapter 4 of this dissertation, may be used by design engineers. Additionally, recognizing that ALDOT has transitioned fully to the use of the AASHTO LRFD Bridge Design Specifications, it is preferable that the final recommendations of this section be compatible with the provisions of that design specification, if possible.

7.1.1 Chapter Objectives

The primary objective of the research described in this chapter was to evaluate the early-age time-dependent deformational behavior (namely creep and shrinkage) of typical Alabama girder concretes in order to recommend appropriate prediction equations for use at the time of preliminary girder design. Tasks completed in support of this primary objective include the following:

- Evaluate the effect of regionally available coarse aggregates on pre-erection time-dependent deformational behavior;

- Evaluate the effect of varying the age at loading on pre-erection early-age time-dependent deformational behavior;
- Evaluate the effect of the use of varying supplementary cementing material (SCMs) on pre-erection time-dependent deformational behavior; and
- Compare time-dependent deformational behavior predicted by available design models to observed material behavior and determine any warranted adjustments.

7.1.2 Chapter Outline

This chapter begins with a brief background discussion of creep and shrinkage behavior in concrete including general definitions, primary factors contributing to each, and available code-based prediction equations appropriate for use at the preliminary design phase. Then, an experimental creep and shrinkage testing program is detailed. Next, various post-processing techniques are applied to the raw experimental results including detection and removal of flawed measurements, determination of experimental precision and investigation of the repeatability of results, and a discussion on uncontrolled thermal effects. Finally, a comprehensive analysis of experimental results is presented in support of the primary chapter objective.

7.2 Background

As noted by Adam and Taha (2011), the modeling of creep and shrinkage behavior of concrete has been among the most challenging problems in recent concrete history. While it is relatively clear that both phenomena are related to the movement of water within concrete elements, the specific mechanisms behind creep and shrinkage are still very much debated. The focus of this chapter remains on the predictability of creep and shrinkage in typical precast, prestressed concretes–without specific consideration of the

mechanisms behind these phenomena. This section introduces terminology related to creep and shrinkage behavior, before presenting a general review of some primary factors affecting the magnitude of these time-dependent changes. Next, three particular factors (coarse aggregate type, SCM type, and concrete age at loading) are explored in depth. Finally, the creep and shrinkage prediction equations evaluated and calibrated in this study are briefly presented.

7.2.1 Terminology

ACI Committee 209 (2008) defines creep as the time-dependent increase of strain in hardened concrete subjected to a sustained stress. The total observed creep consists of both the basic creep component (creep occurring under conditions of no moisture movement to or from the environment) and drying creep (the portion of creep when moisture movement to or from the environment is allowed to occur). For practical design purposes, it is unnecessary to differentiate between basic creep and drying creep. Laboratory evaluation of creep and shrinkage in concrete cylinders is performed in accordance with the *Standard Test Method for Creep of Concrete in Compression* (ASTM C512 2002). The two most common metrics of time-dependent load-induced deformational behavior are the creep coefficient and compliance. The creep coefficient, most commonly denoted by v_t, is defined as the ratio of the observed creep strain to the initial strain and is a function of concrete age at loading, t_i, and duration of loading, t (ACI Committee 209 2005). An ultimate creep coefficient of 2.5 for a particular concrete means that it is expected that ultimate displacement will be 2.5 times the magnitude of the initially observed elastic displacement. An equation relating (1) stress applied at time of loading, (2) concrete elastic modulus at time of loading, and (3) concrete creep

coefficient to (4) total load-induced strain (for a given duration of loading) is shown in Equation 7-1.

$$\varepsilon_{load-induced}(t,t_i) = \frac{\sigma_{applied}}{E_c}\left[1+\nu_t(t,t_i)\right] \tag{7-1}$$

where

t = duration of loading;

t_i = concrete age at loading;

$\sigma_{applied}$ = stress applied at time of loading;

E_c = elastic modulus of concrete at time of loading;

$\nu_t(t,t_i)$ = creep coefficient for a considered duration of loading, t; and

$\frac{\sigma_{applied}}{E_c}$ = initial elastic strain upon loading.

The other common metric for describing time-dependent load-induced deformational behavior is compliance, most commonly denoted as J. ACI Committee 209 (2008) defines compliance as "the total load-induced strain (elastic strain plus creep strain) [for a considered duration of loading, t,]…per unit stress caused by a unit uniaxial sustained load since loading age." Dividing the total load-induced strain, $\varepsilon_{load-induced}(t,t_i)$, (Equation 7-1) by the stress applied at time of loading, $\sigma_{applied}$, and simplifying yields

$$J(t,t_i) = \frac{\left[1+\nu_t(t,t_i)\right]}{E_c} \tag{7-2}$$

where

$J(t,t_i)$ = compliance for a considered loading duration and age at loading.

Rearranging Equation 7-2, the creep coefficient, ν_t, can be solved for as a function of compliance and elastic modulus at the time of loading

$$\nu_t(t,t_i) = E_c J(t,t_i) - 1 \tag{7-3}$$

The primary difference between the two presented metrics of time-dependent deformation is that while the creep coefficient describes time-dependent behavior as a ratio of the creep deformation to the initial elastic deformation, compliance includes the initial elastic deformation and therefore describes the total load-induced deformational behavior (both elastic and time-dependent). For design purposes, the distinction between creep coefficient and compliance is inconsequential, as Equations 7-2 and 7-3 (along with an "expected" value of E_c) allow designers to translate freely between these two parameters of time-dependent deformations.

Practically speaking, it is not possible during creep testing to differentiate between the portion of the observed early deformation attributed to instantaneous elastic strain and that portion attributed to early creep effects (ACI Committee 209 2008). While the creep coefficient parameter is particularly sensitive to intrinsic errors in early testing, compliance, by nature of it being normalized to the applied stress, tends to be a more measurable metric of time-dependent deformation. In this research effort, compliance is used as the primary metric for creep behavior with the understanding that, as long as the elastic modulus of a given concrete is known (or predicted accurately) at the time of prestress transfer, one can freely transition between creep coefficient and compliance. Hubler, Wender, and Bazant (2015) have endorsed the use of the compliance metric for the reporting of all experimental creep and shrinkage work in lieu of the creep coefficient.

Shrinkage is defined as the time-dependent decrease in volume of an unloaded, hardened concrete specimen (ACI Committee 209 2008). Typically measured in dimensionless strain units, the total shrinkage consists of the drying shrinkage (due to moisture loss from the concrete), autogenous shrinkage (due to self-desiccation of cement), and carbonation shrinkage (due to carbonation of various cement hydration products). For design purposes, it is not necessary to differentiate among these sources of shrinkage as long as the net result can be satisfactorily predicted. Shrinkage is typically measured as part of creep testing conducted in accordance with the requirements of ASTM C512-02 or independently in concrete standard rectangular prism testing conducted in accordance with the requirements of the *Standard Test Method for Length Change of Hardened Hydraulic-Cement Mortar and Concrete* (ASTM C157 2008).

7.2.2 Primary Factors Affecting Creep

ACI Committee 209 (ACI Committee 209 2005) outlines three major groups of factors known to affect creep including (1) mixture proportions, (2) environment, and (3) construction and structural design. Each of these groupings is briefly discussed in this section prior to a more in-depth review of three specific parameters explored as part of the experimental work presented later in this chapter. More comprehensive reviews of the factors affecting creep are given by *Factors Affecting Shrinkage and Creep of Hardened Concrete* (ACI Committee 209 2005) and He (2013).

Although the mechanisms behind creep are not fully understood, it is the general consensus that creep behavior is governed by the properties of the cement paste and the quantity and properties of aggregate within a concrete mixture. Generally speaking, a concrete mixture with increased aggregate volume (and corresponding reduced paste

content) will tend to exhibit less creep than a high paste content mixture (ACI Committee 209 2005). Similarly, stiffer aggregates tend to more effectively restrain time-dependent deformational behavior and, therefore, result in less creep. It is also clear that increased water content of a mixture and increased air content both correlate to increased creep. Finally, the presence of various supplementary cementing materials (SCMs) within a mixture has also been found to affect creep magnitude (ACI Committee 209 2005). Two of the above-referenced parameters (aggregate type and SCM use) are discussed in more detail in the subsequent sections.

The next major grouping of factors known to affect creep behavior is the environment in which concrete is cast, cured, and loaded. The magnitude of creep is particularly sensitive to the relative humidity conditions of the concrete sample. Increased relative humidity correlates to slower creep development and less ultimate creep (ACI Committee 209 2005). Creep is also very much temperature-dependent with higher temperatures being generally correlating to increased rates of creep development (ACI Committee 216 2014). In terms of the testing conducted in this dissertation, the above environmental factors are generally well-controlled in accordance with the requirements of ASTM C512-02 and, therefore, are not intended as experimental variables in this work.

Finally, various construction and structural design practices are also known to be primary factors affecting creep of concrete. First, the magnitude of the applied stress linearly correlated to the creep response for values up to approximately 40–60 percent of ultimate compressive strength (ACI Committee 209 2005). The size and shape of the concrete element (particularly the volume-to-surface-area ratio) is another key factor.

Thinner concrete sections, tending to more-easily allow moisture loss to the surrounding environment, typically experience more creep than thicker concrete sections. Creep behavior is also sensitive to the duration and type of curing for a given concrete. Generally, an increased period of moist curing is correlated to lower creep development, while steam-curing is known to reduce the ultimate creep magnitude by up to 30 percent (ACI Committee 209 2005). Finally, age at loading is also important, with concretes loaded at later ages generally exhibiting less overall creep. While the majority of the construction and structural practices reviewed above are fairly well-controlled within precast, prestressed concrete construction, the variation of age at loading (time to prestress release) is quite variable (as discussed in Section 4.5.2) and, therefore, investigated as a primary factor in the experimental work of this dissertation.

7.2.2.1 Coarse Aggregate Type

In the earliest available published work on the topic, Davis and Davis (1931) concluded that the aggregate type had a significant effect on the magnitude of observed creep in loaded concrete specimens. By controlling for aggregate-cement ratio, water-cement ratio, and applied stress among mixtures prepared with varying aggregate mixtures, Davis and Davis (1931) concluded that limestone and quartz aggregates tended to limit the magnitude of long-term creep deformation, while sandstone and basalt aggregates contributed to greater long-term creep. As shown in Figure 7-1, it was reported that the use of sandstone aggregates tended to cause roughly double the magnitude of time-dependent creep as compared to limestone aggregates.

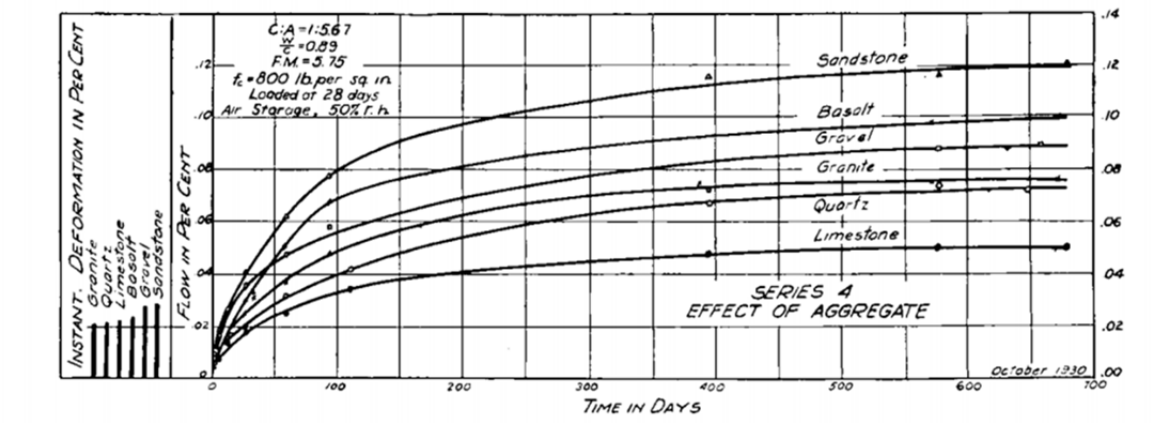

Figure 7-1: Findings of Davis and Davis (1931) Regarding Effect of Aggregate on Creep Behavior

A follow-up study by Troxell, Raphael, and Davis (1958) confirmed the same findings for an extended measurement period of up to 30 years. Neville (2013) explains that the observed differences in creep behavior for varying aggregates are primarily due to differing aggregate stiffness. As creep is a phenomenon that manifests within the paste phase, stiffer aggregates likely better restrain the bulk concrete against the external manifestation of creep behavior. The explanation proposed by Neville has generally been accepted and recently affirmed by other researchers (He [2013], Liu and Tia [2012]). The experimental program detailed in this chapter allows for direct comparisons among creep behavior of concretes made with three coarse aggregate types.

7.2.2.2 Use of Supplementary Cementing Materials (SCMs)

There is little consensus among researchers on the effect of the use of supplementary cementing materials (SCMs) on the creep behavior of concrete. While the work of various researchers is reviewed in this section, it is important to note that there is a relatively large amount of variation intrinsic to the testing of creep in hardened concrete. Neville (2013) attributes the great variety in research findings (and corresponding lack of

consensus on this issue) to a failure by some researchers to recognize the intrinsic limitations of creep testing, namely those of experimental precision and repeatability of results. This topic is discussed further in Section 7.4.3, where experimental precisions are determined for the creep testing described in this dissertation.

ACI 209R.1 (ACI Committee 209 2005) notes that the use of slag cement in concrete generally causes a decrease in the basic creep component, but causes little change in total observed creep. Brooks (1999), whose earlier work is the primary reference for ACI 209R.1 on this topic, later contended that for increasingly large substitution percentages, slag cement replacement causes a distinct decrease in total creep. Similarly, Levy, Barnes, and Schindler (2010) observed a reduction in creep for concretes containing slag cement. Conversely, Chern and Chan (1989) and He (2013) found that increasingly large slag cement replacement caused an increase in total creep. Tia, Liu, and Brown (2005) concluded that the creep coefficient of concrete with slag was generally less than that for a comparable fly ash mixture.

With regards to the effect of fly ash on the creep of hardened concrete, there are somewhat more consistent results reported. ACI 209R.1 (ACI Committee 209 2005) contends that there is a net reduction in observed creep for concrete mixtures using a substitution percentage of more than 10 percent. This recommendation is in agreement with the previous work of Brooks (1999), Ghosh and Timusk (1981), and Lane and Best (1982) —although contrary to the work of He (2013).

ACI 209R.1 (ACI Committee 209 2005) cites a general increase in the creep tendency of concrete for silica fume replacements of less than 7.5 percent. Conversely, Brooks (1999) and Khatri and Sirivivatnanon (1995) observed a net reduction in creep

behavior for replacements of cement with silica fume of less than 15 percent, with a net increase in creep behavior noted for percentage substitutions exceeding 15 percent.

7.2.2.3 Age at Loading

ACI 209.R1 (ACI Committee 209 2005), citing early work by L'Hermite, contends that there is a net decrease in creep for increasing concrete age at load application, but provides little guidance for age at loading of less than seven days. Keske (2014) observed a reduction in creep for specimens loaded at a chronological age of 365 days as compared to specimens loaded at typical prestress release ages (18-24 hours)—further finding that the age at loading provisions of various prediction models satisfactorily predicted the observed reduction due to age at loading over this extreme range. There appears to be no previous research work that explicitly explores the effect of different ages at loading for very early ages (i.e. an attempt to differentiate between 18 and 24 hours creep responses) perhaps, in part, due to a combination of (1) the difficulty in identifying a significant difference given the inherent variability in creep testing results and (2) difficulties in conducting creep testing that isolates age at loading from other inherently-related parameters (e.g. compressive strength at loading, maturity at loading, etc.).

7.2.3 Primary Factors Affecting Shrinkage

The three major groups of factors affecting creep discussed above are also applicable to concrete shrinkage and include (1) mixture proportions, (2) environment, and (3) design and construction practices. Again, each grouping is briefly discussed in this section with a more in-depth review of the three primary factors examined in this research project to follow.

ACI Committee 209 (2005) states the most important factor affecting the potential shrinkage of a given concrete is the total volume of aggregate present in the mixture. Similar to the theory previously discussed for creep, the relatively stiff aggregate acts to restrain the shrinkage tendency that originates primarily in the cement paste. The increasing size of aggregate in a given concrete mixture can also affects shrinkage by dictating a decrease in required paste content for a given workability and, therefore, a corresponding reduction in observed shrinkage. Increasing water content of a mixture generally corresponds to increased shrinkage as more pore water is available within the concrete. The effect of SCMs on concrete shrinkage is somewhat unclear and is discussed in more detailed in subsequent sections.

Concrete shrinkage is especially sensitive to environmental changes in relative humidity and temperature, with decreased shrinkage observed for concrete stored in elevated humidity conditions and an increase in both the time-rate and ultimate shrinkage of concrete subjected to elevated temperatures (ACI Committee 209 2008). Environmental variables were closely controlled (in accordance with applicable testing standards) in the shrinkage testing conducted in this study.

The final grouping of factors affecting shrinkage of concrete according to ACI 209.R1 is design and construction factors. Generally speaking, extended periods of moist curing reduce the expected amount of drying shrinkage. The use of steam curing can significantly reduce drying shrinkage by as much as 30 percent (ACI Committee 209 2005). Finally, the size and shape of the concrete element influence the rate and magnitude of shrinkage. Larger and thicker members typically experience a slower rate

of moisture loss, and therefore a corresponding lower rate of shrinkage development and less ultimate shrinkage.

7.2.3.1 Aggregate Type

The effect of aggregate type on shrinkage is virtually identical to the effect discussed previously for creep with similar behavior again reported by Davis and Davis (1931) and confirmed by Troxell et al. (1958). Generally speaking, stiffer aggregates examined corresponded to reduced rates and ultimate values of concrete shrinkage.

7.2.3.2 Use of Supplementary Cementing Materials (SCMs)

ACI 209.1R (ACI Committee 209 2005) notes that at high replacement values, the use of slag cement may result in increased shrinkage. Work by Khatri and Sirivivatnanon (1995), Chern and Chan (1989), and He (2013) provide similar conclusions. However, as a result of a review of seven studies, Brooks (1999) concluded that the magnitude of concrete shrinkage for a given concrete is largely unaffected by the use of slag cement partial replacement. More recently, Aly and Sanjayan (2008) showed that concrete mixtures containing slag cement exhibit an expansion during curing, which leads to less total shrinkage than mixtures not containing slag cement.

ACI 209.R1 (ACI Committee 209 2005), Brooks (1999), and Lane and Best (1982) agree that the use of fly ash in concrete causes no appreciable change in shrinkage characteristics. While the work of Ghosh and Timusk (1981) provides partial agreement for moderate percent substitutions of fly ash, they also observed lower ultimate shrinkage values corresponding to high fly ash replacement percentages. He (2013) found that shrinkage tends to decrease for substitution percentages of up to 30 percent.

Research work exploring the effect of silica fume usage in concrete is largely inconclusive. ACI 209.R1 notes that at low percent replacement (less than 7.5 percent), a decrease in shrinkage should be expected. Khatri and Sirivivatnanon (1995) found that silica fume replacement generally caused a higher early rate of shrinkage, but a lesser ultimate value when compared to control mixtures. Brooks (1999) concluded that shrinkage behavior remained largely unaffected by the use of silica fume replacement.

7.2.4 Available Creep Prediction Equations

In this research effort, creep prediction equations were selected on the basis of ease of use for designers of precast, prestressed concrete elements. Previous related work by Schrantz (2010) and Isbiliroglu (2014) considered the design-friendly prediction models of the following: (1) AASHTO LRFD Bridge Specifications (hereafter termed "AASHTO 2014 method"), (2) ACI 209R-92 (hereafter termed "ACI 209 method") and (3) the *fib* Model Code 2010 method (hereafter termed "Model Code 2010 method"). This section briefly introduces the basic form of each model and highlights the recommendations of previous researchers regarding the use of each model. Readers interested in the intricacies of prediction model application are referred to the primary reference for each model (i.e. AASHTO [2014], ACI 209R [2008], or *fib* Model Code [2010]) or to the previous work of Keske (2014) and Ellis (2012) for a more thorough comparison of each model than is presented here.

7.2.4.1 AASHTO 2014

The most current of the AASHTO LRFD Bridge Design Specification (AASHTO 2014) contains a relatively simple creep prediction model based on the work of Huo et al. (2001), Al-Omaishi (2001), Tadros et al. (2003), and Collins and Mitchell (1991). The prediction model uses a series of factors to modify an ultimate creep coefficient of 1.9 as shown in Equation 7-4.

$$\psi(t,t_i) = 1.9k_s k_{hc} k_f k_{td} t_i^{-0.118} \tag{7-4}$$

where

k_s = factor for the effect of the volume-to-surface ratio of the component;

k_{hc} = humidity factor for creep;

k_f = factor for the effect of concrete strength;

k_{td} = time-development factor; and

t_i = chronological age accelerated cured concrete at time of load application (days).

While the time index above, t_i, relies on chronological time (and also assumes accelerated curing conditions), the time factor, t, nested within the time-development factor, k_{td}, recommends the use of the maturity (in days) to express the temperature-adjusted time duration of loading. Previous research work by Rizkalla et al. (2011), Keske (2014), Hinkle (2006), and Tadros et al. (2011) endorse the use of this prediction model for use in predicting the time-dependent behavior of precast, prestressed concrete flexural elements. Rosa et al. (2007) also endorse the use of this method, although suggest a modification factor of 1.4 be used to amplify the predicted result to provide more accurate results for typical WSDOT concretes.

7.2.4.2 ACI 209

ACI Committee 209 (2008) first adopted a consensus creep prediction model in 1992. An assumed creep coefficient is modified by a series of parameters as shown in Equation 7-5.

$$v_t = \left(2.35 \cdot \gamma_{la} \cdot \gamma_{\lambda} \cdot \gamma_{vs} \cdot \gamma_{\psi} \cdot \gamma_s \cdot \gamma_a\right)\left(\frac{t^{0.60}}{10 + t^{0.60}}\right) \tag{7-5}$$

where

γ_{la} = loading age correction factor;

γ_{λ} = ambient relative humidity correction factor;

γ_{vs} = volume-surface ratio correction factor;

γ_{ψ} = fine aggregate percentage factor;

γ_s = slump correction factor;

γ_a = air content correction factor; and

t = time after loading (days).

The use of the ACI 209 method for predicting creep behavior in precast, prestressed concrete elements was endorsed in experimental findings of French and O'Neill (2012), while Stallings et al. (2003) found that this method tended to over-predict creep behavior for high-performance concrete if a measured slump (post-HRWRA) is used in the slump correction factor, γ_s.

7.2.4.3 *fib* Model Code 2010

The Model Code 2010 (fib 2010) creep prediction equation is the most complex of the three prediction models considered in this work. A notional creep coefficient is first computed as the sum of the basic and drying creep components, before being modified by a time-development factor as shown in Equation 7-6.

$$\varphi = \varphi_0 \cdot \beta_c(t, t_0) \tag{7-6}$$

φ_0 = notional creep coefficient; and

$\beta_c(t, t_0)$ = time-development coefficient.

Computation of the notional creep coefficient, φ_0, requires knowledge of the following parameters: (1) ambient relative humidity, (2) notional size of member, (3) mean 28-day compressive strength, (4) concrete strength class, and (5) the temperature and cement type adjusted age[5] of concrete at loading. Computation of the time-development coefficient, $\beta_c(t, t_0)$, requires above parameters 1–3 as well as the duration of loading expressed as unadjusted chronological time. The Model Code 2010 method is especially lengthy in formulation, and thus, is not included here in its entirety.

7.2.5 Available Shrinkage Prediction Equations

Typical design practice dictates that provisions of the same model (or governing specification) be used for the computation of creep and shrinkage behavior of concrete for design of a given project. Accordingly, the concrete shrinkage prediction methods corresponding to the three previously considered creep models are briefly outlined in this section.

[5] Hofrichter (2014) showed that the equivalent-age relationship contained in the *fib* Model Code 2010 parallels the equivalent-age maturity method of ASTM C1074 - calibrated for a datum temperature of 20°C and activation energy of 33.2 kJ/mol.

7.2.5.1 AASHTO 2014

The AASHTO 2014 (AASHTO 2014) model relies on an assumed ultimate shrinkage value of 480 microstrain, that is then modified by applicable factors as shown in Equation 7-7.

$$\varepsilon_{sh} = k_s k_{hs} k_f k_{td} 0.48(10^{-3}) \tag{7-7}$$

where

k_s = factor for the effect of the volume-to-surface ratio of the component;

k_{hs} = humidity factor for shrinkage;

k_f = factor for the effect of concrete strength; and

k_{td} = time-development factor.

AASHTO (2014) specifies that for concrete exposed to drying before five days of curing have elapsed, the shrinkage determined by Equation 7-7 should be increased by 20 percent. Schrantz (2012) and Isbiliroglu (2014) adapted the above recommendation (suspected as intended for non-accelerated cured concrete) for accelerated-cured concrete by computing an approximate corresponding age of first drying of 17 hours (5/7 days). In discussing the development of their AASHTO shrinkage provisions, Al-Omaishi et al. (2009) offer no clarification on the applicability of the 20 percent shrinkage increase for accelerated-cured concrete. Practically speaking, implementation of the above requirement for accelerated-cured concrete is questionable because (1) the curing temperature (and therefore, the rate of maturity development) of accelerated-cured concrete is not uniform over time as it is for non-accelerated concrete, (2) therefore, the growth in maturity of a non-accelerated cured concrete for a given non-accelerated curing period (e.g. days 5 to 6) is a different proportion of the overall maturity than the

corresponding maturity growth of an accelerated cured concrete occurring over a similar accelerated curing period (e.g. 17 to 20.5 hours), and (3) the piecewise formulation of the provision (as opposed to a smoother equation-based transition) does not match the expectation of observed behavior. Due to the lack of clarity regarding the applicability of the 20 percent shrinkage amplification and the rarity with which it is applicable in regional precast, prestressed concrete production, it is neither used in the analyses of this dissertation nor recommended for use in camber prediction procedures.

7.2.5.2 ACI 209

The ACI 209 shrinkage prediction model (ACI Committee 209 2008) employs a similar approach to the AASHTO 2014 method, by modifying an assumed ultimate value of 780 microstrain as shown in Equation 7-8.

$$\left(\varepsilon_{sh}\right)_t = \left(780 \cdot 10^{-6} \cdot \gamma_\lambda \cdot \gamma_{vs} \cdot \gamma_\psi \cdot \gamma_s \cdot \gamma_c \cdot \gamma_a\right)\left(\frac{t}{55+t}\right) \tag{7-8}$$

where

γ_λ = ambient relative humidity correction factor;

γ_{vs} = volume-surface ratio correction factor;

γ_ψ = fine aggregate percentage correction factor;

γ_s = slump correction factor;

γ_c = cement content correction factor;

γ_a = air content correction factor; and

t = chronological days after loading (days).

7.2.5.3 *fib* Model Code 2010

The Model Code 2010 method for shrinkage prediction is again the most complex of the three considered methods, relying on independent computation of the relative contributions of both autogenous and drying shrinkage as shown in Equation 7-9.

$$\varepsilon_{cs}(t,t_s) = \varepsilon_{cas}(t) + \varepsilon_{cds}(t,t_s) \tag{7-9}$$

where

$\varepsilon_{cas}(t)$ = autogenous shrinkage component and

$\varepsilon_{cds}(t,t_s)$ = drying shrinkage component.

Time inputs nested within the above expression (concrete age at start of drying and duration of drying) exclusively use chronological time in contrast to those inputs of Equation 7-4 relying on temperature-adjusted time. Computation of the autogenous shrinkage component requires knowledge of (1) mean compressive strength at 28 days, (2) type of cement, and (3) concrete age in days. The time-development of autogenous shrinkage as predicted by MC 2010 is independent of the duration of curing and starts at the time of initial concrete production rather than at the time of first drying. This distinction results in the need to subtract the portion of autogenous shrinkage occurring prior to first measurement when comparisons are made to experimental work. Computation of the drying shrinkage component requires knowledge of (1) concrete age in days, (2) concrete age at the beginning of drying, (3) mean compressive strength at 28 days, (4) ambient relative humidity, (5) cement type, and (6) notional side of member.

7.3 Experimental Program

This section describes the experimental program conducted to explore the creep and shrinkage behavior of concrete mixtures typical of the Alabama precast, prestressed

bridge girder industry. First, a brief summary of work is presented, followed by a discussion of the various candidate mixtures examined. Next, the accelerated curing procedures used in this work are reviewed—including the computation of equivalent age maturities for each trial run. Then, fresh and hardened concrete properties, as relevant to this effort and later use in candidate creep prediction models, are presented. Finally, the experimental procedures for testing the creep and shrinkage behavior of cylindrical specimens and the shrinkage behavior of rectangular prismatic specimens are discussed.

7.3.1 Summary of Work

In this laboratory study, six concrete mixtures were proportioned to represent mixtures typical of Alabama precast, prestressed work. These six mixtures included three regional coarse aggregates and three varying combinations of supplementary cementing materials (SCMs) in typical substitution percentages. By maintaining a uniform 18-hour compressive strength, paste content, and sand-to-total aggregate ratio (by volume) for all mixtures, certain key variables of interest were isolated. Sampled cylindrical specimens were then exposed to accelerated curing practices mimicking those of accelerated curing methods used in precast, prestressed production, while rectangular prismatic specimens were exposed to standard curing conditions. After the completion of the initial curing period (either 18 or 24 hours), cylindrical specimens were tested in accordance with ASTM C512-02 (ASTM 2002) to evaluate the creep and shrinkage behavior of each mixture for two ages at loading for a period of 250 days. Concurrently, rectangular prismatic specimens were tested in accordance with ASTM C157-08 (ASTM 2008) to also evaluate shrinkage behavior also for a period of 250 days. To ensure the precision and repeatability of results, the first three tests were duplicated.

7.3.2 Concrete Mixtures

The laboratory work presented in this chapter was performed concurrently with the laboratory work previously detailed in Chapter 6 of this dissertation. Accordingly, the six trial mixtures included in this testing program are those detailed in Table 6-1, reproduced here for convenience. Each of these six mixtures is characterized by identical sand/total aggregate ratio (by volume), total paste content, and 18-hour strength. Three of these mixtures, the DL-III, CL-III, and GG-III mixtures are identical mixtures with exception of differing coarse aggregates. The three remaining mixtures, the DL-SL, DL-FA, and DL-FA/SF, each utilize an identical coarse aggregate, but include different substitutions of SCMs.

Table 6-1: Laboratory Phase Concrete Mixture Proportions

Mixture ID	Type III Cement (pcy)	Grade 120 Slag Cement (pcy)	Class F Fly Ash (pcy)	Silica Fume (pcy)	Water (pcy)	*w/cm*	Coarse Agg. SSD (pcy)	Fine Agg. SSD (pcy)	*sand/total agg. (volume)*	*total agg. vol. (%)*	*paste vol.* (ft^3/cy)	HRWRA (oz/cwt)	HSA (oz/cwt)
DL-III	878	0	0	0	281	0.32	1,860	1,048	0.37	64	9.0	7.50	1
CL-III	878	0	0	0	281	0.32	1,860	1,048	0.37	64	9.0	7.75	1
GG-III	878	0	0	0	281	0.32	1,823	1,038	0.37	64	9.0	7.50	1
DL-SL	746	130 (15%)	0	0	278	0.32	1,860	1,048	0.37	64	9.0	6.75	1
DL-FA	754	0	132 (15%)	0	262	0.30	1,860	1,048	0.37	64	9.0	7.50	1
DL-FA/SF	606	0	142 (18%)	63 (8%)	276	0.34	1,860	1,048	0.37	64	9.0	7.75	1

Notes:

1. Percent substitutions noted for supplementary cementing materials (SCMs) are by weight of total cementitious materials.
2. HRWRA = Glenium 7700 and HSA = Masterset Delvo.

7.3.3 Accelerated Curing Procedures

While briefly discussed previously in Section 6.3.1.4, this section more completely details the accelerated curing procedures used for cylindrical specimens in this portion of the work and also describes the computation of the various metrics of maturity necessary for inclusion in the candidate creep and shrinkage prediction models summarized earlier in this chapter. While all three models require some metric of age at loading, the *fib* Model Code 2010 is the only model explicitly requiring the use of maturity for computation of creep and shrinkage, as computed herein.

As previously discussed in Chapter 6, two ages of simulated prestress release were selected based on the historic data set compiled by Hofrichter (2014) documenting the chronological time to prestress release for 1,917 girder concrete placement events. These two chronological ages were 18.0 hours (the approximate average of the primary peak of Figure 4-10) and 24.0 hours (an upper-bound value capturing 99.5 percent of the data of the same primary peak). The complete temperature history for each of fifteen tests through the time of loading is shown in Figure 7-2.

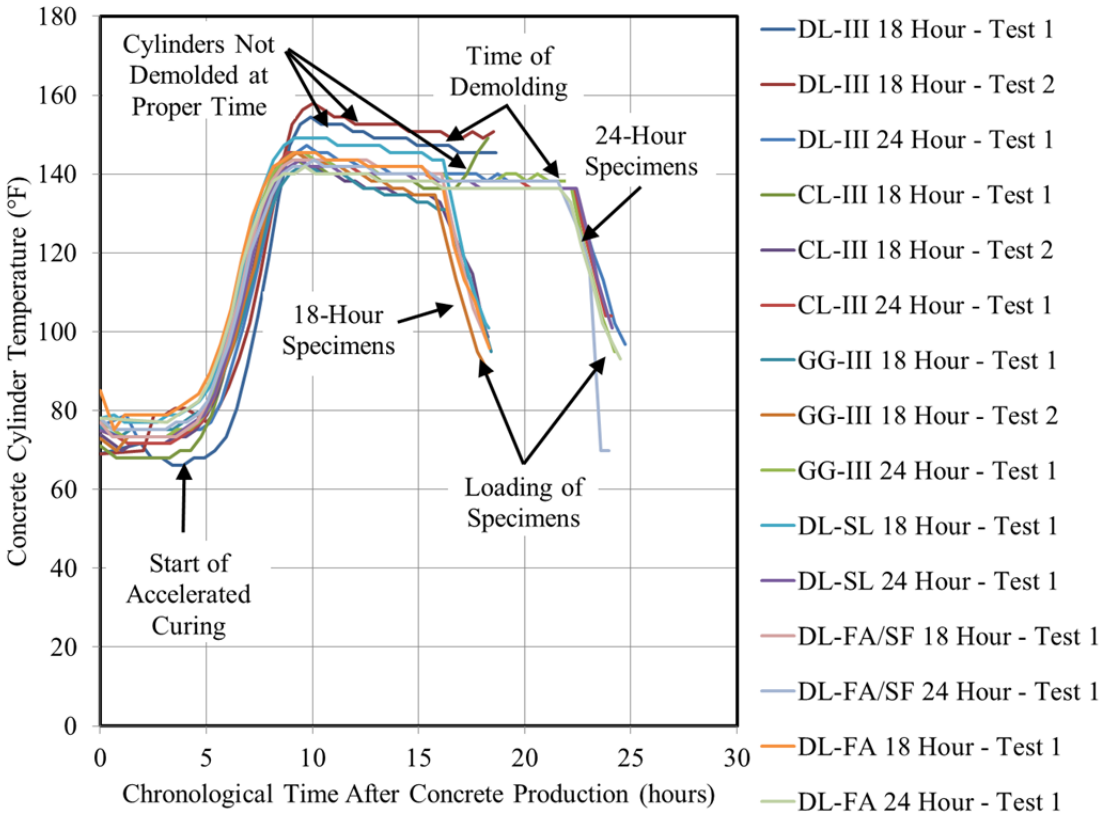

Figure 7-2: Temperature History for Laboratory Tests

As shown, the accelerated curing treatment began four hours after concrete production with curing temperature linearly increasing at an hourly rate of approximately 20.5°F up to a maximum temperature of approximately 150°F. Then, specimens were demolded and prepared for testing in accordance with ASTM C512-02. During the period after demolding and prior to testing, specimens were exposed to ambient laboratory conditions (68-70°F) and allowed to cool accordingly. In three tests (DL-III 18 Hour Test 1+2 and CL-III 18 Hour Test 1), the companion thermocouple cylinders used to record temperature were not demolded at the proper time, as represented in Figure 7-2 by the roughly horizontal lines immediately prior to loading for these three tests. For this reason, the computed maturity for the DL-SL 18 Hour Test 1 was used as a typical 18-hour loading maturity for each of the three tests noted above.

The temperature profiles shown in Figure 7-2 were used to compute two metrics of maturity necessary for creep and shrinkage prediction models. First, the equivalent-age maturity was computed for each test in accordance with *fib* Model Code 2010. Computed values for the equivalent age at the time of loading are shown in the third column of Table 7-1 for each test. Next, to include the effect of cement type and curing temperature as required by the provisions of the *fib* Model Code 2010, the adjusted equivalent-age maturity was computed for each test as shown in the fourth column of Table 7-1.

Table 7-1: Equivalent-Ages at Time of Loading by Test

Test ID	Chronological Age at Loading (days)	Equivalent Age[b] At Loading (days)	Adjusted Equivalent Age[c] of Loading (days)
DL-III 18 Hour – Test 1	0.78	3.0[a]	7.6
DL-III 18 Hour – Test 2	0.77	3.0[a]	7.6
DL-III 24 Hour – Test 1	1.03	4.0	8.9
CL-III 18 Hour – Test 1	0.76	3.0[a]	7.6
CL-III 18 Hour – Test 2	0.76	2.5	7.0
CL-III 24 Hour – Test 1	1.00	3.9	8.8
GG-III 18 Hour – Test 1	0.77	2.5	7.0
GG-III 18 Hour – Test 2	0.76	2.5	7.0
GG-III 24 Hour – Test 1	1.01	3.9	8.8
DL-SL 18 Hour – Test 1	0.76	3.0	7.7
DL-SL 24 Hour – Test 1	1.00	3.8	8.7
DL-FA/SF 18 Hour – Test 1	0.76	2.7	7.3
DL-FA/SF 24 Hour – Test 1	1.00	3.8	8.7
DL-FA 18 Hour – Test 1	0.76	2.8	7.4
DL-FA 24 Hour – Test 1	1.02	3.8	8.7

Notes: [a] = DL-SL 18 Hour – Test 1 temperature profile used;
[b] = Computed in accordance with *fib* MC 2010 (datum temperature = 20°C and AE = 33.2 kJ/mol); and
[c] = Computed in accordance with *fib* MC 2010 accounting for cement type.

7.3.4 Fresh Concrete Properties

For each of fifteen tests, fresh concrete temperature, slump, and air content were measured as shown in Table 7-2. The fresh concrete temperature for each test was used

in the computation of the equivalent-age maturities computed in Section 7.3.3 for the time period between initial mixing of concrete and the time of cylinder sampling.

Table 7-2: Fresh Concrete Properties by Test

Test ID	Temperature (°F)	Slump (in.)	Air Content (%)
DL-III 18 Hour – Test 1	69	9.0	2.5
DL-III 18 Hour – Test 2	69	8.0	3.0
DL-III 24 Hour – Test 1	76	8.0	2.5
CL-III 18 Hour – Test 1	71	9.0	3.0
CL-III 18 Hour – Test 2	74	8.0	3.6
CL-III 24 Hour – Test 1	75	8.25	2.8
GG-III 18 Hour – Test 1	75.5	8.5	3.0
GG-III 18 Hour – Test 2	73	9.0	3.9
GG-III 24 Hour – Test 1	77	8.50	2.5
DL-SL 18 Hour – Test 1	76	8.0	2.8
DL-SL 24 Hour – Test 1	75	8.0	2.5
DL-FA/SF 18 Hour – Test 1	77	8.5	5.0
DL-FA/SF 24 Hour – Test 1	78	8.0	4.0
DL-FA 18 Hour – Test 1	78	8.5	2.9
DL-FA 24 Hour – Test 1	78	7.5	2.8

7.3.5 Hardened Concrete Properties

For each of 15 tests, concrete compressive strength and elastic modulus at the time of loading were tested in accordance with ASTM C39 (ASTM 2010) and ASTM C469 (ASTM 2010), respectively. Results for each test are shown in Table 7-3.

Table 7-3: Hardened Concrete Properties by Test

Test ID	Compressive Strength, f_c, at Loading (psi)	Elastic Modulus, E_c, at Loading (ksi)	Compressive Strength, f_c, at 28 Days (psi)
DL-III 18 Hour – Test 1	6,420	5,700	9,900
DL-III 18 Hour – Test 2	6,520	5,600	9,910
DL-III 24 Hour – Test 1	6,900	6,350	9,010
CL-III 18 Hour – Test 1	6,610	5,700	9,520
CL-III 18 Hour – Test 2	6,170	5,750	9,010
CL-III 24 Hour – Test 1	7,220	6,100	9,640
GG-III 18 Hour – Test 1	7,400	3,700	10,070
GG-III 18 Hour – Test 2	6,850	3,500	9,650
GG-III 24 Hour – Test 1	7,940	3,900	10,440
DL-SL 18 Hour – Test 1	6,870	6,600	10,080
DL-SL 24 Hour – Test 1	7,260	6,400	9,860
DL-FA/SF 18 Hour – Test 1	6,900	6,050	9,850
DL-FA/SF 24 Hour – Test 1	7,270	6,100	9,800
DL-FA 18 Hour – Test 1	6,860	6,100	10,240
DL-FA 24 Hour – Test 1	7,360	6,100	10,200

7.3.6 Creep and Shrinkage Testing Procedures

Creep and shrinkage testing was conducted in accordance with the general requirements of the *Standard Test Method for Creep of Concrete in Compression,* ASTM C512-02. Testing in accordance with this specification requires the application of a sustained stress equal to 40 percent of the compressive strength at the time of loading and monitoring specimens for long-term changes in strain. In absence of specification requirements or guidance, the following experimental procedures were selected to tailor creep and shrinkage testing efforts to regional precast, prestressed industry practices:

- Due to the early age of testing, the use of sulfur capping was impractical and instead, the ends of cylindrical specimens were ground flat and true with an automated diamond grinder intended for use on concrete cylinders;
- Two ages at loading (18 hours and 24 hours) and an accelerated curing protocol were used in this research program to simulate both the average loading maturity observed in the field and an upper-bound value;

- The accelerated curing protocol was terminated roughly two hours prior to creep frame loading to allow preparation of the specimens (demolding, grinding, and *DEMEC* application). During this time period, the specimens were exposed to ambient temperature, but maintained in a moist enclosure;
- The elevated temperature of cylinders at the time of loading was recorded throughout the early life of the test—until the specimens reached ambient specified temperature conditions;
- In addition to the testing of compressive strength immediately prior to the time of loading as required by ASTM C512-02, the elastic modulus was tested at the time of loading in accordance with ASTM C469;
- Creep and shrinkage testing was performed for a period of 250 days, well in excess of the anticipated pre-service life of bridge girder; and
- Demountable mechanical (*DEMEC)* strain gages were used to monitor both concrete cylinder strains and also tension in the steel bars of creep loading frames. *DEMEC* gages were used to monitor steel bar strains to preclude long-term drift associated with electrical-resistance strain gages.

A detailed narrative of creep and shrinkage testing procedures in accordance with ASTM C512-02 is described in previous work of Ellis (2012) and Kavanaugh (2008), who each previously conducted creep and shrinkage testing using identical apparatuses to those used in this experimental effort. Key steps in the creep testing procedure are shown in Figure 7-3.

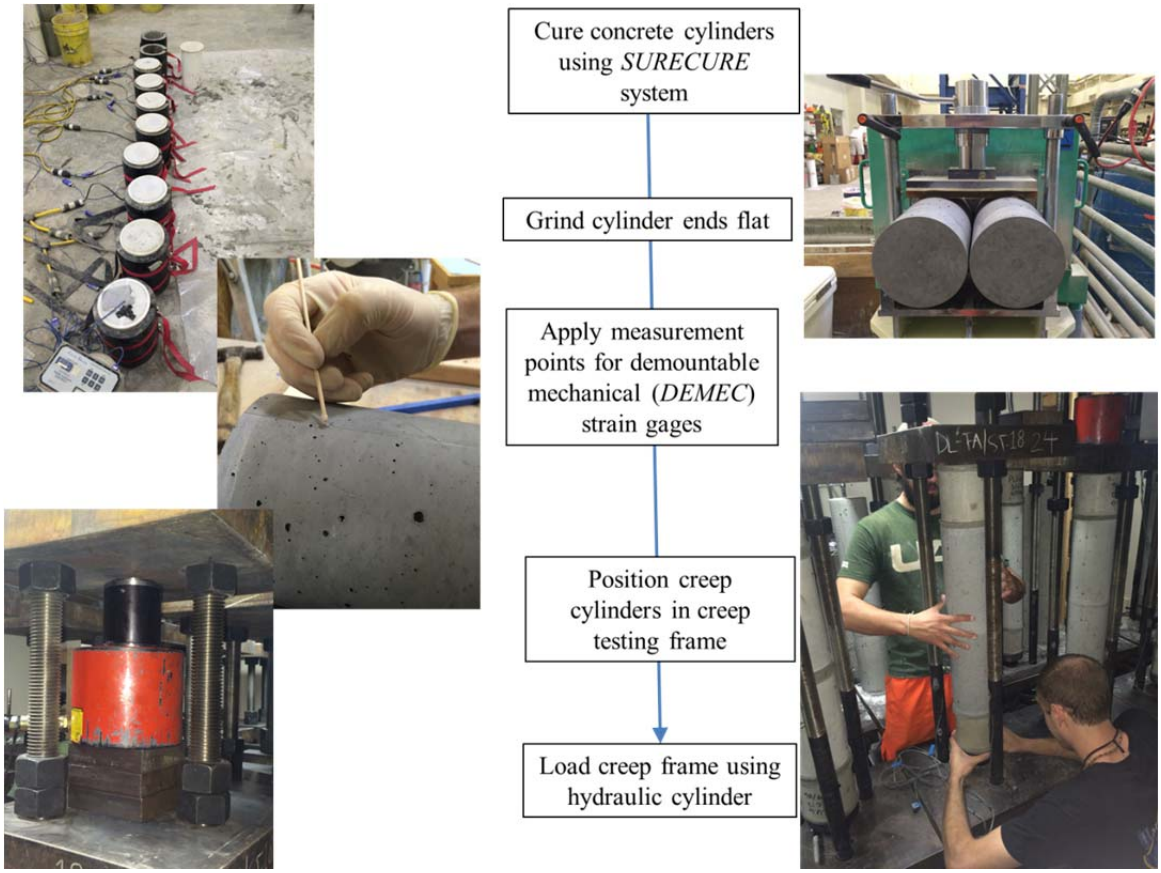

Figure 7-3: Creep Testing Procedure

7.3.7 Shrinkage Testing Procedures

In addition to the shrinkage testing performed on accelerated cured cylindrical specimens detailed above, shrinkage properties were also evaluated for each candidate concrete mixture using standard-cured concrete rectangular prisms in accordance with the requirements of ASTM C157-08. In absence of specification requirements or guidance, the following experimental procedure adjustment was selected to best tailor shrinkage testing efforts to regional precast, prestressed industry practices:

- Benchmark shrinkage readings were first recorded upon exposure to ambient conditions at the end of an initial standard curing period of 7 days. A value of 7 days was selected to coincide with the default assumptions for the length of initial

standard (non-accelerated) curing period as reflected in the ACI 209 and AASHTO 2014 shrinkage prediction models.

7.4 Post-Processing of Measured Data

This section details various post-processing efforts aimed at affirming the accuracy of recorded data, determining the experimental precision of the laboratory creep and shrinkage testing setup, and accounting for temperature effects at the time of loading. The full experimental data set resulting from the creep and shrinkage testing efforts of this research study is presented in Section 7.5; only limited results related to the topic of this section are included here.

7.4.1 Detection and Removal of Climate Control System Failures

As discussed earlier in this chapter, creep and shrinkage behavior of concrete is extremely sensitive to environmental factors, namely temperature and relative humidity. For this reason, ASTM C512-02 and ASTM C157-08 each require strict control over temperature and relative humidity throughout the duration of testing. Ambient temperature during testing must be 73.4 ± 1.5°F, while relative humidity is permitted to range from 46-54 percent. Due to the extended period of testing (250 days) conducted in this research effort, brief failures of the climate control system were inevitable due to power outages and unexpected malfunctions of the climate control system. The date and time of all climate control system malfunctions were noted and repairs were completed expediently. Nonetheless, various failures of the climate control system did compromise certain measurements throughout the course of the project. An iterative procedure (as detailed in Appendix E) was developed for the detection and removal of data points that were compromised by documented failures of the climate control system.

7.4.2 Determination of Experimental Precision for Creep and Shrinkage Testing of Cylindrical Specimens

It is important to determine the experimental precision of the creep and shrinkage testing of cylindrical specimens conducted in this research effort to allow for accurate analysis of experimental data. Without a clear understanding of the precision and repeatability of the experimental methods used herein, it may not be possible to attribute observed variation to the key variables of interest (i.e. age at loading, coarse aggregate type, and SCM use) instead of to intrinsic variability of the test method. This section focuses on determining an approximate level of experimental precision for cylindrical specimen testing that is used in the subsequent data analysis efforts of this chapter. Readers should note that this effort is necessary because of the limited availability of data (n=1 or n=2 at best for given variable combination) precludes the use of inferential statistics. The first portion of this section focuses on systematically determining the experimental precision for compliance of cylindrical specimens, while the later portions focus on estimating the experimental precision for shrinkage testing of cylindrical concrete specimens.

ASTM C512-02 notes that the results of two properly conducted creep and shrinkage tests by the same operator on material cast from different batches should not differ by more than 13 percent of their average (ASTM 2002). The computed compliance, J, for each of three duplicate tests conducted in this experimental effort is shown in Figure 7-4. As shown, the results of duplicate tests qualitatively appear quite similar, with each set of tests satisfying the precision statement noted above (a maximum variation from average of 6 percent is observed for the GG-III tests).

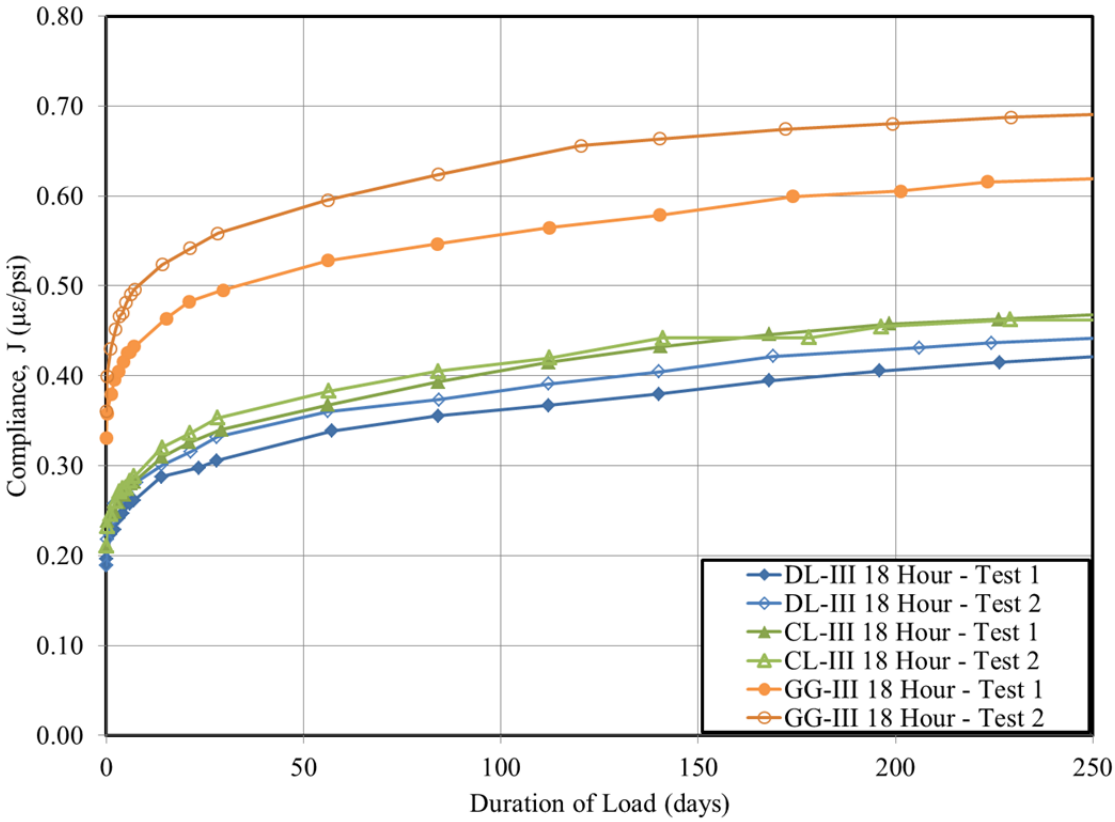

Figure 7-4: Compliance Behavior of Duplicate Tests

The compliance data of Figure 7-4 is displayed in tabulated form for four key ages in Table 7-4. The ages of interest include the following times: (1) immediately after loading, (2) lower-bound girder erection estimate = 60 days, (3) upper-bound girder erection estimate = 120 days, and (4) 250 days. As shown, the duplicate tests for the DL-III concrete exhibit a uniform difference between subsequent tests of 0.02 με/psi at all considered ages, while the CL-III tests exhibit a similar uniform difference of 0.01 με/psi between subsequent verification tests. For the dolomitic limestone mixtures considered in this effort, a precision of 0.02 με/psi is assumed for analysis purposes—that is, any measured compliance value is assumed to be precise to within ± 0.02 με/psi for a given

Table 7-4: Compliance Behavior of Duplicate Tests

Test ID	Initial Compliance, *J*, (με/psi)	Difference Between Duplicate Tests (με/psi)	60-Day Compliance, *J*, (με/psi)	Difference Between Duplicate Tests (με/psi)	120-Day Compliance, *J*, (με/psi)	Difference Between Duplicate Tests (με/psi)	250-Day Compliance, *J*, (με/psi)	Difference Between Duplicate Tests (με/psi)
DL-III 18 Hour – Test 1	0.19	0.00	0.34	**0.02**	0.37	**0.02**	0.42	**0.02**
DL-III 18 Hour – Test 2	0.19		0.36		0.39		0.44	
CL-III 18 Hour – Test 1	0.21	0.00	0.37	0.01	0.41	0.01	0.47	0.01
CL-III 18 Hour – Test 2	0.21		0.38		0.42		0.46	
GG-III 18 Hour – Test 1	0.33	0.03	0.53	0.07	0.56	**0.10**	0.62	0.07
GG-II 18 Hour – Test 2	0.36		0.60		0.66		0.69	

Note: Approximate error derived from instrument precision = 0.003 με/psi.

test[6]. Conversely, the difference between the two GG-III duplicate tests is more pronounced, ranging from 0.03 to 0.10 με/psi at various ages. At first consideration, it is tempting to assume experimental difficulties may be to blame for the larger observed differences between duplicate tests. However, no apparent anomalies were detected within either loading frame. Given that (1) the observed variation for the GG-III duplicate tests remains well within the precision of the test, (2) the GG-III mixture exhibited unexpectedly low stiffness (perhaps due to high levels of deleterious substances), and (3) one of the GG-III tests appears to exhibit an uncharacteristically high early rate of compliance, the computed precision values of 0.03 to 0.10 με/psi is used to evaluate the GG-III tests in the remainder of this report.

A similar procedure was used to determine the experimental precision for shrinkage testing of cylindrical specimens. A graph of experimental results for the duplicate shrinkage tests is shown in Figure 7-5, with values at key ages displayed in Table 7-5. By the nature of testing early-age accelerated-cured concrete specimens, there is slight variability in the temperature of specimens at the age at loading, which increases the variability of measured results. This topic is discussed more thoroughly in Section 7.4.5.

[6] Without knowing which of two duplicate loading cycles is most accurate, it was not possible to compute a percent difference between measured values. Instead, the difference between values is selected as a measure of experimental precision.

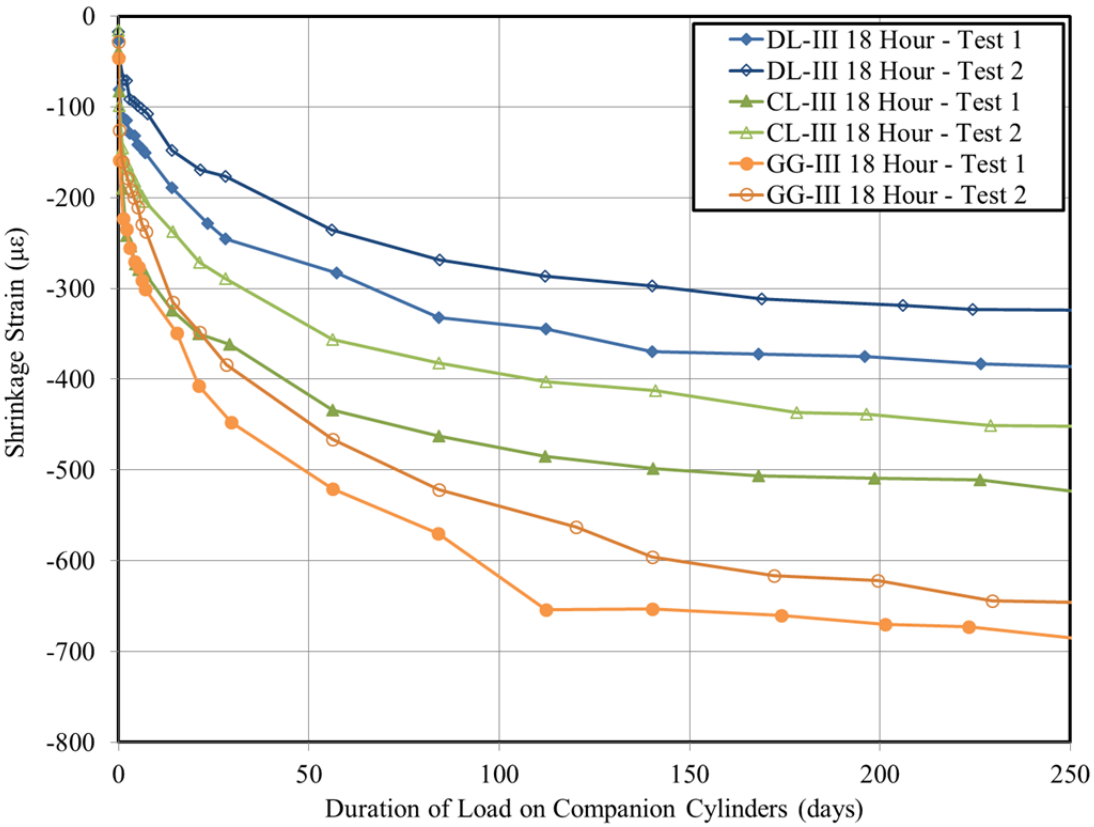

Figure 7-5: Cylinder Shrinkage Behavior of Duplicate Tests

Table 7-5: Cylinder Shrinkage Behavior of Duplicate Tests

Test ID	Initial Shrinkage[a], (με)	Difference Between Duplicate Tests (με)	60-Day Shrinkage, (με)	Difference Between Duplicate Tests (με)	120-Day Shrinkage, (με)	Difference Between Duplicate Tests (με)	250-Day Shrinkage, (με)	Difference Between Duplicate Tests (με)
DL-III 18 Hour - Test 1	-27	9	-288	48	-352	63	-386	62
DL-III 18 Hour – Test 2	-18		-240		-289		-324	
CL-III 18 Hour – Test 1	-39	23	-438	78	-489	84	-524	**90**
CL-III 18 Hour – Test 2	-16		-360		-405		-452	
GG-III 18 Hour – Test 1	-46	17	-528	54	-653	**90**	-685	39
GG-II 18 Hour – Test 2	-29		-474		-563		-646	

[a] = Initial shrinkage is the measured shrinkage occurring between pre-loading and post-loading and is predominately due to the cooling of specimens (as is discussed in Section 7.4.4).

Note: Approximate error from instrument precision = 8 με**.**

Examining the data of Table 7-5, a maximum difference between duplicate tests of 90 με is observed and an approximate average value of 60 με exceeds all but four of the shown differences. This value serves as an average precision for the cylinder shrinkage testing conducted in this study, although engineering judgment is also used to identify possible significant trends in experimental data.

7.4.3 Determination of Experimental Precision for Rectangular Shrinkage Prism Testing

The experimental precision for rectangular shrinkage prism testing was determined in similar fashion to above using the experimental results shown in Figure 7-6 and Table 7-6. Despite the rectangular shrinkage prism data exhibiting more distinct and clear clustering of experimental results, the precisions between duplicate tests are similar to those of cylindrical specimens. In this case, three tests are available for the DL-III and GG-III sample groups due to the identical treatment of rectangular shrinkage prisms regardless of 18- or 24-hour age at loading. The CL-III sample group contains only two tests due to experimental difficulties with the rectangular prisms from the CL-III 18 Hour – Test 2. As shown in Table 7-6, a maximum difference between duplicate results of 92 με is observed for the DL-III tests, while the average value of observed difference lingers again around 70 με. This value serves as an average precision for the rectangular prism shrinkage testing conducted in this study, although engineering judgment may also be used to identify possible significant trends in experimental data. For typical design values of prestressing strand modulus of elasticity and jacking stresses, a variation of 140 με (±70 με) in unrestrained shrinkage corresponds to less than a 2 percent change in the effective prestress force, thereby having a small effect on computed camber values.

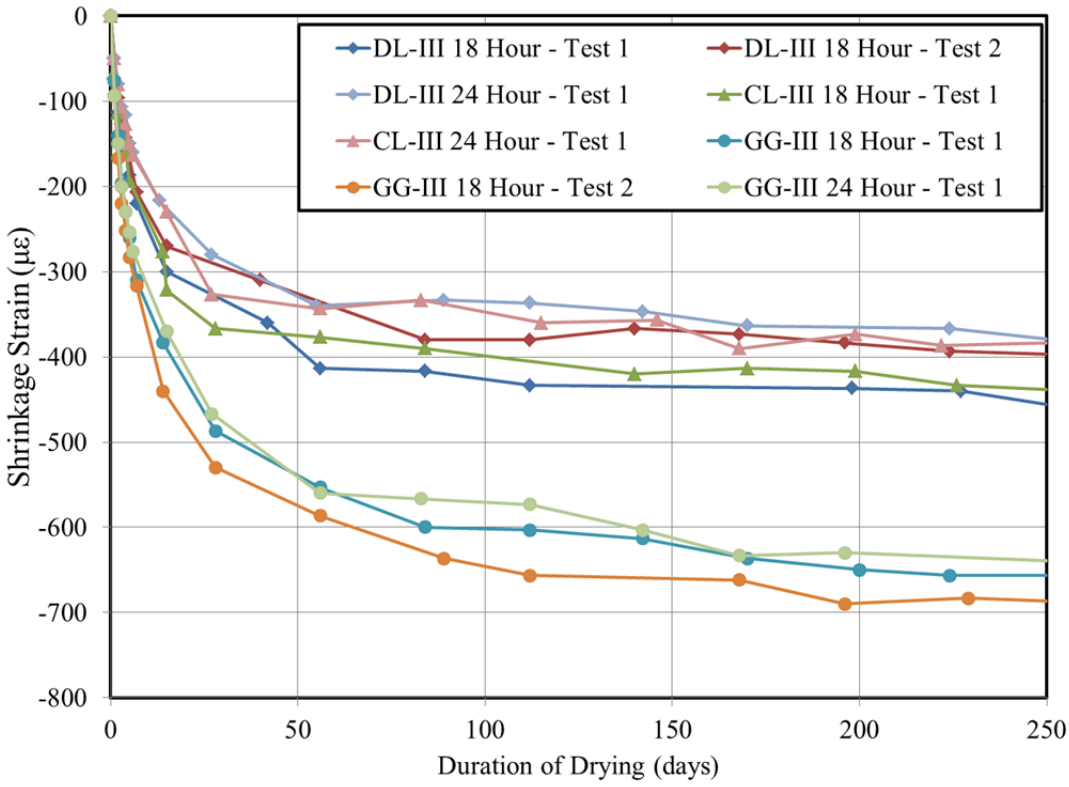

Figure 7-6: Rectangular Prism Shrinkage Behavior for Duplicate Tests

Table 7-6: Rectangular Prism Shrinkage Behavior of Duplicate Tests

Test ID	1-Day Shrinkage, (με)	Max. Difference Among Duplicate Tests (με)	60-Day Shrinkage, (με)	Max. Difference Among Duplicate Tests (με)	120-Day Shrinkage, (με)	Max. Difference Among Duplicate Tests (με)	250-Day Shrinkage, (με)	Max. Difference Among Duplicate Tests (με)
DL-III 18 Hour - Test 1	-73	23	-414	75	-432	**92**	-456	77
DL-III 18 Hour – Test 2	-50		-341		-376		-396	
DL-III 24 Hour – Test 1	-50		-339		-340		-379	
CL-III 18 Hour – Test 1	-67	17	-379	37	-409	50	-438	55
CL-III 24 Hour – Test 1	-50		-342		-359		-383	
GG-III 18 Hour – Test 1	-77	16	-560	33	-606	77	-657	47
GG-III 18 Hour – Test 2	-93		-593		-658		-687	
GG-III 24 Hour – Test 1	-93		-561		-581		-640	

Note: Approximate error from instrument precision = 10 με.

7.4.4 Effect of Concrete Temperature at Loading

As noted by ACI Committee 209 (2008) any effects of thermal strain should be avoided entirely or otherwise removed from measured creep and shrinkage data. By virtue of the early concrete age at loading and accelerated curing methods typical of precast, prestressed concrete construction, it is unavoidable that elevated temperatures be present at the time of loading in both field-testing and laboratory-testing efforts. Previous researchers most often ignore the presence of thermal strains at and immediately following loading and, therefore, reported shrinkage values measured on cylindrical specimens actually represent a combination of shrinkage strains and thermal strains. Conveniently, because these shrinkage and thermal strains are subtracted from the loaded cylinders, compliance is unaffected by the presence of these thermal strains. Kelly, Bradberry, and Breen (1987) attempted to manually remove the effect of thermal strains at the time of loading from measured cylinder shrinkage strains—although their methods relied on an assumed coefficient of thermal expansion for typical precast, prestressed concretes. Without precisely knowing the coefficient of thermal expansion (CTE) of the concrete at loading (which is expected to be a function of moisture content), precise decoupling of shrinkage strains and thermal strains is not possible.

In this research project, the decision was made to disregard the effect of thermal strains at and immediately following the time of loading in laboratory testing for the following reasons:

- The thermal strains observed and induced in this research effort simulated those likely present during field-fabrication and thus, should be included in design predictions of shrinkage[7];
- Nearly all previous researchers conducting creep and shrinkage testing of precast, prestressed concretes have similarly ignored the presence of the effect of early thermal strains in their reported shrinkage results;
- ACI 209 (2008) notes that the rate of creep and shrinkage are temperature-dependent, thereby suggesting that the superposition method used by Kelly et al. (1987) may not fully remove the influence of temperature on experimental measurements; and
- Coefficient of thermal expansion (CTE) values as required for the superposition method used by Kelly at al. (1987) are difficult to estimate accurately at the time (and moisture state) at loading.

In addition to the above practical reasons, a more theoretical justification for the decision to neglect the presence of thermal strains in shrinkage measurements is offered herein. The intent of this experimental effort is to evaluate the effect of various material properties (either assumed, expected, or known) on the camber of precast, prestressed concrete girders. In computing camber, the effect of shrinkage is assumed to act uniformly on a given cross section as is discussed in Chapter 9 (i.e. unrestrained shrinkage strains do not vary with girder height). In accordance with this assumption, a uniform shrinkage will not tend to directly influence the magnitude of camber in a precast, prestressed girder. Instead, concrete shrinkage behavior tends to induce only

[7] ACI 209 (2008) notes that no prediction method can yield better results than testing actual materials under conditions similar to those expected in the field.

minor changes to camber due to (1) eccentric restraint of reinforcement and (2) by reducing the effective prestressing force of the element (as is discussed and clarified in Chapter 8). For this reason, it seems permissible and perhaps even advantageous to include the effect of early thermal strains in measured shrinkage values.

7.5 Presentation and Analysis of Results

This dissertation section first broadly presents the experimental results of the creep and shrinkage testing conducted as part of this effort. Then, the relative effect of each of the three main variables of interest (coarse aggregate type, age at loading, and SCM usage) is explored, while using the previously computed experimental precisions to identify significant results. Next, three candidate creep and shrinkage prediction models are implemented and compared to experimental behavior. Finally, the three candidate creep and shrinkage prediction models are modified (calibrated) by the use of a multiplier to yield most accurate results for typical regional concretes.

7.5.1 Compliance

As previously mentioned, the preferred metric for time-dependent load-induced deformation in this dissertation is compliance. Compliance, as presented in this section, is computed directly from the following measured parameters: (1) the total strain of creep specimens after loading at a given time, (2) the total strain of companion shrinkage specimens after loading at a given time, and (3) the magnitude of the applied load. Due to the large amount of data generated from the experimental efforts of this chapter, visualization of data in a clear and concise manner is somewhat challenging. Graphical depictions of compliance curves are selected as the preferred metric of data display, with selected values shown in tabulated form as required for quantitative comparisons. Where

tabulated values are used to analyze and compare data, the following important durations of load are again used: 60 days, 120 days, and 250 days.

7.5.1.1 Presentation of Measured Results

Compliance results for each of 15 tests included in this project are displayed in Figure 7-7, grouped by coarse aggregate type for clarity. As shown, compliance results from the crushed granite concrete mixture appear distinctly separate from the dolomitic limestone mixtures and are thus considered a separate group for the remainder of data visualization purposes.

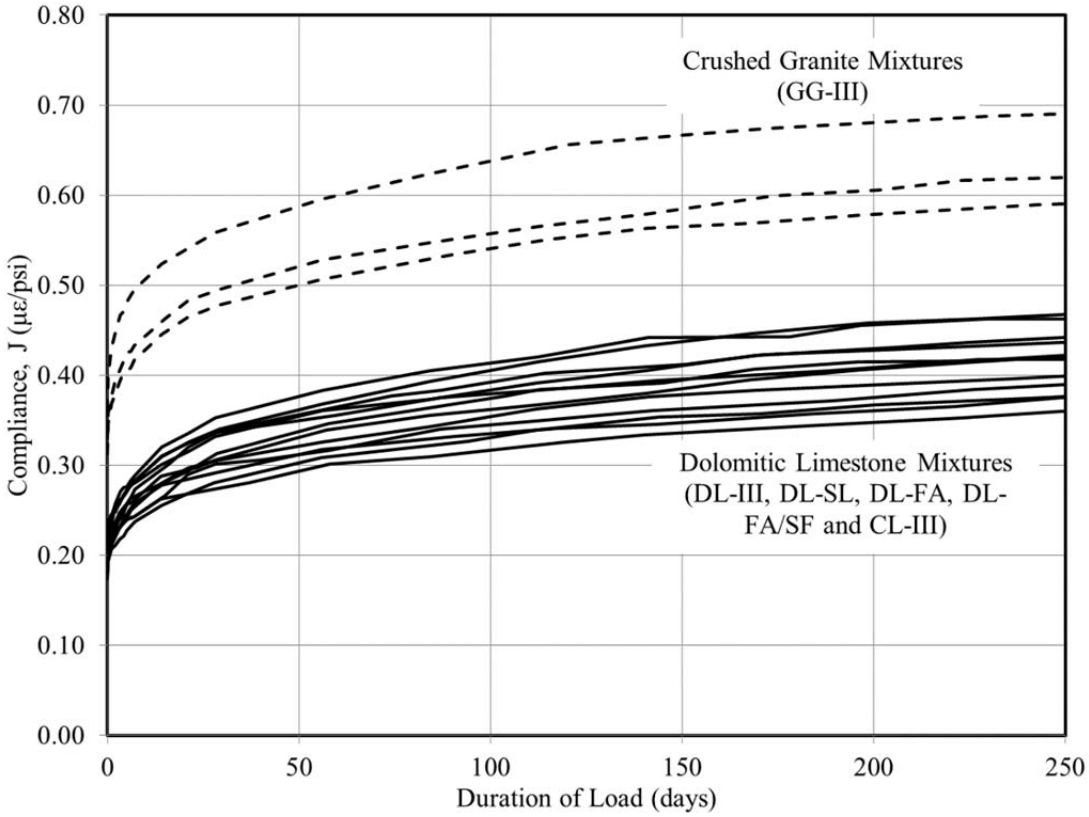

Figure 7-7: Compliance Results by Aggregate Type

For each of the above subgroups, results of the no-SCM variant (i.e. GG-III, DL-III, and CL-III) tests are displayed in Figures 7-8 and 7-9, identified by age at loading. For

convenience in preliminary comparisons of each subgroup, dashed lines identify 18-hour tests and solid lines denote 24-hour tests.

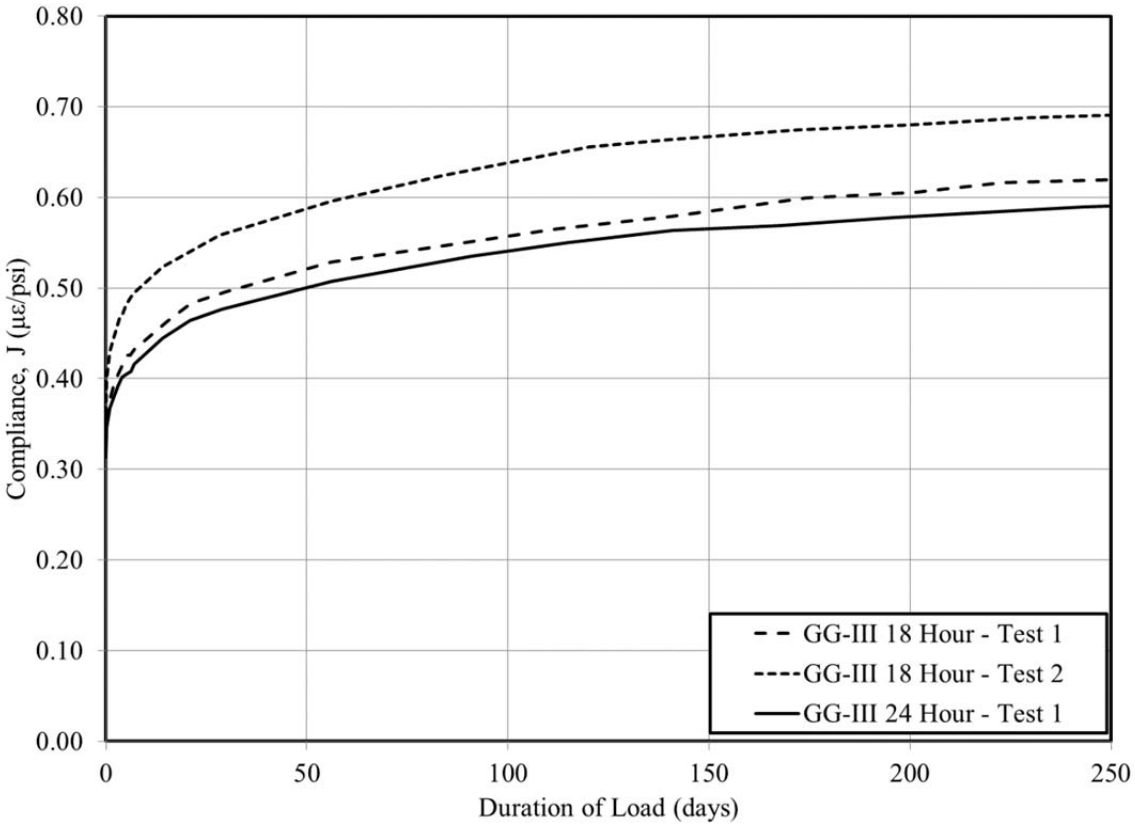

Figure 7-8: Compliance for No-SCM Variant Crushed Granite Tests

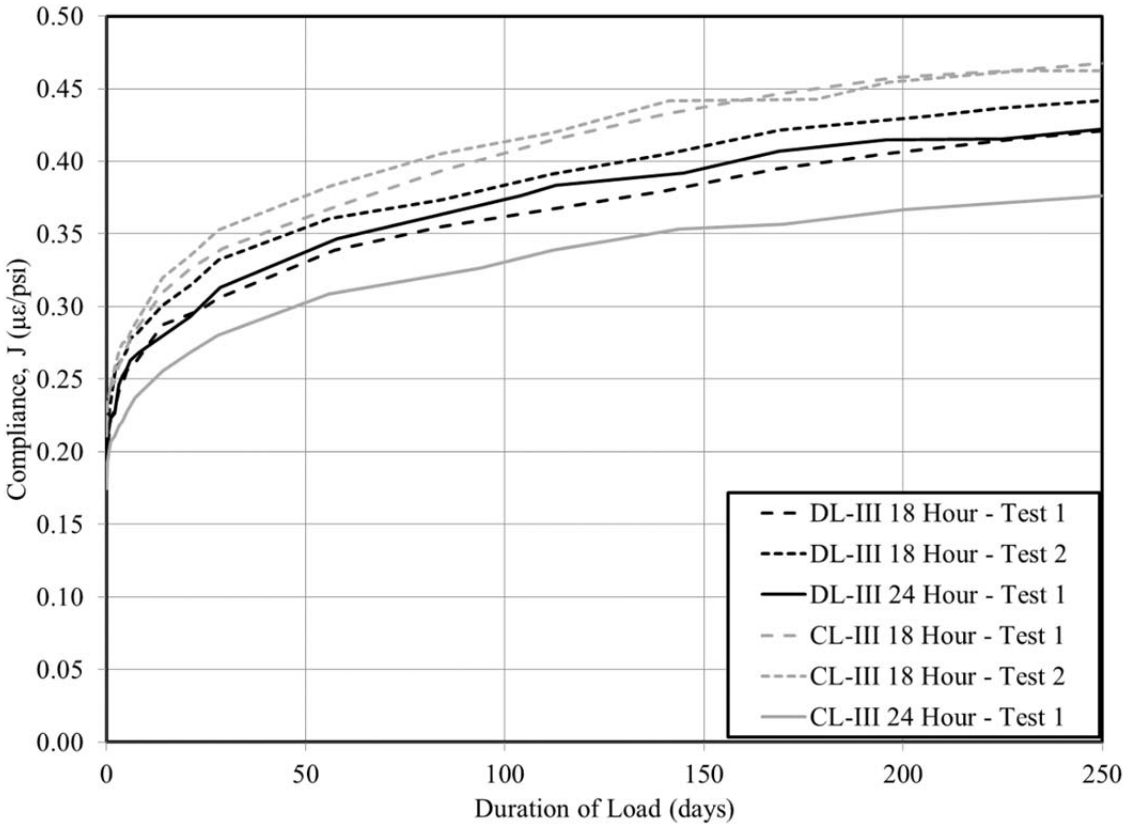

Figure 7-9: Compliance for No-SCM Variant Dolomitic Limestone Tests

Figures 7-8 and 7-9 collectively depict nine of the fifteen total tests conducted as part of this research effort. The remaining six tests represent the SCM variants and are displayed in Figure 7-10, along with the companion dolomitic limestone no-SCM variants for comparison.

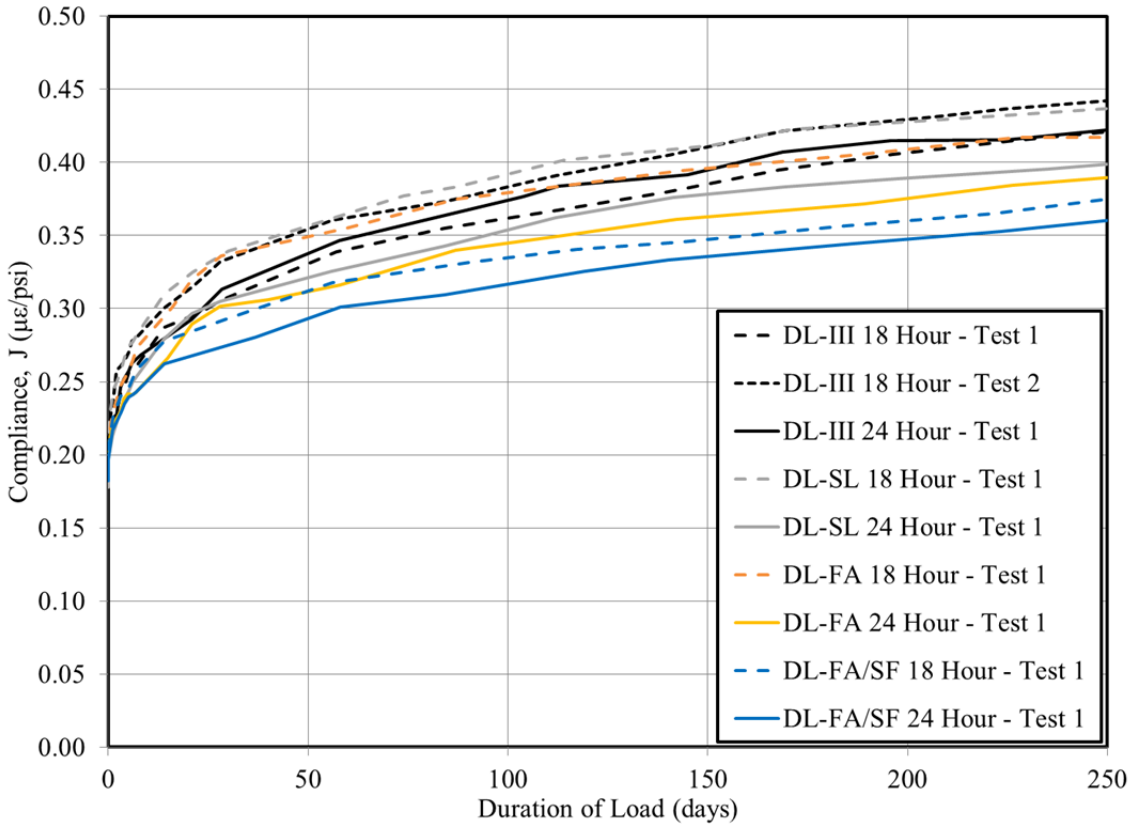

Figure 7-10: SCM-Variant Dolomitic Limestone Tests

Although the above figures display the experimental data set in the most convenient subgrouping for analysis purposes, the complete unsorted data set is also shown in Figure 7-11 for reference.

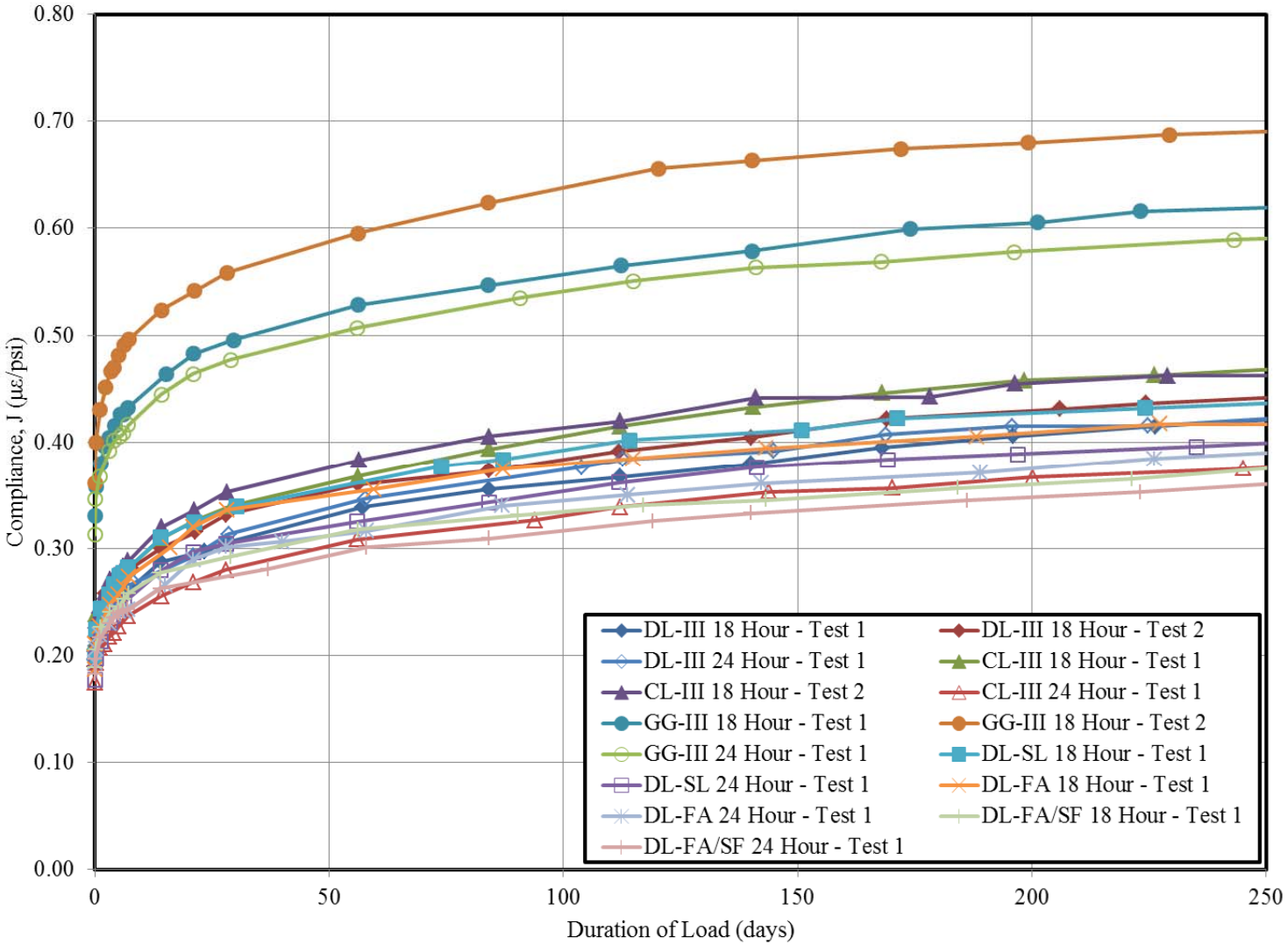

Figure 7-11: Unsorted Creep and Shrinkage Experimental Data Set

7.5.1.2 Effect of Coarse Aggregate Type

To isolate any potential effect of coarse aggregate type on compliance, it is most reasonable to compare only the no-SCM experimental variants (DL-III, CL-III, and GG-III) for each of two ages at loading, independently. Significant trends in experimental data are first identified by the use of error bands corresponding to the experimental precisions determined in Section 7.4.2. Then, tabulated results are presented as necessary to quantify significant trends. Compliance results for each of the three no-SCM variants for an age at loading of 18 hours are shown in Figure 7-12.

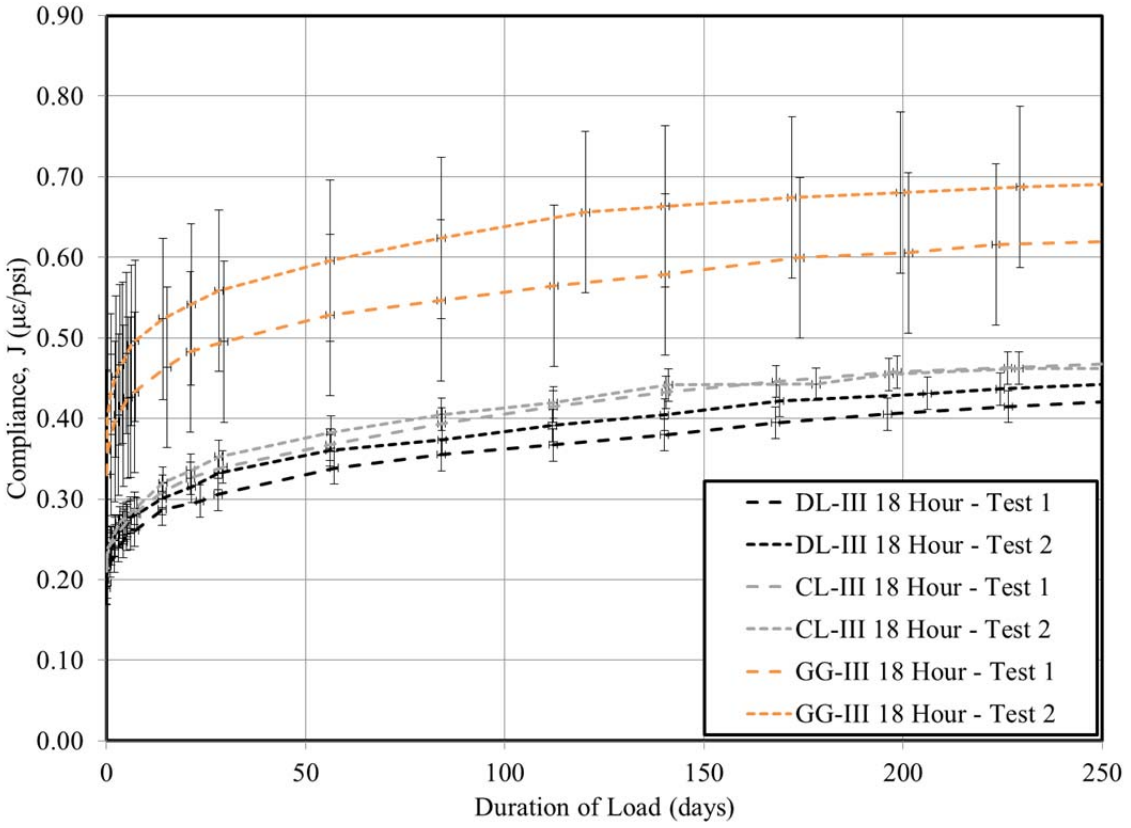

Figure 7-12: Compliance by Aggregate Type for 18 Hour Tests

Error bands are also shown denoting the experimental precisions of ±0.02 με/psi and ±0.10 με/psi for dolomitic limestone and crushed granite tests, respectively. No significant difference in compliance is detectable between the two considered dolomitic

limestone mixtures for an age at loading of 18 hours. Conversely, however, there is a significant difference between the dolomitic limestone mixtures (represented by four tests) and the crushed granite mixtures (represented by two tests). Tabulated values for selected 18-hour age at loading data are shown in Table 7-7.

Table 7-7: Effect of Aggregate Type on Compliance for 18 Hour Loading

Test ID	Initial Compliance[a], *J*, (με/psi)	60-Day Compliance, *J*, (με/psi)	120-Day Compliance, *J*, (με/psi)	250-Day Compliance, *J*, (με/psi)
DL-III 18 Hour - Test 1	0.19	0.34	0.37	0.42
DL-III 18 Hour – Test 2	0.19	0.36	0.39	0.44
CL-III 18 Hour – Test 1	0.21	0.37	0.41	0.47
CL-III 18 Hour – Test 2	0.21	0.38	0.42	0.46
Dolomitic Limestone Average	**0.20**	**0.36**	**0.40**	**0.45**
GG-III 18 Hour – Test 1	0.33	0.53	0.56	0.62
GG-II 18 Hour – Test 2	0.36	0.60	0.66	0.69
Crushed Granite Average	**0.35**	**0.57**	**0.61**	**0.66**

Note: [a] Corresponds to the compliance at the end of load application.

The crushed granite mixtures exhibited substantially increased compliance when compared to the dolomitic limestone mixtures. On average, the observed compliance for the crushed granite mixtures exceeded the dolomitic limestone mixtures by 58 percent. Similar conclusions follow for the compliance behavior by aggregate for the 24-hour tests shown in Figure 7-13 and Table 7-8. In this case, the average observed compliance for the crushed granite mixtures exceeded the dolomitic limestone mixtures by 55 percent.

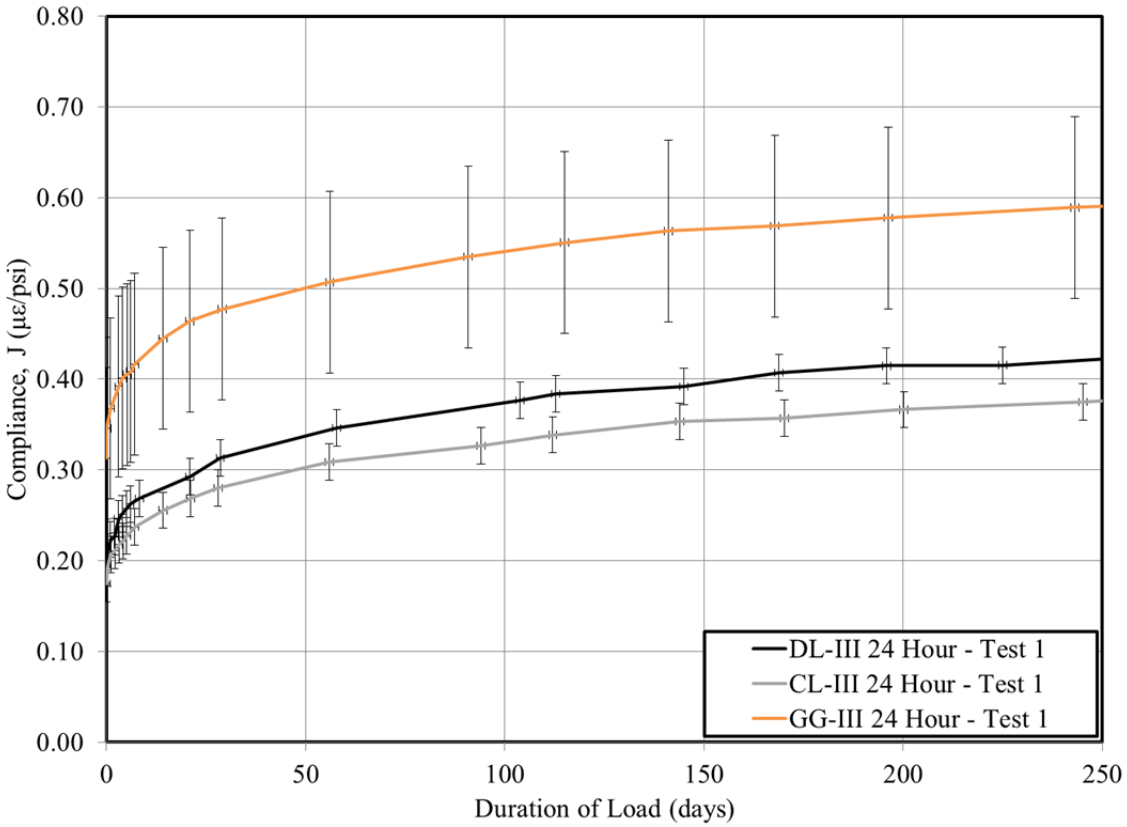

Figure 7-13: Compliance by Aggregate Type for 24 Hour Tests

Table 7-8: Effect of Aggregate Type on Compliance for 24 Hour Loading

Test ID	Initial Compliance[a], *J*, (με/psi)	60-Day Compliance, *J*, (με/psi)	120-Day Compliance, *J*, (με/psi)	250-Day Compliance, *J*, (με/psi)
DL-III 24 Hour - Test 1	0.20	0.35	0.38	0.42
CL-III 24 Hour – Test 1	0.17	0.31	0.34	0.38
Dolomitic Limestone Average	**0.19**	**0.33**	**0.36**	**0.40**
GG-III 24 Hour – Test 1	0.31	0.51	0.55	0.59
Crushed Granite Average	**0.31**	**0.51**	**0.55**	**0.59**

Note: [a] Corresponds to the compliance at the end of load application.

7.5.1.3 Effect of Age at Loading

In order to isolate the effect of age at loading on compliance behavior, each of the six candidate mixtures (unless already shown to be substantially similar as in the case of the DL-III and CL-III) must be independently evaluated using the previously determined experimental precisions. The compliance behavior for the crushed granite tests conducted at ages at loading of 18 and 24 hours are shown in Figure 7-14.

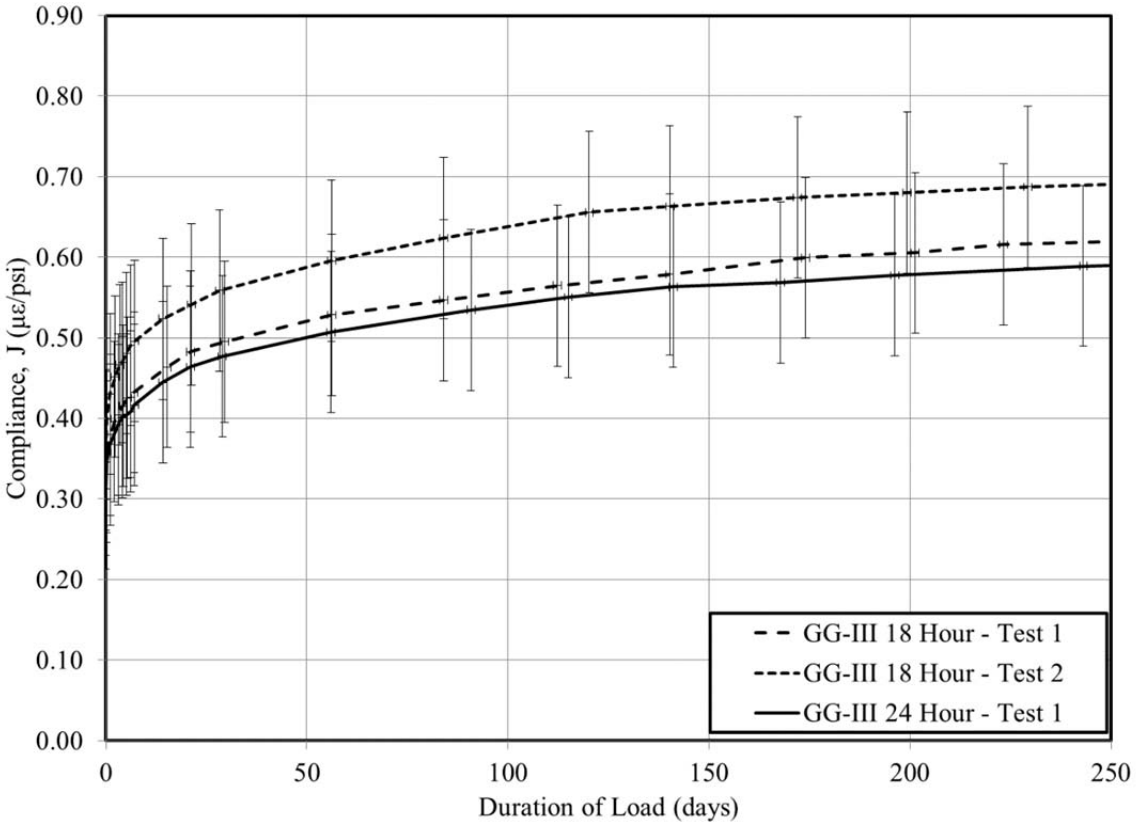

Figure 7-14: Compliance Behavior of Crushed Granite Tests by Age at Loading

As demonstrated by the overlapping error bands, there is no clearly discernable effect of age at loading on compliance behavior for the crushed granite mixtures included in this study. However, although still formally within the precision of the testing program, the 24-hour age at loading tended to exhibit slightly less compliance than the 18-hour ages. Similar conclusions are evident from the no-SCM dolomitic limestone tests shown in

Figure 7-15. (Although the error bands of the CL-III 18-hour tests do not overlap the CL-III 24-hour tests, they do overlap the DL-III 24-hour test, which Section 7.5.1.2 affirmed was largely the same as the CL-III 24-hour test.)

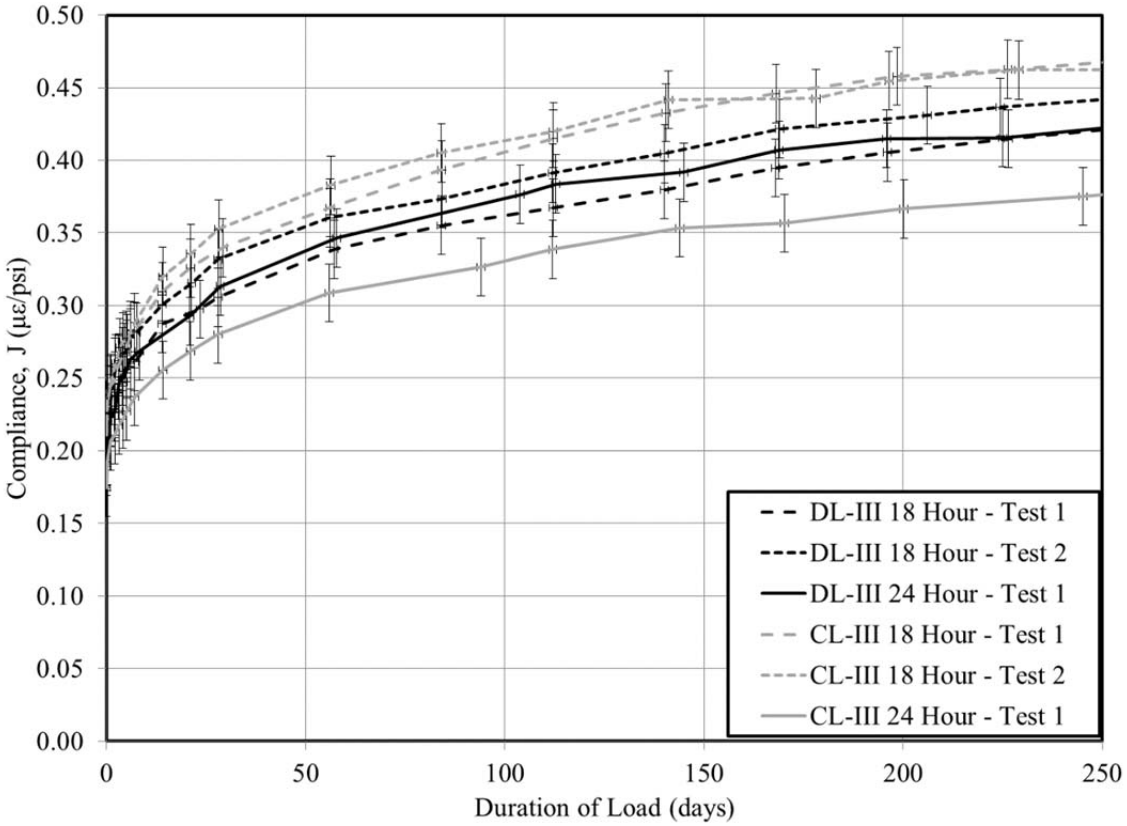

Figure 7-15: Compliance Behavior of No-SCM Variant Dolomitic Limestone Tests by Age at Loading

Again, despite the precision of the experimental program prohibiting the detection of a significant effect of varying ages at loading, all tests with exception of DL-III 18 Hour – Test 1 exhibited the trend that later ages of loading correspond to reduced compliance. Finally, the compliance behavior for each of the SCM-variant tests is shown in Figure 7-16. Similarly, no clear effect of age at loading is detected, although the trend of reduced compliance behavior for later ages at loading is again affirmed.

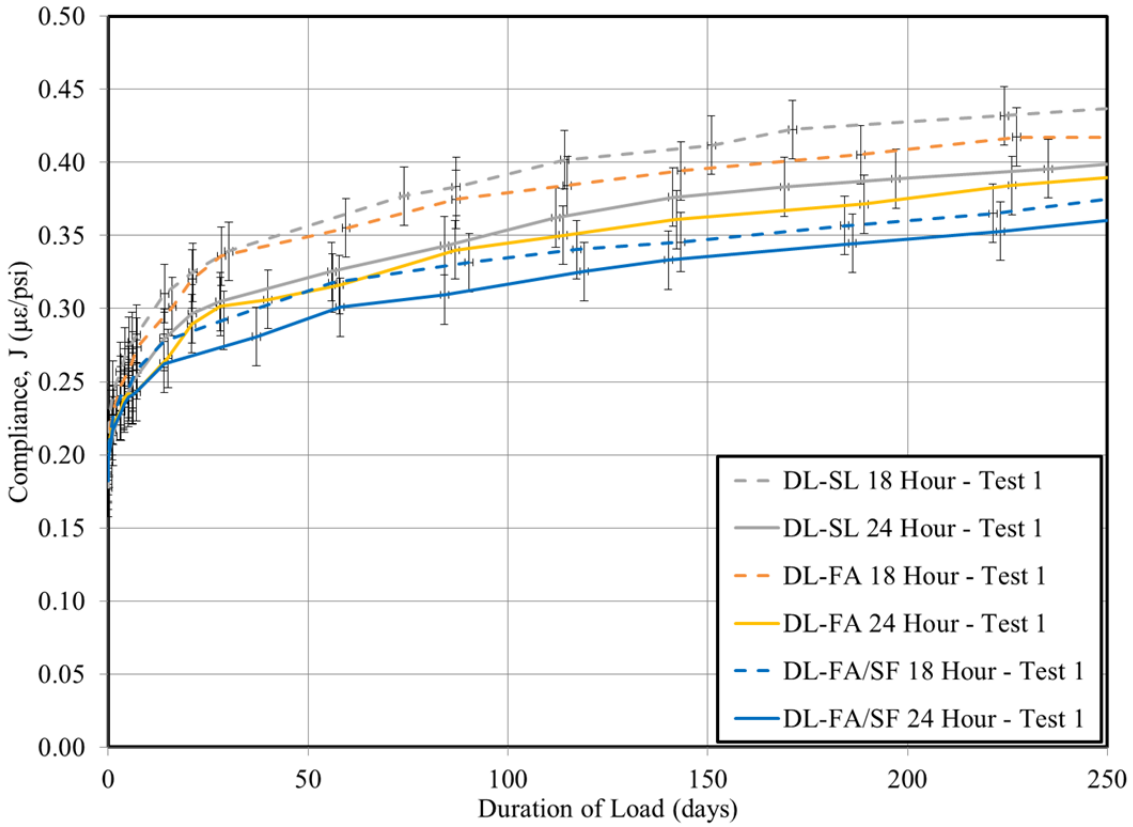

Figure 7-16: Compliance Behavior for SCM-Variant Dolomitic Limestone Tests by Age at Loading

Despite the precision of the creep and shrinkage testing conducted as part of this research effort being better than values included in the precision and bias statement of ASTM C512-02, an effect of age at loading on observed compliance was not detectable for a six hour time difference (18 hour versus 24 hour). In fact, the AASHTO 2014 model predicts a mere 3.5 percent decrease in the computed creep coefficient for an increase in age at loading from 18 hours to 24 hours. Similarly, the 2010 Model Code predicts a 2.9 percent decrease in the computed creep coefficient (for a corresponding shift in adjusted equivalent age from 7.0 to 9.0 days).

7.5.1.4 Effect of Supplementary Cementing Materials (SCMs)

A similar analysis was conducted to explore the potential effect of the use of supplementary cementing materials (SCMs) on compliance, with results shown in Figure 7-17.

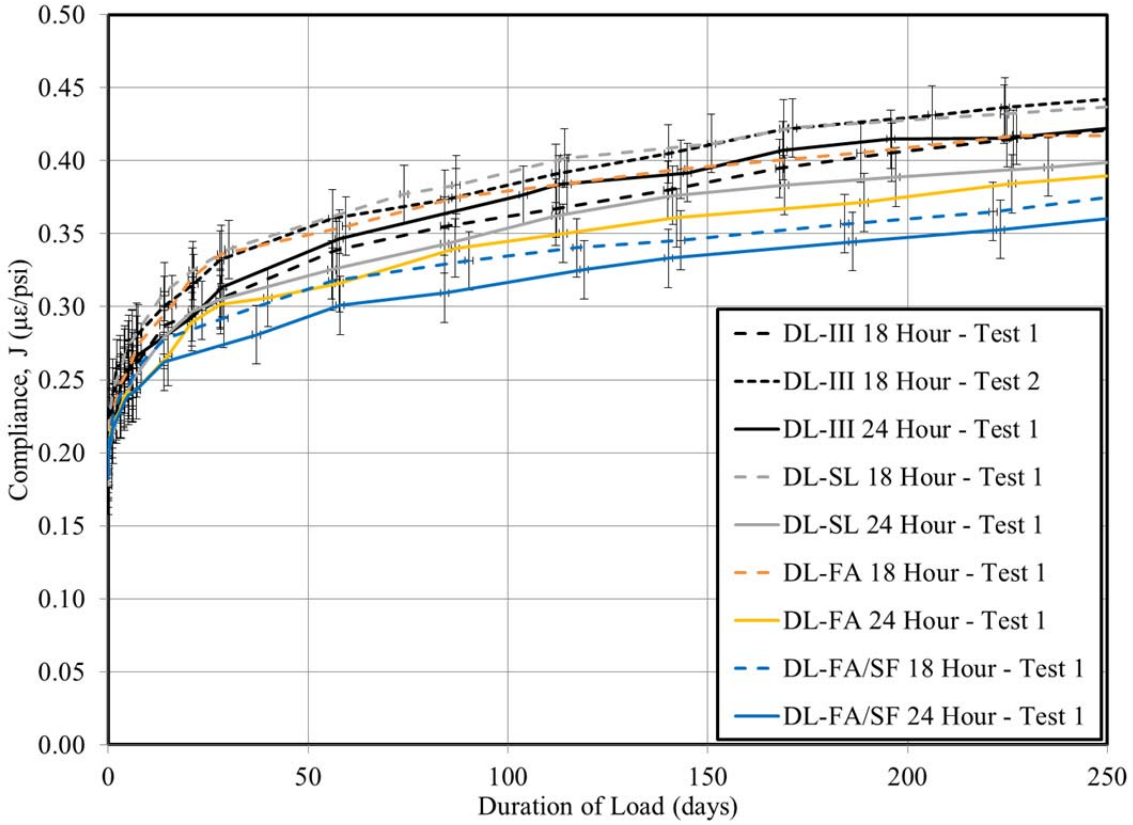

Figure 7-17: Compliance Behavior for All Dolomitic Limestone Tests by Age at Loading

As shown, the DL-SL and DL-FA tests are likely not significantly different from the no-SCM variant experimental control tests. These conclusions are largely in agreement with previous findings, (Section 7.2.2.2) which noted that the use of slag cement tends to have a negligible effect on total observed creep behavior and the influence of fly ash varies by previous researcher. However, despite approaching limits of experimental precision, the overall average of the DL-FA tests exhibited less creep than the overall average of the DL-III tests, perhaps suggesting a small reduction in creep behavior for the fly ash

substitution percentage (15 percent) utilized in this research effort. In contrast to the above discussion, tests of the ternary mixture, DL-FA/SF, exhibited a clearly reduced magnitude of compliance through the testing period. Tabulated values are displayed in Table 7-9.

Table 7-9: Effect of SCM Usage on Compliance

Test ID	Initial Compliance[a], *J*, (με/psi)	60-Day Compliance, *J*, (με/psi)	120-Day Compliance, *J*, (με/psi)	250-Day Compliance, *J*, (με/psi)
DL-III 18 Hour - Test 1	0.19	0.34	0.37	0.42
DL-III 18 Hour - Test 2	0.19	0.36	0.39	0.44
DL-III 24 Hour - Test 1	0.20	0.35	0.38	0.42
No-SCM Variant Average	**0.19**	**0.35**	**0.38**	**0.43**
DL-FA/SF 18 Hour – Test 1	0.19	0.32	0.34	0.38
DL-FA/SF 24 Hour – Test 1	0.18	0.30	0.33	0.36
Fly Ash / Silica Fume Ternary Average	**0.19**	**0.31**	**0.34**	**0.37**

Note: [a] Corresponds to the compliance at the end of load application.

From the data presented in Table 7-9, the use of fly ash and silica fume in ternary mixtures in the substitution percentages utilized in this study (18 percent and 8 percent, respectively) was associated with an average reduction of between 9-12 percent in observed compliance behavior. This conclusion is in agreement with the previous work of Brooks (1999) and Khatri and Sirivivatnanon (1995), who also observed a net reduction in creep behavior for mixtures using silica fume in percent replacements less than 15 percent.

7.5.1.5 Application of Candidate Prediction Models

The three candidate creep prediction models previously described in Section 7.2.4 were implemented for each test to generate predictions of creep coefficients using the assumptions and inputs as summarized in Table 7-10. Then, the initial elastic strain was computed for each test using the measured value of the induced creep frame load and (2) the measured value of elastic modulus at the time of loading as tested by ASTM C469-10. Finally, using the computed initial elastic strain and creep coefficient, compliance was computed for each test. Typical results for a dolomitic limestone test are shown in Figure 7-18, with Appendix F containing a similar plot for each of the 15 tests.

Table 7-10: Creep Prediction Model Summary of Inputs

AASHTO 2014		ACI 209		Model Code 2010	
Input	***Justification***	***Input***	***Justification***	***Input***	***Justification***
Relative humidity = 50 percent	ASTM C512-02	Relative humidity = 50 percent	ASTM C512-02	Relative humidity = 50 percent	ASTM C512-02
Volume-to-surface ratio = 1.5	Computed excluding cylinder ends not exposed to atmosphere	Volume-to-surface ratio = 1.5	Computed excluding cylinder ends not exposed to atmosphere	Cement and temperature – adjusted age at loading	Table 7-1
Chronological age at loading	Table 7-1	Slump = 0.5 in.	Assumed pre-admixture slump in agreement with Keske (2014) and Ellis (2012)	28-day measured compressive strength	Table 7-3
Compressive strength at loading	Table 7-3	Sand-to-aggregate weight ratio	Computed from Table 6-1	Notional size = 76.2 mm.	Computed by MC 2010 provisions.
		Cement factor	Assumed total powder content , Table 6-1	Rapid-hardening high-strength cement assumed	In accordance with Keske (2014) and recommendations of ACI 209 (2008).
		Air content	Table 7-2		

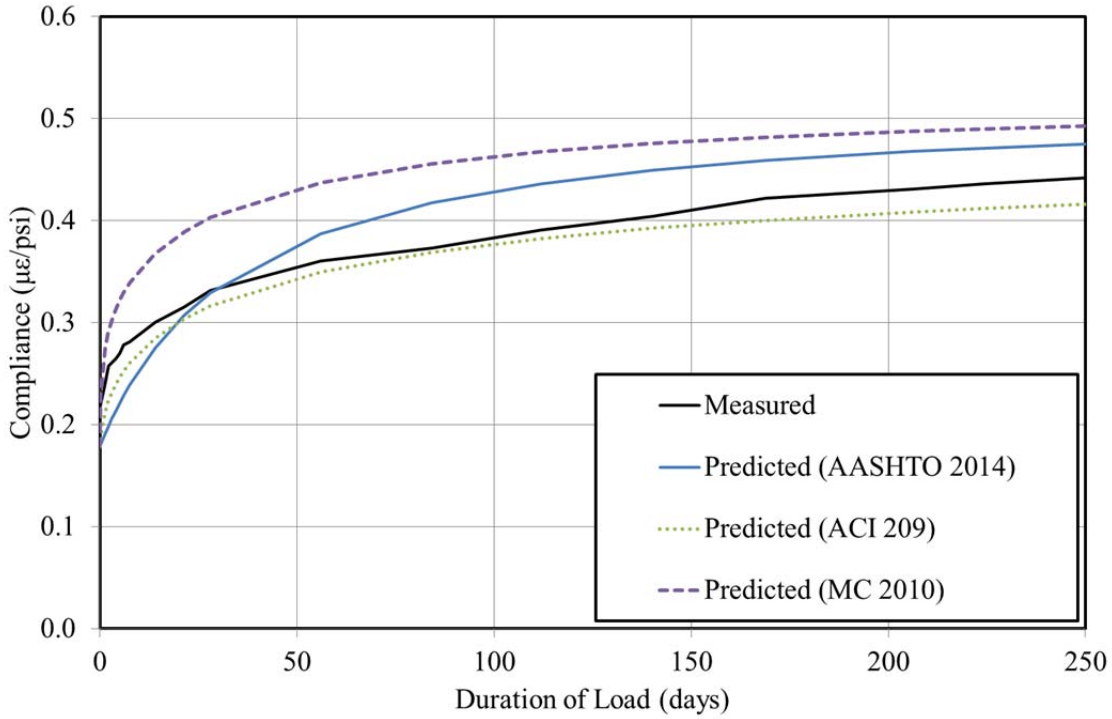

Figure 7-18: Comparison between Experimental Results and Unadjusted Prediction Models for Compliance of a Typical Dolomitic Limestone Test.

In general, for dolomitic limestone concrete mixtures, it appears that the MC 2010 prediction model most frequently tends to over-predict compliance for early ages (less than 100 days), whereas, the AASHTO 2014 and ACI 209 models show relatively good agreement with experimental results at these early ages. For later ages (up to 250 days), the three prediction models yield largely similar results, approaching the precision of the experimental testing conducted in this study. The relative accuracy of each prediction model is explored systematically in the following section.

7.5.1.6 Relative Goodness-of-Fit

As noted by ACI 209.2R (2008), there exists no consensus as to a preferred analytical technique for evaluating the relative goodness-of-fit of prediction models to measured data. Due to the nonlinear measurement timing required by ASTM C512, conventional

methods such as the sum-of-squares error are prone to excessive bias and, therefore, are not preferred. In this section, a technique proposed by Bazant and Panula, as summarized in Appendix B of ACI 209.2R (2008), is used as the preferred scalar metric of goodness-of-fit. Previous similar work by Keske (2014) also utilized this analysis technique.

The basic premise of the analytical technique employed herein is the computation of a time-weighted coefficient of variation, denoted as ϖ_j, intended to evaluate the accuracy of the prediction models in terms of the relative sizes of the squared residuals and outcome values. By grouping data points into logarithmic decades (0 to 9.9 days, 10 to 99.9 days, etc.) and assigning relative weight to each decade based on the number of measurements, the potential for bias from a disproportionate number of early-age measurements is minimized. In general, lower ϖ_j values correspond to improved correlation between predicted and measured data, with a perfect correlation represented by $\varpi_j = 0$ percent. For reference, the range of ϖ_j values reflected in ACI 209.2R (2008) for various endorsed creep prediction models (as compared to experimental compliance data from the RILEM database) is from 23 to 58 percent. Therefore, any ϖ_j value less than 23 percent for compliance reflects an exceptional fit. The details of the application of this procedure are given in Appendix B of ACI 209.2R (2008). Computed values for the coefficient of variation, ϖ_j, for each test of this study are shown in Table 7-11, with the most accurate prediction model noted in bold for each test. The overall coefficient of deviation, ϖ_{BP}, proposed by ACI 209.2R (2008) for all tests within this study is also shown in Table 7-11.

Table 7-11: Relative Goodness-of-Fit of Unadjusted Candidate Prediction Models to Experimental Data for Compliance

	Coefficient of Variation, ϖ_j (%)		
Test ID	**AASHTO 2014**	**ACI 209**	**Model Code 2010**
DL-III 18 Hour - Test 1	13.5	**3.5**	23.0
DL-III 18 Hour - Test 2	11.6	**6.2**	18.6
DL-III 24 Hour - Test 1	**12.2**	13.3	14.0
CL-III 18 Hour - Test 1	**10.1**	11.7	14.7
CL-III 18 Hour - Test 2	**11.4**	13.5	16.0
CL-III 24 Hour - Test 1	10.7	**3.8**	27.7
GG-III 18 Hour - Test 1	13.3	**7.0**	22.5
GG-III 18 Hour - Test 2	14.6	**11.1**	17.2
GG-III 24 Hour - Test 1	12.1	**7.8**	15.6
DL-SL 18 Hour - Test 1	18.3	21.3	**5.0**
DL-SL 24 Hour - Test 1	10.6	**9.8**	11.9
DL-FA/SF 18 Hour - Test 1	15.9	**6.1**	26.9
DL-FA/SF 24 Hour - Test 1	15.2	**7.9**	29.2
DL-FA 18 Hour - Test 1	11.0	11.1	**10.0**
DL-FA 24 Hour - Test 1	9.5	**4.6**	18.9
Overall Average	12.7	**9.3**	18.1
Overall Coefficient of Variation, ϖ_{BP} (%)	12.9	**10.3**	19.2

As shown, all unadjusted creep prediction models reflect fairly good fits of experimental results, with a maximum ϖ_j value of 29.2 percent. For the tests conducted in this project, the unadjusted ACI 209 creep prediction model tended to yield the most accurate results with an overall coefficient of variation, ϖ_{BP}, of 10.3 percent, followed next by the AASHTO 2014 and Model Code 2010 models with overall coefficients of variation of 12.9 and 19.2 percent, respectively.

7.5.1.7 Optimization of Prediction Models to Measured Data

To optimize each prediction model to reflect the results of each test, a creep coefficient modification factor was introduced into the prediction models. For each model and test, a value for the creep coefficient modification factor was determined iteratively using a

GRG nonlinear solver to minimize the corresponding coefficient of variation, ϖ_j. This analysis method essentially minimized the difference between predicted and measured compliance by means of varying the predicted creep coefficient. Computed creep coefficient modification factors for each test and candidate prediction model are summarized in Table 7-12.

Table 7-12: Creep Coefficient Modification Factors to Calibrate Candidate Prediction Equations to Experimental Data

	Modification Factor		
Test	**AASHTO 2014**	**ACI 209**	**Model Code 2010**
DL-III 18 Hour - Test 1	0.83	1.03	0.70
DL-III 18 Hour - Test 2	0.89	1.09	0.75
DL-III 24 Hour - Test 1	1.12	1.27	0.81
CL-III 18 Hour - Test 1	1.01	1.23	0.81
CL-III 18 Hour - Test 2	1.00	1.28	0.79
CL-III 24 Hour - Test 1	0.85	0.94	0.65
GG-III 18 Hour - Test 1	0.89	1.01	0.69
GG-III 18 Hour - Test 2	0.95	1.15	0.76
GG-III 24 Hour - Test 1	0.99	1.03	0.77
DL-SL 18 Hour - Test 1	1.24	1.48	1.04
DL-SL 24 Hour - Test 1	1.07	1.18	0.84
DL-FA/SF 18 Hour - Test 1	0.80	0.96	0.65
DL-FA/SF 24 Hour - Test 1	0.80	0.89	0.62
DL-FA 18 Hour - Test 1	1.02	1.21	0.86
DL-FA 24 Hour - Test 1	0.93	1.02	0.73
Overall Average	**0.96**	**1.12**	**0.76**
Overall Range	**0.44**	**0.59**	**0.42**
Average of Mixtures Similar to Current Regional Mixtures (DL-SL+DL-FA/SF)	0.98	1.13	0.79
Overall Average Excluding DL-FA/SF	0.98	1.15	0.78
Average for DL-FA/SF	0.80	0.93	0.64

As shown, each of the three candidate prediction models requires different average creep coefficient modification factors to provide a best fit to experimental data. The overall average modification factor for the AASHTO 2014 model is closest to 1.0. The Model

Code 2010 model requires an overall average factor of 0.76 to yield most accurate results, while the ACI 209 model requires an average factor of 1.12. An average modification factor is also computed including only those mixtures most similar to current ALDOT precast, prestressed concrete mixtures (DL-SL and DL-FA/SF), although, the modification factor values similar to the overall averages for each model. Also computed are average adjustment factors after segregating the ternary mixture due to the significant difference found in Section 7.5.1.4. Here, the overall average for the AASHTO 2014 model creep coefficient modification factor is closer to 1.0, while the suggested correction factor for the ternary mixture is 0.80.

For each test included in this study, the creep coefficient modification factors of Table 7-12 were used to re-compute compliance (i.e. a factor of 0.83 was applied to the creep coefficient predicted using the AASHTO 2014 model with inputs from DL-III 18 hour – Test 1). Graphical comparisons between these adjusted prediction models and experimental data are included in Appendix G for each test, with a typical result for dolomitic limestone mixtures shown below in Figure 7-19.

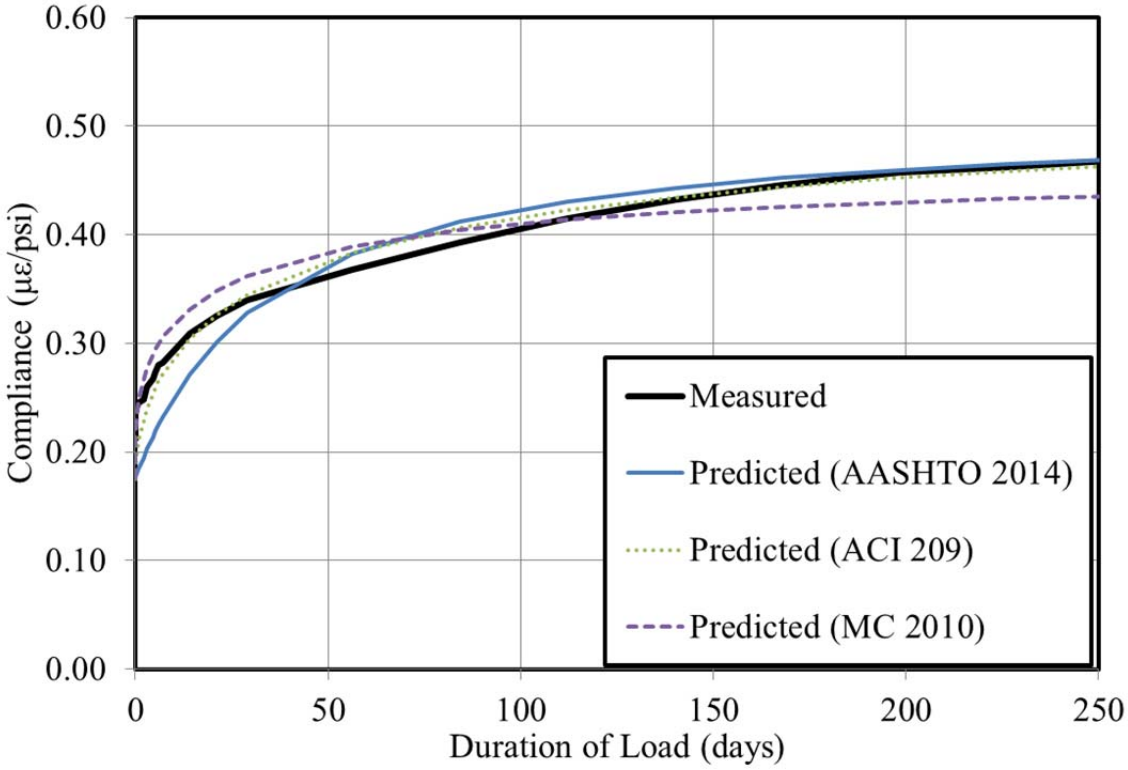

Figure 7-19: Comparison between Experimental Results and Adjusted Prediction Models for Compliance of a Typical Dolomitic Limestone Test.

Similarly to those computed in Section 7.5.1.6 for unadjusted prediction models, revised coefficients of variation for the adjusted models for each test are summarized in Table 7-13.

Table 7-13: Relative Goodness-of-Fit of Adjusted Candidate Prediction Models to Experimental Data

	Coefficient of Variation, ϖ_j (%)		
Test ID	**AASHTO 2014**	**ACI 209**	**Model Code 2010**
DL-III 18 Hour - Test 1	8.4	**3.3**	6.0
DL-III 18 Hour - Test 2	9.8	**4.2**	4.9
DL-III 24 Hour - Test 1	10.7	5.5	**5.3**
CL-III 18 Hour - Test 1	10.0	**5.0**	6.4
CL-III 18 Hour - Test 2	11.4	5.1	**4.5**
CL-III 24 Hour - Test 1	6.3	**2.4**	5.5
GG-III 18 Hour - Test 1	11.9	7.0	**3.5**
GG-III 18 Hour - Test 2	14.4	8.9	**3.7**
GG-III 24 Hour - Test 1	12.0	7.7	**3.8**
DL-SL 18 Hour - Test 1	14.3	8.2	**4.3**
DL-SL 24 Hour - Test 1	10.0	**4.7**	4.8
DL-FA/SF 18 Hour - Test 1	10.5	5.7	**3.2**
DL-FA/SF 24 Hour - Test 1	9.3	4.9	**3.9**
DL-FA 18 Hour - Test 1	11.0	5.5	**3.7**
DL-FA 24 Hour - Test 1	8.8	**4.5**	4.8
Overall Average	10.6	5.5	**4.6**
Overall Coefficient of Variation, ϖ_{BP} (%)	10.8	5.8	**4.7**

As demonstrated by the lowest average coefficient of variation, ϖ_j, the adjusted Model Code 2010 method provides the best fit of experimental data. This is somewhat expected as this model is by far the most complex of the three considered models. Next most accurate is the ACI 209 method, which is the second most complex model, requiring certain concrete mixture-specific inputs (i.e. air content and slump). Finally, the AASHTO 2014 model exhibited the least accurate results of the adjusted models, with an accuracy only slightly improved as compared to the unadjusted AASHTO 2014 model.

7.5.1.8 Design Recommendations

ACI 209.2R (2008) notes that measured creep testing results should, at best, be expected to match prediction models within ±20 percent, while the AASHTO LRFD Bridge Design Specifications (2014) suggest agreement between measured and predicted responses within ±50 percent is typical. Given that agreement of all three unadjusted candidate models is well within the expected range of variation, it can be concluded that the unadjusted creep prediction models provide acceptable agreement for the purposes of camber prediction during initial girder design. Of the unadjusted models, the AASHTO LRFD model is preferable due to its agreement with the experimental data of this study and the simplicity of implementation during the girder design phase. When more refined estimates of girder creep development are desired after a concrete mixture selection is made, (i.e. producer verifications of camber predictions) use of the appropriate creep coefficient modification factor, as summarized in Table 7-14, is recommended.

Table 7-14: Design Recommendations for Creep Coefficient Modification Factors

	Proposed Creep Coefficient Modification Factors	
Prediction Model	**When ternary mixtures are used**	**For all other mixture compositions (or unknown)**
AASHTO LRFD	**0.80**	1.00
ACI 209[b]	**0.95**	**1.15**
Model Code 2010[c]	**0.65**	**0.80**

[a] = Ternary mixtures refer to those mixtures containing fly ash and silica fume.
[b] = Requires mixture-specific input parameters including fine aggregate percent, slump, air content.
[c] = Requires estimate of adjusted maturity at the time of prestress transfer.

Implementation of the ACI 209 model or Model Code 2010 with creep coefficient modification factors as summarized in Table 7-14 yield predictions of similar accuracy and therefore, the prediction model choice is left to designer preference.

7.5.2 Cylinder and Rectangular Prism Shrinkage

This section presents and analyzes the results of the shrinkage testing including both shrinkage of cylindrical specimens (conducted in accordance with ASTM C512-02) and concrete rectangular prisms (in accordance with ASTM C157-08). As previously discussed, the relative influence of concrete shrinkage on the camber of prestressed concrete girders is significantly less than the influence of creep. Accordingly, the discussions and analysis of this section are slightly more abbreviated than those of Section 7.5.1, with less effort devoted to identifying trends in results approaching the limits of experimental precisions. The purpose of the shrinkage testing performed on cylindrical specimens was primarily to provide a means to decouple the effects of creep behavior from early-life temperature effects and shrinkage behavior—not necessary to provide comparisons among experimental tests and variables. For this purpose, the rectangular prism shrinkage testing efforts provide more repeatable and accurate results as is evident in the following sections.

7.5.2.1 Presentation of Measured Results

The full data sets representing the shrinkage testing conducted in this effort are shown in Figures 7-20 and 7-21 for cylindrical specimens and rectangular prismatic specimens, respectively. For cylindrical specimens, the horizontal axis (time) reflects duration of load (days) because readings were taken during creep testing and a small portion of the shrinkage occurred prior to first reading. For rectangular shrinkage prism results, the horizontal axis reflects actual duration of drying (days) because the first measurement of shrinkage was taken immediately upon removal from curing conditions.

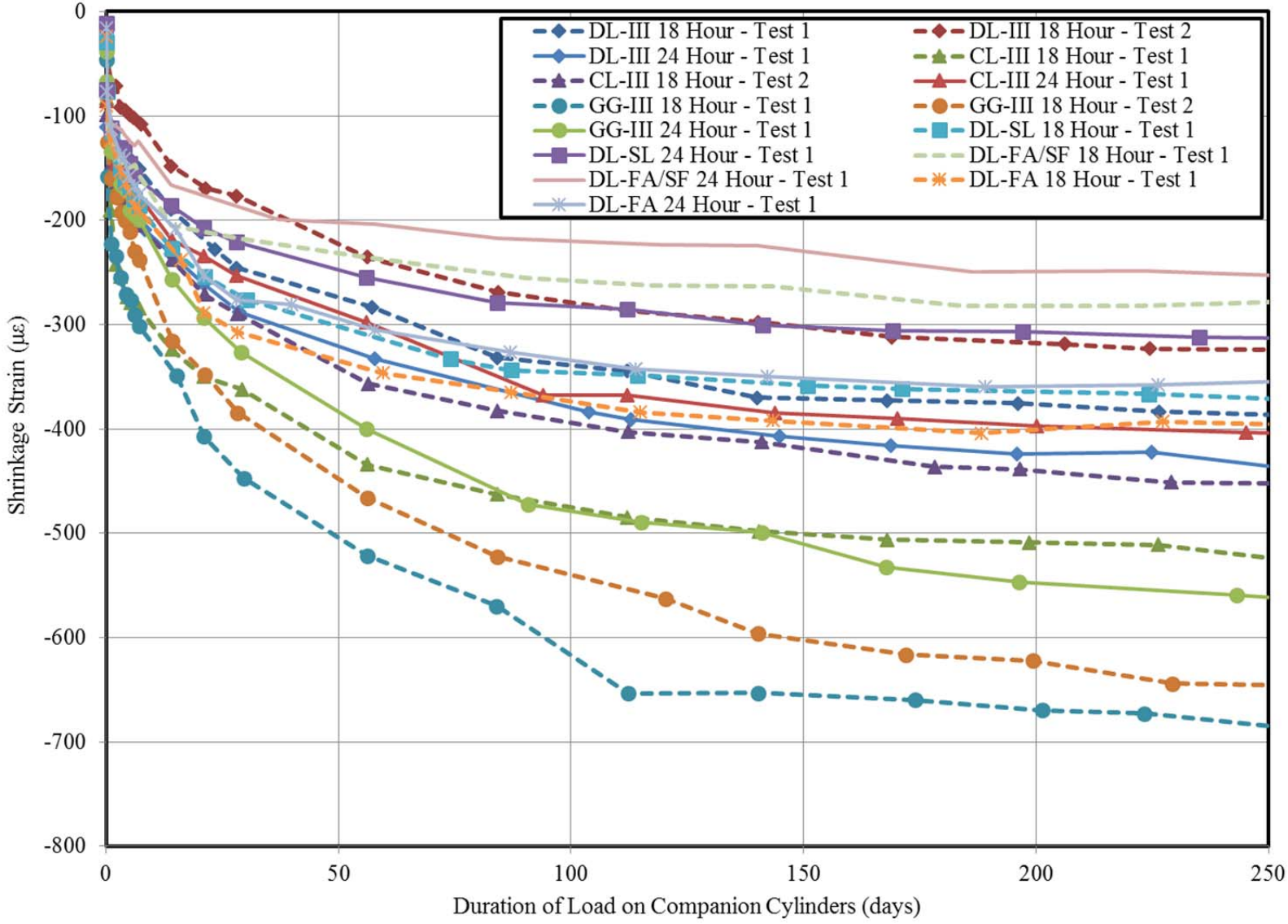

Figure 7-20: Shrinkage Test Results for Cylindrical Specimens

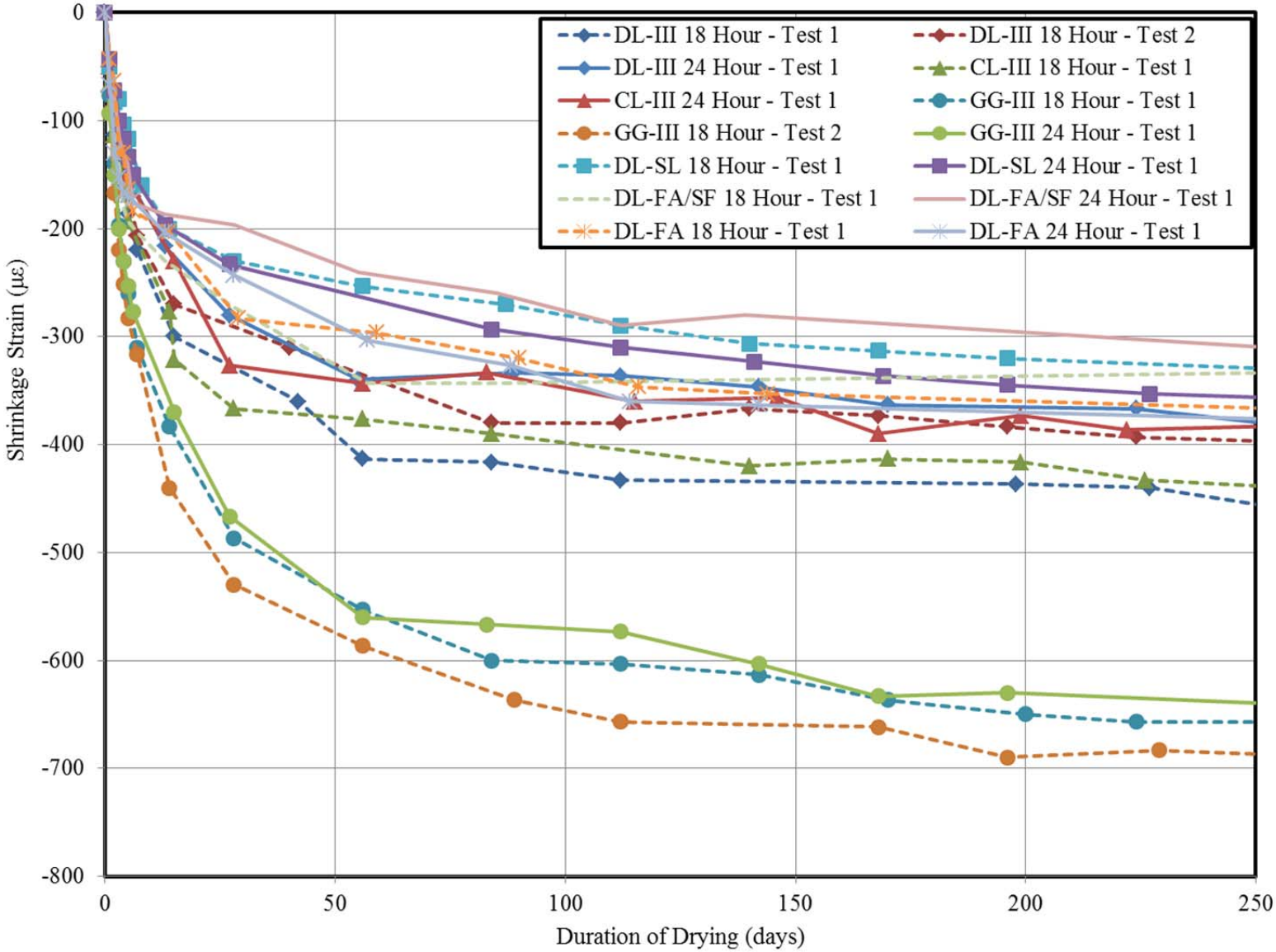

Figure 7-21: Shrinkage Test Results for Rectangular Prismatic Specimens

Dashed lines in Figures 7-20 and 7-21 denote 18-hour tests. As demonstrated by the more distinct clustering of repeated tests in Figure 7-21 than in Figure 7-20, there appears to be more variability in the testing results for cylindrical specimens as compared to rectangular prismatic specimens, likely due to (1) the unavoidable inclusion of early thermal effects in benchmark cylindrical specimen readings and (2) the use of different measuring equipment (*DEMEC* gage versus standard length comparator) for each type of specimen. The following sections describe analyses aimed at identifying significant trends among the three key variables of interest (coarse aggregate type, age at loading, and use of SCMs). Analytical procedures are similar to those of Section 7.5.1 except the appropriate experimental precisions as determined in Sections 7.4.2 and 7.4.3 are used to identify significant trends.

7.5.2.2 Effect of Coarse Aggregate Type

Similar to the previous compliance analysis, the no-SCM variants were compared for each of two ages at loading, independently. Errors bands in this analysis use an average experimental precision value of ±70 με. Cylinder shrinkage testing results, grouped by coarse aggregate type, are shown for the 18-hour age at loading in Figure 7-22. While there appears to be no clear difference between the DL-III and CL-III tests, both CL-III 18-hour tests are located below the DL-III 18-hour tests, possibly suggesting an increased shrinkage tendency. The GG-III mixtures appear to demonstrate more shrinkage as compared to the DL-III and CL-III mixtures, although the difference approaches the experimental precision.

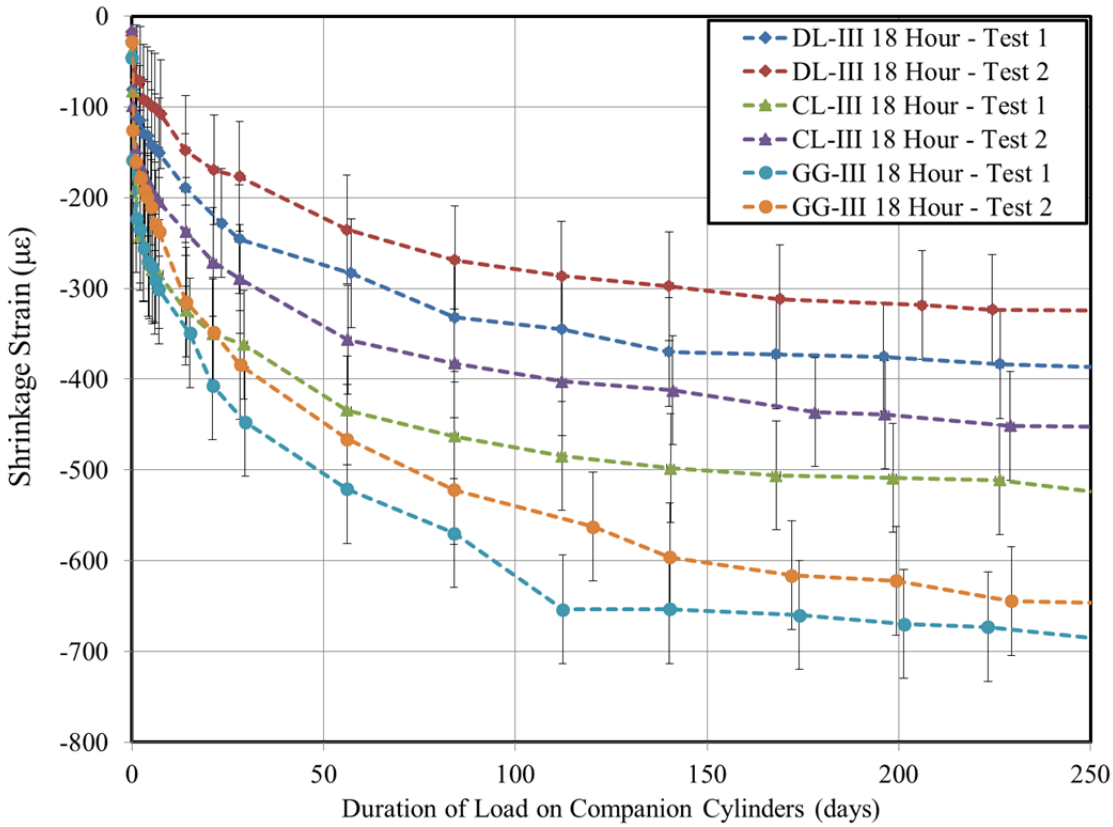

Figure 7-22: Cylinder Shrinkage by Aggregate Type for 18 Hour Tests

Similar results for rectangular prism specimens are shown in Figure 7-23. Here, no differences are detectable among DL-III and CL-III tests, although a significant increased shrinkage tendency is discovered for the GG-III tests when compared to dolomitic limestone tests. Identical results are found when considering shrinkage results from the 24-hour age at loading, as shown in Figures 7-24 and 7-25 for cylinders and rectangular prisms, respectively. Tabulated values used to quantify these qualitatively-identified trends are shown in Table 7-15.

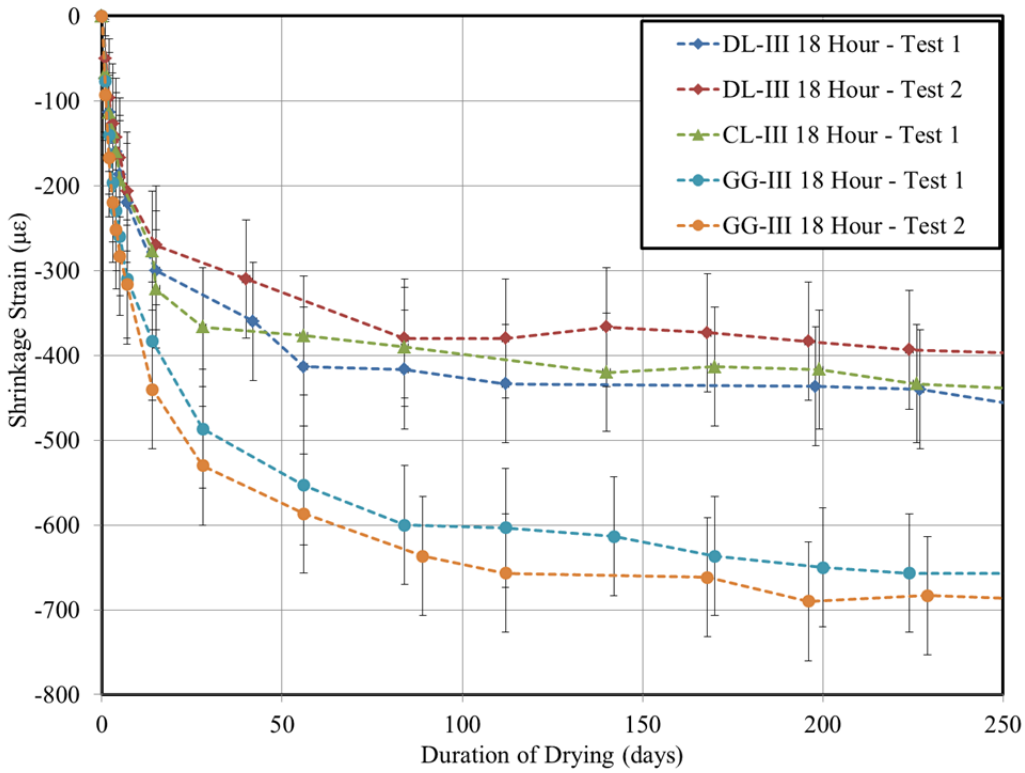

Figure 7-23: Rectangular Prism Shrinkage by Aggregate Type for 18 Hour Tests

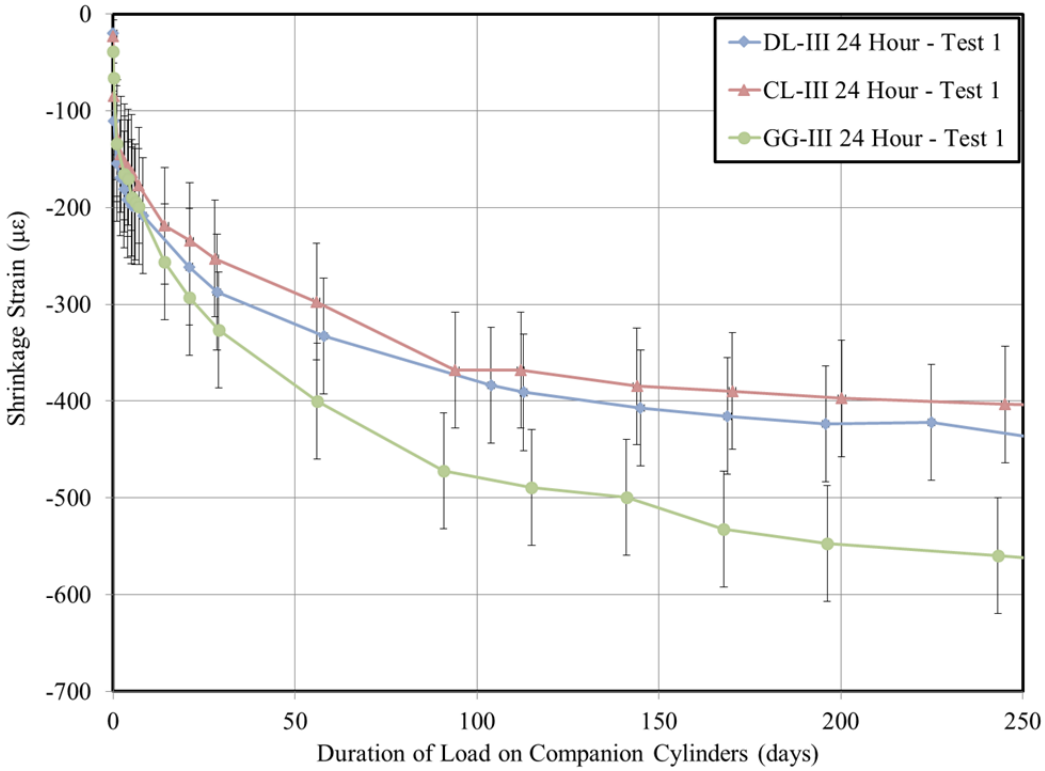

Figure 7-24: Cylinder Shrinkage by Aggregate Type for 24 Hour Tests

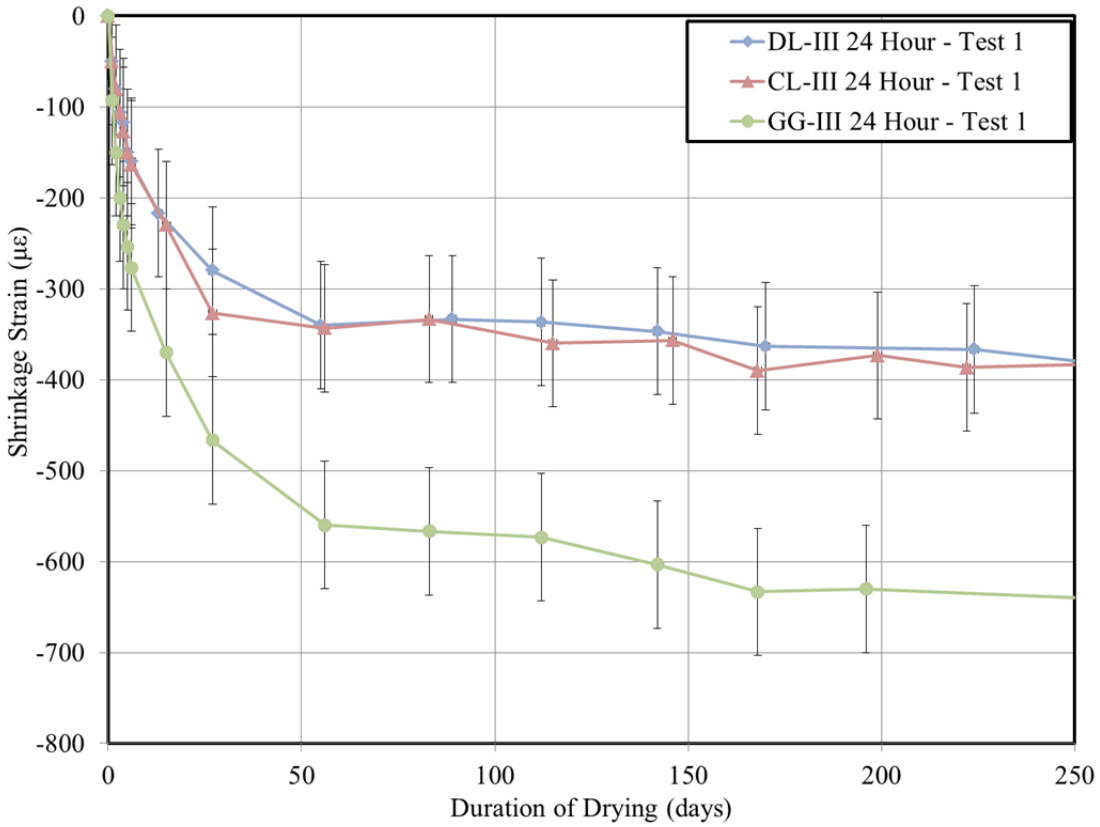

Figure 7-25: Rectangular Prism Shrinkage by Aggregate Type for 24 Hour Tests

Table 7-15: Effect of Aggregate Type on Shrinkage Behavior for 18 and 24 Hour Tests

Test ID	Initial[a] (or 1-Day) Shrinkage, (με)		60-Day Shrinkage, (με)		120-Day Shrinkage, (με)		250-Day Shrinkage, (με)	
	Cylinder	Prism[b]	Cylinder	Prism[b]	Cylinder	Prism[b]	Cylinder	Prism[b]
DL-III 18 Hour – Test 1	-27	-73	-288	-414	-352	-433	-386	-457
DL-III 18 Hour – Test 2	-18	-50	-239	-342	-289	-376	-324	-397
CL-III 18 Hour – Test 1	-39	-67	-438	-379	-488	-409	-525	-438
CL-III 18 Hour – Test 2	-16	n/a	-361	n/a	-405	n/a	-452	n/a
Dolomitic Limestone 18 Hour Average	**-25**	**-63**	**-332**	**-378**	**-384**	**-406**	**-422**	**-431**
GG-III 18 Hour – Test 1	-46	-77	-528	-560	-654	-606	-685	-657
GG-III 18 Hour – Test 2	-29	-93	-474	-593	-563	-658	-646	-687
Crushed Granite 18 Hour Average	**-38**	**-85**	**-501**	**-577**	**-609**	**-632**	**-666**	**-672**
DL-III 24 Hour – Test 1	-20	-50	-335	-339	-395	-340	-436	-380
CL-III 24 Hour – Test 1	-23	-50	-304	-341	-372	-359	-404	-384
Dolomitic Limestone 24 Hour Average	**-22**	**-50**	**-320**	**-340**	**-384**	**-350**	**-420**	**-382**
GG-II 24 Hour – Test 1	-38	-93	-408	-561	-491	-581	-562	-640
Crushed Granite 24 Hour Average	**-38**	**-93**	**-408**	**-561**	**-491**	**-581**	**-562**	**-640**

[a] = For cylindrical specimens, initial shrinkage reflects predominately cooling effects during loading. For prismatic specimens, 1-day shrinkage values are reported.

[b] = Prism specimens received uniform curing treatment and timing to exposure regardless of the age at loading designation of the associated test.

For the 18-hour age at loading, the GG-III cylindrical specimens exhibited a 50 percent net increase in shrinkage when compared to the dolomitic limestone tests, while the rectangular prismatic specimens exhibited a similar 53 percent increase. For the 24-hour age at loading, the GG-III cylindrical specimens showed roughly 40 percent net increased shrinkage as compared to dolomitic limestone specimens, whereas the GG-III prismatic specimens exhibited a substantially greater increase of over 70 percent. These results are generally in agreement with the discussion of Section 7.2.3.1 affirming that less stiff aggregates allow more shrinkage, likely due to their reduced ability to restrain the shrinkage tendency of the cement paste.

7.5.2.3 Effect of Age at Loading

When analyzing results for the effect of age at loading, it is important to recall that rectangular prism specimens received uniform curing treatment and duration regardless of the age at loading designation of the associated test. Therefore, the effect of age at loading is only able to be examined through analysis of cylindrical specimen results. Cylinder shrinkage results, grouped by age at loading, are shown for the dolomitic limestone no-SCM variants in Figure 7-26. As shown, no discernable effect of age at loading is readily apparent, as the 18-hour tests for CL-III tests tend to exhibit increased shrinkage as compared to 24-hour tests, with the opposite trend occurring for DL-III tests. Conversely, cylinder shrinkage results for the GG-III tests and dolomitic limestone SCM-variant tests (shown in Figures 7-27 and 7-28, respectively) tend to suggest that the 18-hour tests may exhibit slightly increased shrinkage as compared to 24-hour tests. However, experimental precision prohibits the identification of a clear trend in this case.

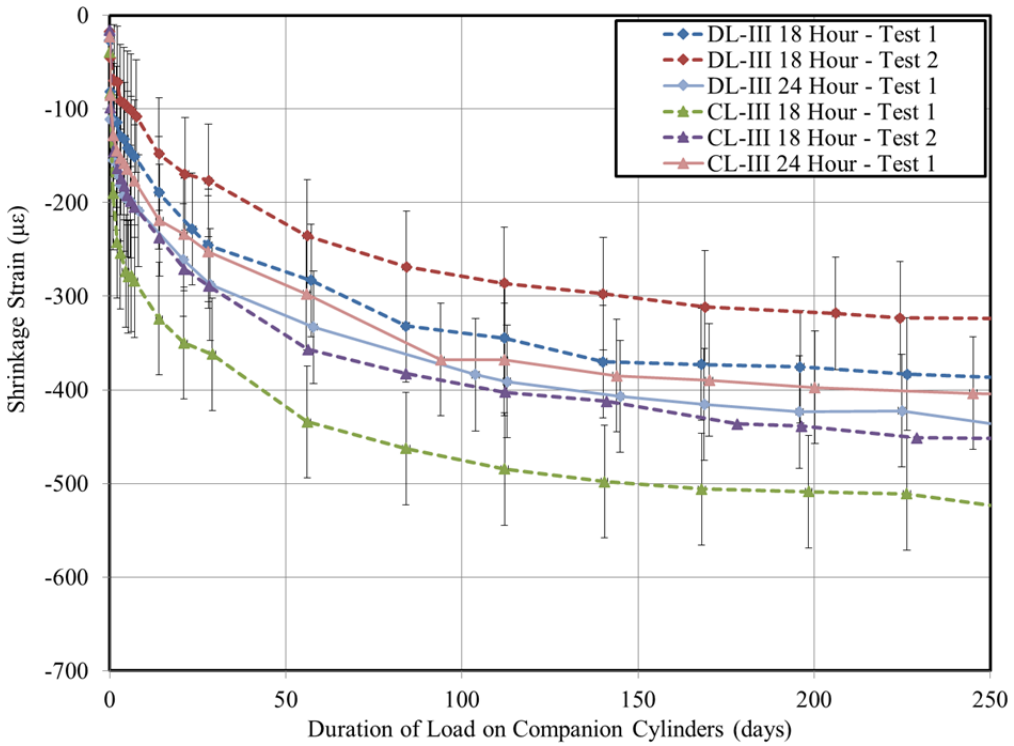

Figure 7-26: Cylinder Shrinkage Behavior of No-SCM Variant Dolomitic Limestone Tests by Age at Loading

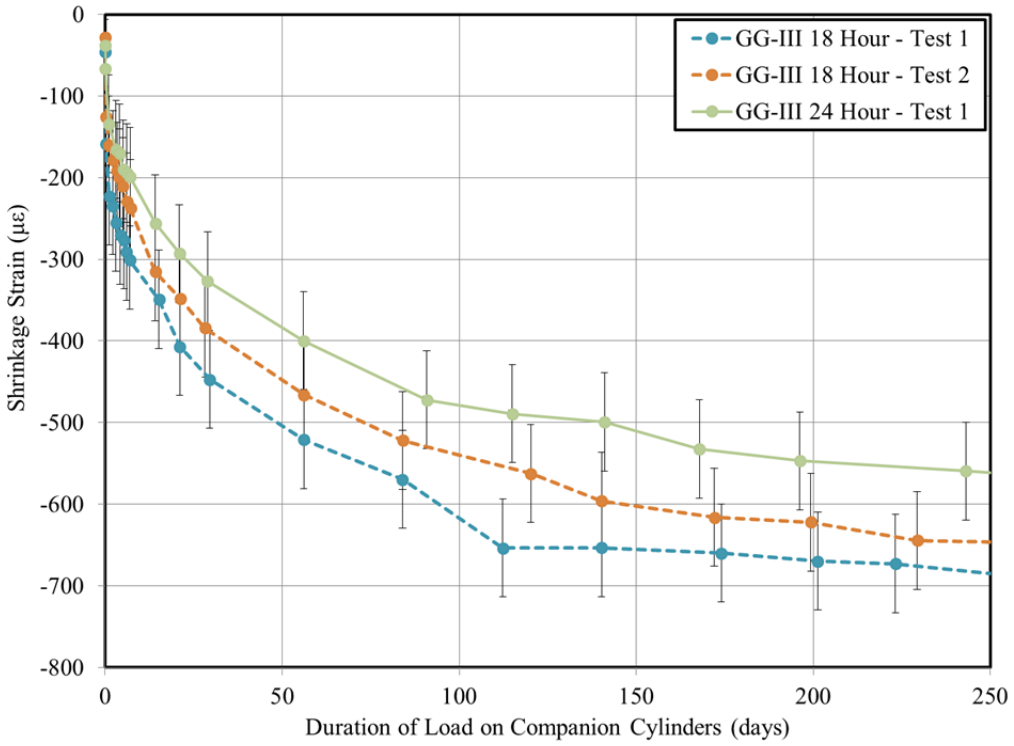

Figure 7-27: Cylinder Shrinkage Behavior of Crushed Granite Tests by Age at Loading

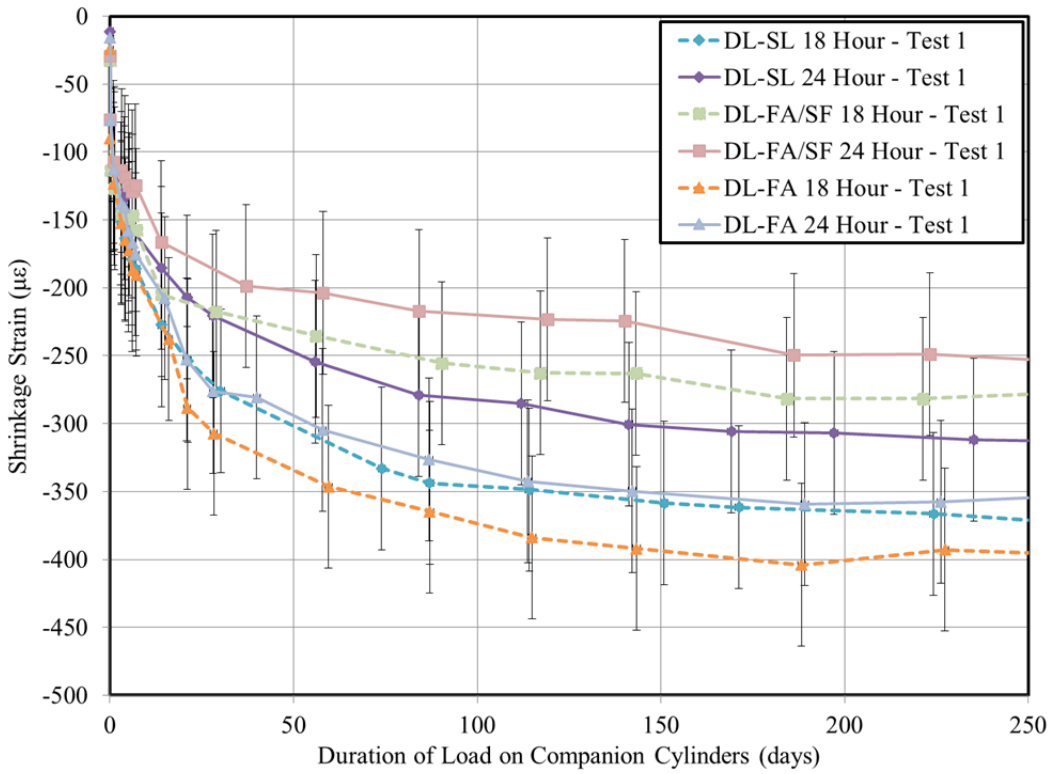

Figure 7-28: Cylinder Shrinkage Behavior of SCM-Variant Dolomitic Limestone Tests by Age at Loading

7.5.2.4 Effect of Supplementary Cementing Materials (SCMs)

Experimental shrinkage results are shown in Figure 7-29 and 7-30 for cylinder and rectangular prism specimens, respectively, along with the no-SCM variant experimental control tests for comparison. There exists no clearly discernable difference between the DL-III and DL-FA tests, suggesting that the effect of fly ash in the percent substitution used in this study is negligible. Similar results are seen for the slag cement mixtures (DL-SL), although a slight reduction in shrinkage of approximately the same order of experimental precision may be seen. Finally, results for the ternary mixture (DL-FA/SF) give the most evidence of a reduced shrinkage as compared to the no-SCM control (DL-III), although again, the observed reduction approaches the magnitude of the experimental precision.

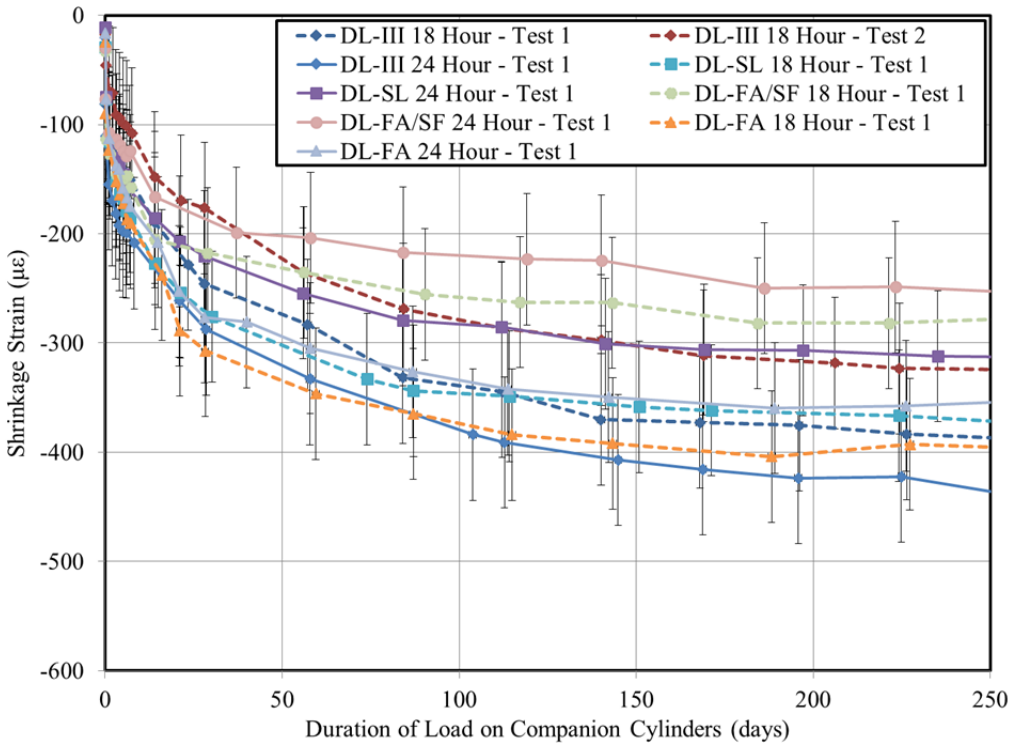

Figure 7-29: Cylinder Shrinkage Behavior of SCM-Variant Tests by Age at Loading

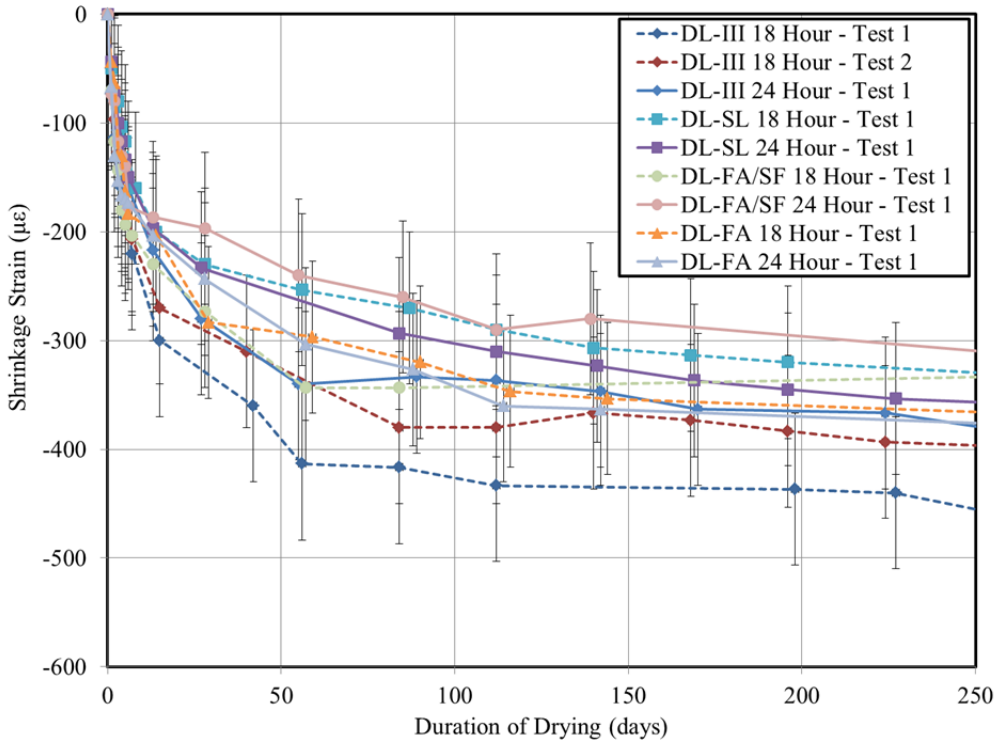

Figure 7-30: Rectangular Prism Shrinkage Behavior of SCM-Variant Tests by Age at Loading

Although more rigorous analytical techniques may be able better justify an observed difference in shrinkage behavior among tests, differences on the order reflected in experimental results (a total range of approximately 150 με) have a minimal effect on the magnitude of camber in prestressed concrete girders (as discussed in Section 7.4.3), and thus, are not of primary interest to the main objectives of this dissertation.

7.5.2.5 Application of Candidate Prediction Models

The three candidate prediction models previously described in Section 7.2.5 were implemented for each test to generate predictions of shrinkage strains using the assumptions and inputs summarized in Table 7-16. Typical results for cylinder shrinkage and rectangular prism shrinkage are shown in Figures 7-31 and 7-32, respectively, with full results for each test available in Appendix H. Major conclusions drawn from the plots of Appendix H are:

- Despite a slight tendency towards overprediction, cylinder and prism shrinkage predictions of the three candidate models are relatively accurate for the dolomitic limestone non-SCM variants;
- Predictions for the slag replacement and fly ash replacement mixtures tended to slightly exceed observed shrinkage behavior similarly in both cylinders and prisms;
- Predictions for the ternary mixture (fly ash and silica fume replacement) tended to substantially exceed observed shrinkage behavior in both cylinders and prisms; and
- Predictions for the crushed granite mixture tended to substantially underpredict observed response in both cylinders and prisms.

Table 7-16: Shrinkage Prediction Model Summary of Inputs

AASHTO 2014		ACI 209		Model Code 2010	
Input	***Justification***	***Input***	***Justification***	***Input***	***Justification***
Relative humidity = 50 percent	ASTM C512-02	Relative humidity = 50 percent	ASTM C512-02	Relative humidity = 50 percent	ASTM C512-02
Volume-to-surface ratio for cylinder = 1.5	Computed excluding cylinder ends not exposed to atmosphere	Volume-to-surface ratio = 1.5	Computed excluding cylinder ends not exposed to atmosphere	Cement and temperature – adjusted age at loading	Table 7-1
Volume-to-surface ratio for rectangular prism = 0.66	Computed including all six sides exposed to atmosphere	Volume-to-surface ratio for rectangular prism = 0.66	Computed including all six sides exposed to atmosphere	28-day measured compressive strength	Table 7-3
Chronological age at loading	Table 7-1	Slump = 0.5 in.	Assumed pre-admixture slump in agreement with Keske (2014) and Ellis (2012)	Notional size = 76.2 mm. for cylinders, = 38.1 mm. for rectangular prisms given ASTM C157 standard rectangular prism sizing.	Computed by MC 2010 provisions.
Compressive strength at loading	Table 7-3	Sand-to-aggregate weight ratio	Computed from Table 6-1	Rapid-hardening high-strength cement assumed	In accordance with Keske (2014) and recommendations of ACI 209 (2008).
		Cement factor	Assumed total powder content , Table 6-1	Concrete age at beginning of drying for rectangular prisms = 7 days	MC 2010 commentary notes chronological age to be used
		Air content	Table 7-2	Concrete age at beginning of drying for cylinders	Cylinder demolding occurred 2 hours prior to specimen loading time.
		Appropriate time-growth equation selected for 1-3 day steam cure or 7-day moist cure			

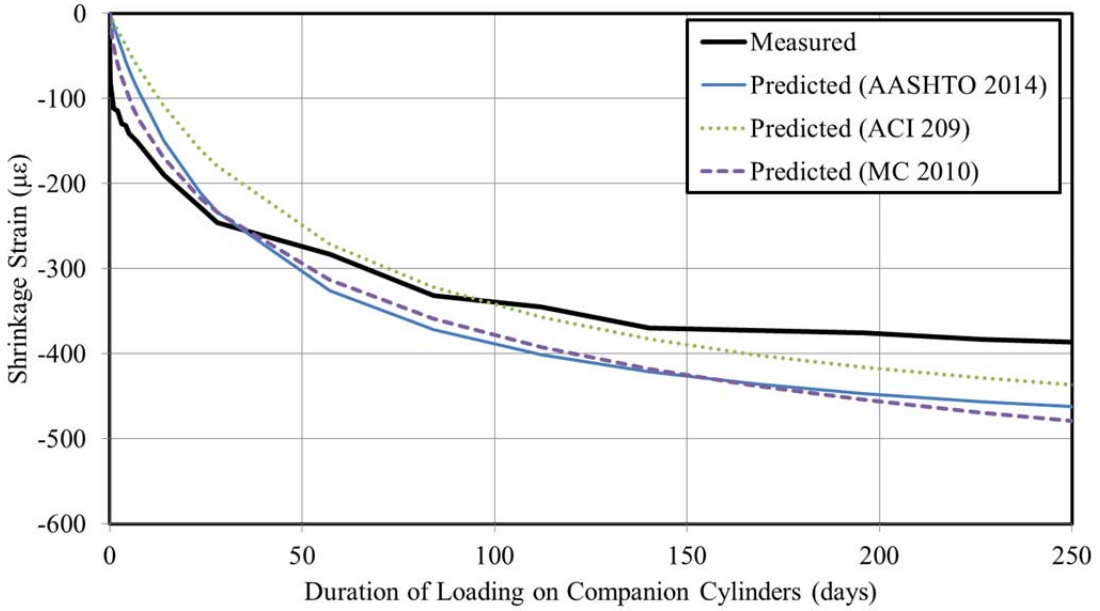

Figure 7-31: Comparison between Experimental Results and Prediction Models for Cylinder Shrinkage of Typical Dolomitic Limestone Test

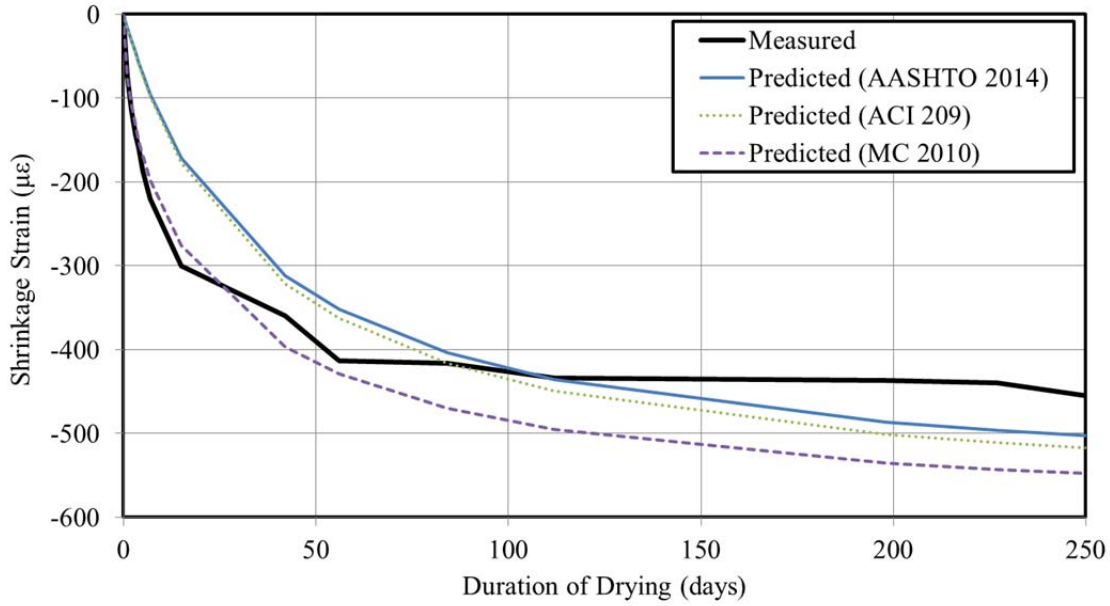

Figure 7-32: Comparison between Experimental Results and Prediction Models for Rectangular Prism Shrinkage of Typical Dolomitic Limestone Test

7.5.2.6 Relative Goodness-of-Fit

Similar to the discussion of Section 7.5.1.6, the time-weighted coefficient of variation, ϖ_j, is used as the preferred metric to evaluate goodness-of-fit. For reference, the

general range of ϖ_j values reflected in ACI 209.2R (2008) for endorsed shrinkage prediction models range from 34 to 55 percent. Therefore, any value less than 34 percent reflects an exceptional fit of a prediction model to experimental data. Computed values for the coefficients of variation for cylinder and rectangular prism shrinkage are shown in Table 7-17 for each test of this study. Also included is the overall coefficient of deviation, ϖ_{BP}, for each model.

Table 7-17: Relative Goodness-of-Fit of Unadjusted Candidate Prediction Models to Experimental Data

Test ID	Coefficient of Variation, ϖ_j (%)					
	AASHTO 2014		ACI 209		Model Code 2010	
	Cylinder	Prism	Cylinder	Prism	Cylinder	Prism
DL-III 18 Hour - Test 1	25.3	24.2	26.7	24.2	21.8	18.6
DL-III 18 Hour - Test 2	43.5	28.8	34.8	31.8	45.0	35.3
DL-III 24 Hour - Test 1	27.7	28.3	34.7	36.2	23.0	54.6
CL-III 18 Hour - Test 1	38.7	27.4	46.0	28.4	33.5	26.1
CL-III 18 Hour - Test 2	25.8	n/a	33.5	n/a	20.7	n/a
CL-III 24 Hour - Test 1	21.7	23.9	27.5	32.4	20.3	42.1
GG-III 18 Hour - Test 1	52.4	48.4	54.7	40.3	45.5	26.2
GG-III 18 Hour - Test 2	42.7	48.2	47.8	43.1	36.7	28.9
GG-III 24 Hour - Test 1	38.8	48.0	39.4	37.8	29.3	25.1
DL-SL 18 Hour - Test 1	27.3	45.8	32.9	57.2	26.9	72.0
DL-SL 24 Hour - Test 1	36.3	32.7	40.7	47.6	44.3	61.9
DL-FA/SF 18 Hour - Test 1	51.8	42.1	50.7	50.2	56.2	55.6
DL-FA/SF 24 Hour - Test 1	63.8	48.7	63.2	63.5	75.8	82.7
DL-FA 18 Hour - Test 1	26.0	31.0	33.3	39.5	24.7	46.5
DL-FA 24 Hour - Test 1	24.9	26.7	32.2	37.6	26.4	42.9
Overall Average	**36.4**	**36.0**	**39.9**	**40.7**	**35.3**	**44.2**
Overall Coefficient of Variation, ϖ_{BP} (%)	**38.4**	**37.3**	**41.2**	**42.0**	**38.4**	**47.9**

Of the unadjusted shrinkage prediction models considered in this effort, the AASHTO 2014 model represents the best combined fit with an overall coefficient of variation of

38.4 percent for cylinder specimens and 37.3 percent for rectangular prisms. While the ACI 209 prediction model is the next most accurate for rectangular prismatic specimens, the Model Code 2010 prediction method proves approximately as accurate as the AASHTO model for cylinder specimens. Overall, the accuracy provided by the AASHTO 2014 model approaches the lower bound of the range cited by ACI Committee 209 (2008) and is therefore a reasonable estimate for girder design purposes.

7.5.2.7 Optimization of Prediction Models to Measured Data

A GRG nonlinear solver was used to calibrate the three considered prediction models to reflect experimental results by means of a shrinkage correction factor. In this analysis, the correction factor was applied directly to the shrinkage strain as predicted by a given model. By iterating the shrinkage correction factor in order to minimize the coefficient of variation, ϖ_j, values for the shrinkage correction factor, as shown in Table 7-18, were computed for each prediction model and test. Where the term "average of above" is used, the computed shrinkage correction factors for cylindrical and rectangular prismatic specimens were averaged[8]. After computing this factor for a given prediction method and test, shrinkage predictions were then recomputed including the shrinkage correction factor. Graphical comparisons between calibrated prediction models and experimental data are provided in Appendix I.

[8] The analytical techniques of this section result in shrinkage correction factors for cylinders and rectangular shrinkage prisms—two types of specimens with different surface area to volume ratios. Although the surface area to volume ratio of 6"x12" cylinders more closely approach those of PCI girder shapes, the decision was made to average the computed shrinkage correction factors for a given test to reflect calibrations representing a variety of curing conditions (e.g. moist curing and accelerated curing).

Table 7-18: Shrinkage Modification Factors to Calibrate Candidate Prediction Equations to Experimental Data

Test ID	Shrinkage Modification Factors					
	AASHTO 2014		ACI 209		Model Code 2010	
	Cylinder	Prism	Cylinder	Prism	Cylinder	Prism
DL-III 18 Hour - Test 1	0.89	1.00	0.99	0.98	0.89	0.88
DL-III 18 Hour - Test 2	0.74	0.89	0.80	0.86	0.72	0.77
DL-III 24 Hour - Test 1	1.07	0.87	1.13	0.80	0.99	0.68
CL-III 18 Hour - Test 1	1.28	0.99	1.38	0.94	1.24	0.83
CL-III 18 Hour - Test 2	1.02	n/a	1.15	n/a	1.01	n/a
CL-III 24 Hour - Test 1	1.02	0.94	1.04	0.84	0.94	0.74
GG-III 18 Hour - Test 1	1.76	1.60	1.76	1.40	1.60	1.27
GG-III 18 Hour - Test 2	1.52	1.60	1.59	1.47	1.43	1.32
GG-III 24 Hour - Test 1	1.45	1.64	1.40	1.37	1.29	1.26
DL-SL 18 Hour - Test 1	0.94	0.74	0.99	0.68	0.91	0.61
DL-SL 24 Hour - Test 1	0.82	0.82	0.82	0.73	0.75	0.65
DL-FA/SF 18 Hour - Test 1	0.72	0.80	0.75	0.74	0.69	0.68
DL-FA/SF 24 Hour - Test 1	0.65	0.73	0.66	0.66	0.60	0.58
DL-FA 18 Hour - Test 1	1.03	0.85	1.07	0.78	0.99	0.72
DL-FA 24 Hour - Test 1	0.97	0.91	0.97	0.80	0.90	0.73
Overall Average	**1.06**	**1.03**	**1.10**	**0.93**	**1.00**	**0.84**
Average of Above	**1.04**		**1.02**		**0.92**	
Overall Range	**1.11**	**0.91**	**1.10**	**0.81**	**1.00**	**0.74**
Average of Mixtures Similar to Current Regional Mixtures (DL-SL+DL-FA/SF)	**0.78**	**0.77**	**0.81**	**0.70**	**0.74**	**0.63**
Average of Above	**0.78**		**0.75**		**0.68**	
Overall Average Excluding GG-III Tests	**0.93**	**0.87**	**0.98**	**0.80**	**0.89**	**0.72**
GG-III Tests Average	**1.58**	**1.61**	**1.58**	**1.41**	**1.44**	**1.28**
Average of Above	**1.6**		**1.5**		**1.4**	

In considering only the overall average of the shrinkage correction factors computed for all tests included in this effort, it appears that (1) no changes to shrinkage prediction equations are justified for AASHTO LRFD and ACI 209 prediction models, and (2) a shrinkage modification factor of 0.90 may be appropriate for use with the Model Code 2010 method. However, upon closer inspection of the computed correction factors, it is apparent that in the overall average approach discussed above, the tendency to overpredict shrinkage for ternary mixtures tends to cancel with the tendency to underpredict shrinkage for the crushed granite mixtures. This effect becomes more evident when considering the average of the shrinkage correction factors for only those mixture types currently used in regional precast, prestressed production (DL-SL and DL-FA/SF). Here, average shrinkage correction factors of 0.78, 0.75, and 0.68 are computed for the AASHTO LRFD, ACI 209, and Model Code 2010 prediction methods, respectively. Isolating the GG-III tests from other results yields average shrinkage correction factors for crushed granites of 1.6, 1.5, and 1.4 for the AASHTO LRFD, ACI 209, and Model Code 2010 prediction models, respectively. The improved relative goodness-of-fits, computed for each of the tests using the shrinkage correction factors shown in Table 7-18, are presented in Table 7-19 (i.e. a shrinkage correction factor of 0.89 was applied to the AASHTO shrinkage prediction method for comparison to experimental data from DL-III -18 Hour Test 1 for cylindrical specimens).

Table 7-19: Relative Goodness-of-Fit of Adjusted Candidate Prediction Models to Experimental Data

Test ID	Coefficient of Variation, ϖ_j (%)					
	AASHTO 2014		ACI 209		Model Code 2010	
	Cylinder	Prism	Cylinder	Prism	Cylinder	Prism
DL-III 18 Hour - Test 1	21.5	24.2	26.6	24.0	16.7	10.0
DL-III 18 Hour - Test 2	16.0	25.8	21.4	25.8	11.0	11.5
DL-III 24 Hour - Test 1	26.7	22.6	32.4	23.3	23.0	8.8
CL-III 18 Hour - Test 1	31.0	27.4	36.3	27.6	26.4	13.7
CL-III 18 Hour - Test 2	25.7	n/a	30.6	n/a	20.6	n/a
CL-III 24 Hour - Test 1	21.6	22.7	27.2	23.9	19.1	10.7
GG-III 18 Hour - Test 1	22.8	21.5	29.2	23.1	19.3	8.0
GG-III 18 Hour - Test 2	18.8	23.6	24.7	24.2	14.4	9.4
GG-III 24 Hour - Test 1	16.0	20.0	23.2	22.6	14.2	7.9
DL-SL 18 Hour - Test 1	26.6	21.4	32.9	21.9	24.5	7.8
DL-SL 24 Hour - Test 1	27.1	21.3	33.7	22.6	26.8	7.0
DL-FA/SF 18 Hour - Test 1	33.2	33.0	38.6	33.7	29.7	19.2
DL-FA/SF 24 Hour - Test 1	29.7	26.6	35.4	27.6	28.3	13.4
DL-FA 18 Hour - Test 1	25.9	23.3	32.6	23.8	24.7	9.9
DL-FA 24 Hour - Test 1	24.7	24.3	32.0	25.4	23.5	11.3
Overall Average	**24.5**	**24.1**	**30.4**	**25.0**	**21.5**	**10.6**
Overall Coefficient of Variation, ϖ_{BP} (%)	**25.0**	**24.3**	**30.8**	**25.1**	**22.2**	**11.1**

Here, it becomes evident that with the exception of the Model Code 2010 shrinkage prism predictions, the accuracies of predictions furnished by all calibrated prediction models are similar.

7.5.2.8 Design Recommendations

Recommendations for shrinkage correction factors for use with the three shrinkage prediction models considered in this study are summarized in Table 7-20. For the purposes of preliminary girder design, use of the AASHTO LRFD model is recommended due to its simplicity in application prior to concrete mixture selection.

Table 7-20: Design Recommendations for Shrinkage Modification Factors

	Proposed Shrinkage Modification Factors	
Prediction Model	**For use with slag and ternary[a] mixtures with limestone coarse aggregate (or unknown)**	**For use with crushed granite aggregate**
AASHTO LRFD	**0.80**	1.6
ACI 209[b]	0.75	1.5
Model Code 2010[c]	0.70	1.4

[a] = Ternary mixtures refer to those containing fly ash and silica fume.
[b] = Requires mixture-specific input parameters including fine aggregate percentage, cement content, slump, and air content.
[c] = Requires estimate of adjusted maturity at the time of prestress release and cement type.

For typical precast, prestressed concretes of the region (slag replacement or fly ash/silica fume replacement ternary mixtures) with limestone coarse aggregate, a shrinkage correction factor of 0.80 for use with the AASHTO LRFD prediction method is recommended at the time of initial girder design. This recommendation is in agreement with previous work of Keske (2014).

7.5.3 Comparison of Elastic Modulus as Computed from Creep Loading Frame to ASTM C469 Testing Results

An inevitable difficulty in conducting experimental creep testing is the tendency to "miss" a portion of the near-instantaneous creep behavior in experimental measurements due to the finite time period required for load application and recording measurements. Unfortunately, the rate of creep development is most active during this initial time period and thus, benchmark creep readings may be influenced by such errors. Recall, it is partially for this reason that compliance was selected as the preferred metric of time-dependent load-induced deformation in this dissertation. By relying on compliance, the above-referenced error is confined to the first post-loading compliance value only, without being propagated through each measurement as would occur in the case of a computed creep coefficient.

For the experimental work reflected in this chapter, the elastic modulus was tested directly using companion cylinders in accordance with the requirements ASTM C469. However, an effective elastic modulus (as discussed in Section 7.4.2) was also computed from creep frame data using the measured values of applied stress and corresponding imposed deformation for each given test. Fundamentally, both methods of measuring concrete stiffness are similar, requiring imposing a load of 40 percent of the compressive strength at time of loading and measuring associated deformation. However, ASTM C469 requires strict adherence to specified loading rates, while ASTM C512 does not specify required loading rates[9]. Values for the elastic modulus for each of the above methods are shown in Table 7-21, grouped by test. As shown by the comparison ratios, elastic modulus values computed from creep frame loading data are, on average, 14

[9] The rate of loading for the creep testing performed in this work was similar to the loading rate specified by ASTM C469, with a given loading cycle for either method taking approximately 1-3 minutes.

percent lower than those tested in accordance with ASTM C469. Although somewhat puzzling at first consideration, this observed trend is in indeed in agreement with the discussion of the previous paragraph. Recognizing that (1) initial creep strain readings taken as close as practicable after creep frame loading inevitably represent the combined effect of initial elastic deformation and early creep behavior (i.e. recorded strain values are greater than if measurement was instantaneous) and (2) the applied stress is independent of the slight lag in measurement time, the value of elastic modulus computed from creep frame data (stress divided by strain) is expected to be less than that tested in accordance with ASTM C469. Also shown in Table 7-21 are initial compliance values, computed as the inverse of the measured elastic modulus for each given testing method. It is evident that despite the noted trend of a reduced apparent elastic modulus computed from creep frame data, these differences are hardly significant in initial compliance results for each testing method.

Table 7-21: Comparison of Elastic Modulus Measurements by Test

Test ID	Elastic Modulus At Loading		E_{cf}/E_c	Compliance at Loading[a]	
	As Tested by ASTM C469, E_c (ksi)	As Computed from Creep Frame, $E_{c,f}$ (ksi)		$J_o = E_c^{-1}$ (με/psi)	$J_{o,f} = E_{c,f}^{-1}$ (με/psi)
DL-III 18 Hour - Test 1	5,700	5,300	0.93	0.18	0.19
DL-III 18 Hour - Test 2	5,600	5,300	0.95	0.18	0.19
DL-III 24 Hour - Test 1	6,350	5,100	0.80	0.16	0.20
CL-III 18 Hour - Test 1	5,700	4,700	0.82	0.18	0.21
CL-III 18 Hour - Test 2	5,750	4,750	0.83	0.17	0.21
CL-III 24 Hour - Test 1	6,100	5,750	0.94	0.16	0.17
GG-III 18 Hour - Test 1	3,700	3,050	0.82	0.27	0.33
GG-III 18 Hour - Test 2	3,500	2,800	0.80	0.29	0.36
GG-III 24 Hour - Test 1	3,900	3,200	0.82	0.26	0.31
DL-SL 18 Hour - Test 1	6,600	5,000	0.76	0.15	0.20
DL-SL 24 Hour - Test 1	6,400	5,650	0.88	0.16	0.18
DL-FA/SF 18 Hour - Test 1	6,050	5,300	0.88	0.17	0.19
DL-FA/SF 24 Hour - Test 1	6,100	5,500	0.90	0.16	0.18
DL-FA 18 Hour - Test 1	6,100	5,350	0.88	0.16	0.19
DL-FA 24 Hour - Test 1	6,100	5,200	0.85	0.16	0.19
Overall Average	-	-	**0.86**	**-**	**-**

[a] = Compliance at loading computed as inverse of elastic modulus at loading. $E_{c,f}^{-1}$ values correspond to those initial compliance values included in the analysis of Section 7.5.1.

7.6 Summary and Conclusions

7.6.1 Summary

In this laboratory study, six concrete mixtures were proportioned to represent mixtures typical of Alabama precast, prestressed girder production. These six mixtures included three regional coarse aggregates and three combinations of supplementary cementing materials (SCMs). A uniform 18-hour compressive strength, paste content, and sand-to-total aggregate ratio (by volume) were maintained for all mixtures. Sampled concrete cylinders were exposed to accelerated curing practices mimicking those of precast, prestressed plants, while rectangular prism specimens were exposed to standard curing conditions. At the completion of initial accelerated curing (either 18 or 24 hours), cylindrical specimens were tested in accordance with ASTM C512-02 (ASTM 2002) to determine creep and shrinkage behavior for a period of 250 days. Concurrently, ASTM C157-08 (ASTM 2008) tests were performed to determine shrinkage behavior for a period of 250 days. To ensure the precision and repeatability of results, the first three tests were duplicated. Trends were then identified in experimental results and comparisons were made between various prediction models—ultimately resulting in design recommendations to accurately predict time-dependent deformations of typical concretes within the study region.

7.6.2 Conclusions and Recommendations

The following are primary research findings relating to concrete creep:

- No significant difference was detected for the two dolomitic limestone aggregates included in this study (DL-III and CL-III);

- Concrete mixtures using crushed granite aggregate exhibited 55-58 percent more creep than corresponding dolomitic limestone mixtures. However, this difference is primarily due to the reduced elastic modulus of the crushed granite aggregate and is not attributable to a significant difference in time-dependent creep behavior;
- Specimens loaded at 24 hours appeared to exhibit slightly reduced creep, although, approaching the limits of experimental precision;
- The use of slag cement (15 percent substitution) had a negligible effect on creep, while the use of fly ash (15 percent substitution) may have caused a slight reduction in creep although again, approaching experimental precision;
- The use of fly ash and silica fume (18 percent and 8 percent substitution, respectively) resulted in a reduced creep tendency of between 9-12 percent;
- Of the unadjusted candidate creep prediction models, the ACI 209 and AASHTO 2014 models provided relatively accurate predictions for the concretes considered in this study, with BP coefficients of variation of 10.3 and 12.9, respectively;
- For the purposes of camber prediction during initial girder design, the unadjusted AASHTO LRFD, ACI 209, and MC 2010 models predict creep behavior with reasonable accuracy for the concretes considered in this study. Of these models, the AASHTO LRFD is the simplest;
- If a more refined estimate of creep is desired, the following creep coefficient modifications may be applied to the unadjusted models, with most accurate predictions offered by the Model Code 2010 method:

Table 7-22: Design Recommendations for Creep Coefficient Modification Factors

	Proposed Creep Coefficient Modification Factors	
Prediction Model	**When ternary mixtures are used**	**For all other mixture compositions (or unknown)**
AASHTO LRFD	**0.80**	1.00
ACI 209[b]	**0.95**	**1.15**
Model Code 2010[c]	**0.65**	**0.80**

[a] = Ternary mixtures refer to those mixtures containing fly ash and silica fume.
[b] = Requires mixture-specific input parameters including fine aggregate percent, slump, air content.
[c] = Requires estimate of adjusted maturity at the time of prestress transfer.

- Elastic modulus, as computed from creep frame loadings in accordance with ASTM C512, tended to be 14 percent lower than those measured in companion cylinders by ASTM C469 at the time of loading—suggesting that a portion of the early creep is "missed" during typical ASTM C512 testing; and
- The "missed" portion of early creep corresponds to negligible differences in compliance, and thus, affirms the preference to consider compliance as the primary metric of time-dependent load-induced deformation.

The following are primary research findings relating to concrete shrinkage behavior:

- No significant difference in shrinkage behavior was detected for the two dolomitic limestones included in this study;
- Crushed granite mixtures tended to exhibit between 40-70 percent increased shrinkage when compared to dolomitic limestone mixtures;
- Specimens loaded at 18-hour ages exhibited a slightly increased shrinkage tendency, although approaching experimental precision;
- No significant effect of fly ash or slag (for the substitution percentages used) on shrinkage behavior was detected;

- The ternary mixture exhibited slightly decreased shrinkage, although approaching experimental precision;
- Of the three unadjusted candidate prediction models, the AASHTO 2014 method is most accurate of the considered models with a BP coefficient of variation of 36 percent;
- For most accurate prediction of concrete shrinkage, the following shrinkage modification factors are suggested for use with each prediction model:
- **Table 7-20: Design Recommendations for Shrinkage Modification Factors**

	Proposed Shrinkage Modification Factors	
Prediction Model	**For use with slag and ternary[a] mixtures with limestone coarse aggregate (or unknown)**	**For use with crushed granite aggregate**
AASHTO LRFD	**0.80**	1.6
ACI 209[b]	0.75	1.5
Model Code 2010[c]	0.70	1.4

- [a] = Ternary mixtures refer to those containing fly ash and silica fume.
- [b] = Requires mixture-specific input parameters including fine aggregate percentage, cement content, slump, and air content.
- [c] = Requires estimate of adjusted maturity at the time of prestress release and cement type.
- The AASHTO LRFD method modified by the shrinkage modification factor of 0.80 is recommended for initial design in the absence of more detailed information.

The following summarize recommendations for future researchers:

- The use of sound post-processing techniques to eliminate erroneous data points and to detect loading anomalies is encouraged;
- Experimental precisions and repeatability of measurements should be determined by duplicate tests to allow identification of significant experimental results;

- If conducting testing intended to simulate precast, prestressed concrete element production, an accelerated curing system should be used to introduce expected temperature profiles before and at the time of creep loading; and
- The comparison of concrete elastic modulus as computed by loading frame data and also by testing of companion material testing can be used to affirm the soundness of testing procedures and validate the accuracy of benchmark readings.

Chapter 8: Effect of Diurnal Temperature Changes on Girder Camber

8.1 Introduction

After production, the introduction of nonuniform temperature variations along the height of hardened girders can induce transient changes in cross-sectional curvatures, thereby also causing relative changes to camber and other girder deflections. These nonuniform vertical temperature variations (also called profiles or gradients) are typically introduced in concrete girders by ambient conditions (temperature variations and differential solar radiation) and are collectively referred to as diurnal (daily) temperature variations.

Typical design predictions of girder deflections neglect the presence of these temperature-induced deflections, thereby assuming constant temperatures throughout structural elements. This practice is defensible for a variety of reasons including (1) difficulties in projecting future temperatures at a given time, (2) difficulties in precisely predicting the thermal response of materials (i.e. coefficient of thermal expansion) at various stages of construction, and (3) the relatively high computational cost of such analyses. Instead of explicitly accounting for these temperature-induced deflections in design computations, it is expected that appropriate levels of design or construction tolerance for camber are included in design documents to accommodate such transient changes in deformation.

This dissertation addresses the topic of diurnal temperature-induced deformations in precast, prestressed girders in detail for a variety of reasons. By thoroughly understanding and validating the mechanism(s) of transient temperature-induced

deformations, improved comparisons can be made among measured field cambers recorded under differing ambient conditions, and recommendations can be made regarding the anticipated degree of camber variation likely to be observed in field measurements due to transient temperature-induced effects.

This chapter describes an analytical and experimental exploration of the structural response of girders exposed to temperature changes. Measured results of a field investigation were used to determine the "effective" or in-place coefficient of thermal expansion (CTE) of girder concrete. The analytical procedures utilized in this chapter are incorporated into the final analyses of Chapter 10.

8.1.1 Chapter Objectives

The primary objective of this chapter is to determine the effect that temperature variations in precast, prestressed concrete girders have on deformational behavior, and specifically on midspan camber. Tasks completed in support of the primary objective of this chapter include the following:

- Improve the implementation of an existing girder temperature-correction methodology;
- Conduct field testing to affirm and validate an existing temperature-correction procedure and recommend most efficient practices for future instrumentation in research applications (i.e. number and location of gages); and
- Identify rational deflection tolerances that reflect expected camber variations for girders in storage due to regionally-appropriate temperature conditions.

8.1.2 Chapter Outline

This chapter begins with a general discussion of the concept of a curvature-based temperature-correction algorithm—providing a thorough derivation of the governing mathematical equations and a description of algorithm refinements and improvements implemented as part of this research effort. Then, a summary of an in-plant experimental program consisting of the monitoring of internal concrete temperatures and various measures of induced deformational responses (i.e. concrete strains and girder deflections/end rotations) is presented. Next, results from each of three experimental tests are presented as necessary to affirm the soundness of recorded data and identify regional trends in girder temperature profiles. Then, an analysis is detailed aimed at (1) determination of an average effective coefficient of thermal expansion (CTE) for each field test, (2) comparison of observed cross-sectional and global deformational responses to predicted behavior, (3) implementation of various simplifications to the temperature-correction procedure utilized herein, and (4) determination of the approximate magnitude of expected variations in the prestressing force caused by temperature-induced girder deformations. Finally, the findings of the analyses of this chapter are relied on to determine appropriate tolerance limits for girder camber to account for the effect of transient temperature variations.

8.1.3 Exclusions

The focus of this chapter and the related experimental program is exploring the effect of transient diurnal temperature profiles on deformations of precast, prestressed concrete girders. Investigation of (1) early-age prestress losses due to temperature effects, (2) changes in the time-dependent rates of creep and/or shrinkage due to elevated

temperatures, or (3) investigation of the effect of differential CTE of constituent materials is outside the scope of this investigation. These topics have been largely studied by others (Roller et al. 2003, French and O'Neill 2012, and Barr and Angomas 2010), who generally conclude that (1) the magnitude of early-age temperature losses is heavily dependent on regional construction practices and assumptions of the timing of steel to concrete bonding (which has not been extensively studied), (2) reductions in the prestressing force caused by early-age temperature losses are typically relatively small (between two to six percent of the initial jacking stress), and (3) the net variation in camber caused solely by temperature-induced prestressed force reductions is relatively small, limited to approximately 5 percent of the overall camber value in one parametric study (French and O'Neill 2012).

8.2 Curvature-Based Temperature-Correction Algorithm

The curvature-based temperature-correction algorithm employed in this dissertation is derived directly from fundamental structural mechanics, specifically engineering beam theory and linear thermal expansion. The purpose of the temperature-correction algorithm is to compute the expected change in two key cross-sectional parameters, centroidal strain and curvature, corresponding to a given change in cross-sectional temperature profile. Most typically, this algorithm is used to compute the expected deformation associated with a change from a given (typically measured) cross-sectional temperature profile to a uniform vertical profile and, thus, the term "temperature-correction" is used. The key parameters, change in centroidal strain and change in curvature, are computed by balancing the thermal expansion tendencies within a cross section with any induced mechanical stresses (often called self-equilibrating stresses) to

ultimately yield a linear strain profile in accordance with equilibrium and deformation constraints. While changes in cross-sectional curvature are of primary interest to this research effort due to their ability to directly induce changes to flexural deformations, cross-sectional centroidal strain was also evaluated.

8.2.1 Background

The use of temperature-correction procedures similar to that used in this dissertation first appear in the literature in the mid-1980's as applicable to evaluating the effect of thermal gradients in concrete flexural members. Primary resources on this topic include a now withdrawn report by ACI Committee 435 titled *Report on Temperature-Induced Deflections of Reinforced Concrete Members* (ACI Committee 435 1997) and an NCHRP publication titled *Report 276: Thermal Effects in Concrete Bridge Superstructures* (Imbsen et al. 1985). Both of these reports contain similar derivations to those contained in Section 8.2.2 of this work, although each uses different notation, different sign conventions, and implements the basic concept somewhat differently. As is shown later in this chapter, the full application of the temperature-correction algorithm as implemented herein can be quite computationally expensive, likely explaining why early temperature-correction efforts employed simplifying approximations (i.e. only considering a single linear temperature profile) and, therefore, were less useful for a variety of temperature profiles than more recent temperature-correction efforts.

8.2.2 Assumptions and Derivation

Various governing assumptions allow the derivation of the curvature-based temperature correction used herein. These assumptions, as summarized from NCHRP Report 276 (1985) include the following: (1) constitutive materials are homogenous and exhibit

isotropic behavior, (2) material properties are independent of temperature, (3) constitutive materials are governed by linear stress-strain and temperature-strain relations, (4) initially plane sections remain plane, and (5) temperature variations are only present with depth, but constant at all points of equal depth (i.e. no transverse gradients considered). A complete derivation, beginning with fundamental principles of structural mechanics is presented below:

Assume a sign convention that positive is downward from the elastic neutral axis with the zero point at the centroid location. At each depth (y) within a given cross section, the linear thermal strain, $\varepsilon_{th}(y)$, if not restrained, is given as

$$\varepsilon_{th}(y) = \alpha_T \cdot \Delta T(y) \tag{8-1}$$

where

α_T = coefficient of thermal expansion and

$\Delta T(y)$ = temperature at a given depth within cross section.

Expressed incrementally, Equation 8-1 becomes the following:

$$\Delta\varepsilon_{th}(y) = \alpha_T \cdot \Delta T(y) \tag{8-2}$$

The total strain at a given cross section, $\varepsilon_{tot}(y)$, can be expressed as

$$\varepsilon_{tot}(y) = \varepsilon_0 + \phi \cdot y \tag{8-3}$$

where

ε_0 = strain at the centroidal axis location for a given cross section,

ϕ = cross-sectional curvature, and

y = depth within a cross section.

Expressed incrementally:

$$\Delta\varepsilon_{tot}(y) = \Delta\varepsilon_0 + \Delta\phi \cdot y \tag{8-4}$$

The mechanical strain at a given cross section, $\Delta\varepsilon_{mech}(y)$, can be expressed as

$$\Delta\varepsilon_{mech}(y) = \frac{\Delta\sigma(y)}{E} \tag{8-5}$$

where

$\Delta\sigma(y)$ = change in stress at a given girder depth, and

E = modulus of elasticity of girder material.

The total strain in a cross section is the sum of the thermal and mechanical strain.

$$\Delta\varepsilon_{tot}(y) = \Delta\varepsilon_{th}(y) + \Delta\varepsilon_{mech}(y) \tag{8-6}$$

Substituting and solving for stress yields:

$$\Delta\sigma(y) = E\left[\Delta\varepsilon_{tot}(y) - \Delta\varepsilon_{th}(y)\right] \tag{8-7}$$

Substituting

$$\Delta\sigma(y) = E\left[\left(\Delta\varepsilon_0 + \Delta\phi \cdot y\right) - \left(\alpha_T \cdot \Delta T(y)\right)\right] \tag{8-8}$$

Imposing equilibrium for a given cross section in a beam with no change in axial force due to restraint:

$$0 = \int \Delta\sigma(y)dA = \int_A E\left(\left[\Delta\varepsilon_0 + \Delta\phi \cdot y\right] - \left[\alpha_T \cdot \Delta T(y)\right]\right)dA \tag{8-9}$$

Simplifying

$$0 = \int_A E\left(\Delta\varepsilon_0 + \Delta\phi \cdot y - \alpha_T \cdot \Delta T(y)\right)dA \tag{8-10}$$

Dividing into three separate integrals and simplifying:

$$0 = E\int_A \Delta\varepsilon_0 dA + E\int_A \left(\Delta\phi \cdot y\right)dA - E\int_A \left(\alpha_T \cdot \Delta T(y)\right)dA \tag{8-11}$$

By virtue of the centroidal axis where y=0, the second term equals zero.

$$0 = E\int_A \Delta\varepsilon_0 dA + 0 - E\int_A \left(\alpha_T \cdot \Delta T(y)\right)dA \tag{8-12}$$

Removing constants from integrals:

$$0 = E\Delta\varepsilon_0 \int_A dA - E\alpha_T \int_A \left(\Delta T(y)\right)dA \tag{8-13}$$

Recognizing that the first integral is equal to the cross-sectional area:

$$0 = E\Delta\varepsilon_0 A - E\alpha_T \int_A \left(\Delta T(y)\right)dA \tag{8-14}$$

Simplifying further yields the governing equation for change in centroidal strain:

$$\Delta\varepsilon_0 = \frac{\alpha_T}{A}\int_A \left(\Delta T(y)\right)dA \tag{8-15}$$

Modifying differential element, dA , to vary with width:

$$dA = dy \cdot w(y) \tag{8-16}$$

where

$w(y)$ = width at a given cross section at height y.

Substituting, yields the first governing equation:

$$\Delta\varepsilon_0 = \frac{\alpha_T}{A}\int_y \left(\Delta T(y)\right)w(y)dy \tag{8-17}$$

Similarly, the change in incremental curvature can be derived. Equations 8-1 through 8-8 are applicable and imposing moment equilibrium yields:

$$0 = \int y\Delta\sigma dA = \int_A yE\left(\left[\Delta\varepsilon_0 + \Delta\phi \cdot y\right] - \left[\alpha_T \cdot \Delta T(y)\right]\right)dA \tag{8-18}$$

Simplifying:

$$0 = \int_A yE\left(\Delta\varepsilon_0 + \Delta\phi \cdot y - \alpha_T \cdot \Delta T(y)\right)dA \tag{8-19}$$

Dividing into three separate integrals and simplifying:

$$0 = E\int_A \Delta\varepsilon_0 y dA + E\int_A \left(\Delta\phi \cdot y^2\right) dA - E\int_A \left(\alpha_T \cdot \Delta T(y)\right) y dA \tag{8-20}$$

By virtue of the centroidal axis where y=0, the first term now equals zero.

$$0 = 0 + E\int_A \left(\Delta\phi \cdot y^2\right) dA - E\int_A \left(\alpha_T \cdot \Delta T(y)\right) y dA \tag{8-21}$$

Simplifying the second and third terms and removing constants from integrals yields:

$$0 = E\Delta\phi\int_A \left(y^2\right) dA - E\alpha_T \int_A \left(\Delta T(y) \cdot y\right) dA \tag{8-22}$$

Recognizing that the first integral is the second moment of area (moment of inertia), I :

$$0 = E\Delta\phi I - E\alpha_T \int_A \left(\Delta T(y) \cdot y\right) dA \tag{8-23}$$

Solving for incremental curvature, $\Delta\phi$:

$$\Delta\phi = \frac{\alpha_T \int_A \left(\Delta T(y) \cdot y\right) dA}{I} \tag{8-24}$$

Simplifying and substituting yields the second governing equation:

$$\Delta\phi = \frac{\alpha_T}{I} \int_y \left(\Delta T(y) \cdot y \cdot w(y)\right) dy \tag{8-25}$$

The above two governing equations, Equation 8-17 and 8-25, jointly define the temperature-correction procedure employed in the remainder of this chapter. These equations are applicable to each cross section within a beam if unique temperature profiles are known for each girder cross section. By integrating Equation 8-25 for all cross sections within a girder, an incremental camber (i.e. the camber variation caused by the induced temperature profile) can be computed. Most typically, a single midspan

temperature profile is assumed to sufficiently represent the cross-sectional temperature profiles present at all other sections within a girder.

8.2.3 Related Previous Work by Others

After the initial appearance of curvature-based temperature-correction procedures in the literature in the mid-1980's, there was a relative absence of further developments and refinements of these procedures until the mid-2000's—apparently spurred by research interest in evaluating the accuracy of camber predictions in precast, prestressed concrete girders. First to implement temperature-correction procedures for the purpose of adjusting field measurements of camber in simple span concrete girders appears to be Cook and Bloomquist (2005) in their FDOT-sponsored effort to verify the accuracy of prefabrication camber estimates. Cook and Bloomquist implemented an analytical model based on the recommendations of NCHRP Report 276 and, in combination with (1) measurements of girder camber and concrete surface temperature profiles and (2) assumptions for the CTE of concrete, used this temperature-correction procedure to facilitate comparisons between predicted and measured camber in production girders.

Next to focus on temperature correction of precast, prestressed concrete girders was Barr et al. (2005), with similar results later republished by Barr and Angomas (2010). A portion of the work of Barr et al. explored the effect of in-service temperature variations and thus, a temperature-correction procedure similar to that used by Cook and Bloomquist (2005) was implemented. An effort was made to validate the temperature-correction procedure using field-gathered data, although it is not clear if an effort was made to calibrate the procedure (by means of an effective CTE or otherwise) or if standard values of thermal material properties were assumed. A similar implementation

of a temperature-correction procedure was implemented by Lee (2010) in his analytical study. This work included a verification effort of the temperature-correction procedure using finite element modeling methods; typical values of concrete CTE were assumed in the absence of field measurements or calibrations.

A study by Rizkalla et al. (2011) also included a similar temperature-correction effort intended to modify field-measured girder cambers, except simplifying assumptions of linear temperature profiles were relied on. Rizkalla et al., using assumed values of concrete CTEs for this analytical work, concluded that (1) temperature-correction procedures are somewhat unreliable, (2) to minimize error, field measurements should be taken at dawn, and (3) no adjustments were recommended due to the transient nature of temperature-induced changes to girder deformations.

Prior to the work contained in this dissertation, four prior researchers also conducting work sponsored by ALDOT have implemented temperature-correction procedures similar to those discussed above. Johnson (2012) first derived a temperature-correction algorithm that served as a precursor to the derivations contained in Section 8.2.2 of this dissertation. Included in Johnson's work were various assumptions to simplify the analysis including (1) a simplified cross-sectional shape and (2) assumptions of standard temperature profile shape given recorded values at four specific depths within a section. Next, Keske (2014) expanded on the prior efforts by (1) conducting laboratory testing to determine appropriate ranges of CTE for girder concretes (SCC and VC) and (2) expanding the applicability of Johnson's work to composite girders. Isbiliroglu (2014) implemented a similar temperature-correction procedure to evaluate historical testing results of noncomposite girders from four previous projects. Finally, Neal (2015),

in concert with the work of Keske (2014), analytically determined values of an "effective" concrete coefficient of thermal expansion (CTE) that yielded best agreement between predicted and measured field responses of full-size girders. The joint work of Neal (2015) and Keske (2014) is most similar to the analytical techniques employed in this dissertation, although the more detailed field instrumentation included in this effort allows for improved comparisons between predicted and measured field responses.

8.2.4 Algorithm Refinements and Improvements in this Work

A major objective of this dissertation was to implement various algorithm refinements and improvements to address weaknesses of the studies referenced above. These refinements were focused in two areas: (1) improved understanding of regionally-induced temperature gradients, and (2) inclusion of actual girder cross-sectional widths without the use of simplifications.

In order to implement a temperature-correction procedure, it is first necessary to have a thorough understanding of the vertical temperature profiles induced in candidate girders. Previous work by others typically monitored temperature readings at certain key depths within a cross section and made assumptions to define the temperature profile for other intermediate depths. In previous AUHRC research on this topic, the typical simplifying assumptions regarding temperature profiles are (1) a uniform temperature is assumed within the top flange, (2) a uniform temperature is assumed within the bottom flange and (3) a single linear gradient is assumed within the height of the web, not necessarily matching the top and bottom flange temperatures at the boundaries. An example of a fitted temperature profile from the previous work of Keske (2014) is shown in Figure 8-1. Given that only limited guidance is available in the literature regarding the

likely shape of vertical temperature profiles in noncomposite precast, prestressed girder shapes (primarily from Lee 2010 and Kelly et al. 1987), the previous assumptions of ALDOT-sponsored researchers were logical.

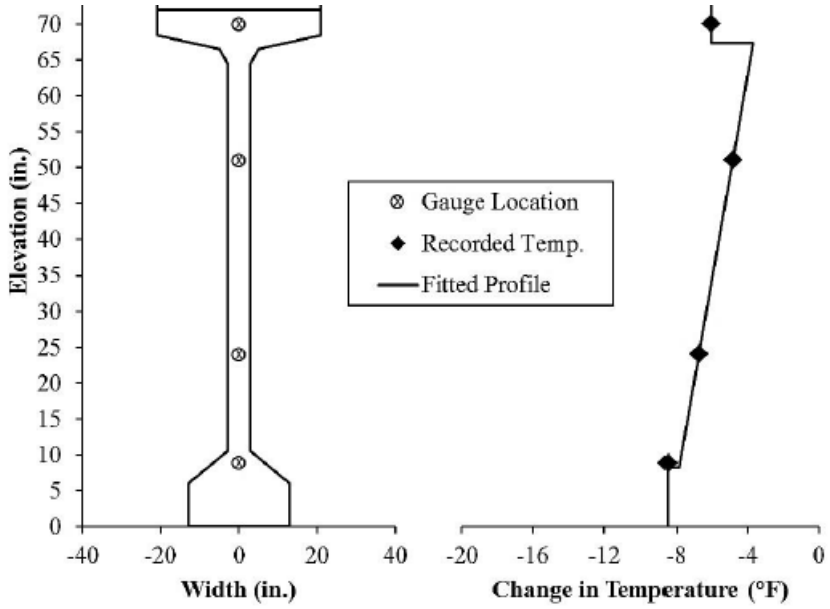

Figure 8-1: Fitted Temperature Profile from Keske (2014)

In the experimental effort detailed in this dissertation, various girder cross sections were heavily instrumented with temperature sensors to more precisely characterize diurnal temperature profiles at different times. Accordingly, the revised implementation of the temperature-correction algorithm used in this project is capable of accepting a nearly unlimited number of vertical temperature measurements at different elevations. The algorithm linearly interpolates between adjacent temperature measurements along the height of the girder and also extrapolates linearly to the extreme top and bottom fibers using the nearest interpolated gradient as shown in Figure 8-2.

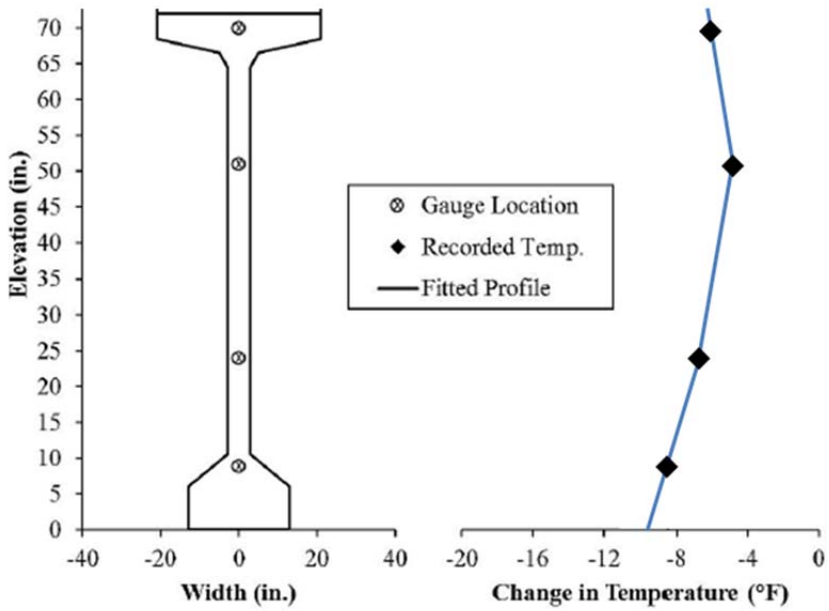

Figure 8-2: Fitted Temperature Profile of Revised Temperature-Correction Algorithm

The flexibility to accept varying numbers of temperature measurements along a girder height was advantageous in allowing the various analysis iterations conducted in Section 8.5 aimed at identifying best (and most efficient) girder instrumentation practices for future research implementation.

Another key improvement implemented in the temperature-correction algorithm used in this chapter was the ability to use true girder widths at any given height within a cross section. Previous work by ALDOT-sponsored researchers relied on a simplification of the bulb-tee girder shape by approximating the cross section as three rectangles with dimensions such that key cross-sectional geometric parameters (e.g. area and moment of inertia) were accurately preserved. In doing so, evaluation of the two integrals of Equation 8-17 and 8-25 is greatly simplified, although perhaps at a cost of computation accuracy. This magnitude of error introduced by the use of an equivalent cross section,

as well as other previous assumptions, is explored thoroughly in Section 8.5 of this chapter.

While the inclusion of (1) the capability to accept additional temperature measurement inputs within a cross section and (2) the use of actual widths at all depths within a cross section were all welcomed improvements of the revised temperature-correction algorithm, these additions came at an increased computational cost. Where previous researchers were able to evaluate the dual integrals of Equations 8-17 and 8-25 relatively simply by approximate methods, the revised temperature-correction algorithm demanded the use of numerical integration. In conducting the numerical integration for a single cross section, large matrices (at least as large as the number of vertical differential elements by the number of height-dependent parameters within Equation 8-17 and 8-25) become necessary. By virtue of these large matrices, it is challenging and computationally expensive to repeatedly evaluate numerical integrals for rapidly changing temperature profiles (e.g. to evaluate temperature-induced changes in deformations every two minutes for a 24-hour period). To address these challenges, the temperature-correction algorithm used herein was programmed as a series of layered functions in an engineering calculation software package. Structuring the algorithm as such facilitated the efficient post-processing of large amounts of field-gathered data, thereby allowing the breadth of the analyses offered later in this chapter. For reference, Appendix J contains samples of the layered functions used in the implementation of the temperature-correction algorithm.

8.3 Experimental Program

This section details the field experimental program conducted as part of this research effort to evaluate the effects of diurnal ambient temperature exposure on the deformations of three production girders during in-plant storage. First, a general overview of the experimental program is provided. Next, the experimental procedure is presented and additional details of each test are provided as required for subsequent analyses conducted later in this chapter. Finally, a comprehensive instrumentation plan is provided detailing both internal concrete and external instrumentation monitored during on-site testing.

8.3.1 Summary of Work

In this field monitoring study, the deformational responses of three hardened bulb-tee girders subjected to diurnal temperature profiles during in-plant storage were continuously monitored—at increments of two minutes—for a period of approximately 24 hours. During this testing period, temperature sensors (previously installed during girder production) monitored internal concrete temperatures at 15 depths within the midspan cross section and four depths within the 1/6-span cross section. In addition, various metrics of girder deformation (four internal concrete strains at midspan and 1/6-span cross sections, vertical deflection at three intermediate locations along each girder, and girder end rotations) were also monitored throughout each testing period.

8.3.2 Experimental Procedure and Field Test Details

The experimental procedure employed in this research effort had several steps:

- Prepare and bench test all sensors and data collection equipment utilized in this effort to verify sensor accuracy and compatibility of measurement ranges with anticipated field responses;

- Install internal girder sensors prior to and during initial girder production. Cap and protect protruding wires for later use;
- Identify candidate testing date(s) most likely to induce extreme diurnal temperature fluctuations[1] of girder concrete and coordinate field-availability with girder producers during these times;
- Approximately one week prior to performing each 24-hour in-plant test, coordinate relocation of candidate girder(s) from typical position in storage yard to a position of (a) relatively unobstructed solar exposure and (b) support conditions similar to those of final installation;
- Arrive on-site, install external girder sensors and connect all gages to data collection system; and
- Continuously monitor data collection effort throughout 24-hour testing period to ensure (a) shading of temperature-sensitive instrumentation from solar exposure, (b) protection of sensors from precipitation, (c) continuous power supply, and (d) proper operation of data collection system.

Details for each girder specimen and field test, as relevant to implementation of the temperature-correction algorithm herein, are displayed in Table 8-1 for each of three tests.

[1] In-plant tests were conducted during winter months due to both researcher/producer availability and the potential for extreme fluctuations of girder concrete temperatures due to diurnal exposures (i.e. colder nights and warmer days with unobstructed solar exposure).

Table 8-1: Test Details for 24-Hour In-Plant Tests

Test No.	Girder Shape	Girder Length[a]	Casting Date	Testing Date	Chronological Age of Girder at Testing (days)	Test Duration (hours)
1	BT-72	139'-5.7"	10/9/13	12/15/13-12/16/13	67	23.9
2	BT-72	137'-9.5"	7/24/13	12/17/13-12/18/13	146	32.1
3	BT-63	130'-0"	9/23/14	12/15/14-12/16/14	83	23.9

[a] = SI girder lengths are converted to English units.

8.3.3 Instrumentation Plan

In accordance with recommendations for the instrumentation of concrete girders provided by both FHWA Report SA-96-075 (Holt 1996) and previous AUHRC researchers (Johnson [2012] and Keske [2014]), an instrumentation plan was developed to support the experimental effort of this research phase. Instrumentation consisted of both internal and external girder sensors labelled according to the convention shown in Figure 8-3.

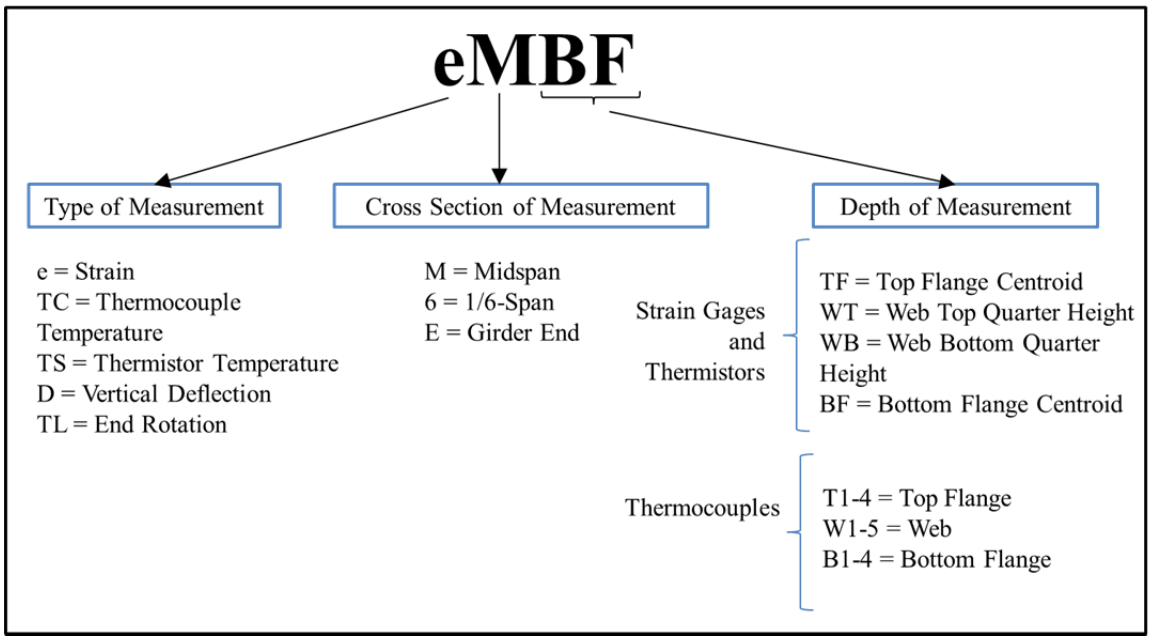

Figure 8-3: Label Convention for Instrumentation

Internal sensors installed at girder midspan consisted of both vibrating-wire strain gages (VWSGs) equipped with companion thermistors and Type T thermocouples

positioned within girder concrete as shown in Figure 8-4. Vibrating-wire strain gages were installed at the approximate geometric centroids of the bottom and top flanges and at upper and lower quarter-points of the girder web height. Type T thermocouple locations at the midspan cross section are also shown in Figure 8-3, consisting of either eleven or thirteen thermocouples dependent on the test. In selecting thermocouple positions, an effort was made to capture temperature profiles at changes in the cross-sectional width, as well as to concentrate sensors in areas expected to experience extreme temperature variations (i.e. extreme top and bottom fibers of girder).

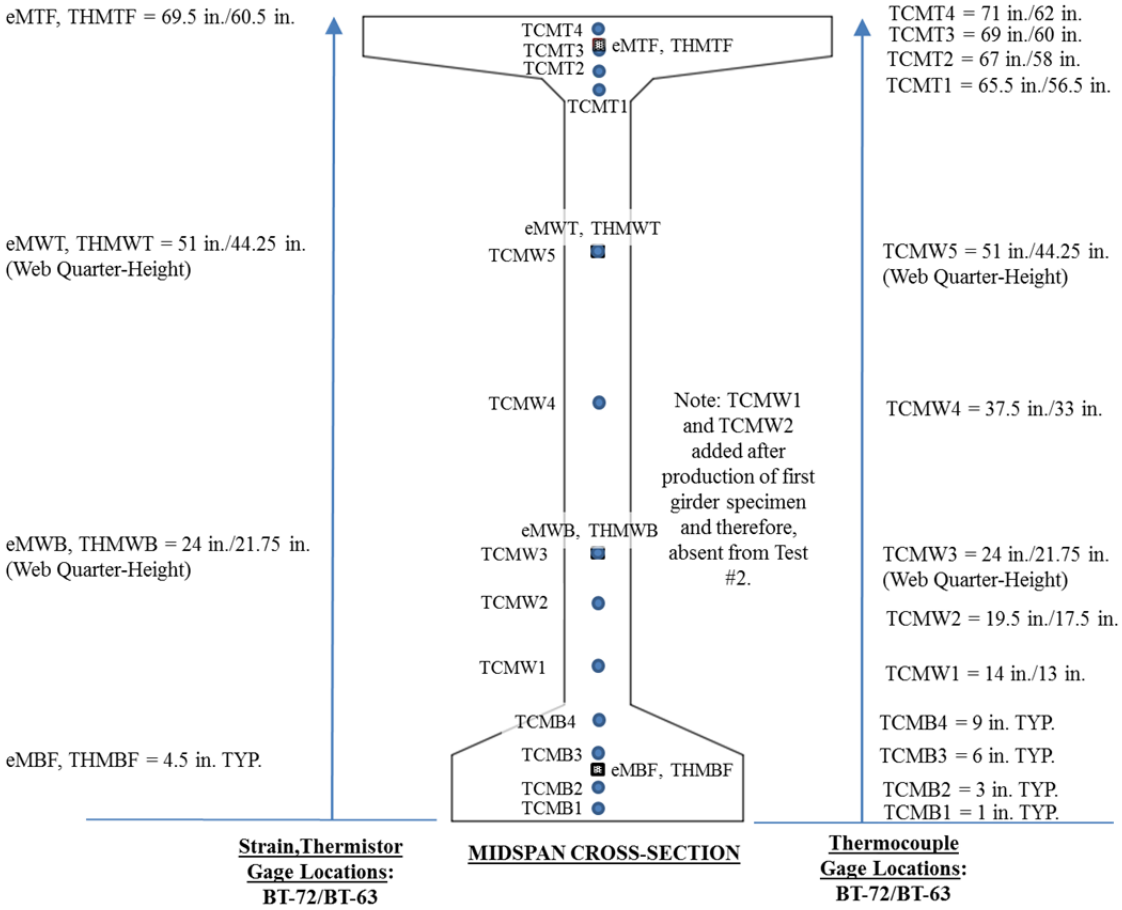

Figure 8-4: Typical Internal Instrumentation at Midspan Cross Section

Vibrating-wire strain gages were also installed at the 1/6-span cross section of girders specimens at similar depths. The primary purpose of these gages was to verify if

different cross sections behaved similarly as hypothesized by the temperature-correction procedure for camber. The locations of the four additional 1/6-span gages are displayed in Figure 8-5.

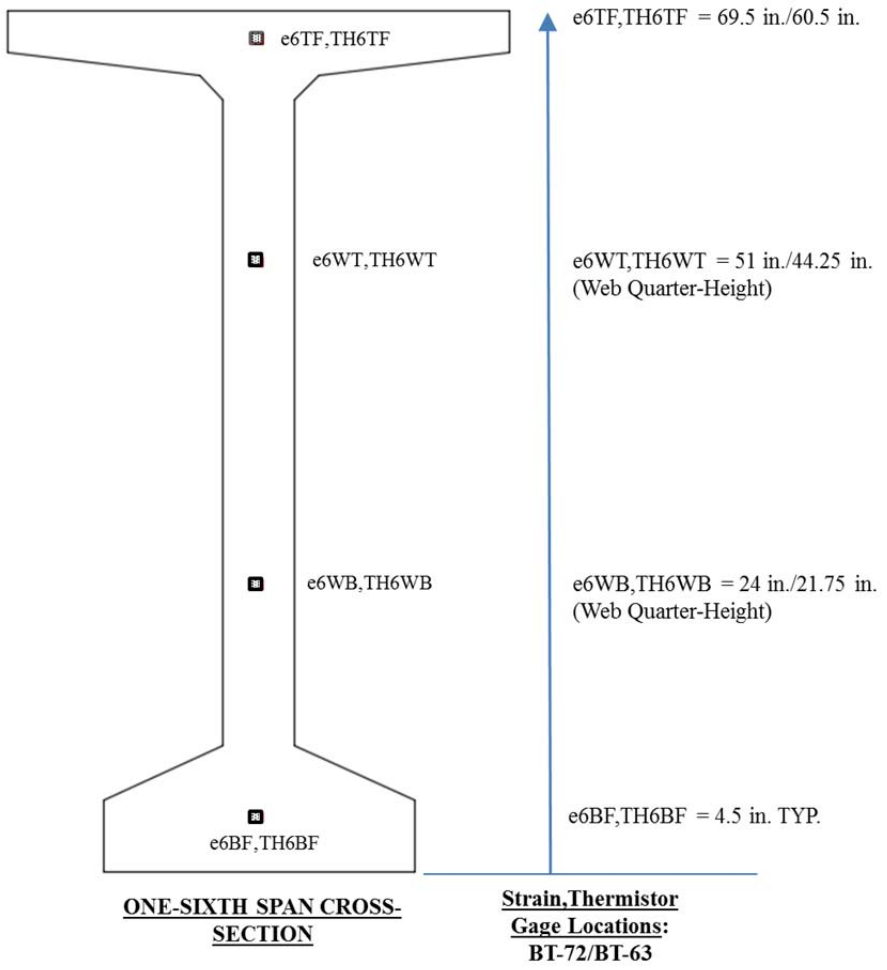

Figure 8-5: Typical Internal Instrumentation at 1/6-Span Cross Section

Both Figures 8-4 and 8-5 show the locations of internal gages measured from girder bottom for both specimen cross-sectional shapes included in this effort (BT-72 and BT-63 sections). A typical midspan installation of gages prior to concrete placement is shown in Figure 8-6.

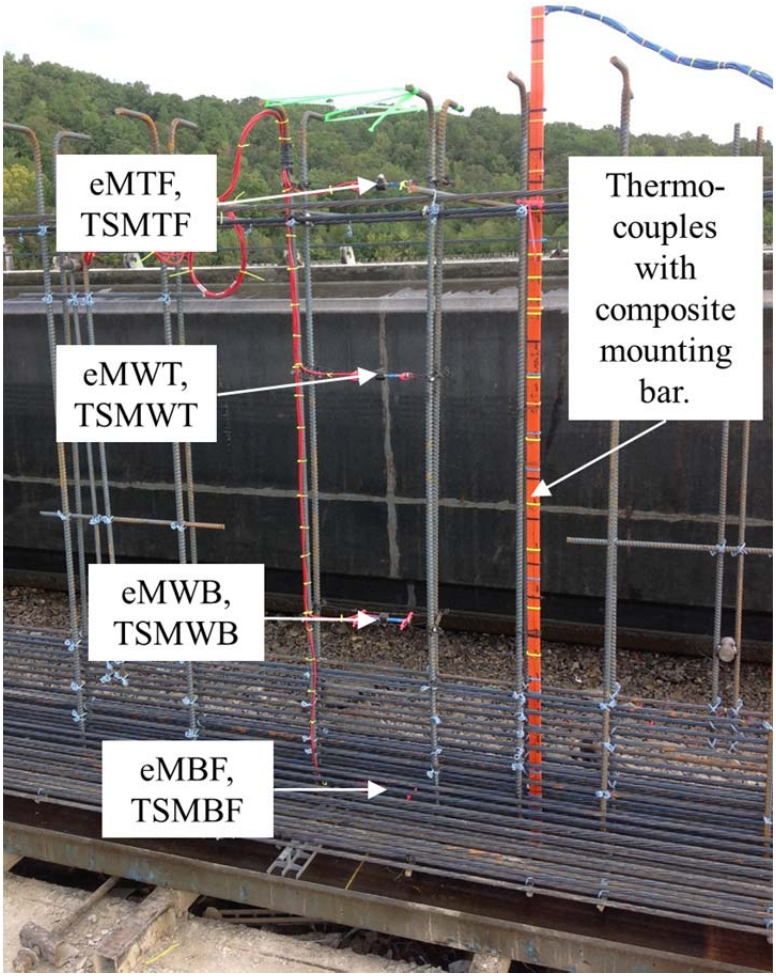

Figure 8-6: Typical Midspan Internal Instrumentation Prior to Concrete Placement

In contrast to the internal sensors which were installed during girder production, the external sensors were temporarily affixed to girder specimens during field monitoring. External sensors consisted of displacement gages attached to the girder bottom flange and tiltmeters affixed to the girder end as shown in Figure 8-7. A slightly modified spacing of the bottom-flange displacement gages was mistakenly used in Tests #1-2, but later corrected for Test #3.

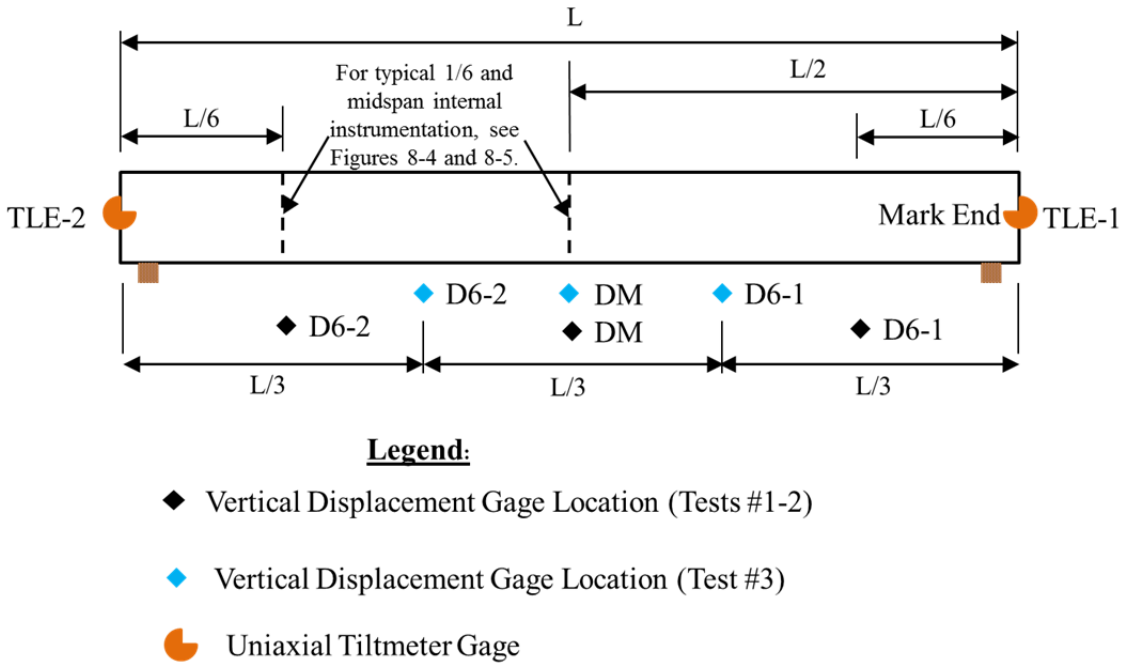

Figure 8-7: Typical Girder External Instrumentation for 24-Hour Tests

A typical 24-hour test in progress is shown in Figure 8-8 with all relevant instrumentation noted and the data acquisition vehicle also visible.

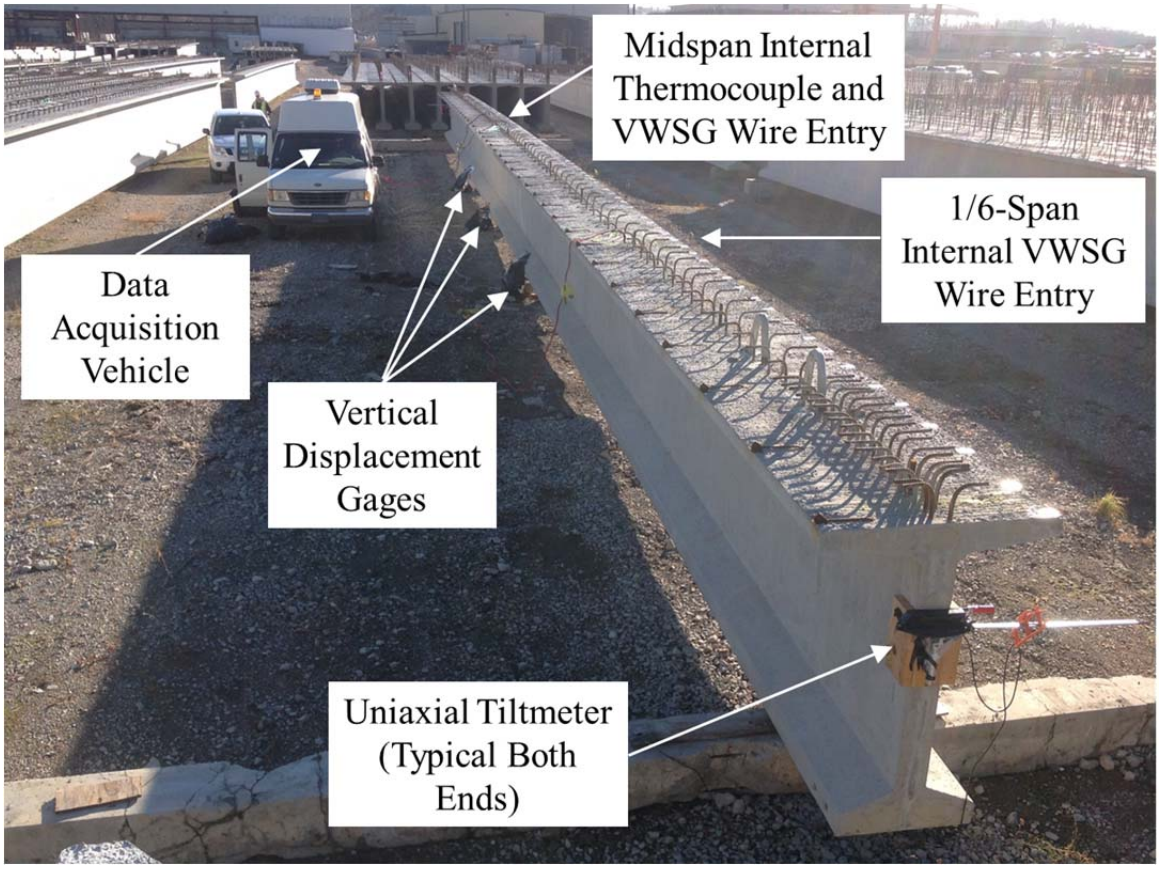

Figure 8-8: 24-Hour Test #3 in Progress

For data collection purposes, a custom data collection system was designed and assembled as shown in Figure 8-9. Key hardware features of the data collection system included (a) a battery backup capable of powering all instrumentation for the duration of each test, (b) a wireless link allowing real-time monitoring of experimental results from a mobile computer or tablet, (c) capability to monitor up to 32 VWSGs, (d) capability to monitor up to 32 thermocouple sensors, and (e) capability to monitor two tiltsensors.

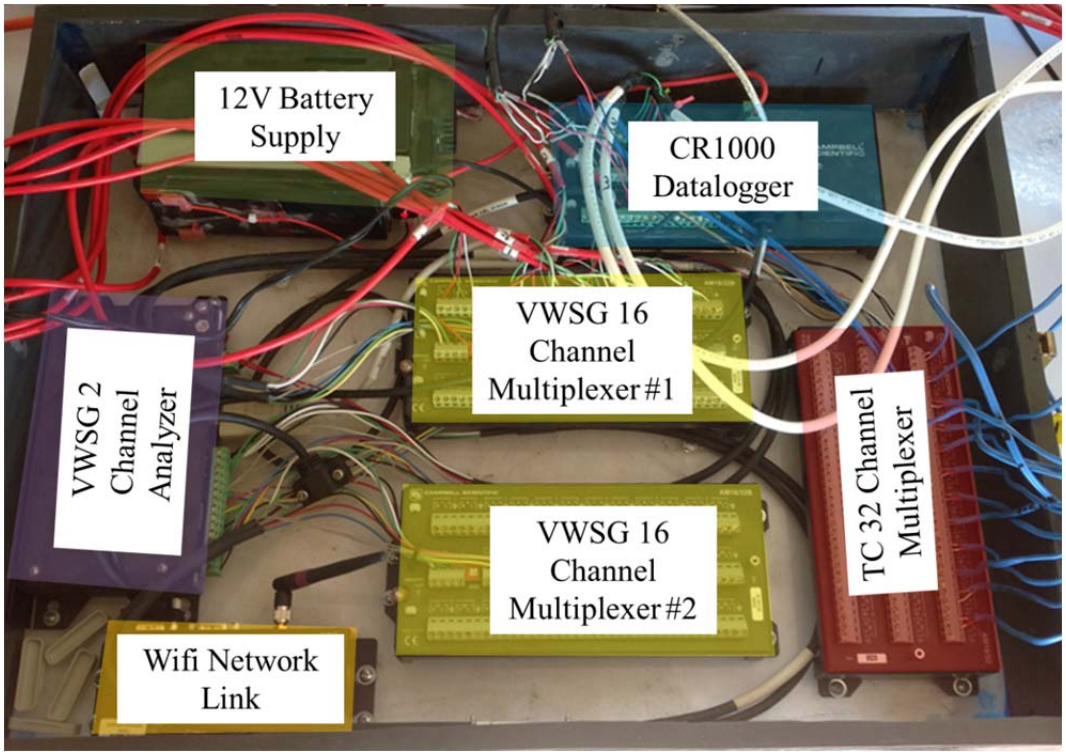

Figure 8-9: Typical Data Collection System for 24-Hour Tests

A custom sampling program was coded that monitored all sensors in 120-second intervals for the duration of each testing period. Details of both the data collection system components and the types/models of sensors used in this investigation are listed in Table 8-2.

Table 8-2: Sensor and Data Collection System Component Details

Type of Gage/Instrumentation	**Manufacturer and Model #**
Vibrating-Wire Strain Gage (VWSG) with Thermistor	Geokon 4200 Series
Draw Wire Displacement Sensor	Micro-Epsilon WDS-150-P60-CR-P
Type T Thermocouple	Varies
Data Collection System Components	**Campbell Scientific Model #**
Data Logger	CR1000
2-Channel Vibrating-Wire Spectrum Analyzer	AVW200
Three 16/32 Channel Multiplexers	AM16/32B
Wireless Network Link Interface	NL240

8.4 Presentation and Post-Processing of Raw Data

The purpose of this section is to present all data gathered as part of this experimental effort, while also detailing any post-processing efforts necessary to prepare the raw data for the analysis later described in Section 8.5 of this dissertation. Major post-processing efforts included (a) detection and dismissal of flawed measurements, (b) examination of the linearity of measured strain profiles to confirm proper function and positioning of internal strain gages, and (c) validation of duplicate measurements (i.e. examining similarities between adjacent thermistor and thermocouple gages). Then, various observations are offered on the magnitude and typical shapes of the diurnal temperature profiles observed in this study and previous research work by others.

8.4.1 Presentation of Raw Data by Test

Raw experimental results for Test #1 are displayed in Figures 8-10 through 8-13. Measured internal concrete temperatures at both midspan (all thermocouple and thermistor measurements) and 1/6-span (thermistor measurements) are shown in Figure 8-10. Also shown on this plot (and all other plots in this section) are the approximate timings of dawn and dusk during the test duration. For reference, the horizontal axis of all plots displayed herein begins at the start of the test (time t = 0) and extends through the duration of the test.

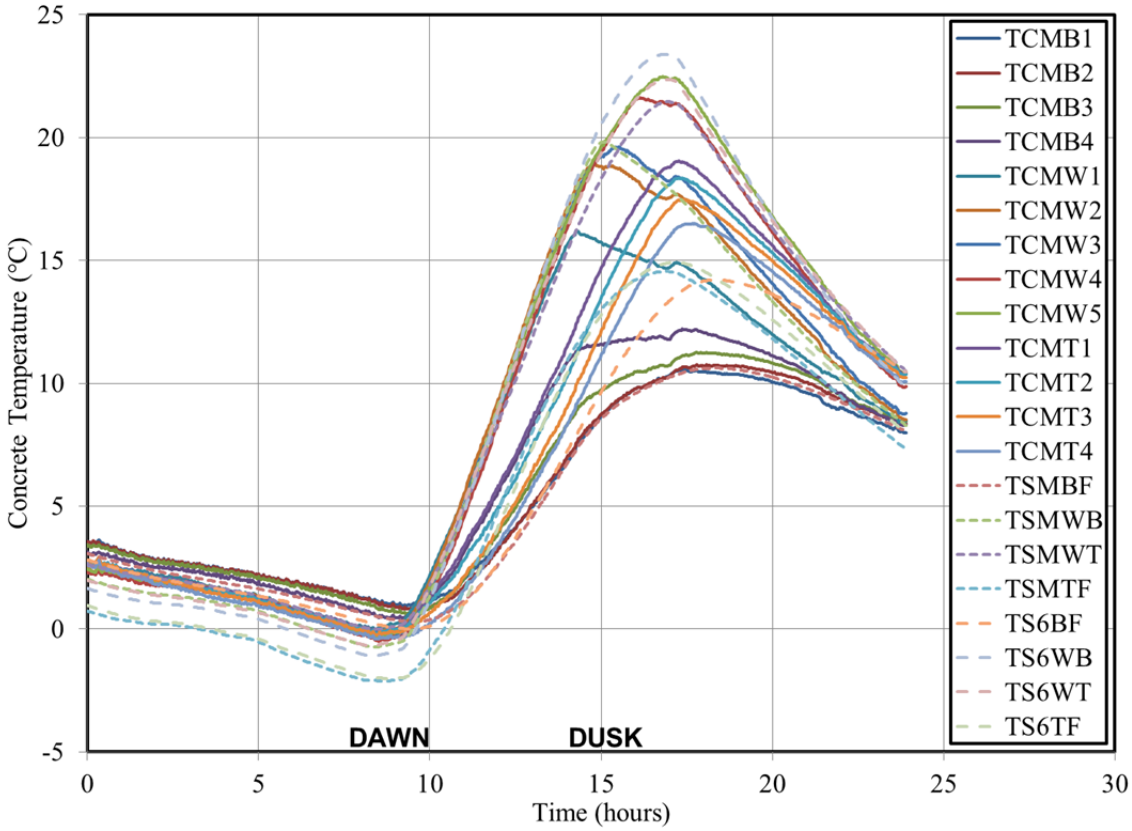

Figure 8-10: Test #1 Recorded Concrete Temperatures

Although Figure 8-10 conveniently displays all recorded temperature data from Test #1 in a single plot, the form of this plot is not conducive to the identification of specific trends within the recorded data set. For this purpose, Section 8.4.3 later displays recorded temperature data in a more useful format to allow discussion and comment on recorded data. Changes in internal concrete strain at both midspan (eM-series) and 1/6-span (e6-series) for Test #1 are displayed in Figure 8-11. These strain values are unprocessed with the exception of the use of a manufacturer-specified gage temperature-correction factor and zeroing of readings with respect to the initial (t=0) reading.

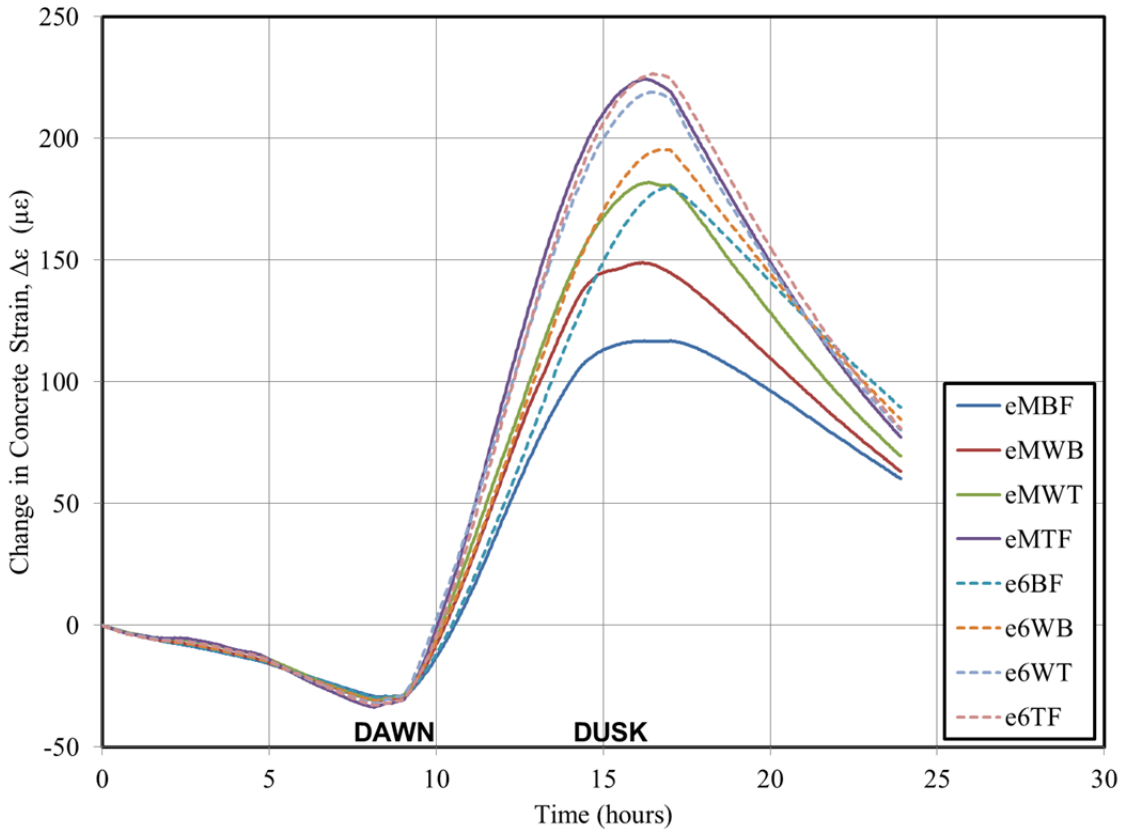

Figure 8-11: Test #1 Recorded Concrete Strains

Recorded vertical displacements for Test #1 are shown in Figure 8-12. As shown, the precision of the displacement sensors utilized in this investigation (approximately 0.01 inches) is visible in the plot. Girder response appears relatively symmetric with peak displacement values occurring at midspan as expected. Raw readings of girder end rotations are shown in Figure 8-13.

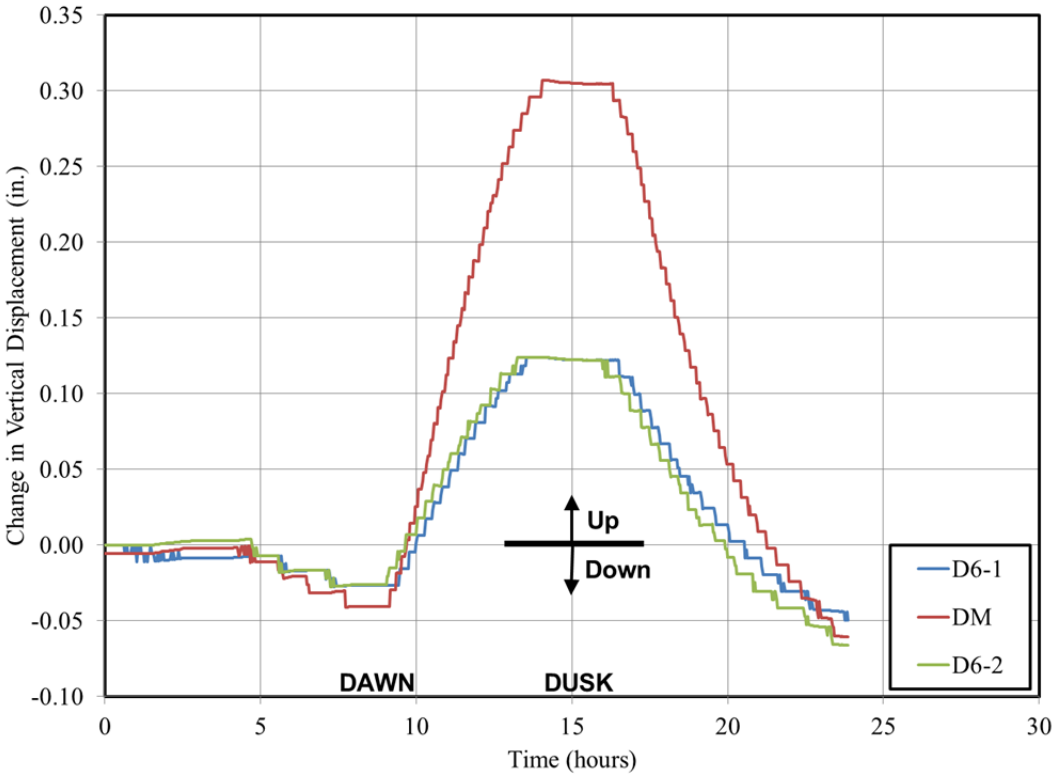

Figure 8-12: Test #1 Recorded Vertical Displacements

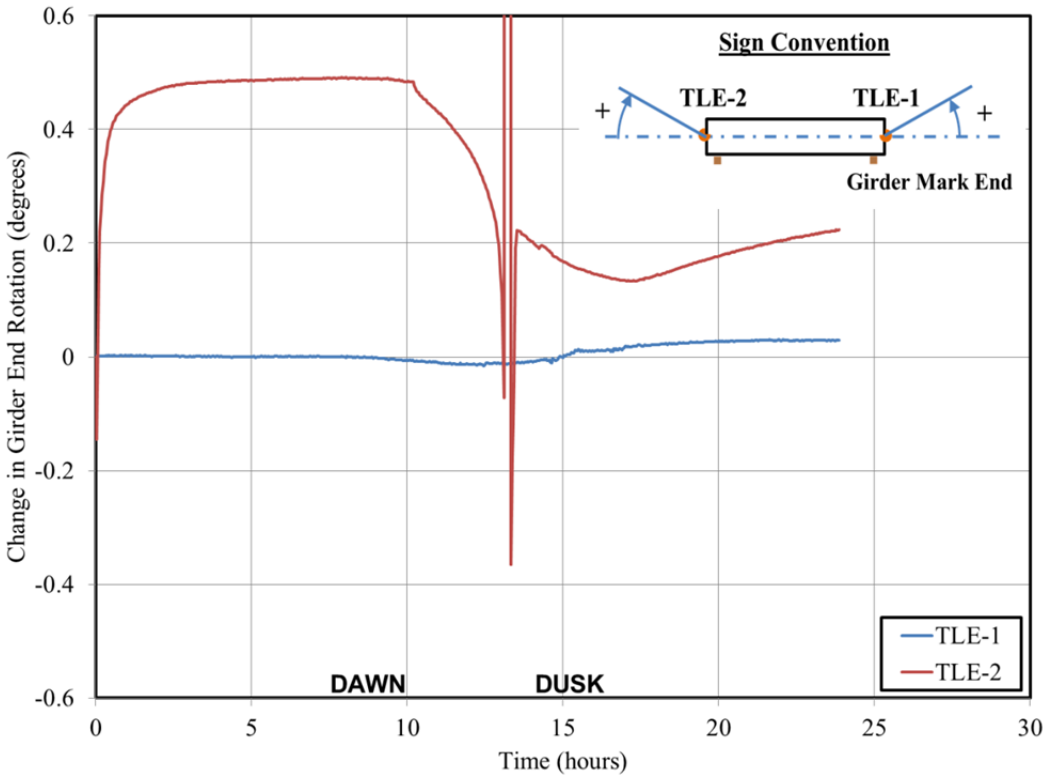

Figure 8-13: Test #1 Recorded Girder End Rotations

The readings from sensor TLE-2 were compromised as a result of the failure of an adhesive[2] used to affix sensor TLE-2 to the girder specimen. Additionally, close inspection of the girder end rotations recorded for sensor TLE-1 show disagreement with the observed vertical displacement trends of Figure 8-12. For instance, girder end rotation readings of gage TLE-1 fail to consistently return to benchmark values (t=0) at times when other measures of girder deformation (e.g. vertical deflection) return to zero (t=10 hours and t=20 hours)—suggesting an apparent drift of tiltmeter readings throughout the testing period. For this reason, the readings of the tiltmeters used in this investigation were found to be unreliable and despite being reported in this section, were omitted from remaining analyses. Similar results are shown in Figures 8-14 through 8-17 for Test #2. Recall, Test #2 utilized only 11 thermocouple sensors at midspan as opposed to the 13 sensors present in Tests #1 and 3.

[2] The epoxy used to attach the tiltmeter mounting bracket to the skewed girder web failed to sufficiently chemically activate due to below-freezing temperatures during test setup.

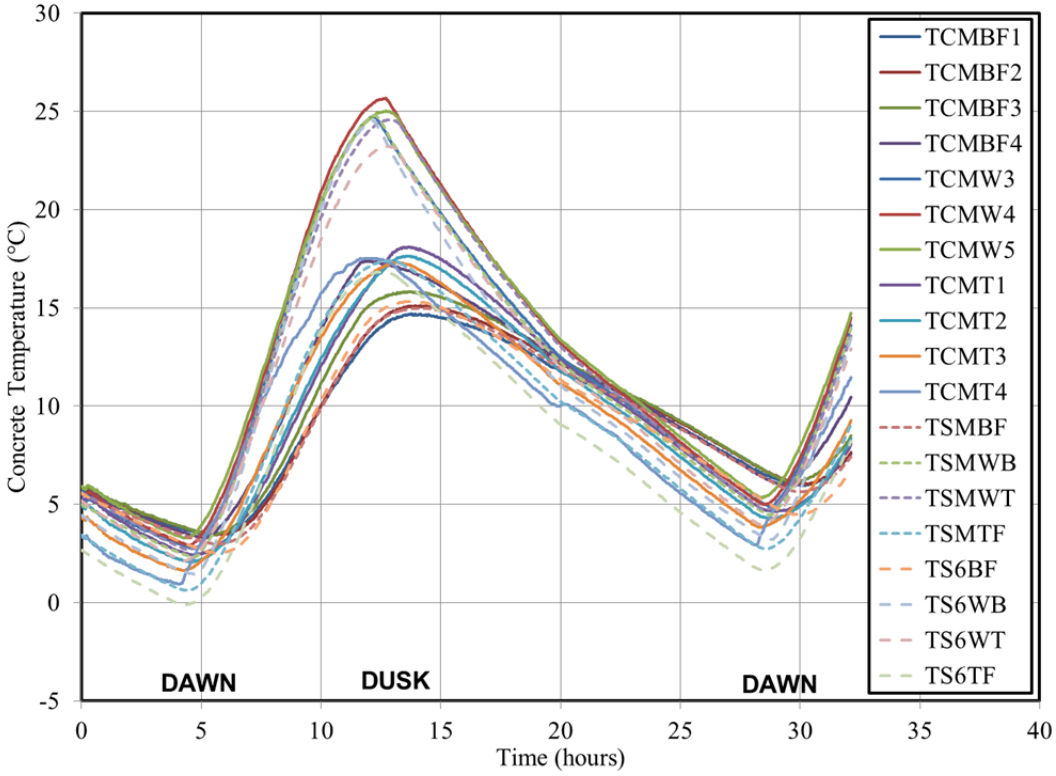

Figure 8-14: Test #2 Recorded Concrete Temperatures

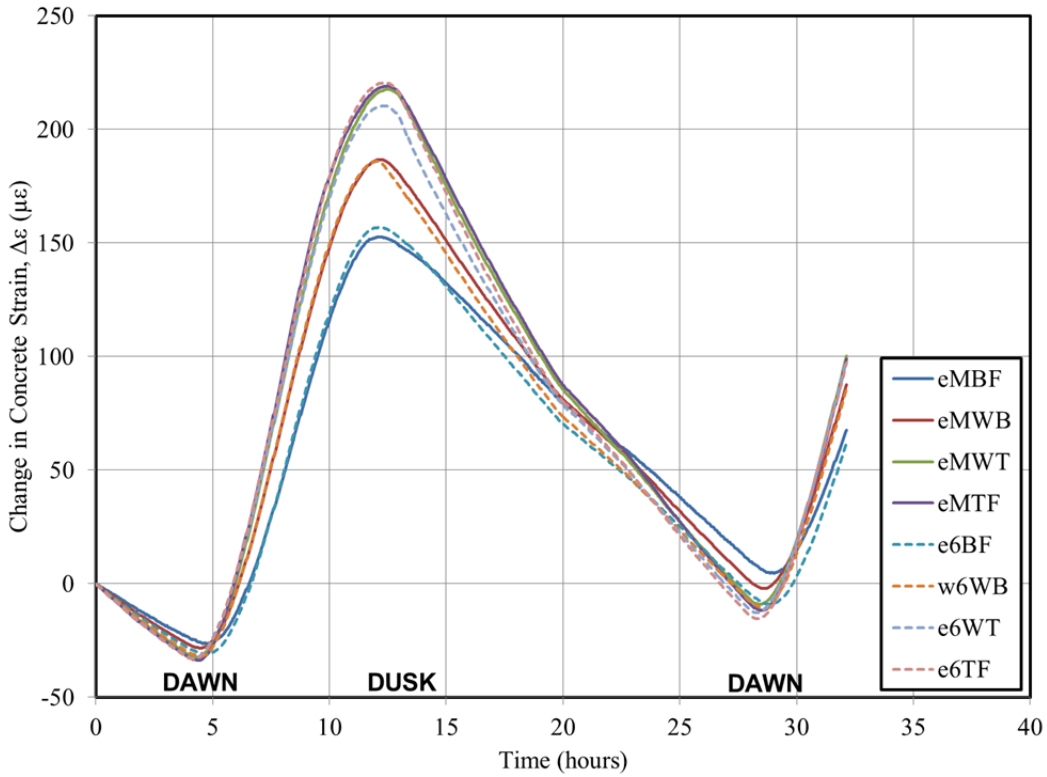

Figure 8-15: Test #2 Recorded Concrete Strains

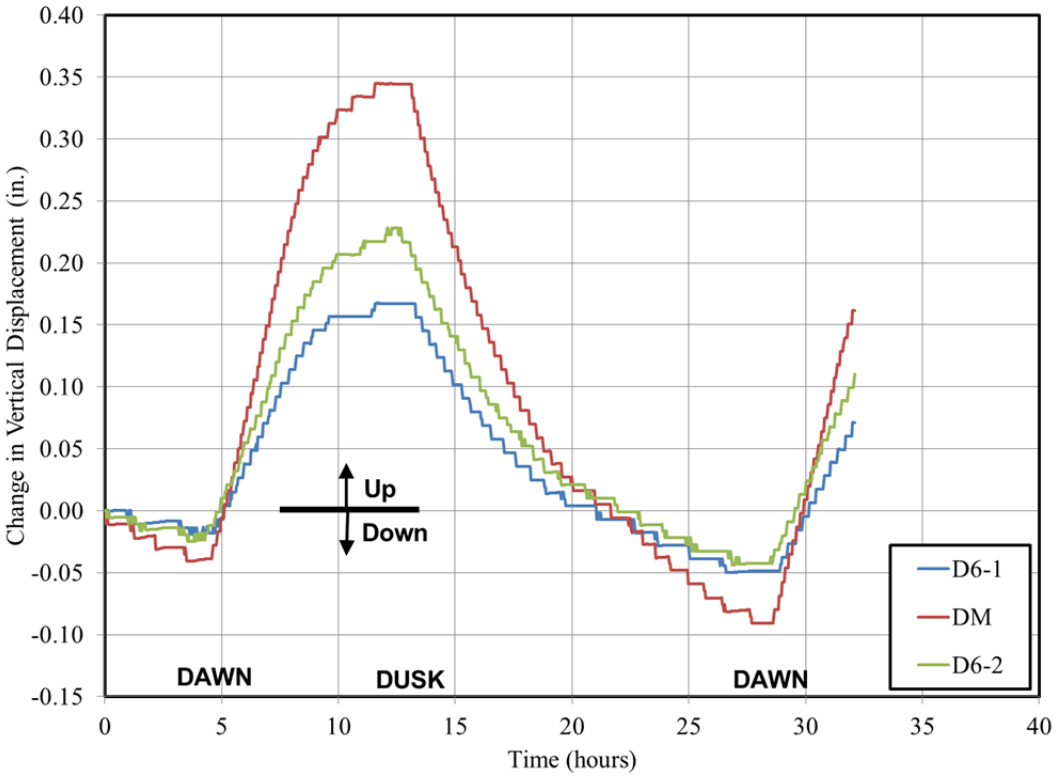

Figure 8-16: Test #2 Recorded Vertical Displacements

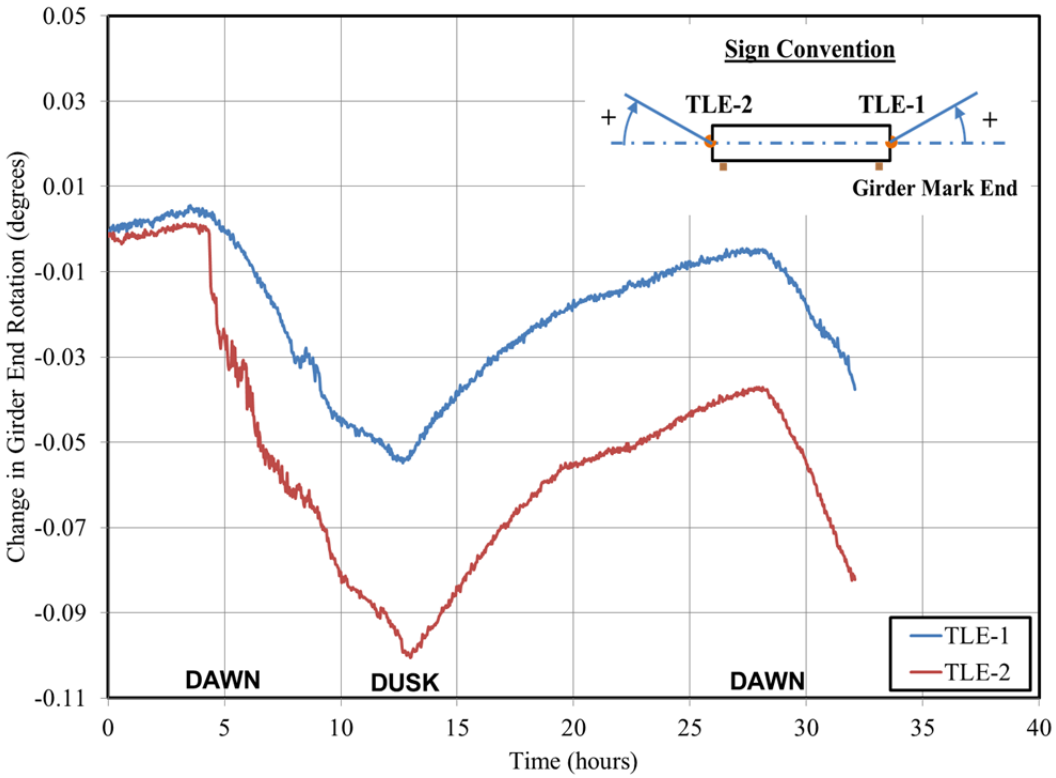

Figure 8-17: Test #2 Recorded Girder End Rotations

Similar plots are displayed in Figures 8-18 through 8-21 for Test #3. As noted on each plot, a change in the ambient weather conditions occurred approximately 5 hours into the test during Test #3 with the ambient temperature first slightly increasing, then rapidly decreasing 6°C in the five-hour period coinciding with testing hours 5 through 15. This weather change affords an opportunity to evaluate the accuracy of the temperature-correction procedure with respect to a change in ambient temperature independent of solar radiation.

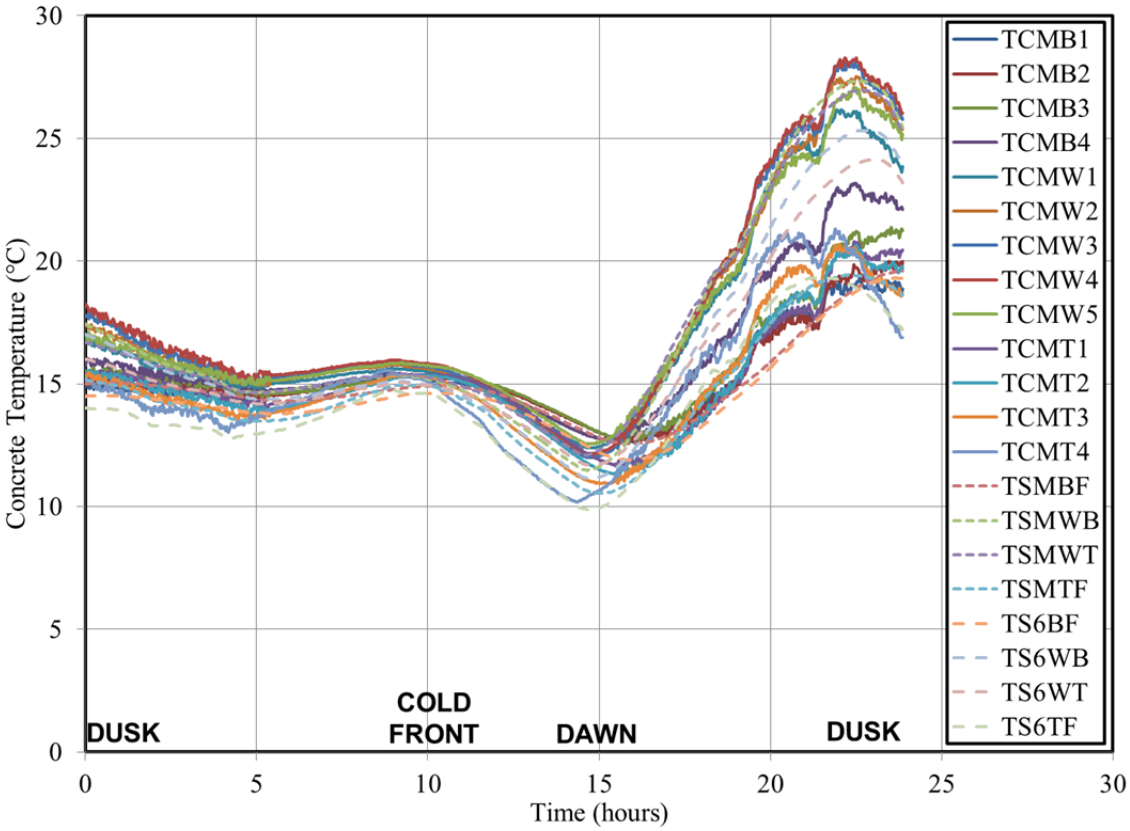

Figure 8-18: Test #3 Recorded Concrete Temperatures

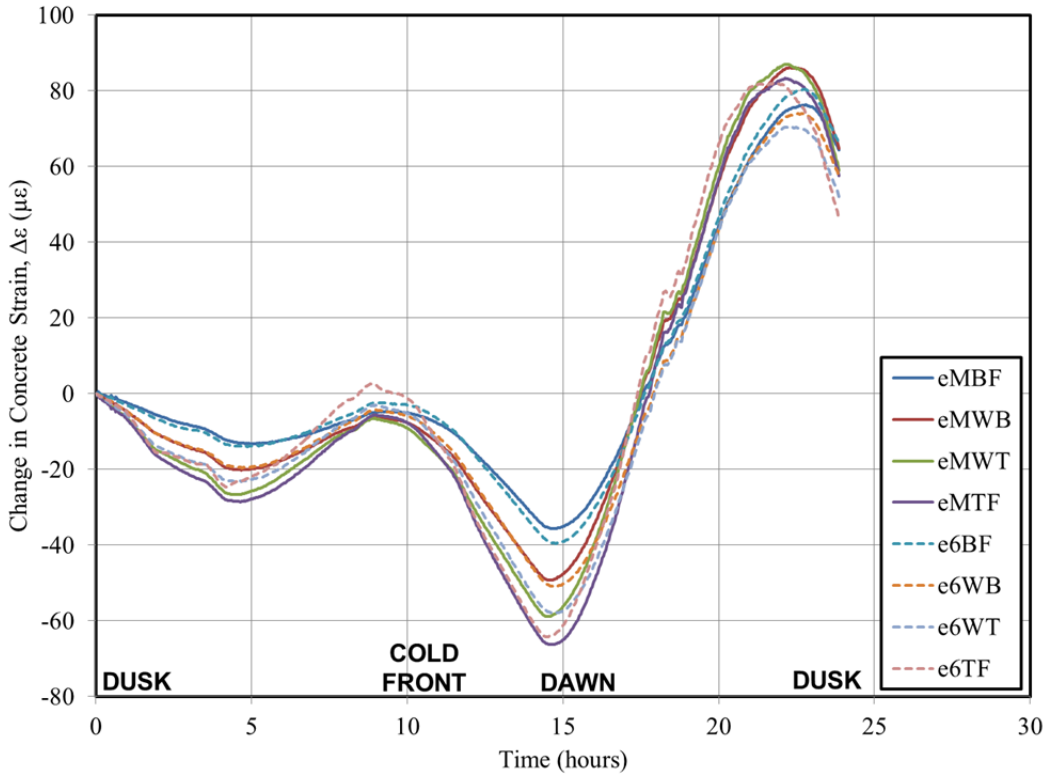

Figure 8-19: Test #3 Recorded Concrete Strains

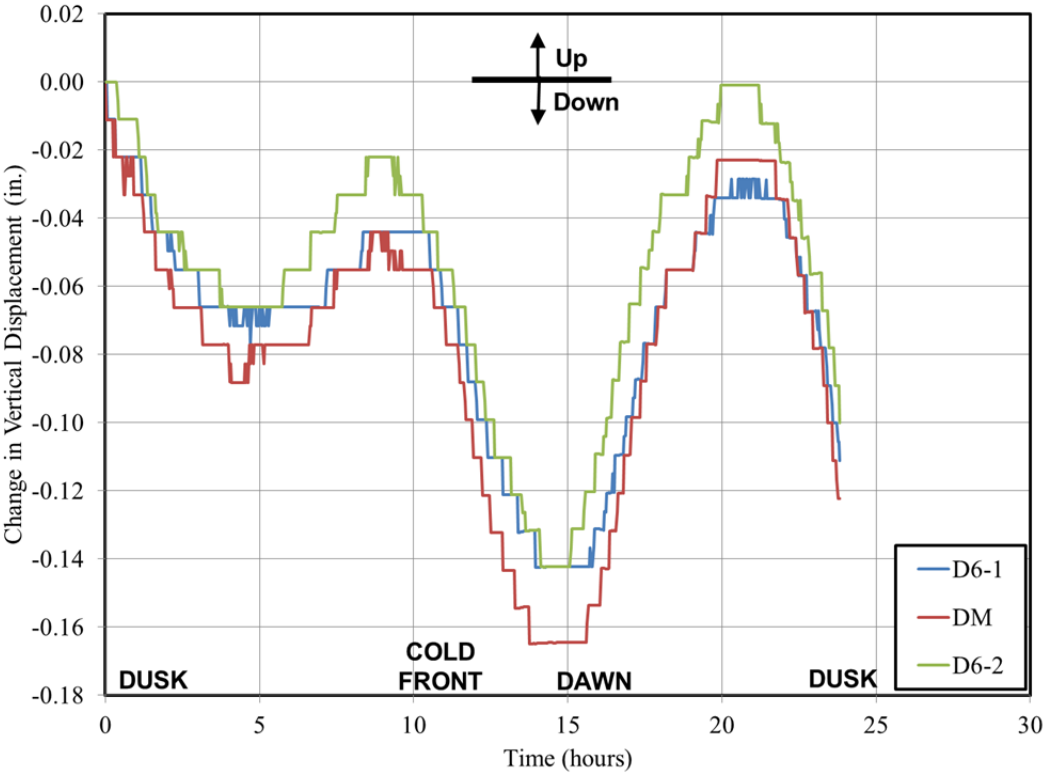

Figure 8-20: Test #3 Recorded Vertical Displacements

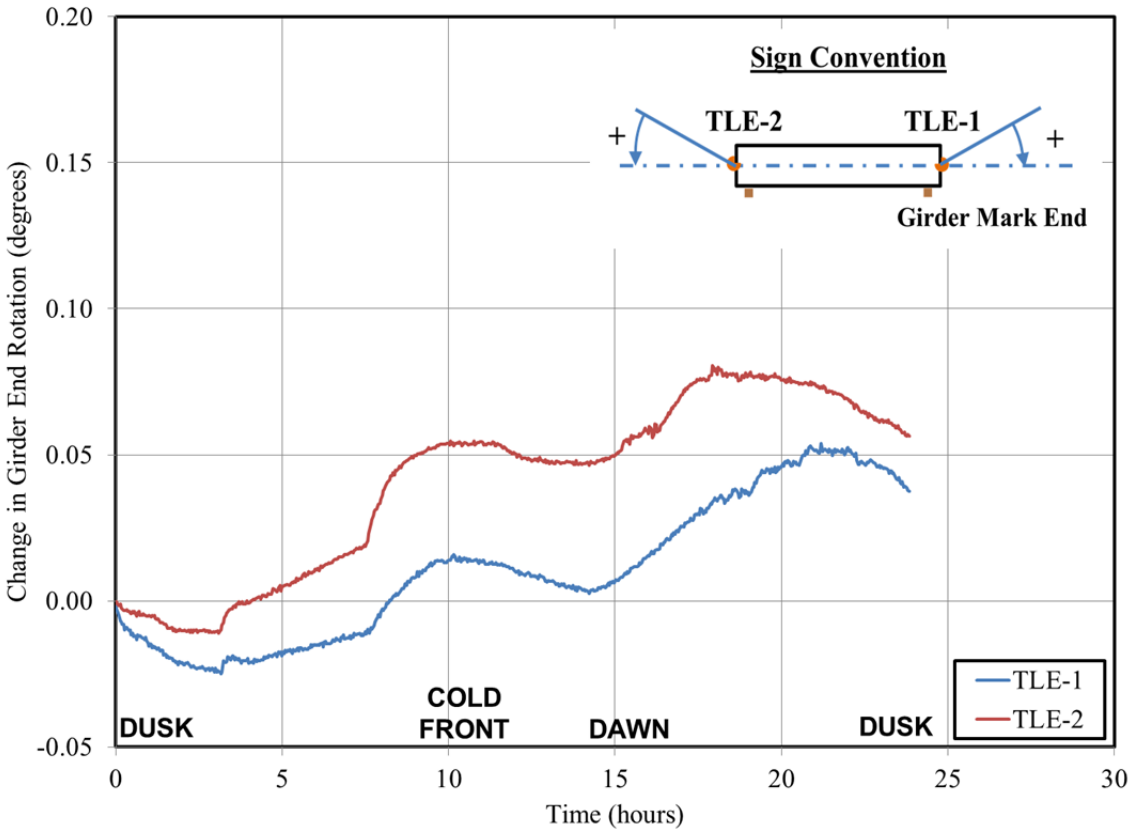

Figure 8-21: Test #3 Recorded Girder End Rotations

The following general observations are based on consideration of the raw data shown in Figures 8-10 through 8-21:

- Tests #1 and 2 appear to have captured the most extreme temperature-induced deformational behavior, followed by Test #3;
- Maximum observed fluctuations in internal concrete temperature of nearly 25°C (44°F) were recorded throughout Tests #1 and 2, with a maximum range within the cross section at a single time of roughly 15°C;
- Maximum observed temperature-induced changes in internal concrete strains of approximately 250 microstrain were observed, with a maximum range within the cross section at a single time of roughly 120 microstrain;

- Maximum observed temperature-induced changes to midspan displacement of approximately 0.45 inches were recorded;
- With the exception of the readings of tilt sensors, a preliminary inspection of all readings does not warrant dismissal of any additional values; and
- The deformational response of the girder, as manifested in external displacement measures, indicates relatively symmetric behavior of girder specimens in response to observed diurnal temperature profiles.

8.4.2 Validation of Recorded Data

During the placement of concrete in the fabrication of precast, prestressed concrete girders, there exists the potential for damage to internally-positioned sensors, primarily by shifting of gages by fresh concrete and incomplete consolidation in the vicinity of gages. Two methods were employed to validate the accuracy of recorded data: (1) confirmation of the linearity of recorded strain measurements across a cross-section depth, and (2) comparisons of readings from adjacent sensors.

A procedure was developed to confirm proper positioning and operation of the vibrating-wire strain gages installed during the fabrication of the three specimens included in this study. The basic premise of this method was to confirm the linearity of strain profiles induced during deformation. A convenient statistical metric for this purpose is the use of the coefficient of determination, R^2. In general, the coefficient of determination is an indicator of the proportion of the observed variation accounted for by a fitted statistical model. In the application used herein, a linear model was fitted to measured strain values (recorded at four depths within a girder) and a corresponding value of R^2 was then computed. For reference, values approaching 1.0 indicate an

exceptionally good linear fit of experimental data. While relatively simple in application, a complication of this analysis procedure arises for experimental data sets representing vertical (or nearly vertical) lines. In this case, the dependent variable, strain, does not vary as a function of the independent variable, height within girder. For this reason, the coefficient of determination is not a valid indicator of the goodness-of-fit of a linear model for vertical lines. To avoid this complication, it was decided to compute the coefficient of determination of linear fit at only a single time for each set of readings—the time of maximum temperature-induced curvature. Values of the coefficient of determination for these situations are summarized in Table 8-3 and also depicted graphically in Figure 8-22.

Table 8-3: Verification of Linearity of Installed Strain Gages

	R^2 of Linear Fit to Measured Strain Readings at Time of Maximum Temperature-Induced Curvature	
Test #	**Midspan**	**1/6-Span**
1	0.99	0.97
2	0.93	0.98
3	0.98	0.98

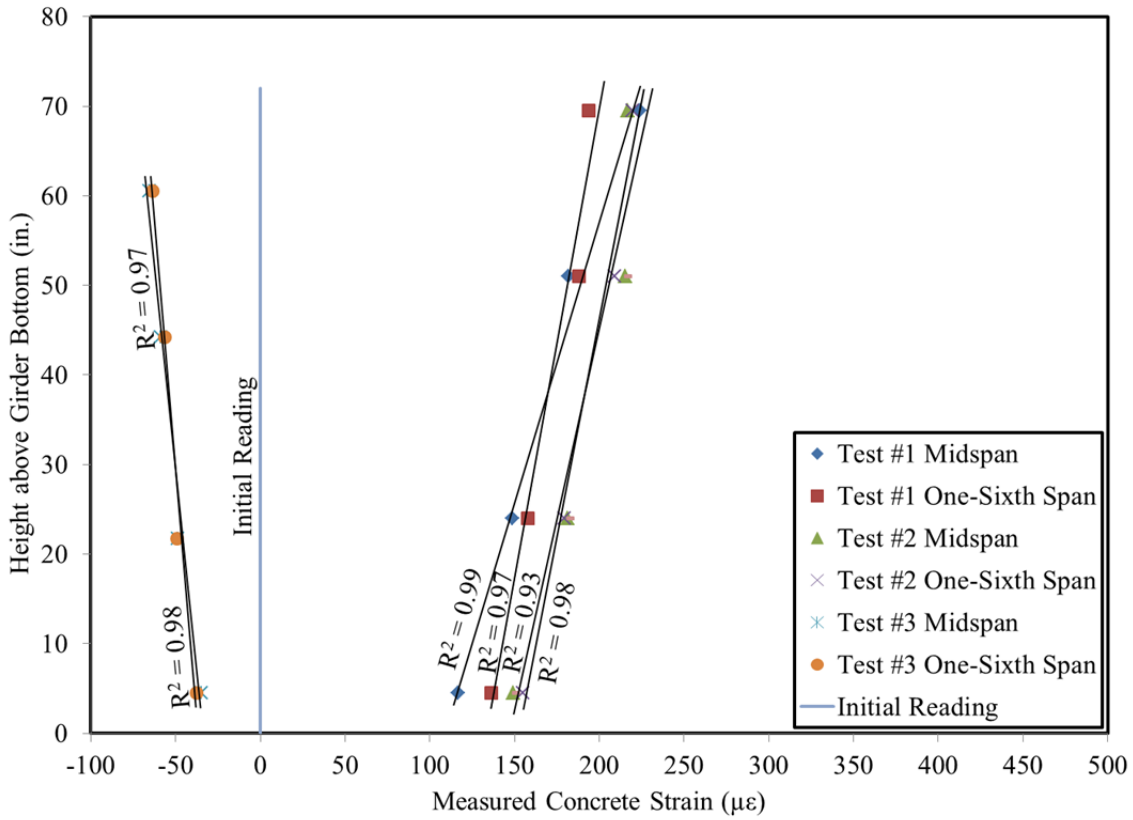

Figure 8-22: Verification of Linearity of Installed Strain Gages

As shown in Figure 8-22, the linear fit of Test #2 midspan data represents the poorest fit, with an R^2 value of 0.925. After a thorough review of site notes, photographs, and gage readings during concrete placement, it became apparent that the top midspan gage (eMTF) may have shifted during concrete placement as a result of the failure of reinforcement ties during girder fabrication. The observed failure, as illustrated in Figure 8-23, resulted from the following mechanism: (a) researchers instructed plant staff to avoid placing concrete directly on to gages to avoid damage, (b) plant staff accommodated the request, resulting in an area void of concrete within the two stirrup bays containing gages, (c) as concrete attempted to flow inward to fill the void during internal vibration, stirrup ties connecting the stirrup to the prestressing strands failed to resist the unbalanced lateral force applied by the concrete, resulting in (d) rotation of the

stirrup as shown. During placement, an attempt was made to reposition the stirrup after the unintentional relocation, although the top vibrating-wire strain gage may not have been returned to its intended location.

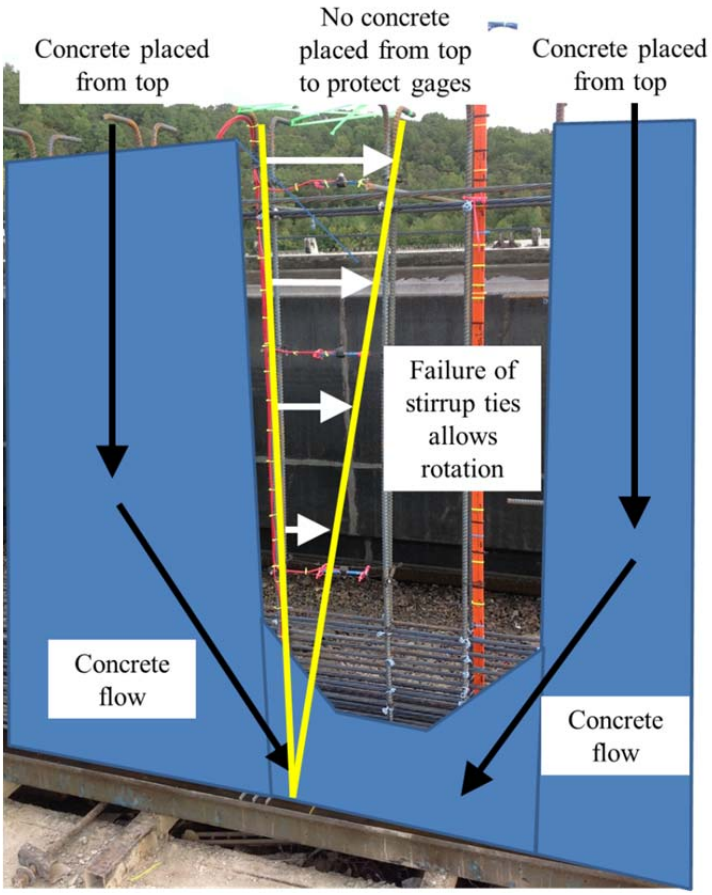

Figure 8-23: Observed Failure Mechanism of Midspan Gages

To avoid failures in future gage installations, the research team (1) separated the location of the vibrating-wire strain gage assembly from the location of the thermocouple assembly by at least 2–3 stirrup bays to allow concrete placement from above between the gage assemblies (thereby, reducing hydrostatic pressure differentials) and (2) inserted timber dunnage as shown in Figure 8-24 to shield installed gages from overhead concrete placement and prevent lateral translation of stirrups. Future researchers placing gages

within girders are advised to consider a similar system to reduce the incidence of damaged gages during concrete placement.

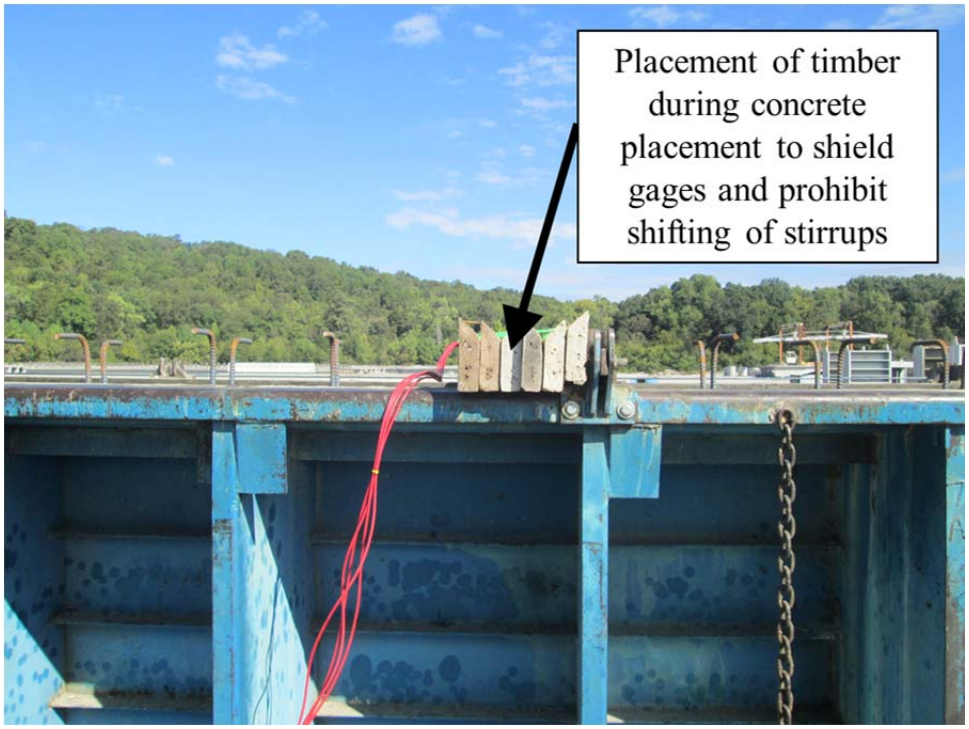

Figure 8-24: Placement of Timber to Avoid Gage Damage during Concrete Placement

Despite the coefficient of determination determined for the linear regression of Test #2 midspan strain measurements being somewhat less than for other similar tests and locations, preservation of the reading from the eMTF gage did cause a substantial change in the results of subsequent analyses performed in this chapter and, therefore, for completeness this reading is included in the remaining analyses of this chapter.

In order to confirm proper positioning and operation of installed thermocouple sensors, a more simple analysis method was used than that detailed above for strain measurements. By directly comparing readings of adjacent sensors, that is, sensors of different types positioned at similar locations, the validity of measured field temperature

data was evaluated. Comparisons of temperature measurements recorded by both thermocouples and thermistors are displayed in Figures 8-25 through 8-27.

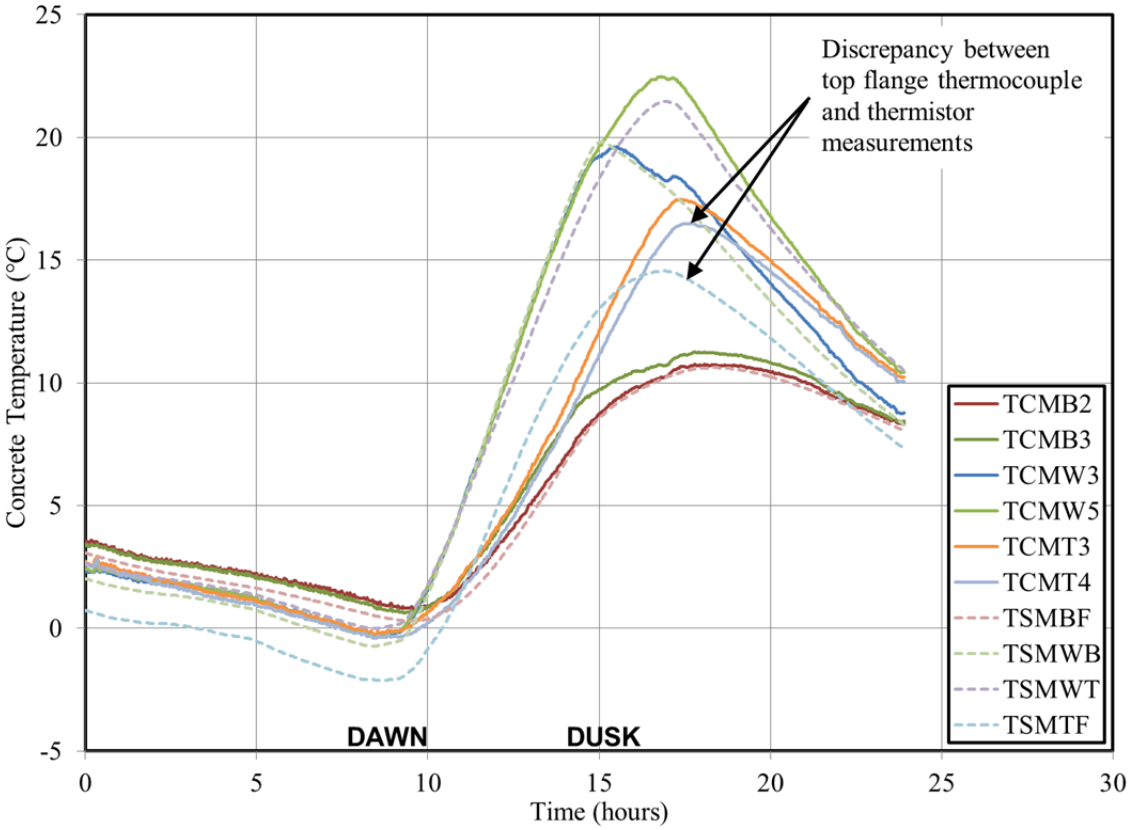

Figure 8-25: Test #1 Measured Temperatures

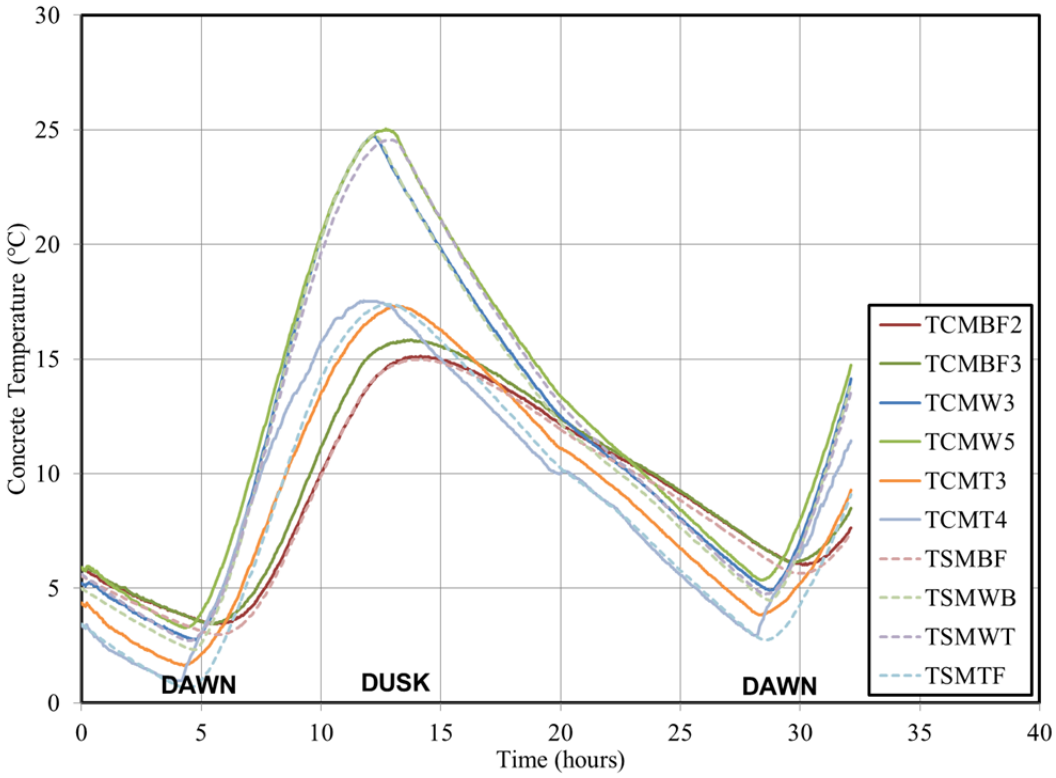

Figure 8-26: Test #2 Measured Temperatures

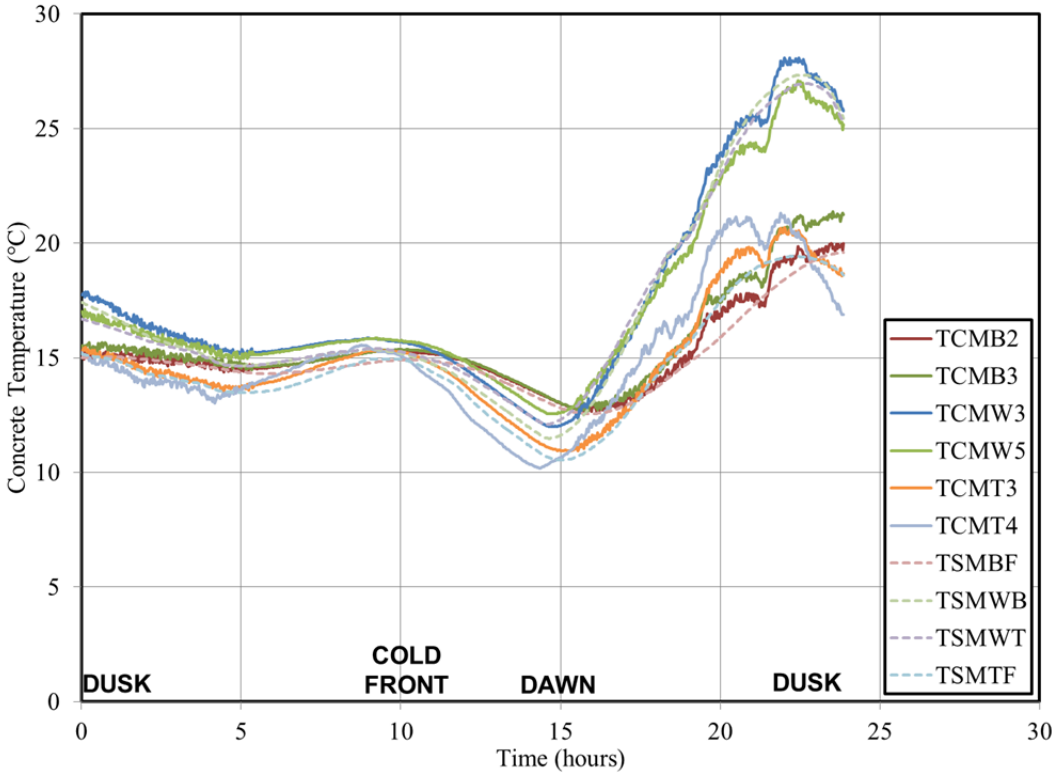

Figure 8-27: Test #3 Measured Temperatures

Readings of gage TSMBF are expected to fall between readings of gages TCMB2 and TCMB3, readings of gage TSMWB and TSMWT are expected be nearly identical to readings of TCMW3 and TCMW5, respectively, and readings of gage TSMTF are expected to fall between readings of TCMT3 and TCMT4. In general, agreement among measured temperature results was largely as expected, although there did exist a suspicious discrepancy among the top flange readings (TSMTF, TCMT3, and TCMT4) in Test #1. In addition, an analysis of the thermocouple sensor readings from Test #3 shows that at various times within the test, increased electrical noise was detected in the sensor signals. While this increased noise does not appear to compromise the results, this noise appears only during operation of the on-site computer and thus is likely a result of interference caused by either the AC adapter wiring of the laptop computer or the RS232 data transfer cable. For reference, a photograph of the test setup inside the mobile laboratory, with possible sources of electrical interference labelled, is shown in Figure 8-28. Future researchers conducting similar on-site testing are advised to not only confirm sensor readings are within expected ranges after experimental setup, but also to evaluate a series of continuous measurements to identify any electrical interference presence in sensor signals.

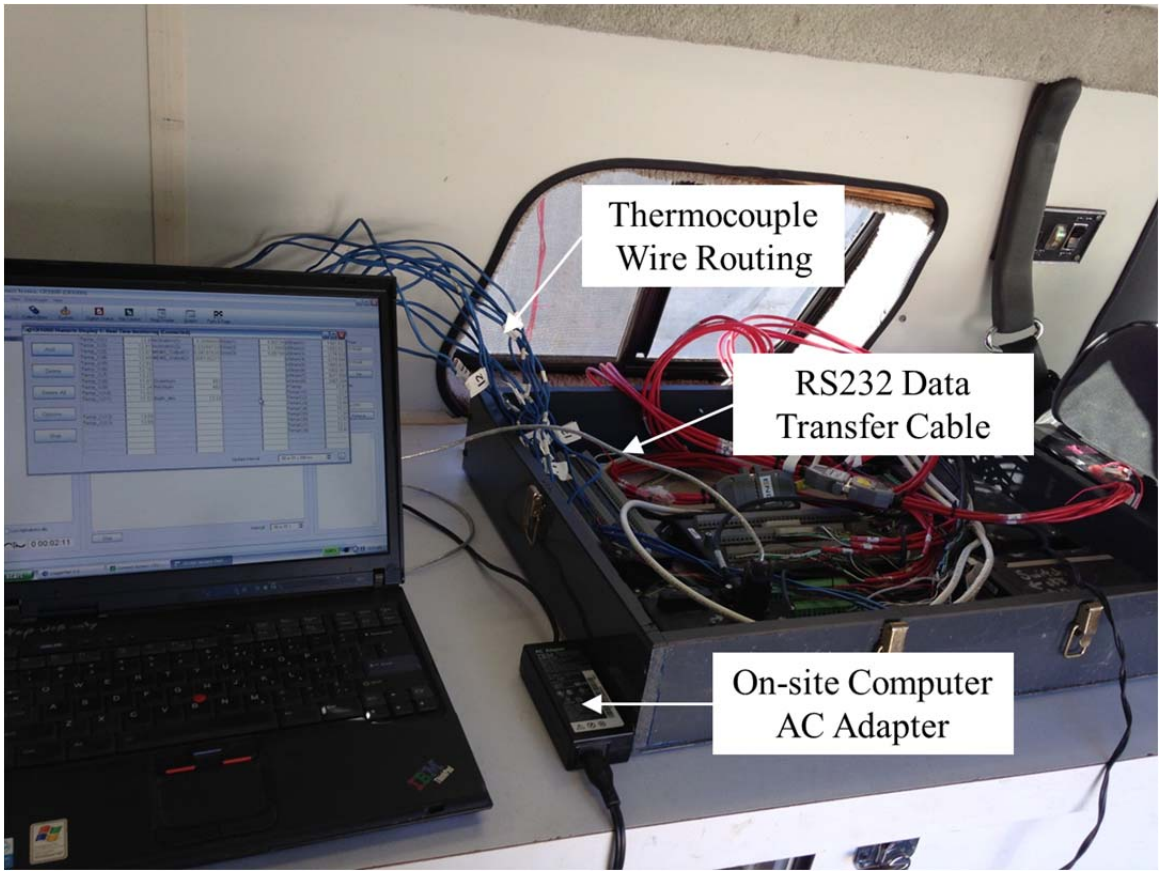

Figure 8-28: Data Acquisition Setup for Test #3

8.4.3 Discussion of Observed Vertical Temperature Profiles

The visualizations of the measured internal concrete temperature data contained in Figures 8-10, 8-14, and 8-18 are not ideal for identification of vertical temperature profiles within girders at various times throughout each test. For this purpose, the data of these figures are displayed in a somewhat more convenient form in this section. Then, a discussion summarizing the observed trends in experimental data is presented and comparisons are made to previous work by others.

For each test, three separate plots are presented, reflecting (1) midspan thermocouple gages, (2) midspan VWSG thermistor gages, and (3) 1/6-span VWSG thermistor gages. Results of Test #1 are shown in Figure 8-29 through 8-31. The vertical axis of each plot represents elevation within the girder cross section, while the horizontal

axis displays internal concrete temperature at a given location. For each hour of the test duration, the internal vertical temperature profile is displayed. Arrows and key hours of timing within the test are shown overlayed on each plot to help clarify the progression of vertical temperature profiles as a function of time. To progress chronologically through the data presented in Figure 8-29 through 8-31, readers should use the following steps: (a) begin at the time t=0 hours, proceeding left to t=8 hours by following solid lines, (b) proceed right following dashed lines until t=17 hours is reached, and finally, (c) proceed left following solid lines until test completion (t=24 hours). Similar plots detailing the recorded temperature readings of Tests #2 and 3 are shown in Figures 8-32 through 8-34 and Figures 8-35 through 8-37, respectively. Trends similar to those identified in Test #1 are seen for Test #2. The results of Test #3, as shown in Figures 8-35 through 8-37, are somewhat more difficult to interpret because four temperature reversals (as shown on superimposed arrows) occur during this test.

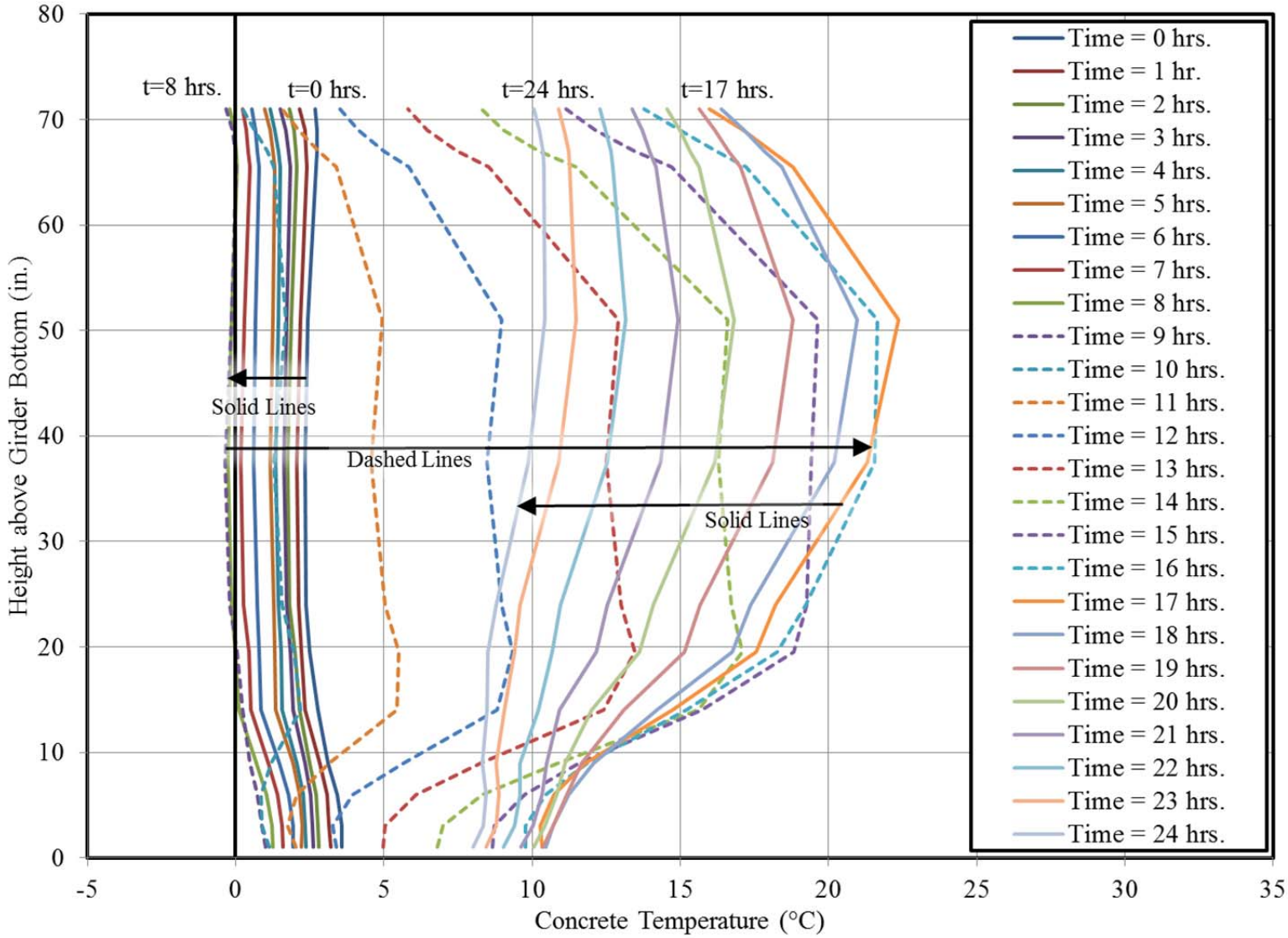

Figure 8-29: Midspan Thermocouple Results (TCM-Series) for Test #1

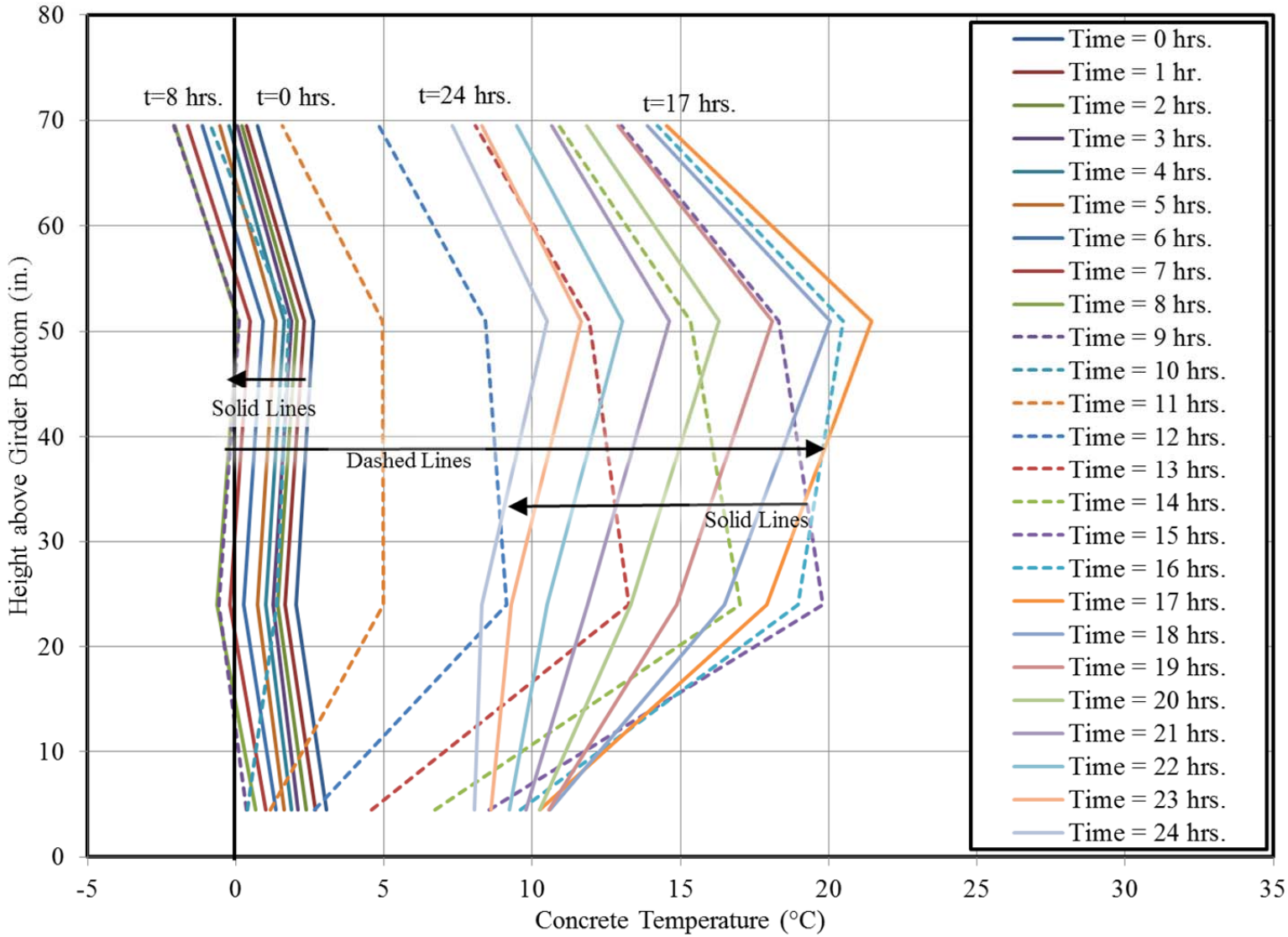

Figure 8-30: Midspan Thermistor (TSM-Series) Results for Test #1

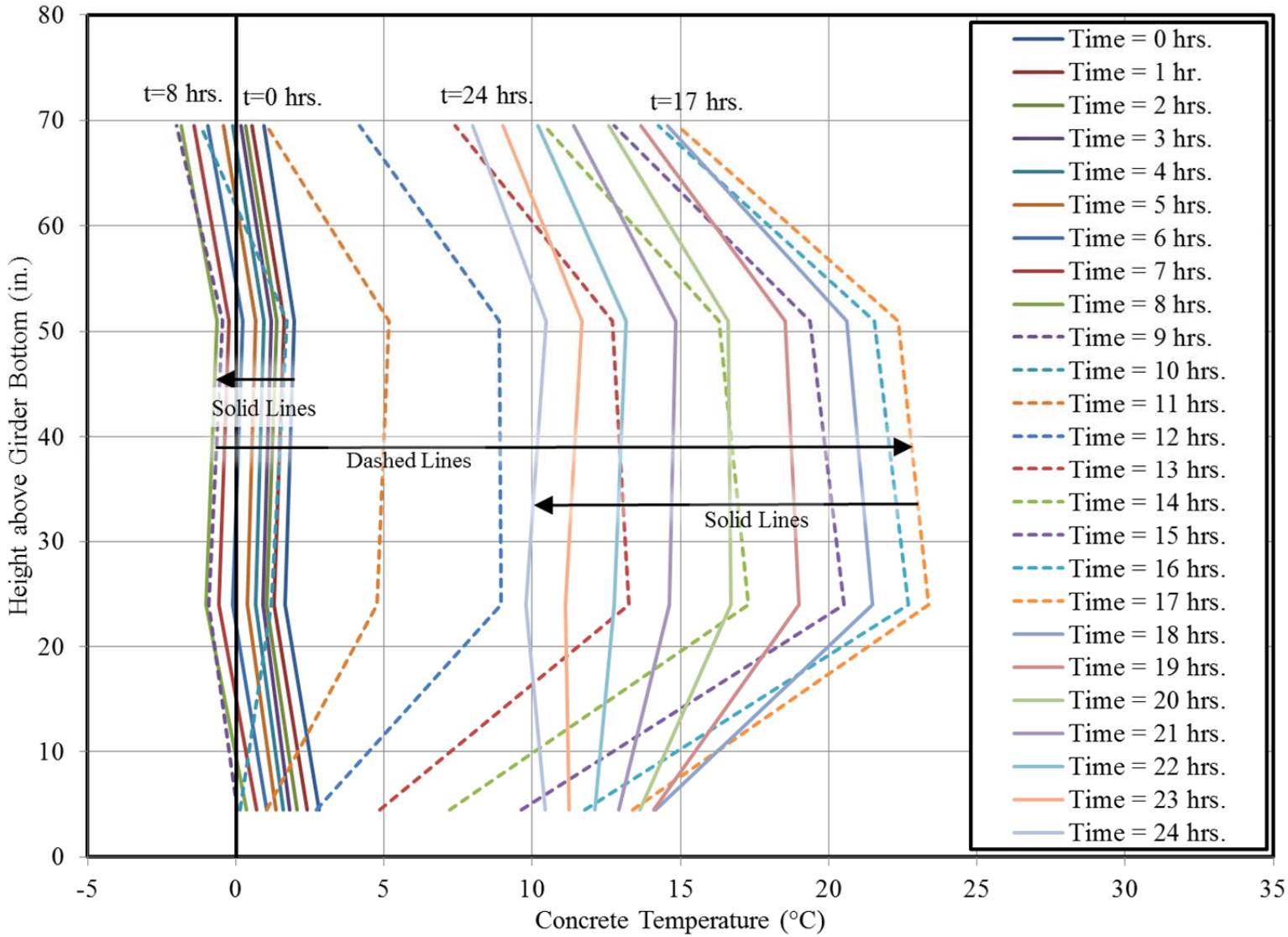

Figure 8-31: 1/6-Span Span Thermistor (TS6-Series) Results for Test #1

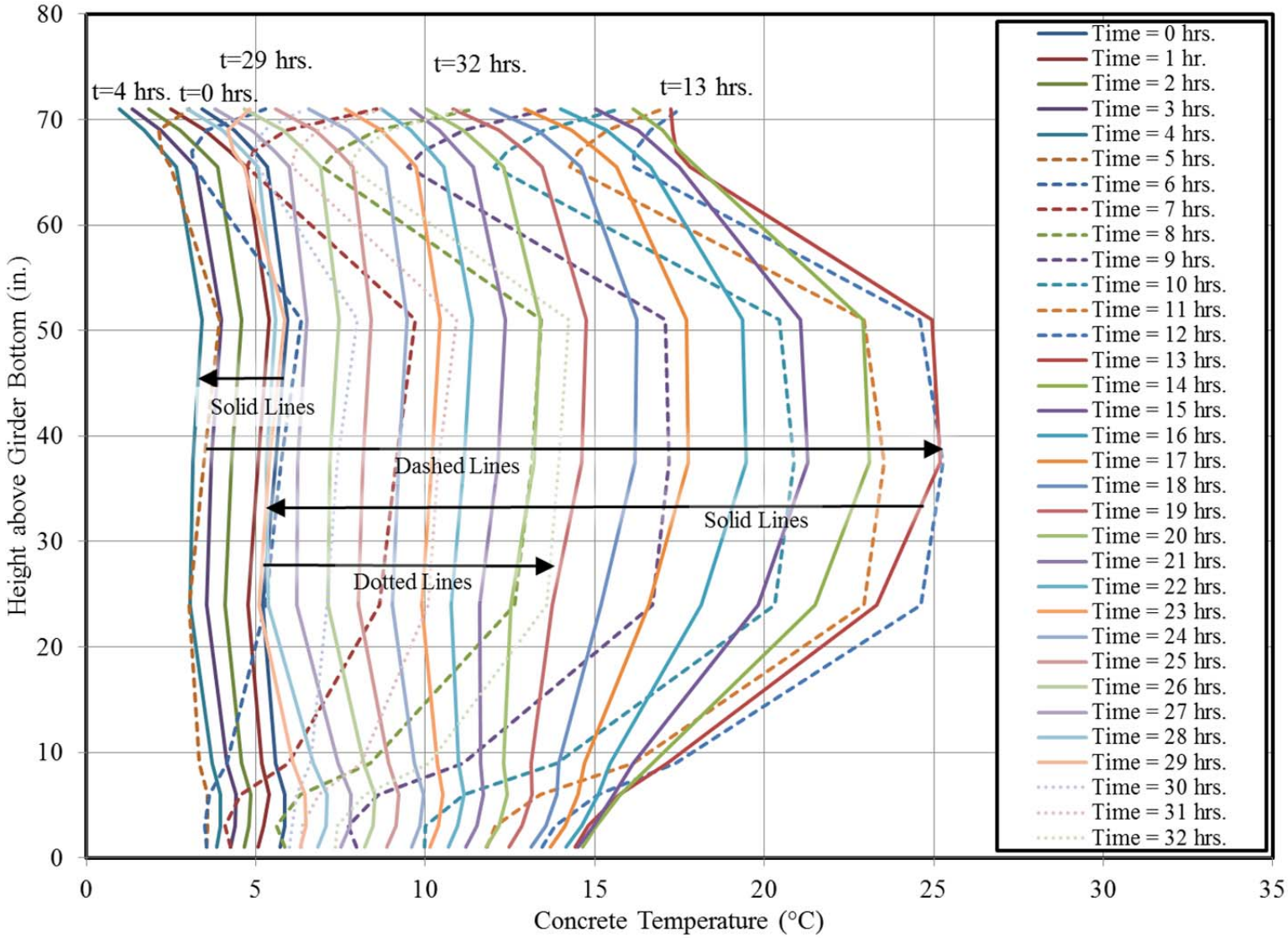

Figure 8-32: Midspan Thermocouple (TCM-Series) Results for Test #2

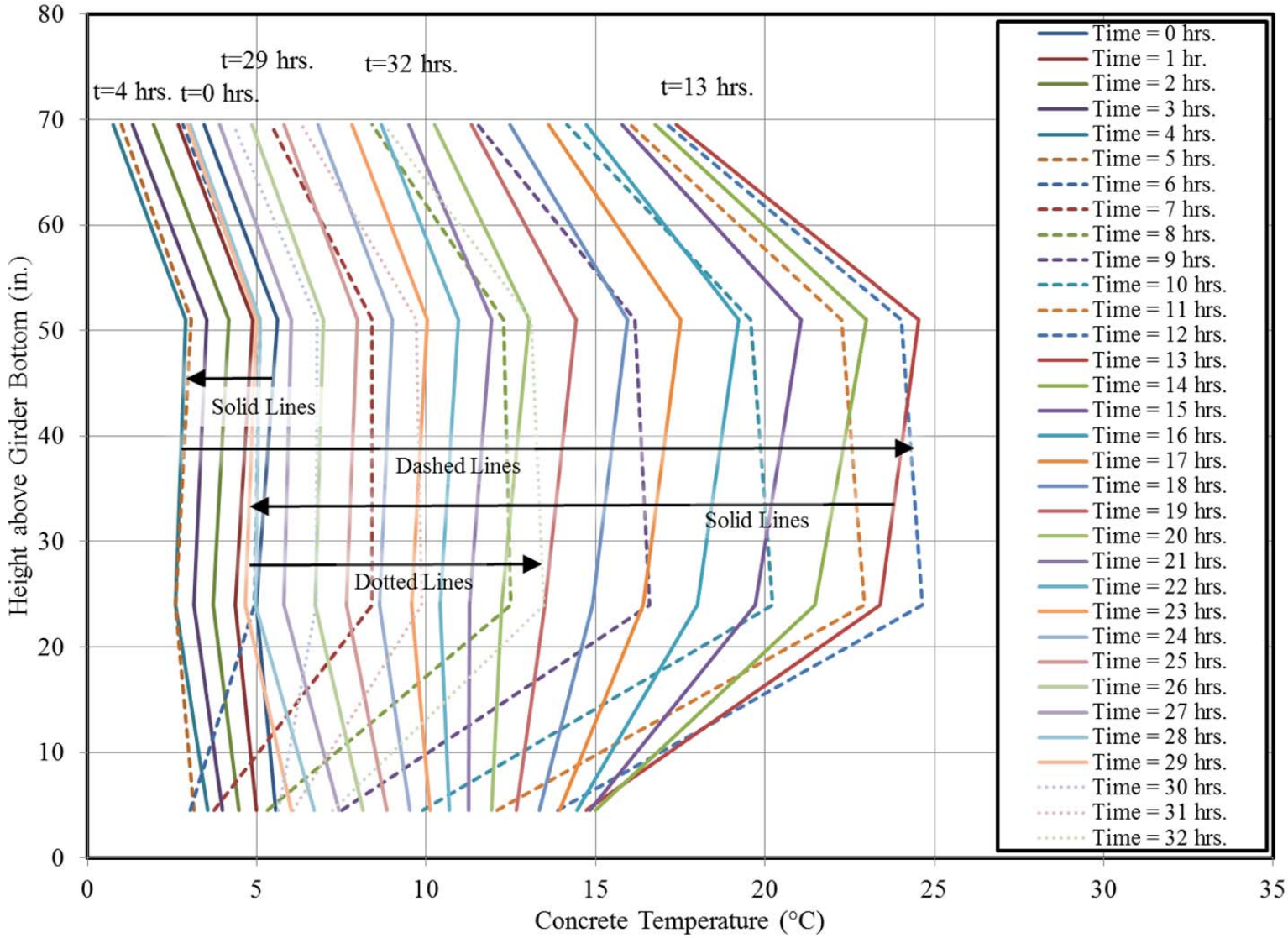

Figure 8-33: Midspan Thermistor (TSM-Series) Results for Test #2

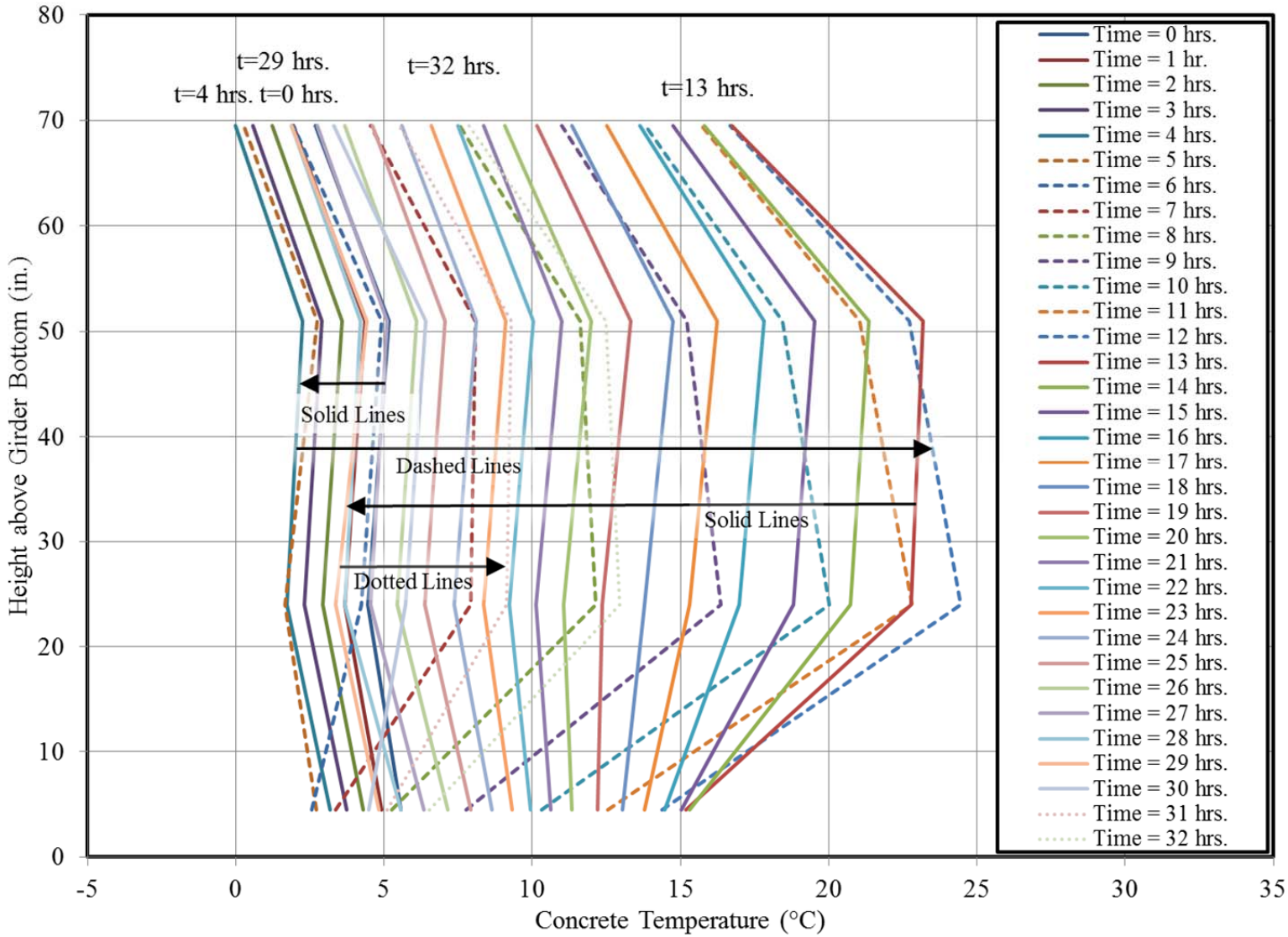

Figure 8-34: 1/6-Span Thermistor (TS6-Series) Results for Test #2

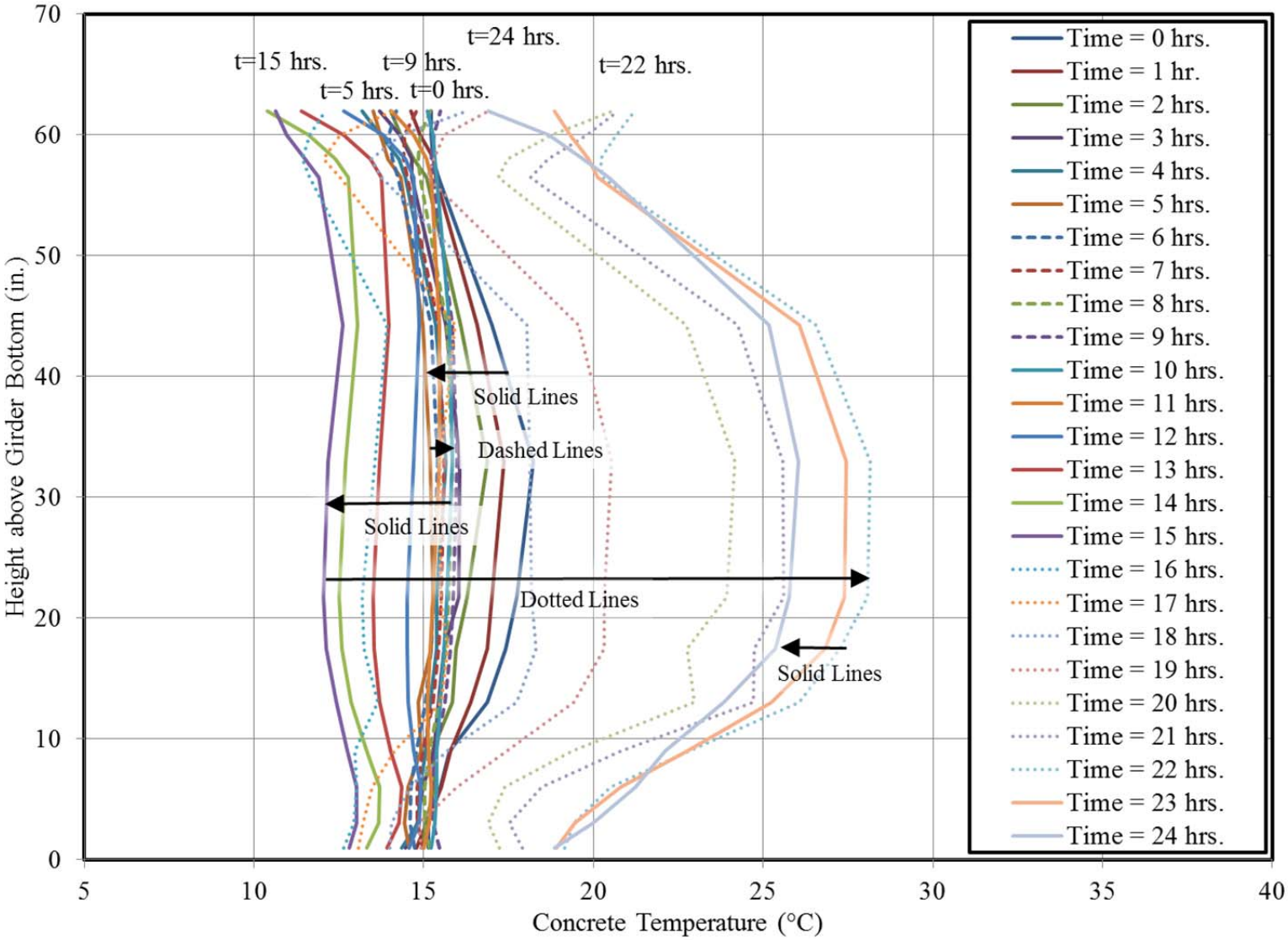

Figure 8-35: Midspan Thermocouple (TCM-Series) Results for Test #3

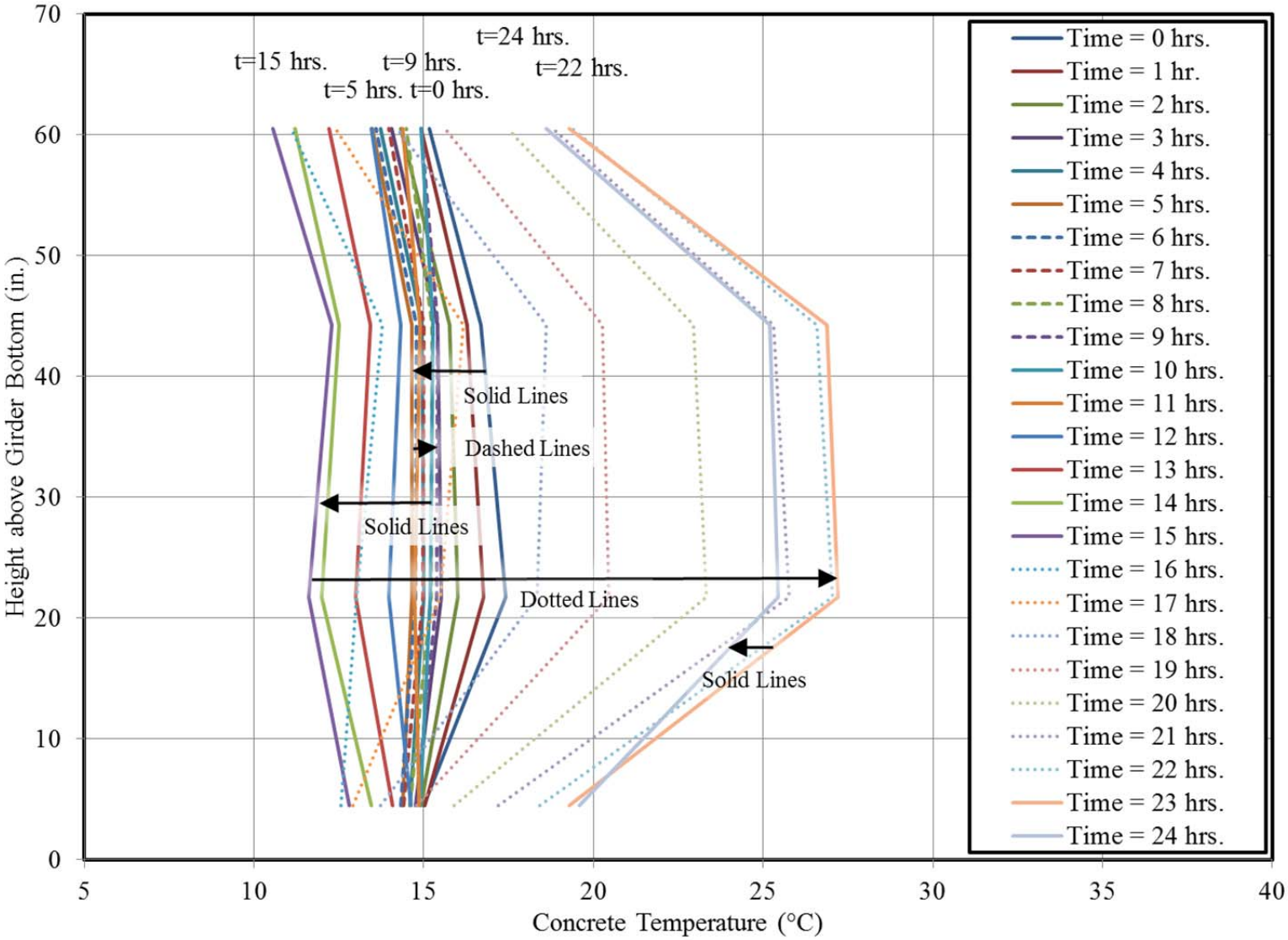

Figure 8-36: Midspan Thermistor (TSM-Series) Results for Test #3

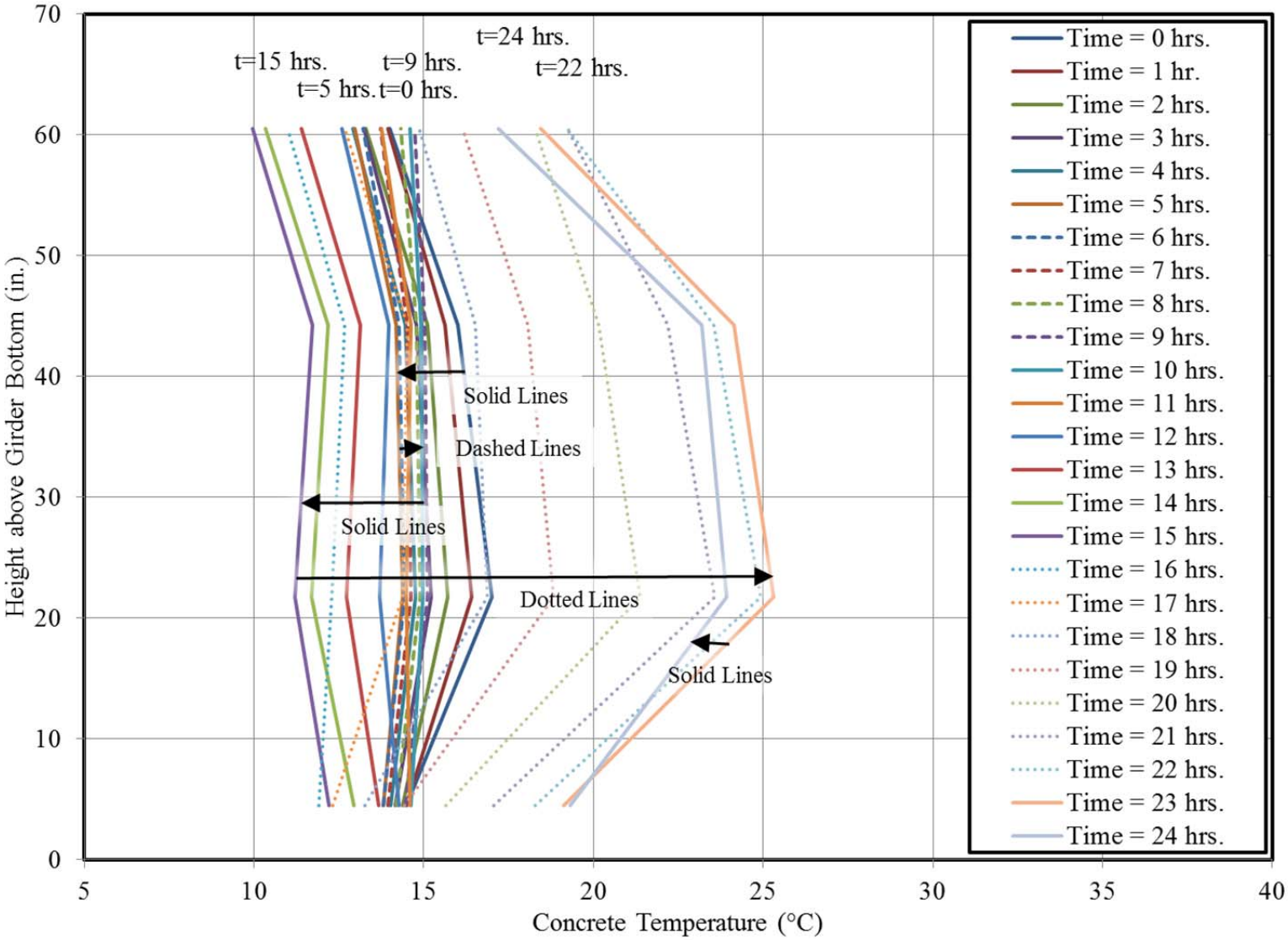

Figure 8-37: 1/6-Span Thermistor (TS6-Series) Results for Test #3

The following observations result from the inspection of Figures 8-29 through 8-37:

- The general shape of temperature profiles at all locations (midspan and 1/6-span) are similar, with extreme temperature changes being induced in the girder web for all tests;
- There is relatively close agreement between midspan gage groups (thermocouples and thermistors) for each of the three tests;
- The positioning of the thermistor gages at one-quarter points within the girder web appear to approximate the reversals of the temperature profile occurring within the girder web relatively well;
- The most detailed instrumentation (TCM-series) seem to better capture temperature trends at the extreme top and bottom depths within the girder when compared to the more limited in quantity midspan thermistor gages (TSM-series); and
- Recorded temperature profiles from midspan and 1/6-span are similar in both relative shape and magnitude.

Further discussion of recommended gage locations for future work is presented later in this chapter in the context of the effect of gage location on the accuracy of temperature-correction procedures.

While the relative magnitudes of the temperatures observed in this study are similar to previous work by others (Kelly et al. [1987] and Lee [2010]), the shapes of the extreme temperature profiles observed during the tests differ from those previously reported. The typical shape for measured vertical temperature profiles in noncomposite bulb-tee girders as reported by Lee (2010) is shown in Figure 8-38. Previous results of

Kelly et al. (1987) and Cook and Bloomquist (2005) also report similar temperature profile shapes for noncomposite girders in storage prior to erection. As shown, the top and bottom flanges typically reflect the highest recorded temperatures, with lesser or constant temperatures being reported throughout the girder web.

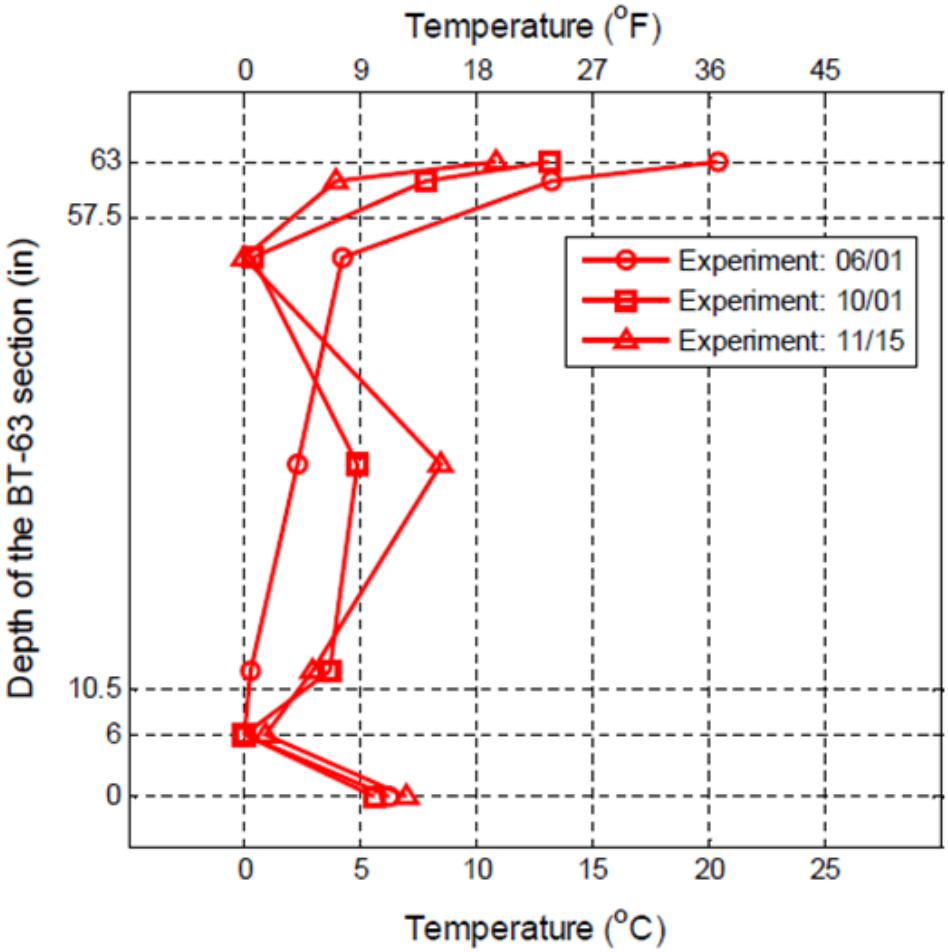

Figure 8-38: Measured Vertical Temperature Gradients in BT-63 Girder in Atlanta, Georgia (Lee 2010)

In the three tests conducted as part of the research effort of this dissertation, a substantially different shape of induced temperature profile was observed than that reported by previous researchers. In this study, peak temperatures were typically observed within the girder web, with lesser temperatures reported in the girder top and bottom flanges. This unexpected temperature profile shape likely results from (a) the

timing of the field-testing occurring during the colder winter months, (b) unseasonably cold ambient temperatures on testing days, (c) the reduced solar incident angle typical of winter months in the study region, (d) relatively unobstructed exposure of the girder webs to solar radiation (i.e. minimal shading by adjacent girders), and (e) orientation of the girders parallel to the direction of the sun's trajectory. It is likely that the lower incident angle of solar exposure caused disproportionate heating of the thinner girder web, while also minimizing solar exposure of the top and bottom flanges.

8.5 Analysis of Results

This section details the analyses conducted to (1) validate the use of the temperature-correction procedure, (2) solve for values of the effective concrete CTE for each field test, and (3) compare the effects of various simplifications on the accuracy of the temperature-correction algorithm.

8.5.1 Analytical Assumptions

The following assumptions are either explicitly or implicitly included in the analytical techniques used in this chapter:

- Where cross-sectional curvatures are computed from measured strain data, a linear regression of four strain gage readings is performed using the least-squares method of analysis;
- It is assumed that the effects of transverse temperature profiles can be decoupled from the effects of vertical temperature profiles, as verified analytically by Lee (2010);
- It is assumed that all cross sections along the girder length experience the same diurnal induced temperature profiles at a specific time; and

- In relating induced cross-sectional changes in curvature to global girder deformations, simple supports are assumed and elastic beam theory is relied on.

8.5.2 Analytical Iterations

Various analytical iterations are employed in this study and referenced throughout the remainder of this chapter. These iterations represent unique analysis procedures that rely on (a) differing analytical assumptions regarding cross-sectional girder shape and temperature profile shape, or (b) differing inputs of measured temperatures and measured concrete strains. These iterations are labelled in accordance with the convention shown in Figure 8-39, with a complete tabulated list of all considered iterations included in Table 8-4.

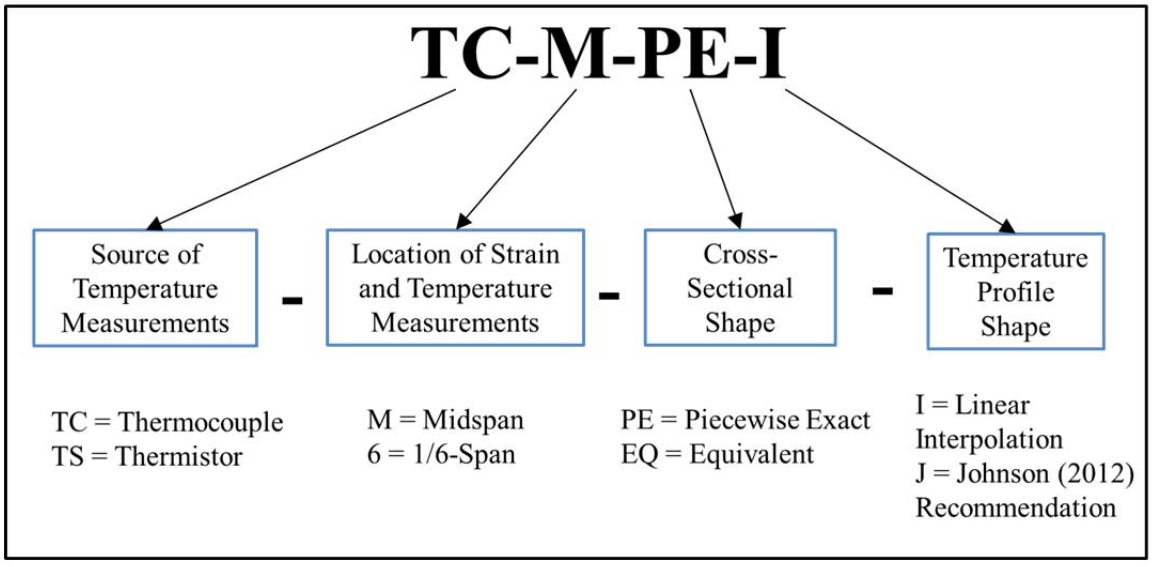

Figure 8-39: Analysis Procedure Labelling Convention

Table 8-4: Analytical Procedure Iterations

Iteration ID	Source of Temperature Measurements	Location of Strain and Temperature Measurements	Cross-Sectional Shape	Temperature Profile Shape
TC-M-PE-I	Thermocouples (TCM-Series)	Midspan	Piecewise Exact	Linear Interpolation
TS-M-PE-I	Thermistors (TSM-Series)	Midspan	Piecewise Exact	Linear Interpolation
TS-6-PE-I	Thermistors (TS6-Series)	1/6-Span	Piecewise Exact	Linear Interpolation
TS-M-EQ-I	Thermistors (TSM-Series)	Midspan	Equivalent Cross Section by Johnson (2012)	Linear Interpolation
TS-M-EQ-J	Thermistors (TSM-Series)	Midspan	Equivalent Cross Section by Johnson (2012)	Simplified Profile by Johnson (2012)

For each analytical iteration, the girder cross-sectional geometry is defined using one of two techniques:

- *Piecewise Exact* (PE): The exact specified geometry of the girder cross section is utilized, programmed as a piecewise exact width function; or
- *Equivalent Cross Section* (EQ): The simplified cross section comprising three rectangles as previously proposed by Johnson (2012) is utilized.

Similarly, the temperature profile shape is generated from recorded temperature data in one of the following two ways:

- *Linear Interpolation* (I): Adjacent measured temperatures at different depths are interpolated between, with results extrapolated linearly to the girder extreme surfaces (i.e. top or bottom) as shown in Figure 8-2; or

- *Simplified Profile* (J): The simplified profile[3] proposed by Johnson (2012), later used by Keske (2014), is utilized—resulting in uniform temperatures through each of the flanges and a single linear trend through the girder web as shown in Figure 8-1;

Iteration TC-M-PE-I represents the most detailed analysis performed in this investigation, relying on (a) between 11–13 thermocouple measurements from the midspan section, (b) four strain measurements from the midspan section, (c) a piecewise exact formulation of the girder cross section, and (d) linear interpolation to define the temperature profile shape. Iterations TS-M-PE-I and TS-6-PE-I represent the next most rigorous analytical iterations. Iteration TS-M-PE-I is identical to the most detailed iteration (TC-M-PE-I) with the exception that it relies on four thermistor measurements to define the temperature profile shape and magnitude instead of the more extensive thermocouple measurements. Iteration TS-6-PE-I is similar, except it relies on measurements of strain and temperature from the 1/6-span cross section. The TS-M-EQ-I iteration incorporates the simplification of girder cross section proposed by Johnson (2012), but is otherwise identical to iteration TS-M-PE-I. Finally, in an effort to replicate the temperature-correction procedure used by Johnson (2012), iteration TS-M-EQ-J incorporates both the effect of the simplified cross section and the effect of the assumed temperature profile assumed by Johnson.

[3] The fitted temperature profile as used by Johnson (2012) and Keske (2014) relied on a bottom flange temperature reading taken at the centroid of the prestressing strand, whereas the bottom flange temperature measurement recorded in this study was located at the approximate centroid of the girder bottom flange.

8.5.3 Effective Coefficient of Thermal Expansion (CTE) Determination

To begin the analyses of this chapter, it was necessary to select one of the analysis iterations introduced in Section 8.5.2 for use in solving for an effective or apparent CTE observed during each field test. This apparent CTE represents the coefficient of thermal expansion that minimizes the error between the theoretical predicted response (caused by a measured temperature profile) and the observed girder response throughout each test. Iteration TC-M-PE-I was selected for this purpose because it represents the most detailed analytical method included in this study and utilizes data from the most detailed instrumentation included in this study. The procedure summarized in Figure 8-40, in conjunction with a GRG nonlinear solver, was used to systematically compute the effective CTE for each field test by minimizing the standard error of the estimate.

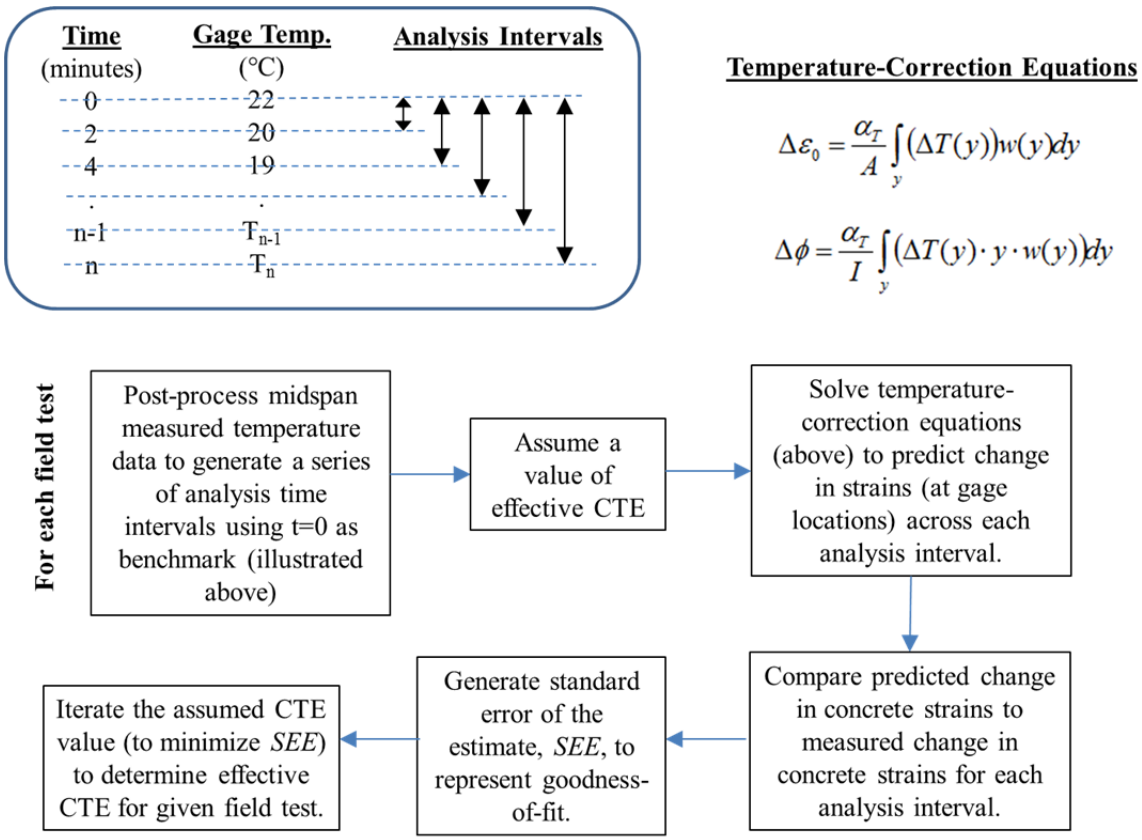

Figure 8-40: Analysis Procedure to Determine Effective CTE for each Field Test (using Iteration TC-M-PE-I)

Effective values for the concrete coefficient of thermal expansion, as determined by the procedure outlined above for the TC-M-PE-I analysis iteration, are tabulated in Table 8-5, along with corresponding values for the standard error of the estimate (*SEE*) for each strain gage.

Table 8-5: Effective CTE by Field Test (TC-M-PE-I)

Gage ID	Gage Location	Standard Error of the Estimate, *SEE*			
		Test #1	Test #2	Test #3	Units
eMTF	Top Flange	26.4	6.8	4.3	με
eMWT	Web Top	16.0	11.3	6.5	με
eMWB	Web Bottom	11.6	12.1	6.6	με
eMBF	Bottom Flange	4.9	10.6	6.8	με
Effective CTE (Determined by minimizing *SEE*)		**12.3**	**13.5**	**13.2**	($\mu\varepsilon/°C$)

While Schinder et al. (2010) recommend an average CTE value of 9.94 με/°C as a result of laboratory testing of regional dolomitic limestone concretes, the *effective* CTE values

reported in Table 8-5 (12.3–13.5 με/°C) exceed this recommendation by up to 36 percent. Reasons for the disparity between laboratory-measured CTE values and the *effective* CTE values determined from field testing may include (a) the effect of varying moisture contents at the time and cross-sectional location of consideration, (b) inaccuracies related to assumptions of cross-sectional and longitudinal temperature profiles or other analytical procedures, or (c) other sources of variation inherent to full-scale field testing of concrete girders. For a more complete discussion of potential causes of variation in CTE values, readers are directed to the work of Keske (2014). Comparisons between predicted and measured concrete strains for each gage location are shown in Figures 8-41 through 8-43 for each field test.

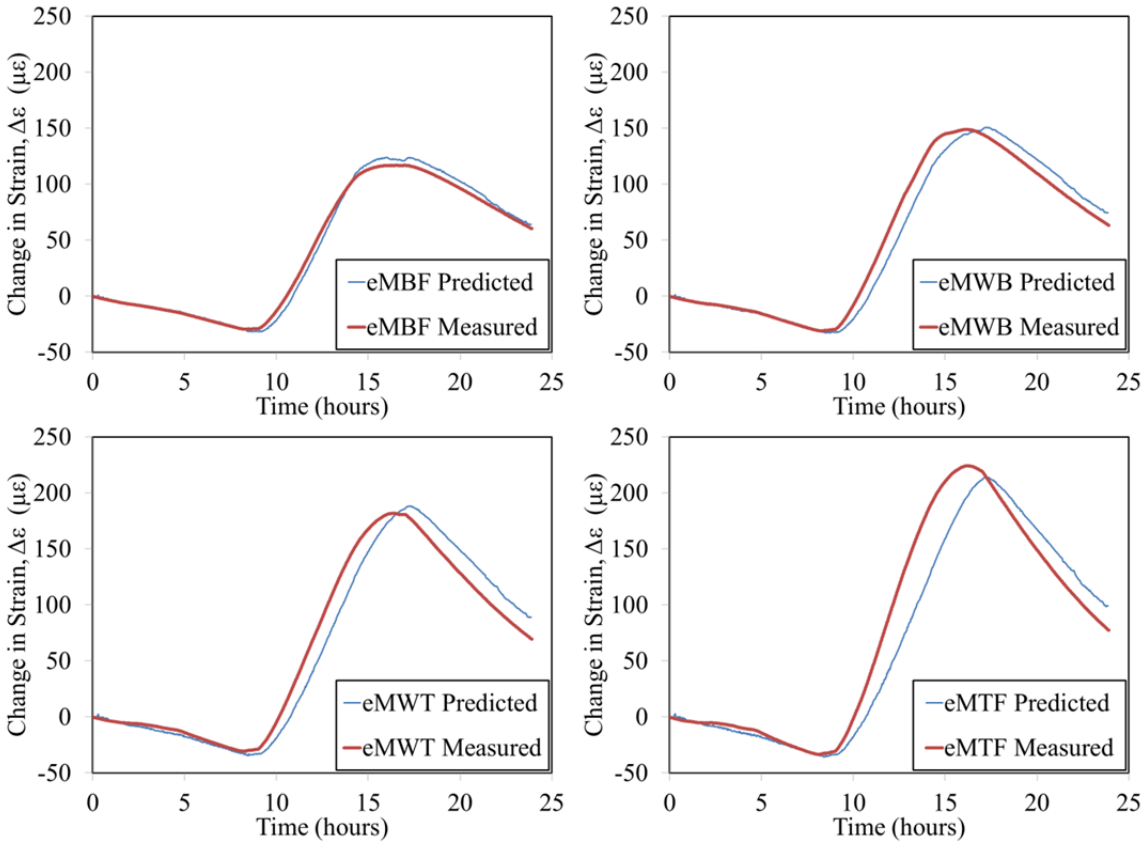

Figure 8-41: Predicted vs. Measured Strains for Test #1 (α_T=12.3)

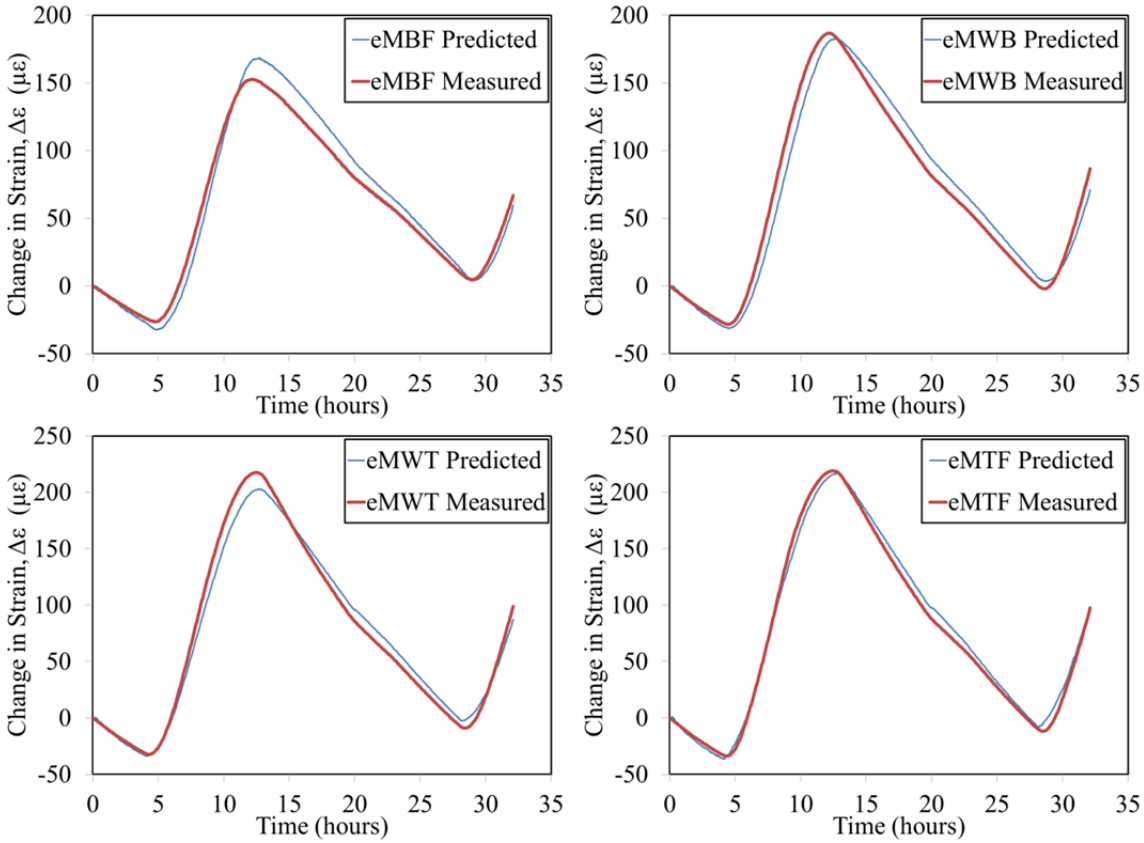

Figure 8-42: Predicted vs. Measured Strains for Test #2 (α_T=13.5)

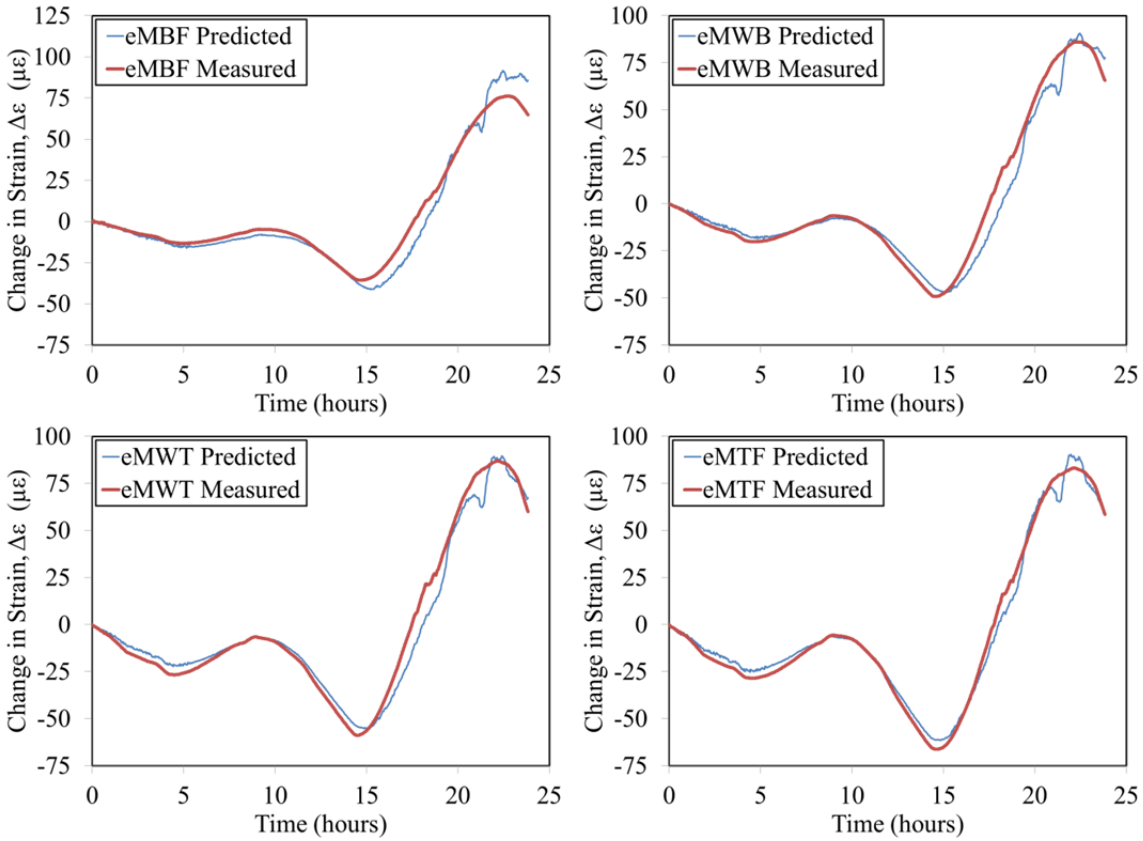

Figure 8-43: Predicted vs. Measured Strains for Test #3 (α_T=13.2)

As shown and indicated by the magnitude of the *SEE* in Table 8-5, the predicted and measured concrete strains show best agreement for Test #3 with a maximum *SEE* of 6.8 microstrain. Test #2 and #3 show the next best agreement between predicted and measured strains with maximum *SEE* of 12.1 microstrain and 26.4 microstrain, respectively. Although certain trends in curvature may be noted by inspection of concrete strain comparisons (i.e. strain comparisons becoming successively less accurate for gage readings towards the extreme top or bottom of section), inspection of concrete strains in this manner does not allow for direct comparisons of curvature—which is the parameter most closely tied to changes in girder camber. For this purpose, Figure 8-44 shows predicted and measured girder curvatures for each field test.

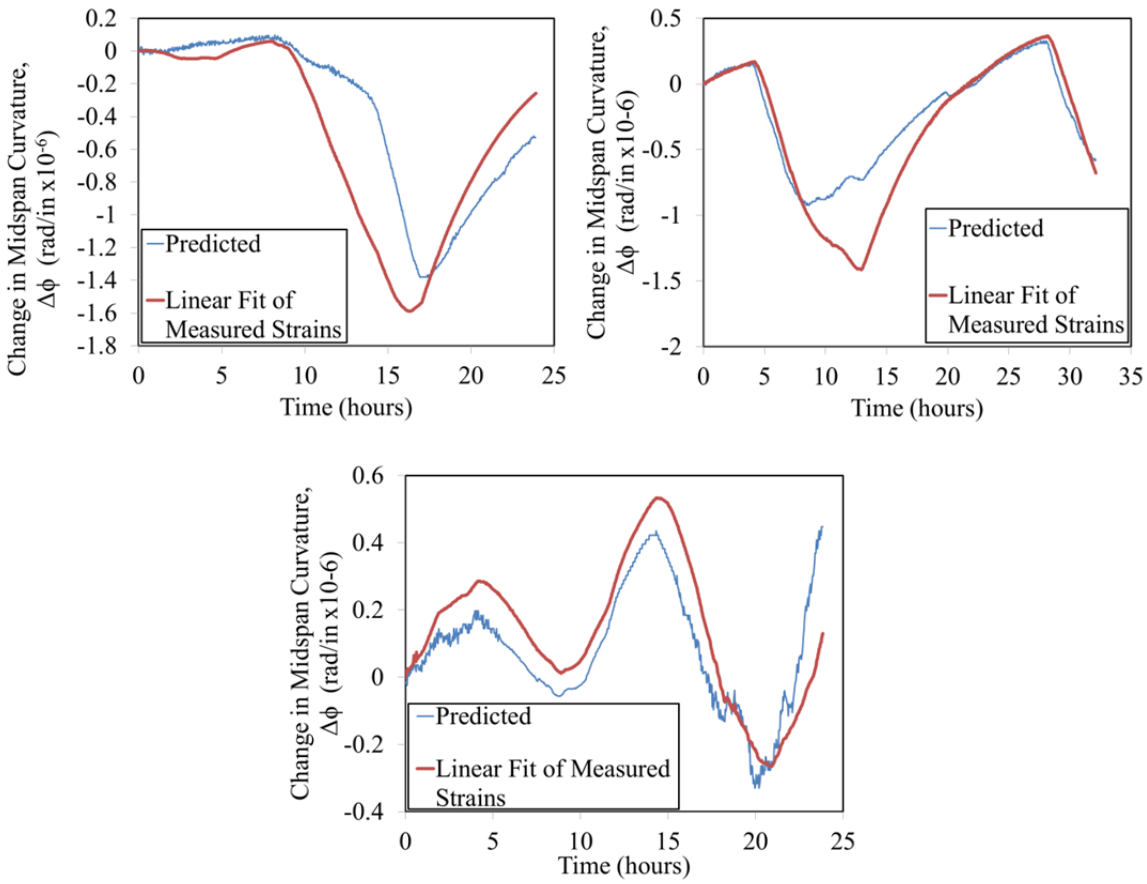

Figure 8-44: Predicted vs. Measured Midspan Curvatures for Test #1 (upper left), Test #2 (upper right), and Test #3 (bottom).

As shown, predicted curvatures for Tests #1–2 show some variations in shape from the measured responses, while predicted curvatures for Test #3 show good agreement with measured response. The discrepancy in curvature shape observed in Test #1 beginning approximately 10 hours into the test was apparently caused by the discrepancy between top flange temperature readings previously noted in Section 8.4.2. This topic is discussed further in Section 8.5.4.

In addition to the cross-sectional comparisons of girder strains and curvatures discussed above, corresponding global girder responses (e.g. vertical deflection at three girder cross sections) were computed using the tabulated expressions of Table 8-6 for comparison to measured girder vertical deflections.

Table 8-6: Engineering Beam Theory Relationships to Relate Cross-Sectional Curvature to Global Behavior

Test No.	Expression used to relate typical change in cross-sectional curvature to:		
	Midspan deflection	1/6-span deflection	One-third span deflection
1-2	$\Delta\phi\left(\frac{l^2}{8}\right)$	$\Delta\phi\left(\frac{5l^2}{72}\right)$	-
3	$\Delta\phi\left(\frac{l^2}{8}\right)$	-	$\Delta\phi\left(\frac{l^2}{9}\right)$

Note: 1. The length used for computation of global deflections is the actual span length.

Comparisons of predicted and measured girder deflections at girder midspan and 1/6-span for each of the three field tests are shown in Figures 8-45 through 8-47.

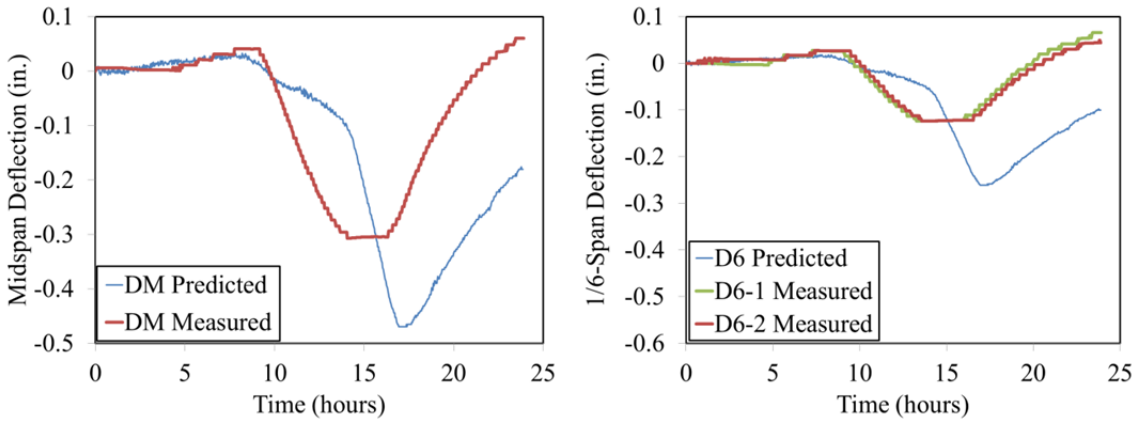

Figure 8-45: Predicted vs. Measured Deflections for Test #1 (α_T=12.3)

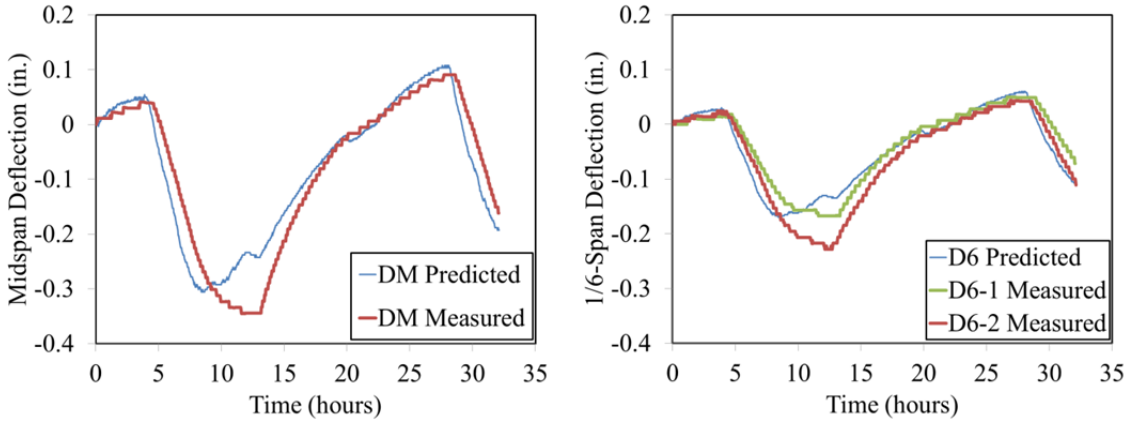

Figure 8-46: Predicted vs. Measured Deflections for Test #2 (α_T=13.5)

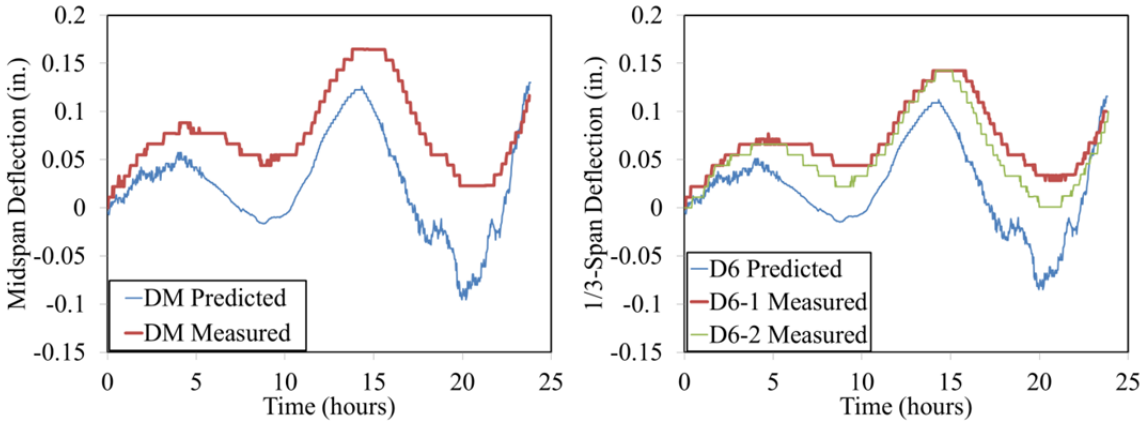

Figure 8-47: Predicted vs. Measured Deflections for Test #2 (α_T=13.2)

Relatively good agreement between predicted and measured vertical deflections is observed for Tests 2–3, although the previously-noted discrepancy in predicted curvature appears to negatively influence the accuracy of predictions for Test #1. The standard errors of the estimate, *SEE*, for each vertical deflection gage location are shown in Table 8-7.

Table 8-7: Standard Error of the Estimate for Global Deflections (TC-M-PE-I)

Gage ID	Gage Location	Standard Error of the Estimate, *SEE*			
		Test #1	Test #2	Test #3	Units
DM	Midspan	0.16	0.05	0.06	in.
D6-1	1/6-Span	0.10	0.03	0.06	in.
D6-2	1/6-Span	0.10	0.03	0.04	in.

As indicated by the small values of the standard errors for Tests #2–3 (between 0.04 and 0.06 in.), these tests represent the best fits between predicted and measured vertical deflections. The vertical deflections predictions for Test #1 are substantially less accurate than for the other two tests, with standard errors approaching triple those of the Tests #2–3.

The following observations regarding the implementation of the temperature-correction algorithm for the most detailed analysis iteration (TC-M-PE-I) are offered:

- The relative agreement between predicted and observed temperature-induced deformation in the precast, prestressed concrete girders included in this study provides support for the soundness and accuracy of the temperature-correction algorithm derived and implemented in this study;
- Best agreement between predicted and measured temperature-induced deformational responses were observed for Tests #2 and 3, with the predictions of Test #1 being less accurate and exhibiting an apparent discrepancy between predicted and measured curvature (and vertical deflection) shape;
- For the most accurate tests included in this study (Tests #2–3), effective CTE values of 13.5 and 13.2 με/°C were found to minimize the error between predicted and measured internal concrete strains;
- For Test #1, an effective CTE of 12.3 provided best agreement between predicted and measured internal concrete strains; and
- A previously noted discrepancy in top flange temperature readings for Test #1 may be to blame for the reduced accuracy of the predictions of temperature-induced deformational responses for this test. This hypothesis is explored further in Section 8.5.4, where comparisons are made to analytical iterations using alternate sources of measured temperatures.

The effective CTE values determined in this section are similar to—but slightly higher than—those values computed previously by the joint work of Keske (2014) and Neal (2015).

8.5.4 Effect of Varying Analytical Methods on Accuracy of Temperature-Correction Algorithm

A key task of this chapter was to evaluate the effect of various analytical simplifications and differing field-measured inputs on the accuracy of the temperature-correction effort implemented in this dissertation. To this end, the various analytical iterations previously described in Section 8.5.2 (reproduced below) were implemented and standard errors of the estimate were computed for each field test and gage location to represent the goodness-of-fit to measured results. In the implementation of each of these iterations, the previously determined effective CTE for each field test was utilized.

Table 8-4: Analytical Procedure Iterations

Iteration ID	Source of Temperature Measurements	Location of Strain and Temperature Measurements	Cross-Sectional Shape	Temperature Profile Shape
TC-M-PE-I	Thermocouples (TCM-Series)	Midspan	Piecewise Exact	Linear Interpolation
TS-M-PE-I	Thermistors (TSM-Series)	Midspan	Piecewise Exact	Linear Interpolation
TS-6-PE-I	Thermistors (TS6-Series)	1/6-Span	Piecewise Exact	Linear Interpolation
TS-M-EQ-I	Thermistors (TSM-Series)	Midspan	Equivalent Cross Section by Johnson (2012)	Linear Interpolation
TS-M-EQ-J	Thermistors (TSM-Series)	Midspan	Equivalent Cross Section by Johnson (2012)	Simplified Profile by Johnson (2012)

Comparisons between predicted and measured bottom flange strains, top flange strains, and midspan vertical deflection are shown in Figures 8-48 through 8-56 for each iteration and test, with a summary of the standard errors of the estimate for each case tabulated in Table 8-8.

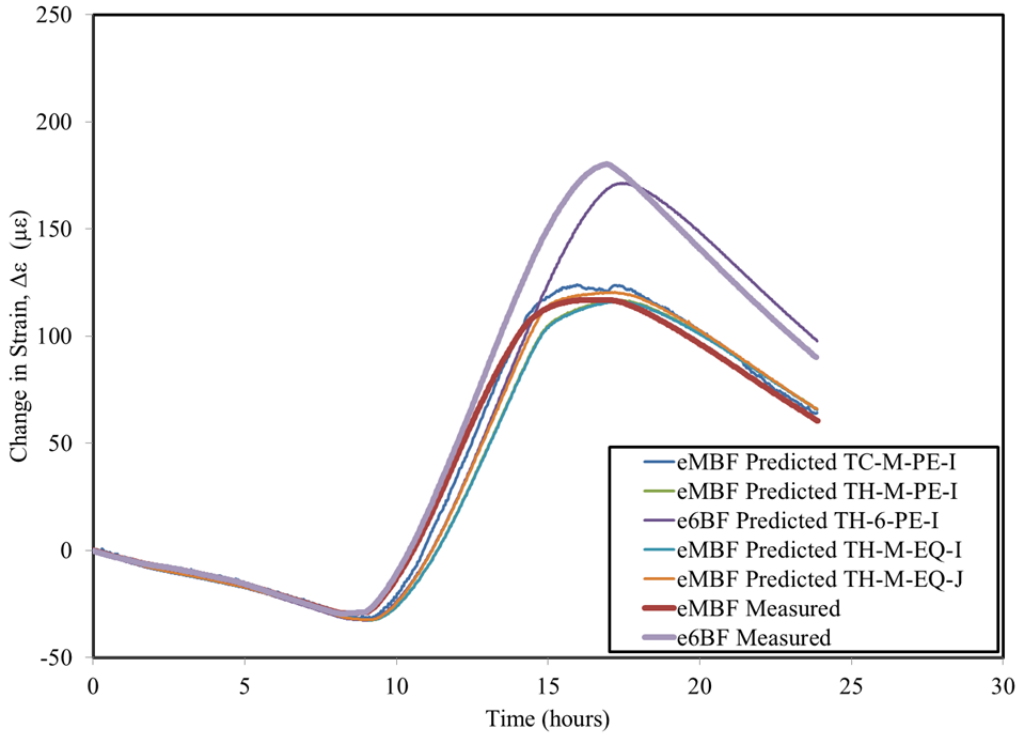

Figure 8-48: Predicted and Measured Bottom Flange Strains for Test #1 by Analysis Procedure (α_T=12.3)

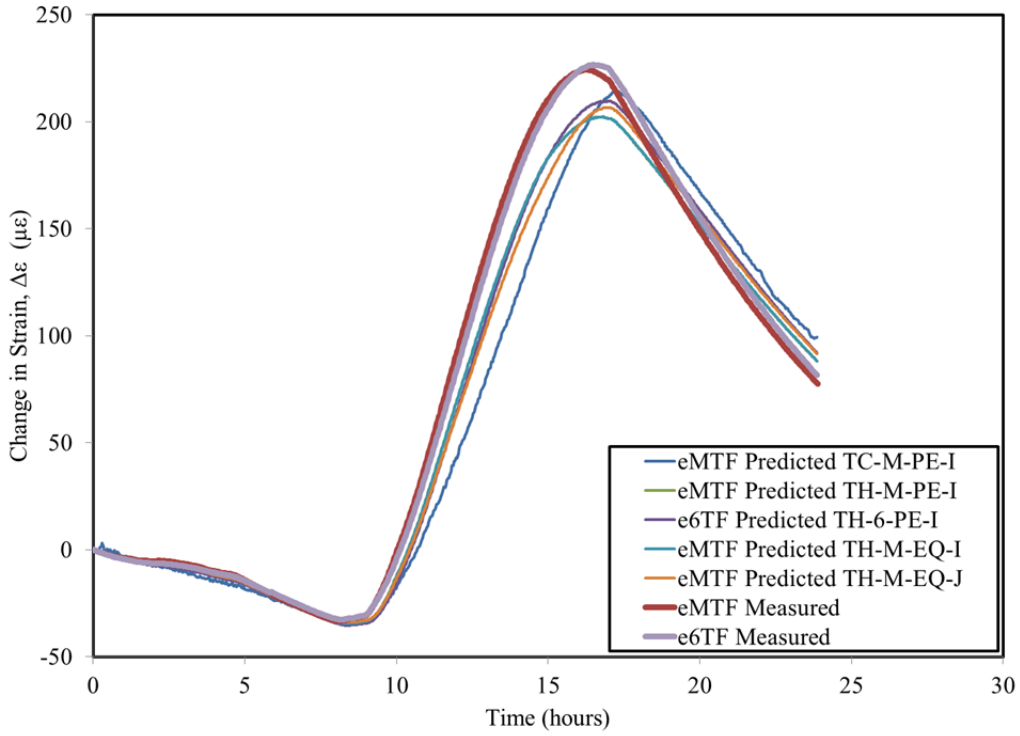

Figure 8-49: Predicted and Measured Top Flange Strains for Test #1 by Analysis Procedure (α_T=12.3)

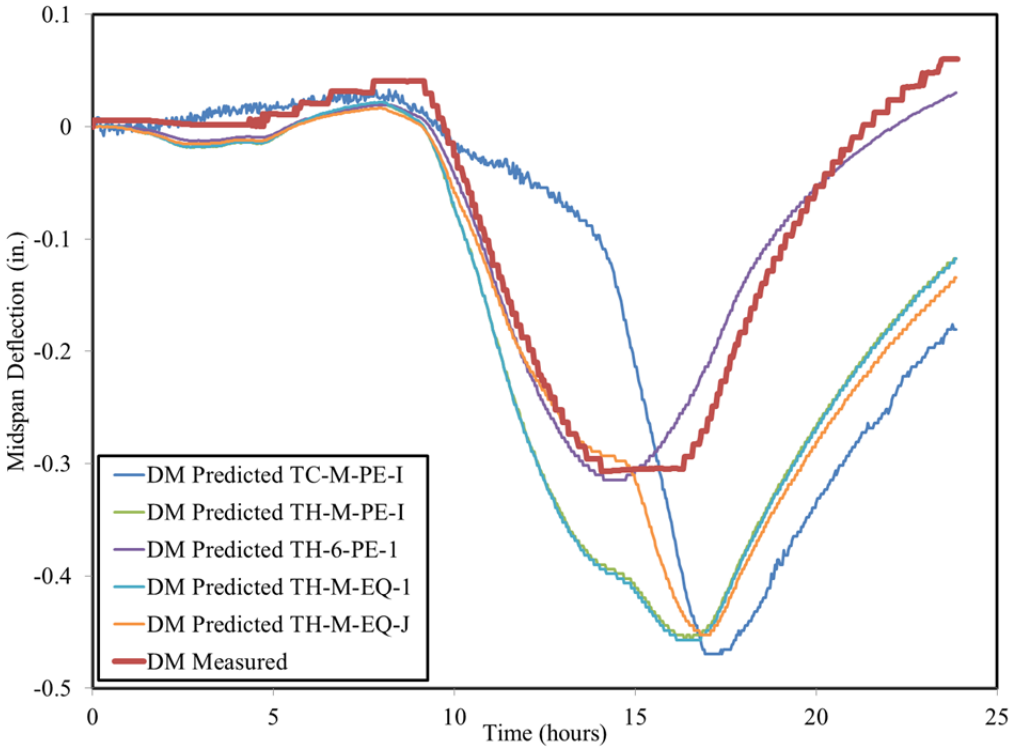

Figure 8-50: Predicted and Measured Midspan Deflection for Test #1 by Analysis Procedure (α_T=12.3)

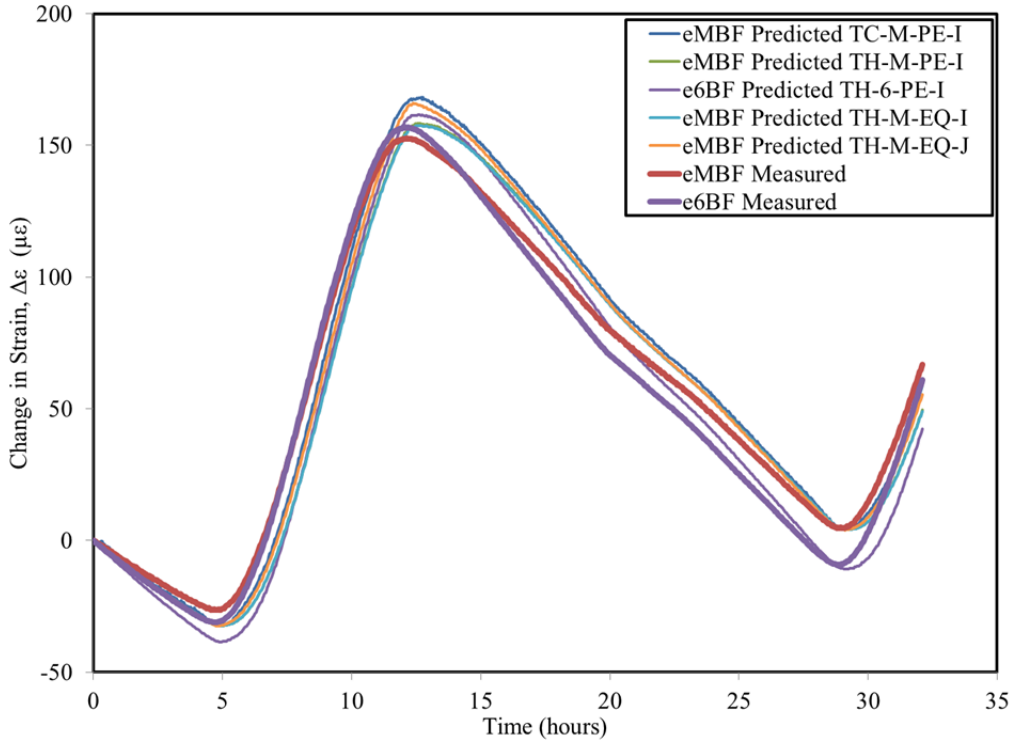

Figure 8-51: Predicted and Measured Bottom Flange Strains for Test #2 by Analysis Method (α_T=13.5)

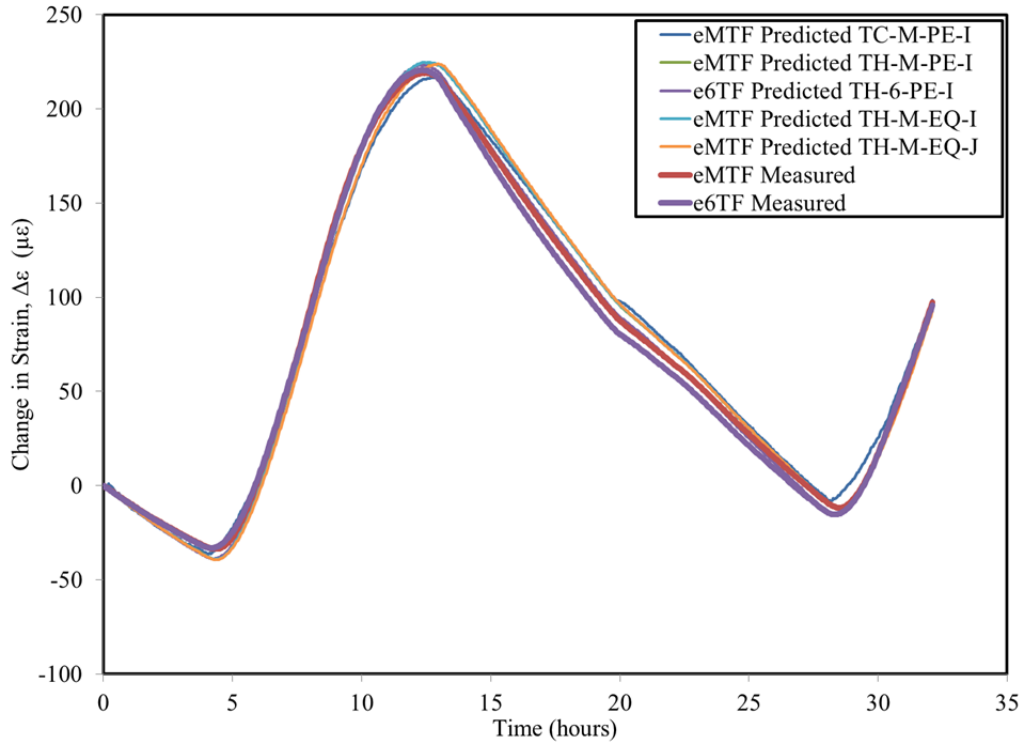

Figure 8-52: Predicted and Measured Top Flange Strains for Test #2 by Analysis Method (α_T=13.5)

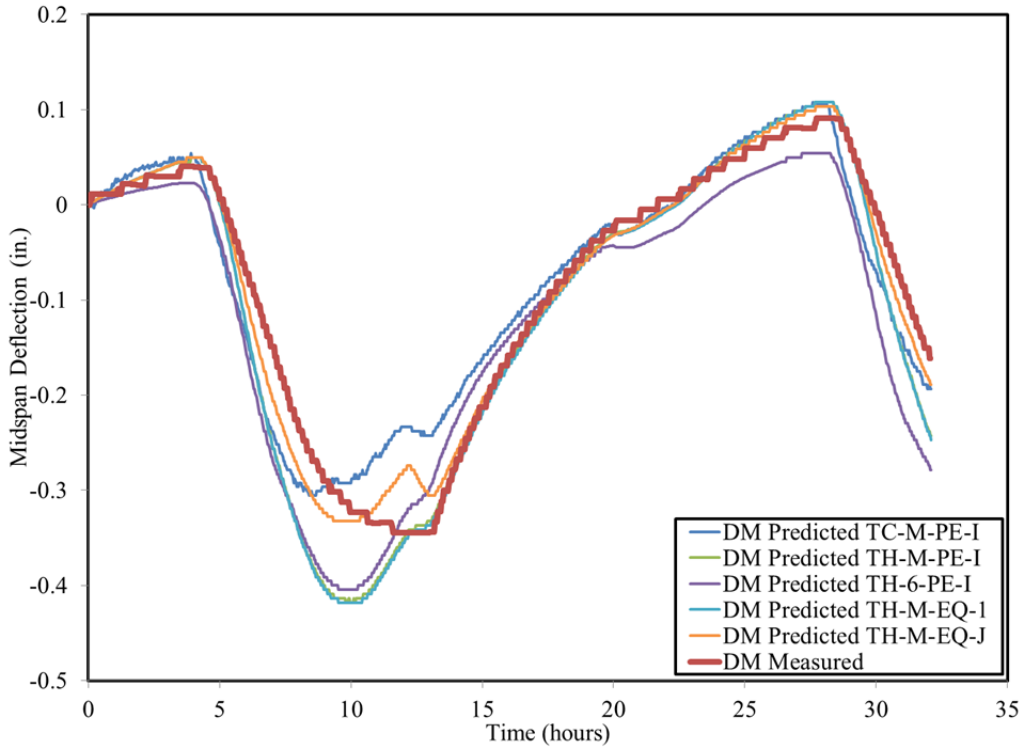

Figure 8-53: Predicted and Measured Midspan Deflection for Test #2 by Analysis Method (α_T=13.5)

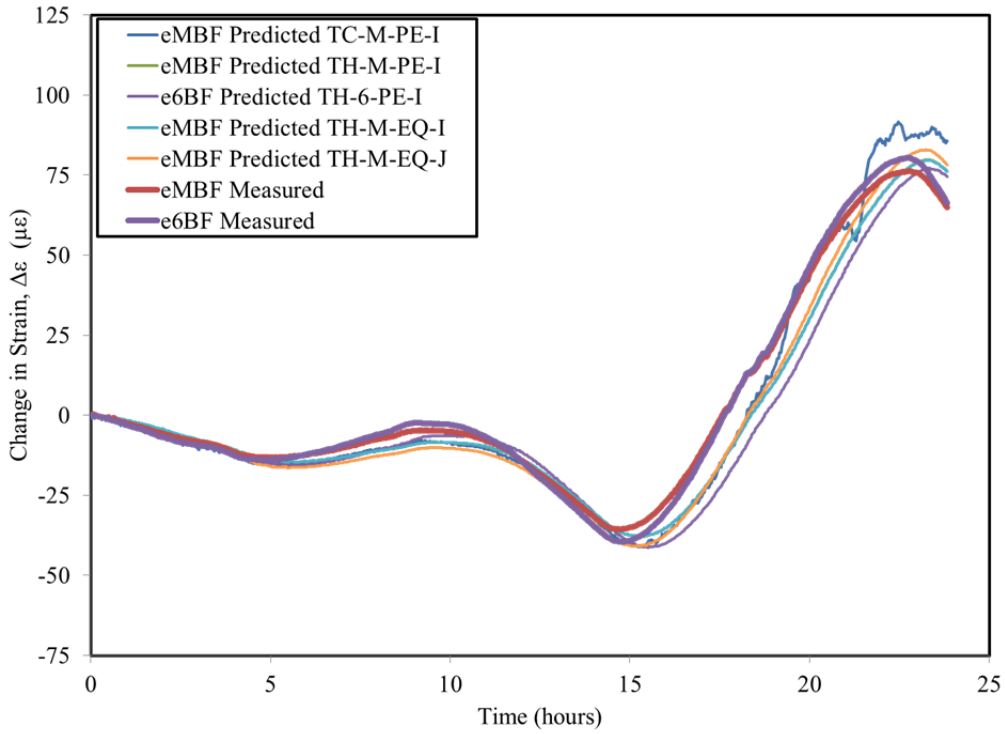

Figure 8-54: Predicted and Measured Bottom Flange Strains for Test #3 by Analysis Method (α_T=13.2)

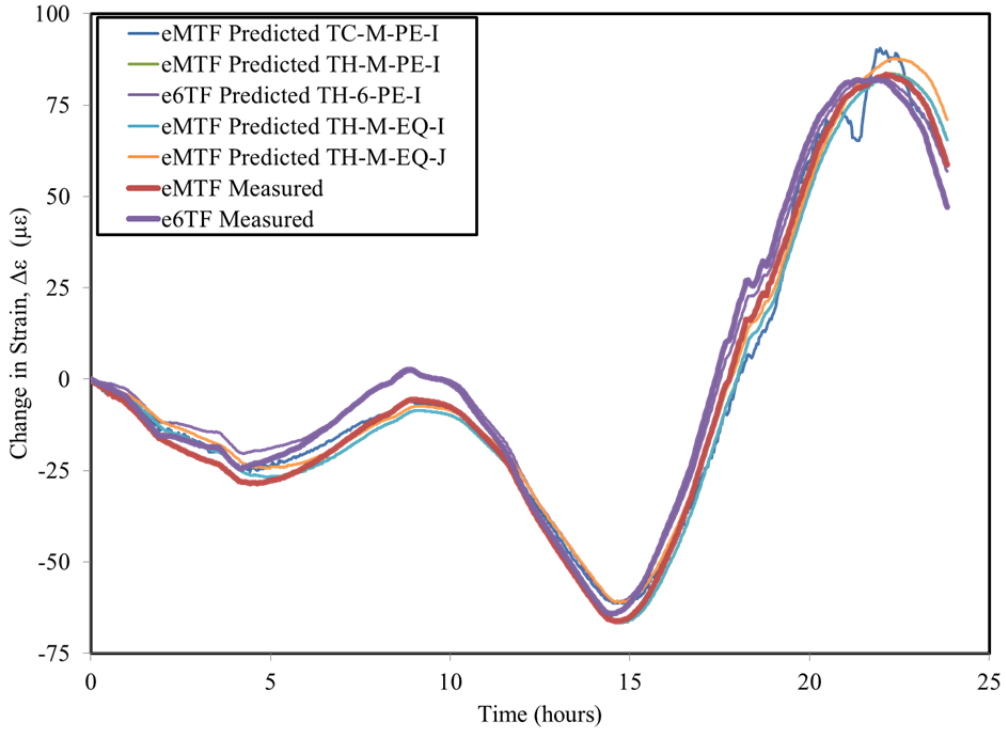

Figure 8-55: Predicted and Measured Top Flange Strains for Test #3 by Analysis Method (α_T=13.2)

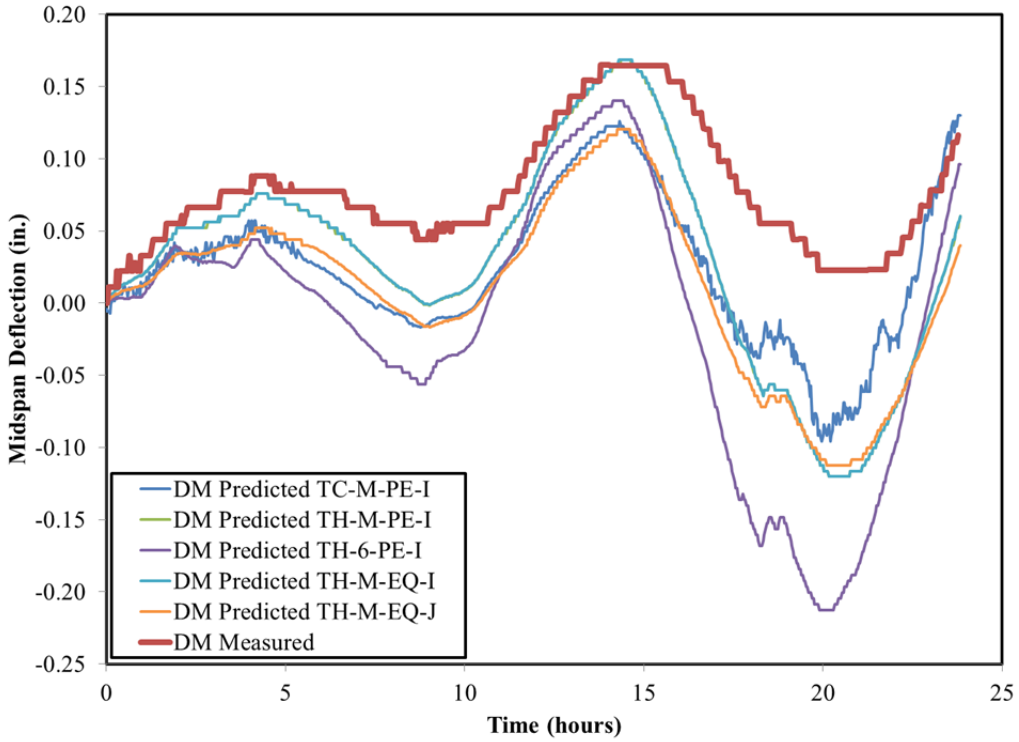

Figure 8-56: Predicted and Measured Midspan Deflection for Test #3 by Analysis Method (α_T=13.2)

Table 8-8: Standard Error of the Estimate for Various Analysis Iterations

Analysis Procedure	Gage ID	Standard Error of the Estimate, *SEE*			
		Test #1	Test #2	Test #3	Units
TC-M-PE-I (Most Detailed)	**eMTF**	26.4	6.8	4.3	με
	eMWT	16.0	11.3	6.5	με
	eMWB	11.6	12.1	6.6	με
	eMBF	4.9	10.6	6.8	με
	DM	0.16	0.05	0.06	in.
	D6-1	0.10	0.03	0.06	in.
	D6-2	0.10	0.03	0.04	in.
TH-M-PE-I	**eMTF**	13.7	6.4	3.3	με
	eMWT	8.3	10.1	7.2	με
	eMWB	12.7	14.5	8.5	με
	eMBF	10.6	12.4	6.6	με
	DM	0.12	0.04	0.07	in.
	D6-1	0.09	0.03	0.06	in.
	D6-2	0.09	0.02	0.05	in.
TH-6-PE-I	**e6TF**	12.0	6.3	3.1	με
	e6WT	18.3	9.6	4.9	με
	e6WB	15.0	14.7	4.7	με
	e6BF	13.1	13.1	10.2	με
	DM	0.02	0.06	0.12	in.
	D6-1	0.03	0.04	0.11	in.
	D6-2	0.03	0.03	0.09	in.
TH-M-EQ-I	**eMTF**	13.7	6.5	3.4	με
	eMWT	8.3	10.1	7.2	με
	eMWB	12.8	14.5	8.5	με
	eMBF	10.8	12.4	6.6	με
	DM	0.12	0.05	0.07	in.
	D6-1	0.09	0.04	0.06	in.
	D6-2	0.10	0.02	0.05	in.
TH-M-EQ-J	**eMTF**	17.0	8.1	4.0	με
	eMWT	10.2	11.2	6.2	με
	eMWB	11.7	13.4	7.2	με
	eMBF	8.2	11.3	6.5	με
	DM	0.12	0.02	0.08	in.
	D6-1	0.09	0.02	0.07	in.
	D6-2	0.09	0.02	0.05	in.

In consideration of the results presented in Figures 8-48 through 8-56 and summarized in Table 8-8, the following observations are offered:

- Relatively good agreement between predicted and measured deformations (e.g. strains and vertical deflection), in shape and magnitude, was observed for Tests #2 and 3 for each analytical iteration —with somewhat less accurate results evident for Test #1;
- Best agreement between predicted and measured cross-sectional strains was observed for Test #3, while most accurate predictions of vertical deflections were observed for Test #2;
- When comparing predicted and measured results between the midspan and 1/6-span analysis sections, the accuracy of strain, curvature, and deflection predictions were similar in shape and magnitude—with the exception of Test #1;
- The most detailed analysis iteration (TC-M-PE-I) used in this study (which relied on between 11–13 thermocouple measurements at midspan and an exact cross section definition) generated the most accurate predictions of girder deformations for Tests #2 and 3;
- The most detailed analysis iteration (TC-M-PE-I) generated the least accurate predictions of any analysis iteration in this study for Test #1—suggesting that the top flange thermocouple temperature measurements (previously noted to have differed from thermistor readings at the same location) were likely flawed. The effective CTE computed for Test #1 of 12.3 με/°C may have been affected by these flawed readings;

- Similar analytical iterations conducted using measured data from different cross sections (i.e. TH-M-PE-I at midspan and TH-6-PE-I at 1/6-span) generated largely similar results, with no consistent discernable trends evident with regards to prediction accuracy;
- By comparing similar analytical iterations using varying definitions of girder cross section (TH-M-PE-I and TH-M-EQ-I), it is evident that use of the simplified equivalent cross section proposed by Johnson (2012) resulted in negligible error when compared to use of an exact cross section definition;
- For tests where most significant top flange temperature gradients were observed (Tests #2–3), the use of the simplified temperature profile proposed by Johnson (TH-M-EQ-J) generated strain predictions only slightly less accurate than those of the most detailed analysis (TC-M-PE-I). For these same tests, a similar analytical iteration utilizing linear interpolation to define the temperature profile shape (TS-M-PE-I) resulted in predictions of strain and vertical deflection slightly less accurate than use of the temperature profile by Johnson; and
- The effective CTE values previously computed for Tests #2 and 3 (13.5 and 13.2 με/°C, respectively) generated satisfactory predictions of temperature-induced girder deformations for all analytical iterations included in this study. In the absence of more detailed information, an effective CTE value of between 13.0 and 13.5 με/°C should be expected to yield sufficiently accurate results in conjunction with the analytical iterations utilized in this study.

8.6 Expected Magnitude of Transient Temperature-Induced Camber Variations For Girders in Storage

The shape of the extreme vertical temperature profiles observed during the three field tests performed in this study differed from the typical vertical temperature profile shape previously reported by others (e.g. Lee 2008, Barr et al. 2005, Kelly et al. 1987, and Neal 2015). Where others generally report extreme temperatures in the girder top flange, the vertical profiles observed in the three winter tests of this study were generally defined by extreme temperatures in the girder web. As a result, the limited temperature data compiled in this study is likely not representative of the most extreme temperature-induced girder camber variations. To explore this topic further, a design vertical temperature profile proposed by a previous researcher and the code-prescribed design profiles of AASHTO 2014 were used to estimate the magnitude of extreme temperature-induced camber variations to be expected for precast, prestressed concrete girders in storage.

The positive design profile[4] by Lee (2008) resulted from an extensive field study and corresponds to the maximum upward deflection expected in PCI bulb-tee girder shapes as a result of warming of the girder top flange. Lee's work was based on field observations of pre-erection behavior (i.e. during girder storage and transportation) and, thus, his design recommendations are useful to estimate the magnitude of temperature-induced camber variations for girders in storage. The AASHTO 2014 code-prescribed design profiles were also included in this analysis for comparison—although these vertical temperature profiles are primarily intended for use in girders with concrete decks.

[4] In agreement with AASHTO 2014 terminology, vertical temperature profiles corresponding to an increase in top flange temperature (e.g. 0 to 20 °C) are called "positive" temperature profiles.

The three design vertical temperature profiles utilized in this analysis are shown in Figure 8-57.

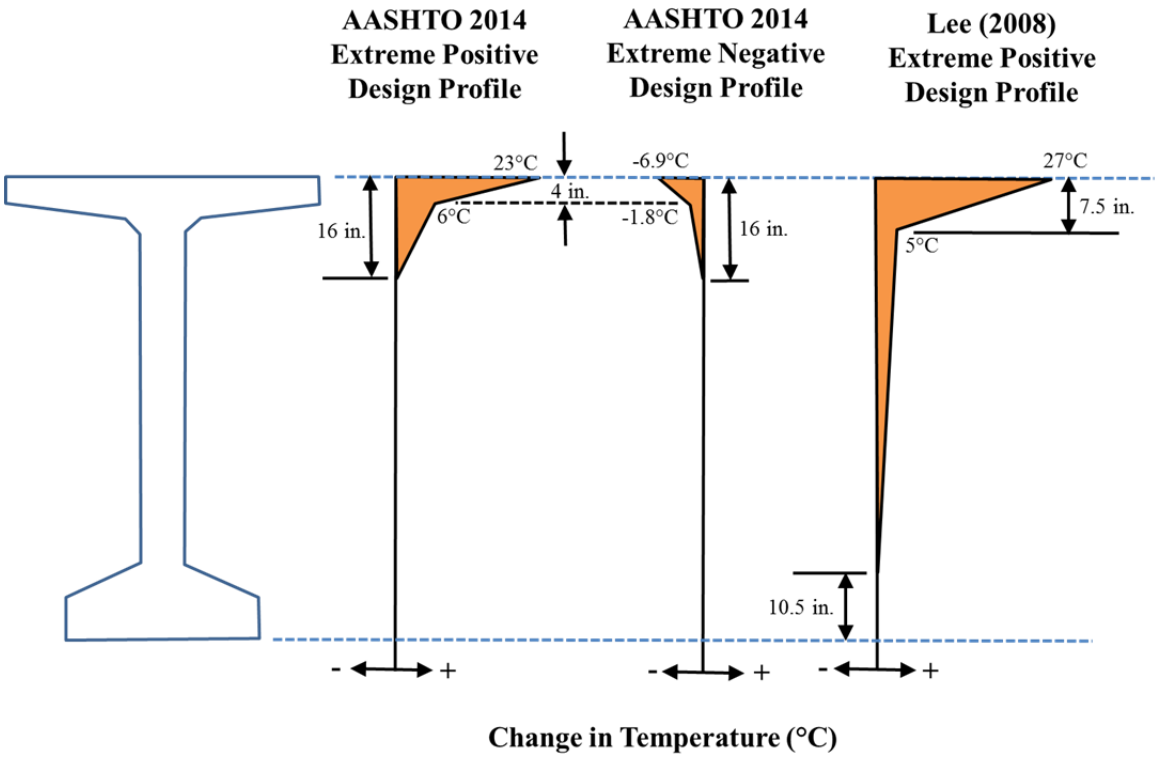

Figure 8-57: Extreme Positive and Negative Vertical Temperature Profiles

The positive design profiles (AASHTO and Lee [2008]) above tend to cause increases in girder camber, while the negative profile (AASHTO) tends to cause a decrease in girder camber. In general, positive design profiles are caused by exposure to solar radiation (i.e. heating of the top flange), while negative design profiles can be caused by other conditions (e.g. differential cooling due to wind or decreasing ambient temperature) in the absence of solar exposure. Using the temperature-correction algorithm implemented in this dissertation, the curvature induced by each design vertical temperature profile was computed as shown in Table 8-9.

Table 8-9: Induced Curvature by Design Temperature Profile

Direction of Midspan Induced Deflection Change	Temperature Gradient Source	Deck Present?	Induced Curvature ($x10^{-6}$ rad/in.)		
			BT-54	BT-63	BT-72
Upward	AASHTO 2014 (Positive)	Yes	-3.3	-2.7	-2.2
	Lee (2010)	No	-5.0	-4.1	-3.4
Downward	AASHTO 2014 (Negative)	Yes	<+1.0	<+1.0	<+1.0
Total Range	AASHTO 2014 (Computed)	Yes	4.3	3.7	3.2
	Observed in this Study	No	n/a	<1.0	<2.0

Notes:
1. An effective CTE of 13.0 με/°C was assumed.
2. Negative curvature corresponds to increased girder camber.

As shown, the design profile of Lee (2008) tended to induce the maximum changes in curvature—approximately 50 percent greater than those computed using the AASHTO 2014 positive design profile. The magnitude of the induced change in curvature corresponding to the negative AASHTO temperature profile was less than $1.0x10^{-6}$ rad/in. The total range of curvature change observed in this study was significantly less than the maximum computed using the AASHTO 2014 design profiles. Using assumed girder lengths and a transverse girder-to-girder spacing (each as noted in Table 8-10), changes to midspan camber were computed corresponding to the curvatures noted above and are shown in Table 8-10.

Table 8-10: Induced Changes in Midspan Camber by Design Temperature Profile

Direction of Midspan Induced Deflection Change	Temperature Gradient Source	Deck Present?	Induced Change in Midspan Camber (in.)		
			BT-54	BT-63	BT-72
Upward	AASHTO 2014 (Positive)	Yes	+0.9	+0.9	+1.0
	Lee (2010)	No	+1.3	+1.3	+1.5
Downward	AASHTO 2014 (Negative)	Yes	-0.3	-0.3	-0.4
Total Range	AASHTO 2014	Yes	1.2	1.2	1.4
	Observed in This Study	No	n/a	0.3	0.9

Notes:
1. Transverse girder-to-girder spacing of 6.5 ft is assumed.
2. Maximum span lengths for BT-54, BT-63, and BT-72 assumed as 120 ft, 135 ft, and 155 ft, respectively, in accordance with PCI design guidelines (PCI 2011).

A number of trends are evident from the results of Table 8-10:

- As a result of two opposing trends ([1] less deep girders exhibited more induced curvature than deeper girders for an identical vertical temperature profile, and [2] changes in cross-sectional curvature tended to cause larger changes in midspan camber for longer span lengths), expected temperature-induced changes in midspan camber are somewhat more independent of girder cross section than was the case for the curvatures previously reported in Table 8-9;
- The positive design temperature profiles of AASHTO 2014 and Lee (2010) are expected to cause maximum transient increases in midspan camber of 1.0 in. and 1.5 in., respectively, for typical PCI bulb-tee girders;
- The negative design temperature profile of AASHTO 2014 is expected to cause a maximum transient decrease in midspan camber of less than 0.5 in. for typical PCI bulb-tee girders; and

- The changes in midspan camber observed during the three field tests performed in this study were substantially less than the maximum values computed using the vertical design profiles of AASHTO or Lee (2008).

The transient change in upward camber computed from the design profile of Lee (2008) is most appropriate as an upper-bound estimate for expected upward camber variation because of the similarities between the experimental conditions used by Lee and typical girder storage practices (i.e. outdoor, unshaded ambient exposure with no concrete deck installed.) For the purpose of estimating the maximum expected downward transient change in midspan camber, use of the AASHTO negative profile is the default option. Although the AASHTO negative temperature profile is not strictly intended for application to girders without concrete decks, application as such is likely less error prone than if the AASHTO positive temperature profile were relied on similarly for a section without a concrete deck. As previously discussed, the heat transfer mechanisms associated with negative temperature profiles tend to be independent of solar exposure and, therefore, the presence of a concrete deck likely does little to change the magnitude or shape of the AASHTO negative temperature profile. Future research work may be justified in this area to better quantify negative temperature profiles in girders prior to concrete deck placement—although the resulting deformations are relatively small and likely of minimal consequence. Recommendations in agreement with the preceding discussion are summarized in Table 8-11.

Table 8-11: Transient Changes to Theoretical Midspan Camber

Expected Transient Temperature-Induced Changes to Theoretical Midspan Camber	
Upward	<+1.5 in.
Downward	<-0.5 in.

8.7 Summary and Conclusions

8.7.1 Summary

In this chapter, a curvature-based temperature-correction algorithm was developed and implemented to analytically predict the behavior of precast, prestressed concrete bridge girders upon exposure to vertical diurnal temperature variations. After derivation of the basic concept, results of a field-monitoring study were used to validate the algorithm and to calibrate values of an "effective" coefficient of thermal expansion providing best agreement between predicted and measured girder deformations. Finally, the magnitudes of expected transient changes in midspan girder camber were estimated using the temperature-correction procedure implemented in this chapter in conjunction with available design extreme vertical temperature profiles published by others.

8.7.2 Conclusions and Recommendations

Key observations and recommendations regarding the temperature-correction algorithm implemented in this dissertation include the following:

- As implemented in this study, the curvature-based temperature-correction algorithm demonstrated good agreement with field measured results—with the exception of where testing anomalies were detected (e.g. Field Test #1);
- For the concrete girders monitored in this study, an effective CTE value of between 13.0 and 13.5 με/°C was found to provide best agreement between predicted and measured deformational responses for girders in unshaded outdoor storage;
- Maximum temperature-induced changes to midspan camber of approximately 0.45 inches were observed in the field testing of this study;

- The general shapes of vertical temperature profiles at all locations (midspan and 1/6-span) were similar, with extreme temperature changes being induced in the girder web for the field tests conducted in this effort;
- Positioning of temperature gages at one-quarter points within the girder web of bulb-tee sections appeared to approximate the reversals of the temperature profile occurring within the girder web relatively well;
- The most detailed analysis iteration (TC-M-PE-I) used in this study (which relied on between 11–13 thermocouple measurements at midspan and an exact cross section definition) tended to generate the most accurate predictions of girder deformations (with the exception of where testing anomalies were detected)—although at the greatest computational cost;
- Analytical iterations conducted using measured data from different cross sections (i.e. TH-M-PE-I at midspan and TH-6-PE-I at 1/6-span), but identical analytical methods generated largely similar results;
- Use of the simplified equivalent cross section proposed by Johnson (2012) resulted in negligible error when compared to use of an exact cross section definition;
- Use of the simplified temperature profile proposed by Johnson (TH-M-EQ-J) generated strain predictions only slightly less accurate than those of the most detailed analysis included in this study (TC-M-PE-I). The use of linear interpolation to define the temperature profile shape (TS-M-PE-I) resulted in predictions of strain and vertical deflection only slightly less accurate than use of the temperature profile by Johnson (2012);

- For the purposes of temperature-correction of field camber measurements, use of the temperature-correction algorithm derived in Section 8.2.2 is appropriate with either (a) the procedures and assumptions implemented by Johnson (2012), (b) the procedures and assumptions implemented in this study, or (c) any combinations thereof;
- Maximum expected transient temperature-induced deformations for PCI bulb-tee girder sections (without decks) in unshaded outdoor storage are summarized in Table 8-11.

Table 8-11: Transient Changes to Theoretical Midspan Camber

Expected Transient Temperature-Induced Changes to Theoretical Midspan Camber	
Upward	<+1.5 in.
Downward	<-0.5 in.

Chapter 9: Camber Prediction Software (*ALCAMBER* v1.0) Development

9.1 Introduction

A key objective of this research effort was to publish a user-friendly camber prediction software capable of implementing the recommendations of this dissertation with regards to predicting expected concrete strength (Chapter 5), concrete stiffness behavior (Chapter 6), and time-dependent concrete behavior (Chapter 7). This chapter serves as a basic introduction to the camber prediction software package, *ALCAMBER*, developed as part of this research project. Finer details of the software development have been documented by Schrantz (2012), Johnson (2012), and Isbiliroglu (2014).

9.1.1 Chapter Outline

First, a general background description of the incremental-time steps method for computing long-term girder deflections is discussed (Section 9.2). Next, various fundamental concepts and assumptions are utilized to derive the two governing equations for the incremental-time step method implemented in this research effort. Finally, the program algorithm is described along with the four key classes of computations performed.

9.2 Background

As introduced briefly in Chapter 2, the incremental time-steps method is an analysis method based on combining the computation of deformations with those of effective prestress and concrete stresses due to time-dependent creep, shrinkage, and relaxation

(ACI Committee 435 2003). By dividing the life of the flexural element into discrete time increments, changes in shrinkage, creep, and relaxation can be computed for each time increment. Effective prestress force and deformations and stresses are then updated at the end of each time increment. By subdividing the flexural element into multiple cross sections and integrating the deformations along the length of the element, girder displacements and rotations can also be computed (ACI Committee 435 2003).

9.2.1 Application of Incremental Time-Steps Method

For the purposes of this research effort, the incremental time-steps method is applied to a simple-span, precast, prestressed concrete beam. Assuming symmetry about midspan, half of the girder is segmented by forty analysis cross sections. For each cross section, the initial strain distribution and corresponding curvature at the time immediately after prestress release is first computed from fundamental mechanics principles using transformed section properties to accurately include the steel stiffness. This initial strain distribution includes the effects of elastic shortening, pre-release relaxation of the prestressing strand, and the portion of concrete shrinkage occurring before prestress release.

The varying constituent girder materials (concrete and steel) exhibit time-dependent deformational tendencies—some of which begin as early as the time of initial strand tensioning. If fully unrestrained and independent of one another, the following responses from the girder constituent materials would be expected after prestress release:

- The tensile stresses (and corresponding forces) in the steel strands would reduce as a result of continued relaxation;

- Due to creep caused by a sustained stress, strains in the concrete would tend to increase in proportion to the relative magnitude of the sustained stress at a given depth within the section; and
- The strain in the concrete would tend to decrease (contract) as a result of unrestrained shrinkage of the concrete.

However, independent consideration of the material responses summarized above *would not* satisfy compatibility and equilibrium for a given cross section. Instead, these time-dependent material changes are interrelated and must be dealt with accordingly.

Two governing relationships can be used to compute the incremental change in cross-sectional strain and curvature that satisfy equilibrium and strain compatibility for a single time increment. Knowing the initial strain and curvature of each analysis section and the incremental change to these parameters within an increment (time step), the total strain and stresses can be updated for each cross section. By iterating this process, that is, using the results from the previous time step as the starting conditions for the subsequent time step, strains and curvatures can be computed at each analysis section for each time step, while accurately incorporating the *interaction* of creep, shrinkage, and steel relaxation on the cross section. Finally, using moment-area theorems for flexural deformations, the cross-sectional stresses and curvatures for each analyzed cross section can be numerically integrated to compute camber at a considered time.

9.3 Derivation of Incremental Strain and Curvature Expressions

The incremental time-steps method, as implemented in this research effort, relies on two closed-form relationships to compute the incremental strain and curvature at a given cross section across a time step. Due to their importance to the development of the

ALCAMBER software package, this section presents the derivations of these two governing equations beginning from basic principles of mechanics. These expressions, as derived by Schrantz (2012), are documented more thoroughly herein.

9.3.1 Key Assumptions

The following key assumptions are implicit to the *ALCAMBER* software package:

- Girders are assumed to be relatively slender, simply-supported, and symmetric about midspan;
- Deflections are computed from the time of prestress release until the estimated time of erection only, without consideration for post-erection behavior;
- Linear-elastic strain response to applied stress, as is uncracked section behavior;
- Strain compatibility between steel reinforcement and adjacent concrete is assumed; and
- The effect of prestressing strand transfer length is assumed to be limited to the end bonded segment of each group of strands (fully bonded or debonded) in the discretized girder.

9.3.2 Fundamental Principles

When the above assumptions are satisfied, it is permissible to utilize the fundamental principles listed here to derive the incremental strain and curvature equations: (1) plane sections remain plane and perpendicular to the longitudinal axis during deformation, (2) the total strain change in a material is equal to the sum of the stress-dependent (mechanical) strains and the stress-independent strains, and (3) cross-sectional equilibrium between internal stresses and external forces and moments.

9.3.3 Incremental Strain Expression Derivation

This section reviews the derivation of the equation for incremental strain as used in the incremental time-steps procedure implemented in the software *ALCAMBER*. The sign convention is as shown in Figure 9-1.

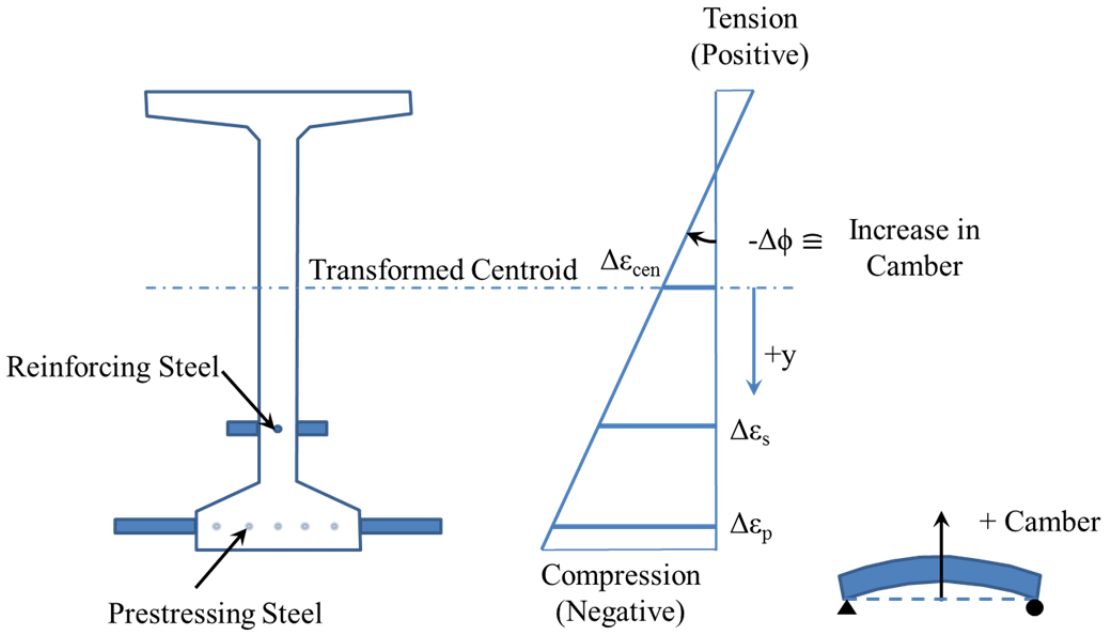

Figure 9-1: Sign Convention and Notation for Derivation

The strain profile shown is characteristic of a typical precast, prestressed girder at the time of prestress release. While the majority of the section remains in compression, any tensile strains at the top of the section remain below code-prescribed thresholds. Positive *y* is defined as downward from the transformed centroid, with negative *y* values upward. Using the fundamental principle of "plane sections remain plane", the following three equations describe the change in strain at all vertical locations in all constituent materials within a cross section:

$$\Delta\varepsilon_c = \Delta\varepsilon_{cen} + \Delta\phi(y) \tag{9-1}$$

$$\Delta\varepsilon_s = \Delta\varepsilon_{cen} + \Delta\phi(y_s) \tag{9-2}$$

$$\Delta\varepsilon_p = \Delta\varepsilon_{cen} + \Delta\phi(y_p) \tag{9-3}$$

where

$\Delta\varepsilon_c$ = change in concrete strain at a given depth within a cross section (in./in.);

$\Delta\varepsilon_{cen}$ = change in concrete strain at the transformed centroid (in./in.);

$\Delta\phi$ = change in curvature of a given cross section;

y = depth from the centroid of the transformed section to a given location within a cross section (in.);

$\Delta\varepsilon_s$ = change in strain in reinforcing steel (in./in.);

y_s = depth from the centroid of the transformed section to the steel location within a cross section (in.);

$\Delta\varepsilon_p$ = change in strain in prestressing steel (in./in.); and

y_p = depth from the centroid of the transformed section to the prestressing steel location within a cross section (in.).

Equilibrium with applied axial loads can be applied by integrating the changes in stress over the cross-sectional area:

$$\Delta N = \int_A \Delta\sigma dA = \int_{A_c} \Delta f_c dA_c + \int_{As} \Delta f_s dA_s + \int_{A_p} \Delta f_p dA_p \tag{9-4}$$

where

f_x = the stress at a given height in a material [where x = c (concrete), s (steel), or p (prestressing steel)];

A_x = the total cross-sectional area of a material [same subscript convention used above for stress];

$\int_{A_c} \Delta f_c dA_c$ = representation of the change in cross sectional force in the concrete;

$\int_{As} \Delta f_s dA_s$ = representation of the change in cross-sectional force in the reinforcing steel; and

$\int_{A_p} \Delta f_p dA_p$ = representation of the change in cross sectional force in the prestressing steel.

Equilibrium of applied moments can be applied similarly, except with an added term to represent the distance from the transformed centroid:

$$\Delta M = \int_A y \Delta\sigma dA = \int_{A_c} y_c \Delta f_c dA_c + \int_{A_s} y_s \Delta f_s dA_s + \int_{A_p} y_p \Delta f_p dA_p \tag{9-5}$$

For each time step in the analysis, the externally applied load and moments do not change for a given cross section. Therefore

$$\Delta N = 0 \text{ , } \Delta M = 0 \tag{9-6}$$

Simplifying the integrals for reinforcing steel and prestressing steel terms into discrete sums to represent the discrete potential locations of steel within a cross section:

$$\Delta N = \int_{A_c} \Delta f_c dA_c + \sum \left(\Delta f_s A_s \right) + \sum \left(\Delta f_p A_p \right) = 0 \tag{9-7}$$

$$\Delta M = \int_{A_c} y \Delta f_c dA_c + \sum \left(y_s \Delta f_s A_s \right) + \sum \left(y_p \Delta f_p A_p \right) = 0 \tag{9-8}$$

Equations 9-7 and 9-8, currently written in terms of incremental stresses, can be written in terms of incremental strains using linear-elastic behavior assumptions and the definition of total strain. The total incremental strain in the concrete can be represented

as the sum of the stress-dependent (mechanical) and stress-independent incremental strains as shown in Equation 9-9.

$$\underbrace{\frac{\Delta f_c}{E_c}}_{\text{Stress Dependent}} + \underbrace{\Delta\varepsilon_{c,cr} + \Delta\varepsilon_{c,shr} + \Delta\varepsilon_{c,temp}}_{\text{Stress Independent}} = \Delta\varepsilon_c \tag{9-9}$$

where

$\frac{\Delta f_c}{E_c}$ = the portion of change in concrete strain resulting from linear-elastic stress response;

$\Delta\varepsilon_{c,cr}$ = the portion of the change in concrete strain due to unrestrained creep;

$\Delta\varepsilon_{c,shr}$ = the portion of the change in concrete strain due to unrestrained shrinkage; and

$\Delta\varepsilon_{c,temp}$ = the portion of concrete strain due to unrestrained temperature effects.

Solving for the incremental stress in the concrete, Δf_c, and neglecting thermal strains yields:

$$\Delta f_c = E_c\left(\Delta\varepsilon_c - \Delta\varepsilon_{c,cr} - \Delta\varepsilon_{c,shr}\right) \tag{9-10}$$

Similarly, an expression for the incremental stress in the prestressing steel (considering relaxation) can be derived:

$$\Delta f_p = E_p\Delta\varepsilon_p + \Delta f_{p,relax} \tag{9-11}$$

where

$\Delta f_{p,relax}$ = the change in stress in prestressing steel due to steel relaxation.

Similarly, the stress in the reinforcing steel can be expressed as

$$\Delta f_s = E_s\Delta\varepsilon_s \tag{9-12}$$

Substitution of the three derived expressions for incremental stress (Equations 9-10, 9-11, and 9-12) into the incremental cross-sectional equilibrium equation for axial force (Equation 9-7) yields

$$\begin{aligned}&\int_{A_c}\left[E_c\left(\Delta\varepsilon_c-\Delta\varepsilon_{c,cr}-\Delta\varepsilon_{c,shr}\right)\right]dA_c+\sum\left(\left[E_s\Delta\varepsilon_s\right]A_s\right)+\\&\sum\left(\left[E_p\Delta\varepsilon_p+\Delta f_{p,relax}\right]A_p\right)=0\end{aligned} \tag{9-13}$$

The incremental creep strain (which varies by cross-sectional height in proportion to stress) can be written similarly to Equation 9-1 as

$$\Delta\varepsilon_{c,creep}=\Delta\varepsilon_{cen,creep}+\Delta\phi_{creep}\left(y\right) \tag{9-14}$$

Combining Equations 9-1, 9-2, 9-3, and 9-14 with Equation 9-13 yields

$$\begin{aligned}&\int_{A_c}\left[E_c\left(\left(\Delta\varepsilon_{cen}+\Delta\phi(y)\right)-\left(\Delta\varepsilon_{cen,creep}+\Delta\phi_{creep}(y)\right)-\Delta\varepsilon_{c,shr}\right)\right]dA_c+\\&\sum\left(\left[E_s\left(\Delta\varepsilon_{cen}+\Delta\phi(y_s)\right)\right]A_s\right)+\sum\left(\left[E_p\left(\Delta\varepsilon_{cen}+\Delta\phi\left(y_p\right)\right)+\Delta f_{p,relax}\right]A_p\right)=0\end{aligned} \tag{9-15}$$

Grouping curvature-dependent terms and those independent of location *y* yields

$$\begin{aligned}&0=E_cA_c\left[\Delta\varepsilon_{cen}-\left(\Delta\varepsilon_{cen,creep}+\varepsilon_{c,shr}\right)\right]+\sum\left(E_pA_p\Delta\varepsilon_{cen}\right)+\sum\left(E_sA_s\Delta\varepsilon_{cen}\right)+\\&\sum\left(A_p\Delta f_{p,relax}\right)+E_c\Delta\phi\left[\int_{A_c}ydA_c+\left(\frac{E_p}{E_c}\right)\sum y_pA_p+\left(\frac{E_s}{E_c}\right)\sum y_sA_s\right]-E_c\Delta\phi_{creep}\int_{A_c}ydA_c\end{aligned} \tag{9-16}$$

Recognizing (1) that the bracketed portion of the following term is the first moment of area, and (2) that if y is measured relative to the centroid of the transformed section, the first moment of area is zero:

$$E_c\Delta\phi\left[\int_{A_c}ydA_c+\left(\frac{E_p}{E_c}\right)\sum y_pA_p+\left(\frac{E_s}{E_c}\right)\sum y_sA_s\right]=E_c\Delta\phi\int_{A_c}ydA_{tr}=0 \tag{9-17}$$

Discarding the above term yields

$$\begin{aligned}&0=E_cA_c\left[\Delta\varepsilon_{cen}-\left(\Delta\varepsilon_{cen,creep}+\varepsilon_{c,shr}\right)\right]+\sum\left(E_pA_p\Delta\varepsilon_{cen}\right)+\sum\left(E_sA_s\Delta\varepsilon_{cen}\right)+\\&\sum\left(A_p\Delta f_{p,relax}\right)-E_c\Delta\phi_{creep}\int_{A_c}ydA_c\end{aligned} \tag{9-18}$$

Regrouping

$$0 = \Delta\varepsilon_{cen}\left[E_c A_c + \sum E_p A_p + \sum E_s A_s\right] - E_c A_c\left(\Delta\varepsilon_{cen,creep} + \Delta\varepsilon_{c,shr}\right) + \sum\left(A_p \Delta f_{p,relax}\right) - E_c \Delta\phi_{creep}\int_{A_c} y dA_c \tag{9-19}$$

Solving for $\Delta\varepsilon_{cen}$

$$\Delta\varepsilon_{cen} = \frac{E_c A_c\left(\Delta\varepsilon_{cen,creep} + \Delta\varepsilon_{c,shr}\right) - \sum\left(A_p \Delta f_{p,relax}\right) + E_c \Delta\phi_{creep}\int_{A_c} y dA_c}{\left[E_c A_c + E_p \sum A_p + E_s \sum A_s\right]} \tag{9-20}$$

Recognizing that the denominator is equal to $E_c A_{tr}$

$$\Delta\varepsilon_{cen} = \frac{A_c\left(\Delta\varepsilon_{cen,creep} + \Delta\varepsilon_{c,shr}\right) - \frac{1}{E_c}\sum\left(A_p \Delta f_{p,relax}\right) + \Delta\phi_{creep}\int_{A_c} y dA_c}{A_{tr}} \tag{9-21}$$

Here, the integral with respect to y is non-zero, because it is not defined in terms of the transformed section. Knowing that the transformed area is

$$A_{tr} = A_c + n_p A_p + n_s A_s \tag{9-22}$$

where

$n_p = \frac{E_p}{E_c}$ = the modular ratio of the prestressing steel, and

$n_s = \frac{E_s}{E_c}$ = the modular ratio of the reinforcing steel.

Solving for A_c

$$A_c = A_{tr} - n_p A_p - n_s A_s \tag{9-23}$$

Substituting into the integral of Equation 9-21

$$\int_{A_c} y dA_c = \int_{A_c} y d\left(A_{tr} - n_p A_p - n_s A_s\right) \tag{9-24}$$

Simplifying, recognizing the first term equals zero, and adding appropriate y-subscripts for context

$$\int_{A_c} y dA_c = -\sum n_p A_p y_p - \sum n_s A_s y_s \tag{9-25}$$

Substituting Equation 9-25 into 9-21 and simplifying yields

$$\Delta\varepsilon_{cen} = \frac{A_c}{A_{tr}}\left(\Delta\varepsilon_{cen,creep} + \Delta\varepsilon_{c,shr}\right) - \frac{\Delta\phi_{creep}\left(n_p\sum\left(A_p y_p\right) + n_s\sum\left(A_s y_s\right)\right)}{A_{tr}} - \frac{\frac{1}{E_c}\sum\left(A_p \Delta f_{p,relax}\right)}{A_{tr}} \tag{9-26}$$

Equation 9-26 is used in *ALCAMBER* at each analysis cross section and time step to compute the incremental strain at the centroid across each time increment.

9.3.4 Incremental Curvature Expression Derivation

This section reviews the derivation of the equation for incremental curvature as used in the incremental time-steps procedure implemented in the software *ALCAMBER*. This derivation is again based on the sign convention of Figure 9-1. Beginning with the incremental moment expression of Equation 9-8

$$\Delta M = \int_{A_c} y \Delta f_c dA_c + \sum\left(y_s \Delta f_s A_s\right) + \sum\left(y_p \Delta f_p A_p\right) = 0 \tag{9-8}$$

Substituting the incremental stress expressions of Equation 9-10, 9-11, and 9-12 and neglecting thermal strains;

$$\Delta M = \int_{A_c} y\left(E_c\left(\Delta\varepsilon_c - \Delta\varepsilon_{c,cr} - \Delta\varepsilon_{c,shr}\right)\right)dA_c + \sum\left(\left(E_s \Delta\varepsilon_s\right) y_s A_s\right) + \sum\left(\left(E_p \Delta\varepsilon_p + \Delta f_{p,relax}\right) y_p A_p\right) = 0 \tag{9-27}$$

Substituting the expressions for incremental strain (Equations 9-1, 9-2, 9-3, and 9-14) into Equation 9-27 yields

$$\Delta M = \int_{A_c} \left(E_c \left(\left[\Delta\varepsilon_{cen} + \Delta\phi(y) \right] - \left[\Delta\varepsilon_{cen,creep} + \Delta\phi_{creep}(y) \right] - \Delta\varepsilon_{c,shr} \right) \right) y dA_c + \sum \left(\left(E_s \left[\Delta\varepsilon_{cen} + \Delta\phi(y_s) \right] \right) y_s A_s \right) + \sum \left(\left(E_p \left[\Delta\varepsilon_{cen} + \Delta\phi(y_p) \right] + \Delta f_{p,relax} \right) y_p A_p \right) = 0 \quad (9\text{-}28)$$

Grouping Equation 9-28 into curvature-dependent and curvature-independent terms and simplifying yields

$$\begin{aligned} 0 = {} & \Delta\varepsilon_{cen} E_c \left[\left(\int_{A_c} y dA_c \right) + \frac{E_p}{E_c} \sum y_p A_p + \frac{E_s}{E_c} \sum y_s A_s \right] + \\ & E_c \Delta\phi \left[\left(\int_{A_c} y^2 dA_c \right) + \frac{E_p}{E_c} \sum {y_p}^2 A_p + \frac{E_s}{E_c} \sum {y_s}^2 A_s \right] - \\ & E_c \left[\Delta\varepsilon_{cen,creep} + \Delta\varepsilon_{c,shr} \right] \left[\int_{A_c} y dA_c \right] - E_c \Delta\phi_{cr} \int_{A_c} y^2 dA_c \\ & + \sum \left(y_p A_p \Delta f_{p,relax} \right) \end{aligned} \quad (9\text{-}29)$$

Recognizing that the bracketed portion of the first term is the first moment of area of the transformed section (which is zero) allows this term to be discarded as shown below.

$$\begin{aligned} 0 = {} & E_c \Delta\phi \left[\left(\int_{A_c} y^2 dA_c \right) + \frac{E_p}{E_c} \sum {y_p}^2 A_p + \frac{E_s}{E_c} \sum {y_s}^2 A_s \right] - \\ & E_c \left[\Delta\varepsilon_{cen,creep} + \Delta\varepsilon_{c,shr} \right] \left[\int_{A_c} y dA_c \right] - \\ & E_c \Delta\phi_{cr} \int_{A_c} y^2 dA_c + \sum \left(y_p A_p \Delta f_{p,relax} \right) \end{aligned} \quad (9\text{-}30)$$

The moment of inertia of the transformed section, I_{tr} is

$$I_{tr} = \int_{A_c} y^2 dA_c + n_p \sum {y_p}^2 A_p + n_s \sum {y_s}^2 A_s \quad (9\text{-}31)$$

Simplifying 9-30 accordingly

$$0 = E_c \Delta\phi[I_{tr}] - E_c\left[\Delta\varepsilon_{cen,creep} + \Delta\varepsilon_{c,shr}\right]\left[\int_{A_c} y dA_c\right] - E_c \Delta\phi_{cr} \int_{A_c} y^2 dA_c + \sum\left(y_p A_p \Delta f_{p,relax}\right) \tag{9-32}$$

Combining Equation 9-25 with 9-32 yields

$$0 = E_c \Delta\phi[I_{tr}] - E_c\left[\Delta\varepsilon_{cen,creep} + \Delta\varepsilon_{c,shr}\right]\left[-n_p \sum A_p y_p - n_s \sum A_s y_s\right] - E_c \Delta\phi_{cr} \int_{A_c} y^2 dA_c + \sum\left(y_p A_p \Delta f_{p,relax}\right) \tag{9-33}$$

Next, the only remaining integral term, the second moment of area of concrete about the centroid of the transformed area, $\int_{A_c} y^2 dA_c$, must be evaluated. Solving Equation 9-31 for $\int_{A_c} y^2 dA_c$ yields

$$\int_{A_c} y^2 dA_c = I_{tr} - n_p \sum {y_p}^2 A_p - n_s \sum {y_s}^2 A_s \tag{9-34}$$

Substituting 9-41 into 9-40 and regrouping yields

$$0 = E_c \Delta\phi[I_{tr}] - E_c\left[\Delta\varepsilon_{cen,creep} + \Delta\varepsilon_{c,shr}\right]\left[-n_p \sum A_p y_p - n_s \sum A_s y_s\right] - E_c \Delta\phi_{cr}\left(I_{tr} - \sum n_p {y_p}^2 A_p - \sum n_s {y_s}^2 A_s\right) + \sum\left(y_p A_p \Delta f_{p,relax}\right) \tag{9-35}$$

Further regrouping, a final expression for incremental curvature can be obtained as follows:

$$\Delta\phi = \Delta\phi_{creep}\left[1 - \frac{\left(\left\{n_p \sum A_p {y_p}^2\right\} + \left\{n_s \sum A_s {y_s}^2\right\}\right)}{I_{tr}}\right] - \frac{\left(\Delta\varepsilon_{cen,cr} + \Delta\varepsilon_{c,shr}\right)\left(n_p \sum A_p y_p + n_s \sum A_s y_s\right)}{I_{tr}} - \frac{\frac{1}{E_p} n_p \sum \Delta f_{p,relax} A_p y_p}{I_{tr}} \tag{9-36}$$

In conjunction with the previously derived expression for incremental strain (Equation 9-26), the derived expression for incremental curvature (Equation 9-36) is used in *ALCAMBER* to completely define the incremental strains and curvature at each analysis

cross section for each time step in the analysis, while satisfying equilibrium and compatibility conditions.

9.4 Software Algorithm Description

A brief description of the software algorithm is offered in this section. The *ALCAMBER* software algorithm is divided into four main categories: (1) initial calculations, (2) calculations for each time step and cross section, (3) updated strains and stresses, and (4) incremental and total camber as shown in Figures 9-2 and 9-3. Each of these categories is briefly discussed in this section. For a more complete description of the software algorithm, readers are referred to Isbiliroglu (2014).

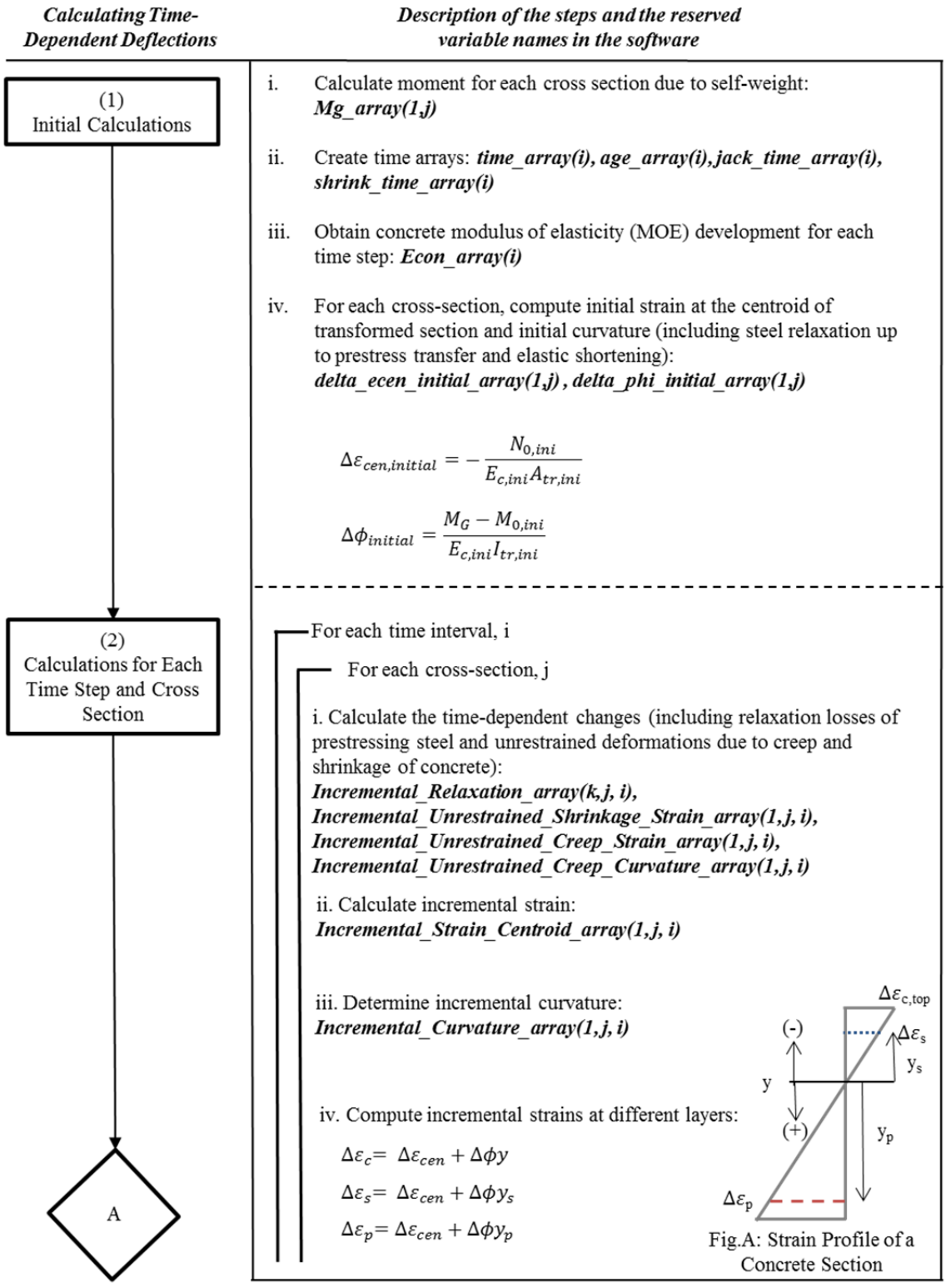

Figure 9-2: *ALCAMBER* Software Program Algorithm – Part 1

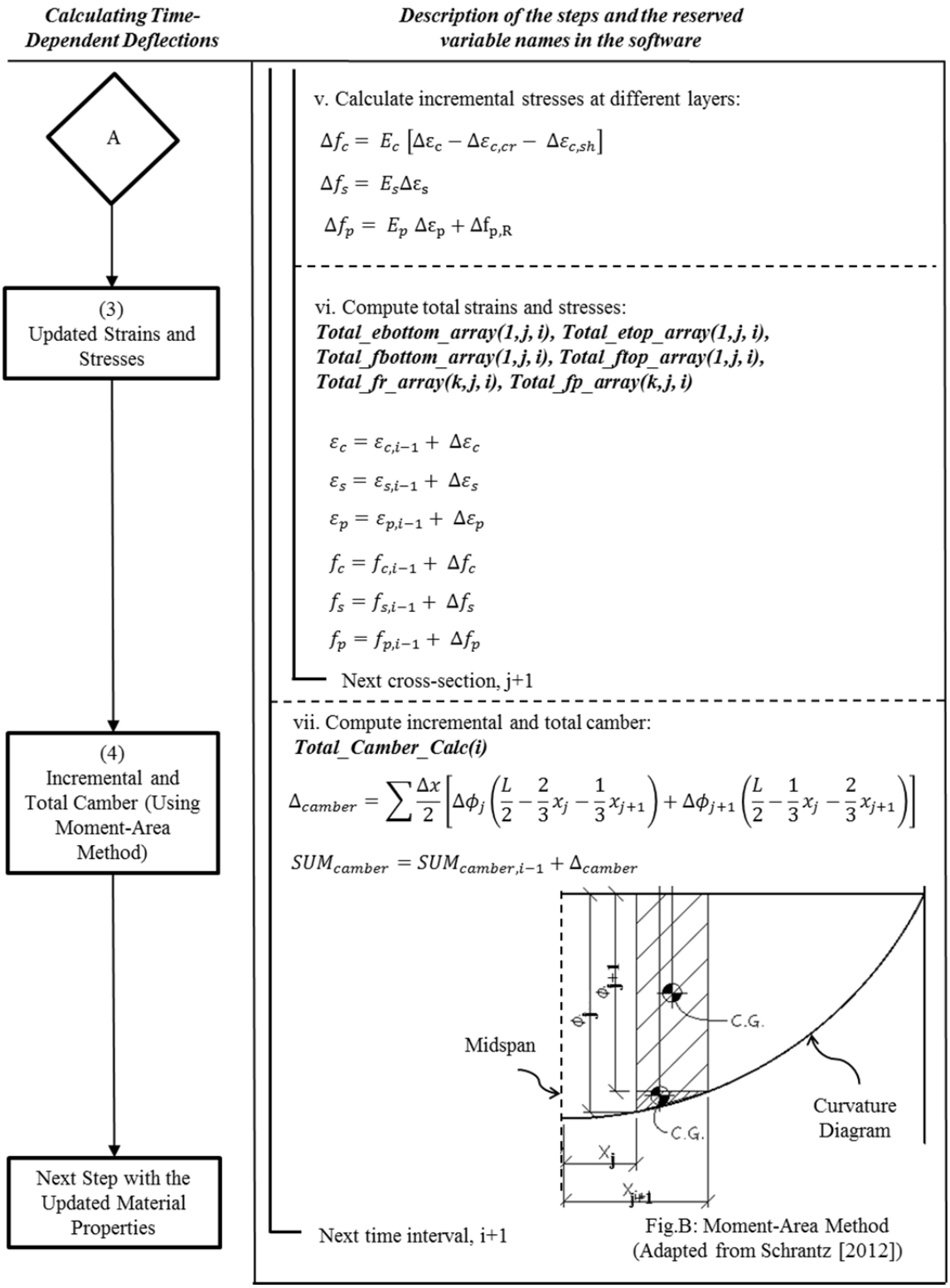

Figure 9-3: *ALCAMBER* Software Program Algorithm – Part 2

9.4.1 Initial Calculations

Prior to beginning the iterations typical of a time-steps analysis, it is first necessary for an analysis starting point to be defined by computing various quantities. First, the moment due to girder self-weight is computed for each cross section. Next, various time indices[5] or arrays are generated to define the progression of time within the program. These time indices are used to represent the chronological timing of construction events, the relative start and analysis end points for time-dependent changes (i.e. creep and shrinkage), and the maturity or equivalent age of concrete (if desired by the user). Next, the concrete modulus of elasticity is computed for each time step in accordance with the user-selected material model. Finally, initial strain and curvature are computed at the centroid of the transformed section at the time of prestress release. These initial strain and curvature computations include the effects of pre-release steel relaxation and elastic shortening. At this point, the initial computations, as necessary to define the starting point for the incremental analysis, are complete.

9.4.2 Calculations for Each Time Step and Cross Section

The next major category of the algorithm defines and executes the various logic loops of the program. As noted in Figure 9-2, there is an outer logic loop (the time loop) and an inner loop (for each cross section). Each of the computations discussed in this paragraph is completed within the inner loop, meaning that these computations are completed for each cross section at each time step. First, the time-dependent losses due to steel relaxation and the time-dependent deformation changes due to unrestrained creep and

[5] Schrantz (2012) details the time array functions utilized within *ALCAMBER* and also contains recommendations for the number of analysis increments and the corresponding effects on prediction accuracy.

shrinkage of concrete are computed. Next, the incremental strain and curvature are computed using the previously derived expressions of Equation 9-26 and 9-36. Using the relationships of Equations 9-1, 9-2, and 9-3, the incremental strains at all locations within a given cross section are next computed. Finally, incremental stresses can be computed for constitutive materials at all layers within a given cross section.

9.4.3 Updated Strains and Stresses

Still within the inner logic loop, the next algorithm category is the computation of updated strains and stresses for each cross section. These updates strains and stresses are computed by adding the incremental change to the strains and stresses associated with a given time step to the values at the end of previous time step. It is critically important to update the strains and stresses at the end of each time step in order to ensure the accuracy of the time-dependent material reflects the new revised stresses over the next time step.

9.4.4 Incremental and Total Camber

The computations of the final category of the software algorithm are located within the outer logic loop (the time loop), but outside of the inner loop (the cross sectional loop). After all cross-sectional analyses are completed within a given time step (e.g. the inner time loop is completed), the fully-defined curvatures allow the use of the moment-area theorems to compute the incremental change in camber occurring across a given time step. By summing the previous incremental changes in camber, the total camber magnitude can be computed for any given age.

9.5 Summary

This chapter details the development of a user-friendly camber prediction software capable of implementing the recommendations of this dissertation with regards to predicting expected concrete strength (Chapter 5), concrete stiffness behavior (Chapter 6), and time-dependent deformational behavior (Chapter 7). Using two key derived relationships, incremental values of centroidal strain and curvature are computed for each analysis cross section for each analysis time step. Using these key parameters, the collective girder deformational response is then defined—allowing predictions of girder camber.

Chapter 10: Selection and Validation of a Revised Camber Prediction Procedure by Limited In-Plant Testing

10.1 Introduction

Previous chapters have focused on systematically addressing inaccuracies intrinsic to the camber prediction problem in precast, prestressed concrete girders. The focus of this chapter is the implementation of the recommendations proposed thus far in this dissertation (with respect to overstrength, modulus of elasticity, creep and shrinkage behavior, and thermal effects) and validation of these recommendations by comparisons to field measurements gathered during and after the production of ALDOT precast, prestressed concrete bridge girders.

10.1.1 Chapter Objectives

The primary objective of this chapter is to validate the effectiveness of various combinations of design recommendations resulting from the experimental work of this study—ultimately in pursuit of a single camber prediction procedure that results in improved predictions during initial girder design. Tasks completed in support of this primary objective include:

- For a variety of prediction trials, compare various metrics of field-observed girder deformation (i.e. camber, curvature, and cross-sectional concrete strains) to predicted girder behavior using different software packages;

- Modify field measurements using the temperature-correction procedure (detailed in Chapter 8) to analytically remove the effect of transient thermal exposure and facilitate appropriate comparisons among measurements;
- Explore the isolated and compounded effects of various design recommendations of previous dissertation chapters; and
- Evaluate the appropriateness of the continued use of the simple multiplier method proposed by Martin (1977) for estimating changes in long-term deflections of Alabama precast, prestressed concrete bridge girders.

10.1.2 Chapter Outline

This chapter begins by detailing an experimental effort conducted on-site at girder production facilities within the study region. Included in the description of the experimental procedure are (1) details of the particular girder production cycles monitored in this study, (2) results of much of the on-site concrete material property testing conducted, and (3) details of techniques utilized to measure girder deformational behavior and internal concrete temperatures. Next, all gathered girder data is first presented unmodified, then subjected to post-processing efforts including (1) computation of concrete equivalent ages at the time of prestress release, (2) verification of the linearity of cross-sectional strain readings, and (3) application of the temperature-correction procedure to remove the effect of transient temperature variations from field measurements. Subsequently, a series of trial camber prediction procedures are implemented and then compared to the measured field responses. Based on these comparisons, the effects of various design recommendations (with respect to concrete overstrength, elastic modulus, and creep and shrinkage) on camber prediction accuracy

are explored and a finalized design procedure is recommended. Finally, the appropriateness of the continued use (or modification) of the PCI multiplier method for predicting time-dependent deformations of Alabama precast, prestressed concrete bridge girders is explored.

10.2 Experimental Program

10.2.1 Summary

In this portion of the study, in-plant testing was conducted for nine girder production cycles, representing a total of twenty-two ALDOT precast, prestressed concrete bridge girders at two production facilities. In-plant testing efforts consisted of (1) measurement of various concrete material properties (e.g. concrete compressive strength and modulus of elasticity) at key ages for various curing conditions, (2) instrumentation of selected girders with internal strain and temperature sensors at the midspan cross section, and (3) measurement of girder camber using the surveying method at various key ages of interest. Using the measured internal concrete temperatures, observed girder camber and internal strain (and curvature) measurements were then corrected to remove the effect of transient thermal effects.

10.2.2 Experimental Procedure

Due to the large number of simultaneous tasks involved in the on-site data gathering performed in this study, this section is divided into three main data collection efforts: (1) concrete material property testing, (2) measurement of girder camber by the surveying method, and (3) measurement of girder strains and temperatures. The experimental work described herein was conducted in parallel with a portion of the efforts discussed in Chapters 6 and 9.

Due to the vital role of concrete material properties in the camber prediction problem, concrete material testing was conducted during nine girder placement events occurring at two regional precast, prestressed concrete girder producers. This included testing concrete compressive strength and concrete elastic modulus in accordance with ASTM C39 and ASTM C469, respectively. The on-site material testing plan is outlined in Figure 10-1 and consisted of sampling 26 6"x12" cylinders for each girder production cycle, exposing these specimens to various curing conditions, and testing at key ages of interest. Additional considerations not explicitly noted in Figure 10-1 include the following:

- Fresh concrete properties, as tested by the girder producer, are also reported in this chapter;
- Field curing of cylinder specimens in this investigation was accomplished by locating cylinders within the girder formwork (between top- and bottom-flange projections) during accelerated curing, and then transferring specimens to preheated, shaded lime-baths exposed to ambient conditions. This method of field-curing cylinders was preferable because (1) it mitigated the rate of heat loss from cylinders upon removal from accelerated curing, thereby avoiding thermal shock, and (2) it avoided exposure of the specimens to direct solar radiation, which can result in artificially elevated temperatures in specimens with volumes substantially less than a girder;
- Hardened property testing consisted of using a cylinder to first conduct elastic modulus testing in accordance with ASTM C469, and then performing compressive strength testing (ASTM C39) on the same cylinder; and

- Concrete maturity, where necessary, was computed using measured internal girder temperatures.

Note:
[a] = Curing tank preheated by exposure to steam prior to insertion of cylinders.
[b] = Hardened testing consists of concrete compressive strength testing and modulus of elasticity testing in accordance with ASTM C39 and ASTM C469, respectively.

Figure 10-1: On-site Concrete Material Testing Procedure

Likely the most critical on-site data collection effort in this study was the measurement of girder camber at various key ages of interest. The procedure for camber measurement, as summarized in Figure 10-2, consisted of the measurement of girder camber by the surveying method. For each girder placement event, metal survey points were installed along the middle of the top flange of each girder during concrete placement in the positions shown in Figure 10-3. Using these permanently anchored points, a two-person team using a surveying instrument and prism rod measured girder camber. Midspan camber was computed as the deviation from a tangent connecting the two outer-most survey points.

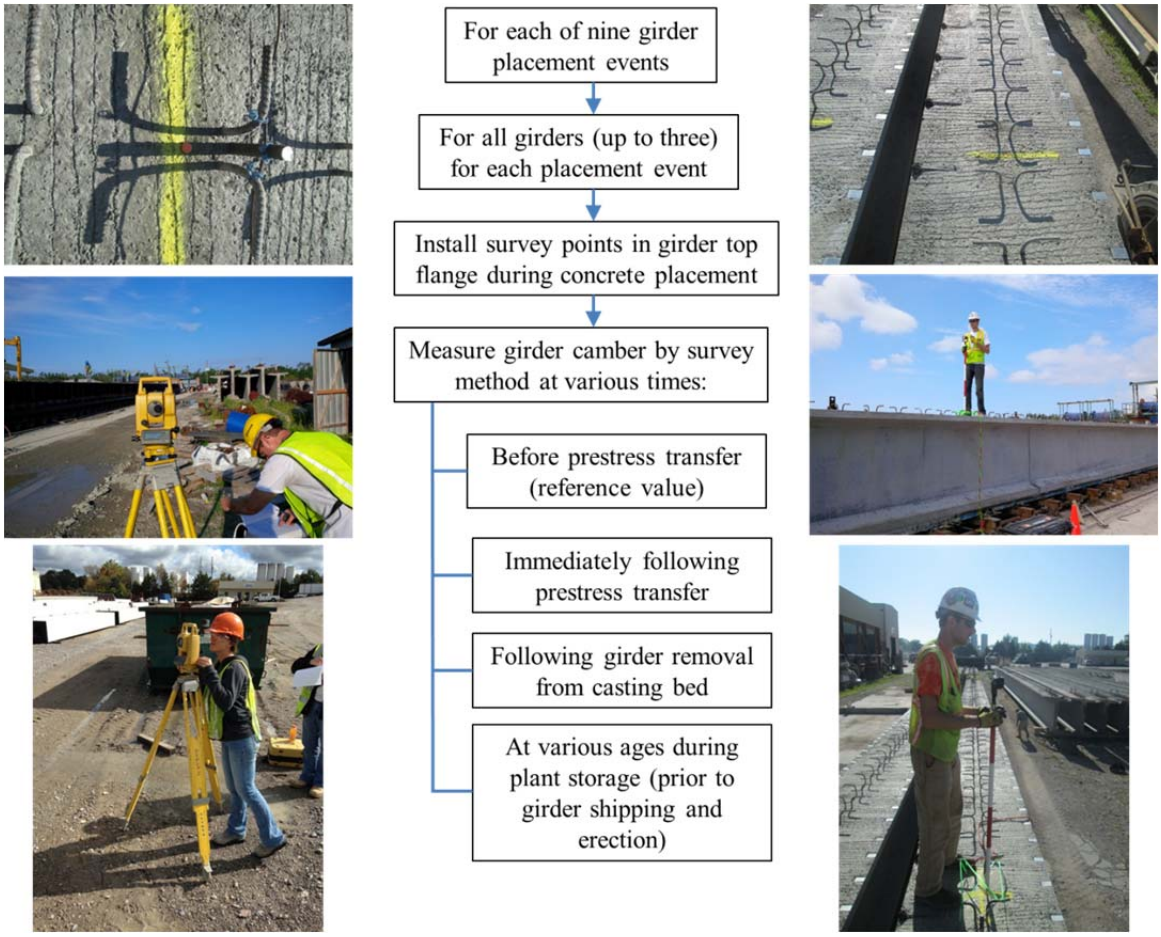

Figure 10-2: Procedure for On-Site Camber Measurement

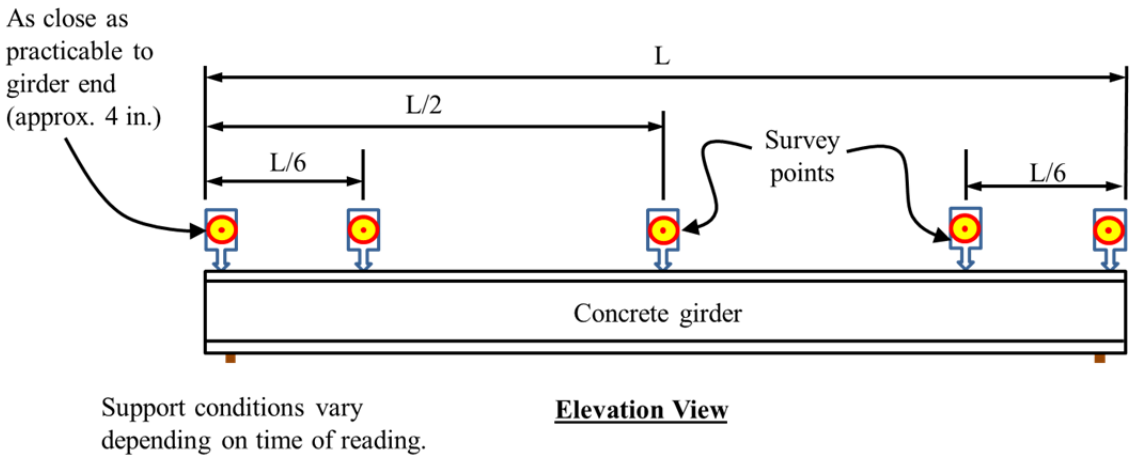

Figure 10-3: Typical Locations of Survey Points along Girder Top Flange

Camber measurements were taken both during the girder production process (to capture instantaneous camber) and also during girder storage (to capture camber growth). To

properly measure camber using the survey method, benchmark measurements must be taken prior to the prestress transfer event. Without these benchmark measurements, it is not possible to differentiate between the portion of elastic camber induced by the effective prestress force and the portion of apparent camber caused by any slope, crown, or other imperfections in the girder top flange concrete.

In order to offer meaningful comparisons among values of camber measured at differing times and ambient conditions, it was necessary to apply the temperature-correction procedure detailed in Chapter 8 of this dissertation to all camber measurements. To perform this correction procedure, internal concrete strains and temperatures were measured at a typical cross section within a representative girder for each concrete placement event. The procedure for monitoring of internal concrete strain and temperatures is summarized in Figure 10-4. During girder production, four vibrating-wire strain gages with thermistors were placed within girder concrete at the midspan cross section in the typical locations shown in Figure 10-5. Then, strains and internal temperatures were monitored continuously during all steps of girder production and also at any time a follow-up measurement of girder camber was recorded. The concrete strain and temperature monitoring work described in this chapter utilized the same data collection system and vibrating-wire strain gage type as discussed in Section 8.3.3.

Figure 10-4: Procedure for On-Site Monitoring of Concrete Strain and Temperature

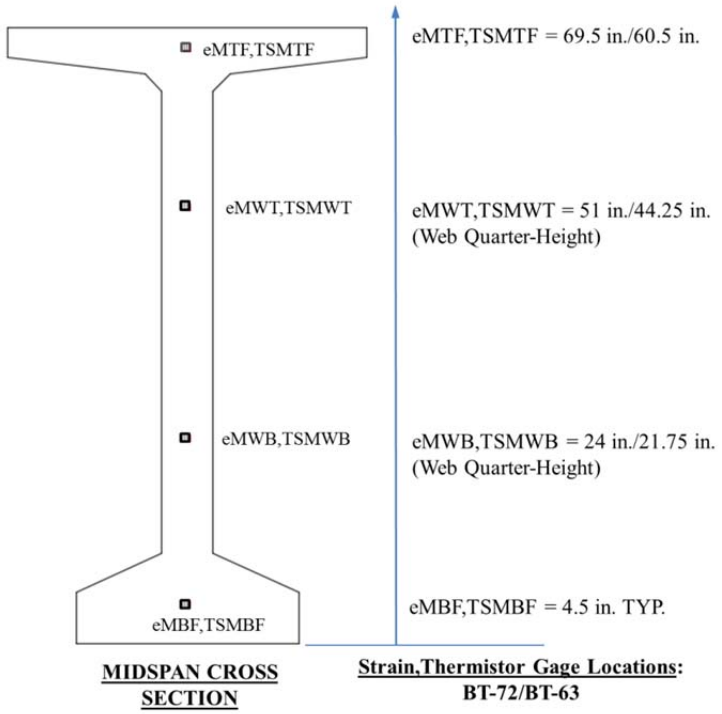

Figure 10-5: Locations of Midspan Concrete Strain and Temperature Sensors

10.2.3 Testing and Girder Details

Nine girder production events were monitored as part of this research effort. Included in this section are (1) general details regarding the girder production events and included girders, (2) timing of critical construction events, (3) girder cross section schematics and prestressing strand details, (4) specified concrete compressive strengths, and (5) concrete mixture designs used.

General details for each of the nine field tests, representing the production of twenty-two precast, prestressed girders, are summarized in Table 10-1. As shown, the girder production events occurred between July, 2013 and September, 2014. Two of the concrete placement events occurred on Mondays (following Friday strand tensioning), while the remainder were standard weekday placement events. There were twelve BT-63 girders and ten BT-72 girders of lengths varying from approximately 1360 in. (113 ft) to 1660 in. (138 ft).

Table 10-1: General Field Testing Information

Field Test ID	Production Date	Girder Cross Section	No. of Girders	Average Girder Length (in.)	Specified Release Strength (psi)	Specified 28-Day Strength (psi)
1[a]	7/8/13	BT-63	3	1357.8	5,600	6,000
2	7/24/13	BT-72	2	1641.0	5,500	7,250
3	7/25/13	BT-72	2	1631.4	5,500	7,250
4[a]	10/7/13	BT-72	2	1659.5	5,500	7,250
5	10/9/13	BT-72	2	1654.6	5,500	7,250
6	10/10/13	BT-72	2	1608.6	5,500	7,250
7	9/23/14	BT-63	3	1537.8	7,000	8,000
8	9/25/14	BT-63	3	1550.5	7,000	8,000
9	9/30/14	BT-63	3	1550.5	7,000	8,000

[a] = Production occurred on Monday following Friday strand tensioning

The timing of various construction events, as recorded by on-site research personnel, is shown in Table 10-2. Where values were not precisely known, estimates were made as noted. There are implicit difficulties encountered when attempting to document the timing of concurrent on-site production events—many with a duration exceeding 1-2 hours. For instance, while the transfer of the prestress force to the concrete occurs over a relatively short time period (approximately 5–30 minutes), the placement of girder concrete occurs gradually over a two hour period, resulting in girders with slightly different ages at the time of prestress release. To address this issue, a best effort was made to estimate average timings of each event and to select typical benchmark events (e.g. concrete placed at midspan gages of instrumented girder) for reporting construction timing.

Table 10-2: Construction Timing for Field Tests

Field Test ID	Age of Strand Tension Prior to Concrete Placement (hours)	Time from Concrete Placement to Prestress Transfer (hours)	Concrete Chronological Age at Prestress Transfer[b] (hours)	Curing Method	Curing Duration[c] (hours)
1	72[a]	42.7	43.0	Moist	40.7
2	24[a]	19.3	19.6	Steam	17.3
3	24[a]	16.1	16.4	Steam	15.1
4	72	19.0	19.3	Steam	17.9
5	24	19.8	20.1	Steam	18.4
6	26	17.7	18.0	Steam	16.4
7	24[a]	20.9	21.2	Steam	18.9
8	24[a]	19.8	20.1	Steam	17.8
9	24[a]	22.2	22.6	Steam	20.2

[a] = Estimated value.
[b] = Concrete mixing time estimated to be 20 minutes prior to placement based on experience.
[c] = Curing duration computed assuming tarp removal 2 hours prior to release unless otherwise documented by on-site researchers.

While the majority of field tests reflect relatively typical plant practices (similar to those reported in Chapter 4), the first production cycle included an abnormally long curing period due to production difficulties encountered by the girder producer. Concrete mixture designs for each girder production cycle, as initially shown in Table 6-3, are reproduced here for reference. Field Test #1 used a mixture similar to the ternary mixture (DL-FA/SF) from the laboratory investigation of Chapters 6 and 7, while the remaining tests used a mixture most similar to the slag SCM mixture (DL-SL) of Chapters 6 and 7. Finally, girder cross sections and prestressing strand details for the three typical girder designers included in this study are shown in Figures 10-6 through 10-8. Included in each figure is the sizing and arrangement of all prestressing strands, strand tensioning details, and strand draping and debonding lengths. For convenience in inputting strand

position into design software, locations of each strand layer are provided relative to the girder bottom.

Table 6-3: Mixture Proportions for On-Site Production Cycles

Field Test ID	Type III Cement (pcy)	Grade 120 Slag Cement (pcy)	Class F Fly Ash (pcy)	Silica Fume (pcy)	Water (pcy)	*w/cm*	Coarse Agg. SSD (pcy)	Fine Agg. SSD (pcy)	*sand/total agg. (volume)*	*total agg. vol. (%)*	*paste vol.* (ft^3/cy)	HRWRA #1 (oz/cwt)	HRWRA #2 (oz/cwt)	HSA (oz/cwt)
Test 1	745	0	135 (14%)	75 (8%)	258	0.27	1,665 (#78 Dolomitic Limestone)	1,085 (#100 River Sand)	0.40	61	9.4	5.25	N/A	1.25
Tests 2-6	751	133 (15%)	0	0	282	0.32	1,861 (#67 Dolomitic Limestone)	1,048 (#100 Natural Sand)	0.37	62	9.1	6.0	4.50	1.0
Tests 7-9	751	133 (15%)	0	0	277	0.31	1,861 (#67 Dolomitic Limestone)	1,048 (#100 Natural Sand)	0.38	63	9.0	9.0	N/A	1.0

Notes:

1. Percent substitutions noted for supplementary cementing materials (SCMs) are by weight of total cementitious materials.
2. Test 1: HRWRA #1 = Glenium 7700 and HSA = Pozzolith 100-XR.
3. Tests 2-6: HRWRA #1 = ADVA Cast 575, HRWRA #2 = ADVA Cast 555, HSA = Recover
4. Tests 7-9: HRWRA #1 = Glenium 7700, HSA = Delvo

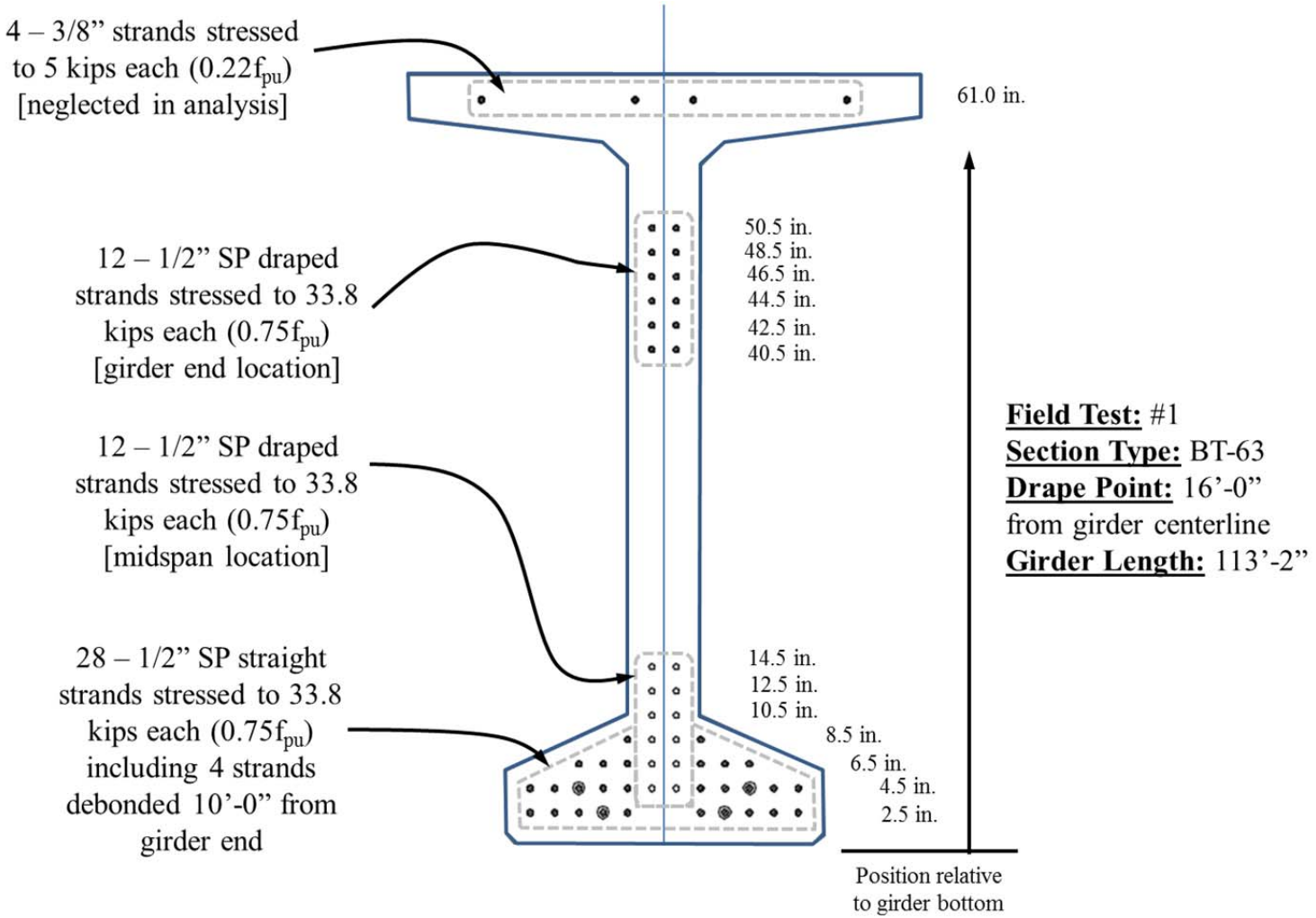

Figure 10-6: Girder and Prestressing Strand Details for Field Test #1

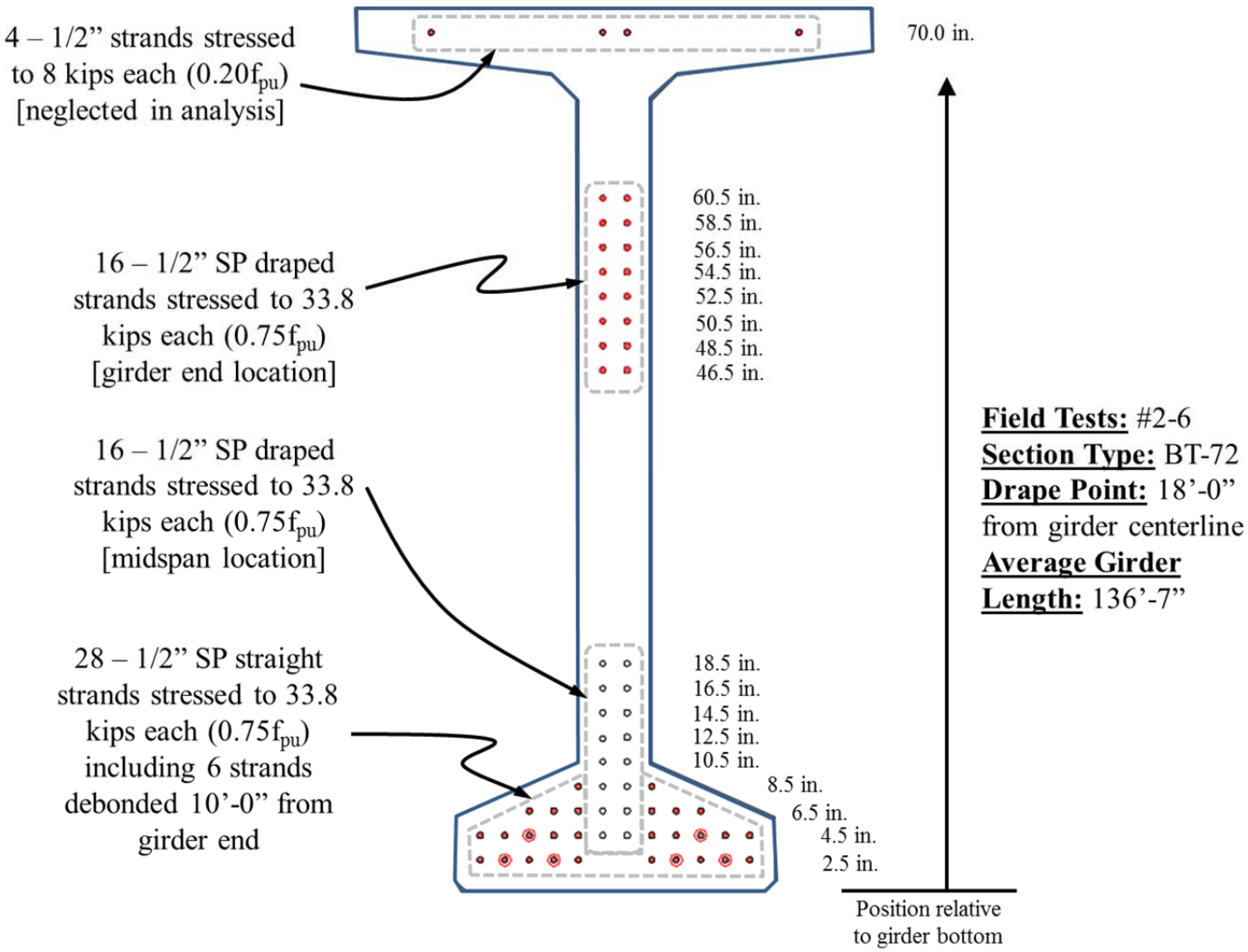

Figure 10-7: Girder and Prestressing Strand Details for Field Tests #2-6

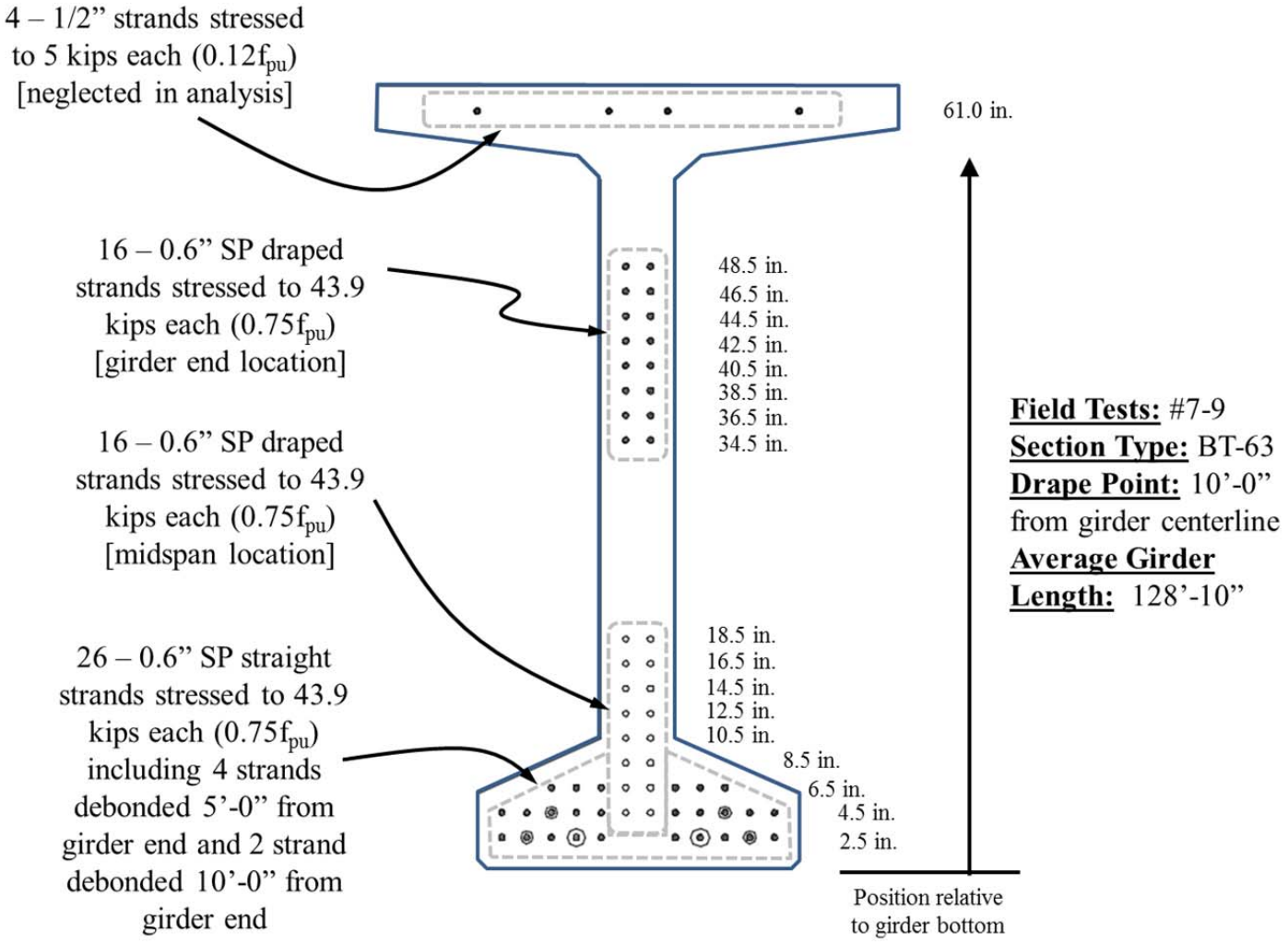

Figure 10-8: Girder and Prestressing Strand Details for Field Tests #7-9

10.3 Presentation and Post-Processing of Raw Field Data

This section begins with results of on-site concrete materials testing including fresh and hardened concrete properties. Next, internal girder temperature data is presented for each field test and computed concrete maturity at the time of prestress release is reported. Then, measured values of girder camber and cross-sectional deformation are presented for each field test. Finally, by applying the temperature-correction procedure previously implemented in Chapter 8, measured camber and cross-sectional deformation parameters are adjusted to values reflecting a standard reference temperature condition to allow for meaningful comparisons to predictions of girder behavior.

10.3.1 Fresh and Hardened Concrete Properties

Fresh concrete properties for each field test, as tested by producer staff and supervised by ALDOT inspectors, are shown in Table 10-3. The fresh properties observed during the on-site data gathering effort were in agreement with the historical observations and general comments offered in Chapter 4 of this dissertation. Producers tend to target the upper limit of allowable slump (9 in.) and the lower allowable limit for air content (2.5 percent).

Table 10-3: Concrete Fresh Properties for Field Tests

Field Test ID	Concrete Temperature, (°F)	Slump (in.)	Air Content, (%)
1	89.5	7.0	3.3
2	88.0	9.0	2.8
3	88.0	8.5	3.3
4	84.0	8.5	2.8
5	82.5	9.0	3.3
6	87.0	8.0	4.2
7	83.0	9.0	2.7
8	86.0	9.0	3.5
9	86.0	8.5	2.7

Note: 1. All readings represent average of two sampling locations

Results of concrete compressive strength and elastic modulus testing for field-cured cylinders are summarized in Table 10-4. Measured compressive strengths for both the time of prestress release and 28 days after production well exceeded specified values. Additionally, as previously discussed in Chapter 4, concretes typical of the precast, prestressed concrete industry within the study region tend to exhibit relatively stiff behavior, with measured elastic moduli mostly greater than 6,000 ksi at transfer.

Table 10-4: Hardened Concrete Properties for Field-Cured Cylinders

Field Test ID	At Prestress Release			At 28 Days		
	Specified Strength, (psi)	Measured Strength (psi)	Measured Elastic Modulus (ksi)	Specified Strength (psi)	Measured Strength (psi)	Measured Elastic Modulus (ksi)
1	5,600	6,770	5,100	6,000	9,420	6,250
2	5,500	8,450	6,700	7,250	11,160	7,650
3	5,500	7,570	5,900	7,250	10,780	7,850
4	5,500	9,280	6,700	7,250	11,040	7,650
5	5,500	8,510	6,500	7,250	10,180	7,200
6	5,500	8,330	6,450	7,250	9,860	6,750
7	7,000	8,300	6,400	8,000	10,960	7,250
8	7,000	8,310	6,350	8,000	10,250	7,500
9	7,000	8,470	6,600	8,000	10,940	7,550

Notes: 1. Strength and modulus testing cylinders field-cured in shaded lime bath.
2. Measured values represent averages of two sampling locations.

The results from the standard-cured cylinders, summarized in Table 10-5, reflect largely similar trends to the field-cured cylinders—although greater 28-day strengths and moduli are attained. The relatively high strengths and stiffnesses obtained during the materials testing portion of this study reflect the properties of the dolomitic limestone coarse aggregate available within the study region. As shown, certain 28-day test results unexpectedly exceeded the 12,000 psi limit for the use of unbonded caps in accordance with ASTM C1231.

Table 10-5: Hardened Concrete Properties for Standard-Cured Cylinders

Field Test ID	At 28 Days		
	Specified Strength (psi)	Measured Strength (psi)	Measured Elastic Modulus (ksi)
1	6,000	10,040	6,500
2	7,250	12,750	8,100
3	7,250	11,990	7,900
4	7,250	12,610	7,900
5	7,250	11,430	7,450
6	7,250	11,710	7,750
7	8,000	12,200	7,800
8	8,000	11,590	7,750
9	8,000	12,410	8,000

Notes: 1. Cylinders cured in temperature-controlled limebath at producer facilities, then transported to AU laboratory and stored in curing room.
2. Measured values represent averages of two sampling locations.

10.3.2 Measured Girder Temperatures and Computed Equivalent Age

In order to compute the equivalent age of girder concrete at the time of prestress release, a complete temperature-history record of the girder concrete is needed beginning at the time of initial concrete mixing. These required temperature records were established using the following procedure:

- The fresh concrete temperature (as reported in Table 10-3) was assumed to extend for a 20-minute period from mixing until the time the concrete was placed in the girder formwork at the midspan of the instrumented girder; and
- The average of the four thermistor measurements (located across the depth at midspan of each instrumented girder) was assumed to be a representative temperature for use in computing concrete maturity for the entire girder.

Complete concrete temperature history plots for each field test are shown in Figure 10-9. Peak average girder temperatures approached, but did not exceed, the ALDOT maximum allowable curing temperature of 160°F. Recall, field test #1 was not steam cured and

included an abnormally long curing period due to difficulties encountered by the girder producer.

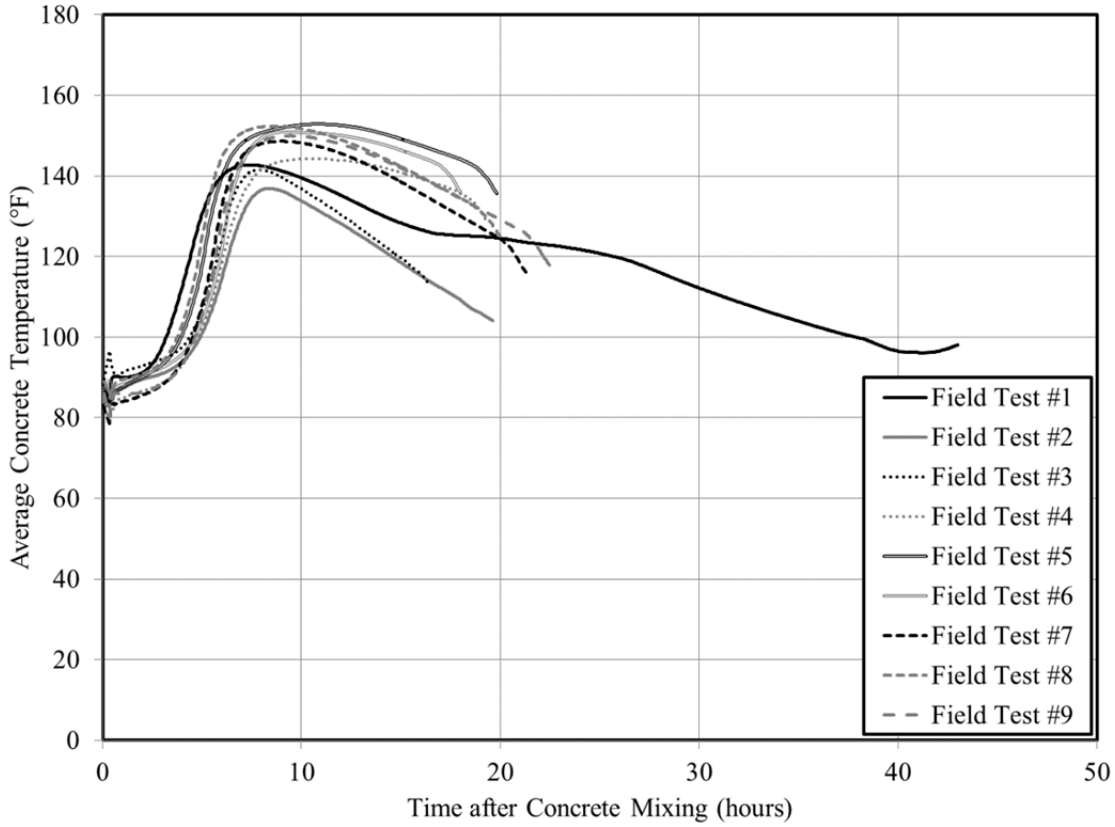

Figure 10-9: Temperature Histories of Girder Concrete

Values from the above-referenced temperature-history plots were used to compute the equivalent age of girder concrete at the time of prestress release yielding results shown in Table 10-6. Recall, for the purposes of camber prediction, equivalent age maturity is only used for the time-dependent portion of the *fib* MC 2010 provisions, as the other time-dependent models rely on chronological concrete age. Accordingly, maturity computations were conducted (similarly to those discussed in Chapter 7) in accordance with the requirements of MC 2010 utilizing a datum temperature of 20°C and an activation energy of 33.2 kJ/mol. The equivalent ages computed here range from 2.4 to 6.0 days and show good agreement with those reported earlier.

Table 10-6: Maturity of Girder Concrete for Field Tests

Field Test ID	Chronological Time from Concrete Placement to Prestress Transfer (hours)	Concrete Chronological Age at Prestress Transfer (hours)	MC2010 Temperature-Adjusted Concrete Age, t_T, at Prestress Transfer[a] (days)	MC2010 Adjusted Equivalent Age at Prestress Transfer[b], t_o (days)
1	42.7	43.0	6.0	11.1
2	19.3	19.6	2.6	7.1
3	16.1	16.4	2.4	6.8
4	19.0	19.3	3.3	8.1
5	19.8	20.1	4.1	9.1
6	17.7	18.0	3.4	8.3
7	20.9	21.2	3.7	8.6
8	19.8	20.1	3.9	8.9
9	22.2	22.6	4.1	9.0

[a] = Computed from datum temperature = 20°C and AE = 33.2 kJ/mol
[b] = Accounting for cement type and curing temperature.

In addition to monitoring temperature during concrete placement for the purpose of computing concrete maturity at the time of prestress release, the experimental plan called for the monitoring of internal girder temperatures each time camber was measured to allow for temperature correction of measured deformations. This practice generated a large amount of data that is presented in its entirety in Appendix K.

10.3.3 Raw Measurements of Girder Deformations

The raw measurements of girder deformations recorded in the field-monitoring portion of this study included midspan camber and midspan concrete strains. Similarly to the temperature data previously mentioned, strain readings were recorded each time camber was measured. Because it is difficult to present the large amount of compiled data in a space-conscious manner, the full raw data set, as directly output from the data collection system is included in Appendix L. All raw strain measurements were well within the measurable range of the sensors utilized in the investigation. Prior to displaying a

condensed tabulated version of the full data set, the data set was processed in a number of ways. First, the manufacturer's gage temperature correction was applied to all recorded strain measurements. Next, strain readings were zeroed to the pre-release survey event to provide a consistent reference for comparison of future measurements to. Then, using the least-squares method of linear fit and relying on the principle that plane sections remain plane, the linearity of measured strain profiles was evaluated for each instrumented girder at the time of maximum induced curvature. Finally, the two key cross-sectional parameters necessary to fully define midspan strains at a given time (strain at the centroid of the section and curvature) were computed.

Girder deformations, as modified by the above procedure, are shown in Tables 10-7 and 10-8. Bottom flange centroid strain readings are intended as an indication of the accuracy of prestress loss computations. The values displayed in Tables 10-7 and 10-8 are referred to as "unadjusted" measurements, as they have yet to be temperature corrected according to the analytical procedures of Chapter 8.

Table 10-7: Measurements of Girder Deformations–Tests 1-5

Field Test ID	Girder No.	Verification of Linearity of Strain Gages[a]	Time After Release (days)	Midspan Camber[b] (in.)	Computed Midspan Curvature[c] ($x10^{-6}$ rad/in.)	Computed Midspan Centroidal Strain[d] (με)	Computed Midspan Bottom Flange Centroidal Strain[d] (με)
1[d]	1	0.99	0.0	2.05	-8.52	-314	-546
			0.1	2.53	-10.05	-323	-598
	2		0.0	2.00	-8.36	-311	-538
			0.1	2.30	-10.11	-322	-599
	3		0.0	1.97	-7.87	-321	-535
			0.1	2.34	-9.62	-334	-596
2	1	0.99	0.0	1.18	-5.76	-285	-487
			0.1	2.04	Data Collection System Malfunction		
			74.0	2.41	-10.70	-845	-1,232
			231.2	2.93	-11.63	-930	-1,358
	2		0.0	0.95	-5.66	-285	-484
			0.1	1.56	Data Collection System Malfunction		
			74.0	2.16	-10.65	-850	-1,236
			145.2	2.65	-11.97	-887	-1,327
			231.2	2.70	-11.58	-936	-1,364
3	1	0.99	0.0	0.79	-4.01	-378	-503
			0.1	1.39	-5.70	-463	-642
			73.2	1.70	-7.61	-999	-1,231
			230.3	2.38	-9.17	-1,108	-1,386
	2		0.0	0.52	-4.07	-383	-510
			0.1	1.12	-5.76	-459	-641
			73.2	1.38	-7.65	-993	-1,226
			230.3	1.94	-9.21	-1,102	-1,382
4	1	0.90	0.0	0.74	-3.68	-345	-441
			0.1	1.19	-5.44	-424	-576
			156.3	2.46	-9.62	-1,030	-1,298
	2		0.0	1.03	-3.89	-346	-449
			0.1	1.51	-5.58	-417	-574
			156.3	3.00	-9.73	-1,018	-1,295
5	1	0.99	0.0	1.09	-3.04	-328	-431
			0.1	1.33	-4.77	-397	-555
			67.1	2.16	-7.05	-1,087	-1,322
			154.2	2.69	-8.58	-1,029	-1,313
	2		0.0	0.98	-3.24	-327	-437
			0.1	1.55	-4.90	-386	-548
			154.2	2.81	-8.69	-1,013	-1,300

[a] = Linearity verification performed for maximum observed curvature for each instrumented girder.
[b] = Positive camber corresponds to upward deflection
[c] = Negative curvature corresponds to concave-down flexure.
[d] = Negative concrete strain corresponds to a relative shortening of girder concrete.

Table 10-8: Measurements of Girder Deformations–Tests 6-9

Field Test ID	Girder No.	Verification of Linearity of Strain Gages	Time After Release (days)	Midspan Camber[a] (in.)	Computed Midspan Curvature[b] ($x10^{-6}$ rad/in.)	Computed Midspan Centroidal Strain[c] (με)	Computed Midspan Bottom Flange Centroidal Strain[c] (με)
6	1	0.99	0.0	1.22	-4.24	-362	-497
			0.1	1.67	-5.61	-434	-612
			153.3	2.70	-8.89	-1,072	-1,342
	2		0.0	1.13	-4.00	-358	-485
			0.1	1.42	-5.50	-445	-620
			153.3	3.10	-8.77	-1,084	-1,350
7[d]	1	0.99	0.0	1.74	-8.24	-458	-678
			0.1	2.39	-10.28	-542	-818
			43.0	3.07	-14.34	-1,020	-1,408
			82.1	3.14	-14.71	-1,144	-1,544
	2		0.0	1.76	-8.64	-465	-696
			0.1	2.10	-10.41	-537	-816
			43.0	2.93	-14.42	-1,010	-1,400
			82.2	3.13	-14.94	-1,130	-1,536
	3		0.0	1.92	-8.77	-450	-685
			0.1	2.34	-10.56	-524	-808
			43.0	3.14	-14.55	-996	-1,390
			82.2	3.38	-15.14	-1,114	-1,525
8[d]	1	0.99	0.0	2.00	-7.96	-458	-664
			0.1	2.59	-9.26	-518	-759
			41.1	3.62	-13.07	-1,047	-1,388
			80.2	3.80	-13.33	-1,076	-1,428
	2		0.0	2.11	-8.24	-459	-672
			0.1	2.38	-9.42	-512	-757
			41.1	3.42	-13.20	-1,037	-1,382
			80.2	3.74	-13.49	-1,064	-1,420
	3		0.0	2.03	-8.50	-458	-679
			0.1	2.38	-9.56	-504	-754
			41.1	3.54	-13.33	-1,028	-1,377
			80.2	3.95	-13.62	-1,053	-1,413
9[d]	1	0.99	0.0	1.86	-7.21	-484	-680
			0.1	2.47	-9.27	-553	-804
			36.1	3.68	-14.10	-1,059	-1,434
			75.3	3.79	-15.00	-1,121	-1,527
	2		0.0	1.72	-7.54	-500	-704
			0.1	2.36	-9.41	-542	-798
			36.1	3.26	-14.23	-1,043	-1,422
			75.3	3.55	-15.08	-1,110	-1,518
	3		0.0	1.24	-7.52	-479	-683
			0.1	1.96	-9.53	-532	-791
			36.1	2.88	-14.33	-1,031	-1,413

Note: Subscript definitions provided in Table 10-7 apply here also.

The following summarizing remarks are offered as a result of the review of the data presented in Tables 10-7 and 10-8:

- Several girders (Field Tests #1, 7, 8, and 9) shipped without notice prior to final measurement of pre-shipping camber;
- The linearity of midspan strain gages installed in each test was good to excellent with values ranging from 0.90 to 0.99—suggesting that gages remained in intended locations and were largely undisturbed by concrete placement activities; and
- The longest period of camber measurement included in this study was 231 days after the prestress transfer event.

10.3.4 Temperature Correction of Field-Measured Values

Using the recorded internal temperatures and measurements of girder deformations discussed in the preceding two sections, the temperature-correction procedure described in Chapter 8 was used to adjust measured values to reflect a standard uniform vertical temperature profile of 20°C. Recall, as shown in Figure 10-10, the temperature-correction procedure consists of two governing equations (Equation 8-17 and 8-25, reproduced below) that jointly define changes in girder cross-sectional centroidal strain and curvature attributed to a given change in vertical temperature profile.

$$\Delta\varepsilon_0 = \frac{\alpha_T}{A}\int_y \left(\Delta T(y)\right) w(y)\,dy \tag{8-17}$$

$$\Delta\phi = \frac{\alpha_T}{I}\int_y \left(\Delta T(y)\cdot y\cdot w(y)\right) dy \tag{8-25}$$

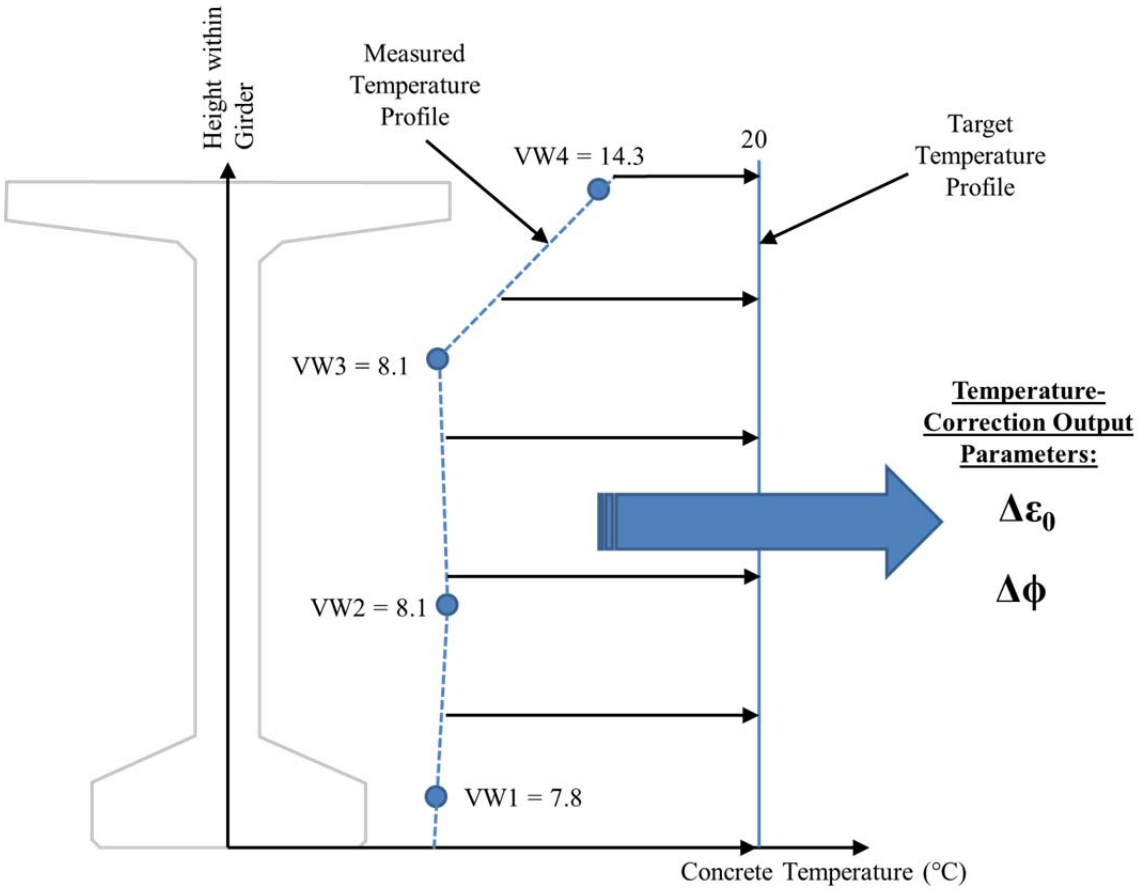

Figure 10-10: Temperature Correction of Field-Measured Girder Deformation Parameters

For the temperature correction performed in this section, the following analytical assumptions and procedures (in agreement with the recommendations of Chapter 8) were used:

- An effective CTE value of 13.0 με /°C was assumed;
- A piecewise-exact cross-sectional shape definition was assumed; and
- Linear interpolation between adjacent temperature measurements was used to define the vertical temperature profile.

Final values of temperature-corrected girder deformations are displayed in Tables 10-9 and 10-10. Where measurements of internal concrete strains and temperatures were not

available due to data collection system malfunction (e.g. Field Test #2, t=0.1 hours), missing values were estimated using the following procedure: (1) the ratio of each deformation metric (e.g. camber, curvature, bottom flange strain, or centroidal strain) was computed for other similar field tests between adjacent ages (0 and 0.1 days), and (2) the average of the computed ratios was used to modify the intact reading (t=0 hours) to estimate the missed reading (t=0.1 hours). The magnitude of the temperature-corrected values observed here are in agreement with those expected by the previous analyses conducted in Chapter 8 of this dissertation.

Table 10-9: Temperature-Corrected Measurements of Girder Deformations–Tests 1-5

Field Test ID	Girder No.	Time After Release (days)	Midspan Camber (in.)	Computed Midspan Curvature (x10^{-6} rad/in.)	Computed Midspan Centroidal Strain (με)	Computed Midspan Bottom Flange Centroidal Strain (με)
1	1	0.0	1.89	-7.82	-332	-544
		0.1	2.27	-8.90	-358	-602
	2	0.0	1.84	-7.67	-327	-536
		0.1	2.03	-8.90	-359	-602
	3	0.0	1.76	-6.98	-338	-527
		0.1	2.01	-8.21	-371	-595
2	1	0.0	1.17	-5.74	-273	-474
		0.1[a]	2.03	-8.33	-290	-559
		74.0	2.39	-10.60	-537	-923
		231.2	2.82	-11.30	-519	-937
	2	0.0	0.94	-5.64	-268	-466
		0.1[a]	1.55	-8.18	-286	-550
		74.0	2.14	-10.60	-536	-921
		145.2	2.17	-10.60	-503	-897
		231.2	2.59	-11.30	-518	-935
3	1	0.0	0.86	-4.22	-354	-485
		0.1	1.53	-6.11	-387	-579
		73.2	2.03	-8.60	-632	-895
		230.3	2.32	-9.01	-616	-890
	2	0.0	0.58	-4.27	-361	-494
		0.1	1.22	-6.09	-389	-580
		73.2	1.68	-8.54	-634	-895
		230.3	1.86	-8.97	-618	-890
4	1	0.0	0.85	-3.99	-310	-415
		0.1	1.35	-5.91	-330	-496
		156.3	1.91	-8.03	-432	-654
	2	0.0	1.12	-4.15	-314	-425
		0.1	1.64	-5.96	-329	-498
		156.3	2.44	-8.10	-431	-655
5	1	0.0	1.19	-3.34	-297	-410
		0.1	1.50	-5.27	-324	-498
		67.1	1.99	-6.55	-330	-549
		154.2	2.20	-7.16	-376	-615
	2	0.0	1.04	-3.41	-307	-422
		0.1	1.66	-5.23	-324	-497
		154.2	2.24	-7.04	-378	-612

Note: A coefficient of thermal expansion of 13.0 με /°C was used in the temperature-correction procedure as determined in the analysis of Chapter 8.

[a] = For analysis purposes, missed values were estimated from similar field tests.

Table 10-10: Temperature-Corrected Measurements of Girder Deformations–Tests 6-9

Field Test ID	Girder No.	Time After Release (days)	Midspan Camber (in.)	Computed Midspan Curvature (x10^{-6} rad/in.)	Computed Midspan Centroidal Strain (με)	Computed Midspan Bottom Flange Centroidal Strain (με)
6	1	0.0	1.31	-4.49	-337	-480
		0.1	1.86	-6.19	-356	-554
		153.3	2.46	-8.14	-441	-687
	2	0.0	1.23	-4.31	-327	-465
		0.1	1.65	-6.21	-356	-554
		153.3	2.91	-8.19	-440	-687
7	1	0.0	1.89	-8.74	-407	-641
		0.1	2.56	-10.90	-435	-726
		43.0	3.01	-14.10	-574	-956
		82.1	3.18	-14.80	-572	-975
	2	0.0	1.88	-9.04	-418	-660
		0.1	2.22	-10.80	-435	-726
		43.0	2.83	-14.10	-575	-955
		82.2	3.07	-14.70	-574	-973
	3	0.0	1.98	-8.97	-422	-662
		0.1	2.40	-10.80	-438	-727
		43.0	2.99	-14.00	-578	-957
		82.2	3.24	-14.60	-577	-975
8	1	0.0	2.14	-8.41	-410	-628
		0.1	2.81	-9.97	-428	-688
		41.1	3.70	-13.30	-551	-899
		80.2	3.89	-13.60	-545	-905
	2	0.0	2.23	-8.62	-417	-640
		0.1	2.56	-10.00	-429	-691
		41.1	3.46	-13.30	-552	-901
		80.2	3.79	-13.60	-548	-908
	3	0.0	2.12	-8.81	-422	-652
		0.1	2.52	-10.00	-431	-694
		41.1	3.55	-13.30	-554	-904
		80.2	3.95	-13.60	-551	-912
9	1	0.0	2.00	-7.67	-435	-643
		0.1	2.66	-9.89	-459	-727
		36.1	3.54	-13.60	-623	-985
		75.3	3.62	-14.40	-651	-1,040
	2	0.0	1.84	-7.95	-448	-664
		0.1	2.49	-9.84	-461	-728
		36.1	3.05	-13.50	-625	-984
		75.3	3.34	-14.40	-653	-1,040
	3	0.0	1.30	-7.74	-448	-658
		0.1	2.03	-9.79	-465	-731
		36.1	2.61	-13.40	-629	-986

Note: A coefficient of thermal expansion of 13.0 με /°C was used in the temperature-correction procedure.

Percent differences between temperature-corrected data (Tables 10-9 and 10-10) and unadjusted measured data (Tables 10-7 and 10-8) for each time of measurement are displayed in Tables 10-11 and 10-12. The denominator in the percent differences computed below is the temperature-corrected value—meaning the percent differences indicate the variation that would remain unaccounted for if a temperature correction was not performed.

Table 10-11: Percent Difference of Temperature-Corrected Girder Deformations– Tests 1-5

Field Test ID	Girder No.	Time After Release (days)	Change in Midspan Camber (%)	Change in Midspan Curvature (%)	Change in Midspan Centroidal Strain (%)	Change in Midspan Bottom Flange Centroidal Strain (%)
1	1	0.0	8.5	9.0	-5.4	0.4
		0.1	11.5	12.9	-9.8	-0.7
	2	0.0	8.7	9.0	-4.9	0.4
		0.1	13.3	13.6	-10.3	-0.5
	3	0.0	11.9	12.8	-5.0	1.5
		0.1	16.4	17.2	-10.0	0.2
2	1	0.0	0.9	0.3	4.4	2.7
		0.1	0.5	Initial Readings Unavailable		
		74.0	0.8	0.9	57.4	33.5
		231.2	3.9	2.9	79.2	44.9
	2	0.0	1.1	0.4	6.3	3.9
		0.1	0.6	Initial Readings Unavailable		
		74.0	0.9	0.5	58.6	34.2
		145.2	22.1	12.9	76.3	47.9
		231.2	4.2	2.5	80.7	45.9
3	1	0.0	-8.1	-5.0	6.8	3.7
		0.1	-9.2	-6.7	19.6	10.9
		73.2	-16.3	-11.5	58.1	37.5
		230.3	2.6	1.8	79.9	55.7
	2	0.0	-10.3	-4.7	6.1	3.2
		0.1	-8.2	-5.4	18.0	10.5
		73.2	-17.9	-10.4	56.6	37.0
		230.3	4.3	2.7	78.3	55.3
4	1	0.0	-12.9	-7.8	11.3	6.3
		0.1	-11.9	-8.0	28.5	16.1
		156.3	28.8	19.8	138.4	98.5
	2	0.0	-8.0	-6.3	10.2	5.6
		0.1	-7.9	-6.4	26.7	15.3
		156.3	23.0	20.1	136.2	97.7
5	1	0.0	-8.4	-9.0	10.4	5.1
		0.1	-11.3	-9.5	22.5	11.4
		67.1	8.5	7.6	229.4	140.8
		154.2	22.3	19.8	173.7	113.5
	2	0.0	-5.8	-5.0	6.5	3.6
		0.1	-6.6	-6.3	19.1	10.3
		154.2	25.4	23.4	168.0	112.4

Table 10-12: Percent Difference of Temperature-Corrected Girder Deformations Tests–6-9

Field Test ID	Girder No.	Time After Release (days)	Change in Midspan Camber (%)	Change in Midspan Curvature (%)	Change in Midspan Centroidal Strain (%)	Change in Midspan Bottom Flange Centroidal Strain (%)
6	1	0.0	-6.9	-5.6	7.4	3.5
		0.1	-10.2	-9.4	21.9	10.5
		153.3	9.8	9.2	143.1	95.3
	2	0.0	-8.1	-7.2	9.5	4.3
		0.1	-13.9	-11.4	25.0	11.9
		153.3	6.5	7.1	146.4	96.5
7	1	0.0	-7.9	-5.7	12.5	5.8
		0.1	-6.6	-5.7	24.6	12.7
		43.0	2.0	1.7	77.7	47.3
		82.1	-1.3	-0.6	100.0	58.4
	2	0.0	-6.4	-4.4	11.2	5.5
		0.1	-5.4	-3.6	23.4	12.4
		43.0	3.5	2.3	75.7	46.6
		82.2	2.0	1.6	96.9	57.9
	3	0.0	-3.0	-2.2	6.6	3.5
		0.1	-2.5	-2.2	19.6	11.1
		43.0	5.0	3.9	72.3	45.2
		82.2	4.3	3.7	93.1	56.4
8	1	0.0	-6.5	-5.4	11.7	5.7
		0.1	-7.8	-7.1	21.0	10.3
		41.1	-2.2	-1.7	90.0	54.4
		80.2	-2.3	-2.0	97.4	57.8
	2	0.0	-5.4	-4.4	10.1	5.0
		0.1	-7.0	-5.8	19.3	9.6
		41.1	-1.2	-0.8	87.9	53.4
		80.2	-1.3	-0.8	94.2	56.4
	3	0.0	-4.2	-3.5	8.5	4.1
		0.1	-5.6	-4.4	16.9	8.6
		41.1	-0.3	0.2	85.6	52.3
		80.2	0.0	0.1	91.1	54.9
9	1	0.0	-7.0	-6.0	11.3	5.8
		0.1	-7.1	-6.3	20.5	10.6
		36.1	4.0	3.7	70.0	45.6
		75.3	4.7	4.2	72.2	46.8
	2	0.0	-6.5	-5.2	11.6	6.0
		0.1	-5.2	-4.4	17.6	9.6
		36.1	6.9	5.4	66.9	44.5
		75.3	6.3	4.7	70.0	46.0
	3	0.0	-4.6	-2.8	6.9	3.8
		0.1	-3.4	-2.7	14.4	8.2
		36.1	10.3	6.9	63.9	43.3

As shown, the largest percent differences (in magnitude) are observed in midspan strains (up to 229 percent), while corresponding temperature-induced changes to camber and midspan curvature tended to be significantly less—approaching maximum percent differences of 30 and 25 percent, respectively.

10.4 Comparison of Field Measurements to Design Prediction Trials

This section focuses primarily on comparisons among various trial camber prediction procedures and temperature-corrected measured field results for considered deformation metrics. First, the analytical procedure—including various trial camber prediction procedures utilized in this investigation—is presented and described in Section 10.4.1. Next, a summary of any relevant material model inputs used within prediction trials is provided. Finally, relevant comparisons are made for each prediction trial for four key midspan parameters of girder deformation (camber, curvature, centroidal strain, and bottom flange strain) to identify the isolated and compounded (combined) effects of varying camber prediction practices.

10.4.1 Analytical Procedure and Details

Trial camber prediction procedures, as utilized in this research effort, are labelled in accordance with the notation of Figure 10-11. The full list of considered trial prediction procedures—accompanied by an outline of the analytical logic implemented herein—is shown in Figure 10-12. The various trial camber prediction procedures considered in this chapter were selected (1) to identify a best prediction procedure for use in ALDOT girder design, and (2) to evaluate the relative effects of varying assumptions (e.g. analysis method, concrete compressive strength, elastic modulus, and creep and shrinkage) on camber prediction accuracy.

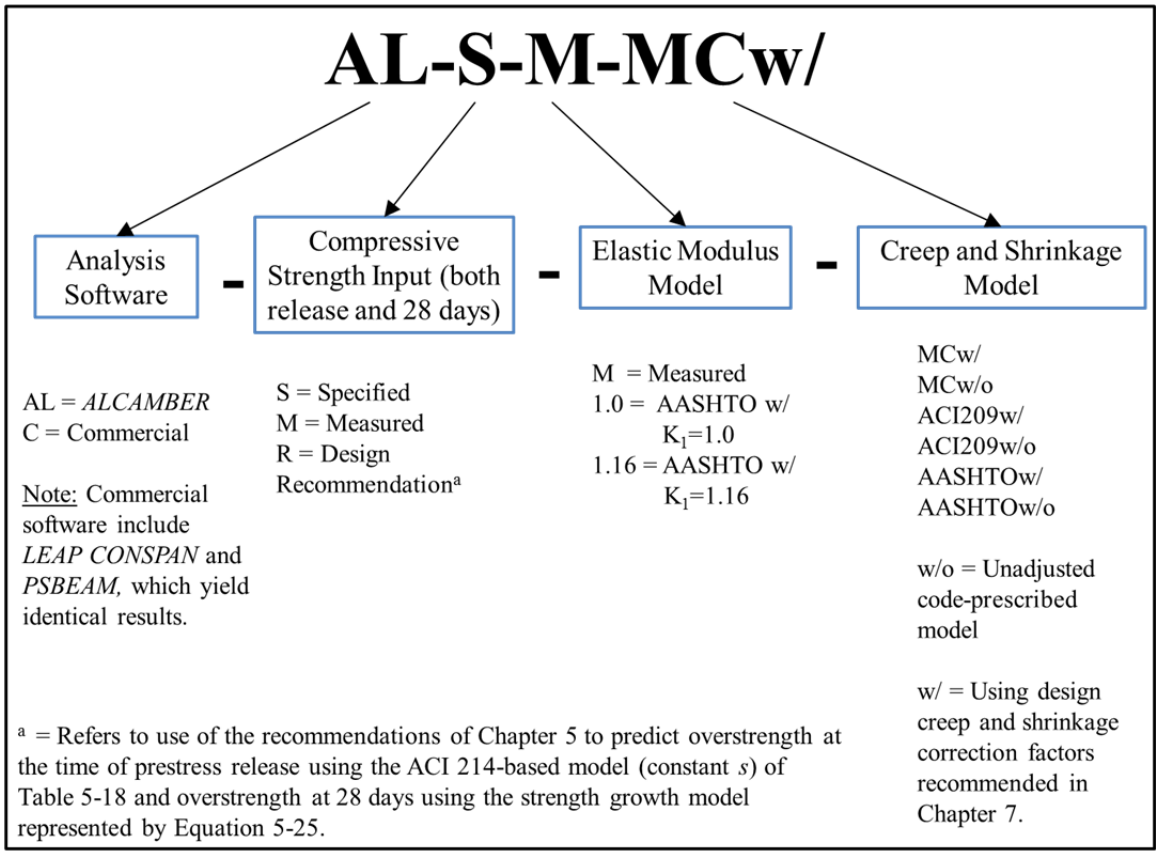

Figure 10-11: Trial Camber Prediction Procedure Labelling Notation

Step 1: Generate best predictions of girder deformations using measured on-site data and three calibrated creep and shrinkage models.

AL-M-M-MCw/ **AL-M-M-ACI209w/** **AL-M-M-AASHTOw/**

Step 2: Compare above predictions to measured deformations to determine *best overall prediction procedure* (including best time-dependent model[a]), to provide benchmark for comparison to subsequent trial procedures–likely **AL-M-M-MCw/**.

Step 3: Generate predictions of girder deformations using measured on-site data and three *uncalibrated* creep and shrinkage models to isolate effect of calibration of models.

AL-M-M-MCw/o **AL-M-M-ACI209w/o** **AL-M-M-AASHTOw/o**

Step 4: Generate predictions of girder deformations necessary to isolate effect of various elastic modulus predictions [on predominately instantaneous deformations].

AL-M-1.16-MCw/ **AL-M-1.0-MCw/**

Step 5: Generate predictions of girder deformations necessary to isolate effect of various compressive strength predictions.

AL-S-M-MCw/ **AL-R-M-MCw/**

Step 6: Generate predictions of deformations [using trial procedures] to capture the compounded (combined) effects of selected changes in compressive strength, elastic modulus, and time-dependent models prediction practices–relative to the previously selected benchmark procedure (likely **AL-M-M-MCw/**).

AL-S-1.16-MCw/	Captures effect of various compressive strength and elastic modulus prediction practices [on both instantaneous and time-dependent behavior].
AL-S-1.0-MCw/	
AL-R-1.16-MCw/	Likely design recommendation.
AL-S-1.0-AASHTOw/o	Most similar to current design practice.

Step 7: Using commercial software, generate predictions of initial deformations to capture the compounded effects of selected changes in compressive strength, elastic modulus, and time-dependent models prediction practices.

C-R-1.16	Using recommended estimate of overstrength and aggregate stiffness modifier.
C-S-1.16	Using only aggregate stiffness modifier.
C-S-1.0	Current design practice.

[a] = MC2010w/ assumed as most accurate time-dependent model for illustration purposes.

Figure 10-12: Analysis Procedure and Trial Prediction Procedures

Predictions of girder deformations (e.g. midspan camber, curvature, bottom flange strain, and centroidal strain) were generated for 17 trial prediction procedures for each of nine field tests using a combination of the following design software programs: *ALCAMBER*, *LEAP CONSPAN*, or *PSBEAM.*

In order to compare the accuracy of predicted girder deformations to observed field behavior for each trial prediction procedure, a standard metric of prediction accuracy is required. Where the standard error of the estimate, *SEE*, was used in previous chapters for similar purposes, the standard error of the estimate fails to indicate if predictions tend to fall above or below the observed response. For this reason, the metric of percent difference from observed values was selected as the preferred metric of prediction procedure accuracy—computed as follows for each time of field measurement:

$$\%Diff = \left[\frac{D_{predicted} - D_{observed}}{D_{observed}} \right] * 100 \qquad (10\text{-}1)$$

where

$D_{predicted}$ = the predicted response of a selected deflection metric (e.g. camber, curvature, bottom flange strain, or centroidal strain) for a given trial prediction procedure; and

$D_{observed}$ = the observed response (either measured or computed from measurements) of the same deflection metric considered above.

A positive percent difference computed in accordance with Equation 10-1 indicates an overprediction of a given parameter.

A final analytical assumption was necessary to facilitate comparisons between predicted and observed early life girder deformations. Recall, in this study, midspan deformation measurements (e.g. camber and concrete strains) were recorded immediately

after prestress release (on the prestressing bed), and shortly thereafter, following girder relocation to a finishing station. For the comparisons of this chapter, the first deformation reading is taken as the average of the reading taken on the prestressing bed and the subsequent reading after girder relocation. It is assumed that by virtue of (1) initial readings likely underestimating deformations due to friction with the prestressing bed (as noted by Rosa et al. [2007]) and (2) readings taken after girder relocation likely overestimating deformations due to the inclusion of a portion of early-age creep and shrinkage deformations, these opposing trends largely cancel and provide a consistent indicator of initial girder deformations.

10.4.2 Prediction Model Summary of Inputs

Various inputs and details regarding the implementation of code-prescribed models are displayed in Tables 10-13 through 10-15. Collectively, the data contained in these tables (and referenced previous tables) represent all input data necessary to generate camber predictions for each trial prediction procedure.

Table 10-13: Elastic Modulus Model Summary of Inputs

AASHTO 2014	
Input	***Justification***
$K_1 = 1.16$	Recommendation of Ch. 6
Concrete unit weight = 150 pcf	In accordance with ALDOT standard practice and current design practice review of Ch. 4
Strength growth development (where necessary) = Backcalculated using ACI 209R-92 formulation by Isbiliroglu[a] (2014)	Yields most accurate prediction of elastic modulus growth at release and 28 days

[a] = Isbiliroglu (2014) derived a function within the *ALCAMBER* software to backcalculate the concrete strength growth curve based on known concrete strengths at two times (typically prestress release and 28 days after production).

Table 10-14: Creep Prediction Model Summary of Inputs

AASHTO 2014		ACI 209		Model Code 2010	
Input	***Justification***	***Input***	***Justification***	***Input***	***Justification***
Relative humidity = 70 percent	AASHTO / ALDOT Recommendation	Relative humidity = 70 percent	AASHTO / ALDOT Recommendation	Relative humidity = 70 percent	AASHTO / ALDOT Recommendation
Volume-to-surface ratio = 3.01 in.	Computed by girder geometry (same for BT-54, BT-63, and BT-72)	Volume-to-surface ratio = 3.01 in.	Computed by girder geometry (same for BT-54, BT-63, and BT-72)	Notional size = 6.02 mm.	Computed per MC 2010 provisions
Chronological age at loading	Table 10-2	Slump = 0.5 in.	Assumed pre-admixture slump in agreement with Keske (2014) and Ellis (2012)	MC2010 concrete maturity at loading, t_t [a]	Table 10-6
Compressive strength at loading	Table 10-4	Sand-to-aggregate weight ratio	Computed from Table 6-3	28-day measured compressive strength	Table 10-4
Creep coefficient correction factor = 1.00	Recommendations of Ch. 7 (for unknown mixture compositions)	Cement factor	Assumed total powder content, Table 6-3	Rapid-hardening high-strength cement assumed	Per Keske (2014) and recommendations of ACI 209 (2008).
		Air content	Table 10-3	Creep coefficient correction factor = 0.80	Recommendations of Ch. 7 (for unknown mixture compositions)
		Creep coefficient correction factor = 1.15	Recommendations of Ch. 7 (for unknown mixture compositions)		

[a] = The *ALCAMBER* software computes the MC2010 cement- and temperature-adjusted age, t_o, based on (1) input of concrete maturity, t_t, and (2) selection of cement properties.

Table 10-15: Shrinkage Prediction Model Summary of Inputs

AASHTO 2014		ACI 209		Model Code 2010	
Input	***Justification***	***Input***	***Justification***	***Input***	***Justification***
Relative humidity = 70 percent	AASHTO / ALDOT Recommendation	Relative humidity = 70 percent	AASHTO / ALDOT Recommendation	Relative humidity = 70 percent	AASHTO / ALDOT Recommendation
Volume-to-surface ratio for cylinder = 3.01 in.	Computed by girder geometry (same for BT-54, BT-63, and BT-72)	Volume-to-surface ratio = 3.01 in.	Computed by girder geometry (same for BT-54, BT-63, and BT-72)	Notional size =6.02 mm	Computed per MC 2010 provisions
Chronological age at loading	Table 10-2	Slump = 0.5 in.	Assumed pre-admixture slump in agreement with Keske (2014) and Ellis (2012)	28-day measured compressive strength	Table 10-4
Compressive strength at loading	Table 10-4	Sand-to-aggregate weight ratio	Computed from Table 6-3	MC2010 concrete maturity at loading, t_t [a]	Table 10-6
Shrinkage correction factor = 0.80	Recommendations of Ch. 7 (for unknown mixture compositions)	Cement factor	Assumed total powder content, Table 6-3	Rapid-hardening high-strength cement assumed	Per Keske (2014) and recommendations of ACI 209 (2008).
		Air content	Table 10-3	Concrete age at beginning of drying for cylinders	Table 10-2
		Shrinkage correction factor = 0.75	Recommendations of Ch. 7 (for unknown mixture compositions)	Shrinkage correction factor = 0.70	Recommendations of Ch. 7 (for unknown mixture compositions)

[a] = The *ALCAMBER* software computes the MC2010 cement- and temperature-adjusted age, t_o, based on (1) input of concrete maturity, t_t, and (2) selection of cement properties.

10.4.3 Estimate of Girder Deformations Using Measured Material Properties and Calibrated Time-Dependent Models

It is logical to assume that the most accurate predictions of girder deflections will result from use of measured concrete compressive strength, elastic modulus, and creep and shrinkage behavior. In this section, results of on-site material testing and calibrated laboratory creep and shrinkage models (representative of girder concretes) are used to generate predictions of girder deformations. The focus of the analyses of this chapter remains predominately on midspan camber—although average percent differences (from observed) for midspan curvature, bottom flange strain, and centroidal strain are also reported. Percent differences from observed midspan camber (averaged for up to three girders in a single field test and measurement time) are shown for the three most comprehensive prediction trials in Figure 10-13.

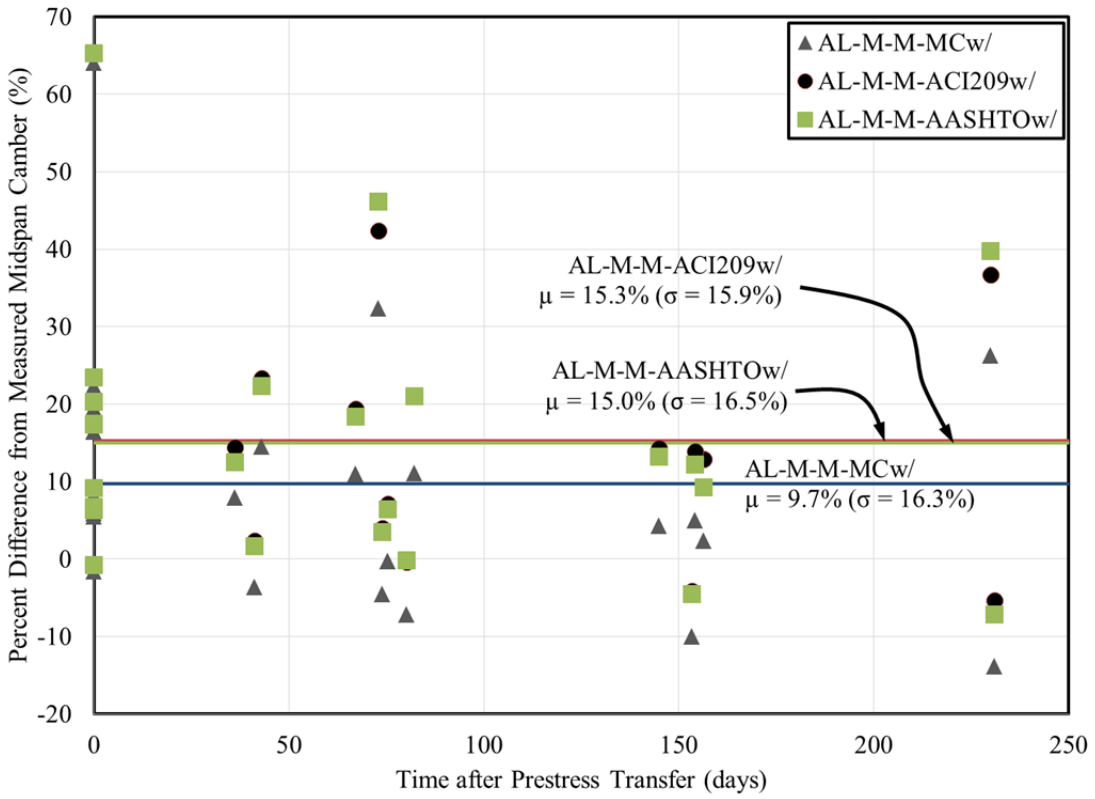

Figure 10-13: Accuracy of Girder Camber Predictions for Selected Trial Procedures

Averages and standard deviations (of percent difference) are also shown on the plot for each prediction trial. Use of the calibrated MC2010 creep and shrinkage model with measured material properties (AL-M-M-MCw/) yielded the overall most accurate prediction of camber—averaging 9.7 percent greater than measured for the girder production cycles monitored in this study. Use of the calibrated AASHTO and ACI 209 creep and shrinkage models yielded somewhat less accurate results—tending to overestimate camber, on average, by approximately 15 percent. Similar average summary statistics are shown in Table 10-16 for other considered metrics of deformation including midspan (a) curvature, (b) bottom flange strain, and (c) centroidal strain.

Table 10-16: Accuracy of Deflection Predictions for Selected Prediction Trials

Trial Prediction Procedure	Percent Difference from Measured Values for All Midspan Measurements (%)							
	Camber		Curvature		Bottom Flange Strain		Centroidal Strain	
	μ	σ	μ	σ	μ	σ	μ	σ
AL-M-M-MCw/	+9.7	+16.3	-12.7	+12.8	+5.5	+16.1	+16.9	+24.6
AL-M-M-ACI209w/	+15.3	+15.9	-8.2	+12.1	+0.1	+14.9	+5.5	+20.7
AL-M-M-AASHTOw/	+15.0	+16.5	-8.7	+12.3	+8.3	+19.9	+19.0	+30.6

Predictions of midspan bottom flange strains tended to be the most accurate of any predicted deformation metric for all considered prediction trials, with lesser levels of accuracy observed for midspan curvatures and centroidal strains. The largest variability in results (as represented by the standard deviation) was observed in centroidal strain comparisons. Where most metrics tended to be overpredicted (e.g. camber, and cross-sectional strains), curvature tended to be underpredicted. For the remainder of this analysis, the most accurate of the above prediction trials (AL-M-M-MCw/) is used for comparison to subsequent prediction trials implementing varying levels of approximations of measured materials properties.

10.4.4 Effect of Calibration of Time-Dependent Models on Prediction Accuracy

To isolate the influence of the calibration of creep and shrinkage models on prediction accuracy for the metrics of deformation considered in this study, prediction trials similar to those discussed in Section 10.4.3 were generated, except omitting creep and shrinkage correction factors. Results for both calibrated and uncalibrated prediction trials for each of the three creep and shrinkage models considered in this study are shown in Figures 10-14 through 10-17.

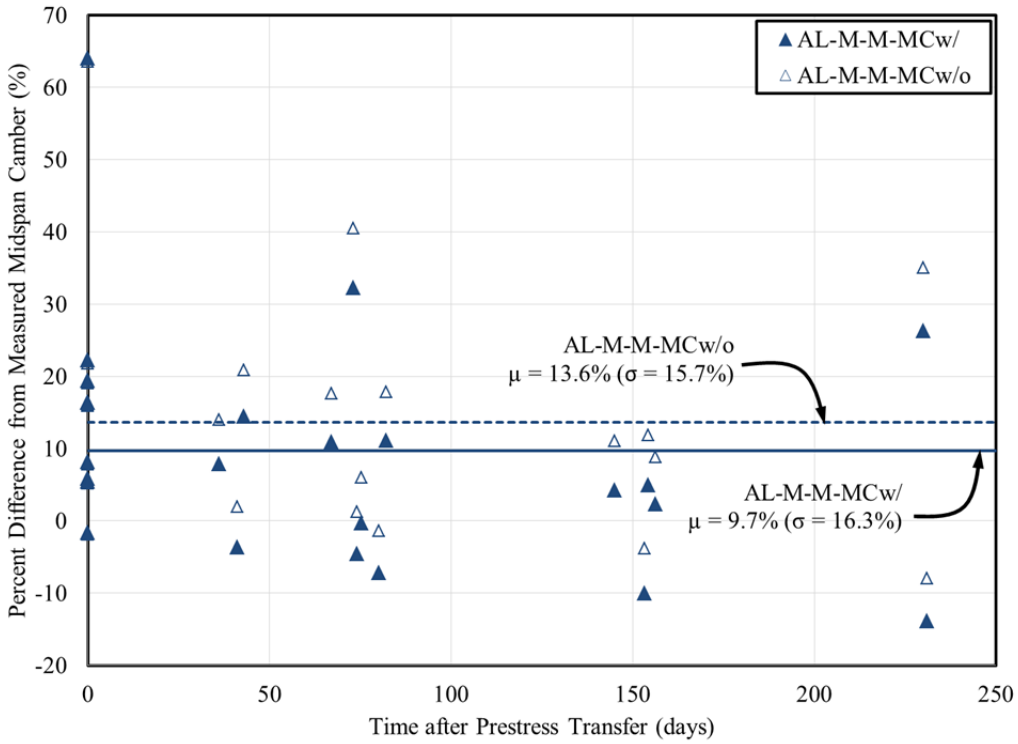

Figure 10-14: Effect of Calibration of MC2010 Creep and Shrinkage Models on Prediction Accuracy

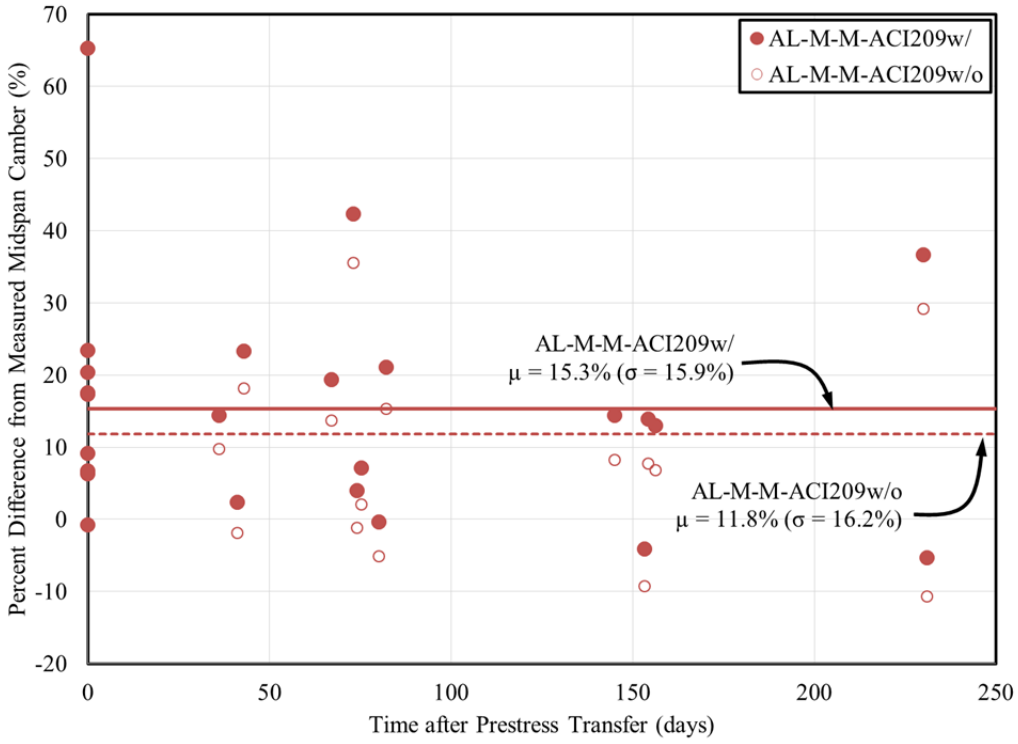

Figure 10-15: Effect of Calibration of ACI 209 Creep and Shrinkage Models on Prediction Accuracy

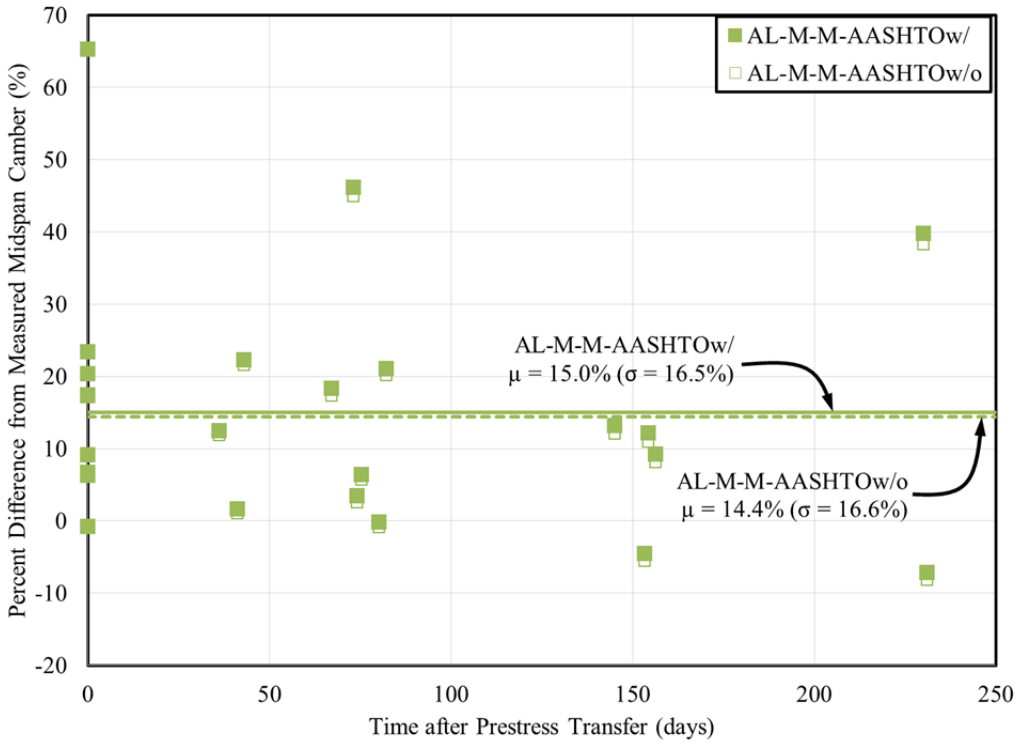

Figure 10-16: Effect of Calibration of AASHTO Creep and Shrinkage Models on Prediction Accuracy

Calibration of the MC2010 creep and shrinkage model tended to increase the accuracy of camber predictions by, on average, approximately 4 percent, while calibration of the ACI 209 creep and shrinkage models tended to reduce camber prediction accuracy by approximately 3.5 percent for the production cycles monitored in this study. Use of the calibrated AASHTO creep and shrinkage models tended to have little effect when compared to use of the uncalibrated models. Average percent differences for other metrics of deformation for the three prediction trials included in this section are summarized in Table 10-17.

Table 10-17: Effect of Calibration of Creep and Shrinkage Models on Deflection Prediction Accuracy

Trial Prediction Procedure	Percent Difference from Measured Values for All Midspan Measurements (%)							
	Camber		Curvature		Bottom Flange Strain		Centroidal Strain	
	μ	σ	μ	σ	μ	σ	μ	σ
AL-M-M-MCw/	+9.7	+16.3	-12.7	+12.8	+5.5	+16.1	+16.9	+24.6
AL-M-M-MCw/o	+13.6	+15.7	-9.8	+12.3	+15.9	+21.8	+31.9	+33.8
AL-M-M-ACI209w/	+15.3	+15.9	-8.2	+12.1	+0.1	+14.9	+5.5	+20.7
AL-M-M-ACI209w/o	+11.8	+16.2	-10.9	+12.4	-1.5	+14.1	+4.6	+20.3
AL-M-M-AASHTOw/	+15.0	+16.5	-8.7	+12.3	+8.3	+19.9	+19.0	+30.6
AL-M-M-AASHTOw/o	+14.4	+16.6	-9.2	+12.3	+11.1	+22.0	+23.9	+34.5

In the above analysis, the differences observed between similar prediction trials reflect differences in only time-dependent behavior, because the initial predictions of girder deformations (at prestress release) remain unaffected by choice of time-dependent model.

10.4.5 Effect of Varying Elastic Modulus Assumptions on Prediction Accuracy

The next series of prediction trials enables investigation of the influence of varying approximations of elastic modulus—independent of approximations in concrete strength or time-dependent behavior. Percent differences from observed midspan camber are shown in Figure 10-17, with summary statistics for other metrics of deformation displayed in Table 10-18.

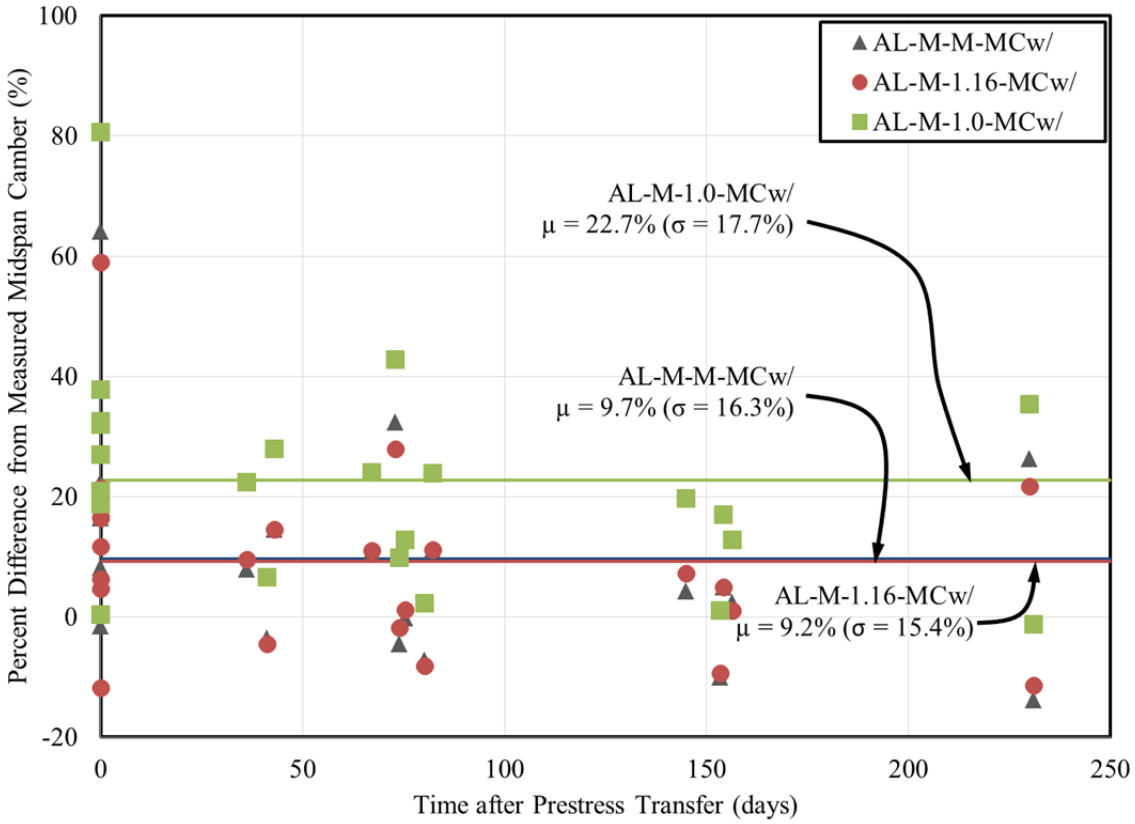

Figure 10-17: Effect of Varying Modulus Assumptions on Camber Prediction Accuracy

Table 10-18: Effect of Varying Modulus Assumptions on Deflection Prediction Accuracy

Trial Prediction Procedure	Percent Difference from Measured Values for All Midspan Measurements (%)							
	Camber		Curvature		Bottom Flange Strain		Centroidal Strain	
	μ	σ	μ	σ	μ	σ	μ	σ
AL-M-M-MCw/	+9.7	+16.3	-12.7	+12.8	+5.5	+16.1	+16.9	+24.6
AL-M-1.16-MCw/	+9.2	+15.4	-13.2	+11.7	+5.1	+15.9	+16.6	+25.0
AL-M-1.0-MCw/	+22.7	+17.7	-2.8	+13.6	+17.2	+16.9	+29.8	+26.6

As shown in Figure 10-17, the computation of elastic modulus with a K_1 factor of 1.16 (using measured strength) yielded results nearly identical to use of measured elastic modulus. Computation of elastic modulus with a K_1 factor of 1.0 (using measured strength) yielded camber predictions that were, on average, 13 percent greater than the most accurate predictions of camber (AL-M-M-MCw/).

10.4.6 Effect of Varying Strength Assumptions on Prediction Accuracy

To explore the effect of varying approximations of concrete compressive strength independent of approximations of elastic modulus, three additional prediction trials were generated. In these cases, changes to the concrete compressive strength tended to only influence the time-dependent deformation predictions due to the inclusion of concrete strength in various creep and shrinkage models. Percent differences for camber predictions for each of the three prediction trials are shown in Figure 10-18, with summary results for other metrics of deformation shown in Table 10-19.

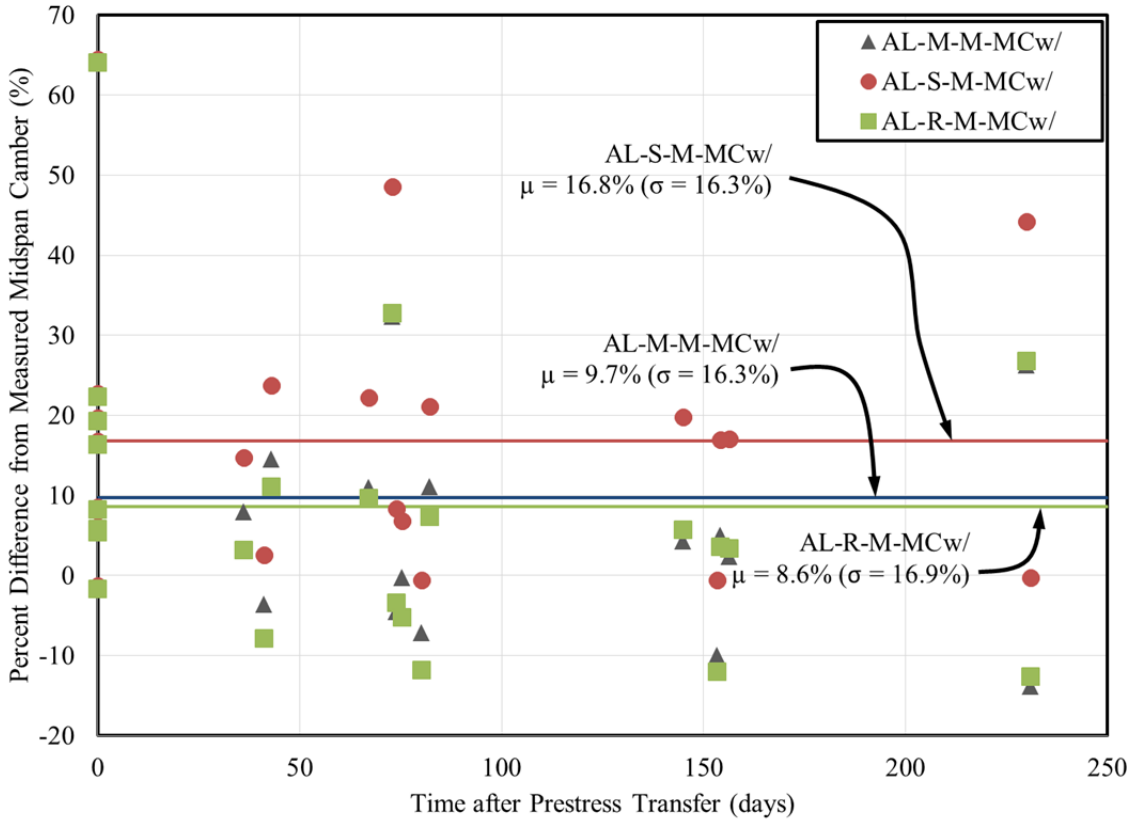

Figure 10-18: Effect of Varying Concrete Strength Assumptions on Camber Prediction Accuracy

Table 10-19: Effect of Varying Concrete Strength Assumptions on Deflection Prediction Accuracy

Trial Prediction Procedure	Percent Difference from Measured Values for All Midspan Measurements (%)							
	Camber		Curvature		Bottom Flange Strain		Centroidal Strain	
	μ	σ	μ	σ	μ	σ	μ	σ
AL-M-M-MCw/	+9.7	+16.3	-12.7	+12.8	+5.5	+16.1	+16.9	+24.6
AL-S-M-MCw/	+16.8	+16.3	-7.3	+11.6	+11.2	+20.4	+22.9	+30.8
AL-R-M-MCw/	+8.6	+16.9	-13.7	+12.5	+4.7	+15.6	+16.2	+24.0

Use of the overstrength recommendations of Chapter 5 in Trial AL-R-M-MCw/ yielded predictions with accuracy similar to those of the overall most accurate prediction trial (AL-M-M-MCw/), while use of specified concrete strengths in prediction trials corresponded to roughly double the percent difference of the overall most accurate prediction trial of this study.

10.4.7 Effects of Selected Compounded Errors Using *ALCAMBER* Software

Where previous sections of this analysis focused on uncoupled (isolated) effects of various approximations of concrete strength, elastic modulus, and creep and shrinkage, this section explores the effect of selected combinations of these approximations. The first two combinations (AL-S-1.16-MCw/ and AL-S-1.0-MCw/) enable investigation of prediction errors associated with approximations of both concrete strength and elastic modulus, while the latter two combinations (AL-R-1.16-MCw/ and AL-S-1.0-AASHTOw/o) correspond to potential and current camber prediction procedures, respectively. Percent differences for camber predictions for each prediction trial are shown in Figure 10-19.

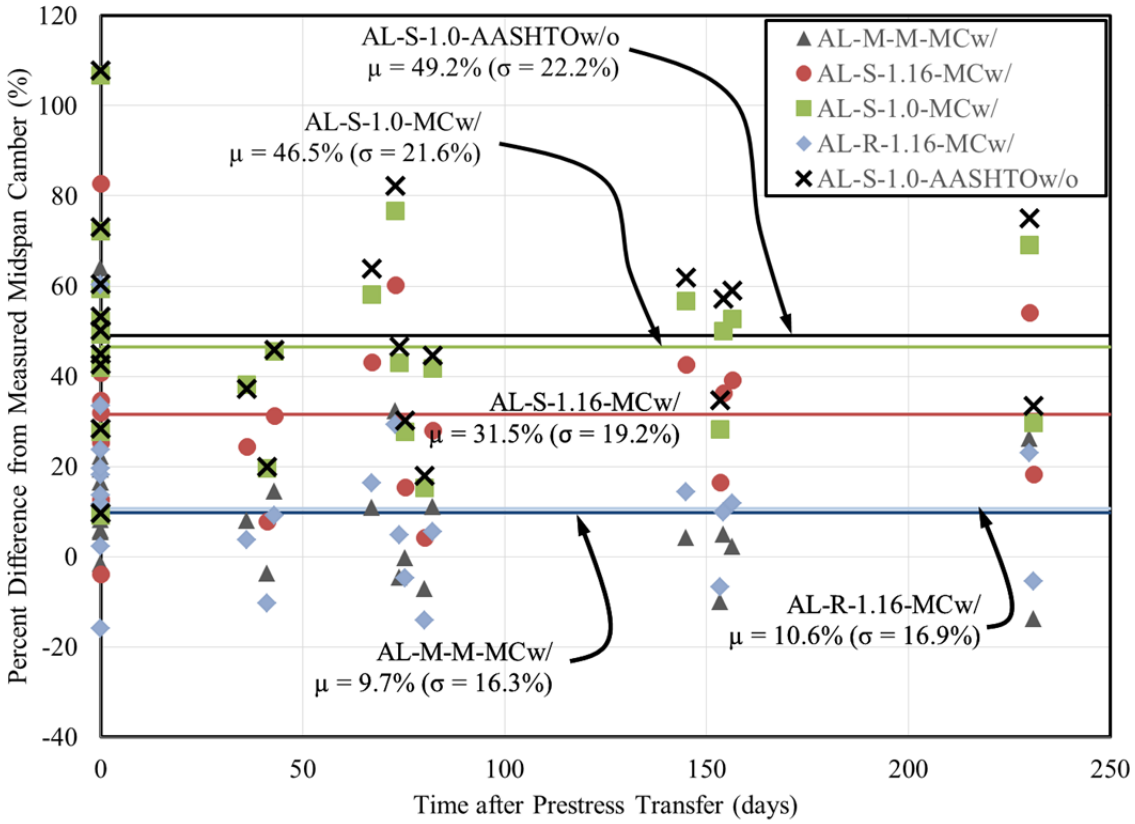

Figure 10-19: Effect of Selected Compounded Approximations on Camber Prediction Accuracy

As shown, the use of specified concrete strength (a lower bound value) with a recommended approximation of elastic modulus (K_1 = 1.16) yields predictions roughly 22 percent less accurate than the best trial procedure (AL-M-M-MCw/) in this study. Use of specified strength and an unadjusted approximation of elastic modulus (K_1 = 1.0), regardless of the choice of time-dependent model, yields camber predictions that are, on average, 40 percent less accurate than best predictions of girder camber. Finally, use of (a) the overstrength recommendations of Chapter 5, (b) a recommended approximation of elastic modulus (K_1 = 1.16), and (c) a calibrated MC2010 time-dependent model yields camber prediction accuracy approximately identical to the best predictions of camber observed in this study. For reference, tabular results for average percent difference for camber and other metrics of girder deformation are displayed in Table 10-20.

Table 10-20: Effect of Selected Compounded Approximations on Deflection Prediction Accuracy Using *ALCAMBER*

Trial Prediction Procedure	Percent Difference from Measured Values for All Midspan Measurements (%)							
	Camber		Curvature		Bottom Flange Strain		Centroidal Strain	
	μ	σ	μ	σ	μ	σ	μ	σ
AL-M-M-MCw/	+9.7	+16.3	-12.7	+12.8	+5.5	+16.1	+16.9	+24.6
AL-S-1.16-MCw/	+31.5	+19.2	+3.5	+12.4	+25.0	+24.6	+38.7	+37.6
AL-S-1.0-MCw/	+46.5	+21.6	+14.9	+14.2	+39.1	+26.0	+54.5	+40.1
AL-R-1.16-MCw/	+10.6	+16.9	-12.4	+11.6	+6.5	+17.4	+18.5	+27.1
AL-S-1.0-AASHTOw/o	+49.2	+22.2	+16.7	+14.6	+49.2	+37.3	+69.8	+58.4

10.4.8 Effects of Selected Compounded Errors on Initial Camber Prediction Using Commercial Design Software

The previous analyses of this section utilized the *ALCAMBER* analysis software to generate predictions of girder deformations at various ages up to an assumed age of girder erection (250 days). This section details a similar limited analysis performed using *LEAP CONSPAN* and *PSBEAM* to explore the effect of various assumptions of concrete strength and elastic modulus on camber prediction accuracy. The comparisons of this section are focused exclusively on *camber* prediction at the time of prestress release because these commercial software programs (a) output only a single time-dependent camber prediction at an approximate age between 30–60 days after production,

and (b) do not directly output other metrics of deformations (e.g. curvature or internal concrete strains). Average summary statistics for the percent difference from measured midspan camber for the three trial prediction procedures included in this analysis are shown in Table 10-21.

Table 10-21: Effect of Selected Compounded Errors on Camber Prediction Accuracy using Commercial Software

Trial Prediction Procedure	Percent Difference from Measured Values for Initial Midspan Camber Measurements (%)	
	μ	σ
C-R-1.16	+25.6	+23.8
C-S-1.16	+41.4	+27.8
C-S-1.0 [Current Practice]	+68.3	+42.7

As shown, the current practice of using specified concrete strength and an unmodified elastic modulus equation ($K_1 = 1.0$) tended to overpredict initial camber by approximately 68 percent when using commercial design software. The use of a recommended elastic modulus equation ($K_1 = 1.16$) tended to reduce the magnitude of the overestimate by 27 percent, while use of both the recommended elastic modulus equation and the Chapter 5 overstrength recommendations tended to reduce the magnitude of the overestimate by 43 percent—to a net overprediction of 25 percent when compared to the field measurements of camber included in this study.

10.5 Design Recommendations

In the above analysis, it is evident that most accurate predictions of girder camber are furnished when using measured material properties for a given production cycle (e.g. concrete compressive strength and elastic modulus) and laboratory calibrated creep and shrinkage models. However, at the time of girder design, these measured properties are not yet available. As an alternative, the trial prediction procedure AL-R-1.16-MCw/ incorporates the design recommendations of Chapters 5, 6, and 7 of this dissertation to predict expected material properties and yields camber predictions nearly as accurate as those computed using measured material properties. For this reason, the trial prediction procedure AL-R-1.16-MCw/, as summarized in Table 10-22, is proposed for use during initial girder design.

Table 10-22: Proposed Camber Prediction Procedure (AL-R-1.16-MCw/) for ALDOT Girder Design

Material Property	**Recommendation**	**Equation(s)**
Concrete Compressive Strength	Estimate expected concrete strength at release, f_{ci}^{*}, using the ACI 214-based overstrength model (constant *s*).	$f_{ci}^{*} = f'_{ci} + 1{,}950$ psi when $f'_{ci} \le 5{,}000$ psi $f_{ci}^{*} = 0.9 f'_{ci} + 2{,}450$ psi otherwise
	Estimate expected concrete strength at 28 days, f_{c}^{*}, using the derived strength-growth model.	$f_{c}^{*} = 1.30 f'_{ci} + 3{,}530$ psi
Modulus of Elasticity	Use the AASHTO modulus of elasticity prediction equation with K_1 = **1.16** for typical regional aggregates for predictions at both release and 28 days.	$E_c = 33{,}000 \cdot K_1 \cdot w^{1.5} \sqrt{f'_c}$ where E_c = static elastic modulus of concrete (ksi); K_1 = correction factor for source of aggregate; = 1.16 for typical regional aggregates;
	Backcalculate the strength-growth curve from computed values at release and 28 days within *ALCAMBER*.	
Creep and Shrinkage Behavior	Use the Model Code 2010 creep prediction model with a creep coefficient correction factor of **0.80.**	---
	Use the Model Code 2010 shrinkage prediction model with a shrinkage correction factor of **0.70.**	---
	In the absence of more detailed information, an MC2010 concrete maturity, t_t, of **3.5** days[a] may be used as *ALCAMBER* input.	---

[a] = Represents the average MC 2010 maturity, t_t, computed for typical field tests of this study.

Summary statistics regarding the accuracy of the proposed camber prediction procedure and a trial procedure similar to current design practice are shown in Table 10-23.

Table 10-23: Summary Statistics for Key Prediction Trials

Trial Prediction Procedure	Percent Difference from Measured Values for All Midspan Measurements (%)							
	Camber		Curvature		Bottom Flange Strain		Centroidal Strain	
	μ	σ	μ	σ	μ	σ	μ	σ
AL-R-1.16-MCw/ **[Proposed Camber Prediction Procedure]**	+10.6	+16.9	-12.4	+11.6	+6.5	+17.4	+18.5	+27.1
AL-S-1.0-AASHTOw/o **[Most Similar to Current Design Practice]**	+49.2	+22.2	+16.7	+14.6	+49.2	+37.3	+69.8	+58.4

As shown above, for the girder production events monitored in this study, use of the proposed camber prediction procedure (AL-R-1.16-MCw/) tended to reduce the net overprediction of girder camber (for all ages) from 49.2 percent to 10.6 percent—thereby eliminating nearly 80 percent of the average error associated with camber prediction by current design practice.

Despite the calibrated MC 2010 creep and shrinkage models providing best agreement with time-dependent behavior observed in both the laboratory portion of this study (Chapter 7) and the field-monitoring portion of this study (Chapter 10), there may be some reluctance regarding the implementation of a camber prediction procedure that relies on MC 2010 time-dependent provisions. In this case, use of the AASHTO creep and shrinkage models (either calibrated or uncalibrated) are an acceptable alternative expected to generate camber predictions that, on average, are approximately 5 percent less accurate than those generated using MC 2010 provisions (as evident from Figures 10-14 and 10-16)—thereby tending to overpredict observed girder camber by

approximately 15 percent instead of the 10.6 percent characteristic of the use of MC 2010 time-dependent provisions.

Despite the analyses of this dissertation thus far confirming that (a) the time-steps analysis approach implemented in the *ALCAMBER* software generates most accurate predictions of girder deformations, and (b) the MC2010 shrinkage provisions (implemented in the *ALCAMBER* software) tend to most closely match early-age shrinkage of typical precast, prestressed concrete girders, certain designers may desire to continue use of existing commercial software for the purposes of camber prediction. In this case, designers are encouraged to manually implement the recommendations of Table 10-22 with regards to computing concrete overstrength and elastic modulus. For the girder production events monitored in this study, manual implementation of these recommendations in commercial software tended to reduce the magnitude of overprediction for camber at prestress transfer from 68 percent to 26 percent—thereby eliminating approximately 60 percent of the average error associated with prediction of camber at prestress transfer by current practice. The next section will briefly examine the suitability of using the PCI multiplier method, as implemented within existing commercial software, for the prediction of time-dependent camber for those who may prefer not to use the *ALCAMBER* software.

10.6 Comparison of PCI Multiplier Method to Recommended Camber Prediction Procedure

The two primary design software programs currently in use by ALDOT bridge designers (*LEAP CONSPAN* and *PSBEAM*) rely on the approximate PCI multiplier method to compute time-dependent midspan camber. This section briefly examines the appropriateness of the continued use of the PCI multiplier by comparing the prediction

results obtained from a commercial design software (*LEAP CONSPAN*) to those predictions generated by the camber prediction procedure (implemented within the *ALCAMBER* software) recommended in Section 10.5. For each of the three typical girder designs observed in the field monitoring effort of this study, predictions of midspan camber are shown in Figure 10-20 for a) the recommended camber prediction procedure (AL-R-1.16-MCw/) and the most similar commercial design prediction procedure (C-R-1.16).

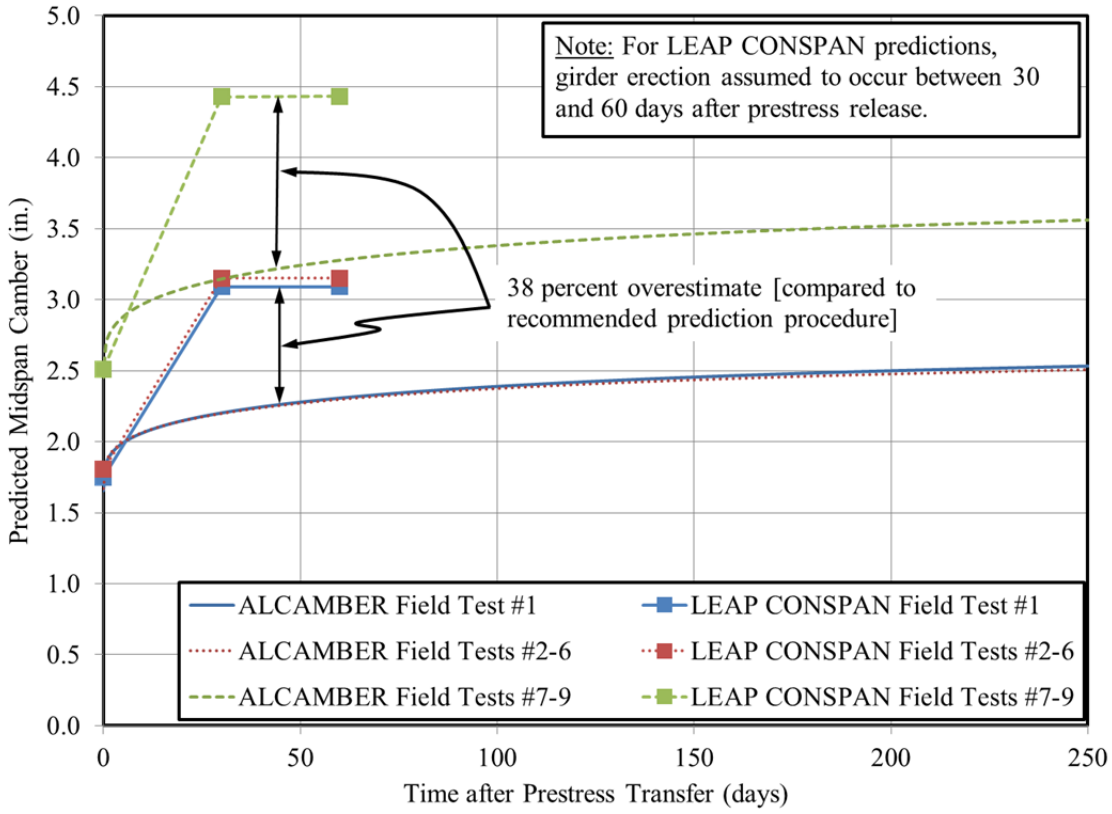

Figure 10-20: Comparison of Predictions by ALCAMBER Recommended Procedure (AL-R-1.16-MCw/) and Commercial Software (C-R-1.16) for Field Test Groups

Predictions of initial camber (t=0 days) were nearly identical for both methods for a given girder design—due to the inclusion of identical overstrength and aggregate stiffness modifiers in each prediction procedure. However, the predictions of time-dependent

camber generated using the approximate PCI multiplier method (for t=40 days) exceeded those predictions generated using the recommended *ALCAMBER* prediction procedure by approximately 38 percent. Because of this discrepancy, use of the PCI multiplier method for the prediction of time-dependent girder deformations is cautioned against—particularly in circumstances where most accurate predictions of girder camber are required to ensure constructability (i.e. midspan camber).

10.7 Summary and Conclusions

10.7.1 Summary

This chapter focused on implementation of the design recommendations of previous chapters (Chapters 5–7) and comparisons of predictions to field measurements of girder deformations for 22 bridge girders produced within the study region. While the beginning portions of this chapter served largely as a compilation of pertinent information from field tests, field results were then post-processed in preparation for comparisons to various trial prediction procedures. By comparing predicted and measured deformational responses for various trials, recommendations were made for the use of a revised camber prediction procedure that is expected to significantly increase the accuracy of initial design predictions of girder deformations.

The following conclusions regarding prediction of girder deformations (at all ages) for the nine girder production events monitored in this study result from the analyses of Chapter 10 conducted within the *ALCAMBER* software:

- Most accurate predictions of girder camber were furnished using measured concrete properties (compressive strength and elastic modulus) for a given field test and a calibrated MC 2010 creep and shrinkage model—resulting in a net

overprediction of girder camber (at all ages) of 10 percent. Similar predictions generated using the calibrated ACI 209 and AASHTO creep and shrinkage models yielded slightly less accurate results (approximately 15 percent overprediction);

- Calibration of creep and shrinkage models tended to, on average, affect prediction accuracy by less than 5 percent;
- Independent of changes in other input variables (e.g. concrete strength and creep and shrinkage models), the use of appropriate stiffness modifiers (K_1 = 1.16) tended to yield prediction accuracies approximately equal to those generated using measured elastic moduli, while omission of stiffness modifiers (K_1 = 1.0) tended to result in predictions 13 percent less accurate than those generated using measured elastic moduli;
- Independent of changes in other variables (e.g. concrete modulus and creep and shrinkage models), the use of recommended overstrength provisions (Ch. 5) tended to yield prediction accuracies on par with those generated using measured compressive strength, while use of specified concrete strength tended to generate predictions roughly half as accurate as those generated using measured compressive strength;
- Use of both appropriate stiffness modifiers (K_1 = 1.16) and recommended overstrength provisions (Ch. 5) tended to generate predictions with accuracy nearly identical to those generated using corresponding measured properties—resulting in a net overprediction of girder camber of approximately 10 percent;

- Use of appropriate stiffness modifiers (K_1 = 1.16), but specified concrete strength (a lower bound value) tended to result in prediction accuracies roughly 22 percent less accurate than those generated using measured material properties; and
- Use of specified strength and an unadjusted approximation of elastic modulus (K_1 = 1.0), regardless of the choice of time-dependent model, tended to yield camber predictions that were, on average, 40 percent less accurate than best predictions observed in this study and represent overpredictions of roughly 50 percent when compared to field measured values.

The following conclusions regarding predictions of girder deformations at prestress transfer for the nine girder production events monitored in this study result from the analyses of Chapter 10 conducted using commercial design software:

- Current design practice tended to overpredict midspan camber at prestress release by approximately 68 percent when compared to field measured values;
- Implementation of an appropriate stiffness modifier (K_1 = 1.16)—while still relying on specified concrete strength—tended to improve the accuracy of initial camber predictions by approximately 27 percent;
- Implementation of both an appropriate stiffness modifier (K_1 = 1.16) and recommended overstrength recommendations (Ch. 5) tended to improve the accuracy of initial camber predictions by approximately 45 percent.

The following conclusions regarding use of the PCI multiplier method result from the analysis of Section 10.6:

- For the three girder designs observed in the field monitoring portion of this study, use of the approximate PCI multiplier method tended to yield predictions of midspan girder camber (at erection) that exceeded best refined predictions (generated using the *ALCAMBER* software) by approximately 38 percent; and
- Use of the PCI multiplier method for the prediction of time-dependent girder deformations is cautioned against—particularly in circumstances where most accurate predictions of camber are required to ensure constructability (i.e. midspan camber).

10.7.2 Design Recommendations

To improve the accuracy of design camber predictions in Alabama, the following design recommendations are proposed:

1. The revised camber prediction procedure summarized in Table 10-24 (and implemented within the *ALCAMBER* software) is recommended for use at the time of girder design to predict girder camber through the time of girder erection. For the nine girder production events monitored in this study, use of the revised camber prediction procedure—in conjunction with the time-steps analysis procedure of the *ALCAMBER* software—eliminated, on average, approximately 80 percent of the error associated with current ALDOT camber prediction practices.
    a. As an alternative to the revised prediction procedure summarized in Table 10-24, designers may instead utilize AASHTO creep and shrinkage models (either calibrated or uncalibrated) within the *ALCAMBER*

Table 10-24: Recommended Camber Prediction Procedure (AL-R-1.16-MCw/) for ALDOT Girder Design

Material Property	**Recommendation**	**Equation(s)**
Concrete Compressive Strength	Estimate expected concrete strength at release, f_{ci}^{*}, using the ACI 214-based overstrength model (constant *s*).	$f_{ci}^{*} = f'_{ci} + 1{,}950$ psi when $f'_{ci} \le 5{,}000$ psi $f_{ci}^{*} = 0.9 f'_{ci} + 2{,}450$ psi otherwise
	Estimate expected concrete strength at 28 days, f_{c}^{*}, using the derived strength-growth model.	$f_{c}^{*} = 1.30 f'_{ci} + 3{,}530$ psi
Modulus of Elasticity	Use the AASHTO modulus of elasticity prediction equation with K_1 = **1.16** for typical regional aggregates for predictions at both release and 28 days.	$E_c = 33{,}000 \cdot K_1 \cdot w^{1.5} \sqrt{f'_c}$ where E_c = static elastic modulus of concrete (ksi); K_1 = correction factor for source of aggregate; = 1.16 for typical regional aggregates;
	Backcalculate the strength-growth curve from computed values at release and 28 days within *ALCAMBER*.	
Creep and Shrinkage Behavior	Use the Model Code 2010 creep prediction model with a creep coefficient correction factor of **0.80.**	---
	Use the Model Code 2010 shrinkage prediction model with a shrinkage correction factor of **0.70.**	---
	In the absence of more detailed information, an MC2010 concrete maturity, t_t, of **3.5** days[a] may be used as *ALCAMBER* input.	---

[a] = Represents the average MC 2010 maturity, t_t, computed for typical field tests of this study.

software—although the accuracy of camber prediction results are expected to be somewhat less accurate (approximately 5 percent);

2. Designers who prefer to continue use of existing commercial software for camber prediction should consider manual implementation of the overstrength and modulus of elasticity adjustments included in Table 10-24. Manual implementation of these recommendations is expected to eliminate approximately 60 percent of the average error associated with current design practice. Designers should also be aware that use of the PCI multiplier, as implemented in existing commercial design software, may tend to overpredict camber at girder erection by approximately 40 percent when compared to predictions of camber furnished by the recommended procedure of Table 10-24.

Chapter 11: Summary, Conclusions, and Recommendations

11.1 Summary of Work

In precast, prestressed concrete construction, the eccentricity of the prestressing force typically results in a net upward girder deflection known as camber. Camber is first observed at the time of prestress transfer and tends to increase thereafter as a function of time-dependent material properties. While accurately predicted levels of camber are desirable to concrete bridge construction, inaccuracies in design camber estimates can result in construction difficulties and the need to modify bridge designs to ensure proper girder fit. To mitigate such troublesome issues, the Alabama Department of Transportation (ALDOT) sponsored an investigation to develop a suggested procedure for use during girder design to more accurately predict pre-erection camber in precast, prestressed concrete bridge girders.

In support of this objective, various laboratory and field studies were conducted to explore relevant regionally-variable concrete material properties (e.g. concrete compressive strength, concrete elastic modulus, and creep and shrinkage behavior), as well as the effect of varying temperature conditions on girder camber. Then, a revised camber prediction procedure was developed, implemented in a standalone computer program (*ALCAMBER*), and validated by comparison to multiple production events of ALDOT precast, prestressed concrete girders. Use of the revised camber prediction procedure developed in this study—in conjunction with the time-steps analysis procedure of the *ALCAMBER* software—eliminated, on average, approximately 80 percent of the

error associated with current ALDOT camber prediction practices for the girder production events monitored in this study.

11.2 Research Conclusions and Recommendations

Conclusions and recommendations are grouped by chapter title—with recommendations of Chapter 10 incorporating relevant design recommendations from earlier chapters.

11.2.1 Current Design and Construction Practices for ALDOT Precast, Prestressed Concrete Bridge Girders

A recommended change to girder design practice supported by work presented in Chapter 4:

- In addition to the 60-day erection midspan camber currently noted on design drawings, ALDOT bridge design plans should also include estimated camber at the time of prestress transfer, thereby facilitating earlier detection of any significant deviations from predicted camber.

11.2.2 Accurately Predicting Expected Concrete Compressive Strength

Conclusions and recommendations are supported by research presented in Chapter 5:

- For design deflection computations, it is appropriate to use an estimate of the "expected" concrete compressive strength rather than the current practice of using the specified strength.
- The existing provisions of ACI 301 and ACI 214R-11 are an appropriate and convenient method for estimating the expected concrete compressive strength as a function of the specified strength.
- The "difference statistic" and the concept of preservation of standard deviation (as summarized below) offer a convenient method to compute a standard deviation

from a historical data set with varying specified concrete strengths that is appropriate for use within the provisions of ACI 301 and ACI 214R-11:

> *For an assumed (or approximated) constant standard deviation value at all considered strength levels, the distribution of the difference statistic is identical regardless of the number of constitutive mixtures or the relative mean strength levels of each mixture.*

Recommendations for use by girder designers, supported by the historical data set compiled in Chapter 5, include the following:

- To predict the expected concrete compressive strength at the time of prestress release, f_{ci}^{*}, the overstrength provisions of ACI 301 and ACI 214 should be applied with a standard deviation as determined by the distribution of the difference statistic for historical records from production events of precast, prestressed products within the region.
    - In the absence of historical data, the standard deviation, *s*, may be assumed to be 1,050 psi based on the results of this study—resulting in the following relationships:

For 4,000 psi $\leq f_{ci} \leq$ 5,000 psi $\qquad f_{ci}^{*} = f'_{ci} + 1{,}950$ psi

For 5,000 psi $< f_{ci} \leq$ 9,000 psi $\qquad f_{ci}^{*} = 0.9 f'_{ci} + 2{,}450$ psi

- The overstrength factor at release, OS_i, corresponding to the above expressions (for concrete strengths exceeding 5,000 psi) can be expressed as

$$OS_i = \frac{f_{ci}^{*}}{f'_{ci}} = 0.9 + \frac{2{,}450}{f'_{ci}}$$

where

OS_i^* = expected overstrength factor at prestress release;

f_{ci}^* = the expected concrete strength at prestress release (psi); and

f'_{ci} = the specified concrete strength at prestress release (psi).

- To predict expected compressive strength at the age of 28 days (for accelerated cured concretes typical of the precast, prestressed industry), the following expression is recommended:

$$f_c^* = 1.3 f'_{ci} + 3{,}500 \text{ psi}$$

where

f'_{ci} = the specified concrete strength at prestress release (psi).

- The expected overstrength at 28 days, OS_{28}^*, corresponding to the above expressions can be computed as

$$OS_{28}^* = 1.3\left(\frac{f'_{ci}}{f'_c}\right) + \frac{3{,}500}{f'_c}$$

where

$\left(\frac{f'_{ci}}{f'_c}\right)$ = the ratio of specified strength at prestress release to 28 days as selected by design engineer; and

f'_c = specified compressive strength at 28 days.

11.2.3 Concrete Modulus of Elasticity Relationships

Conclusions and recommendations are supported by research presented in Chapter 6:

- No statistical difference in elastic modulus was detectable among three laboratory mixtures containing various SCMs (fly ash, slag cement, or silica fume) in typical percent replacements used in Alabama.
- The use of two regional dolomitic limestone aggregates (acquired from an ALDOT-approved source) resulted in concrete stiffnesses greater than those predicted by unmodified AASHTO equations by 16 percent at the time of prestress transfer and by 13 percent 28 days after production.
- The use of a regional crushed granite aggregate (acquired from an ALDOT-approved source) resulted in concretes with less than expected E_c values (K_1 values between 0.68–0.72).
    - Requirements of the *ALDOT Standard Specification for Highway Construction* (ALDOT 2012), specifically with regards to the permissible levels of deleterious substances within coarse aggregate, should continue to be enforced to ensure acceptable concretes for precast, prestressed applications.
- Concrete cylinder temperature (at the time of hardened testing) is a potential source of uncontrolled variability in this research study and, perhaps a cause of the varying K_1 factors observed at different ages of testing.

Recommendations for use by girder designers supported by the research reflected in Chapter 6:

- The AASHTO LRFD Bridge Design Specifications (AASHTO 2014) prediction equation, with the assumptions and calibrations noted below, is most appropriate for design predictions of the elastic modulus for precast, prestressed concrete.

$$E_c = 33{,}000 \cdot K_1 \cdot w^{1.5} \sqrt{f'_c}$$

  where

  E_c = static elastic modulus of concrete (ksi);

  K_1 = correction factor for source of aggregate;

  = 1.16 for dolomitic limestone at release;

  = 1.13 for dolomitic limestone at 28 days;

  w = unit weight of concrete (kcf);

  = assumed equation to 0.150 kcf for design purposes; and

  f'_c = concrete compressive strength (ksi).

- For simplicity, the above K_1 factors may be approximated as $K_1 = 1.15$ in design applications incompatible with the implementation of unique K_1 factors for different ages.

11.2.4 Creep and Shrinkage Behavior of Alabama Precast, Prestressed Concretes

Conclusions and recommendations regarding concrete creep are supported by research presented in Chapter 7:

- No significant difference in concrete creep was detected between the two regional dolomitic limestone aggregates included in this study.

- Concrete mixtures using crushed granite aggregate exhibited 55–58 percent more compliance than corresponding dolomitic limestone control mixtures. However, this difference was primarily due to the reduced elastic modulus of the crushed granite aggregate and is not attributable to a significant difference in time-dependent creep behavior.
- Specimens loaded at 24 hours appeared to exhibit slightly reduced creep in comparison to specimens loaded at 18 hours, although approaching the limits of experimental precision.
- The use of slag cement (15 percent substitution) had a negligible effect on creep, while the use of fly ash (15 percent substitution) may have caused a slight reduction in creep.
- The use of fly ash and silica fume (18 percent and 8 percent substitution, respectively) resulted in a reduced creep tendency of between 9–12 percent.
- Of the unadjusted creep prediction models, the ACI 209 and AASHTO 2014 models provided relatively accurate predictions for the typical regional prestressed concretes considered in this study, with BP coefficients of variation of 10.3 and 12.9, respectively. Of these models, AASHTO LRFD is the simplest.
- Elastic moduli, as computed from creep frame loadings in accordance with ASTM C512, tended to be 14 percent lower than those measured in companion cylinders by ASTM C469 at the time of loading—suggesting that a small portion of early creep is "missed" during typical ASTM C512 testing.

- The “missed” portion of early creep corresponded to negligible differences in compliance, and thus, affirms the preference to consider compliance as the primary metric of time-dependent load-induced deformation.

Conclusions and recommendations regarding concrete shrinkage are supported by research presented in Chapter 7:

- No significant difference in shrinkage behavior was detectable between the two regional dolomitic limestones included in this study.
- Crushed granite mixtures tended to exhibit between 40–70 percent increased shrinkage when compared to dolomitic limestone mixtures.
- Specimens loaded at 18 hour ages exhibited a slightly increased shrinkage tendency when compared to specimens loaded at 24 hour ages, although approaching experimental precision.
- No significant effect of fly ash or slag (for typical regional substitution percentages) on shrinkage behavior was detectable in comparison to control mixtures.
- The ternary mixture (containing fly ash and silica fume) exhibited slightly decreased shrinkage in comparison to control mixtures, although approaching experimental precision.
- Of the three unadjusted candidate prediction models, the AASHTO 2014 method is most accurate of the considered models with a BP coefficient of variation of 36 percent.

The following summarize recommendations for future researchers:

- The use of sound post-processing techniques to eliminate erroneous data points and to detect loading anomalies is encouraged.
- Experimental precisions and repeatability of measurements should be determined by duplicate tests to allow identification of significant experimental trends.
- If conducting testing intended to simulate precast, prestressed concrete element production, an accelerated curing system should be used to introduce expected temperature profiles before and at the time of creep loading.
- The comparison of concrete elastic modulus as computed by loading frame data and also by companion material testing can be used to affirm the soundness of testing procedures and validate the accuracy of benchmark readings.

Recommendations for use by girder designers, supported by the laboratory testing conducted in Chapter 7, include the following:

- For best estimates of creep, the following creep coefficient modifications may be applied to the unadjusted models—with most accurate predictions offered by the Model Code 2010 method:

Table 7-22: Design Recommendations for Creep Coefficient Modification Factors

	Proposed Creep Coefficient Modification Factors	
Prediction Model	**When ternary mixtures are used**	**For all other mixture compositions (or unknown)**
AASHTO LRFD	**0.80**	1.00
ACI 209[b]	**0.95**	**1.15**
Model Code 2010[c]	**0.65**	**0.80**

[a] = Ternary mixtures refer to those mixtures containing fly ash and silica fume.
[b] = Requires mixture-specific input parameters including fine aggregate percent, slump, air content.
[c] = Requires estimate of adjusted maturity at the time of prestress transfer.

- For best predictions of concrete shrinkage, the following shrinkage modification factors are suggested for use with each considered prediction model:

Table 7-20: Design Recommendations for Shrinkage Modification Factors

	Proposed Shrinkage Modification Factors	
Prediction Model	**For use with slag and ternary[a] mixtures with limestone coarse aggregate (or unknown)**	**For use with crushed granite aggregate**
AASHTO LRFD	**0.80**	1.6
ACI 209[b]	0.75	1.5
Model Code 2010[c]	0.70	1.4

[a] = Ternary mixtures refer to those containing fly ash and silica fume.
[b] = Requires mixture-specific input parameters including fine aggregate percentage, cement content, slump, and air content.
[c] = Requires estimate of adjusted maturity at the time of prestress release and cement type.

11.2.5 Effect of Diurnal Temperature Changes on Girder Camber

Conclusions and recommendations are supported by research presented in Chapter 8:

- The curvature-based temperature-correction algorithm, as implemented in this study, demonstrated good agreement with field measured results—with the exception of where testing anomalies were detected (e.g. Field Test #1).
- For the concrete girders monitored in this study, an effective CTE value of between 13.0 and 13.5 με/°C was found to provide best agreement between predicted and measured deformational responses for girders in unshaded outdoor storage.
- Maximum diurnal temperature-induced changes to midspan camber of approximately 0.45 inches were observed in the field testing of this study.
- The general shapes of vertical temperature profiles at all locations (midspan and 1/6-span) were similar, with extreme temperature changes being induced in the girder web for the field tests conducted in this effort.

- Positioning of temperature gages at one-quarter points within the girder web of bulb-tee sections appeared to approximate observed reversals of the temperature profile occurring within the girder web relatively well.
- The most detailed analysis iteration used in this study (which relied on between 11–13 thermocouple measurements at midspan and an exact cross section definition) tended to generate the most accurate predictions of temperature-induced girder deformations (with the exception of where testing anomalies were detected)—although at the greatest computational cost.
- Analytical iterations conducted using measured data from different cross sections (i.e. measured temperatures and strains from midspan and 1/6-span) generated largely similar results.
- Use of the simplified equivalent cross section proposed by Johnson (2012) resulted in negligible error when compared to use of an exact cross section definition.
- Use of the simplified temperature profile proposed by Johnson (2012) generated strain predictions only slightly less accurate than those of the most detailed analysis included in this study.
- The use of direct linear interpolation between measurements to define vertical temperature profile shape resulted in predictions of strains and vertical deflections only slightly less accurate than use of the temperature profile by Johnson (2012).
- For the purposes of temperature-correction of field camber measurements, use of the temperature-correction algorithm derived in Section 8.2.2 is appropriate with

either (a) the procedures and assumptions implemented by Johnson (2012), (b) the procedures and assumptions implemented in this study, or (c) any combinations thereof.

- Maximum expected transient temperature-induced deformations for PCI bulb-tee girder sections (without decks) in unshaded outdoor storage are summarized in Table 8-11.

Table 8-11: Transient Changes to Theoretical Midspan Camber

Expected Transient Temperature-Induced Changes to Theoretical Midspan Camber	
Upward	<+1.5 in.
Downward	<-0.5 in.

11.2.6 Selection and Validation of a Revised Camber Prediction Procedure by Limited In-Plant Testing

Conclusions and recommendations are supported by research presented in Chapter 10:

- Most accurate predictions of girder camber were furnished using the *ALCAMBER* software, measured concrete properties (compressive strength and elastic modulus) for a given field test, and calibrated MC 2010 creep and shrinkage models. For the girder production events monitored in this study, use of this procedure resulted in a net overprediction of midspan camber of 10 percent compared to field-observed values.
- Prediction trials generated using measured concrete properties and either the calibrated ACI 209 or AASHTO creep and shrinkage models tended to yield slightly less accurate results (approximately 15 percent greater than field-observed values).

- In comparison to the use of uncalibrated creep and shrinkage models, use of calibrated models tended to affect prediction accuracy, on average, by less than 5 percent.
- The use of appropriate stiffness modifiers ($K_1 = 1.16$), independent of changes to other input variables (e.g. concrete strength and creep and shrinkage models), tended to yield prediction accuracies approximately equal to those generated using measured elastic moduli, while omission of stiffness modifiers ($K_1 = 1.0$) tended to result in predictions 13 percent less accurate than those generated using measured elastic moduli.
- The use of recommended overstrength provisions (Ch. 5), independent of changes in other variables (e.g. concrete modulus and creep and shrinkage models), tended to yield prediction accuracies on par with those generated using measured compressive strength, while use of specified concrete strength tended to generate predictions roughly half as accurate as those generated using measured compressive strength.
- Use of appropriate stiffness modifiers ($K_1 = 1.16$) and recommended overstrength provisions (Ch. 5) tended to generate predictions with accuracy nearly identical to those generated using corresponding measured properties—resulting in a net overprediction of observed girder camber by approximately 10 percent.
- Use of appropriate stiffness modifiers ($K_1 = 1.16$), but specified concrete strength (a lower bound value) tended to result in prediction accuracies roughly

22 percent less accurate than those generated using measured material properties.

- Use of specified strength and an unadjusted approximation of elastic modulus (K_1 = 1.0), regardless of the choice of time-dependent model, tended to yield camber predictions that were, on average, 40 percent less accurate than best predictions observed in this study (and represent overpredictions of roughly 50 percent when compared to field observed values).
- Current design practice (using commercial design software) tended to overpredict midspan camber at the time of prestress release by approximately 68 percent when compared to field observed values.
- Implementation of an appropriate stiffness modifier (K_1 = 1.16) in commercial design software—while relying on specified concrete strength—tended to improve the accuracy of initial camber predictions by approximately 27 percent when compared to current design practice.
- Implementation of both an appropriate stiffness modifier (K_1 = 1.16) and recommended overstrength recommendations (Ch. 5) in commercial design software tended to improve the accuracy of initial camber predictions by approximately 45 percent when compared to current design practice.
- For the three girder designs observed in the field monitoring portion of this study, use of the approximate PCI multiplier method tended to yield predictions of midspan girder camber (at erection) that exceeded best refined predictions (generated using the *ALCAMBER* software) by approximately 38 percent.

- Use of the PCI multiplier method for the prediction of time-dependent girder deformations is cautioned against—particularly in circumstances where most accurate predictions of deformations are required to ensure constructability (i.e. midspan camber).

To improve the accuracy of design camber predictions in Alabama, the following design recommendations, supported by the complete work of this dissertation, are recommended:

1. The revised camber prediction procedure summarized in Table 10-24 (as implemented within the *ALCAMBER* software) is recommended for use at the time of girder design to predict midspan camber through girder erection. For the nine girder production events monitored in this study, use of the revised camber prediction procedure—in conjunction with the time-steps analysis procedure of the *ALCAMBER* software—eliminated, on average, approximately 80 percent of the error associated with current ALDOT camber prediction practices.
    a. As an alternative to the revised prediction procedure summarized in Table 10-24, designers may instead utilize AASHTO creep and shrinkage models (either calibrated or uncalibrated) within the *ALCAMBER* software if preferred—although the accuracy of camber prediction results is expected to be somewhat less (by approximately 5 percent).
2. Designers who prefer to continue use of existing commercial software for camber prediction should consider manual implementation of the overstrength and modulus of elasticity adjustments included in Table 10-24. Manual

Table 10-24: Recommended Camber Prediction Procedure (AL-R-1.16-MCw/) for ALDOT Girder Design

Material Property	**Recommendation**	**Equation(s)**
Concrete Compressive Strength	Estimate expected concrete strength at release, f_{ci}^{*}, using the ACI 214-based overstrength model (constant *s*).	$f_{ci}^{*} = f'_{ci} + 1{,}950$ psi when $f'_{ci} \le 5{,}000$ psi $f_{ci}^{*} = 0.9 f'_{ci} + 2{,}450$ psi otherwise
	Estimate expected concrete strength at 28 days, f_{c}^{*}, using the derived strength-growth model.	$f_{c}^{*} = 1.3 f'_{ci} + 3{,}500$ psi
Modulus of Elasticity	Use the AASHTO modulus of elasticity prediction equation with K_1 **= 1.16** for typical regional aggregates for predictions at both release and 28 days.	$E_c = 33{,}000 \cdot K_1 \cdot w^{1.5} \sqrt{f'_c}$ where E_c = static elastic modulus of concrete (ksi); K_1 = correction factor for source of aggregate; = 1.16 for typical regional aggregates;
	Backcalculate the strength-growth curve from computed values at release and 28 days within *ALCAMBER*.	
Creep and Shrinkage Behavior	Use the Model Code 2010 creep prediction model with a creep coefficient correction factor of **0.80.**	---
	Use the Model Code 2010 shrinkage prediction model with a shrinkage correction factor of **0.70.**	---
	In the absence of more detailed information, an MC2010 concrete maturity, t_t, of **3.5** days[a] may be used as *ALCAMBER* input.	---

[a] = Represents the average MC 2010 maturity, t_t, computed for typical field tests of this study.

implementation of these recommendations is expected to eliminate approximately 60 percent of the average error associated with initial camber predictions by current design practice. Designers should also be aware that use of the PCI multiplier, as implemented in existing commercial design software, may tend to overpredict camber at girder erection (by up to 40 percent) when compared to predictions of camber furnished by the recommended procedure of Table 10-24.

11.3 Recommendations for Future Research

Based on the research presented in this dissertation, the following recommendations are given for potential future research:

- The temperature of concrete cylinders at the time of hardened testing was identified as a possible reason for the time-dependent nature of aggregate stiffness factors, K_1, as observed in this study and also noted by previous researchers. Future work is recommended in this area to identify potential trends significant to the precast, prestressed concrete community.
- Recalibration of the existing PCI multiplier method to better match the refined predictions of *ALCAMBER* may be useful for preliminary estimates of time-dependent girder camber.
- Public distribution of the *ALCAMBER* v1.0 software at the conclusion of this study will provide a convenient platform for conducting parametric studies regarding the prediction of pre-erection time-dependent girder deformations. Potential topics of future study include the following:

1. The effect of non-standard production schedules (i.e. weekend pours) on predicted camber, and
2. The effect of selected variable concrete properties (e.g. concrete compressive strength, elastic modulus, and creep and shrinkage) on predicted camber.

References

AASHTO. 2014. *AASHTO LRFD Bridge Design Specifications*. 7th ed. Washington, DC: American Association of State Highway and Transportation Officials.

AASHTO. 2012. *AASHTO LRFD Bridge Design Specifications*. 6th ed. Washington, DC: American Association of State Highway and Transportation Officials.

Abrams, D.A. 1927. Water-Cement Ratio as Basis of Concrete Quality. *ACI Journal Proceedings* 23 (2): 452-457.

ACI Committee 211. 2008. Guide for Selecting Proportions for High-Strength Concrete Using Portland Cement and Other Cementitious Materials (ACI 211.4R-08). Farmington Hills, MI: American Concrete Institute.

ACI Committee 301. 2010. Specifications for Structural Concrete (ACI 301-10). Farmington Hills, MI: American Concrete Institute.

ACI Committee 363. 2010. Report on High-Strength Concrete (ACI 363R-11). Farmington Hills, MI: American Concrete Institute.

ACI Committee 209. 2005. Factors Affecting Shrinkage and Creep of Hardened Concrete (ACI 209.1R). Farmington Hills, MI: American Concrete Institute.

ACI Committee 209. 2008. Guide for Modeling and Calculating Shrinkage and Creep of Concrete (ACI 209.2R-08). Farmington Hills, MI: American Concrete Institute.

ACI Committee 209. 2008. Prediction of Creep, Shrinkage, and Temperature Effects in Concrete Structures (ACI 209R-92/08). Farmington Hills, MI: American Concrete Institute.

ACI Committee 214. 2011. Guide to Evaluation of Strength Test Results of Concrete (ACI 214R-11). Farmington Hills, MI: American Concrete Institute.

ACI Committee 216. 2014. Code Requirement for Determining the Fire Resistance of Concrete and Masonry Construction Assemblies (ACI 216.1-14). Farmington Hill, MI: American Concrete Institute.

ACI Committee 318. 2014. Building Code Requirements for Structural Concrete (ACI 318-14). Farmington Hills, MI: American Concrete Institute.

ACI Committee 318. 1971. Building Code Requirements for Reinforced Concrete (ACI-318-71). Detroit, MI: American Concrete Institute.

ACI Committee 435. 1997. Report on Temperature-Induced Deflections of Reinforced Concrete Members (ACI 435.7R-85). Farmington Hills, MI: American Concrete Institute.

ACI. 2013. ACI Concrete Terminology (ACI CT-13). Farmington Hills, MI: American Concrete Institute.

ACI Committee 318. 2011. Building Code Requirements for Structural Concrete (ACI 318-11). Farmington Hills, MI: American Concrete Institute.

ACI Committee 435. 2003. Control of Deflection in Concrete Structures (ACI 435R), Farmington Hills, MI: American Concrete Institute.

ACI Committee 435/Subcommittee 5. 1963. Deflections of Prestressed Concrete Members. *Journal of the American Concrete Institute* 60 (12): 1697-1728.

Adam, I., and M. M. R. Taha. 2011. Identifying the Significance of Factors Affecting Creep of Concrete: A Probabilistic Analysis of RILEM database. *International Journal of Concrete Structures and Materials* 05 (2): 97-111.

Aitcin, P.C., and P.K. Mehta. 1990. Effect of Coarse-Aggregate Characteristics on Mechanical Properties of High-Strength Concrete. *ACI Materials Journal* 82 (2): 103-107.

ALDOT. 2014. Structural Design Manual. Montgomery, AL: Alabama Department of Transportation.

ALDOT. 2014. Bridge Plans Detailing Manual. Montgomery, AL: Alabama Department of Transportation.

ALDOT. 2009. Method of Controlling Concrete Operations for Structural Portland Cement Concrete (Procedure 170). Montgomery, AL: Alabama Department of Transportation.

ALDOT. 2015. Production and Inspection of Precast Non-Prestressed and Prestressed Concrete (Specification ALDOT-367-89). Montgomery, AL: Alabama Department of Transportation.

ALDOT. 2012. Standard Specifications for Highway Construction. Montgomery, AL: Alabama Department of Transportation.

Alexander, M.G., and T.I. Milne. 1995. Influence of Cement Blend and Aggregate Type on Stress-Strain Behavior and Elastic Modulus of Concrete. *ACI Materials Journal* 92 (3): 227-235.

Al-Omaishi, N, M.K. Tadros, and S.J. Seguirant. 2009. Elasticity, Modulus, Shrinkage, and Creep of High-Strength Concrete as Adopted by AASHTO. *PCI Journal* 54 (3):44-63.

Al-Omaishi, N. 2001. *Prestress Losses in High Strength Pretensioned Concrete Girders*. PhD Dissertation, University of Nebraska – Lincoln.

Aly, T. and Sanjayan, J.P. 2008. Factors Contributing to Early Age Shrinkage Cracking of Slag Concretes Subjected to 7-days Moist Curing. *Materials and Structures Journal*: 41(4):633-624.

ASTM C1074. 2011. Standard Practice for Estimating Concrete Strength by the Maturity Method. *ASTM International*. West Conshohocken, PA.

ASTM C192. 2014. Standard Practice for Making and Curing Concrete Test Specimens in the Laboratory. *ASTM International*. West Conshohocken, PA.

ASTM C31. 2009. Standard Practice for Making and Curing Concrete Test Specimens in the Field. *ASTM International*. West Conshohocken, PA.

ASTM C157. 2008. Standard Test Method for Length Change of Hardened Hydraulic-Cement Mortar and Concrete. *ASTM International*. West Conshohocken, PA.

ASTM C512. 2002. Standard Test Method for Creep of Concrete in Compression. *ASTM International*. West Conshohocken, PA.

ASTM C39. 2010. Standard Test Method for Compressive Strength of Cylindrical Concrete Specimens. *ASTM International*. West Conshohocken, PA.

ASTM C469. 2010. Standard Test Method for Static Modulus of Elasticity and Poisson's Ratio of Concrete in Compression. *ASTM International*. West Conshohocken, PA.

Barr, P.J., and F. Angomas. 2010. Differences between Calculated and Measured Long-Term Deflections in a Prestressed Concrete Girder Bridge. *ASCE J. Perform. Constr. Facil*, 24 (6), 603-609.

Barr, P.J., J.F. Stanton, and M.O. Eberhard. 2005. Effects of Temperature Variations on Precast, Prestressed Concrete Bridge Girders." *ASCE Journal of Bridge Engineering*, 10 (2): 186-194.

Baughn, J. 2014. Searchable National Bridge Inventory Data. http://www.uglybridges.com (accessed February 2, 2015).

Bazant, Z.P., and L. Panula. 1980. Creep and Shrinkage for Analyzing Prestressed Concrete Structures." *PCI Journal* 25 (3): 68-117.

Bentley Systems, Inc. 2012. *LEAP CONSPAN User Manual*. Exton, PA.

Boehm, K. 2008. *Structural Performance of Self-Consolidating Concrete*. MS Thesis, Auburn, AL: Auburn University.

Boehm, K.M., R.W. Barnes, and A.K. Schindler. 2010. *Performance of Self-Consolidating Concrete in Prestressed Girders*. Final Project Report, Auburn University Highway Research Center.

Boresi, Arthur P., and Richard J. Schmidt. 2003. *Advanced Mechanics of Materials*. Hoboken, NJ: John Wiley and Sons, Inc.

Branson, D.E. 1977. *Deformations of Concrete Structures*. New York, NY: McGraw-Hill Book Co.

Branson, D.E., and A.M. Ozell. 1961. Camber in Prestressed Concrete Beams. *Journal of the American Concrete Institute* 57 (12): 1549-1574.

Brooks, J.J. 1999. How Admixtures Affect Shrinkage and Creep. *Concrete International*, 21 (4): 35-38.

Brown, K.M. 1998. *Camber Growth Prediction in Precast Prestressed Concrete Bridge Girders*. PhD Dissertation, University of Idaho, Ann Arbor, MI.

Buettner, D.R., and J.R. Libby. 1979. Camber Requirements for Pretensioned Members. *Concrete International* 1 (2): 66-72.

Carino, N.J., and R.C. Tank. 1992. Maturity Functions for Concrete Made with Various Cements and Admixtures. *ACI Materials Journal* 89 (2): 188-196.

Carrasquillo, R.L., A.H. Nilson, and F.O. Slate. 1981. Properties of High Strength Concrete Subject to Short-Term Loads. *ACI Journal* 78(3): 171-177.

Chern, J., and Y. Chan. 1989. Deformations of Concretes Made with Blast-Furnace Slag Cement and Ordinary Portland Cement. *ACI Materials Journal* 86 (4): 372-382.

Collins, M.P., and D. Mitchell. 1991. *Prestressed Concrete Structures.* Englewood Cliffs, NJ: Prentice Hall.

Cook, J.E. 1989. 10,000 psi Concrete. *Concrete International* 11 (10): 67-75.

Cook, J.E. 1982. Research and Application of High-Strength Concrete Using Class C Fly Ash. *Concrete International* 4 (7): 72-80.

Cook, R.A., and D. Bloomquist. 2005. *Field Verification of Camber Estimates for Prestressed Concrete Bridge Girders*. Final Project Report, University of Florida, Tallahassee, FL: Florida Department of Transportation.

Davis, R.E., and H.E. Davis. 1931. Flow of Concrete Under the Action of Sustained Loads. *ACI Journal Proceedings* 27 (3):837-901.

Davison, B. 2014. *Prediction of Time-Dependent Stresses and Deflections in Prestressed, Concrete Girders: From Start of Fabrication to End of Service Life.* MS Thesis, Seattle Washington: University of Washington.

Donza, H., O. Cabrera, and E.F. Irassar. 2002. High-strength Concrete with Different Fine Aggregates. *Cement and Concrete Research* (Pergamon) 32: 1755-1761.

Dunham, E.L. 2011. *Transfer Length in Bulb-Tee Girders Constructed with Self-Consolidating Concrete*. MS Thesis, Auburn, AL: Auburn University.

Ellis, M.A. 2012. *Time-Dependent Deformations of Concrete for Precast/Prestressed Bridge Components*. MS Thesis, Auburn, AL: Auburn University.

Fawzy, F. and K.E. Hanna. 2011. Precast, Prestressed Girder Camber Variability. *PCI Journal* 56 (1): 135-154.

fib. *Model Code 2010*. Design Code, Lausanne, Switzerland: International Federation for Structural Concrete, 2010.

French, C.E., and C. O'Neill. 2012. *Validation of Prestressed Concrete I-Beam Deflection and Camber Estimates*. Final Report, University of Minnesota, St. Paul, MN: Minnesota Department of Transportation.

Freskakis, G.N., R.C. Burrow, and E.B. Debbas. 1979. Strength Properties of Concrete at Elevated Temperatures. *Proceedings of ASCE National Convention Civil Engineering Nuclear Power*. Boston, Massachusetts: American Society of Civil Engineers.

Ghosh, R.S., and J. Timusk. 1981. Creep of Fly Ash Concrete. *ACI Journal* 78 (5): 351-357.

Haranki, B. 2009. *Strength, Modulus of Elasticity, Creep, and Shrinkage of Concrete Used in Florida*. MS Thesis, Gainesville, FL: University of Florida.

He, W. 2013. *Creep and Shrinkage of High Performance Concrete and Prediction of the Long-term Camber of Prestressed Bridge Girders*. MS Thesis, Ames, Iowa: Iowa State University.

Hibbeler, R. C. 2011. *Mechanics of Materials*. Upper Saddle River, NJ: Pearson Prentice Hall.

Hibbeler, R.C. 2006. *Structural Analysis*. Upper Saddle River, NJ: Pearson Prentice Hall.

Hinkle, S.D. 2006. *Investigation of Time-Dependent Deflection in Long Span, High Strength, Prestressed Concrete Bridge Beams*. MS Thesis, Blacksburg, VA: Virginia Polytechnic Institute and State University.

Hofrichter, A. 2014. *Compressive Strength and Modulus of Elasticity Relationships for Alabama Prestressed Concrete Bridge Girders*. MS Thesis, Auburn, AL: Auburn University.

Holland, R.C. 2005. *Silica Fume User's Manual*. Lovettsville, VA: Silica Fume Association.

Holt, R. 1996. *Implementation Program on High Performance Concrete Guidelines for Instrumentation of Bridges*. Research Report, Washington, DC: Federal Highway Administration.

Hubler, M.H., Wendner, R., Bazant, Z.P. 2015. Comprehensive Database for Concrete Creep and Shrinkage: Analysis and Recommendations for Testing and Recording. *American Concrete Institute Materials Journal* 112 (4): 547-558.

Huo, X.S., N. Al-Omaishi, and M.K. Tadros. 2001. Creep, Shrinkage, and Modulus of Elasticity of High Performance Concrete. *ACI Materials Journal* 98 (6): 440-449.

Imbsen, R.A., D.E. Vandershaf, R.A. Schamber, and R.V. Nutt 1985. *Thermal Effects in Concrete Bridge Superstructures* (NCHRP Report 276). Washington, DC: Transportation Research Board.

Isbiliroglu, L. 2014. *Predicting Time-Dependent Deformations in Prestressed Concrete Girders*. MS Thesis, Auburn, AL: Auburn University.

Jayaseelan, H., and B.W. Russell. 2007. *Prestress Losses and the Estimation of Long-Term Deflections and Camber for Prestressed Concrete Bridges*. Final Report, Stillwater, OK: Oklahoma State University.

Johnson, Brandon Ray. 2012. *Time-Dependent Deformation in Precast, Prestressed Bridge Girders*. MS Thesis, Auburn, AL: Auburn University.

Kavanaugh, B.P. 2008. Creep Behavior of Self-Consolidating Concrete. MS Thesis, Auburn, AL: Auburn University.

Kelly, D.J., T.E. Bradberry, and J.E. Breen. 1987. *Time Dependent Deflections of Pretensioned Beams* (Research Report 381-1). The University of Texas at Austin, Austin, TX: Center for Transportation Research.

Keske, S.D. 2014. *Use of Self-Consolidating Concrete in Precast, Prestressed Girders*. PhD Dissertation, Auburn, AL: Auburn University.

Khatri, B.P., and V. Sirivivatnanon. 1995. Effect of Different Supplementary Cementitious Materials on Mechanical Properties of High Performance Concrete. *Cement and Concrete Research* (Elsevier Science Ltd.) 25 (1): 209-220.

Lane, R.O., and J.F. Best. 1982. Properties and Use of Fly Ash in Portland Cement Concrete. *Concrete International* 4 (7): 81-92.

Lee, J.H. 2010. *Experimental and Analytical Investigations of the Thermal Behavior of Prestressed Concrete Bridge Girders Including Imperfections*. PhD Dissertation, Atlanta, GA: Georgia Institute of Technology.

Levy, K. 2007. *Bond Behavior of Prestressed Reinforcement in Beams Constructed with Self-Consolidating Concrete*. MS Thesis, Auburn, AL: Auburn University.

Levy, K., Barnes, R.W., Schindler, A.K. 2010. *Time-Dependent Deformations of Pretensioned, Self-Consolidating Concrete*. Proceedings of the 3rd *fib* International Congress, May 29–June 2, 2010: Washington, DC.

Limeria, J., M. Etxeberria, and D. Molina. 2011. Mechanical and Durability Properties of Concrete Made with Dredged Marine Sand. *Journal o*f *Construction and Building Products* (Elsevier) 25: 4165-4174.

Liu, Yanjan, and Mang Tia. 2012. Creep Property of Concretes with Different Types of Coarse Aggregates. *Journal of Applied Mechanics and Materials* (Trans Tech Publications) 174-177: 308-313.

Magura, D.D., M.A. Sozen, and C.P. Seiss. 1964. A Study of Stress Relaxation in Prestressing Reinforcement. *PCI Journal* 9 (2): 13-57.

Mahmood, O.I. 2013. *Camber Control in Simply Supported Prestressed Concrete Bridge Girders.* MS Thesis, Lexington, KY: University of Kentucky.

Martin, L.D. 1977. A Rational Method for Estimating Camber and Deflection of Precast Prestressed Members. *PCI Journal* 22 (1):100-108.

Mehta, P.K., and P.J.M. Monteiro. 2014. *Concrete Microstructure, Properties, and Materials*. 4th ed. McGraw-Hill Education.

Muller, H.S., I. Anders, R. Breiner, and M. Vogel. 2013. Concrete: Treatment of types and properties in fib Model Code 2010. *Journal of Structural Concrete* (Ernst and Sohn) 4: 320-334.

Naaman, A.E. 2004. *Prestressed Concrete Analysis and Design: Fundamentals*. 2nd ed. Ann Arbor, MI: Techno Press 3000.

Nawy, E.G. 2010. *Prestressed Concrete - A Fundamental Approach*. Upper Saddle River, NJ: Pearson Education, Inc.

Nervig, J. 2014. *Improving Predictions of Instantaneous Camber for Prestressed Concrete Bridge Girders* (Paper 13817). MS Thesis. Iowa State University.

Neville, A.M. 2013. *Properties of Concrete*. New Delhi, India: Dorling Kindersley.

Noguchi, T., F Tomosawa, K.M. Nemati, B.M. Chiaia, and A.P. Fantill. 2009. A Practical Equation for Elastic Modulus of Concrete. *ACI Structural Journal* 106 (5): 690-696.

Omar, W., T. Pui Lai, L. Poh Huat, and R. Omar. 2008. Improved Prediction of Pre-Camber of Post-Tensioned Prestressed I-Beam. *Journal of the Institution of Engineers* 69 (1):32-37.

Pauw, Adrian. 1960. Static Modulus of Elasticity of Concrete as Affected by Density. *Journal of the American Concrete Institute* 57 (2): 679-688.

Philleo, R.E. 1981. Increasing the Usefulness of ACI 214: Use of Standard Deviation and a Technique for Small Sample Sizes. *Concrete International* 3 (9): 71-74.

PCI Committee on Bridges. 2012. Camber FAST Team. Chicago, IL: Precast Prestressed Concrete Institute.

PCI. 2011. *Precast Prestressed Concrete Bridge Design Manual* 3rd ed. Chicago, IL: Precast/Prestressed Concrete Institute.

Rizkalla, S., P. Zia, and T Storm. 2011. *Predicting Camber, Deflection, and Prestress Losses in Prestressed Concrete Members*. Final Project Report, Raleigh, NC: North Carolina State University.

Roller, J.J., H.G. Russell, R.N. Bruce, and B. Hasset. 2003. Effect of Curing Temperature on High Strength Concrete Bridge Girders. *PCI Journal* 48 (2): 72-79.

Rosa, M.A., J. F. Stanton, and M.O. Eberhard. 2007. *Improving Predictions for Camber In Precast, Prestressed Concrete Bridge Girders*. Research Report, University of Washington, Seattle, WA: Washington State Transportation Center (TRAC).

Schindler, A.K, M.L. Hughes, R.W. Barnes, and B.E. Byard. 2010. *Evaluation of Cracking of the US 331 Bridge Deck.* ALDOT Project Report 930-645. Auburn University, Auburn AL: Highway Research Center.

Schrantz, C.E. 2012. *Development of a User-Guided Program for Predicting Time-Dependent Deformations in Prestressed Bridge Girders*. MS Thesis, Auburn, AL: Auburn University.

Schuster, R.L. 1957. *A Review of Research on Deleterious Substances in Concrete Aggregates*. Joint Highway Research Project, Lafayette, Indiana: Purdue University.

Shi-Cong, K., and P. Chi-Sun. 2009. Properties of Concrete Prepared with Crushed Fine Stone, Furnace Bottom Ash, and Fine Recycled Aggregate as Fine Aggregate. *Journal of Construction and Building Materials* (Elsevier) 23:2877-2886.

Stallings, J.M., and S. Eskildsen. 2001. *Camber and Prestress Losses in High Performance Concrete Bridge Girders*. Final Research Report: Project 930-373, Auburn, AL: Auburn University Highway Research Center.

Stallings, J.M., R.W Barnes, and S. Eskildsen. 2003. Camber and Prestress Losses in Alabama HPC Bridge Girders. *PCI Journal* 48 (5): 2-16.

Storm, T.K., S.H. Rizkalla, and P.Z. Zia. 2013. Effects of Production Practices on Camber of Prestressed Concrete Bridge Girders. *PCI Journal* 58 (1): 96-111.

Svirsky, A. National Bridges. 2015. www.nationalbridges.com (accessed February 2, 2015).

Tadros, M.K, N. Al-Omaishi, S.J Seguirant, and J.G. Gallt. 2003. *Prestress Losses in Pretensioned High-Strength Concrete Bridge Girders* (NCHRP Report 496), Washington, DC: National Cooperative Highway Research Program, Project 18-07.

Tadros, M.K., A. Ghali, and A.W. Meyer. 1985. Prestressed Loss and Deflection of Precast Concrete Members. *PCI Journal* 30 (1): 114-141.

Tadros, M.K., F. Fawzy, and K.E. Hanna. 2011. Precast, Prestressed Girder Camber Variability. *PCI Journal* 56 (1): 135-154.

Thoman, W.H., and W. Raeder. 1934. Ultimate Strength and Modulus of Elasticity of High-Strength Portland Cement Concrete. *Journal of the American Concrete Institute* 30 (1).

Tia, M., Y Liu, and D. Brown. 2005. *Modulus of Elasticity, Creep, and Shrinkage of Concrete*. Final Project Report, University of Florida, Tallahassee, FL: Florida Department of Transportation.

Troxell, G.E., J.M. Raphael, and R.E. Davis. 1958. Long-Term Creep and Shrinkage Tests of Plain and Reinforced Concrete. *Proceedings of ASTM Annual Meeting 1958*: 1101-1120.

Vardeman, S.B. and Jobe, J.M. 2001. Basic Engineering Data Collection and Analysis. Pacific Grove, CA: Duxbury Thompson Learning.

Wu, K., B. Chen, W. Yao, and D. Zhang. 2001. Effect of Coarse Aggregate Type on Mechanical Properties of High-Performance Concrete. *Journal of Cement and Concrete Research* (Pergamon) 31: 1421-1425.

Wyffels, T.A., C.E. French, and C.K. Shield. 2000. *Effects of Pre-Release Cracks in High-Strength Prestressed Concrete*. Final Project Report, University of Minnesota, St. Paul, MN: Minnesota Department of Transportation Office of Research Administration.

Appendix A: Predicting Short-Term Camber by Energy Methods

Appendix A details an independent effort undertaken to investigate the feasibility of using energy methods to compute the upward camber tendency in prestressed concrete girders. To date, there is no evidence in literature that energy methods have been employed in the calculation of short-term deflection components in prestressed concrete. This section includes a draft paper, intended for standalone publication.

Title: Reduced Camber Theory in Prestressed Concrete Girders Analyzed using Energy Principles

Authors:

David M. Mante[a], Robert W. Barnes[b], Chai H. Yoo[c]

[a] Graduate Research Assistant, Department of Civil Engineering, 238 Harbert Engineering Center, Auburn University, Auburn, AL 36849-5337 USA (corresponding author). E-mail: dmm0018@auburn.edu. Telephone: (334)-740-6554.

[b] Associate Professor, Department of Civil Engineering, Auburn University, Auburn, AL 36849-5337 USA

[c] Professor Emeritus, Department of Civil Engineering, Auburn University, Auburn, AL 36849-5337 USA

Abstract:

Accurately predicting the net upward deflection or camber in prestressed concrete bridge girders prior to fabrication is critical to ensure the intended functionality of the completed structure. Inaccurate camber predictions often result in adjacent component fit problems, construction delays, and unanticipated costs for the project sponsor. Despite best efforts, significant unexplained disparities often remain between predicted and measured camber values. In this study, a numerical solution method is developed to predict initial elastic camber at prestress transfer in flat strand girders by using a combination of energy principles and geometric relationships. Unique to this numerical solution is the opportunity to include the effect of axial shortening due to flexure on the calculated

initial elastic camber. Using this method, computed elastic cambers are less than those calculated by conventional methods. The authors offer this apparent reduced camber theory as a possible explanation to explain the continued difficulty in achieving accurate initial elastic camber predictions.
Keywords: prestressed concrete, flat strand, camber prediction, deflection

1. Introduction

Camber is a net upward deflection commonly introduced into prestressed concrete girders by eccentrically located prestressed steel strands. Camber is first observed immediately upon the transfer of the prestressing force into the bulk concrete section [1]. The magnitude of the instantaneous elastic camber is typically calculated using simple mechanics principles of elastic structures and thus, is influenced by factors such as girder size, configuration of prestressed reinforcement, concrete stiffness, and other select cross-sectional properties [2]. When accurately predicted during the design phase, appropriate levels of camber are desirable to the bridge construction industry [3]. However, when actual camber values deviate from predicted values, adjacent component fit problems, schedule delays, and cost overruns commonly occur. Even a minor overestimate of camber by a design engineer can result in the need for tens of thousands of dollars of additional deck concrete placement to ensure contractual roadway elevation and slope requirements are satisfied.

2. Background

In recent years, there has been substantial research effort devoted to improving predictions of camber during the girder design phase. Most researchers agree that variability in prestressed concrete girder cambers has increased recently with the implementation of high performance concrete (HPC) and corresponding longer design span lengths [4]. Much of the ongoing research effort is related to more precisely characterizing the material properties and variables used for initial elastic camber computations. In particular, much attention has been focused on more accurately reflecting actual in-place concrete strength and stiffness properties [5,6] more closely estimating the prestress force at time of transfer [7,8] and even more accurately reflecting actual cross-sectional geometric properties [9]. Despite best efforts to improve the accuracy of elastic camber computations, predicted camber magnitudes are universally regarded as estimates at best and prediction error continues to vary by up to 20 percent [1]. In various recent surveys and studies, actual initial cambers most frequently tend to fall below predicted values by widely varying amounts [8,10,11].

While great effort has been devoted to isolating each factor related to elastic camber prediction, comparatively minimal effort has historically been devoted to critically examining computational methods currently used for camber calculation. Limited research in this area generally relies heavily on simple elastic mechanics principles with slight variations [4] or tends to focus primarily on time-dependent modeling of camber as girder materials age.

In this study, an energy principle and various geometric relationships are used to derive a numerical method to predict elastic camber at prestress transfer in flat strand girders. Applying this new method, computed elastic camber values are less than those calculated by other conventional methods. The authors offer this apparent reduced camber theory as a possible explanation to explain the continued difficulty in achieving accurate initial elastic camber predictions.

3. Calculation of Elastic Camber in Flat Strand Girders by Conventional Methods

In prestressed concrete girder design, the geometry and reinforcing of the girder section are typically selected in order to ensure that flexural stresses in the section remain lower than the modulus of rupture of concrete. By ensuring this tensile limit is not exceeded, the section is assumed to exhibit uncracked, linear-elastic material behavior [2]. Under this condition, deflections may be calculated by employing basic principles of mechanics of elastic structures and the principle of superposition is applicable [12]. Superposition is typically used to combine an upward camber tendency due to an eccentric prestress force with the simultaneous downward self-weight deflection due to the end-supported condition of the prestressed beam.

In order to apply basic mechanics principles to the calculation of the upward elastic camber tendency in prestressed concrete construction, an equivalent external loading is typically applied to the girder in order to simulate the forces exerted by the internal prestressing steel strands. This equivalent loading approach is commonly used by designers, researchers, and is suggested by both ACI Committee 435 (2003) [2] and the PCI Bridge Design Manual (2011) [1]. Various available resources [1,2] present illustrations indicating equivalent external loadings corresponding to common prestress patterns. For a prestressed girder with eccentric, flat strands, the equivalent external loading is shown in Fig. 1. As shown, the internal force from the prestressing strand is

idealized as a centroidal compressive force, P, and an end moment acting about the centroid, M, to account for the eccentricity of the prestressing force.

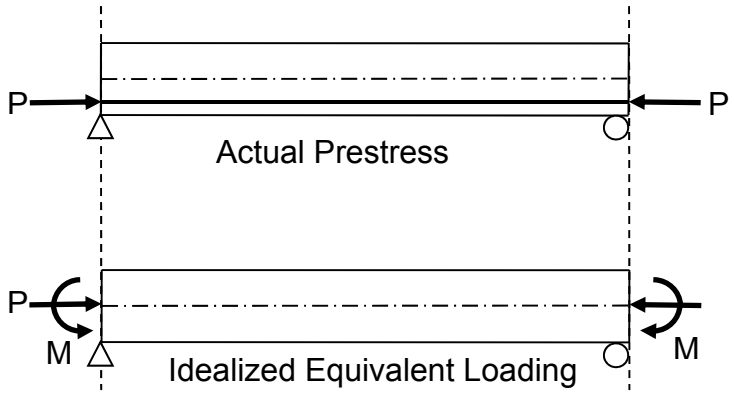

Fig. 1: Idealized Equivalent Loading for Flat Eccentric Strand Pattern

At this point, a discussion of boundary conditions commonly used for analysis is warranted. Available guidance from ACI and PCI resources [1,2] recommend the use of a pin and roller (as shown in Fig. 1) or dual pin assembly for analysis. Although limited experimental research [6] indicates these support conditions may not perfectly reflect actual in-place restraints, the majority of current camber calculations are made using the simply supported beam recommendations noted above. The derivations included later in this report utilize slightly modified boundary conditions as discussed in the following section.

After selecting an idealized equivalent loading, simple elastic mechanics (i.e. moment-area theorems) can be used to solve for the midspan elastic camber tendency due to the applied loading. When considering the eccentric, flat strand prestress pattern shown in Fig. 1, the midspan elastic upward camber component (neglecting the self weight deflection), Δ, can be expressed as

$$\Delta = \frac{PeL^2}{8EI} \text{ or } \Delta = \frac{ML^2}{8EI} \quad (1)$$

where M is the equivalent moment acting about the centroid due to the prestressing force, P, and eccentricity, e; L is the total length of beam, and E and I are the modulus of elasticity of the concrete and the second moment of area of the gross cross section, respectively. Implicit in the formulation of Eq. 1 are the basic assumptions of Euler-Bernoulli beam theory including: (1) small deflection theory and (2) the centroidal axis remains the same length. Eq. (1) is found in both ACI (2003) and PCI (2011) design

guidance [1,2] and is used as a point of comparison for the numerical solution process derived in the remainder of this paper.

4. Numerical Camber Solutions Using Energy Principles

In order to most clearly communicate the numerical solution process and apparent camber reduction theory explored in this investigation, two detailed derivations are included in this paper.

4.1. Conservation of Energy Principle

Neglecting energy terms associated with heat, chemical reactions, and electromagnetic effects, the conservation of energy principle as used in structural mechanics is mathematically expressed as

$$\Delta W = \Delta U \tag{2}$$

where ΔW represents the external work done on a body and ΔU represents the corresponding change in internal strain energy of the body due to deformation. Generally, this direct formulation of the conservation of energy principle has limited applicability and is suited only to solving elementary systems with a single external force or couple moment acting on the structure [13]. However, when geometric relationships are used to relate displacements at the location of applied forces to displacement at other locations, this basic energy approach becomes convenient to solve for midspan camber in prestressed concrete girders.

4.2. Beam Model, Boundary Conditions, and Displacement Function

For the purposes of these analyses, the notation and boundary conditions as reflected in Fig. 2 are assumed. For the simply supported beam, roller supports are used at the beam ends. For stability, a slotted roller is located at midspan to prevent movement of the girder in the horizontal direction at this location, but freely allows shear transfer, moment continuity, and upward camber to occur. While L remains the overall flat length of the beam prior to loading, the term L' is introduced to denote the horizontal projected length of the beam after deflection due to bending effects only. Similarly, the terms δ and θ as shown in Fig. 2 denote the relative horizontal end translation due to bending and end rotation, respectively.

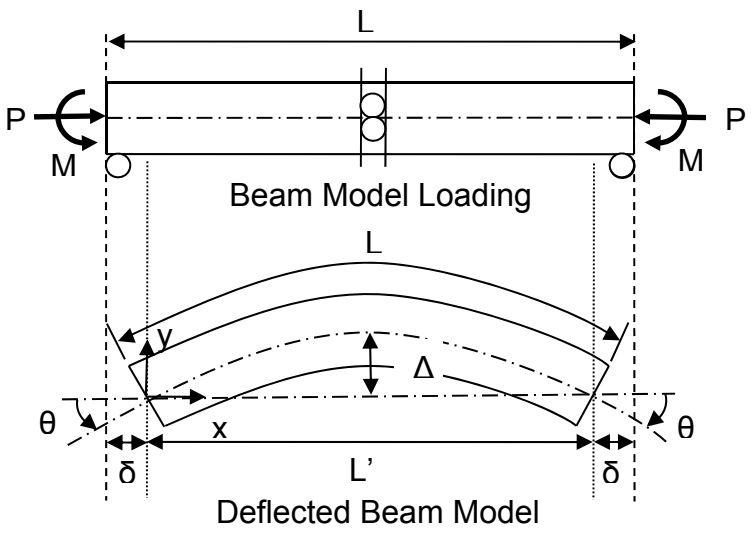

Fig. 2: Beam Model and Notation

A displacement function for the deflected beam model shown above is assumed to be second order parabolic as is appropriate for a beam subjected to a uniform moment condition along the length (i.e. a prestressed concrete beam with a flat strand profile). The displacement function reflecting elastic vertical displacement values for any point along the x-axis is written as

$$y(x) = \frac{4\Delta x(L\prime - x)}{(L\prime)^2} \tag{3}$$

which yields zero displacement at the beam ends (e.g. values of $x = 0$ and $x = L'$) and yields Δ, the peak midspan camber, when $x = L'/2$.

5. Energy Principle Derivation for Camber Neglecting End Translation

This first derivation neglects the effect of end translation due to bending, δ, in the calculation of the external work term, ΔW, and thus provides identical results to conventional beam model approaches calculated by Eq. (1). It is also important to note that in all subsequent analyses, axial shortening effects due to pure compression loading, shear, and torsion are uncoupled from the effects considered and thus can be neglected without affecting the solution. In this first case, external work done on the system occurs only due to end rotations at each beam end and can be calculated as the area under a linear moment-rotation diagram.

$$\Delta W_{rotation} = \frac{2M\theta}{2} = M\theta \tag{4}$$

where $\Delta W_{rotation}$ denotes the external work done on the system due to both end rotations. Taking a first derivative of the displacement function from Eq. (3), an expression can be found for slope at a given cross section as shown in Eq. (5). Using small displacement theory, the terms slope and rotation are interchangeable with respect to the beam ends.

$$\theta(x) = \frac{d}{dx}y(x) = \frac{4\Delta(L'-x)}{(L\prime)^2} - \frac{4\Delta x}{(L\prime)^2} \tag{5}$$

By substituting $x = 0$ or $x = L'$, end rotations can be calculated.

$$\theta(0) = \frac{4\Delta(L'-0)}{(L\prime)^2} - \frac{4\Delta(0)}{(L\prime)^2} = \frac{4\Delta}{L\prime} \tag{6}$$

Summing and collecting terms, the external work term can now be determined as

$$\Delta W_{rotation} = M\theta = M\left(\frac{4\Delta}{L\prime}\right) \tag{7}$$

At this point, the two unknowns in the external work term are the midspan camber, Δ, and the horizontal projection of deformed length, L'.

Next, an expression for the internal strain energy of the system can be found by integrating the internal stresses and strains with respect to the volume.

$$\Delta U = \frac{1}{2}\int \sigma\varepsilon \, dv = \int_0^L \frac{M^2}{2EI} dx \tag{8}$$

The limits of the integral are selected as the full length of the beam since the centroidal axis of the beam remains length L even after the beam deflects through the parabolic displacement function. At this point, it is assumed that all variables in the internal strain energy expression (i.e. internal moment, length, modulus of elasticity, and moment of inertia) are known and can be substituted to calculate a quantity, hereafter denoted as #.

Setting the internal strain energy term, ΔU, equal to the external work term, ΔW, it becomes obvious that two unknowns remain (Δ and L'), but only a single equation is available for solution.

$$M\left(\frac{4\Delta}{L\prime}\right) = \# \tag{9}$$

To gain the additional equation necessary for solution, it is possible to use the arc length formula to provide a relationship between Δ and L' as shown in Eq. (10).

$$L = \int_0^{L'} \sqrt{1 + \left[\frac{d}{dx}y(x)\right]^2} \, dx \tag{10}$$

The arc length formula is extremely complex in this formulation. Using the binomial expansion approximation, Eq. (10) is simplified as shown in Eq. (11).

$$L = \int_0^{L'} 1 + \frac{1}{2}\left[\frac{d}{dx}y(x)\right]^2 dx \tag{11}$$

Collecting terms and numerically approximating Eq. (11), it is found that the elastic midspan camber (neglecting the effects of end translation) is as follows:

$$\Delta = 0.61237\sqrt{L'}\sqrt{L - L'} \tag{12}$$

The accuracy of the above numerical approximation was verified by considering a progressively large number of terms in the binomial expansion series. Accuracy well beyond that required for practical analysis was achieved with a single term approximation as shown in Eq. (11).

Substituting values for a set of known variables and solving the system of equations presented by Eqs. (9) and (12), a numerical solution can be reached for a set of girder inputs. The following example verifies the results of this first derivation and provides an identical solution to that found from the commonly used Eq. (1).

5.1. Example

For a prestressed girder with a flat strand profile and the following set of given properties, calculate the upward elastic camber tendency at midspan. $L = 1174\ in., e = 17.78\ in., P = 1162\ kip, E = 6200\ ksi, and\ I = 268{,}077\ in.^4$ (Note: 1 in. = 0.0254 m., 1 kip = 4.45 kN)

In order to solve using the conventional solution, substitute the above given values in Eq. (1) as follows:

$$\Delta = \frac{PeL^2}{8EI} = \frac{(1162\ kip)(17.78\ in.)(1174\ in.)^2}{8(6200\ ksi)(268{,}077\ in.^4)} = 2.14\ in.\ (5.44\ cm.) \tag{13}$$

To solve using the derived energy approach, the internal strain energy term can be calculated as

$$\Delta U = \int_0^L \frac{(Pe)^2}{2EI}dx = \int_0^{1174} \frac{\left((1162\ kips)(17.78\ in.)\right)^2}{2(6200\ ksi)(267{,}077\ in.^4)}dx = 150.6\ kip - in \tag{14}$$

which can be substituted into Eq. (9) as follows:

$$(1162\ kips)(17.18\ in.)\left(\frac{4\Delta}{L'}\right) = 150.67 \tag{15}$$

Simultaneous solution of Eqs. (12) and (15) gives $L' = 1173.9896\ in.\ (29.82\ m.)$ and $\Delta = 2.14\ in.\ (5.44\ cm.)$

5.2. Commentary

By demonstrating that the above formulation agrees with the conventional solution, the following assumptions are affirmed:

- Small displacement theory is valid,
- The assumed parabolic deflected shape is sufficiently accurate,
- The assumed boundary conditions as outlined in Fig. 2 are valid,
- It is valid to decouple the effects of axial shortening (due to concentric compression), shear, and torsion without affecting the accuracy of the solution,
- The use of the arc length formula (and the corresponding binomial expansion) are justified and provide sufficient accuracy.

Readers will notice that while the elastic upward camber tendency agrees with the conventional solution and the centroidal beam length has remained unchanged, the projected horizontal length, L', has shortened slightly due to the upward camber action. Intuitively, this phenomenon should be expected, but is typically neglected from simplified line beam bending models. While some skeptics of the computation method presented here may contend that an equivalent end shortening may be calculated for any beam (given known values for beam length and a midspan deflection), it is important to note that the horizontal projected length, L', is critical to the formulation of the method, acts as an intermediate variable, and cannot be decoupled from the solution in any way.

In the next derivation, the effect of this end translation due to bending, δ, will also be included in the calculation of the external work term, ΔW, and thus, a more theoretically correct solution will be reached[1].

[1] The practice of accounting for end shortening due to bending can also be used in the derivation of the critical buckling load in columns subject to both axial compression and bending as reviewed in [14].

6. Energy Principle Derivation for Camber Including End Translation Due to Bending

Due to the roller boundary conditions at each end of the beam (as shown in Fig. 2), end translation is an intrinsic effect of the camber motion and should be included in the formulation and derivation of the upward elastic camber. This second derivation includes an additional term for external work, ΔW, which allows for consideration of end translation due to bending. As previously derived, the external work due to rotation was expressed as

$$\Delta W_{rotation} = \frac{2M\theta}{2} = M\left(\frac{4\Delta}{L\prime}\right) \tag{4}$$

which represents twice the area under a linear moment-rotation diagram of the beam end. In this second derivation, an additional term, $\Delta W_{translation}$, is introduced to account for the work performed on the system due to the translation of the axial prestressing force, P. From the notation in Fig. 2, the translation which occurs at each end due to bending only can be expressed as follows:

$$\delta = \frac{L-L\prime}{2} \tag{16}$$

Similar to the derivation of the $\Delta W_{rotation}$ term, $\Delta W_{translation}$ can be computed as twice the area under a linear load deflection diagram of each beam end:

$$\Delta W_{translation} = \frac{2P}{2} = P\left(\frac{L-L\prime}{2}\right) \tag{17}$$

Summing the total external work on the system,

$$\Delta W = \Delta W_{rotation} + \Delta W_{translation} \tag{18}$$

and substituting terms,

$$\Delta W = M\left(\frac{4\Delta}{L\prime}\right) + P\left(\frac{L-L\prime}{2}\right) \tag{19}$$

The internal strain energy term, ΔU, remains unchanged from the first derivation because the deformed shape is the same as that of the previous formulation. By setting the internal strain energy and external work terms equal, the following equation is derived:

$$M\left(\frac{4\Delta}{L\prime}\right) + P\left(\frac{L-L\prime}{2}\right) = \# \tag{20}$$

From this point, the numerical solution process is identical to the previous derivation. An example problem is presented below for clarification.

6.1. Example

For a prestressed girder with a flat strand profile and the following set of given properties, calculate the upward elastic camber tendency at midspan. $L = 1174\ in., e = 17.78\ in., P = 1162\ kip, E = 6200\ ksi, and\ I = 268{,}077\ in.^4$ (Note: 1 in. = 0.0254 m., 1 kip = 4.45 kN)

The solution from the conventional analysis as shown in Eq. (13) $= 2.14\ in.$ (5.44 $cm.$)

To solve using the derived energy approach, the internal strain energy term is again calculated as

$$\Delta U = \int_0^L \frac{(Pe)^2}{2EI}\,dx = \int_0^{1174} \frac{\left((1162\ kips)(17.78\ in.)\right)^2}{2(6200\ ksi)(267{,}077\ in.^4)}\,dx = 150.67\ kip - in \tag{21}$$

which can be substituted into Eq. (20) as follows:

$$(1162\ kips)(17.18\ in.)\left(\frac{4\Delta}{L'}\right) + 1162\ kips\left(\frac{1174\ in. - L'}{2}\right) = 150.67\ kip - in \tag{22}$$

When Eqs. (12) and (22) are simultaneously solved for unknowns by a math evaluation software, $L' = 1173.9903\ in.$ (29.8194 $m.$) and $\Delta = 2.062\ in$ (5.24 $cm.$), as compared to the previously derived solution of $L' = 1173.9896\ in.$ (29.8193$m.$) and $\Delta = 2.141\ in.$ (5.44 $cm.$) In this case, the variation in upward midspan camber components between the two methods approaches 4%. This apparent decrease in midspan upward camber tendency achieved by the second derivation method is hereafter termed a "reduced camber theory."

6.2. Commentary

It is important to note that the above example calculates only the upward camber component of the girder. To calculate the net upward deflection (as would be observed in the field), superposition is used to add the upward camber component to the simultaneous downward self-weight component. The downward self-weight component will always tend to have a cancelling effect on the upward camber component and, therefore, will tend to increase the percent variation when comparing the two computation methods shown above. Eq. (23) shows how a 4% variation in the upward camber component could correspond to a 56% variation in net camber if the girder had a downward self-weight deflection component of 2 in (5.08 cm).

$$\%\ Difference\ in\ Net\ Camber = \left(\frac{(2.141\ in.-2\ in.)-(2.062\ in.-2\ in.)}{2.141\ in.-2\ in.}\right) * 100\ = 56\% \quad (23)$$

7. Discussion of Results

7.1. Computer Implementation

The computational procedures derived in this report are conducive to computer automation to allow efficient modification of inputs and examination of corresponding results. However, the initial setup of a computer procedure can be rather complex and often requires a specific order of steps to allow software to reach a unique solution.

7.2. Comparison of Methods

When using an automated program, it becomes clear that the derived solution for the reduced camber theory approaches the conventional solution as girders decrease in length. Fig. 3 shows a comparison of the two prediction methods for a given set of varying girder lengths, while holding all other noted parameters constant.

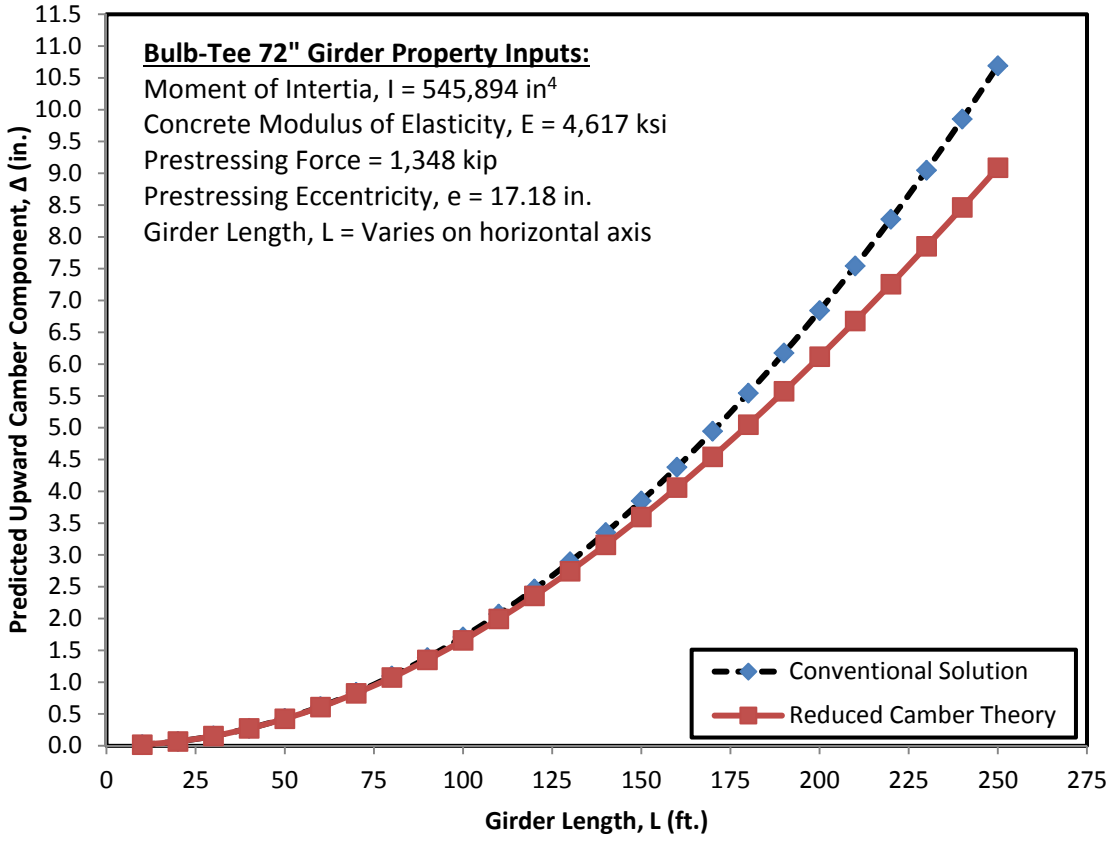

Fig. 3: Comparison of Camber Prediction Methods by Girder Length

For very short girders, the predicted camber values are identical. This is a significant conclusion as it affirms the soundness of the derivation within the bounds of girder lengths historically validated as accurate. For various longer span inputs approaching 300 ft., the conventional method overestimates the upward elastic camber tendency by more than 15% when compared to the reduced camber theory.

7.3. State of the Industry Commentary

After identifying the trends discussed above, it is tempting to examine the prestressed concrete industry as a whole and attempt to draw parallels between any changes in practice which may correspond to worsening camber predictions in recent years. The lack of a historical research focus (pre-2002) on camber prediction in prestressed concrete girders suggests that historically, industry standard practice and tolerance limits were in sync and allowed designers to predict camber with sufficient accuracy to yield functional structures and avoid construction problems. In 2002, Stallings [5] published the first major research study drawing attention to this issue of inaccurate camber predictions. Shortly thereafter, various other entities identified the issue as troublesome and began sponsoring research in this field.

Coincidentally, the early 2000's correspond to a time of great change in the prestressed concrete industry. Most notably, this period was characterized by (1) greatly increased concrete compressive strengths due to the implementation of high-performance concrete (HPC) and (2) expanding research and usage of light-weight aggregate for long span girders [4]. Both of the above mentioned developments allowed engineers to greatly increase design span lengths. In fact, in 2003 as part of the National Cooperative Highway Research Program (NCHRP), Castrodale and White [15] released a report detailing various strategies aimed specifically at extending span ranges of precast prestressed concrete girders.

The reduced camber theory set forth in this paper becomes a convenient way to explain the sudden worsening of the accuracy of camber predictions which has occurred in recent years. As shown in Fig. 3, shorter span girders (lengths less than approximately 130 ft.) show little difference between the prediction methods. However, as span lengths continue to increase to nearly 300 ft. in present day, significant variations exist and may be partly to blame for recent troublesome predictions of camber.

8. Summary and Concluding Remarks

The conventional method of predicting camber in prestressed concrete girders neglects the effect of axial shortening due to bending and may lead to an overestimation of the upward elastic camber component. Through the use of an energy method and geometric relationships, an alternate formulation to predict camber is presented by means of two detailed derivations. The first derivation included in this paper yields identical results to the conventional method, thereby validating various assumptions in the formulation and convincing readers that the methodology of the reduced camber theory is sound. The final derivation and analysis thereof further suggests that the reduced camber theory is valid, agrees with intuitive trends regarding increasing span lengths, and may even correspond to recent changes in the state of the prestressed concrete industry. Although camber prediction in prestressed concrete girders may inherently include a level of uncertainty [1], the apparent reduced camber theory detailed in this paper is offered as a possible explanation for the continued difficulty in achieving accurate initial elastic camber predictions in prestressed concrete girders.

Notation:

The following symbols are used in this paper:

M = end moment acting on the girder (kip-in.);

P = magnitude of the prestress force on the girder end (kips);

Δ = midspan elastic upward camber component (in.);

e = distance from the neutral axis to the centroid of prestressing steel (in.);

L = total beam length (in.);

E = modulus of elasticity of concrete (kips/in^2);

I = moment of inertia of the gross concrete section (in^4);

ΔW = magnitude of external work performed on the system;

ΔU = magnitude of change in internal strain energy;

L' = horizontal projected length after deflection (in.);

δ = relative horizontal end translation at each end (in.);

θ = rotation of beam end (rad);

$y(x)$ = function representing upward elastic camber tendency along beam (in.);

$\Delta W_{rotation}$ = portion of external work due to rotation of the beam end;

$\theta(x)$ = function representing rotation along beam (rad);

σ = stress at a given point within the member (ksi);

ε = strain at a given point within the member (in/in);

V = volume of the beam (in.^{3});

= a unique number able to be computed by equation;

a, b = symbolic limits of the arc length formula; and

$\Delta W_{translation}$ = portion of the external work due to translation of the beam end,

References:

[1] Precast Prestressed Concrete Institute (PCI). Precast Prestressed Concrete Bridge Design Manual. Manual , Chicago, IL: PCI, 2011.
[2] American Concrete Institute Committee (ACI) 435. ACI 435R Control of Deflection in Concrete Structures. Committee Report, Farmington Hills, MI : ACI, 2003.
[3] Buettner, Donald R., and James R. Libby. ""Camber" Requirements for Pretensioned Members." Concrete International, February 1979: 66-72.
[4] Tadros, Maher K., Faten Fawzy, and Kromel E. Hanna. "Precast, Prestressed Girder Camber Variability." Precast Prestressed Concrete Institute Journal, 2011: 135-154.
[5] Stallings, Michael J., Robert W. Barnes, and Sam Eskildsen. "Camber and Prestress Losses in Alabama HPC Bridge Girders." Precast Prestressed Concrete Institute Journal, September 2003: 2-16.
[6] Rosa, Michael A., John F. Stanton, and Marc O. Eberhard. Improving Predictions for Camber In Precast, Prestressed Concrete Bridge Girders. Seattle, WA: Washington State Transportation Center, 2007.
[7] Tadros, Maher K., Stephen J. Seguirant, and James G. Gallt. Report 496: Prestressed Losses in Pretensioned High-Strength Concrete Bridge Girders . National Cooperative Highway Research Program Report, Washington, DC: Transportation Research Board , 2003.
[8] French, Catherine E., and Cullen O'Neill. Validation of Prestressed Concrete I-Beam Deflection and Camber Estimates. Final Report, St. Paul, MN: Minnesota Department of Transportation, 2012.
[9] Storm, Tyler K., Sami H. Rizkalla, and Paul Z. Zia. "Effects of Production Practices on Camber of Prestressed Concrete Bridge Girders." Precast Prestressed Institute Journal, Winter 2013: 96-111.
[10] Precast Prestressed Concrete Institute (PCI). Committee on Bridges - Camber FAST Team. Committee Report, Chicago, IL: Precast Prestressed Concrete Institute, 2012.
[11] Johnson, Brandon Ray. Time-Dependent Deformation in Precast, Prestressed Bridge Girders. MS Thesis, Auburn, AL: Auburn University, 2012.
[12] Nawy, Edward G. Prestressed Concrete - A Fundamental Approach. Upper Saddle River, NJ: Pearson Education, Inc., 2010.
[13] Hibbeler, R. C. Mechanics of Materials. Upper Saddle River, NJ: Pearson Prentice Hall, 2011.
[14] Chajes, Alexander. Principles of Structural Stability Theory. Prentice-Hall, Inc. Englewood Cliffs, NJ. 1974.
[15] Castrodale, R.W., and White, C.D. Extending Span Ranges of Precast Prestressed Concrete Girders: NCHRP Report 517. Transportation Research Board. Washington, D.C. 2004.

Appendix B: Evidence of Preservation of Standard Deviation Concept

Appendix B includes statistical simulations that show that the distribution of the test statistic for concrete strength is identical to the sampled distribution assuming that a constant standard deviation applies in this range.

Proof of Preservation of Standard Deviations

Dave Mante

Tuesday, February 10, 2015

Generate five normal distributions (n=10,000) for concrete mixture trials with varying means and identical standard deviations of 500 psi:

```
mix1<-rnorm(10000,20000,500)

mix2<-rnorm(10000,10000,500)

mix3<-rnorm(10000,5000,500)

mix4<-rnorm(10000,8000,500)

mix5<-rnorm(10000,4000,500)
data<-rbind(mix1,mix2,mix3,mix4,mix5)
datatarget1<-rep(20000,10000)
datatarget2<-rep(10000,10000)
datatarget3<-rep(5000,10000)
datatarget4<-rep(8000,10000)
datatarget5<-rep(4000,10000)
datatarget<-rbind(datatarget1,datatarget2,datatarget3,datatarget4,datatarget5)
```

Compute difference statistic distribution for each mixture:

```
Tmix1=0
Tmix2=0
Tmix3=0
Tmix4=0
Tmix5=0

for (i in 1:10000){
     Tmix1[i]=20000-mix1[i]
     Tmix2[i]=10000-mix2[i]
     Tmix3[i]=5000-mix3[i]
     Tmix4[i]=8000-mix4[i]
     Tmix5[i]=4000-mix5[i]
}
sdmix1<-sd(Tmix1)
sdmix2<-sd(Tmix2)
sdmix3<-sd(Tmix3)
sdmix4<-sd(Tmix4)
sdmix5<-sd(Tmix5)
```

Display the standard deviation of each generated mixture distribution, the standard deviation of each computed difference statistic distribution, and the coefficient of variability for each computed difference statistic distribution:

```
sdmix1
```

```
## [1] 497.5
```

```
sd(mix1)
```

```
## [1] 497.5
```

```
varmix1=sdmix1/20000*100
varmix1
```

```
## [1] 2.487
```

```
sdmix2
```

```
## [1] 499.3
```

```
sd(mix2)
```

```
## [1] 499.3
```

```
varmix2=sdmix2/10000*100
varmix2
```

```
## [1] 4.993
```

```
sdmix3
```

```
## [1] 497.9
```

```
sd(mix3)
```

```
## [1] 497.9
```

```
varmix3=sdmix3/5000*100
varmix3
```

```
## [1] 9.958
```

```
sdmix4
```

```
## [1] 499.7
```

```
sd(mix4)
```

```
## [1] 499.7
```

```
varmix4=sdmix4/8000*100
varmix4
```

```
## [1] 6.246
```

```
sdmix5
```

```
## [1] 496.7
```

```
sd(mix5)
```

```
## [1] 496.7
```

```
varmix5=sdmix5/4000*100
varmix5
```

```
## [1] 12.42
```

It is confirmed that the standard deviation of the inital generated distribution is identical to the standard deviation of the computed difference statistic distribution as expected.

Next, compute the mean for the combined data set, the difference statistic distribution of the combined data set, and the variance of the combined data set.

```
mean.data<-mean(data)
  Tdata=0
for (i in 1:length(data)){
     Tdata[i]=datatarget[i]-data[i]
     }
sd(data)
```

```
## [1] 5736
```

```
sd(Tdata)
```

```
## [1] 498.2
```

```
vardata=sd(data)/mean(data)*100
vardata
```

```
## [1] 61.01
```

```
vardata=sd(Tdata)/mean(data)*100
vardata
```

```
## [1] 5.298
```

We observe that the standard deviation of the full data set is not a valid reflection of the initially generated distributions. Instead, the difference statistic distribution is preferable and is identical to the assumed uniform standard deviation of each of the five generated data sets.

Furthermore, we observe that the variance of the computed difference statistic is not preserved.

Appendix C: Raw Historical Strength Data Set

Appendix C includes the complete condensed raw data set based on the complete data set compiled by Hofrichter (2014). This data set includes all available strength records from four regional precast, prestressed concrete producers as required for the analyses of Chapter 5 of this dissertation. The data set is filtered to include only complete records (that is, values for each column) and records that achieved both the specified prestress release strength and the 28 day strength.

Plant	Specified f`ci (psi)	Specified f`c (psi)	Air Content (%)	Chronological Time to Release (days)	Average Release Breaks (psi)	Average 28-day Breaks (psi)
C	4,000	5,000	4.0	0.61	4,790	7,350
C	4,000	5,000	3.2	0.52	4,750	7,790
C	4,000	5,000	4.0	0.69	5,370	8,130
C	4,000	5,000	3.4	0.61	5,060	8,180
C	4,000	5,000	3.5	0.63	6,730	8,410
A	4,000	5,000	4.2	2.72	8,500	9,860
A	4,000	5,000	4.5	2.83	8,450	9,920
A	4,000	5,000	3.4	0.72	7,940	10,110
B	4,000	5,000	2.9	0.78	7,090	10,580
B	4,000	5,000	2.7	0.75	7,160	10,600
B	4,000	5,000	2.7	0.67	6,990	10,620
D	4,000	5,000	3.0	1.93	8,310	10,620
B	4,000	5,000	2.8	0.69	6,470	10,710
B	4,000	5,000	3.5	0.58	7,970	11,120
D	4,000	5,000	2.6	1.98	8,590	11,170
D	4,000	5,000	2.8	0.89	8,230	11,360
D	4,000	5,000	2.5	0.60	7,130	11,930
D	4,000	5,000	2.5	0.86	8,840	12,020
D	4,000	5,000	2.5	2.83	10,290	12,160

D	4,000	5,000	2.5	0.59	7,200	12,180
D	4,000	5,000	2.6	2.78	10,150	12,290
D	4,000	5,000	2.5	3.01	10,850	12,600
D	4,000	5,000	1.8	2.98	10,990	13,010
C	4,500	5,000	4.5	0.87	5,770	7,690
C	4,500	5,000	4.2	0.66	5,250	8,610
C	4,500	5,000	5.0	5.07	7,620	9,070
C	4,500	5,000	4.2	2.84	7,410	9,400
C	4,500	5,000	5.5	1.90	7,370	10,050
C	4,500	5,000	5.0	0.92	6,980	10,290
B	4,500	5,000	3.1	0.70	7,610	10,640
B	4,500	5,000	3.3	0.71	7,500	10,720
B	4,500	5,000	3.1	0.76	7,630	10,720
B	4,500	5,000	2.8	0.67	7,430	10,890
A	5,000	5,000	4.5	0.74	6,110	8,620
A	5,000	5,000	5.5	0.74	6,230	8,620
A	5,000	5,000	2.6	0.73	6,470	9,000
A	5,000	5,000	4.5	0.73	6,780	9,050
A	5,000	5,000	5.0	0.74	7,040	9,250
A	5,000	5,000	4.2	0.69	6,640	9,530
A	5,000	5,000	4.0	0.70	6,760	9,560
A	5,000	5,000	4.0	0.68	6,850	9,610
A	5,000	5,000	3.0	0.76	7,030	9,650
A	5,000	5,000	3.3	2.80	8,840	9,680
A	5,000	5,000	4.0	0.72	7,370	9,720
A	5,000	5,000	2.5	0.65	6,020	9,750
A	5,000	5,000	3.0	0.72	6,750	9,760
A	5,000	5,000	3.2	0.73	6,930	9,850
A	5,000	5,000	2.9	0.69	6,770	9,870
A	5,000	5,000	2.5	2.77	8,200	9,930
A	5,000	5,000	4.0	0.75	7,220	10,050
A	5,000	5,000	4.0	0.71	7,040	10,120
A	5,000	5,000	2.6	0.71	6,560	10,210
A	5,000	5,000	3.7	0.65	7,040	10,240
A	5,000	5,000	3.0	2.77	8,790	10,260
A	5,000	5,000	3.8	0.72	6,850	10,290
A	5,000	5,000	3.2	0.68	7,000	10,310
A	5,000	5,000	4.0	2.74	8,310	10,320
A	4,495	5,220	4.0	2.87	9,850	11,160
A	4,495	5,220	3.1	2.84	9,590	11,230
A	4,495	5,220	3.1	0.80	9,490	12,110

A	4,495	5,220	3.0	0.82	9,190	12,590
B	4,000	5,500	3.8	0.84	7,790	10,620
B	4,000	5,500	3.5	0.67	7,560	10,630
B	4,000	5,500	3.3	0.68	7,550	10,740
B	4,000	5,500	2.9	0.64	7,620	10,790
B	4,000	5,500	3.8	0.82	7,720	10,790
B	4,000	5,500	3.1	0.66	7,570	10,860
B	4,000	5,500	3.0	0.68	6,360	11,320
B	4,000	5,500	2.6	0.72	6,620	12,140
B	4,500	5,500	3.0	0.69	7,590	10,620
B	4,500	5,500	2.8	0.68	7,860	10,830
B	4,500	5,500	2.9	0.63	5,850	12,660
B	5,000	5,500	2.8	0.62	6,540	10,230
A	5,000	5,500	3.8	0.69	6,960	10,360
B	5,000	5,500	2.7	0.60	6,460	10,410
B	5,000	5,500	2.8	0.61	5,210	10,580
A	5,000	5,500	4.2	0.73	7,200	10,610
B	5,000	5,500	3.4	0.70	7,490	10,610
A	5,000	5,500	3.8	0.71	7,040	10,650
B	5,000	5,500	3.2	0.67	7,380	10,710
B	5,000	5,500	3.2	0.54	5,620	10,720
B	5,000	5,500	3.3	0.63	6,130	10,720
B	5,000	5,500	3.6	0.57	6,850	10,720
B	5,000	5,500	3.1	0.60	5,060	10,800
B	5,000	5,500	2.6	0.84	6,800	10,810
B	5,000	5,500	4.8	0.88	8,120	10,810
B	5,000	5,500	3.2	0.68	7,810	10,820
A	5,000	5,500	3.6	0.72	7,470	10,840
B	5,000	5,500	2.7	0.65	6,330	10,850
A	5,000	5,500	3.8	0.74	7,550	10,880
B	5,000	5,500	2.7	0.62	6,200	10,920
B	5,000	5,500	2.8	0.64	5,890	10,950
B	5,000	5,500	3.3	0.79	6,960	10,960
B	5,000	5,500	2.7	0.76	7,100	11,030
B	5,000	5,500	3.3	0.64	6,790	11,080
B	5,000	5,500	3.8	0.56	5,590	11,110
B	5,000	5,500	3.6	0.54	6,850	11,130
A	5,000	5,500	3.5	0.71	6,870	11,150
B	5,000	5,500	2.8	0.81	6,940	11,190
A	5,000	5,500	3.5	0.76	7,700	11,460
A	5,000	5,500	2.4	0.75	7,850	11,780

B	5,000	5,500	3.4	0.72	7,170	11,800
A	4,500	5,600	3.6	0.68	6,200	8,710
A	4,500	5,600	2.1	2.79	9,080	10,070
B	4,500	5,600	2.7	0.59	7,280	11,060
B	4,500	5,600	2.8	0.66	7,830	11,090
B	4,500	5,600	4.6	2.89	8,270	11,100
B	4,500	5,600	2.6	0.72	7,490	11,720
B	4,500	5,600	2.6	0.81	7,410	12,130
A	4,495	5,800	3.7	0.71	7,750	10,540
A	4,495	5,800	3.6	0.70	8,350	10,750
A	4,495	5,800	3.2	0.71	8,390	11,190
A	4,495	5,800	3.6	0.75	8,310	11,410
A	5,900	5,900	3.9	0.79	6,400	9,910
A	5,990	5,990	3.2	0.86	7,610	11,250
A	5,990	5,990	2.8	0.64	6,560	11,280
A	5,990	5,990	3.1	0.83	6,920	12,290
A	4,000	6,000	2.5	0.79	6,640	8,630
A	4,000	6,000	5.2	0.59	7,330	9,170
B	4,000	6,000	3.8	0.62	7,010	9,480
A	4,000	6,000	3.0	0.82	7,250	9,690
A	4,000	6,000	3.5	0.63	7,520	9,690
A	4,000	6,000	3.1	0.42	8,330	9,740
A	4,000	6,000	3.1	0.84	7,070	10,370
A	4,000	6,000	3.0	0.87	7,430	10,590
A	4,000	6,000	3.3	0.76	6,530	10,730
A	4,100	6,000	5.4	0.83	5,730	8,500
B	4,100	6,000	3.5	0.85	6,810	9,080
A	4,100	6,000	3.5	0.80	6,450	9,190
B	4,100	6,000	3.4	0.70	7,590	10,000
A	4,100	6,000	2.0	0.89	7,000	10,470
A	4,400	6,000	3.8	0.38	7,230	9,230
A	4,400	6,000	3.8	0.68	8,950	10,690
A	4,500	6,000	3.1	0.74	8,130	10,210
A	4,500	6,000	2.8	0.91	8,960	11,070
B	4,500	6,000	3.4	1.08	8,000	11,330
B	4,500	6,000	2.7	2.59	9,400	11,500
A	4,600	6,000	3.6	2.75	7,620	9,160
A	4,600	6,000	3.9	0.80	7,030	9,230
A	4,600	6,000	3.7	0.63	5,840	9,630
A	4,600	6,000	3.7	0.88	8,180	9,970
A	4,600	6,000	3.8	0.65	5,730	10,180

A	4,600	6,000	3.8	2.87	8,400	10,200
A	4,600	6,000	3.7	0.81	7,330	10,300
A	4,600	6,000	3.2	0.70	8,040	10,350
A	4,600	6,000	3.6	0.82	7,480	10,410
A	4,600	6,000	2.8	0.83	8,400	11,300
A	4,600	6,000	2.7	0.78	7,750	11,330
A	4,600	6,000	2.9	0.80	9,380	11,380
A	4,600	6,000	2.9	2.86	9,640	11,920
A	4,600	6,000	2.8	0.68	8,110	12,080
A	4,700	6,000	3.9	0.72	7,220	8,690
A	4,700	6,000	4.0	0.78	6,880	9,150
A	4,700	6,000	3.1	0.75	7,450	9,170
A	4,700	6,000	3.9	0.72	7,630	9,380
A	4,700	6,000	4.1	0.87	7,740	9,690
A	4,800	6,000	3.0	0.86	6,590	9,160
A	4,800	6,000	3.7	0.84	6,780	9,500
A	4,800	6,000	3.2	0.85	7,310	9,730
A	4,900	6,000	3.3	2.75	8,960	8,240
A	4,900	6,000	3.2	2.73	8,480	10,090
A	4,900	6,000	3.5	0.71	7,330	10,480
C	5,000	6,000	4.4	0.95	5,360	7,310
C	5,000	6,000	2.8	0.91	5,230	7,500
C	5,000	6,000	4.5	0.61	5,110	7,760
C	5,000	6,000	5.4	0.83	5,360	7,800
C	5,000	6,000	4.2	0.85	5,560	8,080
C	5,000	6,000	4.2	0.91	5,420	8,310
C	5,000	6,000	4.9	1.74	6,540	8,370
C	5,000	6,000	5.5	0.95	6,460	8,460
C	5,000	6,000	4.2	0.94	5,130	8,600
A	5,000	6,000	4.9	0.72	7,660	8,690
A	5,000	6,000	2.9	0.75	7,040	8,920
A	5,000	6,000	4.0	0.71	7,270	8,980
A	5,000	6,000	4.5	0.68	6,970	9,040
A	5,000	6,000	5.5	0.72	6,490	9,110
A	5,000	6,000	4.5	0.65	5,230	9,150
A	5,000	6,000	4.4	0.78	6,690	9,150
A	5,000	6,000	3.1	0.69	7,460	9,180
A	5,000	6,000	2.8	0.85	6,320	9,260
A	5,000	6,000	3.8	0.63	7,140	9,260
A	5,000	6,000	3.7	0.80	5,530	9,310
A	5,000	6,000	3.2	0.63	7,310	9,310

A	5,000	6,000	3.3	0.66	7,250	9,320
B	5,000	6,000	3.5	0.84	6,730	9,350
A	5,000	6,000	3.1	0.74	6,500	9,420
B	5,000	6,000	3.6	0.81	7,230	9,430
A	5,000	6,000	4.4	0.63	7,040	9,450
A	5,000	6,000	3.2	0.68	7,460	9,450
A	5,000	6,000	3.1	0.68	6,810	9,460
A	5,000	6,000	4.2	0.74	7,380	9,480
C	5,000	6,000	5.5	0.86	6,550	9,540
A	5,000	6,000	3.8	0.68	7,560	9,550
A	5,000	6,000	2.9	2.68	7,840	9,630
A	5,000	6,000	2.5	0.76	6,720	9,660
A	5,000	6,000	3.1	0.67	7,480	9,660
A	5,000	6,000	3.4	2.71	8,340	9,680
A	5,000	6,000	3.8	0.74	6,760	9,750
B	5,000	6,000	3.7	0.82	7,100	9,750
B	5,000	6,000	4.4	0.81	6,770	9,770
C	5,000	6,000	4.5	0.69	6,590	9,810
D	5,000	6,000	3.6	0.65	6,340	9,870
A	5,000	6,000	4.0	0.77	7,620	9,900
C	5,000	6,000	3.6	0.91	7,970	9,960
A	5,000	6,000	2.9	0.68	7,650	9,980
A	5,000	6,000	4.3	2.77	9,540	10,020
A	5,000	6,000	4.8	2.74	8,610	10,060
C	5,000	6,000	3.9	0.66	6,350	10,100
A	5,000	6,000	2.5	0.94	7,150	10,100
B	5,000	6,000	4.3	0.82	6,060	10,170
B	5,000	6,000	4.0	0.68	6,350	10,210
A	5,000	6,000	3.6	0.77	8,000	10,220
A	5,000	6,000	3.7	0.62	6,030	10,250
C	5,000	6,000	2.9	0.55	5,600	10,290
A	5,000	6,000	3.8	0.67	7,150	10,290
A	5,000	6,000	2.5	0.88	8,190	10,290
A	5,000	6,000	4.7	0.86	7,140	10,390
B	5,000	6,000	4.0	0.81	6,650	10,410
A	5,000	6,000	4.6	0.76	7,670	10,450
B	5,000	6,000	3.3	0.74	7,570	10,480
A	5,000	6,000	3.8	0.73	7,100	10,490
A	5,000	6,000	3.0	0.92	7,770	10,500
B	5,000	6,000	3.1	0.72	6,660	10,510
A	5,000	6,000	4.5	0.70	7,020	10,530

B	5,000	6,000	3.5	0.78	7,050	10,530
B	5,000	6,000	3.0	0.73	7,370	10,560
A	5,000	6,000	4.1	0.64	6,600	10,570
B	5,000	6,000	2.9	0.74	7,120	10,600
A	5,000	6,000	2.8	0.62	5,800	10,610
B	5,000	6,000	3.2	0.80	6,930	10,620
B	5,000	6,000	4.5	0.76	7,190	10,620
A	5,000	6,000	3.8	0.67	6,610	10,630
B	5,000	6,000	3.2	0.64	6,220	10,650
A	5,000	6,000	4.1	0.70	6,980	10,650
B	5,000	6,000	3.0	0.62	7,430	10,660
B	5,000	6,000	3.1	0.66	6,220	10,680
B	5,000	6,000	4.2	2.65	8,550	10,710
B	5,000	6,000	3.5	0.60	7,240	10,720
A	5,000	6,000	4.4	0.68	7,310	10,720
B	5,000	6,000	3.3	0.77	7,150	10,730
A	5,000	6,000	3.3	0.75	7,810	10,750
A	5,000	6,000	3.5	0.80	8,070	10,790
A	5,000	6,000	3.9	0.68	7,050	10,800
A	5,000	6,000	2.9	0.69	7,900	10,830
A	5,000	6,000	2.8	0.75	7,990	10,830
A	5,000	6,000	3.0	0.71	8,030	10,830
A	5,000	6,000	2.6	0.84	8,620	10,830
A	5,000	6,000	3.9	0.70	6,930	10,890
A	5,000	6,000	3.8	0.66	7,840	10,890
A	5,000	6,000	3.8	0.65	6,330	10,900
A	5,000	6,000	4.9	0.84	8,170	10,900
A	5,000	6,000	3.1	0.84	7,940	10,920
A	5,000	6,000	4.0	0.65	8,540	10,960
A	5,000	6,000	3.7	0.77	7,600	10,970
A	5,000	6,000	3.8	0.63	7,430	10,980
A	5,000	6,000	3.5	0.75	7,530	10,980
A	5,000	6,000	3.8	0.74	7,680	11,000
A	5,000	6,000	2.5	0.78	7,750	11,000
A	5,000	6,000	2.7	0.92	8,510	11,030
A	5,000	6,000	4.2	0.78	6,860	11,050
A	5,000	6,000	3.6	0.75	7,290	11,080
B	5,000	6,000	3.0	0.65	8,080	11,080
A	5,000	6,000	3.1	0.66	7,800	11,120
A	5,000	6,000	4.1	0.84	7,220	11,160
A	5,000	6,000	3.1	2.91	8,630	11,260

A	5,000	6,000	2.9	2.70	9,700	11,300
A	5,000	6,000	3.0	0.86	8,130	11,330
A	5,000	6,000	2.6	2.71	9,430	11,400
A	5,000	6,000	4.3	0.68	7,150	11,410
A	5,000	6,000	3.3	2.81	9,370	11,430
A	5,000	6,000	2.9	2.85	9,740	11,460
A	5,000	6,000	3.6	0.67	8,060	11,480
B	5,000	6,000	3.9	0.80	6,570	11,540
A	5,000	6,000	2.7	0.66	8,630	11,590
A	5,000	6,000	2.5	0.82	8,690	11,610
A	5,000	6,000	3.0	0.84	8,160	11,650
A	5,000	6,000	3.1	0.65	7,020	11,680
A	5,000	6,000	2.9	2.97	9,730	11,690
A	5,000	6,000	2.9	0.77	7,830	11,740
B	5,000	6,000	2.9	0.78	7,260	11,750
A	5,000	6,000	3.8	0.69	7,290	11,790
A	5,000	6,000	3.2	0.65	7,380	11,940
A	5,000	6,000	2.5	0.84	8,480	11,950
A	5,000	6,000	3.6	0.68	6,020	11,990
A	5,000	6,000	2.6	0.76	9,180	12,010
A	5,000	6,000	2.6	0.73	7,800	12,100
A	5,000	6,000	3.5	0.75	8,410	12,120
A	5,000	6,000	3.3	0.84	8,050	12,200
A	5,000	6,000	2.7	0.80	9,080	12,450
D	5,000	6,000	2.5	0.63	9,270	12,620
A	5,100	6,000	5.2	2.70	7,110	8,980
A	5,100	6,000	4.4	2.76	8,760	9,600
A	5,100	6,000	3.3	0.72	6,820	9,700
A	5,100	6,000	5.0	0.86	6,740	9,980
A	5,100	6,000	3.6	0.74	7,870	10,090
A	5,100	6,000	3.1	0.67	7,360	10,130
A	5,100	6,000	4.1	0.86	7,810	10,300
A	5,100	6,000	3.9	0.80	7,930	10,360
A	5,100	6,000	3.9	0.75	7,760	10,410
A	5,100	6,000	3.1	0.61	7,890	10,430
A	5,100	6,000	4.0	0.72	8,060	10,500
A	5,100	6,000	2.5	0.78	7,220	10,580
A	5,100	6,000	3.8	0.78	8,100	10,580
A	5,100	6,000	3.8	0.88	7,670	10,620
A	5,100	6,000	3.0	0.65	7,880	10,710
A	5,100	6,000	3.7	2.81	9,270	10,750

A	5,100	6,000	4.7	2.80	9,190	10,840
A	5,100	6,000	2.5	0.85	8,250	10,900
A	5,100	6,000	3.1	0.76	7,580	11,130
A	5,200	6,000	4.2	0.75	6,830	9,640
A	5,200	6,000	4.4	0.73	7,480	9,980
A	5,200	6,000	4.5	0.84	7,050	10,280
A	5,200	6,000	3.9	0.83	7,590	10,430
A	5,200	6,000	5.5	0.80	7,450	10,440
A	5,200	6,000	3.3	0.79	7,400	10,610
A	5,200	6,000	3.0	0.83	8,280	10,680
A	5,200	6,000	4.5	0.75	7,650	10,690
A	5,200	6,000	4.0	0.78	7,960	10,760
A	5,200	6,000	2.6	0.84	7,980	10,800
C	5,400	6,000	5.4	2.08	5,780	7,740
A	5,400	6,000	3.7	2.84	8,370	9,860
A	5,400	6,000	4.4	0.71	6,980	9,960
A	5,400	6,000	3.9	0.67	7,790	10,060
A	5,400	6,000	4.2	0.80	6,100	10,160
A	5,400	6,000	5.0	0.74	7,570	10,220
A	5,400	6,000	4.2	0.88	6,750	10,240
A	5,400	6,000	3.6	2.80	7,710	10,320
A	5,400	6,000	4.0	0.77	6,900	10,340
A	5,400	6,000	3.7	0.64	6,300	10,410
A	5,400	6,000	3.7	0.69	7,720	10,490
A	5,400	6,000	3.9	0.67	6,480	10,560
A	5,400	6,000	3.5	2.82	9,130	10,560
A	5,400	6,000	3.6	2.83	7,500	10,650
A	5,400	6,000	2.9	2.79	9,980	10,880
A	5,400	6,000	3.4	0.78	7,280	10,910
A	5,400	6,000	3.6	0.85	7,280	10,940
A	5,400	6,000	2.5	0.75	8,460	10,950
A	5,400	6,000	3.8	0.80	7,910	11,040
A	5,400	6,000	3.4	0.76	8,150	11,040
A	5,400	6,000	2.5	2.81	10,280	11,040
A	5,400	6,000	3.8	0.82	7,890	11,070
A	5,400	6,000	2.8	0.78	8,420	11,070
A	5,400	6,000	3.0	0.82	7,520	11,170
A	5,400	6,000	3.6	0.67	7,360	11,180
A	5,400	6,000	1.7	0.84	8,050	11,180
A	5,400	6,000	3.2	0.80	7,880	11,490
A	5,400	6,000	3.3	0.70	7,190	11,550

A	5,400	6,000	3.5	1.02	8,780	11,830
A	5,400	6,000	2.4	0.82	8,790	11,870
A	5,400	6,000	2.8	1.00	8,410	11,880
A	5,400	6,000	1.9	0.81	8,620	11,990
A	5,400	6,000	2.5	0.79	9,280	12,070
A	5,400	6,000	2.3	0.63	8,340	12,090
A	5,400	6,000	2.4	0.61	8,700	12,220
A	5,400	6,000	2.6	0.74	9,370	12,280
A	5,500	6,000	2.6	0.63	8,300	7,600
A	5,500	6,000	4.1	2.70	8,630	8,150
C	5,500	6,000	5.4	0.91	6,740	8,610
C	5,500	6,000	4.5	0.66	5,850	8,660
A	5,500	6,000	4.9	0.65	7,060	9,240
A	5,500	6,000	2.5	0.67	7,990	9,980
A	5,500	6,000	2.5	0.67	7,760	10,110
B	5,500	6,000	2.5	0.69	6,720	10,120
B	5,500	6,000	3.9	0.83	6,870	10,180
B	5,500	6,000	2.8	0.59	6,700	10,210
B	5,500	6,000	3.5	2.90	8,070	10,260
A	5,500	6,000	2.2	0.88	8,070	10,290
B	5,500	6,000	2.8	0.58	6,320	10,630
B	5,500	6,000	3.1	0.54	6,580	10,650
B	5,500	6,000	3.0	0.80	6,890	10,650
B	5,500	6,000	3.3	0.79	7,120	10,650
B	5,500	6,000	2.9	0.51	7,190	10,660
B	5,500	6,000	3.2	2.59	9,290	10,710
B	5,500	6,000	2.8	0.66	6,780	10,800
B	5,500	6,000	3.8	0.67	7,100	10,940
B	5,500	6,000	3.4	0.55	6,770	11,320
B	5,500	6,000	3.7	0.57	7,040	11,480
B	5,500	6,000	3.2	0.80	7,890	11,870
B	5,500	6,000	2.9	0.70	7,380	12,650
C	5,700	6,000	4.1	1.63	6,610	7,910
C	5,700	6,000	4.7	0.90	6,570	9,500
B	5,700	6,000	3.6	0.68	6,760	10,260
B	5,700	6,000	4.9	0.72	6,700	10,310
B	5,700	6,000	3.1	0.50	5,730	10,370
B	5,700	6,000	3.1	0.83	6,980	10,390
B	5,700	6,000	5.5	0.69	7,230	10,390
B	5,700	6,000	3.0	0.61	6,280	10,460
B	5,700	6,000	3.5	0.74	6,530	10,460

B	5,700	6,000	3.4	0.71	6,880	10,500
B	5,700	6,000	3.2	0.66	6,850	10,530
B	5,700	6,000	3.3	0.67	6,580	10,630
B	5,700	6,000	2.5	0.55	6,630	10,630
A	5,700	6,000	3.2	0.85	8,770	10,630
B	5,700	6,000	2.9	0.64	6,110	10,640
B	5,700	6,000	4.2	0.66	6,260	10,640
B	5,700	6,000	2.5	0.57	6,520	10,640
B	5,700	6,000	3.3	0.57	6,260	10,650
B	5,700	6,000	2.8	2.67	8,800	10,650
B	5,700	6,000	2.9	2.74	8,210	10,660
B	5,700	6,000	3.0	2.59	8,310	10,660
B	5,700	6,000	2.6	0.74	7,160	10,670
B	5,700	6,000	3.5	0.63	7,200	10,670
B	5,700	6,000	3.3	2.87	7,810	10,670
B	5,700	6,000	3.0	0.74	7,440	10,710
B	5,700	6,000	3.7	0.56	6,540	10,720
B	5,700	6,000	3.5	0.66	7,750	10,730
B	5,700	6,000	3.1	0.75	7,020	10,750
B	5,700	6,000	3.0	2.67	9,080	10,750
B	5,700	6,000	2.7	0.74	6,150	10,770
B	5,700	6,000	4.0	0.66	6,570	10,780
B	5,700	6,000	3.1	0.69	7,560	10,780
B	5,700	6,000	3.1	0.74	7,980	10,780
B	5,700	6,000	3.3	0.56	5,860	10,810
B	5,700	6,000	2.6	0.56	7,060	10,910
A	5,700	6,000	2.8	0.93	9,620	11,460
A	5,800	6,000	3.8	0.84	7,170	9,500
A	5,800	6,000	4.7	2.88	8,340	9,630
A	5,800	6,000	3.3	0.83	7,260	9,640
A	5,800	6,000	4.2	0.69	6,320	9,650
A	5,800	6,000	4.3	0.69	6,570	9,740
A	5,800	6,000	4.1	0.67	6,820	9,760
A	5,800	6,000	3.5	0.88	7,880	9,930
A	5,800	6,000	3.8	0.83	9,020	10,690
A	5,800	6,000	4.1	0.66	7,040	11,240
A	6,000	6,000	4.5	0.93	6,230	8,660
C	6,000	6,000	5.5	0.72	6,740	9,160
C	6,000	6,000	2.6	1.68	7,060	10,280
A	6,000	6,000	2.5	0.66	7,170	11,310
A	6,000	6,000	2.6	2.71	9,960	11,410

A	6,000	6,000	2.2	0.77	7,770	11,670
A	6,000	6,000	2.5	0.78	8,930	12,120
A	6,000	6,000	2.7	0.67	8,900	12,770
A	5,394	6,003	4.4	0.71	6,530	9,030
A	5,394	6,003	3.9	0.68	6,000	9,400
A	5,394	6,003	4.4	0.93	6,820	9,400
A	5,394	6,003	4.5	0.79	7,060	9,430
A	5,394	6,003	3.4	0.84	7,220	9,480
A	5,394	6,003	3.5	0.75	6,730	9,490
A	5,394	6,003	4.3	0.72	6,790	9,500
A	5,394	6,003	3.9	2.83	8,070	9,530
A	5,394	6,003	4.0	0.83	7,190	9,560
A	5,394	6,003	3.5	0.88	7,590	9,740
A	5,394	6,003	4.0	0.68	6,340	9,760
A	5,394	6,003	3.5	0.80	6,960	9,760
A	5,394	6,003	4.2	0.83	6,870	9,770
A	5,394	6,003	4.6	0.71	6,380	9,870
A	5,394	6,003	3.1	0.67	6,890	9,940
A	5,394	6,003	3.8	0.79	7,120	10,010
A	5,394	6,003	3.9	0.82	6,690	10,040
A	5,394	6,003	3.7	0.70	6,670	10,050
A	5,394	6,003	3.5	0.86	7,570	10,060
A	5,394	6,003	4.4	0.71	6,580	10,080
A	5,394	6,003	3.9	2.97	8,790	10,080
A	5,394	6,003	3.8	0.79	7,720	10,100
A	5,394	6,003	4.2	2.79	8,400	10,100
A	5,394	6,003	4.0	0.81	6,930	10,140
A	5,394	6,003	4.2	0.78	7,020	10,140
A	5,394	6,003	4.1	0.77	7,060	10,140
A	5,394	6,003	7.0	0.75	7,370	10,140
A	5,394	6,003	3.6	0.85	7,390	10,160
A	5,394	6,003	3.9	2.69	8,390	10,190
A	5,394	6,003	3.8	0.72	7,730	10,220
A	5,394	6,003	4.8	0.85	7,430	10,240
A	5,394	6,003	4.8	0.68	7,740	10,250
A	5,394	6,003	3.7	0.72	7,490	10,260
A	5,394	6,003	4.2	0.82	7,500	10,280
A	5,394	6,003	3.9	0.80	7,630	10,280
A	5,394	6,003	3.1	0.78	7,220	10,340
A	5,394	6,003	3.9	0.75	7,730	10,340
A	5,394	6,003	3.8	0.80	7,940	10,340

A	5,394	6,003	4.0	0.83	7,620	10,360
A	5,394	6,003	4.0	0.81	7,570	10,370
A	5,394	6,003	4.2	0.81	7,700	10,370
A	5,394	6,003	3.6	0.76	7,470	10,390
A	5,394	6,003	3.8	2.78	8,650	10,390
A	5,394	6,003	3.4	0.72	8,040	10,400
A	5,394	6,003	3.6	0.69	7,620	10,410
A	5,394	6,003	5.1	0.81	7,600	10,430
A	5,394	6,003	5.3	0.58	6,850	10,450
A	5,394	6,003	4.4	0.83	8,050	10,450
A	5,394	6,003	4.4	0.78	7,650	10,460
A	5,394	6,003	3.2	0.68	6,890	10,480
A	5,394	6,003	3.5	0.62	7,620	10,480
A	5,394	6,003	3.6	0.64	7,110	10,520
A	5,394	6,003	3.8	0.65	6,850	10,540
A	5,394	6,003	4.2	2.99	8,990	10,540
A	5,394	6,003	4.0	0.70	7,000	10,560
A	5,394	6,003	3.3	0.72	7,260	10,570
A	5,394	6,003	3.6	2.71	8,660	10,570
A	5,394	6,003	3.5	0.75	7,600	10,580
A	5,394	6,003	3.4	0.69	7,720	10,590
A	5,394	6,003	3.8	0.89	7,590	10,660
A	5,394	6,003	3.3	2.73	9,220	10,710
A	5,394	6,003	4.5	0.61	6,700	10,740
A	5,394	6,003	3.5	0.89	7,650	10,740
A	5,394	6,003	4.9	0.75	7,590	10,780
A	5,394	6,003	3.3	0.67	7,090	10,800
A	5,394	6,003	3.4	0.71	7,670	10,820
A	5,394	6,003	4.2	0.68	7,490	10,850
A	5,394	6,003	3.7	0.88	8,010	10,850
A	5,394	6,003	4.8	0.70	7,180	11,010
A	5,394	6,003	3.3	0.67	7,000	11,050
A	5,394	6,003	3.5	0.80	7,960	11,150
A	5,394	6,003	2.8	0.83	8,940	11,170
A	5,394	6,003	5.2	0.61	6,470	11,210
A	5,394	6,003	3.2	0.85	7,970	11,210
A	5,394	6,003	2.0	0.78	8,720	11,210
A	5,394	6,003	3.0	0.73	6,980	11,300
A	5,394	6,003	3.6	0.96	8,120	11,310
A	5,394	6,003	2.9	0.72	7,500	11,330
A	5,394	6,003	3.4	0.82	8,250	11,400

A	5,394	6,003	2.8	0.84	8,350	11,400
A	5,394	6,003	3.0	0.74	7,430	11,430
A	5,394	6,003	3.9	2.65	8,990	11,430
A	5,394	6,003	3.6	0.72	8,080	11,440
A	5,394	6,003	3.4	0.79	8,250	11,500
A	5,394	6,003	2.8	2.72	9,740	11,500
A	5,394	6,003	3.3	2.77	10,290	11,690
A	5,394	6,003	3.2	0.77	7,930	11,920
A	5,394	6,003	2.9	2.69	9,390	12,140
A	5,496	6,090	4.9	0.65	6,710	9,560
A	5,496	6,090	3.2	0.63	6,830	9,940
A	5,496	6,090	3.2	0.73	6,590	10,180
A	5,496	6,090	2.4	2.77	8,400	10,500
A	5,496	6,090	3.0	0.79	7,320	10,590
A	5,496	6,090	3.5	0.69	6,530	10,660
A	5,496	6,090	3.2	0.70	6,970	10,660
A	5,496	6,090	2.5	2.77	9,730	10,700
A	5,496	6,090	2.9	2.81	9,210	10,810
A	5,496	6,090	3.3	0.79	7,310	10,870
A	5,496	6,090	2.5	2.79	8,520	10,900
A	5,496	6,090	3.9	2.77	8,740	10,910
A	5,496	6,090	3.2	0.76	7,520	10,970
A	5,496	6,090	3.0	0.63	6,960	11,290
A	5,496	6,090	2.6	0.65	7,170	11,370
A	5,496	6,090	3.1	0.75	6,500	11,410
A	5,496	6,090	3.2	0.80	7,990	11,430
A	5,496	6,090	2.9	0.67	6,900	11,470
A	5,496	6,090	3.7	0.74	7,860	11,480
A	5,496	6,090	3.4	2.79	9,390	11,520
A	5,496	6,090	3.1	0.71	8,080	11,590
A	5,496	6,090	2.5	0.76	7,690	11,680
A	5,496	6,090	3.3	0.80	7,880	11,740
A	5,496	6,090	4.8	0.89	8,330	11,760
A	5,496	6,090	3.0	0.71	6,770	12,070
A	5,496	6,090	2.8	0.85	8,870	12,130
A	5,510	6,090	3.7	0.86	7,910	10,160
A	5,510	6,090	3.2	0.78	7,690	10,190
A	5,510	6,090	2.6	0.80	8,370	10,450
A	5,510	6,090	3.2	0.92	7,560	10,530
A	5,510	6,090	2.8	0.81	8,050	10,550
A	5,510	6,090	3.1	0.81	7,510	10,570

A	5,510	6,090	3.5	0.94	8,330	10,620
A	5,510	6,090	2.5	0.79	7,610	10,630
A	5,510	6,090	3.0	0.76	7,490	10,660
A	5,510	6,090	3.1	0.89	7,540	10,760
A	5,510	6,090	2.5	0.83	7,760	10,850
A	5,510	6,090	2.9	2.96	9,370	10,890
A	5,510	6,090	3.2	2.92	9,080	10,970
A	5,510	6,090	3.5	0.80	8,300	11,010
A	5,510	6,090	3.0	2.96	9,000	11,020
A	5,510	6,090	2.5	2.98	9,580	11,050
A	5,510	6,090	3.0	0.84	8,480	11,180
A	5,510	6,090	3.3	0.94	7,800	11,220
A	5,510	6,090	3.2	0.99	7,760	11,300
A	5,510	6,090	2.8	0.82	8,420	11,400
A	6,295	6,295	3.8	0.78	6,560	10,220
A	6,295	6,295	3.0	2.79	6,920	11,250
A	6,295	6,295	2.8	0.70	7,240	11,370
A	6,295	6,295	3.0	0.80	8,110	11,710
A	6,300	6,300	2.7	0.81	8,430	9,410
A	6,300	6,300	2.5	0.84	9,100	11,280
A	5,000	6,500	5.5	0.82	6,640	9,150
A	5,000	6,500	3.6	0.66	6,020	9,520
A	5,000	6,500	2.5	0.65	6,810	9,980
B	5,000	6,500	3.1	0.76	7,330	10,410
A	5,000	6,500	2.5	0.83	5,980	10,540
B	5,000	6,500	2.7	0.75	7,580	10,780
A	5,000	6,500	2.5	2.73	7,780	11,010
A	5,200	6,500	3.0	0.85	8,180	10,330
A	5,200	6,500	2.8	0.82	8,370	10,470
A	5,200	6,500	3.2	0.67	7,470	10,650
A	5,200	6,500	3.0	0.64	8,750	10,680
A	5,200	6,500	3.5	0.78	7,530	10,800
A	5,200	6,500	3.6	0.67	7,840	11,150
A	5,200	6,500	4.3	0.70	7,490	11,320
C	5,400	6,500	2.7	0.62	5,780	7,980
C	5,400	6,500	3.1	0.59	7,770	8,500
C	5,400	6,500	3.2	0.57	7,610	8,550
C	5,400	6,500	4.0	0.58	7,440	8,630
C	5,400	6,500	2.8	0.69	8,600	9,120
C	5,400	6,500	3.1	2.70	8,020	9,180
C	5,400	6,500	2.8	2.67	8,090	9,210

C	5,400	6,500	3.0	0.58	7,360	9,300
C	5,400	6,500	3.1	0.71	8,360	9,530
C	5,400	6,500	4.0	0.58	7,080	9,570
C	5,500	6,500	4.1	0.78	5,580	6,690
C	5,500	6,500	2.7	0.57	5,850	7,140
C	5,500	6,500	4.5	3.85	7,150	8,290
A	5,500	6,500	2.5	0.83	7,760	8,610
A	5,500	6,500	3.1	0.75	6,940	8,980
A	5,500	6,500	2.5	0.72	7,440	9,060
A	5,500	6,500	3.8	0.73	6,730	9,150
A	5,500	6,500	2.5	0.72	7,500	9,210
A	5,500	6,500	2.2	2.72	7,710	9,210
A	5,500	6,500	2.9	0.78	7,310	9,230
A	5,500	6,500	2.5	0.77	6,670	9,250
A	5,500	6,500	3.0	0.79	6,350	9,330
A	5,500	6,500	2.5	0.73	7,040	9,380
A	5,500	6,500	2.9	0.70	6,690	9,400
A	5,500	6,500	3.6	0.77	7,230	9,500
A	5,500	6,500	2.5	0.80	7,410	9,550
A	5,500	6,500	4.3	0.77	8,000	9,550
A	5,500	6,500	2.9	0.81	7,620	9,580
A	5,500	6,500	3.6	0.78	7,620	9,630
A	5,500	6,500	3.5	0.73	7,200	9,720
A	5,500	6,500	2.6	0.73	7,210	9,720
A	5,500	6,500	2.5	2.78	8,470	9,810
A	5,500	6,500	2.9	2.80	9,050	9,880
A	5,500	6,500	3.5	0.79	8,450	10,000
A	5,500	6,500	2.8	0.83	6,760	10,080
A	5,500	6,500	4.4	0.90	7,090	10,110
A	5,500	6,500	2.0	0.77	6,560	10,130
A	5,500	6,500	2.8	2.76	7,990	10,260
A	5,500	6,500	2.5	0.73	7,430	10,350
A	5,500	6,500	3.8	0.80	6,260	10,370
A	5,500	6,500	4.0	0.77	8,080	10,410
A	5,500	6,500	4.5	0.85	8,520	10,420
A	5,500	6,500	2.5	0.82	7,790	10,490
A	5,500	6,500	3.1	0.87	7,080	10,510
A	5,500	6,500	4.0	0.79	7,140	10,550
A	5,500	6,500	2.5	0.89	7,750	10,580
A	5,500	6,500	3.8	2.78	9,550	10,640
A	5,500	6,500	3.0	0.73	7,390	10,650

A	5,500	6,500	2.5	0.83	7,650	10,650
A	5,500	6,500	2.7	0.65	6,890	10,670
B	5,500	6,500	4.8	0.61	7,030	10,690
A	5,500	6,500	3.1	0.80	8,560	10,710
A	5,500	6,500	2.8	0.78	8,290	10,730
B	5,500	6,500	2.7	0.58	6,250	10,740
B	5,500	6,500	3.0	0.58	6,090	10,770
A	5,500	6,500	3.1	0.75	7,110	10,780
A	5,500	6,500	2.6	0.66	8,550	10,800
B	5,500	6,500	3.7	0.82	7,520	10,820
A	5,500	6,500	3.7	0.73	8,460	10,830
A	5,500	6,500	2.8	0.82	7,160	10,880
A	5,500	6,500	3.8	0.61	7,660	10,890
A	5,500	6,500	2.9	0.78	7,290	10,900
A	5,500	6,500	3.3	0.51	8,600	10,900
A	5,500	6,500	4.6	0.84	6,270	10,970
A	5,500	6,500	2.9	0.72	9,000	11,010
A	5,500	6,500	3.1	2.79	10,030	11,020
A	5,500	6,500	3.8	0.76	8,590	11,030
A	5,500	6,500	3.9	0.74	6,520	11,060
A	5,500	6,500	2.2	0.85	7,570	11,110
B	5,500	6,500	3.4	0.78	7,580	11,110
A	5,500	6,500	3.0	0.76	9,320	11,120
B	5,500	6,500	2.9	0.70	6,340	11,170
B	5,500	6,500	2.6	0.68	6,220	11,180
A	5,500	6,500	4.0	2.75	9,430	11,270
A	5,500	6,500	3.1	0.64	7,520	11,280
A	5,500	6,500	4.1	0.83	9,500	11,360
A	5,500	6,500	3.0	0.65	8,200	11,450
B	5,500	6,500	3.3	0.66	6,530	11,480
A	5,500	6,500	5.0	0.79	8,150	11,520
B	5,500	6,500	2.9	0.66	6,470	11,630
A	5,500	6,500	3.2	0.70	8,120	11,760
A	5,500	6,500	3.8	0.65	8,030	11,910
A	5,500	6,500	3.3	2.86	9,900	11,940
A	5,500	6,500	2.5	0.83	9,710	12,050
A	5,500	6,500	3.4	0.65	6,430	12,140
B	5,500	6,500	2.8	0.65	6,970	12,470
B	5,500	6,500	2.6	0.62	6,840	12,580
A	5,600	6,500	3.8	0.71	8,620	11,190
A	5,600	6,500	3.9	0.75	7,820	11,230

A	5,600	6,500	4.7	0.77	8,590	11,490
A	5,600	6,500	3.7	0.72	9,100	11,910
A	5,700	6,500	5.5	0.74	6,730	9,820
A	5,700	6,500	4.5	0.74	7,940	10,000
A	5,700	6,500	4.5	0.79	8,010	10,560
A	5,700	6,500	4.3	0.78	8,610	10,910
A	5,700	6,500	4.4	0.79	7,740	11,330
A	5,700	6,500	4.1	0.66	8,080	12,210
A	5,800	6,500	3.0	0.70	8,290	10,500
A	5,800	6,500	2.5	0.70	8,370	10,580
A	5,800	6,500	3.3	0.70	6,940	10,870
A	6,000	6,500	3.8	0.70	6,230	8,790
A	6,000	6,500	4.5	0.90	7,860	9,190
A	6,000	6,500	5.0	0.85	7,070	9,270
A	6,000	6,500	4.6	0.78	7,460	9,440
B	6,000	6,500	2.8	0.65	7,350	9,470
B	6,000	6,500	3.2	0.69	7,010	9,540
A	6,000	6,500	3.3	0.71	6,670	9,550
A	6,000	6,500	5.0	0.78	6,620	9,570
B	6,000	6,500	3.2	0.72	6,920	9,620
A	6,000	6,500	4.3	0.67	6,720	9,660
B	6,000	6,500	2.7	0.75	7,050	9,680
B	6,000	6,500	4.1	0.71	7,030	9,800
A	6,000	6,500	3.6	0.76	6,740	9,810
B	6,000	6,500	3.0	0.62	7,330	9,830
A	6,000	6,500	4.5	0.74	8,270	10,010
A	6,000	6,500	3.3	0.69	6,770	10,030
A	6,000	6,500	3.2	0.78	7,050	10,030
A	6,000	6,500	2.4	0.77	7,270	10,060
B	6,000	6,500	2.5	0.82	6,260	10,140
A	6,000	6,500	2.8	0.94	7,250	10,190
A	6,000	6,500	2.8	0.74	7,060	10,200
B	6,000	6,500	3.1	0.78	7,430	10,200
A	6,000	6,500	3.6	0.82	7,350	10,210
B	6,000	6,500	2.8	2.58	8,530	10,280
A	6,000	6,500	5.0	0.81	6,750	10,300
A	6,000	6,500	3.2	0.70	7,070	10,300
B	6,000	6,500	2.8	0.67	6,950	10,310
A	6,000	6,500	3.0	0.80	7,750	10,310
A	6,000	6,500	3.3	0.70	8,530	10,330
A	6,000	6,500	4.0	0.79	8,310	10,360

A	6,000	6,500	2.5	2.78	8,640	10,360
A	6,000	6,500	5.0	0.69	6,990	10,390
A	6,000	6,500	3.8	0.76	7,000	10,420
A	6,000	6,500	3.2	0.69	9,170	10,500
A	6,000	6,500	3.5	0.64	7,970	10,510
B	6,000	6,500	3.0	0.61	7,350	10,540
A	6,000	6,500	3.0	0.79	8,360	10,540
B	6,000	6,500	2.8	0.64	7,020	10,560
B	6,000	6,500	2.8	0.63	6,200	10,570
A	6,000	6,500	3.5	0.84	7,400	10,570
B	6,000	6,500	2.8	0.61	6,210	10,580
A	6,000	6,500	4.2	0.79	6,910	10,590
B	6,000	6,500	3.2	0.74	6,130	10,640
B	6,000	6,500	3.0	0.72	7,600	10,680
A	6,000	6,500	4.0	0.83	7,880	10,680
B	6,000	6,500	2.7	2.56	8,340	10,680
A	6,000	6,500	3.0	0.73	7,210	10,690
B	6,000	6,500	3.4	0.73	7,650	10,700
B	6,000	6,500	2.9	0.60	6,290	10,730
B	6,000	6,500	3.2	0.83	8,100	10,730
B	6,000	6,500	3.3	0.56	6,650	10,740
B	6,000	6,500	2.8	0.70	7,680	10,790
B	6,000	6,500	2.8	0.69	7,590	10,800
A	6,000	6,500	3.6	0.67	7,790	10,800
B	6,000	6,500	2.8	0.82	7,920	10,800
A	6,000	6,500	3.6	0.83	7,940	10,800
A	6,000	6,500	3.5	0.81	8,110	10,810
A	6,000	6,500	3.4	2.77	8,720	10,810
A	6,000	6,500	3.4	0.79	7,650	10,840
B	6,000	6,500	2.9	0.70	6,230	10,860
A	6,000	6,500	2.9	0.76	7,360	10,870
B	6,000	6,500	2.8	0.75	6,740	10,890
B	6,000	6,500	3.1	0.80	7,720	10,920
B	6,000	6,500	3.0	0.80	7,910	10,940
A	6,000	6,500	3.6	0.68	6,980	11,020
A	6,000	6,500	3.7	0.70	7,470	11,080
A	6,000	6,500	3.8	0.77	7,510	11,130
A	6,000	6,500	3.3	0.86	8,690	11,130
A	6,000	6,500	2.5	0.82	8,710	11,190
B	6,000	6,500	3.5	0.83	7,320	11,280
A	6,000	6,500	3.5	0.91	8,940	11,330

B	6,000	6,500	3.0	0.83	7,560	11,340
B	6,000	6,500	2.8	0.86	7,630	11,340
A	6,000	6,500	3.8	0.74	8,220	11,370
B	6,000	6,500	2.8	0.75	6,910	11,380
A	6,000	6,500	2.9	0.71	7,580	11,380
A	6,000	6,500	2.7	0.90	8,340	11,380
A	6,000	6,500	4.0	0.68	7,410	11,800
A	6,000	6,500	3.5	0.56	8,270	11,810
A	6,000	6,500	3.8	0.91	8,740	11,890
B	6,000	6,500	2.8	0.80	7,020	11,940
A	6,000	6,500	2.9	0.93	8,480	12,070
B	6,000	6,500	3.3	0.84	8,130	12,080
B	6,000	6,500	2.7	0.64	6,010	12,110
B	6,000	6,500	3.5	0.67	6,780	12,170
B	6,000	6,500	3.2	0.81	8,570	12,680
A	6,100	6,500	2.6	0.72	7,950	10,050
A	6,100	6,500	2.7	0.66	6,250	10,230
A	6,100	6,500	2.9	0.84	6,400	10,260
A	6,100	6,500	2.5	0.82	8,170	10,370
A	6,100	6,500	3.6	0.65	7,910	10,450
A	6,100	6,500	2.7	0.70	8,270	10,460
A	6,100	6,500	2.6	0.70	7,810	10,480
A	6,100	6,500	3.4	2.77	8,050	10,550
A	6,100	6,500	2.4	0.84	7,570	10,590
A	6,100	6,500	2.5	0.63	7,680	10,590
A	6,100	6,500	2.8	4.74	7,950	10,610
A	6,100	6,500	2.5	0.80	8,290	10,640
A	6,100	6,500	2.7	0.75	8,330	10,700
A	6,100	6,500	3.3	0.79	8,370	10,710
A	6,100	6,500	2.4	0.63	7,620	10,740
A	6,100	6,500	2.5	0.73	8,320	10,760
A	6,100	6,500	3.0	0.62	8,510	11,020
A	6,100	6,500	2.7	0.76	8,330	11,040
A	6,100	6,500	3.0	0.79	8,280	11,240
A	6,100	6,500	3.3	0.64	8,390	11,400
A	6,200	6,500	3.5	0.80	7,120	8,960
B	6,200	6,500	4.6	0.67	7,110	10,690
B	6,200	6,500	3.5	2.79	9,670	10,790
D	6,500	6,500	2.3	0.73	7,370	9,300
D	6,500	6,500	3.5	0.82	6,670	9,420
D	6,500	6,500	3.2	3.82	7,900	9,460

D	6,500	6,500	2.6	1.78	7,070	9,650
D	6,500	6,500	3.1	0.86	7,360	9,930
D	6,500	6,500	3.5	0.81	8,320	10,210
D	6,500	6,500	3.8	0.88	8,150	10,240
D	6,500	6,500	3.0	0.71	7,690	10,560
D	6,500	6,500	3.1	0.63	7,450	10,590
D	6,500	6,500	2.6	2.74	9,980	10,820
D	6,500	6,500	3.1	0.65	7,470	10,850
D	6,500	6,500	2.6	0.80	9,890	11,270
D	6,500	6,500	2.5	0.76	8,340	11,770
D	6,500	6,500	2.5	1.24	8,390	11,820
A	5,800	6,510	3.0	0.76	6,740	9,520
A	5,800	6,510	4.2	0.87	6,350	10,130
A	5,800	6,510	4.0	0.76	7,800	10,190
A	5,800	6,510	3.8	0.77	7,790	10,230
A	5,800	6,510	4.0	0.87	7,920	10,570
A	5,800	6,510	3.7	0.80	7,290	10,680
A	5,800	6,510	2.5	0.71	7,510	10,690
A	5,800	6,510	2.8	0.88	7,410	10,710
A	5,800	6,510	2.8	0.74	7,800	10,890
A	5,800	6,510	2.7	0.72	7,990	11,150
A	5,800	6,510	2.8	0.88	7,610	11,250
A	5,800	6,510	3.3	0.74	7,730	11,470
A	5,500	6,600	3.8	0.73	7,510	10,580
A	5,500	6,600	3.2	0.71	7,990	11,130
A	5,500	6,600	3.8	0.73	8,430	11,650
B	6,000	6,600	2.5	0.81	6,810	9,060
A	6,000	6,600	5	0.66	6,970	9,120
A	6,000	6,600	3.5	0.76	7,080	9,310
B	6,000	6,600	3.5	0.63	7,010	9,430
B	6,000	6,600	3.4	0.60	7,180	9,470
B	6,000	6,600	4.5	0.68	6,040	9,540
A	6,000	6,600	4	0.78	6,980	9,560
B	6,000	6,600	3.0	0.56	6,790	9,570
B	6,000	6,600	3.5	0.86	6,980	9,790
B	6,000	6,600	2.8	0.66	6,980	9,850
B	6,000	6,600	4.5	0.63	6,890	9,860
A	6,000	6,600	3.5	0.81	6,900	9,860
A	6,000	6,600	4	0.76	6,660	9,980
A	6,000	6,600	3.5	0.63	6,260	10,090
A	6,000	6,600	3.8	0.68	7,680	10,240

A	6,000	6,600	3.5	0.66	6,340	10,270
A	6,000	6,600	3.5	0.73	7,290	10,330
A	6,000	6,600	3.5	0.84	8,070	10,900
A	6,000	6,600	3.3	0.67	7,210	11,170
A	6,000	6,600	4.2	0.69	7,210	11,200
A	6,400	6,600	3.4	0.63	6,570	10,340
A	6,400	6,600	3.5	0.65	6,550	10,540
A	6,400	6,600	2.5	2.73	8,770	10,760
A	6,400	6,600	3	2.75	8,910	11,230
B	5,700	6,700	3.3	0.65	6,680	10,150
B	5,700	6,700	3.4	0.57	6,820	10,430
B	5,700	6,700	2.7	0.74	7,070	10,470
B	5,700	6,700	2.8	0.53	6,400	10,490
B	5,700	6,700	2.5	0.62	7,240	10,520
B	5,700	6,700	2.7	0.88	7,290	10,530
B	5,700	6,700	2.9	0.48	6,410	10,540
B	5,700	6,700	2.4	0.76	7,000	10,540
B	5,700	6,700	3.0	0.50	6,380	10,550
B	5,700	6,700	3.0	0.59	5,720	10,560
B	5,700	6,700	3.3	0.84	7,450	10,570
B	5,700	6,700	2.9	0.61	7,730	10,570
B	5,700	6,700	3.5	0.64	6,680	10,620
B	5,700	6,700	3.4	0.59	7,110	10,640
B	5,700	6,700	3.6	0.58	5,990	10,650
B	5,700	6,700	3.3	0.54	6,830	10,650
B	5,700	6,700	2.9	0.67	6,340	10,660
B	5,700	6,700	2.9	0.54	6,290	10,680
B	5,700	6,700	3.4	0.60	6,890	10,680
B	5,700	6,700	3.1	0.73	7,630	10,710
B	5,700	6,700	3.2	0.59	6,740	10,720
B	5,700	6,700	3.2	0.57	6,500	10,750
B	5,700	6,700	2.9	0.55	6,940	10,750
B	5,700	6,700	3.0	0.51	7,310	10,760
B	5,700	6,700	3.5	0.55	7,390	10,760
B	5,700	6,700	4.0	0.57	6,630	10,770
B	5,700	6,700	2.9	0.53	7,250	10,770
B	5,700	6,700	2.8	0.62	6,830	10,780
B	5,700	6,700	2.7	0.64	7,480	10,790
B	5,700	6,700	3.2	0.53	6,600	10,840
A	5,400	7,000	3.3	0.85	7,030	9,960
A	5,400	7,000	3.5	0.88	8,310	10,100

A	5,400	7,000	3.5	0.87	8,240	11,490
C	5,500	7,000	2.5	1.77	5,720	7,060
C	5,500	7,000	2.5	1.02	5,520	7,520
C	5,500	7,000	5.0	1.72	5,820	7,810
C	5,500	7,000	2.5	0.91	5,570	7,900
C	5,500	7,000	3.5	1.70	5,930	7,970
C	5,500	7,000	4.1	0.82	5,800	8,260
C	5,500	7,000	3.5	0.83	5,620	8,590
C	5,500	7,000	3.4	0.82	5,700	8,900
D	5,500	7,000	3.0	2.69	7,960	9,030
D	5,500	7,000	2.8	2.67	8,900	9,060
D	5,500	7,000	3.4	0.82	6,020	9,070
D	5,500	7,000	2.8	0.73	7,710	9,080
D	5,500	7,000	3.0	0.63	6,950	9,100
D	5,500	7,000	2.7	2.78	9,370	9,110
D	5,500	7,000	3.9	0.64	6,130	9,120
D	5,500	7,000	3.1	0.69	6,690	9,130
C	5,500	7,000	3.3	2.57	7,600	9,130
C	5,500	7,000	4.6	3.06	7,550	9,140
D	5,500	7,000	3.6	2.01	7,530	9,180
D	5,500	7,000	3.0	2.81	9,460	9,180
D	5,500	7,000	3.1	0.87	5,550	9,190
D	5,500	7,000	3.6	2.90	7,430	9,200
D	5,500	7,000	3.6	0.66	5,660	9,210
C	5,500	7,000	4.8	0.81	7,430	9,220
D	5,500	7,000	3.6	2.65	6,100	9,250
D	5,500	7,000	3.4	0.78	6,450	9,260
D	5,500	7,000	2.5	0.84	6,810	9,280
D	5,500	7,000	3.6	0.90	6,630	9,290
D	5,500	7,000	2.8	0.64	6,870	9,290
D	5,500	7,000	3.0	1.62	6,480	9,300
D	5,500	7,000	3.4	1.75	6,970	9,300
D	5,500	7,000	2.7	1.92	9,160	9,340
D	5,500	7,000	3.1	1.71	6,460	9,370
D	5,500	7,000	2.5	0.75	6,560	9,380
D	5,500	7,000	3.0	2.70	8,280	9,480
D	5,500	7,000	3.8	0.91	6,930	9,510
D	5,500	7,000	3.3	0.65	7,070	9,530
D	5,500	7,000	3.2	0.67	6,300	9,560
D	5,500	7,000	3.7	1.76	7,180	9,580
D	5,500	7,000	5.0	0.77	5,600	9,610

D	5,500	7,000	2.7	0.76	7,880	9,620
C	5,500	7,000	4.2	1.60	7,090	9,630
D	5,500	7,000	2.7	0.72	7,350	9,710
D	5,500	7,000	3.4	0.63	6,380	9,770
D	5,500	7,000	3.3	0.75	5,920	9,930
D	5,500	7,000	3.5	0.72	8,050	9,930
D	5,500	7,000	2.5	0.71	6,570	10,100
D	5,500	7,000	3.4	0.70	6,770	10,230
D	5,500	7,000	3.7	2.81	8,220	10,370
D	5,500	7,000	2.5	1.22	7,390	10,490
D	5,500	7,000	4.1	0.67	5,610	10,520
D	5,500	7,000	3.0	0.86	7,570	10,520
B	5,500	7,000	2.5	0.66	6,540	10,530
D	5,500	7,000	3.7	0.65	7,190	10,680
B	5,500	7,000	3.1	0.61	6,370	10,700
B	5,500	7,000	3.0	0.63	6,390	10,740
D	5,500	7,000	2.6	0.66	7,180	10,770
B	5,500	7,000	2.5	0.69	6,200	10,780
D	5,500	7,000	3.2	0.69	6,740	10,780
D	5,500	7,000	3.0	0.70	6,670	10,810
D	5,500	7,000	3.1	0.75	7,890	10,820
D	5,500	7,000	3.0	2.72	7,540	10,880
D	5,500	7,000	3.3	0.81	7,580	10,880
D	5,500	7,000	3.0	2.75	9,330	10,880
B	5,500	7,000	2.9	0.64	6,500	10,910
D	5,500	7,000	3.5	1.58	7,520	10,910
B	5,500	7,000	3.1	0.65	6,850	10,930
D	5,500	7,000	3.7	0.62	6,240	10,950
B	5,500	7,000	3.1	0.70	6,490	11,000
D	5,500	7,000	3.6	0.90	7,680	11,280
D	5,500	7,000	2.5	2.66	8,890	11,320
D	5,500	7,000	3.0	2.86	9,910	11,410
A	5,500	7,000	3.2	2.84	9,420	11,500
D	5,500	7,000	2.5	0.73	8,000	11,520
D	5,500	7,000	2.8	2.76	7,140	11,580
D	5,500	7,000	2.8	0.65	6,900	11,590
A	5,500	7,000	3.1	0.80	8,300	11,590
D	5,500	7,000	3.6	1.08	9,660	11,840
D	5,500	7,000	2.6	0.73	8,360	11,970
A	5,500	7,000	3.6	0.90	7,450	12,050
A	5,500	7,000	3.2	0.66	8,040	12,350

B	5,600	7,000	3.6	2.77	9,310	10,710
B	5,600	7,000	4.6	0.78	7,590	11,300
A	5,700	7,000	3.3	0.72	6,960	9,890
A	5,700	7,000	3.8	0.71	6,650	10,000
A	5,700	7,000	3.2	0.68	7,360	10,270
A	5,700	7,000	3.1	0.69	7,050	10,390
A	5,700	7,000	3.0	0.77	7,440	10,730
A	5,700	7,000	3.3	0.70	8,330	10,760
A	5,700	7,000	2.8	0.81	7,130	11,040
A	5,700	7,000	2.9	0.77	8,150	11,100
A	5,700	7,000	2.2	0.73	7,630	11,140
A	5,700	7,000	2.7	0.75	8,120	11,150
A	5,700	7,000	2.5	0.65	7,470	11,210
A	5,700	7,000	3.0	0.84	7,790	11,260
A	5,700	7,000	2.8	0.82	7,500	11,320
A	5,700	7,000	2.5	0.70	9,110	11,430
A	5,700	7,000	2.2	0.65	7,960	11,460
A	5,700	7,000	2.0	0.67	7,590	11,480
A	5,700	7,000	2.6	0.87	8,490	11,600
A	5,700	7,000	2.9	0.79	7,730	11,610
A	5,700	7,000	2.5	0.68	9,340	11,640
A	5,700	7,000	2.2	0.67	8,930	11,700
A	5,700	7,000	2.2	0.71	8,720	11,890
A	5,700	7,000	4.1	0.80	8,600	11,900
A	5,700	7,000	2.7	0.71	8,070	11,950
A	5,700	7,000	2.6	0.84	9,020	11,960
A	5,700	7,000	2.8	0.70	9,260	12,100
A	5,700	7,000	2.8	0.76	9,110	12,110
A	5,700	7,000	2.5	0.70	7,810	12,160
A	5,700	7,000	2.5	0.77	9,440	12,160
A	5,700	7,000	2.6	0.76	9,110	12,190
A	5,700	7,000	2.5	0.64	9,330	12,300
A	5,700	7,000	3.0	0.78	8,580	12,350
A	5,700	7,000	3.0	0.73	9,220	12,400
A	5,700	7,000	2.5	0.73	9,270	12,480
A	5,700	7,000	3.9	0.76	9,300	12,520
A	5,700	7,000	3.2	0.79	9,390	12,640
A	5,700	7,000	2.8	0.60	9,400	12,950
A	5,700	7,000	2.7	0.76	9,430	13,080
A	5,700	7,000	3.0	0.74	8,540	13,230
A	5,900	7,000	5.0	2.78	7,440	8,780

B	5,900	7,000	3.5	0.54	6,250	10,300
B	5,900	7,000	2.7	0.56	6,440	10,400
B	5,900	7,000	3.5	0.58	7,110	10,510
A	5,900	7,000	3.0	0.81	7,940	10,510
B	5,900	7,000	2.6	0.50	6,030	10,620
B	5,900	7,000	2.8	0.54	6,730	10,630
B	5,900	7,000	2.8	0.57	6,130	10,640
B	5,900	7,000	3.0	0.54	6,370	10,680
B	5,900	7,000	3.5	0.53	7,220	10,710
B	5,900	7,000	3.2	0.54	6,950	10,720
B	5,900	7,000	3.0	0.54	6,180	10,790
B	5,900	7,000	3.1	0.50	6,960	10,790
B	5,900	7,000	3.0	0.51	6,790	10,830
A	5,900	7,000	3.7	0.83	7,880	10,960
A	5,900	7,000	2.0	0.74	6,290	11,070
B	5,900	7,000	3.7	0.65	6,900	11,260
A	5,900	7,000	2.5	0.82	8,180	11,260
B	5,900	7,000	3.7	0.63	7,440	11,790
B	5,900	7,000	3.4	2.58	9,390	12,240
A	5,900	7,000	2.5	0.79	8,500	12,290
B	5,900	7,000	4.1	2.63	9,440	12,680
C	6,000	7,000	3.4	1.18	6,410	7,100
C	6,000	7,000	2.9	0.75	6,440	7,530
B	6,000	7,000	3.0	0.68	7,110	7,560
B	6,000	7,000	3.3	0.65	6,520	7,620
C	6,000	7,000	2.5	0.87	6,470	8,250
C	6,000	7,000	3.4	0.60	7,740	8,250
C	6,000	7,000	4.6	0.61	6,070	8,520
C	6,000	7,000	2.8	0.81	7,380	8,550
C	6,000	7,000	3.0	0.57	6,050	8,570
C	6,000	7,000	2.5	0.84	7,450	8,730
C	6,000	7,000	3.8	0.53	6,860	8,760
C	6,000	7,000	3.5	0.64	7,720	8,900
B	6,000	7,000	2.8	0.65	7,820	8,940
C	6,000	7,000	4.0	0.61	6,960	8,960
D	6,000	7,000	3.0	2.69	7,990	9,020
D	6,000	7,000	2.5	0.65	6,380	9,040
D	6,000	7,000	2.7	0.71	6,410	9,040
D	6,000	7,000	2.7	2.78	7,400	9,050
C	6,000	7,000	3.8	0.59	6,620	9,070
D	6,000	7,000	2.5	0.63	7,470	9,070

D	6,000	7,000	2.5	0.74	8,690	9,080
D	6,000	7,000	2.5	2.76	7,390	9,090
D	6,000	7,000	2.8	0.66	7,740	9,100
D	6,000	7,000	3.2	0.72	7,750	9,110
D	6,000	7,000	3.5	2.80	8,650	9,110
C	6,000	7,000	2.8	0.56	6,760	9,120
C	6,000	7,000	3.2	0.53	7,440	9,120
D	6,000	7,000	3.3	2.81	7,980	9,130
D	6,000	7,000	2.5	2.80	7,860	9,140
D	6,000	7,000	2.6	0.68	7,220	9,150
D	6,000	7,000	3.8	0.74	7,300	9,160
D	6,000	7,000	3.5	2.68	7,590	9,160
C	6,000	7,000	3.0	0.80	8,090	9,180
C	6,000	7,000	2.6	2.71	8,580	9,180
D	6,000	7,000	3.7	0.66	6,510	9,200
D	6,000	7,000	3.2	0.69	7,070	9,200
C	6,000	7,000	4.0	0.83	7,760	9,200
D	6,000	7,000	3.4	0.60	6,890	9,210
D	6,000	7,000	3.4	0.69	6,420	9,220
D	6,000	7,000	3.5	0.71	6,550	9,220
D	6,000	7,000	2.5	0.68	6,790	9,220
D	6,000	7,000	4.6	0.76	6,840	9,230
D	6,000	7,000	2.7	0.79	7,720	9,230
C	6,000	7,000	2.5	2.68	8,650	9,240
D	6,000	7,000	2.5	0.70	7,590	9,250
D	6,000	7,000	3.4	0.84	7,400	9,260
D	6,000	7,000	3.4	0.83	7,490	9,260
C	6,000	7,000	3.3	0.68	7,720	9,280
D	6,000	7,000	2.8	0.66	6,250	9,310
D	6,000	7,000	3.0	0.67	6,570	9,310
D	6,000	7,000	3.0	0.73	7,070	9,310
D	6,000	7,000	3.2	0.90	6,490	9,330
A	6,000	7,000	2.8	0.76	8,980	9,340
D	6,000	7,000	1.7	0.70	7,660	9,350
B	6,000	7,000	2.6	0.70	6,240	9,360
D	6,000	7,000	2.9	0.56	6,080	9,380
D	6,000	7,000	3.5	2.77	8,270	9,380
D	6,000	7,000	4.2	0.72	6,880	9,400
D	6,000	7,000	2.7	0.81	7,610	9,400
D	6,000	7,000	5.0	1.77	6,090	9,420
D	6,000	7,000	3.0	0.70	6,030	9,430

D	6,000	7,000	2.5	0.67	7,870	9,440
C	6,000	7,000	5.1	0.77	6,000	9,490
D	6,000	7,000	3.5	0.92	6,150	9,500
A	6,000	7,000	4.2	0.63	6,130	9,560
D	6,000	7,000	5.1	1.76	6,780	9,610
D	6,000	7,000	2.7	0.88	7,320	9,620
D	6,000	7,000	2.6	0.68	7,460	9,670
B	6,000	7,000	2.8	0.73	6,040	9,680
B	6,000	7,000	2.8	0.80	6,270	9,690
D	6,000	7,000	3.9	0.71	7,420	9,700
B	6,000	7,000	3.6	0.82	6,300	9,710
D	6,000	7,000	2.5	2.69	8,050	9,740
B	6,000	7,000	3.6	0.64	6,350	9,790
D	6,000	7,000	3.8	0.82	7,080	9,870
B	6,000	7,000	4.0	0.69	6,160	9,920
A	6,000	7,000	3.7	2.75	9,220	9,920
D	6,000	7,000	4.1	4.83	9,660	9,940
B	6,000	7,000	3.4	0.60	6,110	9,950
D	6,000	7,000	3.3	1.77	7,930	9,970
D	6,000	7,000	3.2	2.87	7,850	10,030
B	6,000	7,000	3.5	0.59	6,460	10,040
D	6,000	7,000	2.9	2.84	7,850	10,040
D	6,000	7,000	2.8	0.85	8,290	10,040
D	6,000	7,000	3.8	0.73	7,450	10,120
D	6,000	7,000	3.4	0.71	7,200	10,140
D	6,000	7,000	3.1	2.77	8,010	10,190
D	6,000	7,000	3.2	0.92	7,000	10,200
B	6,000	7,000	3.6	0.67	6,710	10,260
D	6,000	7,000	2.7	2.72	7,930	10,320
C	6,000	7,000	3.5	0.82	7,410	10,330
D	6,000	7,000	2.5	0.79	7,560	10,330
B	6,000	7,000	4.5	0.72	7,140	10,340
D	6,000	7,000	2.6	2.67	8,250	10,340
A	6,000	7,000	3.1	0.79	9,110	10,340
D	6,000	7,000	4.1	0.82	6,940	10,390
A	6,000	7,000	3.4	0.76	8,320	10,410
B	6,000	7,000	3.5	1.62	7,750	10,440
B	6,000	7,000	3.5	0.55	6,950	10,450
B	6,000	7,000	3.0	0.62	6,420	10,500
B	6,000	7,000	3.1	0.73	7,790	10,500
B	6,000	7,000	4.2	0.62	6,500	10,540

A	6,000	7,000	4.1	0.82	8,100	10,550
A	6,000	7,000	3.8	0.89	7,580	10,560
D	6,000	7,000	2.0	0.78	7,250	10,570
A	6,000	7,000	3.5	0.78	7,550	10,570
D	6,000	7,000	2.5	0.82	7,620	10,580
D	6,000	7,000	2.8	2.78	7,600	10,600
D	6,000	7,000	3.5	0.68	7,070	10,620
D	6,000	7,000	3.7	0.78	7,200	10,620
B	6,000	7,000	2.7	0.60	6,510	10,630
B	6,000	7,000	3.2	2.63	8,200	10,630
B	6,000	7,000	2.5	0.72	6,730	10,650
D	6,000	7,000	3.7	0.58	6,750	10,650
A	6,000	7,000	3.9	0.88	7,530	10,650
B	6,000	7,000	3.4	0.68	6,800	10,660
B	6,000	7,000	3.0	0.57	6,980	10,660
B	6,000	7,000	3.2	0.55	7,220	10,660
B	6,000	7,000	2.8	0.78	7,600	10,660
B	6,000	7,000	3.3	0.58	6,630	10,670
B	6,000	7,000	3.5	0.60	7,120	10,670
B	6,000	7,000	3.0	0.59	7,260	10,670
A	6,000	7,000	3.0	0.84	8,610	10,670
B	6,000	7,000	3.2	0.69	7,360	10,680
B	6,000	7,000	2.7	0.66	6,590	10,690
B	6,000	7,000	3.0	0.91	7,850	10,690
B	6,000	7,000	3.2	0.57	7,260	10,700
D	6,000	7,000	2.5	0.55	6,560	10,710
D	6,000	7,000	2.5	0.75	6,660	10,730
B	6,000	7,000	2.5	0.62	7,030	10,730
B	6,000	7,000	2.6	0.57	7,110	10,730
B	6,000	7,000	3.1	0.67	7,300	10,730
B	6,000	7,000	4.0	0.82	7,320	10,730
D	6,000	7,000	3.2	0.85	7,780	10,740
D	6,000	7,000	5.5	2.83	7,180	10,750
B	6,000	7,000	3.5	0.72	7,540	10,760
D	6,000	7,000	3.2	0.66	7,030	10,770
B	6,000	7,000	3.3	0.75	7,350	10,770
D	6,000	7,000	2.9	0.72	6,940	10,780
B	6,000	7,000	2.6	0.68	7,690	10,780
D	6,000	7,000	3.6	0.75	7,140	10,790
B	6,000	7,000	3.0	0.65	6,970	10,800
D	6,000	7,000	2.9	0.64	7,720	10,810

B	6,000	7,000	3.4	0.68	6,800	10,820
B	6,000	7,000	3.5	0.66	7,570	10,820
D	6,000	7,000	3.2	0.75	7,680	10,820
B	6,000	7,000	2.8	0.75	7,880	10,820
D	6,000	7,000	2.6	2.81	7,250	10,830
D	6,000	7,000	3.2	0.73	7,390	10,840
B	6,000	7,000	3.0	0.60	6,410	10,850
B	6,000	7,000	3.2	2.78	8,180	10,850
B	6,000	7,000	4.9	0.64	7,220	10,860
D	6,000	7,000	3.3	0.77	7,570	10,870
A	6,000	7,000	2.8	0.81	8,400	10,870
D	6,000	7,000	3.6	0.81	6,550	10,890
B	6,000	7,000	3.2	0.64	6,650	10,890
D	6,000	7,000	2.7	2.75	9,720	10,890
D	6,000	7,000	3.4	0.71	7,520	10,900
D	6,000	7,000	2.7	2.77	7,520	10,900
A	6,000	7,000	2.5	0.70	8,150	10,900
B	6,000	7,000	2.8	0.62	7,260	10,910
A	6,000	7,000	3.2	0.89	8,470	10,910
D	6,000	7,000	3.4	0.69	7,150	10,930
A	6,000	7,000	2.9	0.93	8,410	10,950
D	6,000	7,000	2.7	1.84	7,120	10,960
B	6,000	7,000	2.6	0.63	6,670	10,970
A	6,000	7,000	3.5	0.80	8,460	11,000
B	6,000	7,000	2.5	0.69	7,780	11,010
A	6,000	7,000	3.0	2.81	9,730	11,010
B	6,000	7,000	3.1	0.67	6,420	11,030
B	6,000	7,000	2.5	0.65	6,190	11,040
A	6,000	7,000	3.5	0.86	7,630	11,040
B	6,000	7,000	3.5	0.89	8,100	11,040
B	6,000	7,000	3.4	2.83	9,210	11,060
A	6,000	7,000	3.1	0.74	7,570	11,080
A	6,000	7,000	3.7	0.84	7,900	11,080
B	6,000	7,000	2.9	0.76	7,480	11,090
D	6,000	7,000	3.1	0.82	7,480	11,090
A	6,000	7,000	3.1	0.73	7,690	11,090
D	6,000	7,000	2.5	0.76	7,020	11,110
B	6,000	7,000	3.0	0.91	7,580	11,120
B	6,000	7,000	2.8	0.80	7,090	11,150
B	6,000	7,000	3.0	0.81	7,850	11,150
A	6,000	7,000	3.2	0.78	7,920	11,150

B	6,000	7,000	3.6	1.68	8,190	11,150
A	6,000	7,000	4.2	0.80	8,220	11,160
B	6,000	7,000	3.4	3.72	9,390	11,160
B	6,000	7,000	3.1	3.74	9,300	11,190
B	6,000	7,000	3.3	0.78	8,230	11,200
A	6,000	7,000	3.6	0.69	6,310	11,210
B	6,000	7,000	2.8	0.57	6,630	11,210
A	6,000	7,000	2.5	0.83	8,610	11,210
B	6,000	7,000	2.7	0.64	6,990	11,230
A	6,000	7,000	2.5	0.89	8,480	11,230
B	6,000	7,000	3.5	0.71	6,200	11,240
A	6,000	7,000	3.2	0.79	8,060	11,240
A	6,000	7,000	3.2	0.81	8,490	11,270
D	6,000	7,000	3.1	1.81	7,630	11,280
A	6,000	7,000	3.1	0.86	8,200	11,290
A	6,000	7,000	3.3	0.86	8,880	11,290
A	6,000	7,000	3.2	0.79	8,040	11,310
A	6,000	7,000	3.6	0.85	9,170	11,320
B	6,000	7,000	3.2	0.88	8,180	11,340
A	6,000	7,000	3.2	0.74	8,020	11,360
B	6,000	7,000	3.8	1.65	8,320	11,370
A	6,000	7,000	2.6	0.87	7,020	11,400
B	6,000	7,000	3.1	0.76	7,970	11,410
A	6,000	7,000	3.0	0.73	8,000	11,440
A	6,000	7,000	4.0	0.94	7,840	11,450
A	6,000	7,000	3.4	0.91	8,700	11,490
A	6,000	7,000	3.2	0.69	8,270	11,530
A	6,000	7,000	4.1	2.79	9,650	11,550
A	6,000	7,000	3.9	0.88	7,950	11,560
A	6,000	7,000	3.3	0.71	8,310	11,570
A	6,000	7,000	3.3	2.86	9,640	11,590
A	6,000	7,000	3.0	0.90	8,580	11,660
A	6,000	7,000	3.0	0.92	8,300	11,670
B	6,000	7,000	2.8	0.69	6,700	11,700
A	6,000	7,000	2.8	0.85	8,450	11,700
B	6,000	7,000	2.9	2.75	9,330	11,700
A	6,000	7,000	3.0	0.88	8,690	11,730
A	6,000	7,000	3.2	0.77	7,810	11,740
D	6,000	7,000	4.0	4.83	9,060	11,760
D	6,000	7,000	3.0	0.69	7,180	11,780
A	6,000	7,000	2.5	0.90	8,880	11,800

A	6,000	7,000	3.2	0.87	8,480	11,810
A	6,000	7,000	3.0	0.72	8,090	11,860
A	6,000	7,000	3.4	0.71	6,950	11,890
D	6,000	7,000	3.3	0.54	8,060	11,920
D	6,000	7,000	2.0	0.72	6,840	11,970
A	6,000	7,000	3.1	1.85	10,260	11,970
A	6,000	7,000	3.2	0.85	8,550	11,990
A	6,000	7,000	3.8	1.90	10,170	12,020
A	6,000	7,000	2.6	0.67	8,480	12,060
A	6,000	7,000	3.4	0.75	8,180	12,230
A	6,000	7,000	2.8	0.70	8,140	12,270
A	6,000	7,000	3.7	0.75	7,780	12,360
A	6,000	7,000	3.2	0.72	8,930	12,390
D	6,000	7,000	3.3	2.77	10,280	12,560
A	6,000	7,000	3.1	0.89	8,660	12,710
A	6,000	7,000	3.6	2.70	8,970	12,720
A	6,000	7,000	3.1	2.67	9,150	12,730
A	6,100	7,000	2.6	0.90	7,980	10,620
A	6,100	7,000	2.8	0.76	8,490	10,790
C	6,200	7,000	3.1	1.03	6,220	7,080
C	6,200	7,000	3.8	2.82	6,230	7,540
A	6,200	7,000	3.4	0.76	6,830	7,870
C	6,200	7,000	3.2	1.75	6,220	8,020
C	6,200	7,000	2.6	1.01	7,600	8,240
C	6,200	7,000	2.8	0.68	6,460	8,260
A	6,200	7,000	4.5	2.91	7,130	8,260
C	6,200	7,000	3.5	2.79	6,320	8,280
C	6,200	7,000	2.9	3.56	6,350	8,470
C	6,200	7,000	3.4	1.73	7,180	8,470
A	6,200	7,000	3.5	0.85	7,360	8,470
C	6,200	7,000	4.1	0.58	6,230	8,550
C	6,200	7,000	2.5	0.67	7,920	8,620
C	6,200	7,000	2.5	2.56	6,830	8,870
C	6,200	7,000	2.3	0.57	7,510	8,960
C	6,200	7,000	2.9	0.63	7,910	8,970
C	6,200	7,000	2.7	0.61	7,270	8,990
C	6,200	7,000	2.6	0.60	8,240	9,080
A	6,200	7,000	2.8	0.79	7,570	9,150
C	6,200	7,000	3.2	0.70	6,760	9,220
A	6,200	7,000	4.0	0.81	7,840	9,470
A	6,200	7,000	3.0	0.73	7,450	9,490

A	6,200	7,000	3.1	0.87	7,520	9,580
A	6,200	7,000	3.1	2.80	8,410	9,650
A	6,200	7,000	4.0	0.61	7,200	9,720
A	6,200	7,000	3.0	0.71	7,300	9,730
A	6,200	7,000	2.7	2.52	8,970	9,840
A	6,200	7,000	3.0	0.77	7,450	9,920
A	6,200	7,000	3.5	0.67	7,720	9,990
A	6,200	7,000	3.8	2.76	9,140	10,620
A	6,200	7,000	3.0	0.74	8,920	10,710
A	6,200	7,000	5.0	0.69	7,210	10,800
A	6,200	7,000	3.4	2.76	9,280	11,010
B	6,200	7,000	2.5	0.62	6,890	11,100
B	6,200	7,000	2.6	0.75	7,200	11,130
B	6,200	7,000	2.8	1.08	6,980	11,160
B	6,200	7,000	3.5	1.09	7,170	11,310
B	6,200	7,000	2.8	0.60	6,200	11,390
B	6,200	7,000	3.2	0.60	7,200	11,410
B	6,200	7,000	2.9	2.61	9,140	11,470
B	6,200	7,000	3.0	0.58	7,510	11,600
B	6,200	7,000	3.5	0.67	7,570	11,630
B	6,200	7,000	4.0	2.66	9,480	11,730
B	6,200	7,000	3.2	0.59	7,320	11,740
B	6,200	7,000	3.4	0.73	7,990	11,840
B	6,200	7,000	2.7	0.80	7,700	11,940
B	6,200	7,000	2.7	2.64	9,340	12,100
B	6,200	7,000	3.3	2.55	9,430	12,160
B	6,200	7,000	3.0	0.65	7,320	12,200
B	6,200	7,000	3.0	1.15	7,420	12,240
B	6,200	7,000	3.4	0.91	8,740	12,240
B	6,200	7,000	3.6	0.76	7,950	12,280
B	6,200	7,000	3.3	1.13	7,840	12,510
B	6,200	7,000	3.5	0.87	9,000	13,110
A	6,300	7,000	4.2	1.07	6,390	8,520
A	6,300	7,000	3.9	0.73	6,470	9,400
A	6,300	7,000	3.6	2.69	8,400	9,720
A	6,300	7,000	4.2	0.78	7,340	9,870
A	6,300	7,000	4.6	0.68	7,140	10,190
A	6,300	7,000	2.5	0.81	7,320	10,200
A	6,300	7,000	4.1	0.89	8,360	10,240
A	6,300	7,000	5.5	0.69	7,620	10,250
A	6,300	7,000	3.6	0.82	8,430	10,260

A	6,300	7,000	5.1	0.65	6,500	10,270
A	6,300	7,000	4.6	0.69	7,570	10,430
A	6,300	7,000	2.5	0.66	8,120	10,530
A	6,300	7,000	3.9	0.69	7,610	10,560
A	6,300	7,000	3.3	0.72	7,860	10,590
A	6,300	7,000	4.1	2.73	8,590	10,670
A	6,300	7,000	5.0	2.81	8,150	10,690
A	6,300	7,000	4.0	0.78	7,650	10,930
A	6,300	7,000	3.5	0.90	8,390	11,220
C	6,400	7,000	5.4	2.89	6,610	7,230
C	6,400	7,000	2.0	6.82	6,430	7,630
C	6,400	7,000	3.9	1.86	6,470	7,970
A	6,400	7,000	3.7	0.62	6,620	8,580
A	6,400	7,000	3.4	0.63	7,260	8,750
A	6,400	7,000	2.5	0.64	6,540	8,810
C	6,400	7,000	2.5	1.58	7,030	9,170
C	6,400	7,000	2.5	0.63	6,870	9,240
C	6,400	7,000	3.0	0.61	6,750	9,250
A	6,400	7,000	3.2	0.69	7,730	9,430
C	6,400	7,000	4.9	1.08	6,520	9,990
C	6,400	7,000	3.6	1.06	6,480	10,160
C	6,400	7,000	4.5	0.91	7,120	10,200
B	6,400	7,000	4.0	0.79	7,700	10,860
B	6,400	7,000	4.0	0.79	8,010	11,100
B	6,400	7,000	4.0	0.75	8,010	11,200
A	6,500	7,000	2.5	0.69	6,540	8,690
A	6,500	7,000	3.6	0.66	7,330	9,020
A	6,500	7,000	3.0	0.62	6,550	9,270
A	6,500	7,000	3.0	0.64	6,890	9,280
A	6,500	7,000	3.6	0.66	7,190	9,550
B	6,500	7,000	3.0	0.67	6,820	9,610
A	6,500	7,000	4.2	0.66	7,770	9,720
A	6,500	7,000	3.3	0.64	8,000	9,720
B	6,500	7,000	3.5	0.70	7,050	9,810
A	6,500	7,000	4.5	0.65	7,140	9,830
B	6,500	7,000	3.4	0.78	7,100	10,000
B	6,500	7,000	4.5	0.87	7,250	10,010
B	6,500	7,000	4.5	2.74	8,290	10,010
B	6,500	7,000	2.6	0.82	6,640	10,080
B	6,500	7,000	2.8	0.81	6,590	10,150
A	6,500	7,000	3.6	2.71	8,920	10,180

B	6,500	7,000	3.2	0.79	7,070	10,270
A	6,500	7,000	4.7	2.68	9,040	10,320
B	6,500	7,000	2.7	0.76	7,130	10,530
B	6,500	7,000	2.5	0.67	7,650	10,530
B	6,500	7,000	2.7	0.56	6,830	10,560
A	6,500	7,000	4.5	0.77	7,440	10,560
B	6,500	7,000	3.5	0.58	6,800	10,580
B	6,500	7,000	3.0	0.51	7,080	10,640
A	6,500	7,000	4.0	0.81	7,520	10,640
B	6,500	7,000	3.4	0.91	8,170	10,640
B	6,500	7,000	3.3	0.53	6,900	10,650
B	6,500	7,000	2.9	0.77	7,080	10,660
B	6,500	7,000	3.3	1.55	8,190	10,660
B	6,500	7,000	3.1	0.73	7,140	10,670
B	6,500	7,000	3.3	0.63	7,320	10,670
B	6,500	7,000	3.2	0.55	7,500	10,670
B	6,500	7,000	3.0	0.59	7,640	10,680
B	6,500	7,000	2.9	2.64	8,420	10,690
B	6,500	7,000	3.3	0.53	7,600	10,700
B	6,500	7,000	2.8	0.68	7,040	10,730
B	6,500	7,000	2.8	2.68	8,310	10,750
B	6,500	7,000	2.9	1.61	8,060	10,820
B	6,500	7,000	3.0	1.63	9,100	10,850
A	6,500	7,000	3.3	0.89	7,970	10,910
B	6,500	7,000	2.8	0.60	7,200	10,940
B	6,500	7,000	3.1	0.64	7,800	10,970
A	6,500	7,000	2.5	0.65	7,670	11,000
A	6,500	7,000	2.8	0.85	8,210	11,060
A	6,500	7,000	3.0	0.72	7,850	11,200
A	6,500	7,000	3.0	0.76	8,620	11,230
A	6,500	7,000	3.8	0.77	8,060	11,360
A	6,500	7,000	4.4	0.75	7,950	11,400
A	6,500	7,000	3.5	0.64	8,060	11,430
A	6,500	7,000	3.2	0.74	7,420	11,470
B	6,500	7,000	3.2	0.94	7,480	11,550
A	6,500	7,000	3.2	0.79	7,980	11,600
A	6,500	7,000	2.5	0.70	8,250	11,690
A	6,500	7,000	2.8	0.75	7,990	11,700
A	6,500	7,000	3.0	0.80	8,380	11,770
A	6,500	7,000	2.5	0.74	8,280	11,900
A	6,500	7,000	3.8	0.77	8,470	11,960

B	6,500	7,000	3.0	0.90	8,100	12,220
B	6,500	7,000	2.5	2.78	8,580	12,800
B	6,500	7,000	2.4	2.81	9,010	13,270
A	6,600	7,000	2.5	0.69	7,670	8,970
A	6,600	7,000	2.5	0.65	6,880	9,590
A	6,600	7,000	2.6	2.75	8,930	9,770
A	6,600	7,000	4.0	0.65	8,540	9,870
A	6,600	7,000	2.9	0.71	7,490	9,910
A	6,600	7,000	4.5	2.73	8,960	9,950
A	6,600	7,000	2.1	0.63	7,280	10,040
A	6,600	7,000	2.5	0.65	7,450	10,150
A	6,600	7,000	3.6	0.73	7,370	10,200
A	6,600	7,000	3.0	0.78	8,060	10,260
A	6,600	7,000	3.2	0.60	8,410	10,360
A	6,600	7,000	3.9	0.60	8,390	10,380
A	6,600	7,000	2.9	0.70	7,420	10,420
A	6,600	7,000	2.5	0.71	7,660	10,560
A	6,600	7,000	3.3	0.67	9,030	10,620
A	6,600	7,000	2.6	0.78	8,300	10,660
A	6,600	7,000	3.3	0.74	7,780	10,770
A	6,600	7,000	3.2	0.72	8,420	10,890
A	6,600	7,000	4.4	0.66	8,880	10,910
A	6,600	7,000	3.2	2.74	8,440	11,060
A	6,600	7,000	4.2	2.68	10,210	11,240
A	6,700	7,000	3.1	0.65	8,600	11,480
A	6,700	7,000	2.5	0.65	8,360	11,620
A	6,700	7,000	2.8	0.68	8,540	11,720
A	6,700	7,000	1.8	0.63	8,600	11,730
A	6,700	7,000	3.0	2.75	10,390	11,830
A	6,700	7,000	2.6	2.74	9,420	11,880
A	6,700	7,000	3.3	0.64	8,780	12,090
A	6,700	7,000	2.5	0.70	8,900	12,140
A	6,700	7,000	2.9	0.66	8,660	12,190
A	6,700	7,000	4.1	0.68	8,340	12,360
A	5,220	7,250	3.9	2.83	8,810	10,400
A	5,220	7,250	3.0	0.66	8,670	10,810
A	5,220	7,250	3.2	0.74	8,260	10,820
A	5,220	7,250	3.8	2.79	9,180	10,880
A	5,220	7,250	3.6	0.75	8,330	11,050
A	5,220	7,250	3.7	2.83	9,570	11,110
A	5,220	7,250	5.0	0.74	8,280	11,250

A	5,220	7,250	3.1	0.64	8,320	11,320
A	5,220	7,250	3.2	0.75	7,460	11,470
A	5,220	7,250	3.8	0.77	7,770	11,510
A	5,220	7,250	2.5	0.81	8,990	11,610
A	5,220	7,250	3.0	2.80	9,910	12,020
A	5,220	7,250	3.0	0.76	9,140	12,080
A	5,220	7,250	2.6	0.83	9,130	12,400
A	5,510	7,250	5.0	0.82	6,900	9,370
A	5,510	7,250	3.4	0.96	6,810	9,390
A	5,510	7,250	3.0	0.70	6,320	9,410
A	5,510	7,250	4.3	0.94	7,160	9,550
A	5,510	7,250	3.0	0.75	6,640	9,790
A	5,510	7,250	3.2	0.68	7,120	9,860
A	5,510	7,250	3.3	0.78	6,990	9,880
A	5,510	7,250	3.4	0.78	6,970	10,070
A	5,510	7,250	4.4	0.74	6,820	10,090
A	5,510	7,250	3.0	0.74	6,390	10,160
A	5,510	7,250	3.2	0.80	7,140	10,280
A	5,510	7,250	3.2	0.72	6,830	10,290
A	5,510	7,250	3.7	0.70	7,050	10,300
A	5,510	7,250	2.5	0.77	7,040	10,410
A	5,510	7,250	3.6	0.62	6,760	10,420
A	5,510	7,250	3.9	0.73	7,180	10,810
A	5,510	7,250	4.3	0.78	6,780	10,860
A	5,510	7,250	3.4	0.60	7,580	10,930
A	5,510	7,250	3.3	0.71	7,420	11,500
A	5,655	7,250	3.2	0.82	6,670	9,660
A	5,655	7,250	3.7	0.84	6,230	9,770
A	5,655	7,250	3.6	2.67	8,120	9,850
A	5,655	7,250	3.5	0.89	6,850	9,900
A	5,655	7,250	2.7	0.87	7,110	9,950
A	5,655	7,250	3.5	0.81	7,090	9,970
A	5,655	7,250	3.5	0.82	6,550	10,120
A	5,655	7,250	3.5	0.83	6,500	10,170
A	5,655	7,250	3.5	0.69	7,620	10,430
A	5,655	7,250	2.9	2.78	8,280	10,450
A	5,655	7,250	3.4	0.80	6,850	10,530
A	5,655	7,250	4.1	0.70	7,950	10,590
A	5,655	7,250	4.5	0.83	7,740	10,600
A	5,655	7,250	3.0	0.87	8,710	10,790
A	5,655	7,250	3.1	0.79	7,400	10,840

A	5,655	7,250	4.0	0.73	7,430	10,880
A	5,655	7,250	3.2	0.81	7,240	10,890
A	5,655	7,250	4.8	0.86	7,530	11,010
A	5,655	7,250	3.7	0.70	7,530	11,050
A	5,655	7,250	2.8	0.65	6,860	11,060
A	5,655	7,250	3.0	0.65	7,880	11,070
A	5,655	7,250	5.0	0.82	8,010	11,080
A	5,655	7,250	5.0	0.85	7,530	11,090
A	5,655	7,250	3.7	0.72	7,820	11,090
A	5,655	7,250	2.8	0.62	8,050	11,250
A	5,655	7,250	2.9	0.71	7,540	11,340
A	5,655	7,250	3.2	0.88	8,490	11,340
A	5,655	7,250	4.5	2.96	9,970	11,380
A	5,655	7,250	3.2	0.77	7,070	11,390
A	5,655	7,250	2.9	0.87	7,970	11,430
A	5,655	7,250	3.5	0.73	7,310	11,460
A	5,655	7,250	3.4	0.75	7,440	11,520
A	5,655	7,250	3.8	3.87	10,210	11,610
A	5,655	7,250	3.7	0.71	8,280	11,650
A	5,655	7,250	3.5	0.68	7,890	11,660
A	5,655	7,250	3.6	0.88	8,300	11,680
A	5,655	7,250	3.6	0.70	7,300	11,690
A	5,655	7,250	3.2	0.83	8,480	11,730
A	5,655	7,250	3.2	0.86	8,600	11,730
A	5,655	7,250	3.1	0.64	7,690	11,830
A	5,655	7,250	3.6	2.93	9,580	11,900
A	5,655	7,250	3.0	0.85	7,580	11,910
A	5,655	7,250	3.6	0.69	8,050	12,160
A	5,655	7,250	3.3	3.84	10,620	12,180
A	5,655	7,250	3.3	0.84	8,940	12,250
A	5,655	7,250	3.0	0.83	8,080	12,370
A	5,800	7,250	4.0	0.80	6,260	8,800
A	5,800	7,250	3.2	0.77	6,080	9,080
A	5,800	7,250	4.5	0.75	6,100	9,120
A	5,800	7,250	4.1	0.76	6,450	9,280
A	5,800	7,250	2.9	0.83	6,530	9,380
A	5,800	7,250	2.5	0.70	6,390	9,450
A	5,800	7,250	4.6	0.70	6,640	9,500
A	5,800	7,250	4.2	0.74	6,860	9,540
A	5,800	7,250	4.4	0.80	5,960	9,690
A	5,800	7,250	4.3	2.81	8,280	9,760

A	5,800	7,250	3.4	0.74	6,730	9,790
A	5,800	7,250	3.6	0.73	6,620	9,900
A	5,800	7,250	3.5	0.87	7,140	9,920
A	5,800	7,250	3.3	0.79	7,170	9,930
A	5,800	7,250	3.4	0.75	6,290	9,950
A	5,800	7,250	3.3	0.77	6,730	9,960
A	5,800	7,250	3.3	2.75	8,090	10,050
A	5,800	7,250	3.0	0.74	7,200	10,230
A	5,800	7,250	2.7	0.78	7,530	10,390
A	5,800	7,250	3.4	0.72	7,240	10,410
A	5,800	7,250	3.1	2.78	9,140	10,700
A	5,800	7,250	3.8	0.66	8,330	11,150
A	5,800	7,250	3.2	0.77	8,450	11,290
A	5,800	7,250	3.4	0.68	7,420	11,410
A	5,800	7,250	3.7	2.85	9,510	11,420
A	5,800	7,250	4.3	2.86	10,090	11,640
A	5,800	7,250	3.8	0.84	9,190	11,720
A	5,800	7,250	3.5	0.68	8,320	11,740
A	5,800	7,250	2.6	0.81	8,450	11,770
A	5,800	7,250	2.7	0.83	7,370	11,850
A	5,800	7,250	3.7	0.78	8,310	11,880
A	5,800	7,250	3.5	0.70	8,620	11,890
A	5,800	7,250	3.1	0.79	9,160	12,160
A	5,800	7,250	2.2	2.75	10,800	12,180
A	5,800	7,250	3.5	0.81	9,350	12,190
A	5,800	7,250	3.7	2.73	10,540	12,320
A	5,800	7,250	3.0	0.63	6,240	12,540
A	5,800	7,250	3.5	0.82	9,420	12,860
A	6,090	7,250	3.6	0.70	6,590	9,850
A	6,090	7,250	4.5	0.73	7,230	10,020
A	6,090	7,250	3.6	0.78	6,900	10,040
A	6,090	7,250	3.3	0.80	7,020	10,270
A	6,090	7,250	3.7	0.80	7,110	10,290
A	6,090	7,250	4.7	2.70	9,050	10,310
A	6,090	7,250	3.5	0.83	7,490	10,400
A	6,090	7,250	3.8	0.71	7,040	10,450
A	6,090	7,250	3.5	0.81	7,140	10,490
A	6,090	7,250	3.8	2.79	8,620	10,490
A	6,090	7,250	3.8	0.85	8,790	10,510
A	6,090	7,250	3.5	0.92	7,850	10,540
A	6,090	7,250	3.8	0.85	7,500	10,550

A	6,090	7,250	3.7	0.80	7,160	10,570
A	6,090	7,250	3.2	0.90	7,710	10,570
A	6,090	7,250	3.0	0.69	7,270	10,580
A	6,090	7,250	3.5	2.83	8,760	10,590
A	6,090	7,250	3.1	0.80	7,710	10,640
A	6,090	7,250	3.4	0.84	7,750	10,670
A	6,090	7,250	3.0	0.76	7,420	10,710
A	6,090	7,250	3.7	2.75	8,710	10,710
A	6,090	7,250	3.1	0.84	7,320	10,750
A	6,090	7,250	2.9	0.75	7,760	10,810
A	6,090	7,250	2.9	0.72	7,330	11,080
A	6,090	7,250	3.6	0.87	8,650	11,090
A	6,090	7,250	3.1	0.76	7,690	11,220
A	6,090	7,250	3.8	0.87	8,180	11,280
A	6,090	7,250	4.0	0.83	7,680	11,370
A	6,090	7,250	3.1	2.79	8,950	11,570
A	6,090	7,250	3.1	2.76	9,810	12,010
A	6,530	7,250	3.9	0.77	7,130	9,820
A	6,530	7,250	4.4	0.67	7,200	9,960
A	6,530	7,250	3.1	0.58	6,540	10,080
A	6,530	7,250	2.4	0.67	6,910	10,170
A	6,530	7,250	3.5	0.64	7,870	10,260
A	6,530	7,250	2.5	0.55	7,290	10,560
A	6,530	7,250	4.0	0.77	7,370	10,560
A	6,530	7,250	3.2	0.78	8,590	10,570
A	6,530	7,250	2.4	0.63	7,590	10,610
A	6,530	7,250	3.8	0.58	8,110	10,680
A	6,530	7,250	3.1	0.67	8,000	10,710
A	6,530	7,250	3.3	0.75	7,330	10,770
A	6,530	7,250	4.2	0.74	8,210	10,790
A	6,530	7,250	3.7	0.68	8,920	10,870
A	6,530	7,250	3.6	0.69	7,790	10,900
A	6,530	7,250	3.0	0.72	8,430	10,950
A	6,530	7,250	3.3	0.64	7,170	10,970
A	6,530	7,250	3.2	0.86	8,190	10,980
A	6,530	7,250	3.3	0.66	7,850	11,000
A	6,530	7,250	3.2	0.81	8,610	11,010
A	6,530	7,250	2.5	0.70	7,620	11,020
A	6,530	7,250	2.8	0.75	8,100	11,020
A	6,530	7,250	3.6	0.75	8,190	11,070
A	6,530	7,250	3.7	0.65	8,530	11,090

A	6,530	7,250	3.0	0.70	7,650	11,110
A	6,530	7,250	3.3	0.72	8,530	11,120
A	6,530	7,250	4.5	0.74	7,830	11,150
A	6,530	7,250	4.0	0.74	8,860	11,160
A	6,530	7,250	3.5	0.83	8,660	11,180
A	6,530	7,250	4.0	0.65	8,320	11,220
A	6,530	7,250	4.0	0.68	8,040	11,230
A	6,530	7,250	2.9	0.73	8,090	11,340
A	6,530	7,250	3.4	2.68	9,290	11,340
A	6,530	7,250	3.0	0.73	8,140	11,360
A	6,530	7,250	2.5	0.79	7,900	11,370
A	6,530	7,250	3.2	2.64	10,380	11,500
A	6,530	7,250	3.0	0.71	8,780	11,530
A	6,530	7,250	3.0	0.64	10,120	11,530
A	6,530	7,250	3.5	0.70	8,570	11,590
A	6,530	7,250	3.1	0.65	8,380	11,730
A	6,530	7,250	2.5	0.82	9,280	11,760
A	6,530	7,250	2.8	2.64	9,780	11,770
A	6,530	7,250	4.2	0.75	9,020	11,820
A	6,530	7,250	3.5	0.86	8,290	11,840
A	6,530	7,250	2.5	0.68	9,150	11,880
A	6,530	7,250	3.9	0.67	8,570	11,980
A	6,530	7,250	4.0	2.62	9,890	11,990
A	6,530	7,250	4.5	0.80	9,300	12,000
A	6,530	7,250	2.7	0.67	8,910	12,040
A	6,530	7,250	3.1	0.83	8,790	12,060
A	6,530	7,250	2.5	0.85	9,070	12,070
A	6,530	7,250	3.6	0.71	9,200	12,110
A	6,530	7,250	2.5	0.70	9,120	12,170
A	6,530	7,250	2.3	0.86	9,600	12,260
A	6,530	7,250	3.5	0.74	9,310	12,270
A	6,530	7,250	2.7	0.62	10,340	12,370
A	6,530	7,250	2.6	0.88	9,870	12,500
A	6,530	7,250	3.4	0.81	10,070	12,590
A	6,530	7,250	3.6	0.77	9,970	12,880
B	5,600	7,500	3.3	2.84	8,710	10,910
B	5,600	7,500	2.9	0.55	7,210	11,080
B	5,600	7,500	3.0	0.99	7,490	11,300
B	5,600	7,500	3.0	0.97	7,410	11,310
B	5,600	7,500	3.3	0.56	7,260	11,410
B	5,600	7,500	3.0	2.65	8,970	11,580

B	5,600	7,500	3.0	1.00	7,180	11,670
B	5,600	7,500	2.7	2.66	9,020	11,700
B	5,600	7,500	3.0	0.56	7,350	11,890
B	5,600	7,500	3.0	1.02	7,080	12,000
B	5,600	7,500	3.3	2.82	9,430	12,000
B	5,600	7,500	2.8	0.58	7,620	12,350
B	6,000	7,500	2.4	0.67	7,440	10,790
B	6,000	7,500	3.3	0.72	8,030	10,980
D	6,200	7,500	2.8	0.88	6,390	9,320
D	6,200	7,500	2.3	0.66	7,330	10,730
D	6,200	7,500	2.5	0.82	7,470	10,870
A	6,500	7,500	4.2	0.85	7,600	9,110
A	6,500	7,500	5.0	0.79	6,940	9,420
A	6,500	7,500	4.4	0.84	7,040	9,880
A	6,500	7,500	4.0	0.80	6,960	10,030
A	6,500	7,500	3.5	0.74	7,680	10,130
A	6,500	7,500	4.0	0.80	7,450	10,180
B	6,500	7,500	3.4	0.77	6,870	10,300
B	6,500	7,500	3.6	0.75	6,650	10,350
B	6,500	7,500	3.1	0.75	6,790	10,700
B	6,500	7,500	3.8	0.80	6,710	10,740
B	6,500	7,500	3.0	0.75	6,810	10,990
B	6,500	7,500	3.1	0.63	6,680	11,450
A	7,000	7,500	3.6	0.72	8,100	9,630
A	7,000	7,500	3	0.84	7,570	9,940
A	7,000	7,500	3.3	0.84	7,820	9,980
B	7,500	7,500	4.0	2.84	8,030	10,060
B	7,500	7,500	4.0	0.88	7,720	10,260
B	7,500	7,500	3.5	0.71	7,620	10,470
B	6,000	7,700	3.4	0.80	7,550	10,650
B	6,000	7,700	2.5	0.70	7,100	11,860
B	6,000	7,700	3.0	0.73	7,090	11,880
A	5,800	8,000	2.2	0.75	5,950	9,910
A	5,800	8,000	3.1	0.79	7,610	10,250
A	5,800	8,000	3.7	0.65	7,320	10,420
A	5,800	8,000	4.2	0.77	6,940	10,460
A	5,800	8,000	3.4	0.79	7,740	10,510
A	5,800	8,000	3.6	0.73	7,340	10,540
A	5,800	8,000	2.5	0.77	8,060	10,540
A	5,800	8,000	3.7	0.81	7,010	10,590
A	5,800	8,000	4.2	0.83	7,580	10,700

A	5,800	8,000	4.0	0.83	7,560	10,720
A	5,800	8,000	2.0	0.81	7,450	10,770
A	5,800	8,000	3.5	0.70	7,630	10,820
B	5,800	8,000	4.2	0.55	7,060	10,900
B	5,800	8,000	3.7	0.59	7,450	11,160
A	5,800	8,000	3.3	0.67	7,670	11,360
B	5,800	8,000	2.9	0.65	7,740	11,570
B	5,800	8,000	3.2	0.63	8,150	11,800
A	5,800	8,000	3.8	0.69	7,780	11,850
B	5,800	8,000	3.0	0.86	8,510	12,140
B	5,800	8,000	3.4	0.60	8,010	12,210
B	5,800	8,000	3.0	0.83	8,920	12,420
B	5,800	8,000	2.5	2.98	9,530	12,640
B	5,800	8,000	2.6	3.00	9,190	12,880
A	6,000	8,000	3.1	0.73	7,720	11,470
A	6,000	8,000	2.8	0.65	6,850	12,230
D	6,200	8,000	2.9	0.88	7,390	10,550
D	6,200	8,000	2.2	0.83	7,370	11,240
D	6,200	8,000	2.5	0.70	7,690	11,470
A	6,200	8,000	2.7	0.80	7,900	11,490
D	6,200	8,000	2.0	0.56	9,990	11,780
A	6,200	8,000	3.3	0.74	8,090	11,820
A	6,200	8,000	3.2	0.85	8,490	11,880
D	6,200	8,000	2.5	4.83	10,050	11,930
D	6,200	8,000	2.5	0.87	7,420	12,010
D	6,200	8,000	2.5	0.69	7,050	12,020
A	6,200	8,000	3.0	0.88	8,280	12,160
A	6,200	8,000	2.6	0.72	7,910	12,230
D	6,200	8,000	2.5	0.66	7,340	12,450
D	6,200	8,000	2.5	0.83	7,440	12,590
A	6,400	8,000	2.5	1.69	7,350	9,200
A	6,400	8,000	3.9	0.66	6,480	9,290
A	6,400	8,000	3.2	0.89	6,960	9,480
A	6,400	8,000	3.3	0.82	6,880	9,900
A	6,400	8,000	4.0	0.85	6,860	10,000
A	6,400	8,000	3.0	2.88	8,610	10,090
A	6,400	8,000	5.1	0.74	7,180	10,110
A	6,400	8,000	3.5	0.81	7,300	10,340
A	6,400	8,000	3.0	0.68	7,380	10,570
A	6,400	8,000	3.8	0.73	7,730	10,590
A	6,400	8,000	3.7	0.82	7,730	10,600

A	6,400	8,000	2.7	0.91	7,410	10,650
A	6,400	8,000	3.7	0.87	7,910	10,670
A	6,400	8,000	3.0	0.84	7,560	10,700
A	6,400	8,000	4.5	0.83	7,820	10,870
A	6,400	8,000	3.0	0.62	6,820	10,990
A	6,400	8,000	3.6	0.83	7,370	11,060
A	6,400	8,000	3.2	0.88	7,930	11,360
A	6,400	8,000	2.6	0.74	7,430	11,400
A	6,400	8,000	2.5	0.91	7,710	11,420
B	6,500	8,000	4.2	0.80	7,770	9,310
B	6,500	8,000	3.6	0.65	7,330	9,350
B	6,500	8,000	3.9	0.74	7,240	10,470
A	7,000	8,000	3.2	0.75	8,340	10,040
A	7,000	8,000	3.1	0.77	8,220	10,100
A	7,000	8,000	3.0	0.62	7,150	10,440
A	7,000	8,000	3.0	0.60	8,260	10,500
A	7,000	8,000	2.5	0.77	8,280	10,510
A	7,000	8,000	2.5	0.77	8,460	10,680
A	7,000	8,000	2.8	0.94	8,140	10,750
A	7,000	8,000	2.2	0.70	7,850	10,770
A	7,000	8,000	2.5	2.83	10,490	10,810
B	7,000	8,000	4.3	0.69	9,940	11,000
A	7,000	8,000	2.1	0.72	8,090	11,010
B	7,000	8,000	2.8	0.72	7,690	11,060
A	7,000	8,000	2.8	0.82	8,510	11,100
A	7,000	8,000	2.9	0.84	8,680	11,160
B	7,000	8,000	4.0	0.64	9,750	11,160
A	7,000	8,000	3.0	0.77	8,500	11,190
A	7,000	8,000	3.6	0.80	8,200	11,300
A	7,000	8,000	3.1	0.75	8,750	11,450
B	7,000	8,000	3.2	0.83	8,790	11,510
A	7,000	8,000	2.3	0.73	8,420	11,600
A	7,000	8,000	3.1	0.73	8,460	11,600
A	7,000	8,000	2.8	0.77	8,380	11,610
A	7,000	8,000	3.0	0.79	7,850	11,630
A	7,000	8,000	2.8	0.84	8,610	11,650
A	7,000	8,000	3.3	0.76	8,710	11,670
A	7,000	8,000	3.0	0.74	8,140	11,720
A	7,000	8,000	3.0	0.75	8,550	11,720
A	7,000	8,000	2.5	0.76	8,550	11,890
A	7,000	8,000	3.0	0.77	8,940	11,940

A	7,000	8,000	2.6	2.76	10,270	11,980
A	7,000	8,000	3.0	2.78	10,290	12,000
A	7,000	8,000	2.5	0.82	9,090	12,020
A	7,000	8,000	2.3	0.72	8,810	12,140
A	7,000	8,000	2.2	0.74	8,880	12,160
A	7,000	8,000	3.3	2.76	9,860	12,170
A	7,000	8,000	2.9	0.78	8,800	12,290
A	7,000	8,000	2.5	0.67	8,530	12,300
A	7,000	8,000	2.5	2.79	9,290	12,310
A	7,000	8,000	2.4	0.70	8,580	12,320
A	7,000	8,000	2.8	0.79	9,040	12,370
A	7,500	8,000	3.0	0.79	7,660	10,010
A	7,500	8,000	4.3	2.78	8,680	10,010
A	7,500	8,000	3.4	0.76	7,500	10,050
A	7,500	8,000	3.2	0.73	7,640	10,080
A	7,500	8,000	4	0.82	7,520	10,120
A	7,500	8,000	3.5	0.82	7,810	10,230
A	7,500	8,000	2.9	0.73	8,720	10,300
A	7,500	8,000	4	0.87	7,720	10,350
A	7,500	8,000	3.5	0.85	7,560	10,370
A	7,500	8,000	2.6	0.77	8,830	10,390
A	7,500	8,000	2.5	1.00	7,890	10,430
A	7,500	8,000	2.5	0.75	7,850	10,530
B	7,500	8,000	2.5	0.82	7,600	10,590
A	7,500	8,000	2.8	0.67	7,710	10,590
B	7,500	8,000	2.8	1.63	8,470	10,630
A	7,500	8,000	3.5	0.93	7,500	10,640
B	7,500	8,000	3.5	0.66	7,550	10,640
B	7,500	8,000	2.8	1.66	8,100	10,640
A	7,500	8,000	3.1	0.85	7,820	10,670
B	7,500	8,000	3.5	1.58	8,640	10,680
B	7,500	8,000	3.3	1.62	8,760	10,680
B	7,500	8,000	3.3	0.71	7,760	10,690
A	7,500	8,000	3.6	0.77	7,850	10,690
A	7,500	8,000	2.6	0.76	9,040	10,700
B	7,500	8,000	3.2	0.74	7,530	10,710
A	7,500	8,000	3.4	0.86	8,380	10,730
B	7,500	8,000	3.0	2.51	9,570	10,740
A	7,500	8,000	2.7	0.82	8,410	10,750
B	7,500	8,000	3.2	0.80	7,510	10,760
A	7,500	8,000	3	0.79	7,840	10,760

B	7,500	8,000	3.3	0.70	7,690	10,770
B	7,500	8,000	3.4	0.77	7,700	10,780
B	7,500	8,000	2.4	2.49	9,340	10,790
B	7,500	8,000	2.9	0.74	7,770	10,810
A	7,500	8,000	2.6	0.82	9,070	10,820
A	7,500	8,000	4.0	0.87	7,600	10,870
A	7,500	8,000	3	0.81	7,890	10,930
A	7,500	8,000	2.5	0.82	8,320	11,080
A	7,500	8,000	3.6	0.76	7,800	11,090
A	7,500	8,000	2.7	0.96	8,510	11,110
A	7,500	8,000	2.5	0.85	8,780	11,140
A	7,500	8,000	3.4	0.91	8,800	11,150
A	7,500	8,000	2.8	0.87	8,800	11,160
A	7,500	8,000	3	0.92	7,630	11,230
A	7,500	8,000	3.0	2.73	9,240	11,240
A	7,500	8,000	2.7	0.76	8,270	11,280
A	7,500	8,000	2.5	0.70	7,520	11,290
A	7,500	8,000	2.6	0.80	8,000	11,400
A	7,500	8,000	2.6	0.81	8,470	11,440
A	7,500	8,000	2.2	0.78	8,910	11,450
A	7,500	8,000	2.6	0.97	8,780	11,490
A	7,500	8,000	2.7	0.78	8,420	11,600
A	7,500	8,000	2.9	0.71	8,930	11,630
A	7,500	8,000	2.9	0.73	8,480	11,680
A	7,500	8,000	2.3	0.83	8,610	11,680
A	7,500	8,000	3.3	0.76	8,400	11,750
A	7,500	8,000	3.3	0.83	8,730	11,800
A	7,500	8,000	2.5	0.82	8,190	11,860
A	7,500	8,000	3.0	0.79	9,090	11,940
A	7,500	8,000	2.6	0.83	8,990	11,950
A	7,500	8,000	2.9	0.74	9,060	12,030
A	7,500	8,000	2.9	0.71	8,970	12,260
A	7,500	8,000	2.5	0.69	8,610	12,290
A	7,500	8,000	2.8	0.81	9,490	12,310
C	8,000	8,000	3.0	2.58	8,110	9,440
C	8,000	8,000	4.0	0.97	8,430	9,920
C	8,000	8,000	3.0	2.84	9,050	11,090
C	7,500	8,500	3.0	0.82	8,020	9,450
C	7,500	8,500	3.4	0.80	9,770	9,910
C	7,500	8,500	3.5	0.48	8,230	10,140
C	7,500	8,500	3.0	0.47	7,840	10,270

C	7,500	8,500	4.0	0.79	9,400	10,330
C	7,500	8,500	4.0	0.86	9,160	10,340
C	7,500	8,500	5.5	0.59	8,620	10,350
C	7,500	8,500	3.2	0.76	9,090	10,360
C	7,500	8,500	3.5	0.78	8,560	10,490
C	7,500	8,500	3.7	0.83	10,530	10,500
C	7,500	8,500	3.0	0.75	9,710	10,530
C	7,500	8,500	2.5	0.56	8,590	10,560
D	9,000	9,000	3.9	2.81	9,000	9,220
D	9,000	9,000	2.5	3.92	9,210	10,250
D	9,000	9,000	2.8	2.70	9,280	10,250
D	9,000	9,000	2.7	2.06	9,090	10,260
D	9,000	9,000	3.1	3.76	9,110	10,280
D	9,000	9,000	2.5	1.19	9,010	10,350
D	9,000	9,000	2.7	1.57	10,160	10,970
D	9,000	9,000	2.5	2.65	9,960	11,130
D	9,000	9,000	3.2	2.58	9,980	11,310
D	9,000	9,000	2.6	0.72	9,050	11,500
D	9,000	9,000	3.0	1.93	9,360	11,580
D	9,000	9,000	3.0	1.03	9,000	11,810
D	9,000	9,000	2.5	1.70	10,140	12,060
D	9,000	9,000	3.1	1.74	9,170	12,690
D	9,000	9,000	2.7	0.74	9,110	12,980

Appendix D: Raw Historical Stiffness Data Set

Appendix D includes the raw stiffness-strength data set compiled as part of this research effort and includes 148 data points. Of these data points, 110 were gathered by the field and laboratory component of this research project, while the additional 38 data points represent prior work by Keske (2014) and Boehm et al. (2010).

KEY:		
R	=	Release
28	=	28 Days
DL	=	Dolomitic limestone
GG	=	Crushed granite
FC	=	Field cure (in formwork)
FC-L	=	Field cure (in formwork) followed by field lime-bath
FC-SC	=	Field cure (in formwork) followed by standard cure
SC-SC	=	Standard cure both before and after prestress release
FC-A	=	Field cure (in formwork) followed by ambient exposure

Time of Measurement	Coarse Aggregate Type	Curing Method	Data Source	Unit Weight (pcf)	Chronological Age of Testing (hours)	Measured Compressive Strength (psi)	Measured Modulus of Elasticity (ksi)
R	DL	FC	Hanson, Camber Project Pour #2a	152.1	20.6	8,450	6,700
R	DL	FC	Hanson, Camber Project Pour #2a	152.1	23.5	8,610	6,900
R	DL	FC	Hanson, Camber Project Pour #2b	152.8	20.4	8,350	6,700
R	DL	FC	Hanson, Camber Project Pour #2b	152.8	23.4	8,600	7,050

R	DL	FC	Hanson, Camber Project Pour #3a	150.5	17.7	7,050	5,500
R	DL	FC	Hanson, Camber Project Pour #3a	150.5	23.8	7,240	6,100
R	DL	FC	Hanson, Camber Project Pour #3b	152.8	23.3	8,380	6,300
R	DL	FC	Hanson, Camber Project Pour #3b	152.8	17.1	8,090	6,500
R	DL	FC	Hanson, Camber Project Pour #4a	152.1	20.1	9,160	6,600
R	DL	FC	Hanson, Camber Project Pour #4a	152.1	25	9,580	6,750
R	DL	FC	Hanson, Camber Project Pour #4b	152.8	18.8	9,400	6,800
R	DL	FC	Hanson, Camber Project Pour #4b	152.8	24	9,620	7,300
R	DL	FC	Hanson, Camber Project Pour #5a	150.8	27.7	8,230	6,300
R	DL	FC	Hanson, Camber Project Pour #5a	150.8	24.9	8,530	6,500
R	DL	FC	Hanson, Camber Project Pour #5b	152.4	20	8,780	6,650
R	DL	FC	Hanson, Camber Project Pour #5b	152.4	23.8	9,070	7,000
R	DL	FC	Hanson, Camber Project Pour #6a	149.9	18.4	8,450	6,600
R	DL	FC	Hanson, Camber Project Pour #6a	149.9	23.4	8,590	6,700
R	DL	FC	Hanson, Camber Project Pour #6b	150.5	17.4	8,210	6,350
R	DL	FC	Hanson, Camber Project Pour #6b	150.5	23.9	8,560	7,050
R	DL	FC	Hanson, Camber Project Pour #7a	152.4	25.5	8,950	6,650
R	DL	FC	Hanson, Camber Project Pour #7a	152.4	20.9	8,500	6,600
R	DL	FC	Hanson, Camber Project Pour #7b	152.8	20.4	8,110	6,200
R	DL	FC	Hanson, Camber Project Pour #7b	152.8	24	8,490	6,650
R	DL	FC	Hanson, Camber Project Pour #8a	150.5	24.5	8,740	6,700
R	DL	FC	Hanson, Camber Project Pour #8a	150.5	21.2	8,450	6,850
R	DL	FC	Hanson, Camber Project Pour #8b	152.1	20	7,840	5,850
R	DL	FC	Hanson, Camber Project Pour #8b	152.1	23	7,870	6,550
R	DL	FC	Hanson, Camber Project Pour #9a	152.1	24.7	8,450	6,900
R	DL	FC	Hanson, Camber Project Pour #9a	152.1	22.2	8,190	6,800
R	DL	FC	Hanson, Camber Project Pour #9b	152.8	21.8	8,740	6,350
R	DL	FC	Hanson, Camber Project Pour #9b	152.8	24.1	8,830	7,000
R	DL	FC	Hanson, Sam Keske, Oct 15, Pour F	151.2	23	8,120	5,750
R	DL	FC	Hanson, Sam Keske, Oct 19, Pour G	154.1	23	8,290	6,700
R	DL	FC	Hanson, Sam Keske, Oct 20, Pour H	151.0	20	7,860	5,850
R	DL	FC	Hanson, Sam Keske, Oct 22, Pour I	155.7	23	8,770	7,050
R	DL	FC	Hanson, Sam Keske, Oct 26, Pour J	151.2	23	8,220	5,850
R	DL	FC	Hanson, Sam Keske, Oct 27, Pour K	155.2	20	8,320	6,800
R	DL	FC	Hanson, Sam Keske, Oct 29, Pour L	151.2	18	6,930	5,650
R	DL	FC	Hanson, Sam Keske, Oct 29, Pour L	156.9	20	7,710	6,550
R	DL	FC	Hanson, Sam Keske, Oct 6, Pour E	153.6	24	8,760	6,450
R	DL	FC	Hanson, Sam Keske, Oct 6, Pour E	148.9	23	7,940	6,050
R	DL	FC	Hanson, Sam Keske, Sep 22, Pour A	151.1	24	9,010	6,200
R	DL	FC	Hanson, Sam Keske, Sep 24, Pour B	153.7	25	8,790	7,100

R	DL	FC	Hanson, Sam Keske, Sep 29, Pour C	151.7	24	8,680	6,350
R	DL	FC	Hanson, Sam Keske, Sep 30, Pour D	153.2	23	7,860	6,650
R	DL	FC	Kurtis Boehm, SCC-HS-1	153.6	23.3	10,190	6,750
R	DL	FC	Kurtis Boehm, SCC-HS-2	153.2	23.3	10,720	7,150
R	DL	FC	Kurtis Boehm, SCC-MS-1	148.5	22.8	5,110	5,200
R	DL	FC	Kurtis Boehm, SCC-MS-2	150.3	23.3	4,500	4,950
R	DL	FC	Kurtis Boehm, STD-M-1	151.2	20.6	4,990	6,050
R	DL	FC	Kurtis Boehm, STD-M-2	151.9		4,860	5,550
R	DL	FC	Lab Study CL-III 2/26/2014	150.7	17.9	6,610	5,700
R	DL	FC	Lab Study CL-III 3/3/2014	149.8	17.9	6,170	5,750
R	DL	FC	Lab Study CL-III 3/5/2014	151.1	23.8	7,220	6,100
R	DL	FC	Lab Study DL-FA 4/14/2014	150.4	23.8	7,360	6,100
R	DL	FC	Lab Study DL-FA 4/9/2014	150.4	17.7	6,860	6,100
R	DL	FC	Lab Study DL-FA/SF 5/12/2014	146.5	23.9	7,270	6,100
R	DL	FC	Lab Study DL-FA/SF 5/15/2014	145.1	17.9	6,900	6,050
R	DL	FC	Lab Study DL-III 5/27/2014	151.3	17.9	6,420	5,700
R	DL	FC	Lab Study DL-III 5/29/2014	150.6	18.2	6,520	5,600
R	DL	FC	Lab Study DL-III 6/3/2014	151.4	23.8	6,900	6,350
R	DL	FC	Lab Study DL-SL 7/7/2014	150.9	23.7	7,260	6,400
R	DL	FC	Lab Study DL-SL 7/9/2014	150.9	17.6	6,870	6,600
R	GG	FC	Lab Study GG-III 7/13/2014	148.9	18.0	7,400	3,700
R	GG	FC	Lab Study GG-III 7/15/2014	147.6	18	6,850	3,500
R	GG	FC	Lab Study GG-III 7/17/2014	149.6	24	7,940	3,900
R	DL	FC	Pass Christian, Camber Project Pour #1a	147.2	41.5	6,110	4,800
R	DL	FC	Pass Christian, Camber Project Pour #1a	147.2	18.5	5,050	4,700
R	DL	FC	Pass Christian, Camber Project Pour #1b	148.3	40.9	7,440	5,350
R	DL	FC	Pass Christian, Camber Project Pour #1b	148.3	18.6	6,410	5,150
28	DL	FC - A	Hanson, Sam Keske, Oct 15, Pour F	151.2	672	10,490	6,300
28	DL	FC - A	Hanson, Sam Keske, Oct 19, Pour G	154.1	672	10,770	7,000
28	DL	FC - A	Hanson, Sam Keske, Oct 20, Pour H	151.0	672	10,770	6,350
28	DL	FC - A	Hanson, Sam Keske, Oct 22, Pour I	155.7	672	10,850	7,300
28	DL	FC - A	Hanson, Sam Keske, Oct 26, Pour J	151.2	672	10,550	6,350
28	DL	FC - A	Hanson, Sam Keske, Oct 27, Pour K	155.2	672	11,050	7,650
28	DL	FC - A	Hanson, Sam Keske, Oct 29, Pour L	151.2	672	10,070	6,000
28	DL	FC - A	Hanson, Sam Keske, Oct 29, Pour L	156.9	672	10,510	6,850
28	DL	FC - A	Hanson, Sam Keske, Oct 6, Pour E	148.9	672	10,180	6,150

28	DL	FC - A	Hanson, Sam Keske, Oct 6, Pour E	153.6	672	10,360	6,850
28	DL	FC - A	Hanson, Sam Keske, Sep 22, Pour A	151.1	672	10,240	6,350
28	DL	FC - A	Hanson, Sam Keske, Sep 24, Pour B	153.7	672	10,590	7,350
28	DL	FC - A	Hanson, Sam Keske, Sep 29, Pour C	151.7	672	10,800	6,600
28	DL	FC - A	Hanson, Sam Keske, Sep 30, Pour D	153.2	672	9,670	6,850
28	DL	FC - A	Kurtis Boehm, SCC-HS-1	153.6	672	12,200	7,500
28	DL	FC - A	Kurtis Boehm, SCC-HS-2	153.2	672	12,030	7,550
28	DL	FC - A	Kurtis Boehm, SCC-MS-1	148.5	672	8,390	6,450
28	DL	FC - A	Kurtis Boehm, SCC-MS-2	150.3	672	8,530	6,350
28	DL	FC - A	Kurtis Boehm, STD-M-1	151.2	672	6,330	6,350
28	DL	FC - A	Kurtis Boehm, STD-M-2	151.9	672	6,120	5,800
28	DL	FC - L	Hanson, Camber Project Pour #2a	152.1	672	11,480	8,050
28	DL	FC - L	Hanson, Camber Project Pour #2b	152.8	672	10,830	7,300
28	DL	FC - L	Hanson, Camber Project Pour #3a	150.5	672	10,060	7,750
28	DL	FC - L	Hanson, Camber Project Pour #3b	152.8	672	11,490	7,950
28	DL	FC - L	Hanson, Camber Project Pour #4a	152.1	672	11,540	7,300
28	DL	FC - L	Hanson, Camber Project Pour #4b	152.8	672	10,540	8,000
28	DL	FC - L	Hanson, Camber Project Pour #5a	150.8	672	9,640	6,900
28	DL	FC - L	Hanson, Camber Project Pour #5b	152.4	672	10,730	7,500
28	DL	FC - L	Hanson, Camber Project Pour #6a	149.9	672	10,100	6,750
28	DL	FC - L	Hanson, Camber Project Pour #6b	150.5	672	9,620	6,800
28	DL	FC - L	Hanson, Camber Project Pour #7a	152.4	672	11,250	7,300
28	DL	FC - L	Hanson, Camber Project Pour #7b	152.8	672	10,660	7,150
28	DL	FC - L	Hanson, Camber Project Pour #8a	150.5	672	10,610	7,900
28	DL	FC - L	Hanson, Camber Project Pour #8b	152.1	672	9,900	7,100
28	DL	FC - L	Hanson, Camber Project Pour #9a	152.1	672	10,690	7,400
28	DL	FC - L	Hanson, Camber Project Pour #9b	152.8	672	11,200	7,650

28	DL	FC - L	Pass Christian, Camber Project Pour #1a	147.2	672	8,910	5,950
28	DL	FC - L	Pass Christian, Camber Project Pour #1b	148.3	672	9,930	6,550
28	DL	FC - SC	Lab Study CL-III 2/19/2014	150.7	672	9,940	7,050
28	DL	FC - SC	Lab Study CL-III 2/24/2014	150.7	672	10,150	6,450
28	DL	FC - SC	Lab Study CL-III 2/26/2014	150.7	672	9,520	6,700
28	DL	FC - SC	Lab Study CL-III 3/3/2014	149.8	672	9,010	6,900
28	DL	FC - SC	Lab Study CL-III 3/5/2014	151.1	672	9,640	6,450
28	DL	FC - SC	Lab Study DL-FA 3/17/2014	149.5	672	8,700	6,600
28	DL	FC - SC	Lab Study DL-FA 3/19/2014	150.8	672	9,670	6,800
28	DL	FC - SC	Lab Study DL-FA 3/31/2014	150.4	672	9,993	7,000
28	DL	FC - SC	Lab Study DL-FA 4/14/2014	150.4	672	10,200	6,950
28	DL	FC - SC	Lab Study DL-FA 4/2/2014	151.0	672	10,490	7,100
28	DL	FC - SC	Lab Study DL-FA 4/9/2014	150.4	672	10,240	6,850
28	DL	FC - SC	Lab Study DL-FA/SF 4/16/2014	147.5	672	10,510	7,150
28	DL	FC - SC	Lab Study DL-FA/SF 5/12/2014	146.5	672	9,800	6,600
28	DL	FC - SC	Lab Study DL-FA/SF 5/15/2014	145.1	672	9,850	6,650
28	DL	FC - SC	Lab Study DL-FA/SF 5/7/2014	146.7	672	9,500	6,950
28	DL	FC - SC	Lab Study DL-III 5/21/2014	151.2	672	9,870	6,650
28	DL	FC - SC	Lab Study DL-III 5/27/2014	151.3	672	9,900	6,600
28	DL	FC - SC	Lab Study DL-III 5/29/2014	150.6	672	9,910	7,000
28	DL	FC - SC	Lab Study DL-III 6/3/2014	151.4	672	9,000	7,000
28	DL	FC - SC	Lab Study DL-SL 6/5/2014	150.2	672	10,280	7,150
28	DL	FC - SC	Lab Study DL-SL 6/9/2014	151.0	672	9,350	6,750
28	DL	FC - SC	Lab Study DL-SL 7/7/2014	150.9	672	9,860	6,600
28	DL	FC - SC	Lab Study DL-SL 7/9/2014	150.9	672	10,080	6,700
28	GG	FC - SC	Lab Study GG-III 7/11/2014	148.0	672	9,590	4,250
28	GG	FC - SC	Lab Study GG-III 7/13/2014	148.9	672	10,070	4,000

28	GG	FC - SC	Lab Study GG-III 7/15/2014	147.6	672	9,650	4,000
28	GG	FC - SC	Lab Study GG-III 7/17/2014	149.6	672	10,440	4,050
28	DL	SC - SC	Hanson, Camber Project Pour #2a	152.1	672	12,560	8,050
28	DL	SC - SC	Hanson, Camber Project Pour #2b	152.8	672	12,950	8,150
28	DL	SC - SC	Hanson, Camber Project Pour #3a	150.5	672	11,380	7,850
28	DL	SC - SC	Hanson, Camber Project Pour #3b	152.8	672	12,450	8,000
28	DL	SC - SC	Hanson, Camber Project Pour #4a	152.1	672	12,800	7,800
28	DL	SC - SC	Hanson, Camber Project Pour #4b	152.8	672	12,420	7,950
28	DL	SC - SC	Hanson, Camber Project Pour #5a	150.8	672	10,980	7,200
28	DL	SC - SC	Hanson, Camber Project Pour #5b	152.4	672	12,030	7,650
28	DL	SC - SC	Hanson, Camber Project Pour #6a	149.9	672	11,650	7,450
28	DL	SC - SC	Hanson, Camber Project Pour #7a	152.4	672	12,170	8,050
28	DL	SC - SC	Hanson, Camber Project Pour #7b	152.8	672	12,240	7,900
28	DL	SC - SC	Hanson, Camber Project Pour #8a	150.5	672	11,810	7,650
28	DL	SC - SC	Hanson, Camber Project Pour #8b	152.1	672	11,520	7,900
28	DL	SC - SC	Pass Christian, Camber Project Pour #1a	147.2	672	9,400	6,450
28	DL	SC - SC	Pass Christian, Camber Project Pour #1b	148.3	672	10,670	6,600
28	DL	SC- SC	Hanson, Camber Project Pour #9a	152.1	672	12,440	7,900
28	DL	SC- SC	Hanson, Camber Project Pour #9b	152.8	672	12,380	8,100

Appendix E: Detection and Removal of Climate Control System Failures from Creep and Shrinkage Data Set

The following procedure was used to post-process experimental creep and shrinkage data to remove suspect data points that could be tied to documented failures of the climate control system. This procedure was manually applied to the recorded data sets:

1. Manually step through each directly measured quantity
2. If value changes in the opposite direction of anticipated across a time step:
    a. If time interval is small, (<2 hours) this corresponds to a reloading event. In this case, average the recorded quantities across the time step and approximate as a single data point;
    b. Otherwise, delete first recorded value and see if data now follows expected trend. If so, tentatively dismiss deleted value.
    c. If not, delete next recorded value and see if data now follows expected trend,
    d. If not, delete two recorded values independently deleted above and see if data now follows expected trend,
    e. If not, delete subsequent two recorded values and see if data now follows expected trend.
    f. Ties (situations in which b+c or d+e each resolve the unexpected trend) are resolved by selecting the solution with the smallest gap in time-steps.
    g. If difference in unexpected direction is small and occurs late in testing, attribute to instrument precision and disregard.
3. In order to dismiss any values, identical unexpected trends must be seen in all three measured parameters at a given time (cylinder creep, cylinder shrinkage, and rectangular prism shrinkage) and a documented failure of the climate control system must have occurred.

Appendix F: Relative Goodness-of-Fit of Unadjusted Candidate Creep Prediction Models to Experimental Data

This appendix contains visualizations of the relative goodness-of-fit of the three candidate creep prediction equations for each of 15 testing cycles included in this experimental effort.

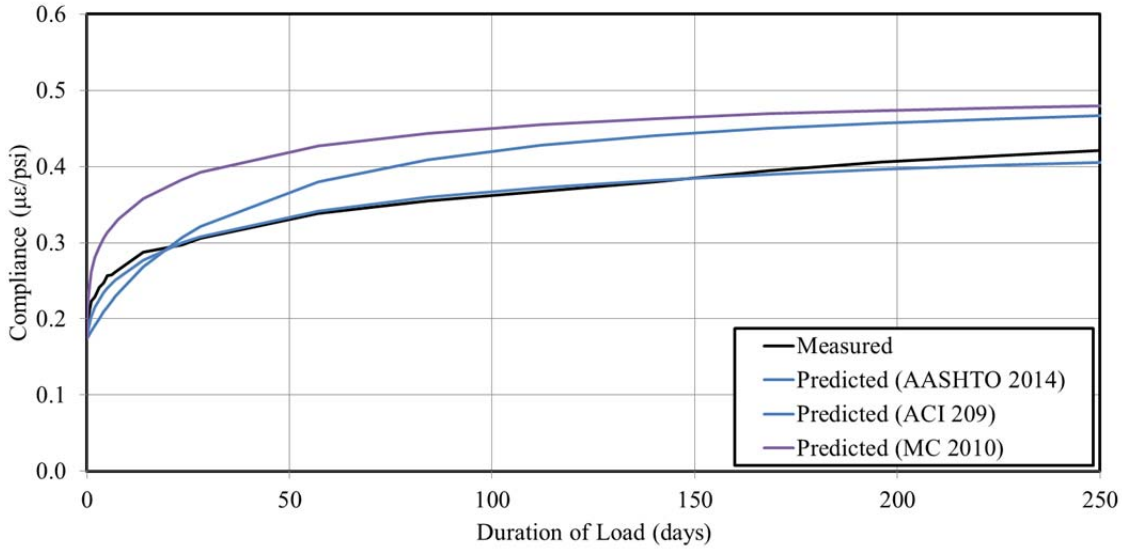

Figure F-1: DL-III 18 Hour – Test 1 Compliance Comparisons

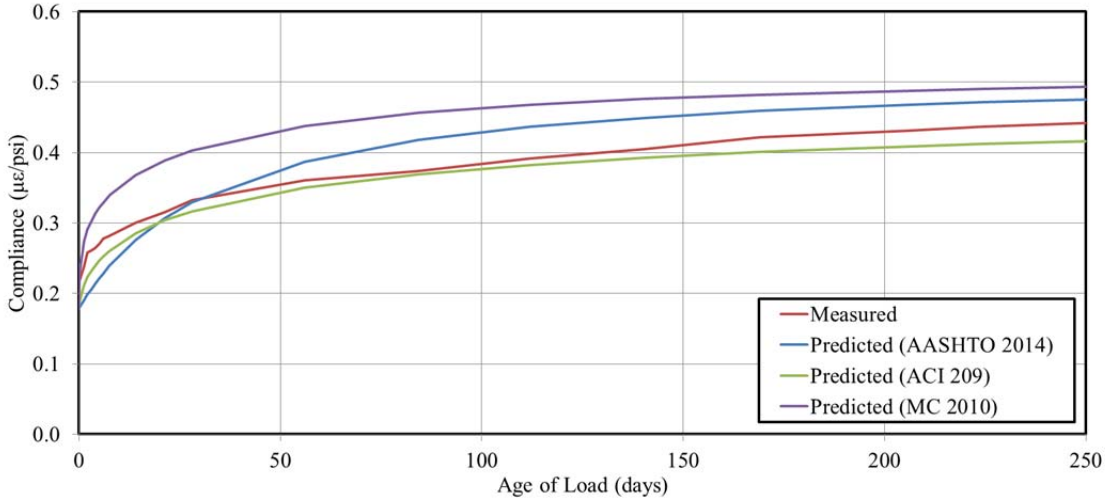

Figure F-2: DL-III 18 Hour – Test 2 Compliance Comparisons

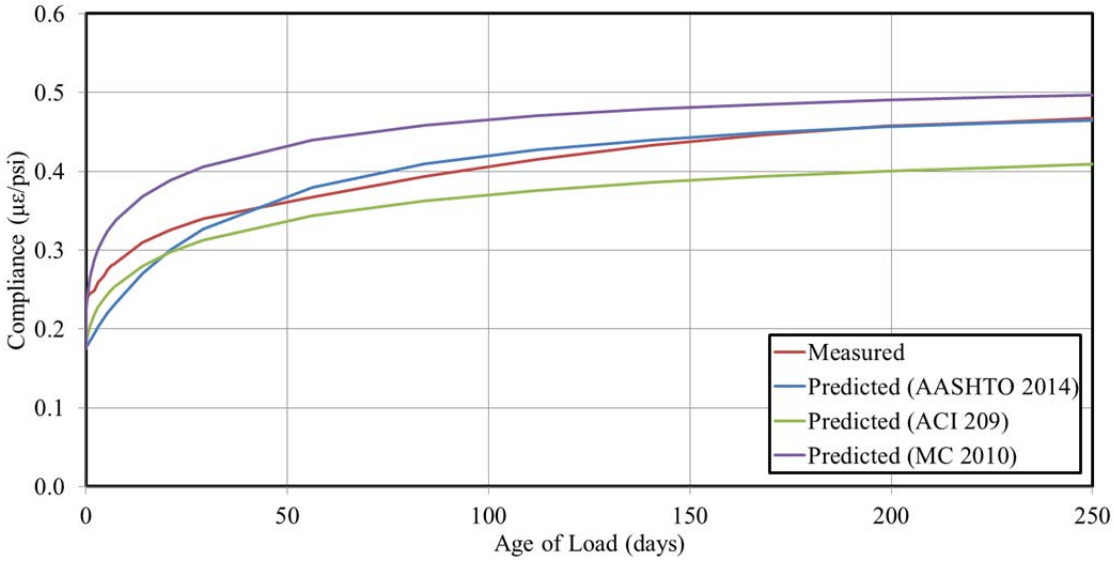

Figure F-3: CL-III 18 Hour – Test 1 Compliance Comparisons

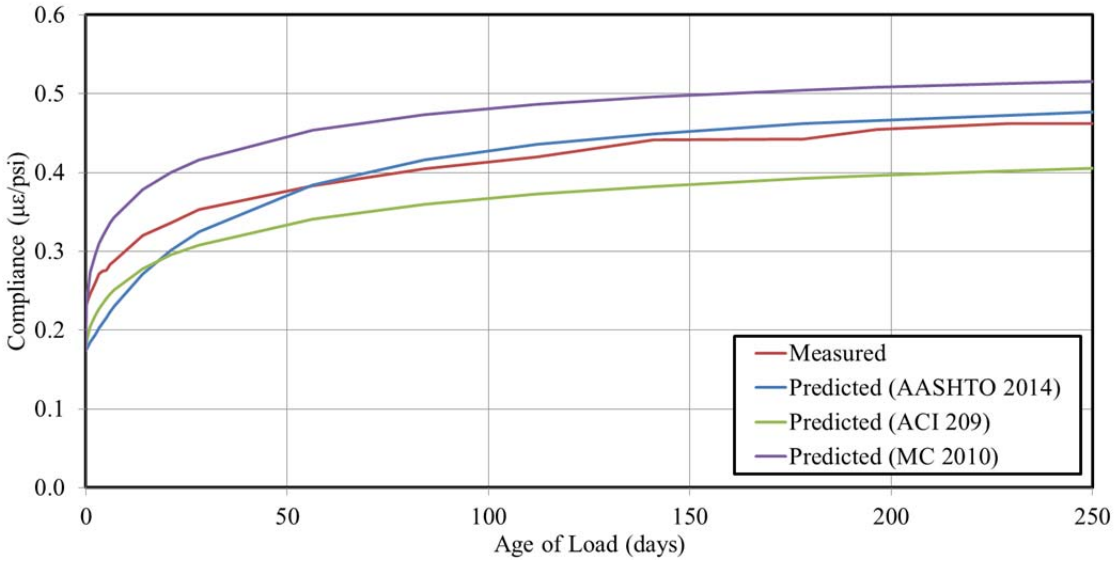

Figure F-4: CL-III 18 Hour – Test 2 Compliance Comparisons

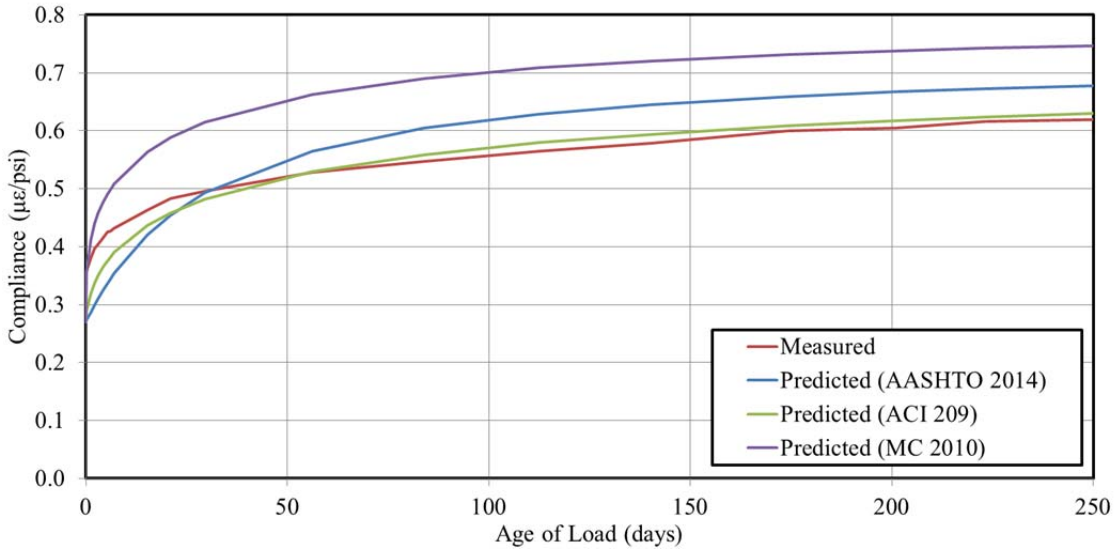

Figure F-5: GG-III 18 Hour – Test 1 Compliance Comparisons

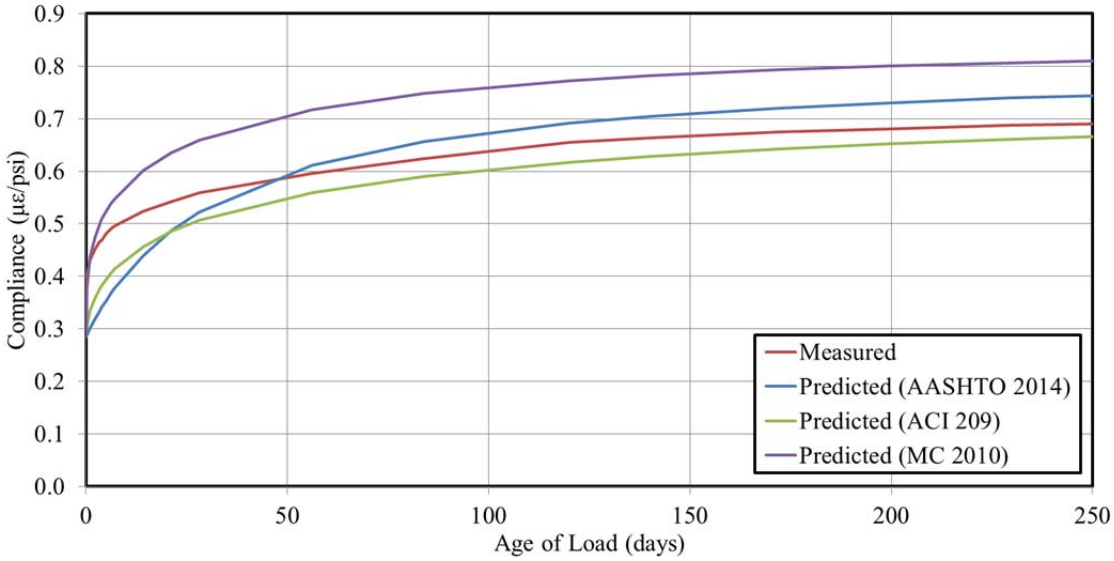

Figure F-6: GG-III 18 Hour – Test 2 Compliance Comparisons

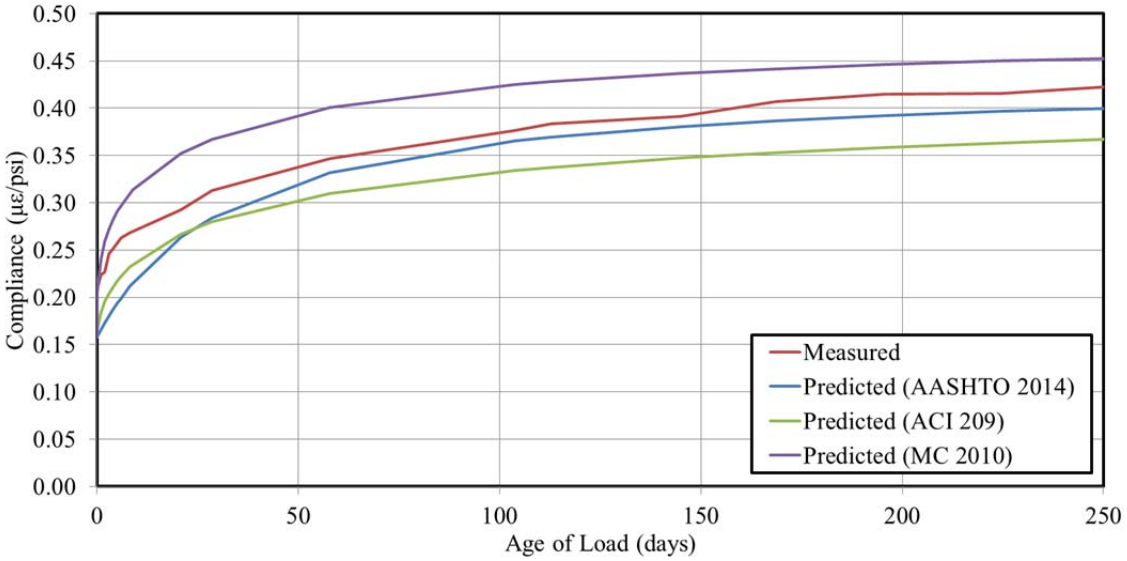

Figure F-7: DL-III 24 Hour – Test 1 Compliance Comparisons

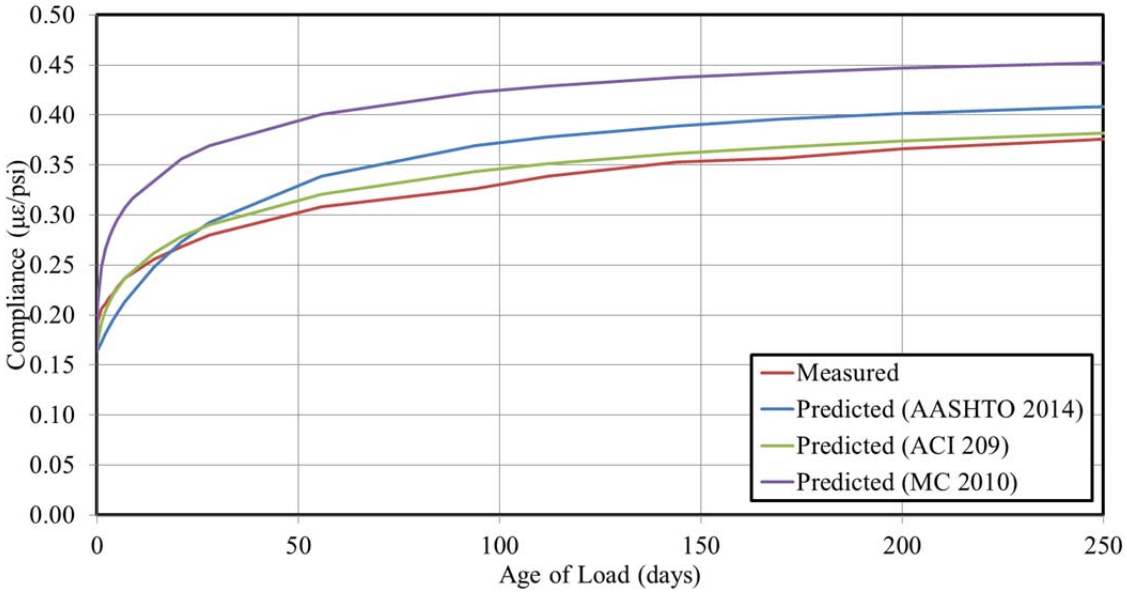

Figure F-8: CL-III 24 Hour – Test 1 Compliance Comparisons

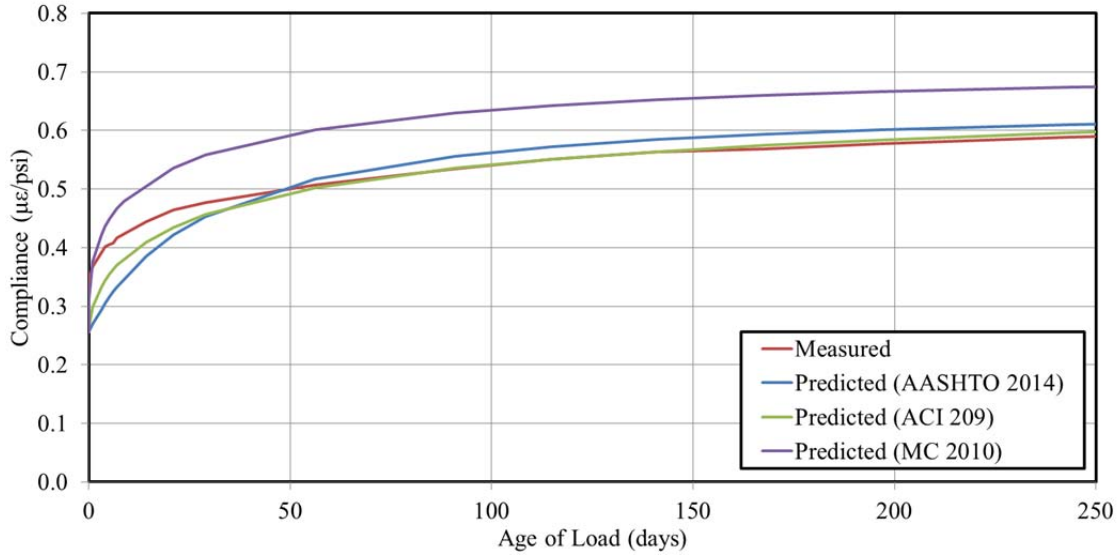

Figure F-9: GG-III 24 Hour – Test 1 Compliance Comparisons

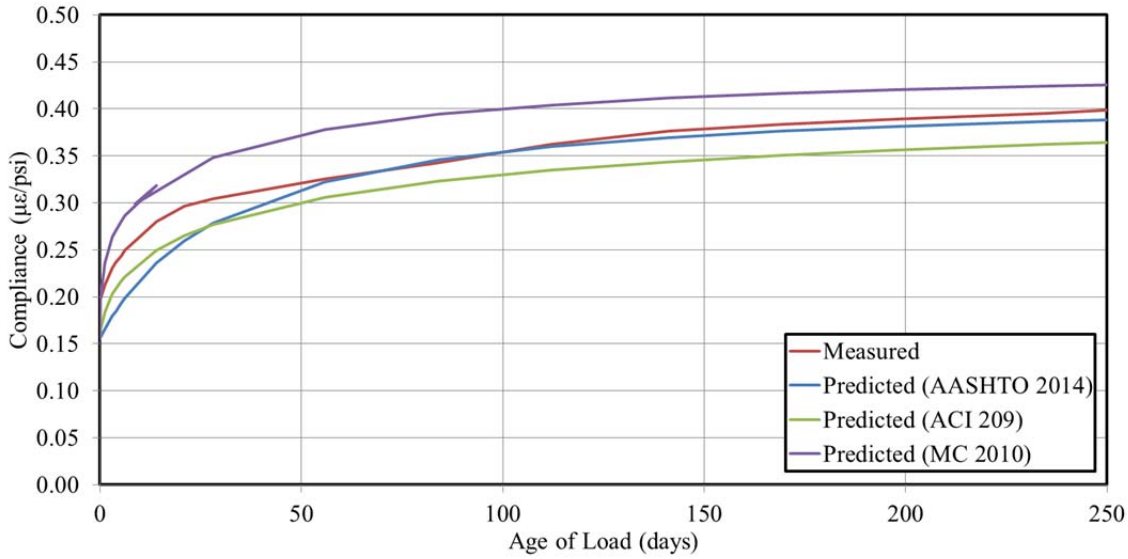

Figure F-10: DL-SL 24 Hour – Test 1 Compliance Comparisons

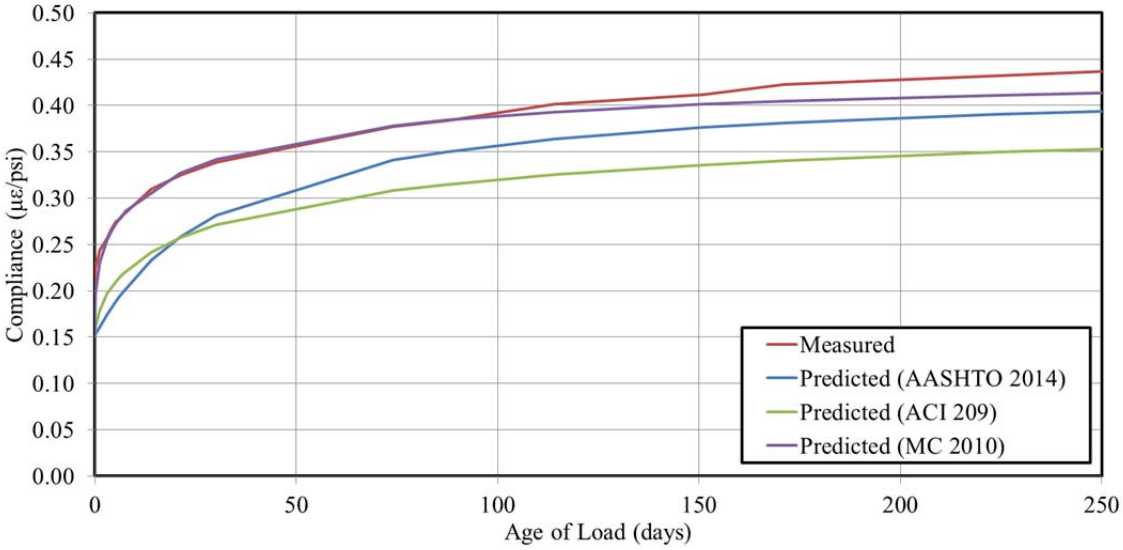

Figure F-11: DL-SL 18 Hour – Test 1 Compliance Comparisons

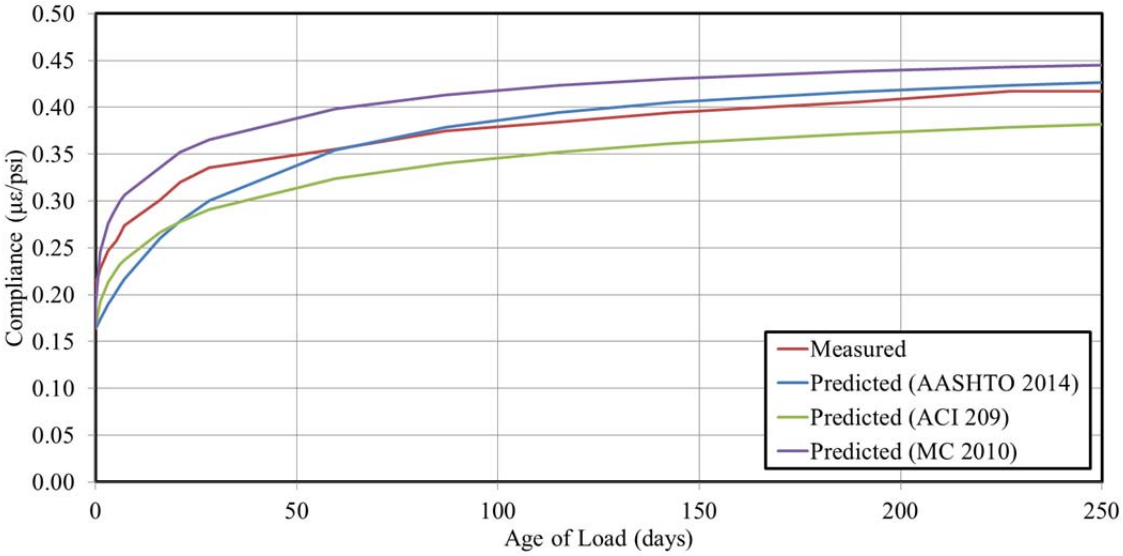

Figure F-12: DL-FA 18 Hour – Test 1 Compliance Comparisons

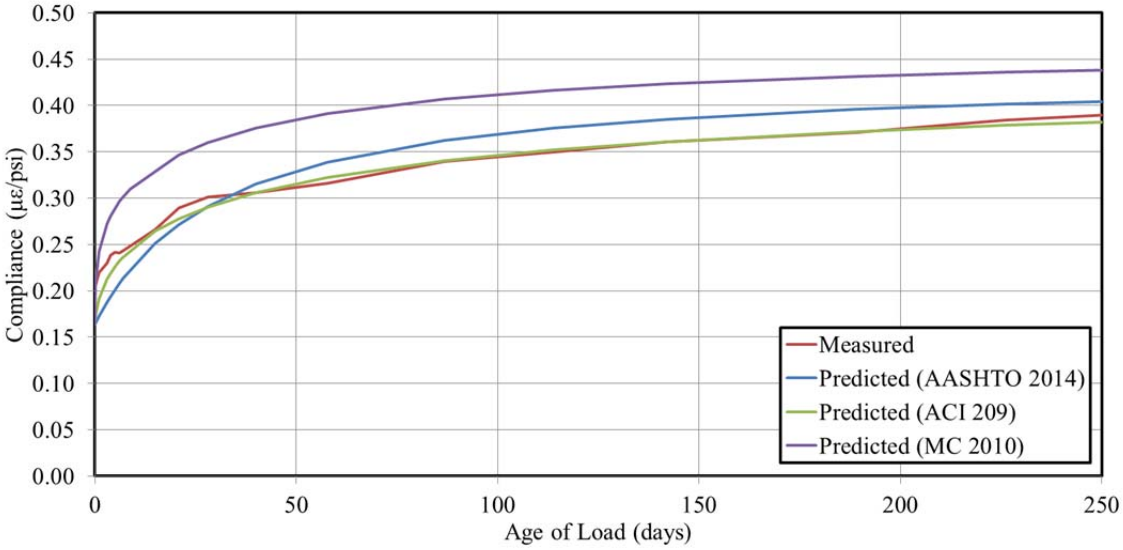

Figure F-13: DL-FA 24 Hour – Test 1 Compliance Comparisons

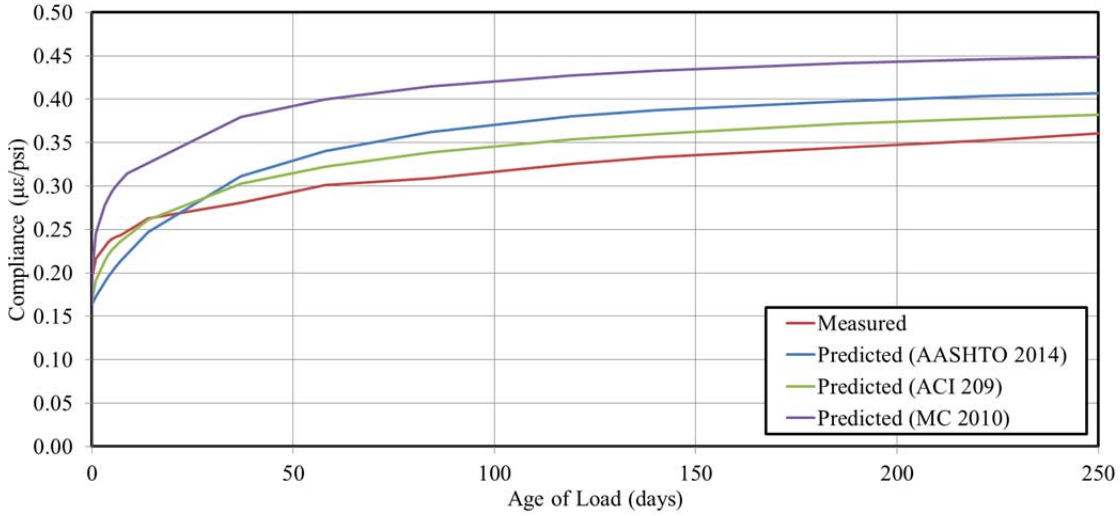

Figure F-14: DL-FA/SF 24 Hour – Test 1 Compliance Comparisons

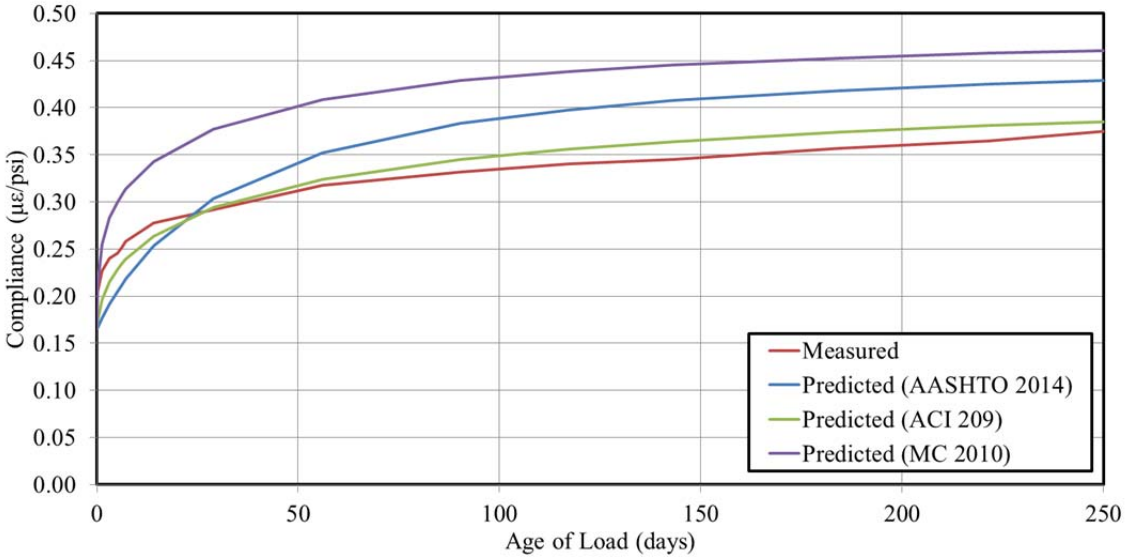

Figure F-15: DL-FA/SF 18 Hour – Test 1 Compliance Comparisons

Appendix G: Relative Goodness-of-Fit of Adjusted Candidate Creep Prediction Models to Experimental Data

This appendix contains visualizations of the relative goodness-of-fit of the three candidate creep prediction equations for each of 15 testing cycles included in this experimental effort, as calibrated to experimental data.

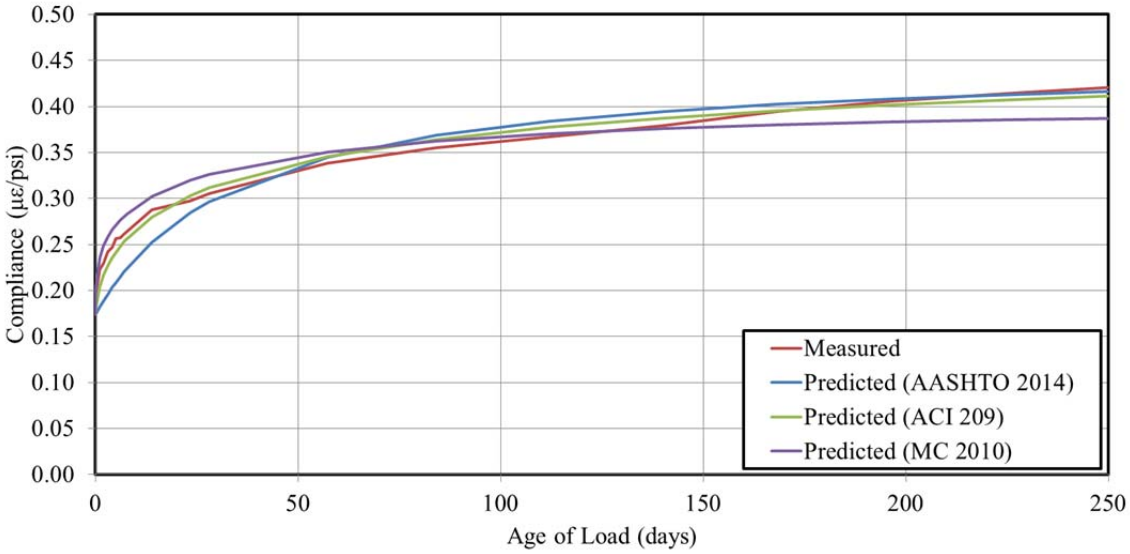

Figure G-1: DL-III 18 Hour – Test 1 Compliance Comparisons

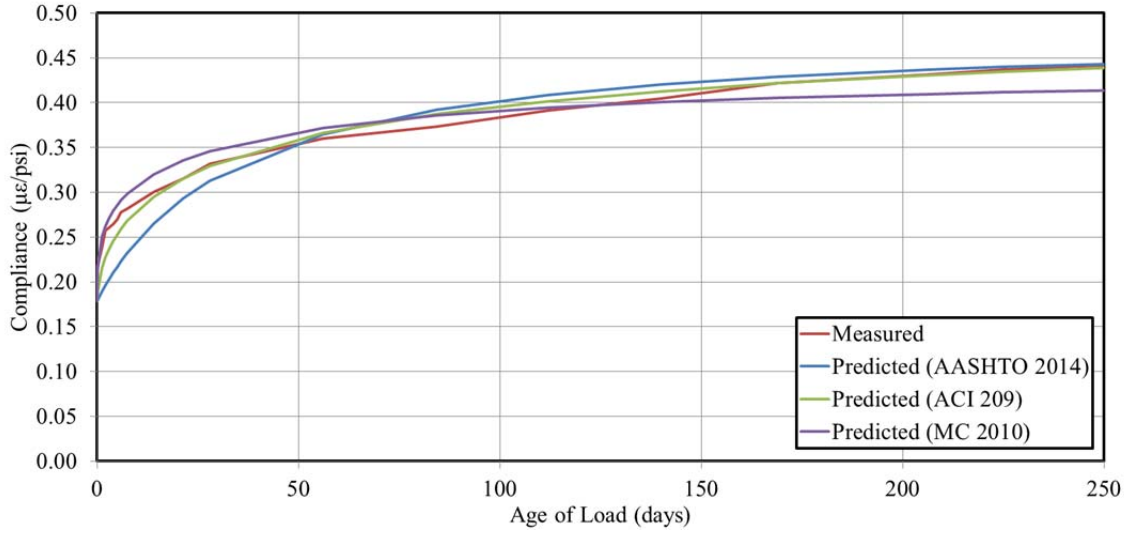

Figure G-2: DL-III 18 Hour – Test 2 Compliance Comparisons

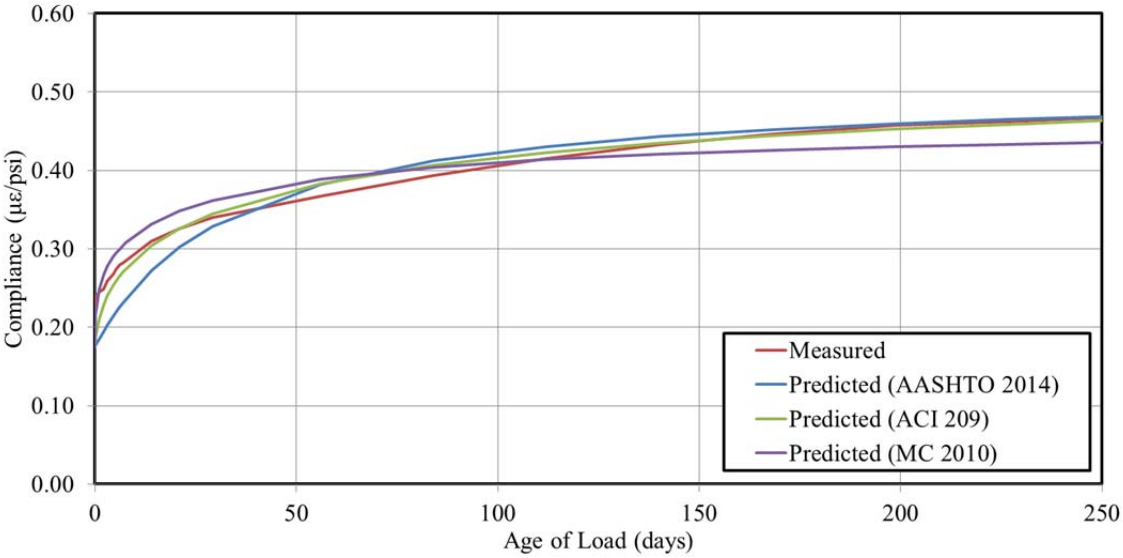

Figure G-3: CL-III 18 Hour – Test 1 Compliance Comparisons

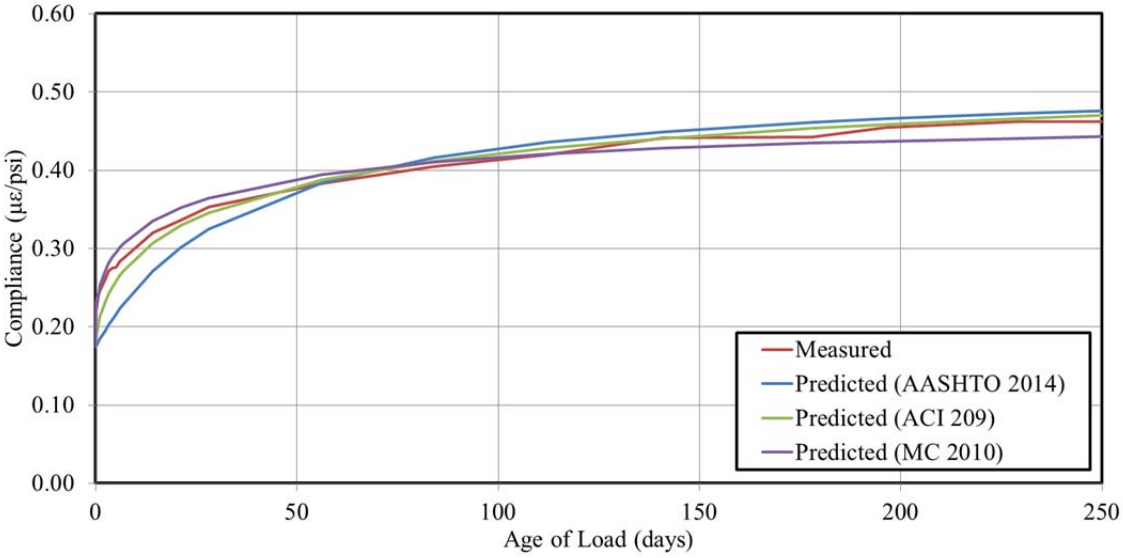

Figure G-4: CL-III 18 Hour – Test 2 Compliance Comparisons

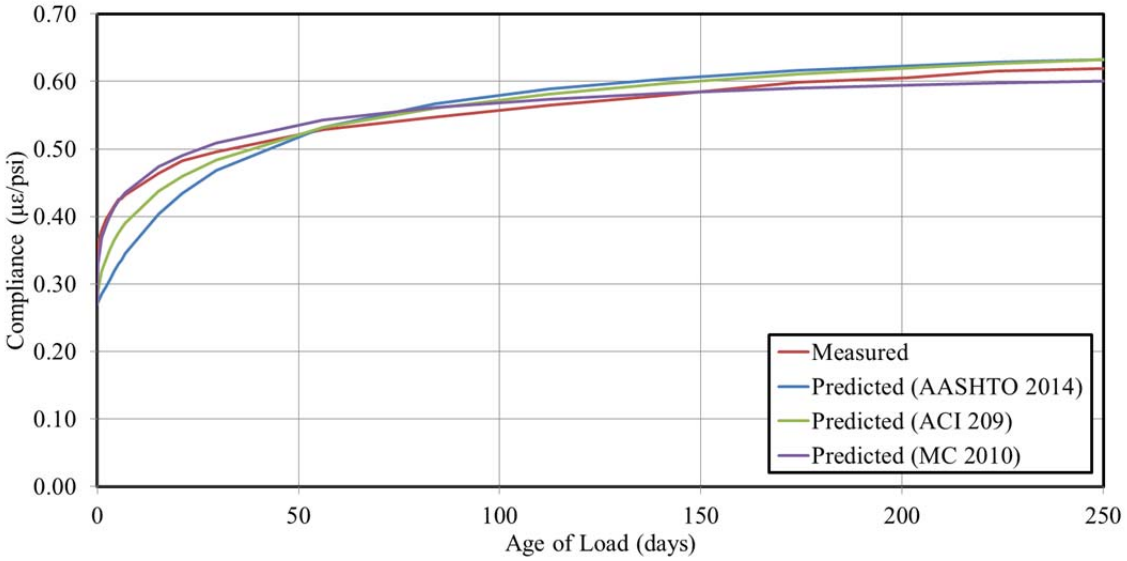

Figure G-5: GG-III 18 Hour – Test 1 Compliance Comparisons

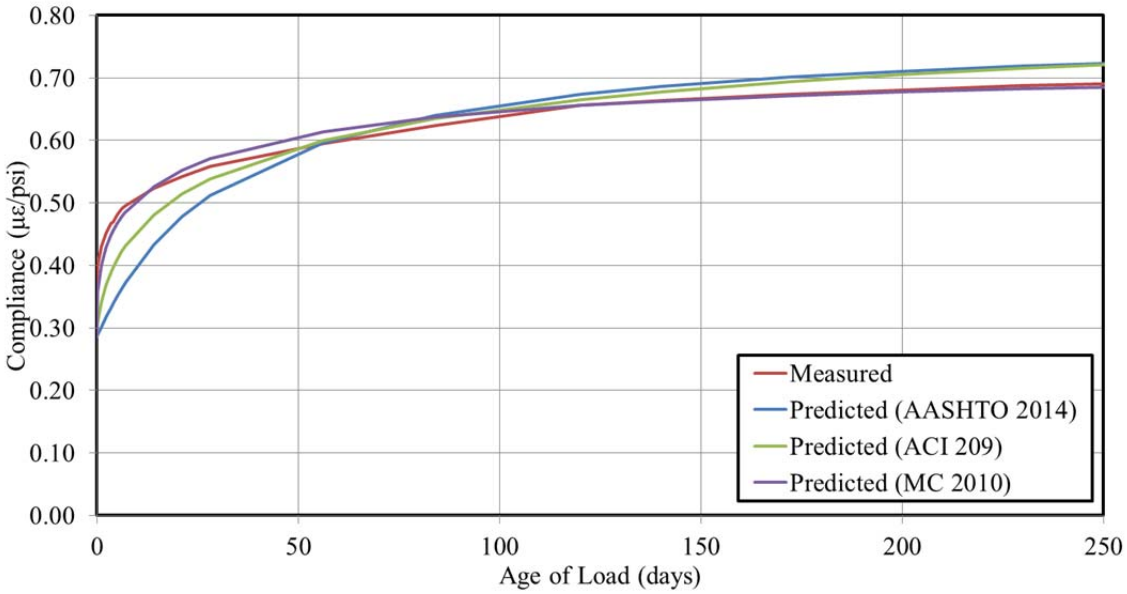

Figure G-6: GG-III 18 Hour – Test 2 Compliance Comparisons

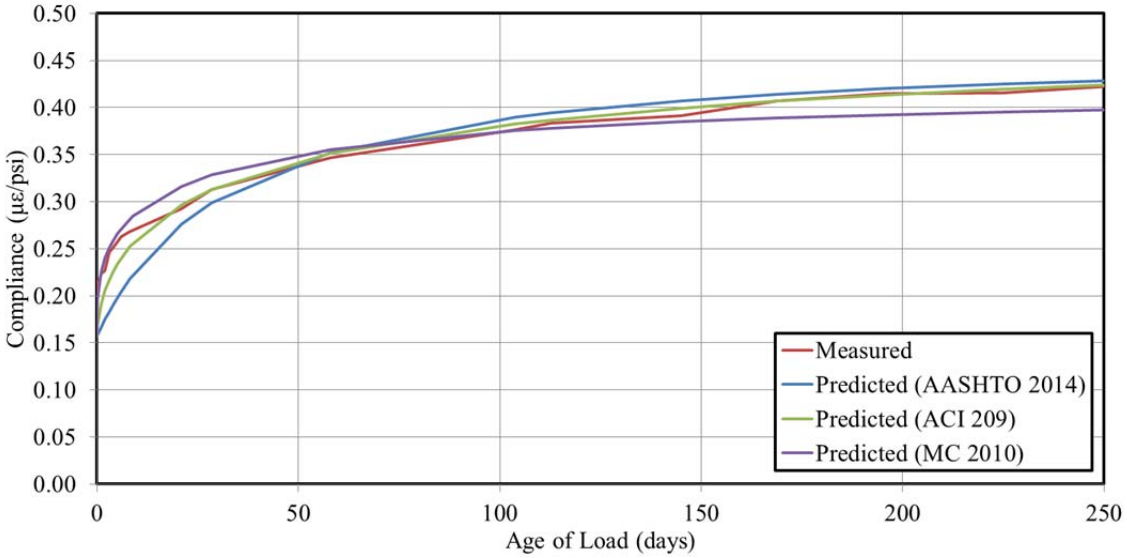

Figure G-7: DL-III 24 Hour – Test 1 Compliance Comparisons

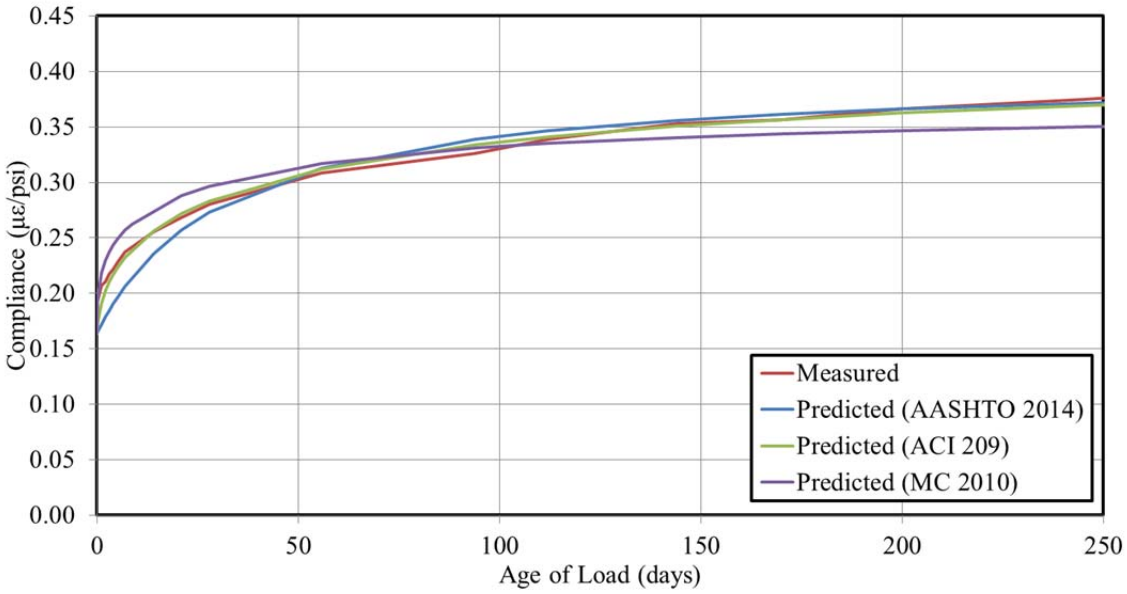

Figure G-8: CL-III 24 Hour – Test 1 Compliance Comparisons

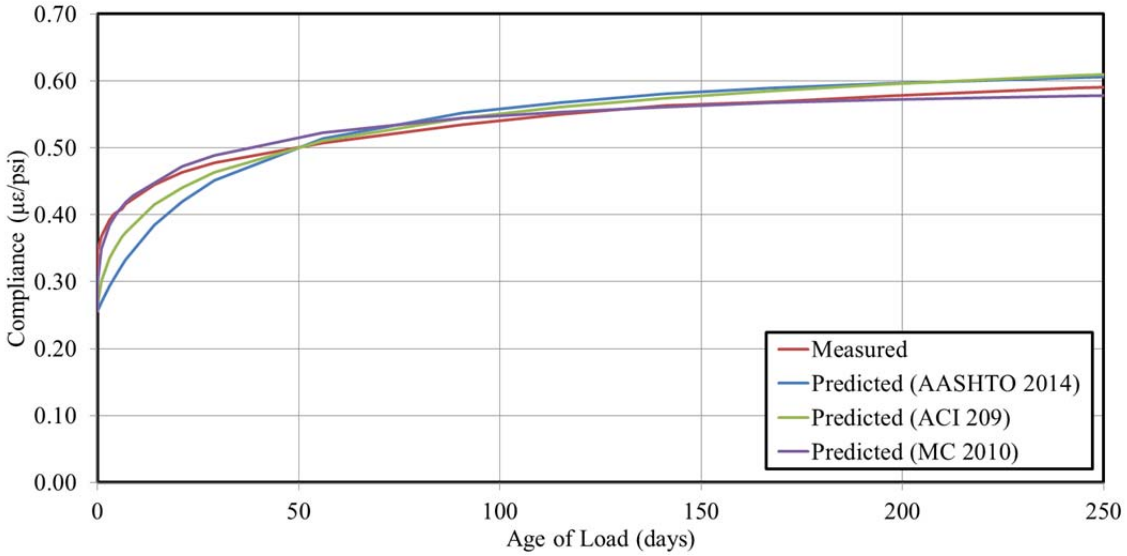

Figure G-9: GG-III 24 Hour – Test 1 Compliance Comparisons

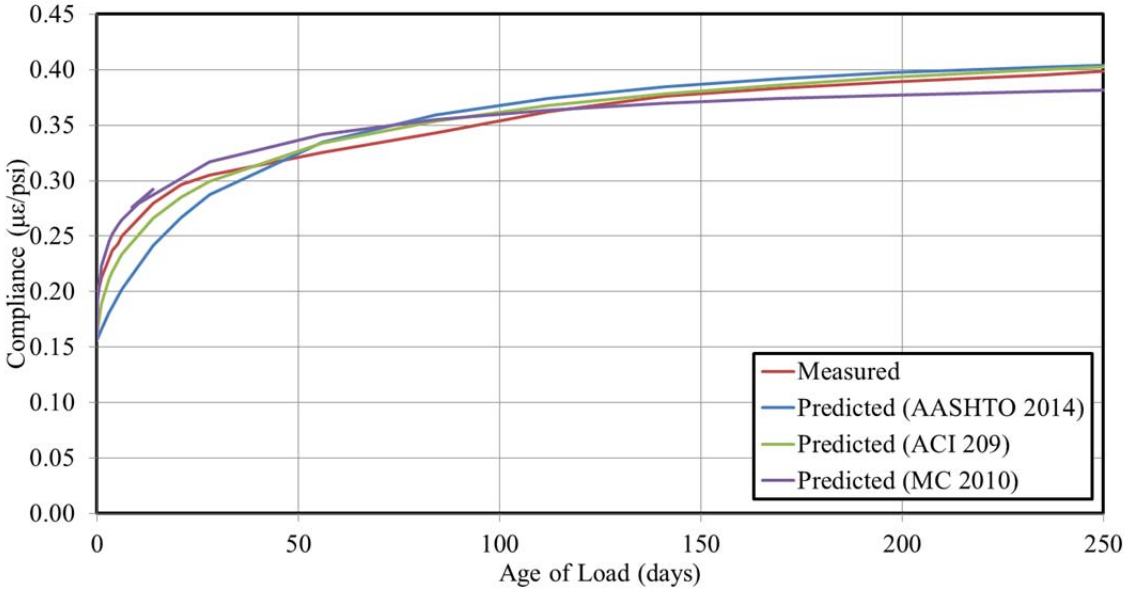

Figure G-10: DL-SL 24 Hour – Test 1 Compliance Comparisons

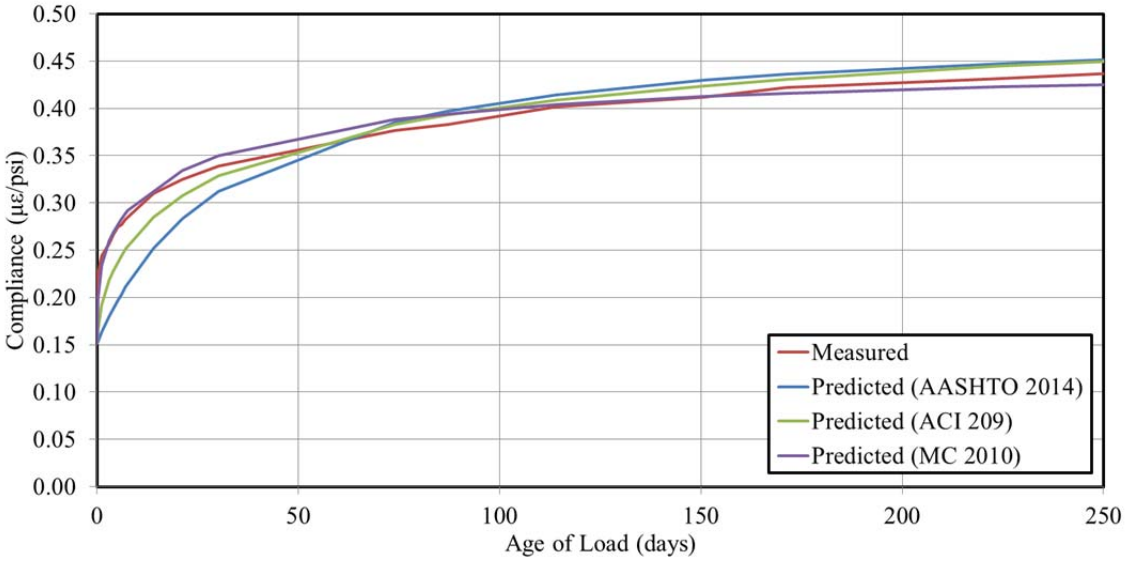

Figure G-11: DL-SL 18 Hour – Test 1 Compliance Comparisons

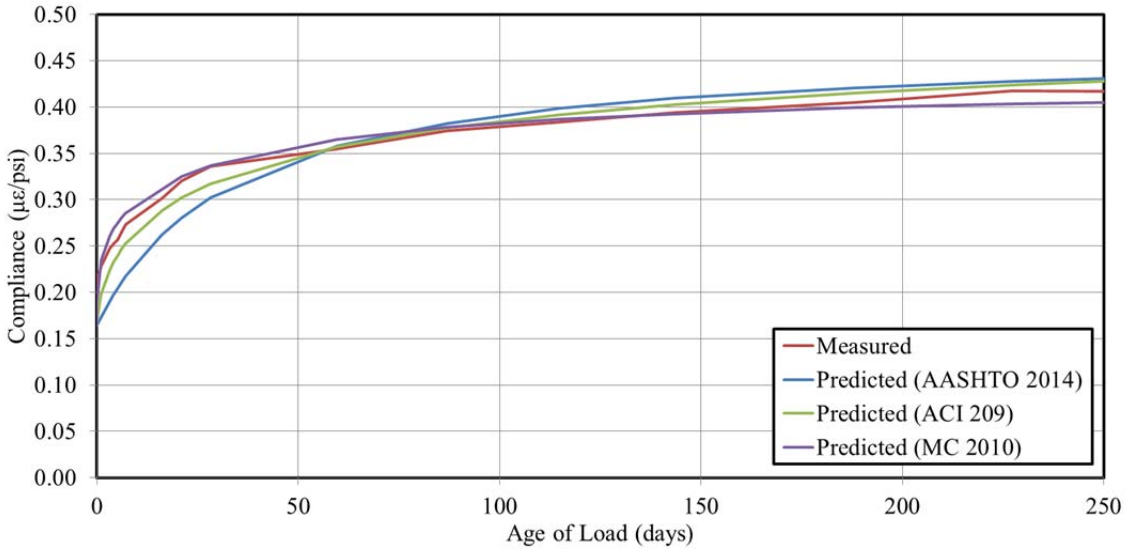

Figure G-12: DL-FA 18 Hour – Test 1 Compliance Comparisons

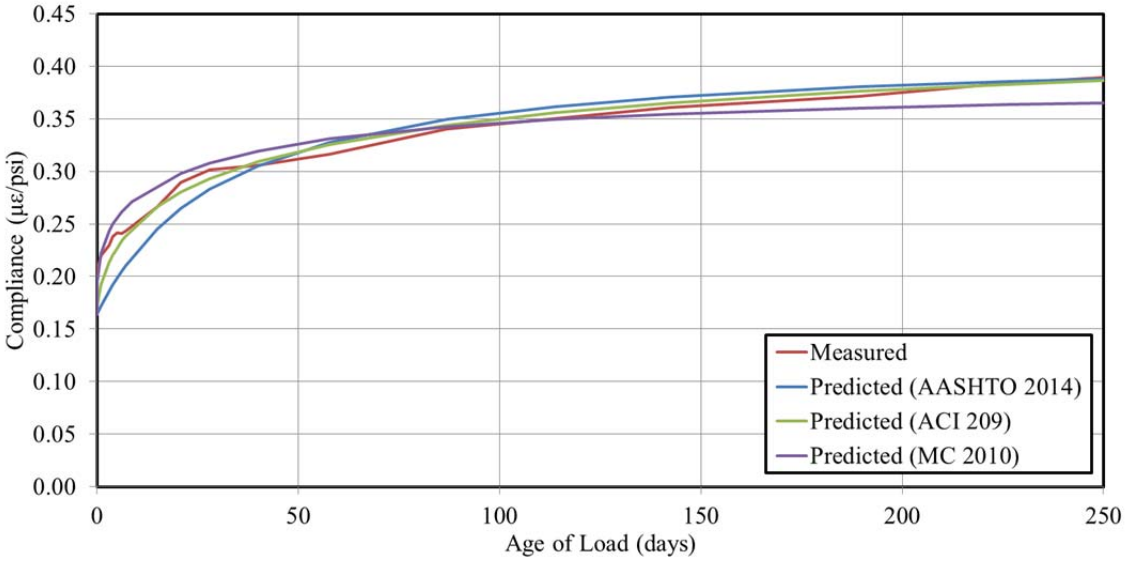

Figure G-13: DL-FA 24 Hour – Test 1 Compliance Comparisons

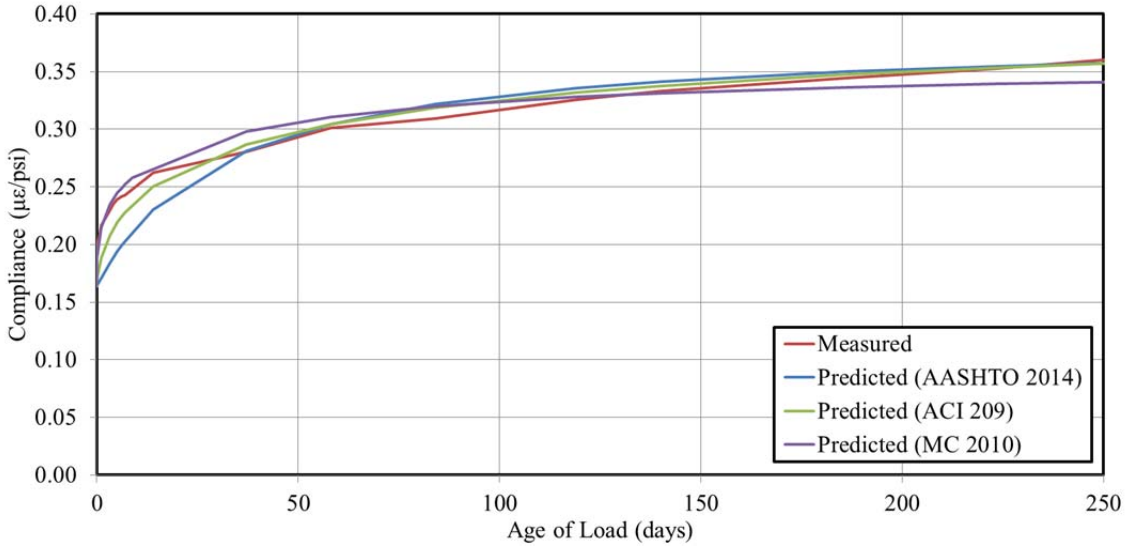

Figure G-14: DL-FA/SF 24 Hour – Test 1 Compliance Comparisons

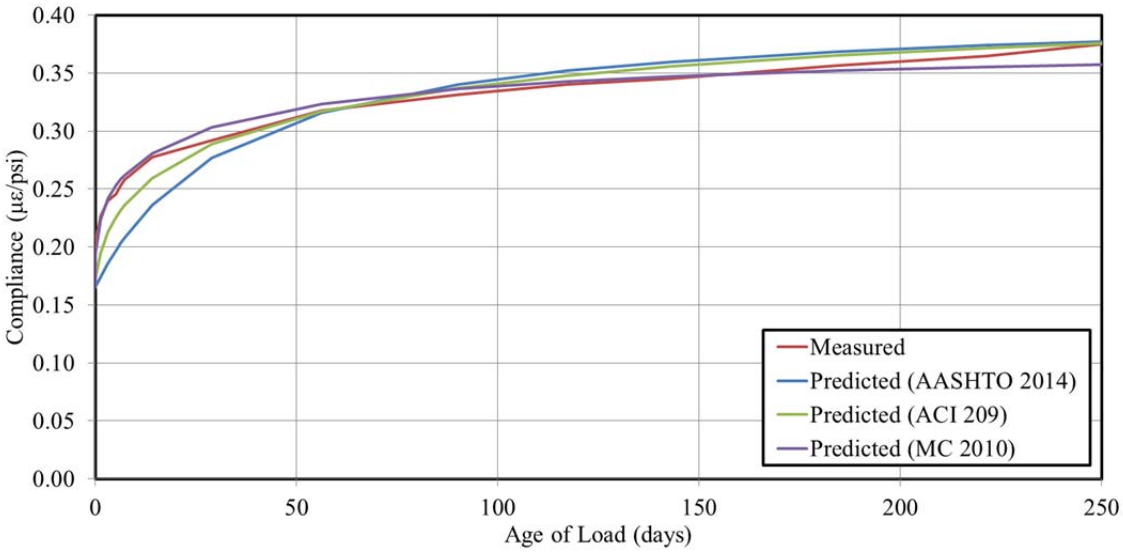

Figure G-15: DL-FA/SF 18 Hour – Test 1 Compliance Comparisons

Appendix H: Relative Goodness-of-Fit of Unadjusted Candidate Shrinkage Prediction Models to Experimental Data

This appendix contains visualizations of the relative goodness-of-fit of the three candidate shrinkage prediction equations for both cylinder and rectangular prismatic specimens for each of 15 testing cycles included in this experimental effort.

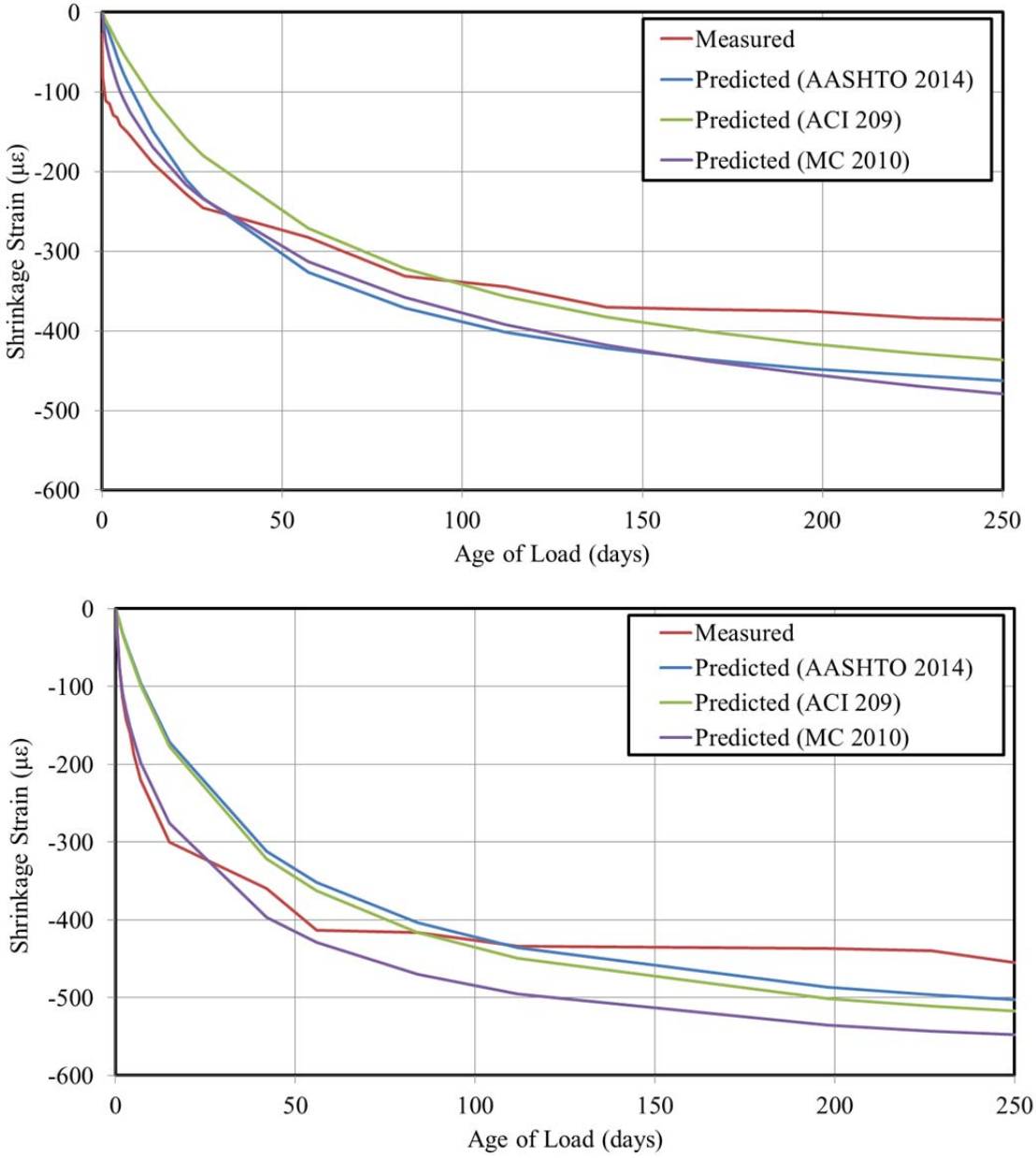

Figure H-1: DL-III 18 Hour – Test 1 Shrinkage Comparisons Cylinder Specimens (Top) and Rectangular Prism Specimens (Bottom)

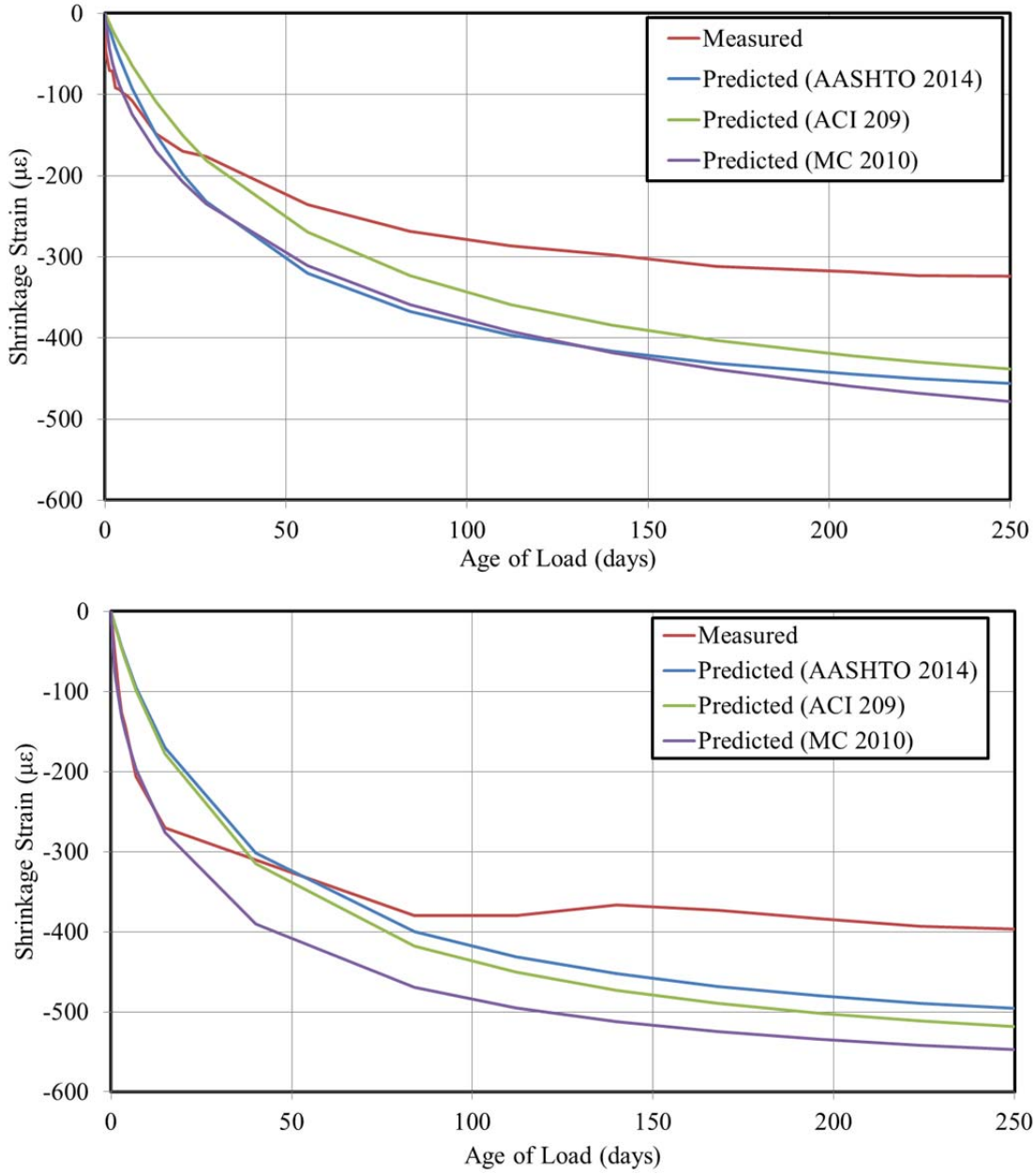

Figure H-2: DL-III 18 Hour – Test 2 Shrinkage Comparisons Cylinder Specimens (Top) and Rectangular Prism Specimens (Bottom)

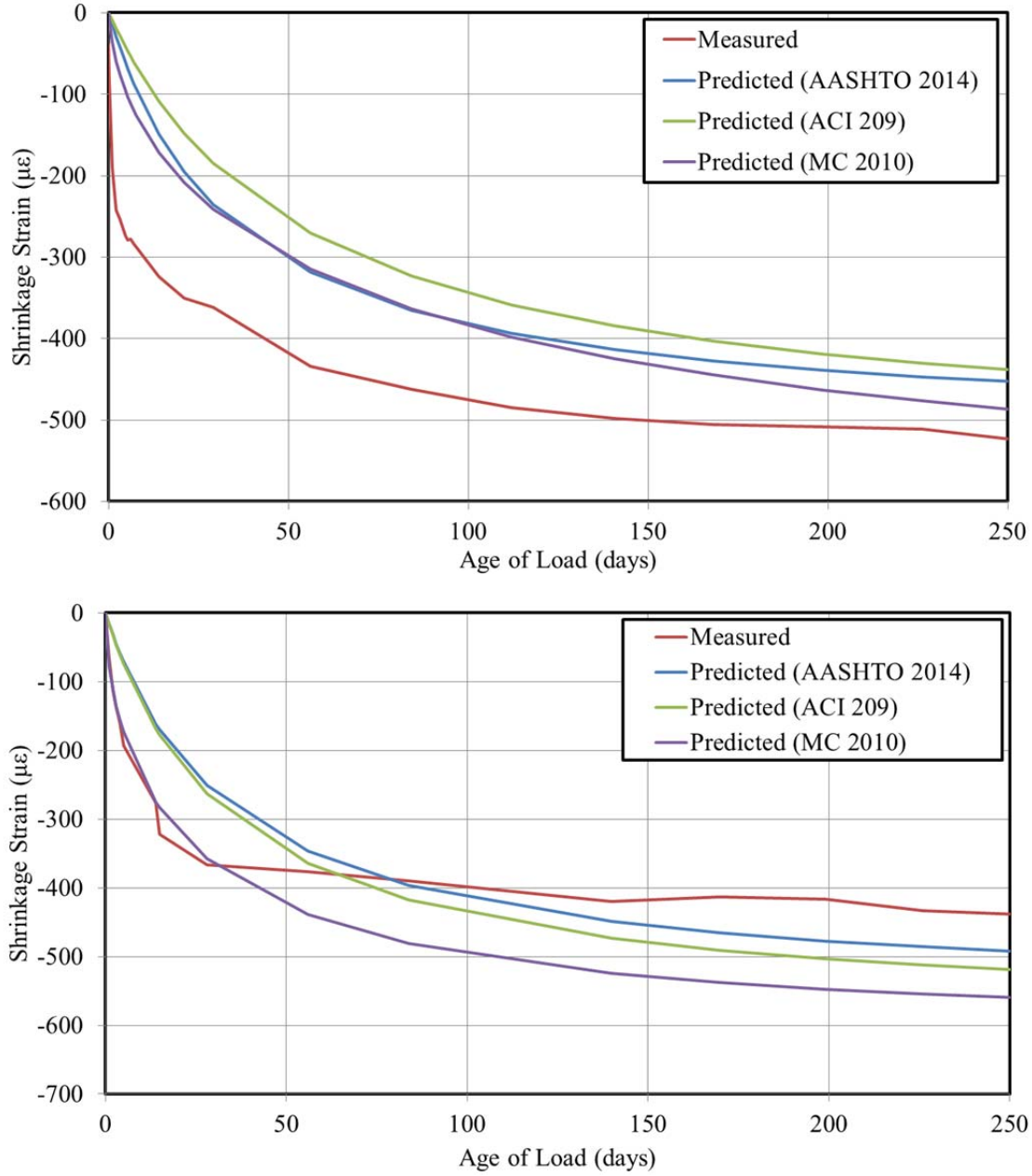

Figure H-3: CL-III 18 Hour – Test 1 Shrinkage Comparisons Cylinder Specimens (Top) and Rectangular Prism Specimens (Bottom)

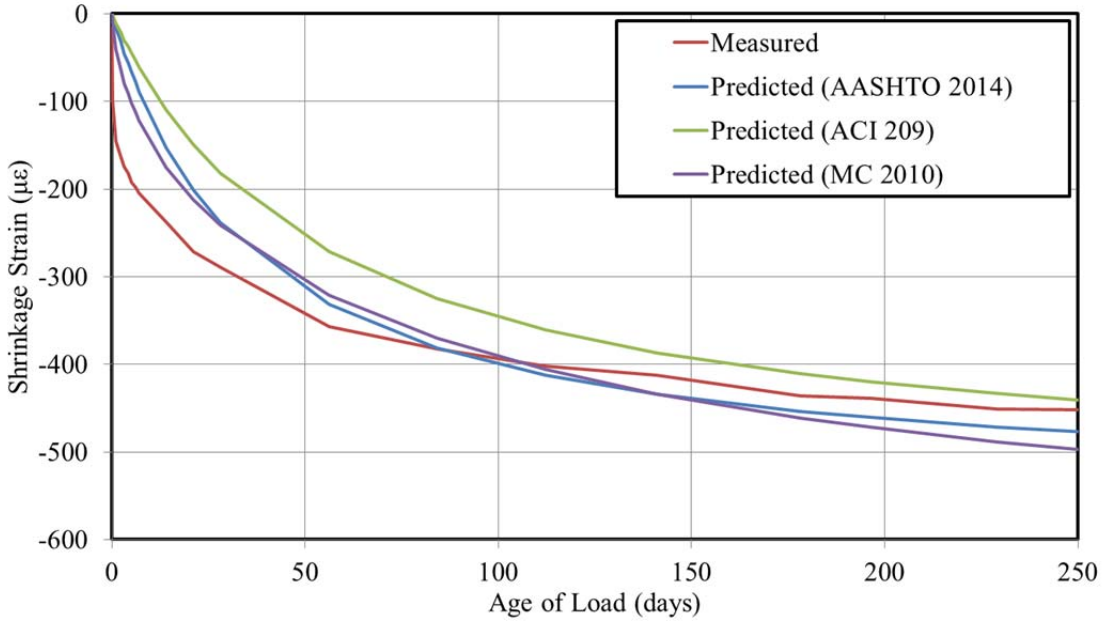

Figure H-4: CL-III 18 Hour – Test 2 Shrinkage Comparisons Cylinder Specimens

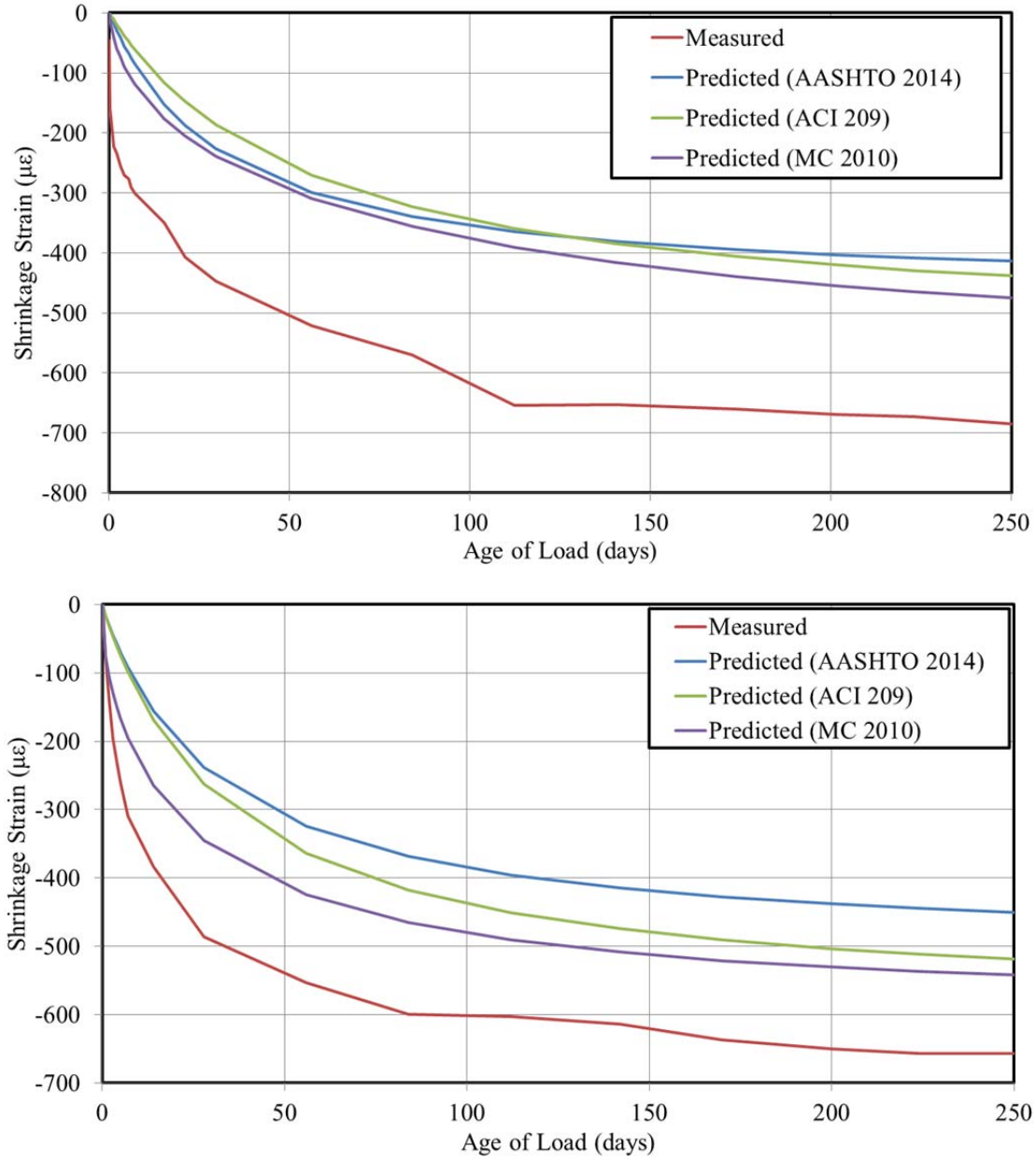

Figure H-5: GG-III 18 Hour – Test 1 Shrinkage Comparisons Cylinder Specimens (Top) and Rectangular Prism Specimens (Bottom)

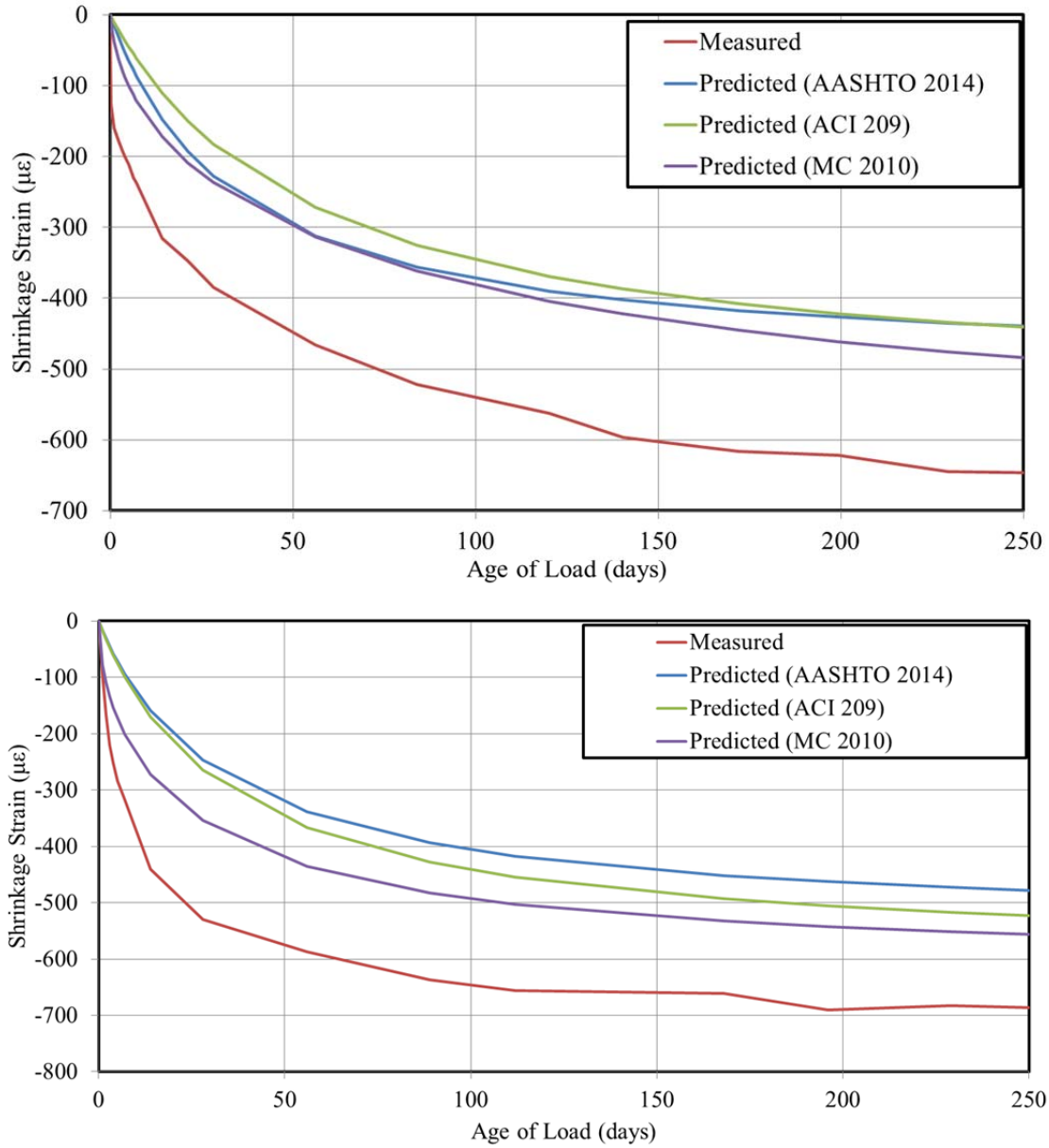

Figure H-6: GG-III 18 Hour – Test 2 Shrinkage Comparisons Cylinder Specimens (Top) and Rectangular Prism Specimens (Bottom)

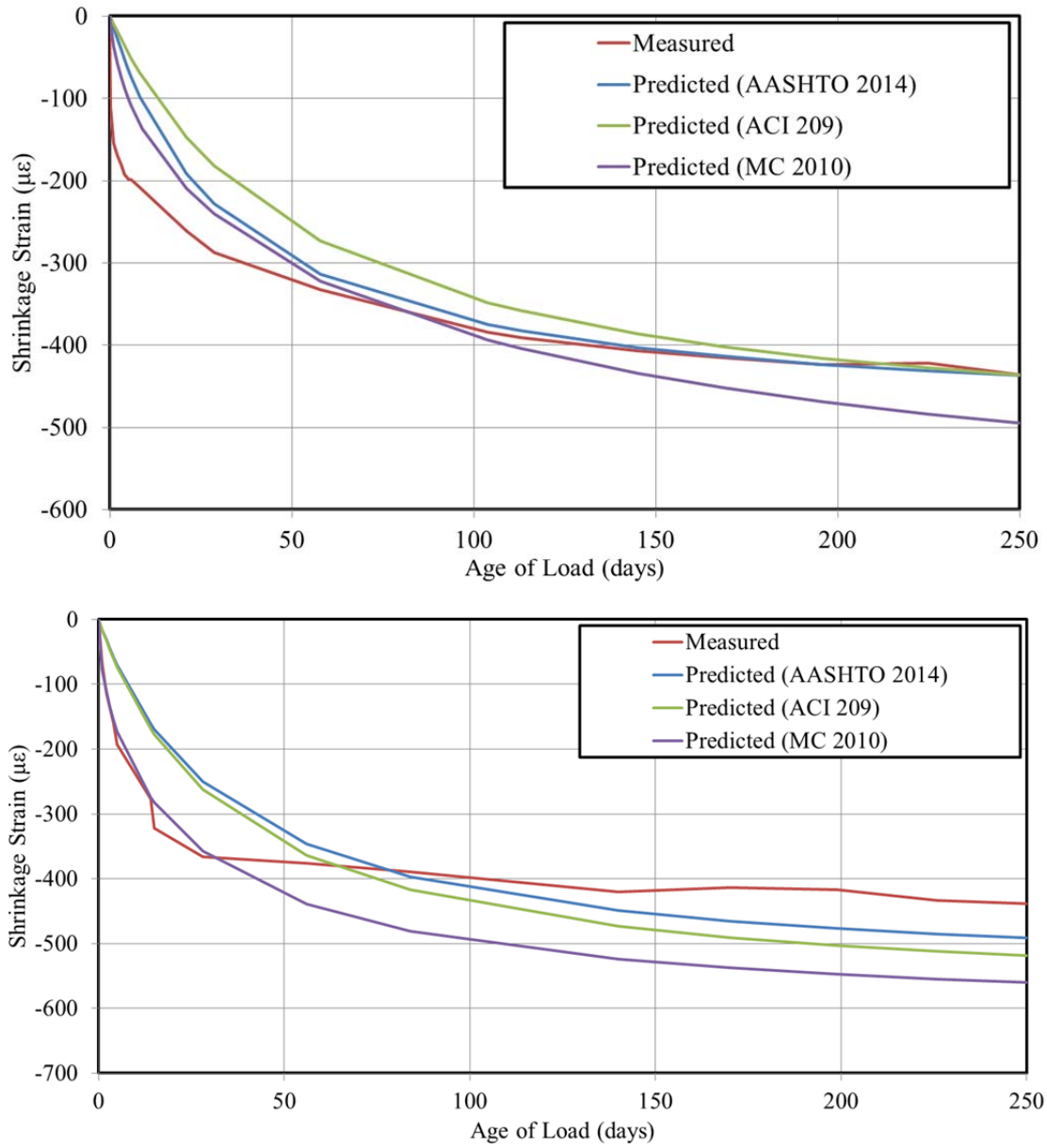

Figure H-7: DL-III 24 Hour – Test 1 Shrinkage Comparisons Cylinder Specimens (Top) and Rectangular Prism Specimens (Bottom)

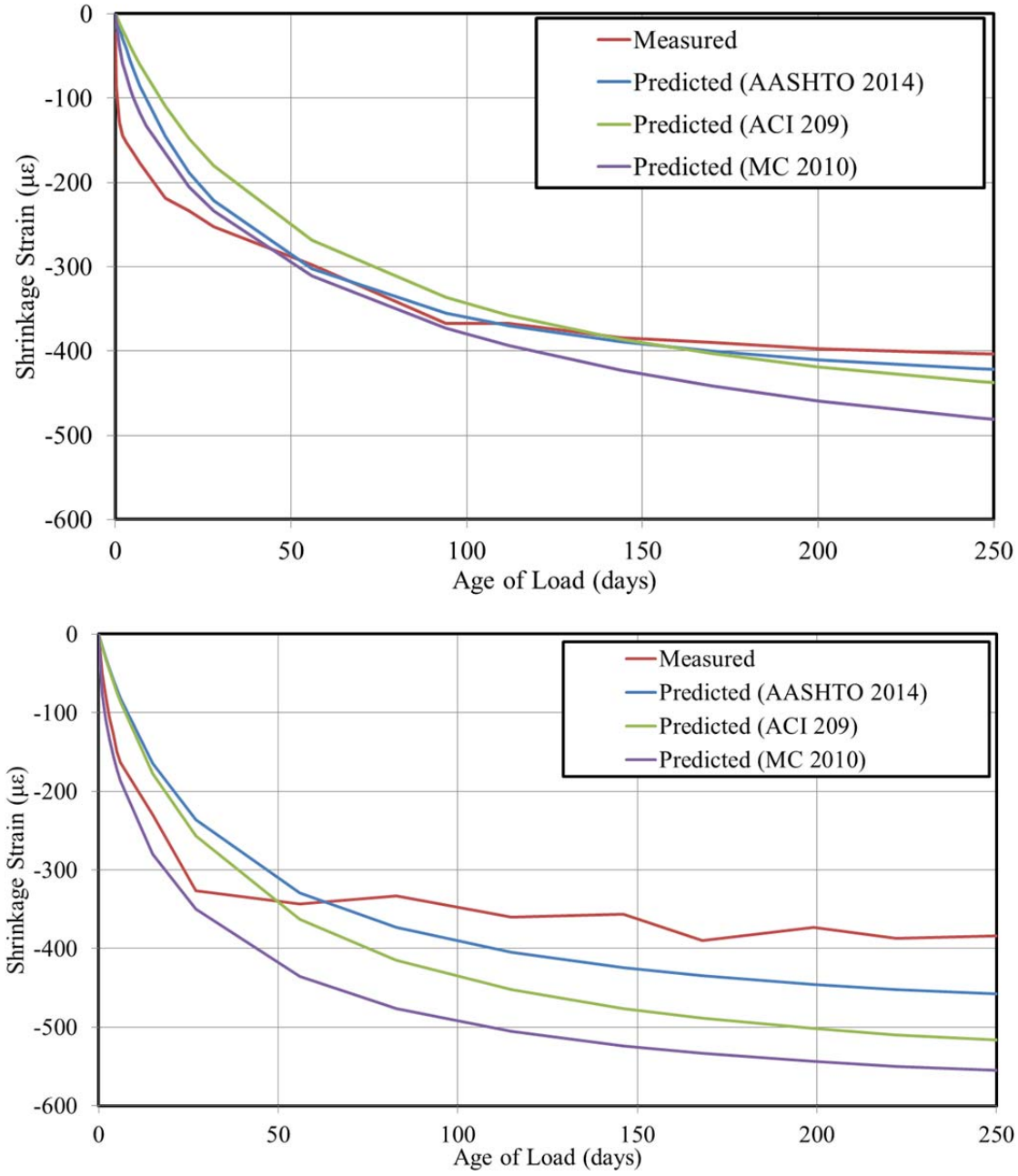

Figure H-8: CL-III 24 Hour – Test 1 Shrinkage Comparisons Cylinder Specimens (Top) and Rectangular Prism Specimens (Bottom)

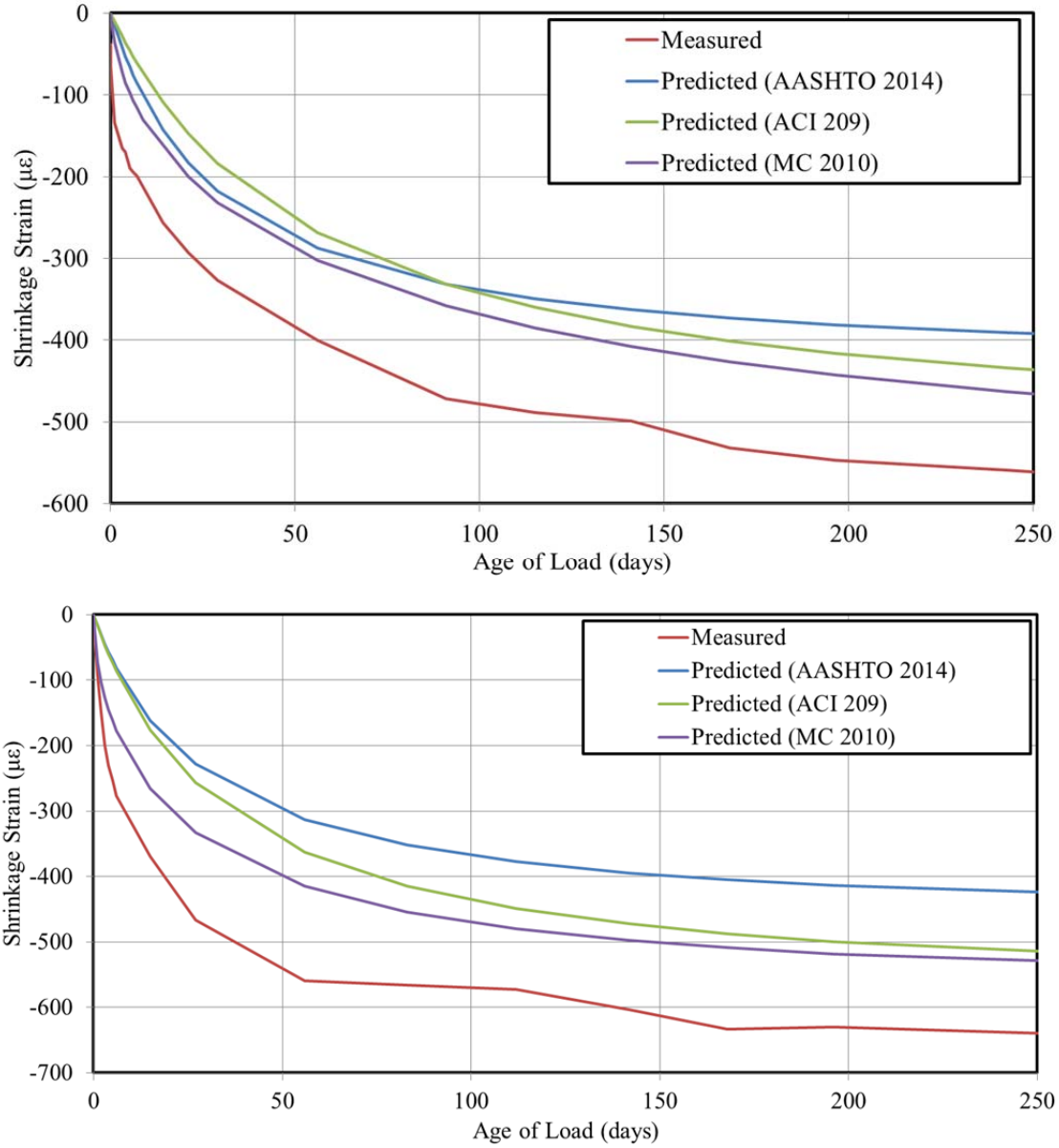

Figure H-9: GG-III 24 Hour – Test 1 Shrinkage Comparisons Cylinder Specimens (Top) and Rectangular Prism Specimens (Bottom)

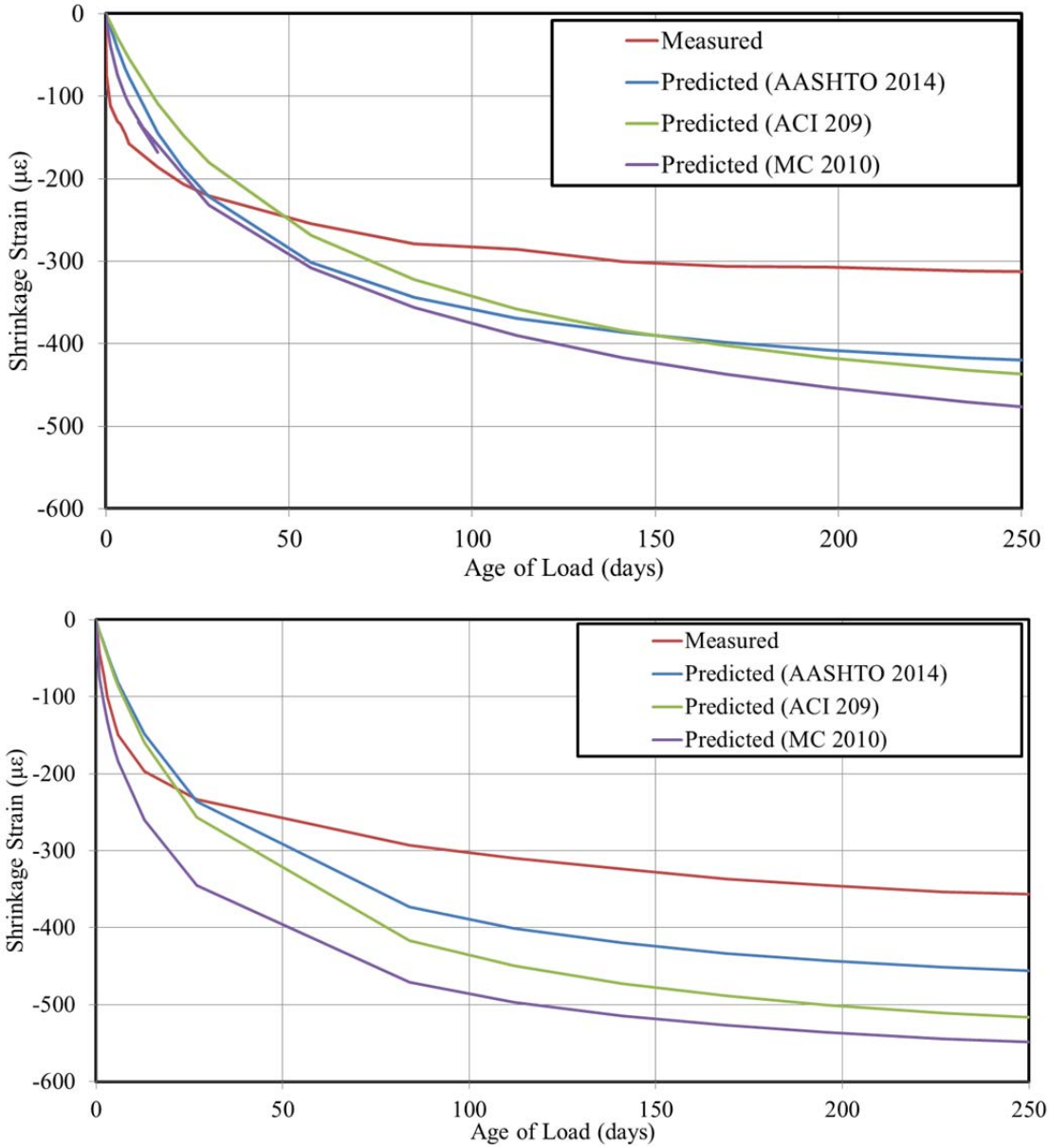

Figure H-10: DL-SL 24 Hour – Test 1 Shrinkage Comparisons Cylinder Specimens (Top) and Rectangular Prism Specimens (Bottom)

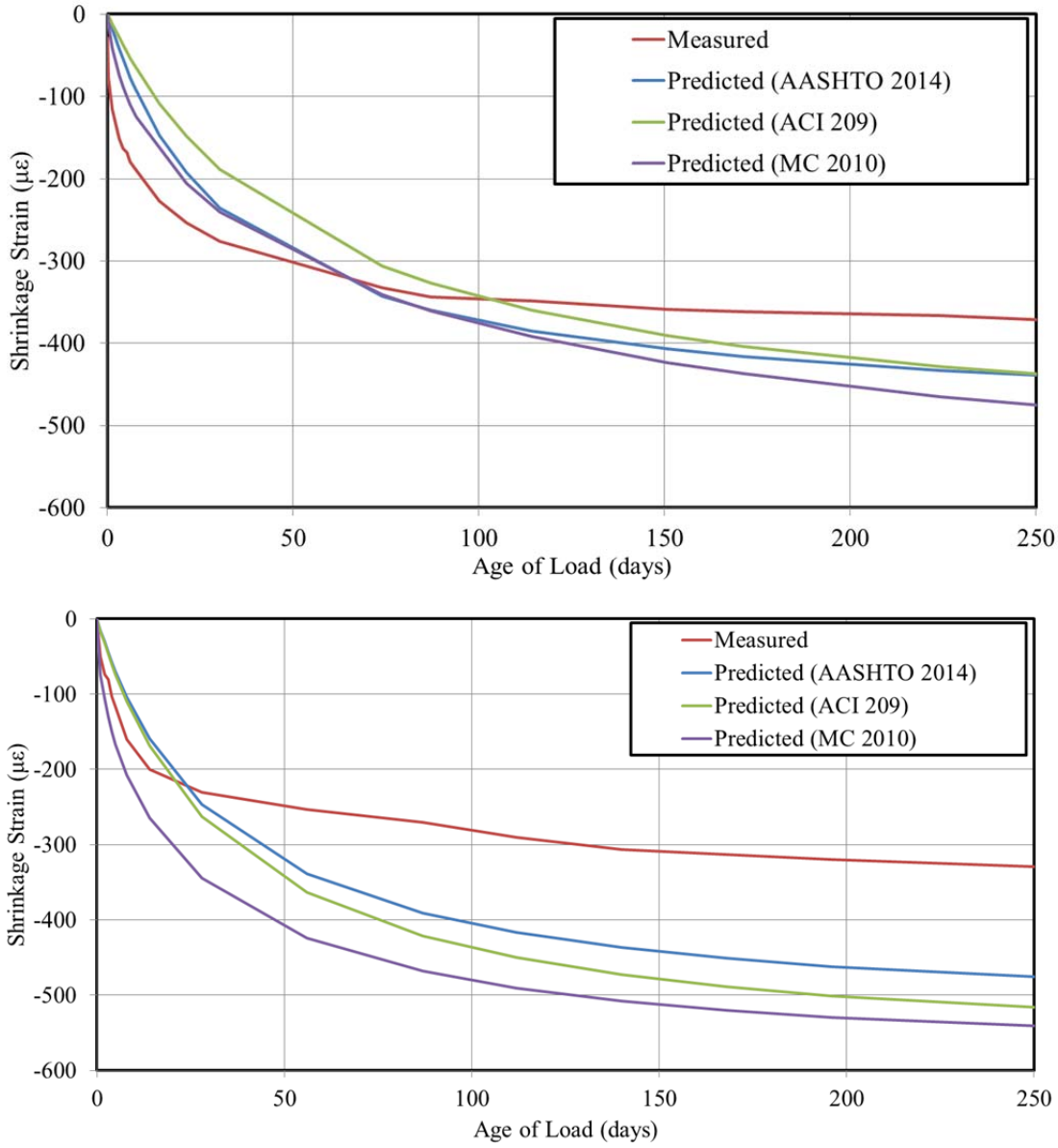

Figure H-11: DL-SL 18 Hour – Test 1 Shrinkage Comparisons Cylinder Specimens (Top) and Rectangular Prism Specimens (Bottom)

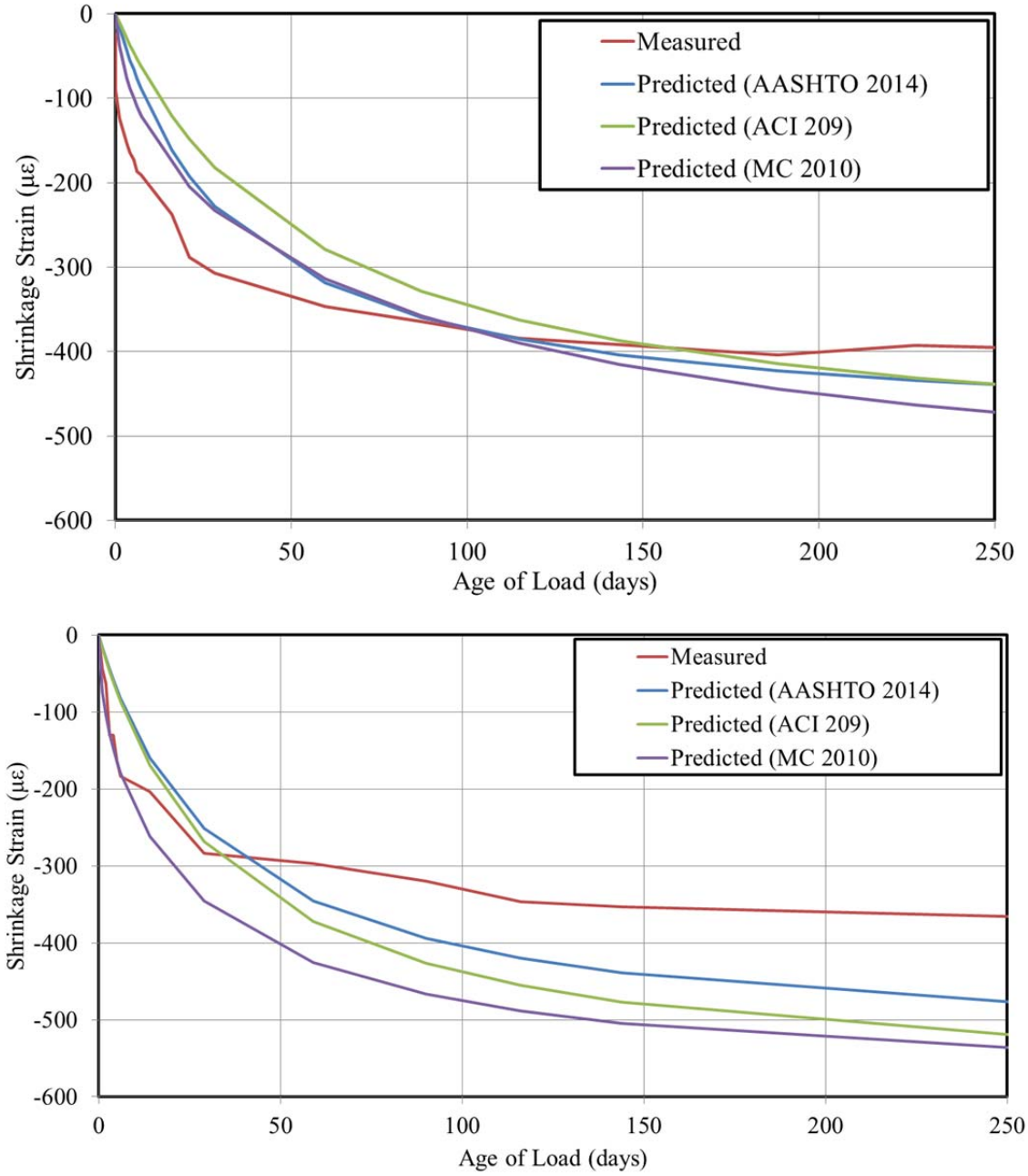

Figure H-12: DL-FA 18 Hour – Test 1 Shrinkage Comparisons Cylinder Specimens (Top) and Rectangular Prism Specimens (Bottom)

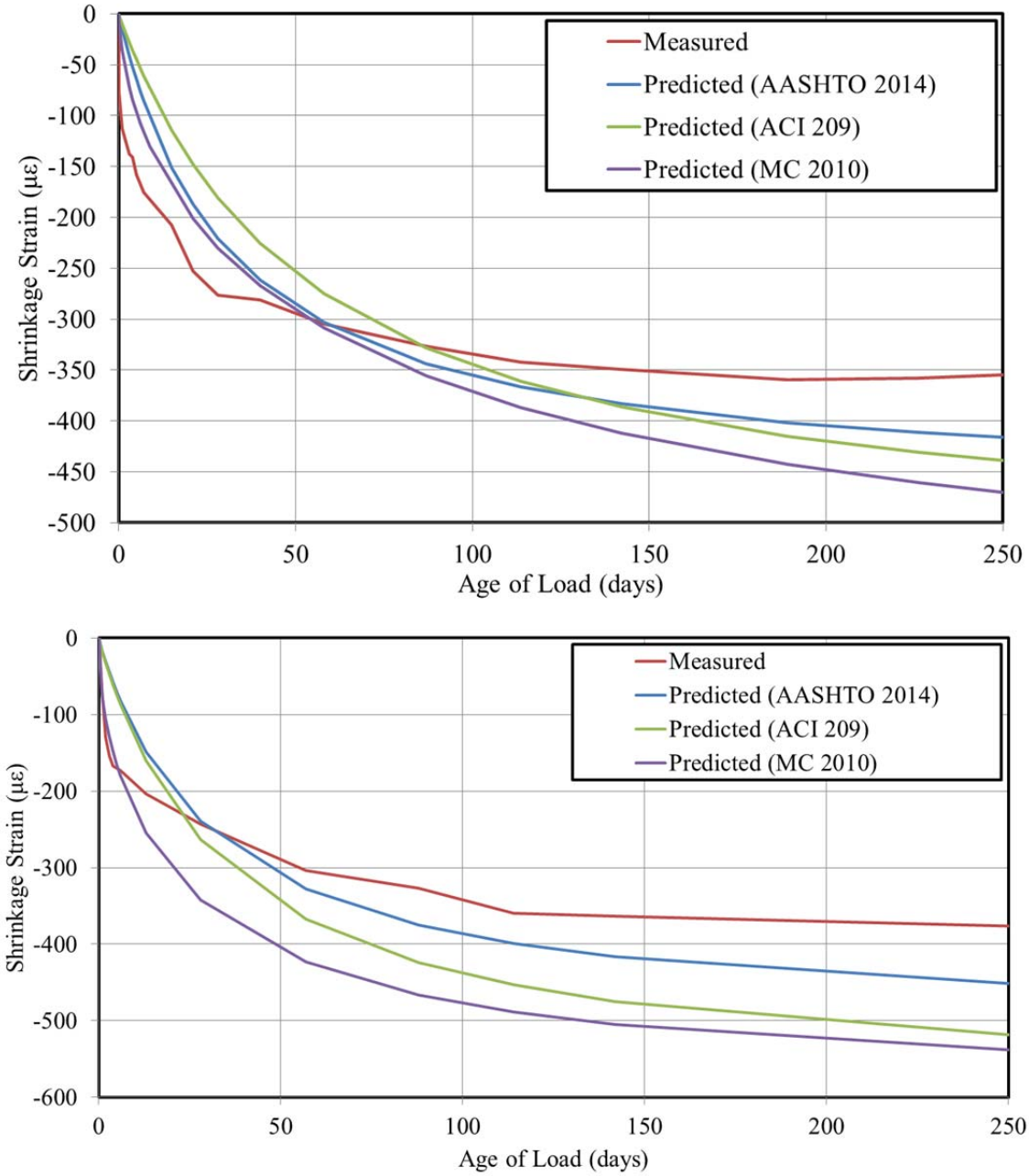

Figure H-13: DL-FA 24 Hour – Test 1 Shrinkage Comparisons Cylinder Specimens (Top) and Rectangular Prism Specimens (Bottom)

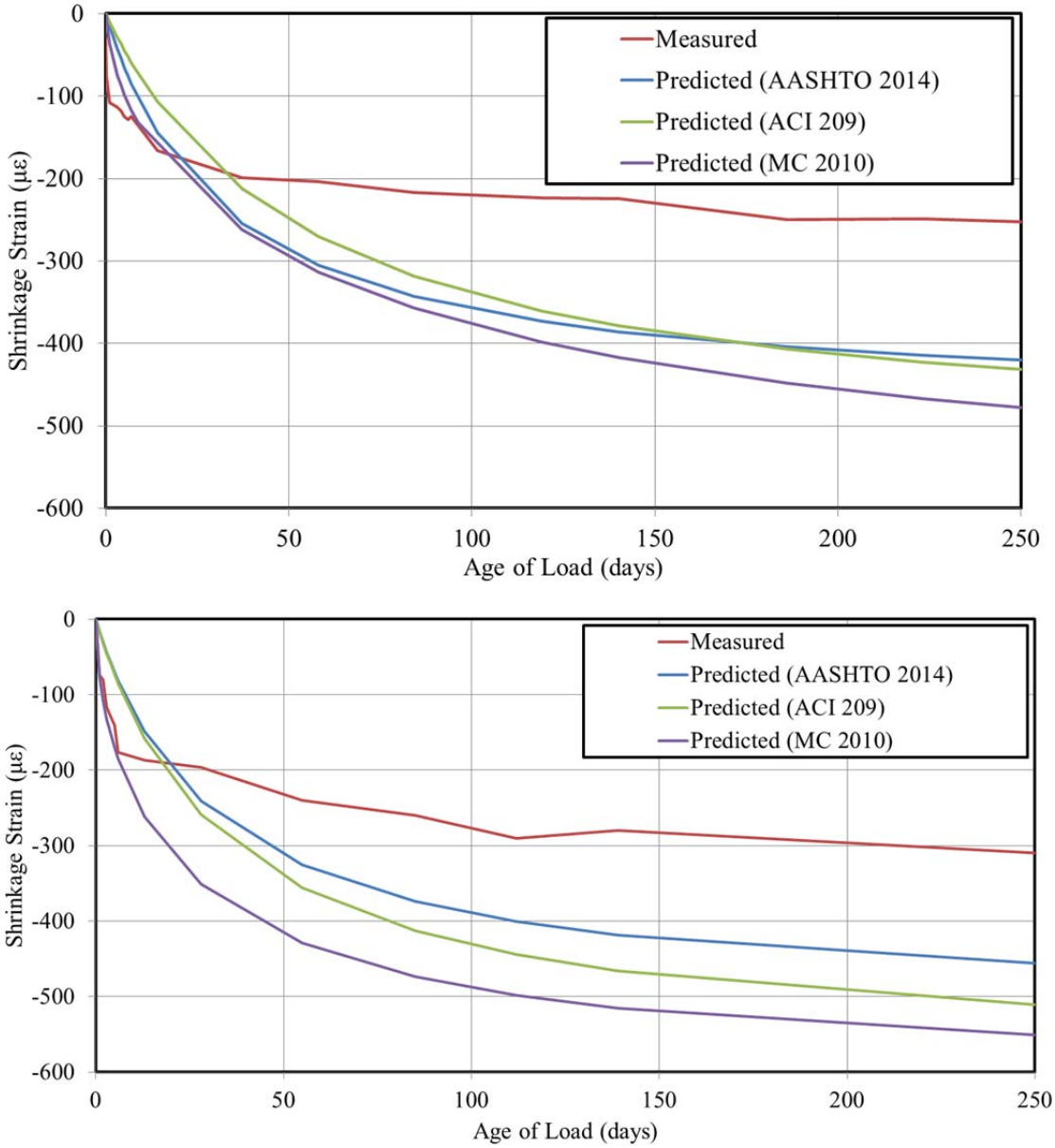

Figure H-14: DL-FA/SF 24 Hour – Test 1 Shrinkage Comparisons Cylinder Specimens (Top) and Rectangular Prism Specimens (Bottom)

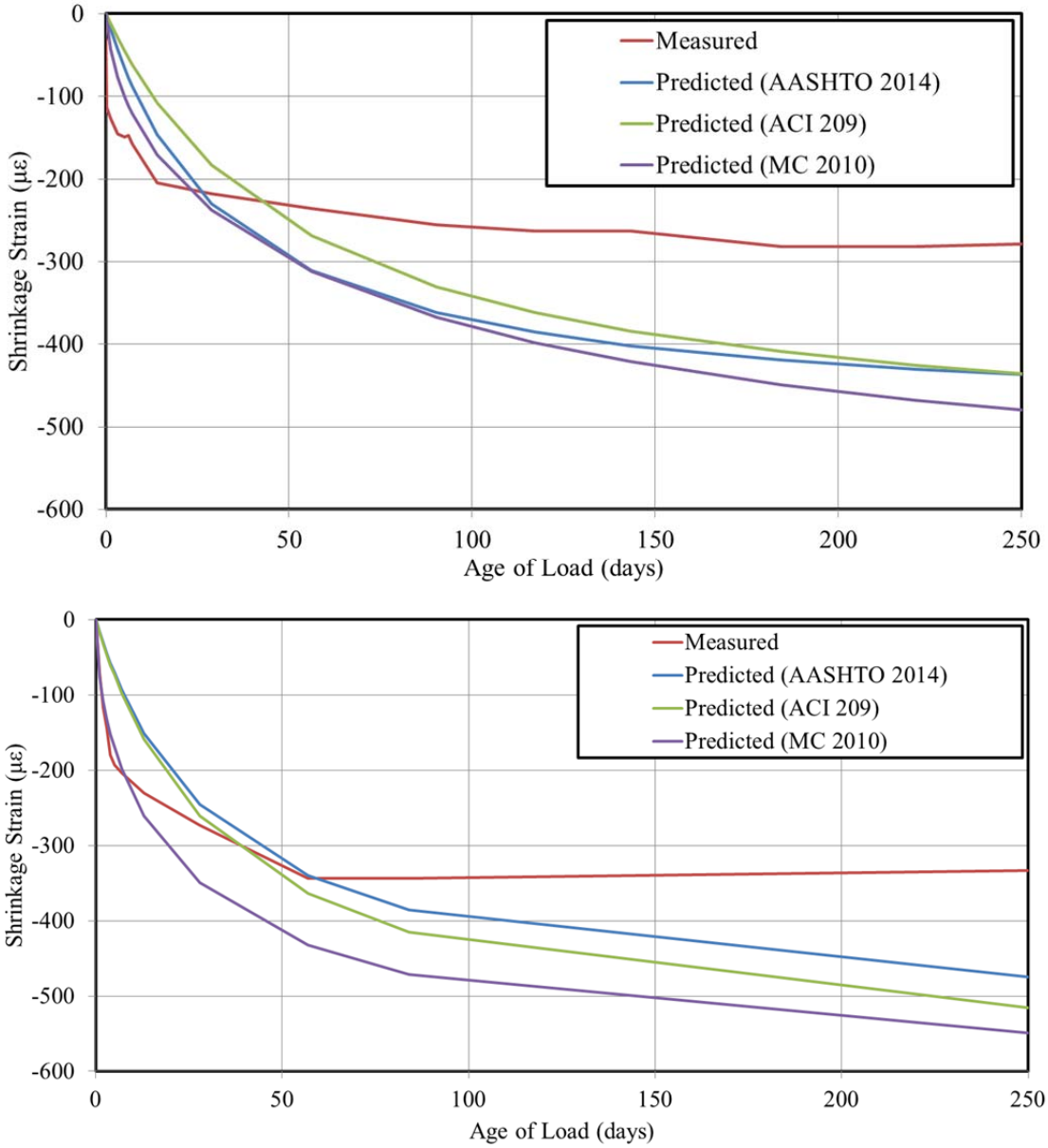

Figure H-15: DL-FA/SF 18 Hour – Test 1 Shrinkage Comparisons Cylinder Specimens (Top) and Rectangular Prism Specimens (Bottom)

Appendix I: Relative Goodness-of-Fit of Adjusted Candidate Shrinkage Prediction Models to Experimental Data

This appendix contains visualizations of the relative goodness-of-fit of the three calibrated candidate shrinkage prediction equations for both cylinder and rectangular prismatic specimens for each of 15 testing cycles included in this experimental effort.

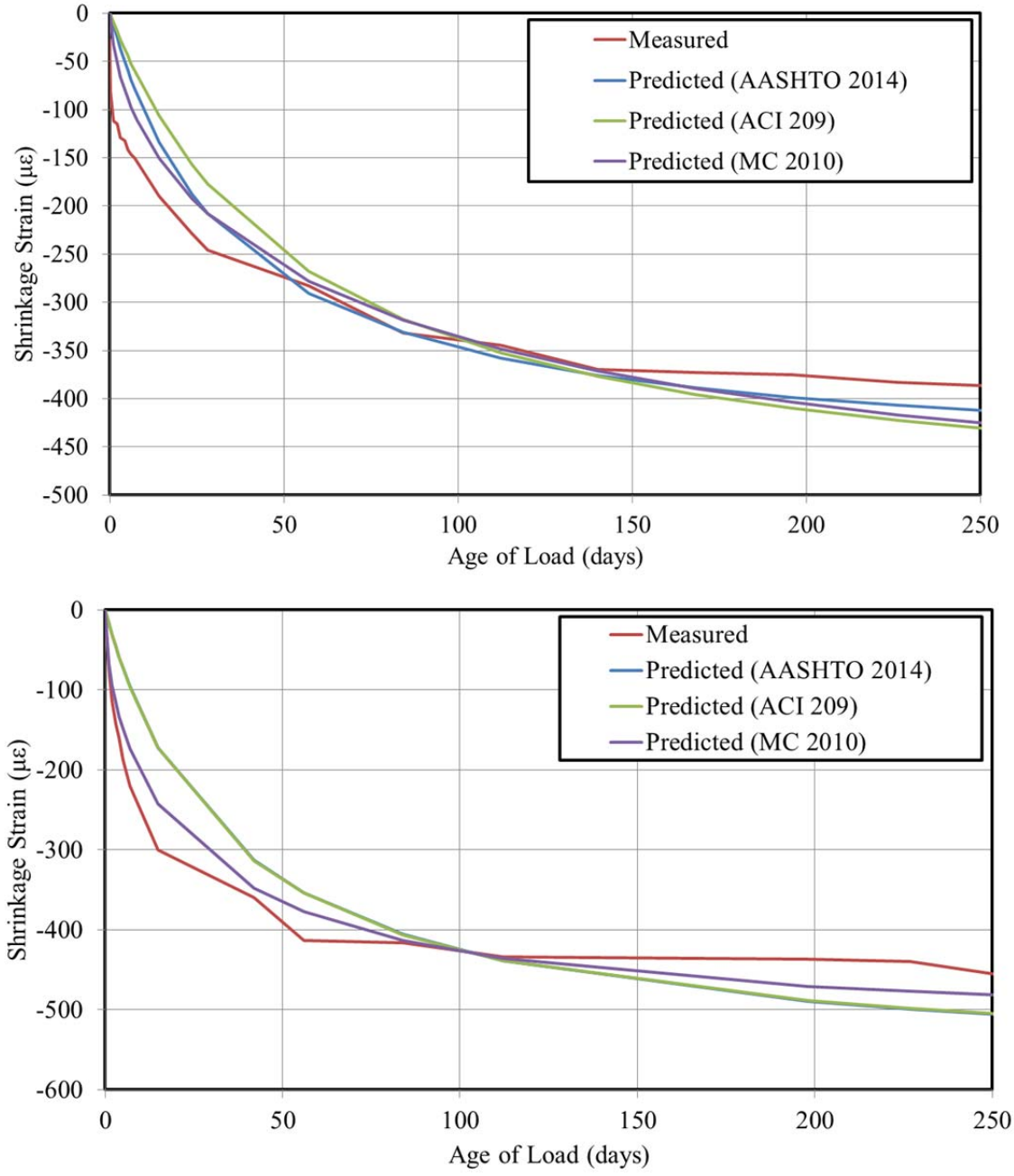

Figure I-1: DL-III 18 Hour – Test 1 Shrinkage Comparisons Cylinder Specimens (Top) and Rectangular Prism Specimens (Bottom)

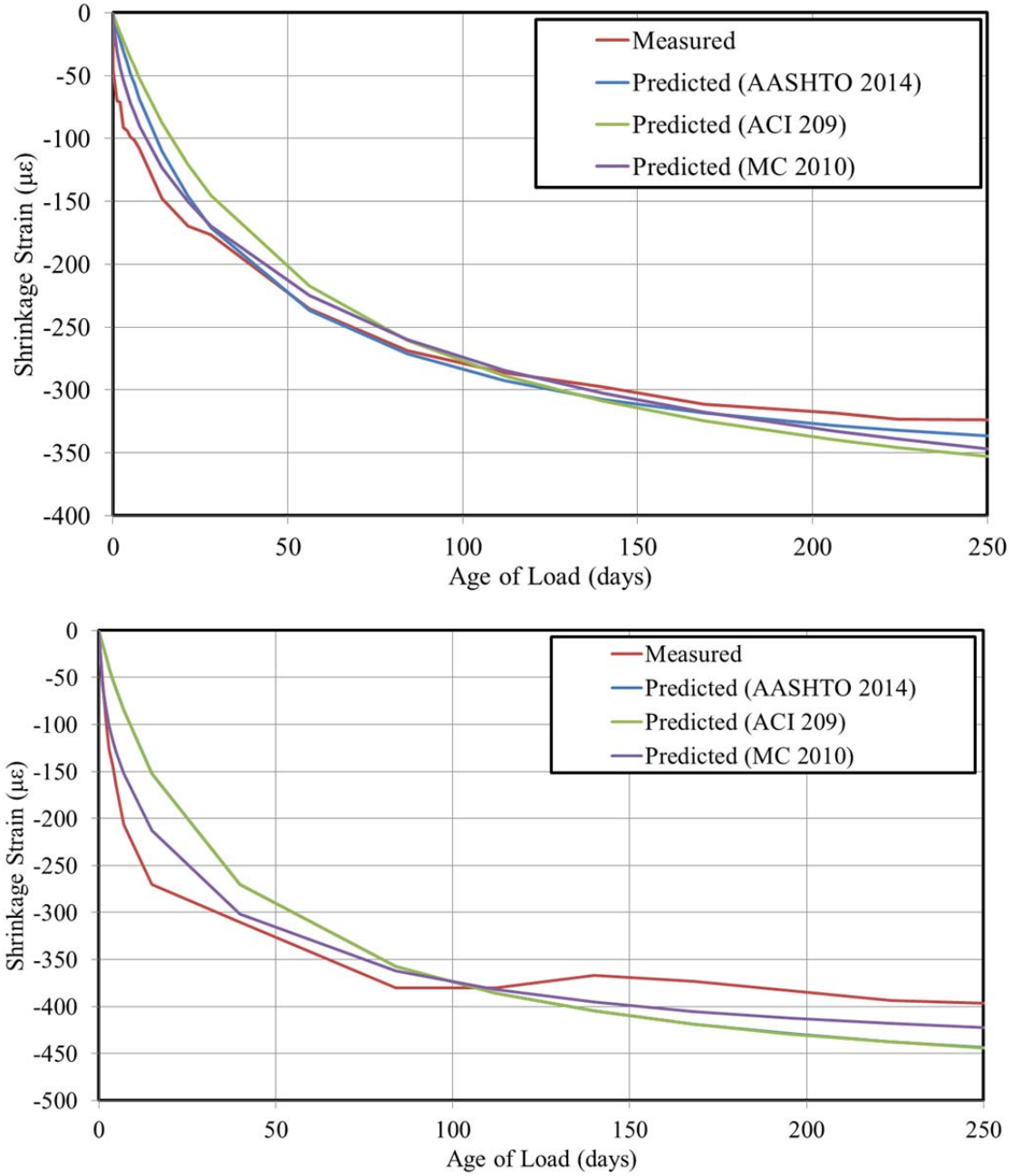

Figure I-2: DL-III 18 Hour – Test 2 Shrinkage Comparisons Cylinder Specimens (Top) and Rectangular Prism Specimens (Bottom)

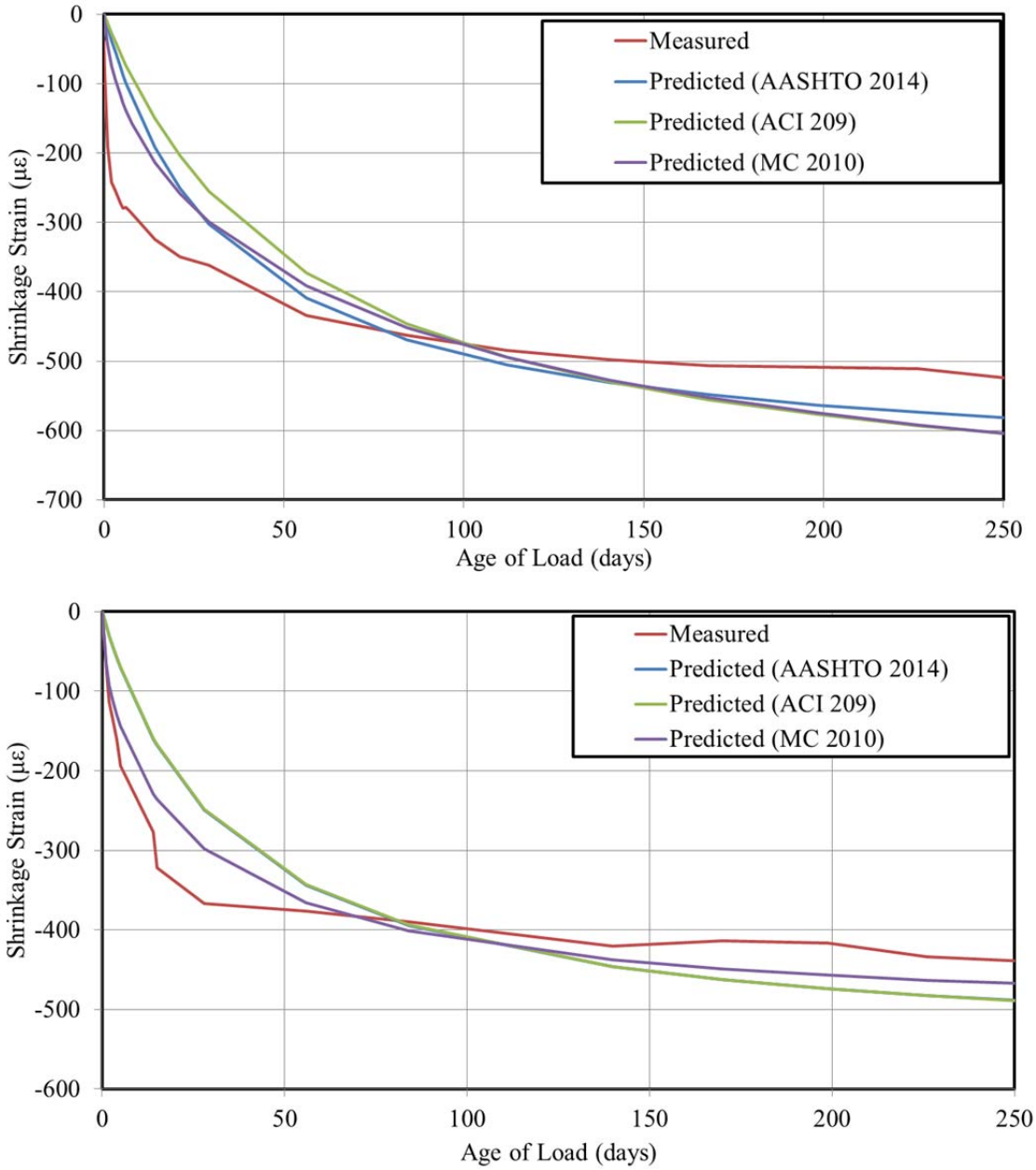

Figure I-3: CL-III 18 Hour – Test 1 Shrinkage Comparisons Cylinder Specimens (Top) and Rectangular Prism Specimens (Bottom)

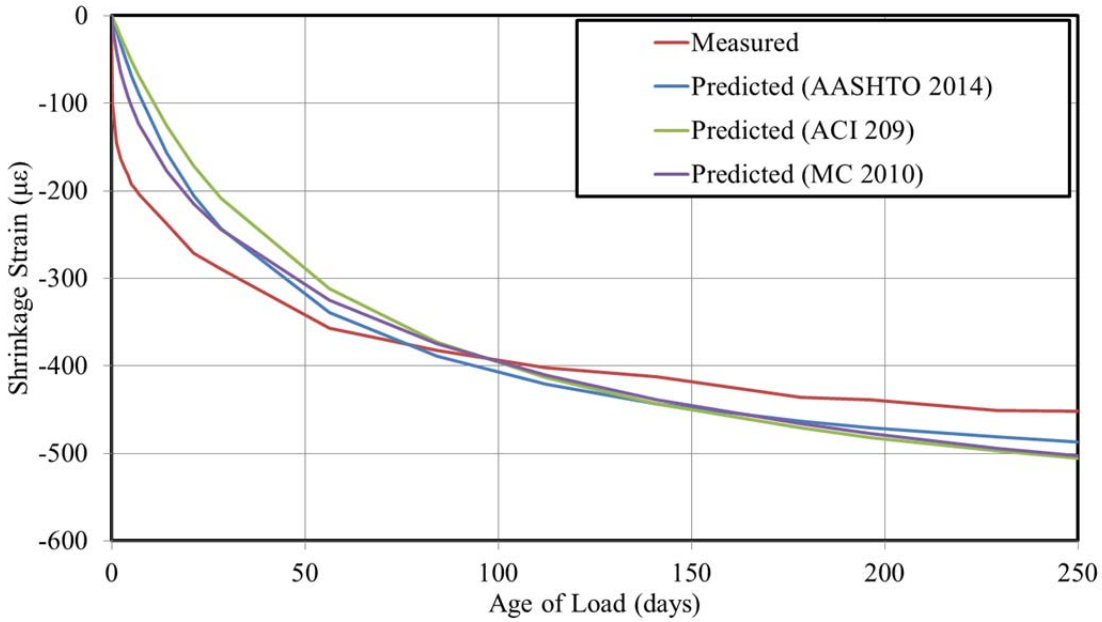

Figure I-4: CL-III 18 Hour – Test 2 Shrinkage Comparisons Cylinder Specimens

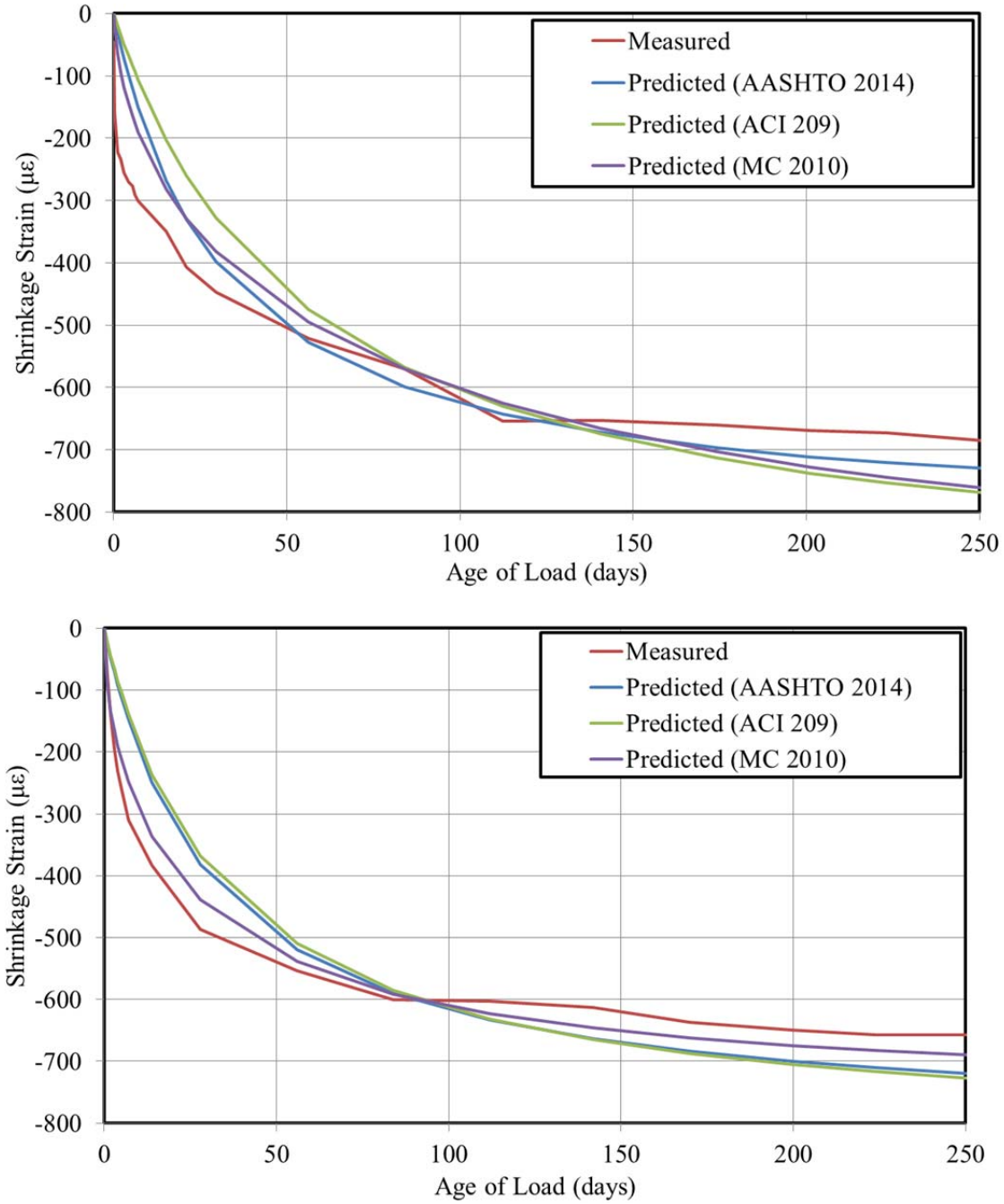

Figure I-5: GG-III 18 Hour – Test 1 Shrinkage Comparisons Cylinder Specimens (Top) and Rectangular Prism Specimens (Bottom)

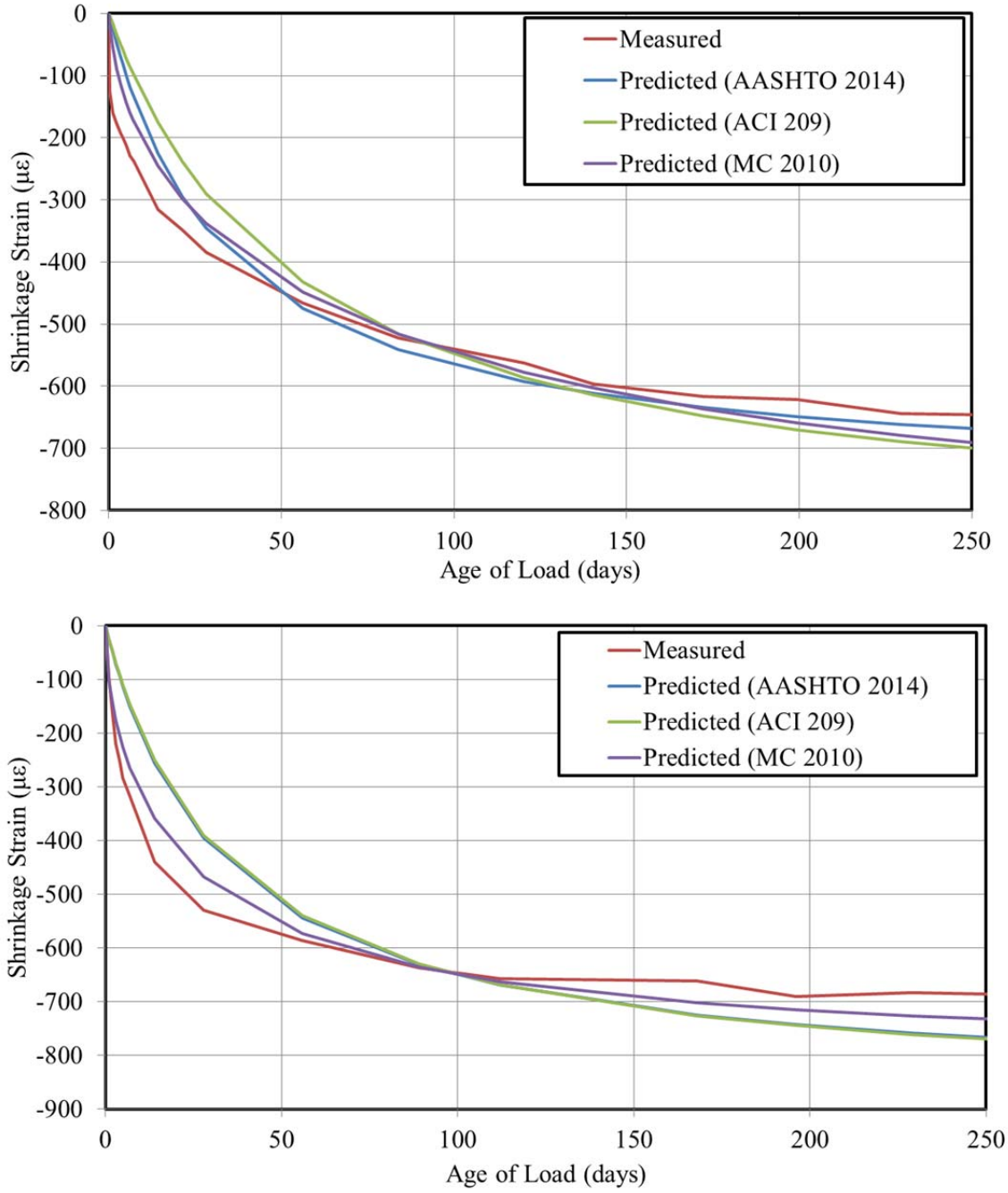

Figure I-6: GG-III 18 Hour – Test 2 Shrinkage Comparisons Cylinder Specimens (Top) and Rectangular Prism Specimens (Bottom)

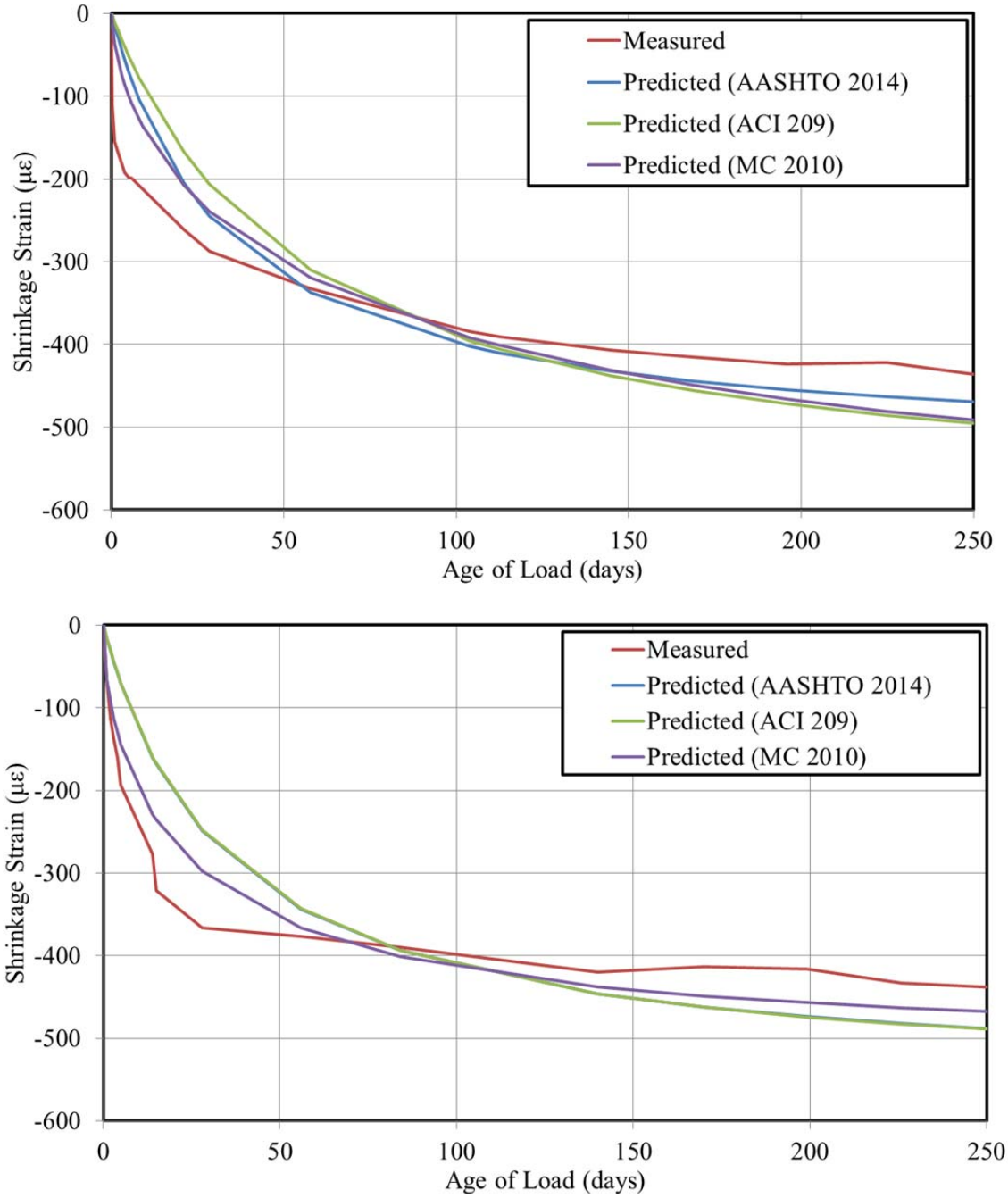

Figure I-7: DL-III 24 Hour – Test 1 Shrinkage Comparisons Cylinder Specimens (Top) and Rectangular Prism Specimens (Bottom)

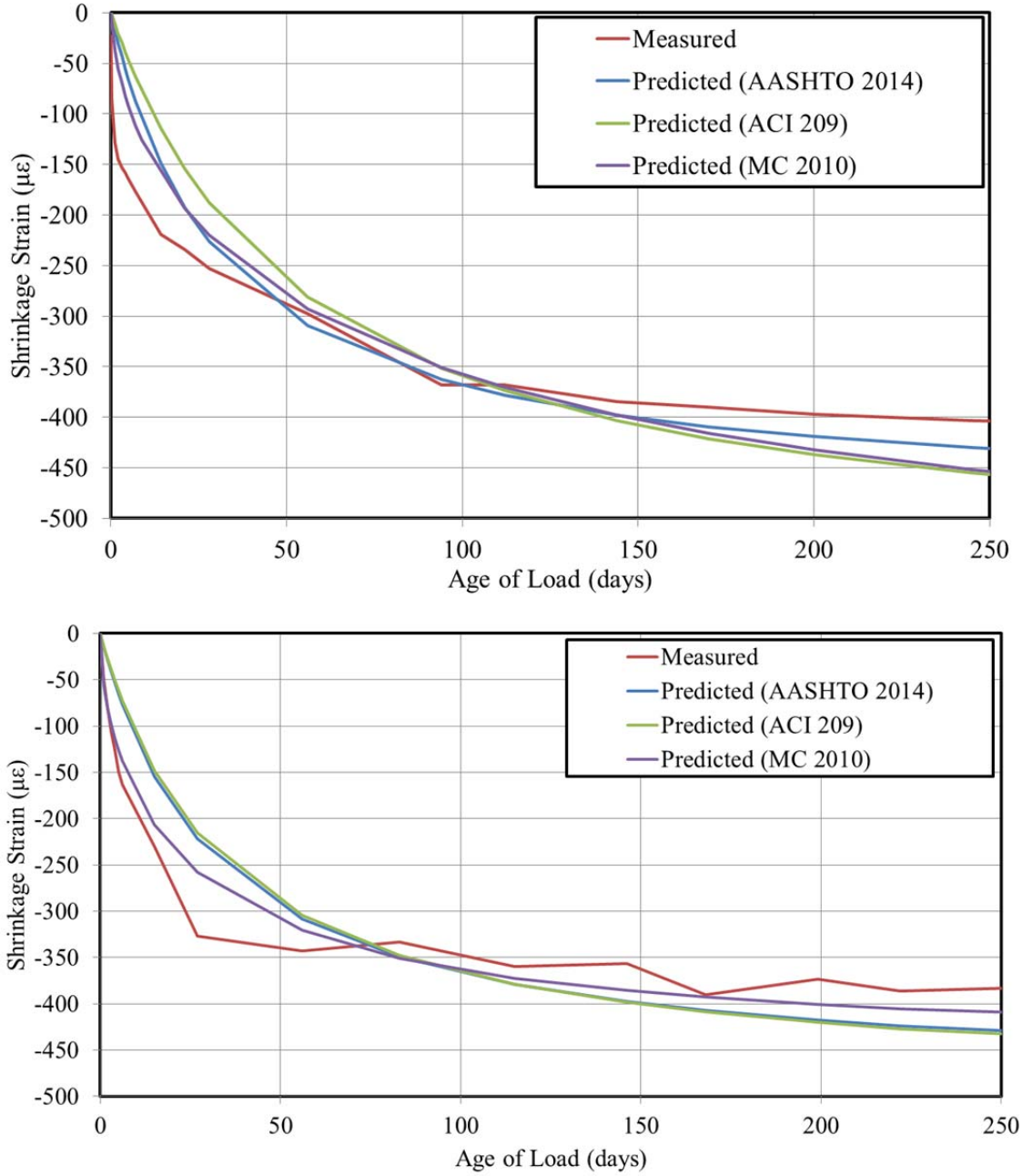

Figure I-8: CL-III 24 Hour – Test 1 Shrinkage Comparisons Cylinder Specimens (Top) and Rectangular Prism Specimens (Bottom)

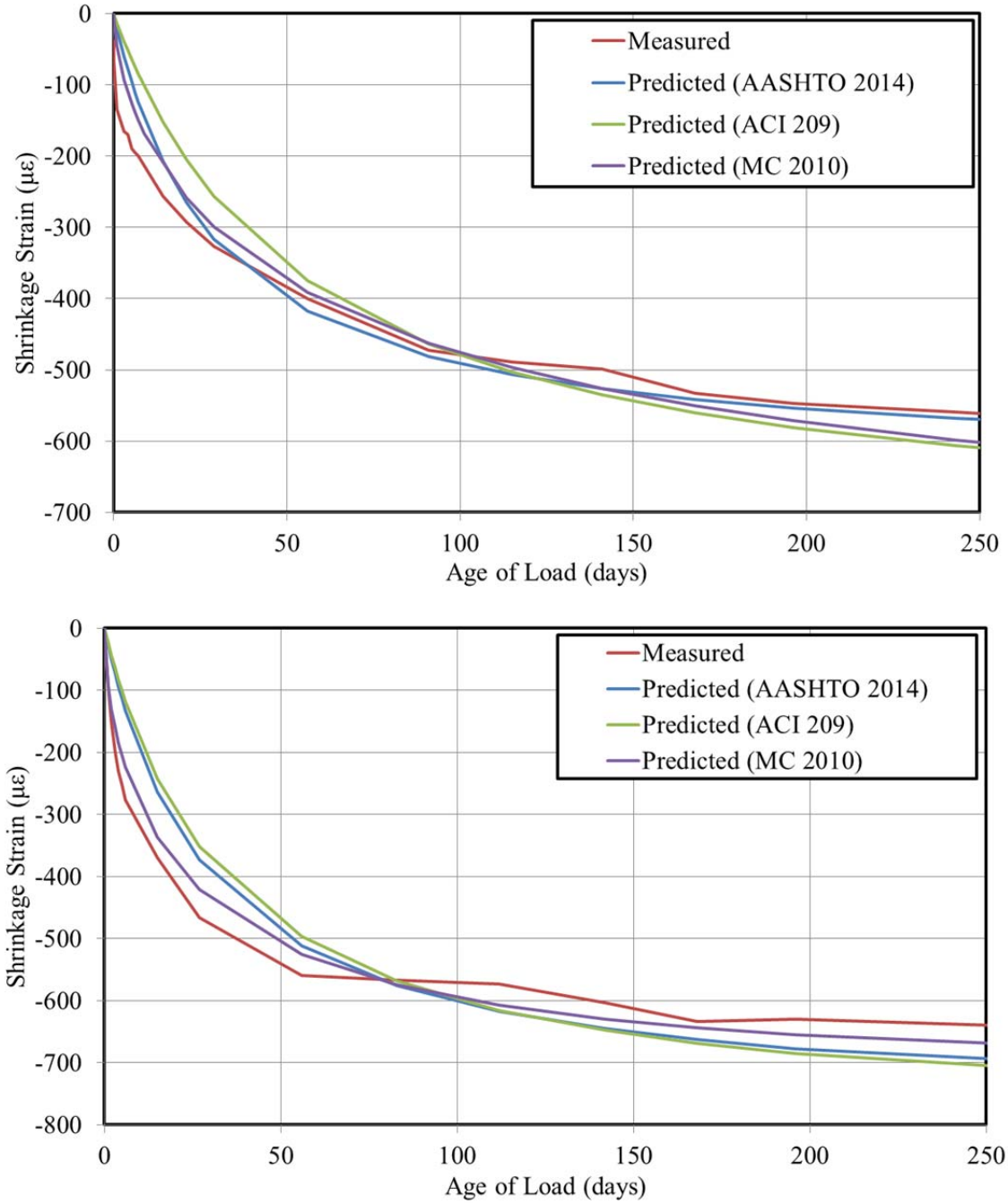

Figure I-9: GG-III 24 Hour – Test 1 Shrinkage Comparisons Cylinder Specimens (Top) and Rectangular Prism Specimens (Bottom)

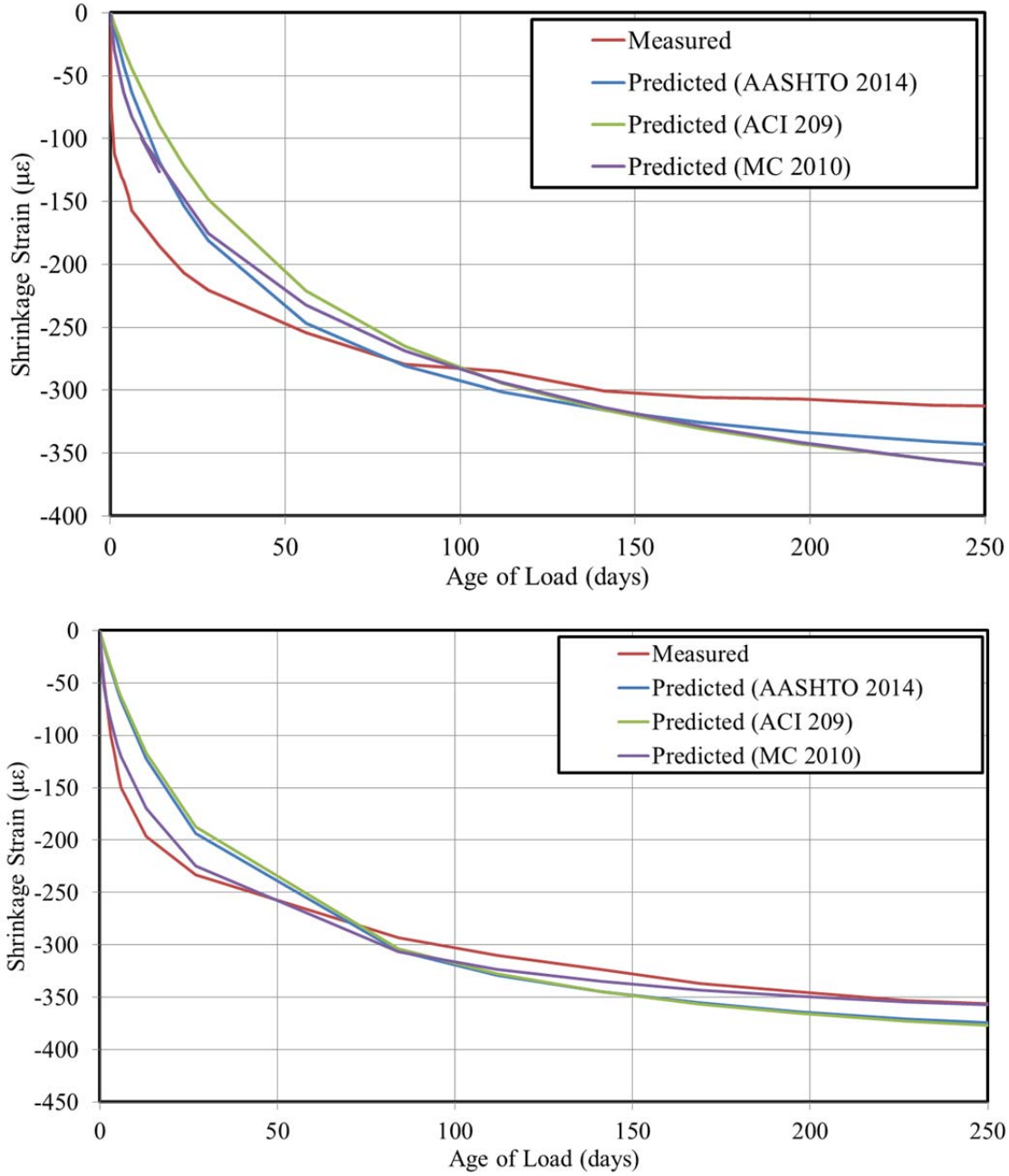

Figure I-10: DL-SL 24 Hour – Test 1 Shrinkage Comparisons Cylinder Specimens (Top) and Rectangular Prism Specimens (Bottom)

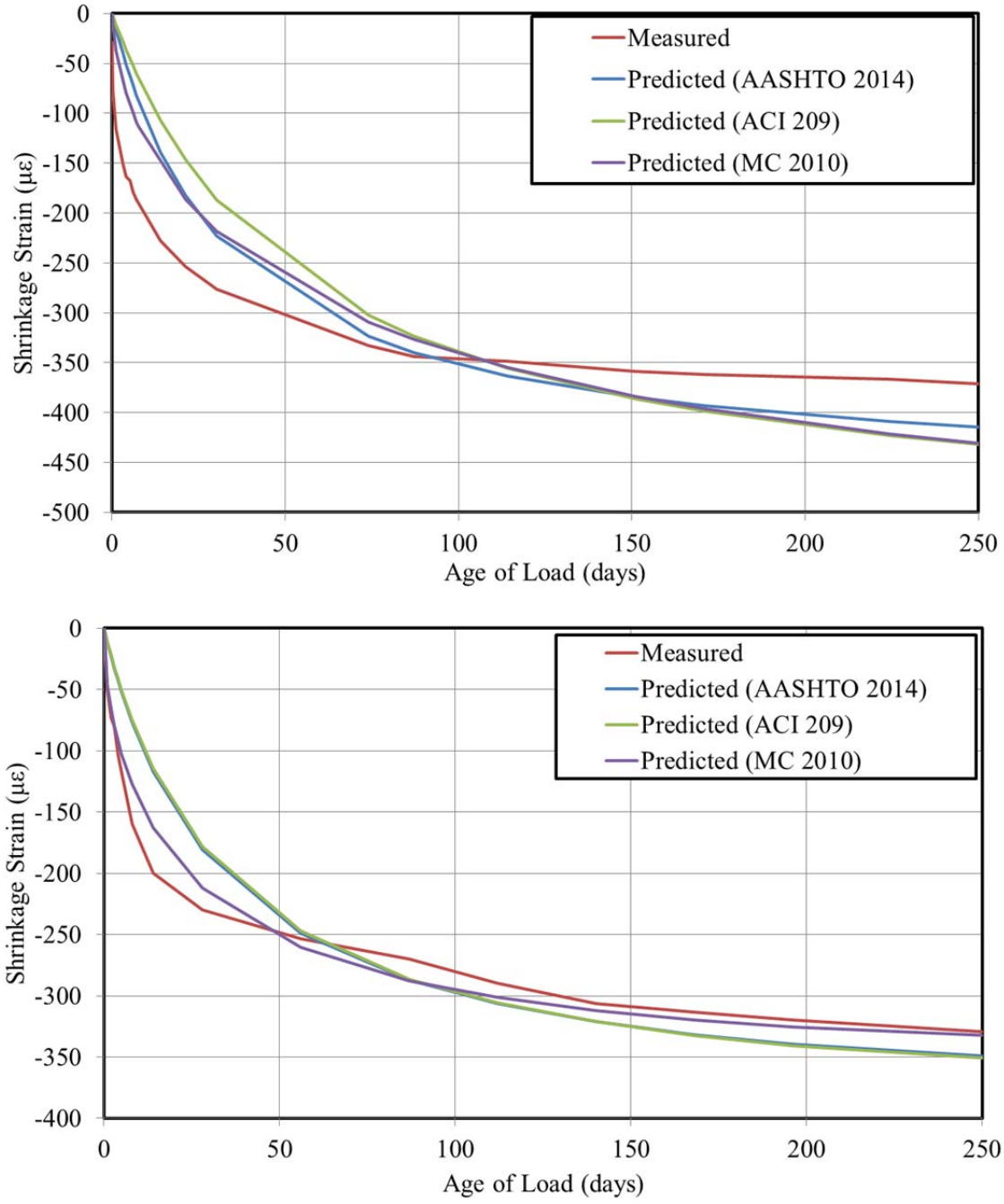

Figure I-11: DL-SL 18 Hour – Test 1 Shrinkage Comparisons Cylinder Specimens (Top) and Rectangular Prism Specimens (Bottom)

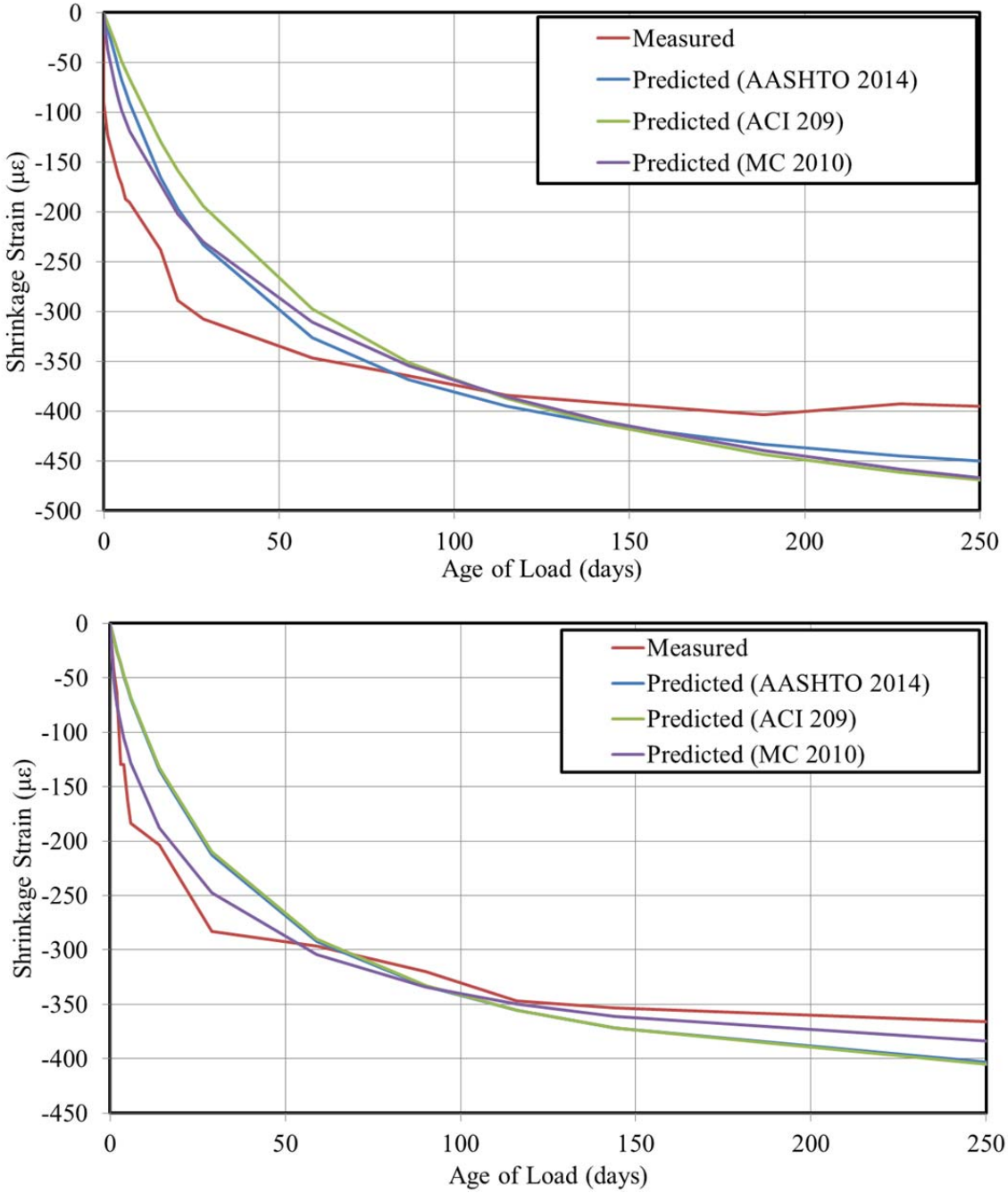

Figure I-12: DL-FA 18 Hour – Test 1 Shrinkage Comparisons Cylinder Specimens (Top) and Rectangular Prism Specimens (Bottom)

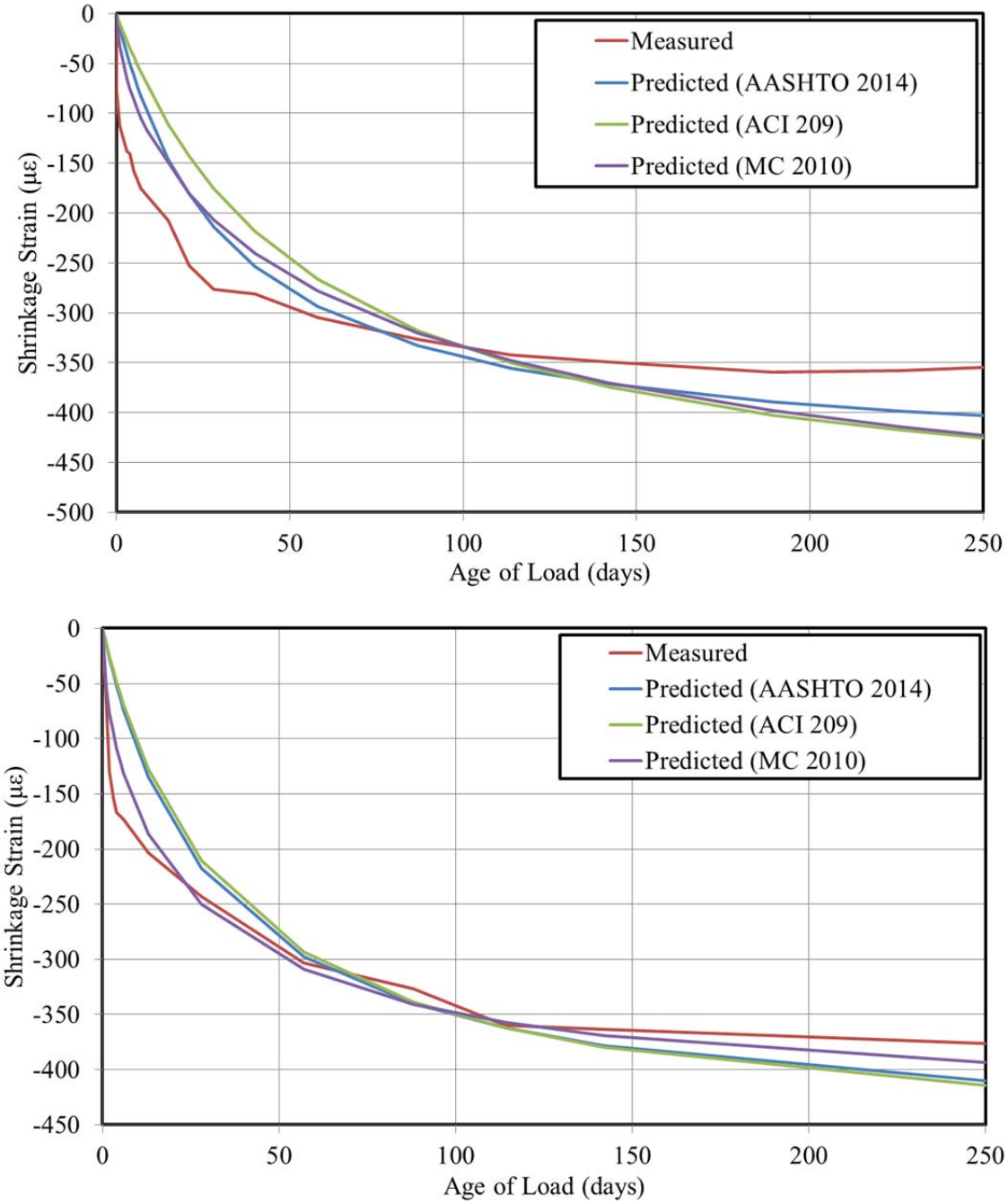

Figure I-13: DL-FA 24 Hour – Test 1 Shrinkage Comparisons Cylinder Specimens (Top) and Rectangular Prism Specimens (Bottom)

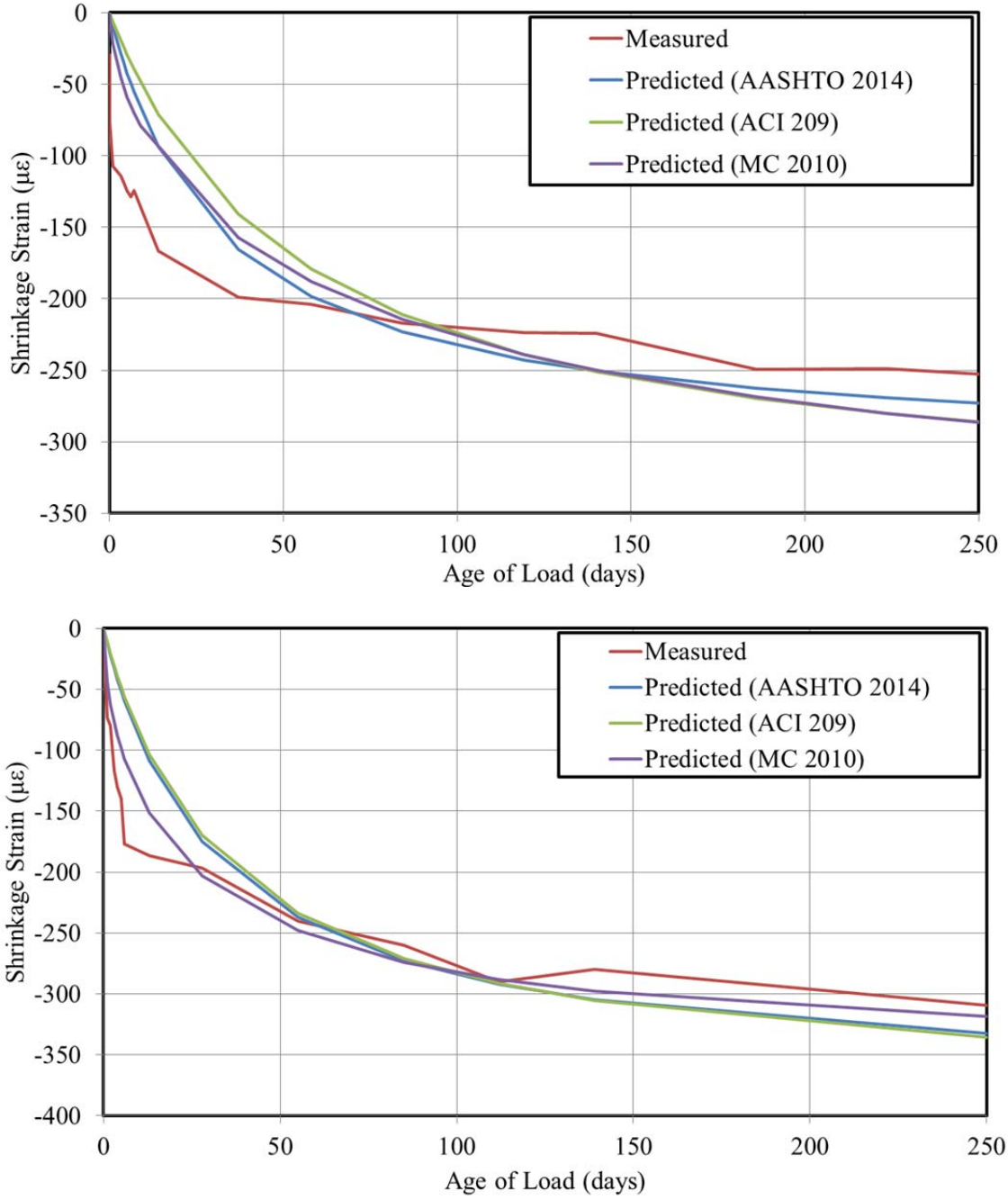

Figure I-14: DL-FA/SF 24 Hour – Test 1 Shrinkage Comparisons Cylinder Specimens (Top) and Rectangular Prism Specimens (Bottom)

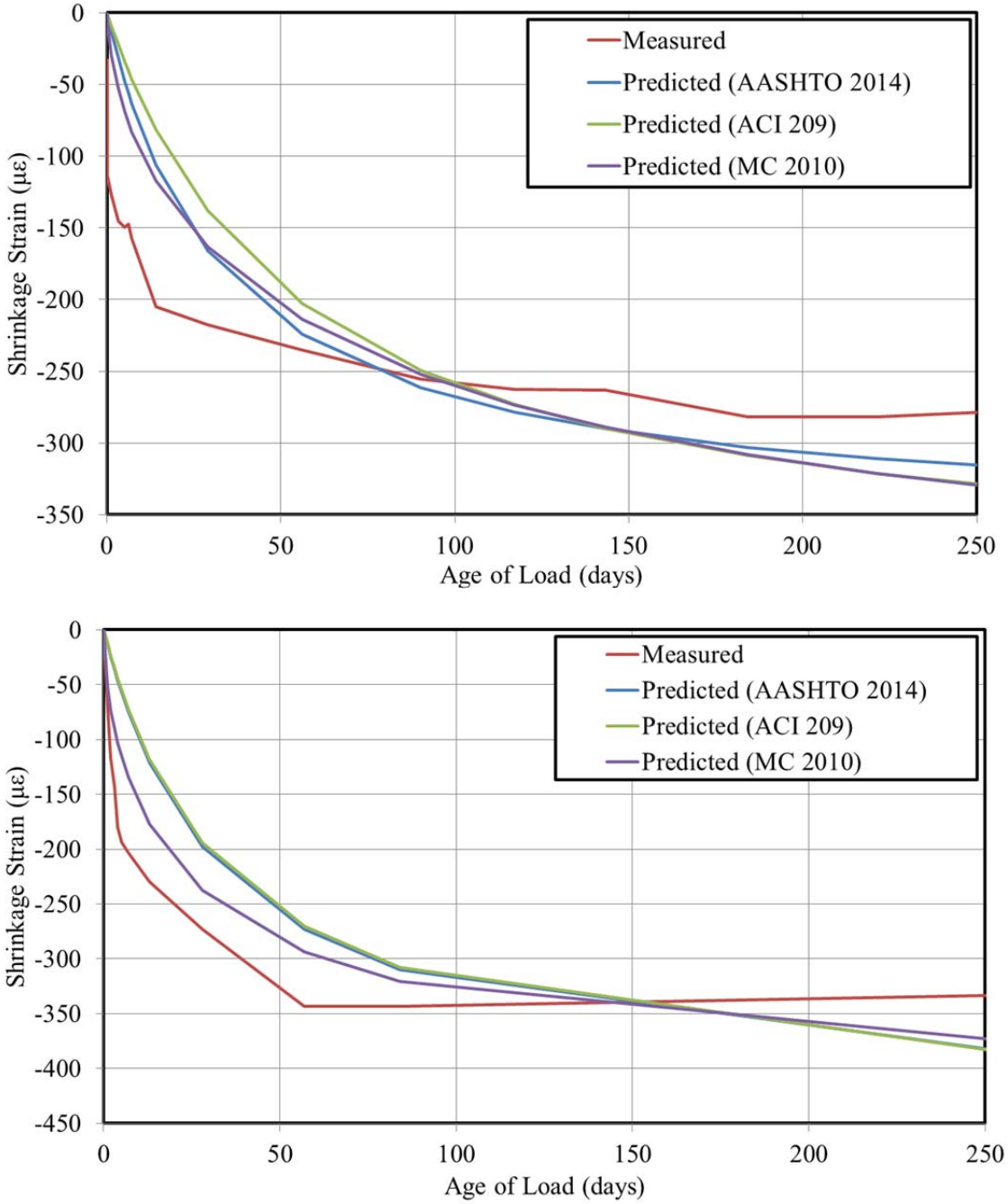

Figure I-15: DL-FA/SF 18 Hour – Test 1 Shrinkage Comparisons Cylinder Specimens (Top) and Rectangular Prism Specimens (Bottom)

Appendix J: Sample Layered Functions of the Implemented Temperature-Correction Algorithm

This appendix contains samples of the layered functions used in the analyses of Chapter 8. The sample layered functions included here were modified as necessary to accommodate differing demands of each analysis (i.e. reduced number of thermocouple gages in testing cycle #2, discarding gage VW4 for testing cycle #2 midspan, etc.)

Function to find centroidal strain from strain profile:

$$\text{centroidalstraindiff}\left(\text{rawstrain0}, \text{rawstrain1}, \text{height}_{\text{strain}}, c_{\text{bot}}\right) := \left(\begin{array}{l} \text{strain} \leftarrow \text{rawstrain1} - \text{rawstrain0} \\ \text{slope} \leftarrow \text{slope}\left(\text{height}_{\text{strain}}, \text{strain}\right) \\ \text{intercept} \leftarrow \text{intercept}\left(\text{height}_{\text{strain}}, \text{strain}\right) \\ \text{output} \leftarrow \text{slope} \cdot c_{\text{bot}} + \text{intercept} \end{array} \right)$$

Function to compute area of section:

$$\text{Area}(\text{height}) := \left(\int_0^{\text{height}} w\left(y_{\text{bot}}, \text{height}\right) dy_{\text{bot}} \right)$$

Function to compute first moment of area of section:

$$Q(\text{height}) := \left(\int_0^{\text{height}} w\left(y_{\text{bot}}, \text{height}\right) \cdot y_{\text{bot}}\, dy_{\text{bot}} \right)$$

Function to compute centroid of section:

$$c_{\text{bot}} := \frac{Q(\text{height})}{\text{Area}(\text{height})} = 36.603$$

Function to compute moment of inertia of section:

$$I(\text{height}) := \left[\int_0^{\text{height}} \left(y_{\text{bot}} - c_{\text{bot}}\right)^2 \cdot w\left(y_{\text{bot}}, \text{height}\right) dy_{\text{bot}} \right]$$

Function to define section width in absolute bottom notation:

$$w(y_{bot}, height) := \left[\begin{array}{l} widths \leftarrow \begin{pmatrix} height & 42 \\ height - 3.5 & 42 \\ height - 5.5 & 10 \\ height - 7.5 & 6 \\ 10.5 & 6 \\ 6 & 26 \\ 0 & 26 \end{pmatrix} \\ a1 \leftarrow slope(submatrix(widths, 5, 6, 1, 1), submatrix(widths, 5, 6, 2, 2)) \\ b1 \leftarrow intercept(submatrix(widths, 5, 6, 1, 1), submatrix(widths, 5, 6, 2, 2)) \\ a2 \leftarrow slope(submatrix(widths, 3, 4, 1, 1), submatrix(widths, 3, 4, 2, 2)) \\ b2 \leftarrow intercept(submatrix(widths, 3, 4, 1, 1), submatrix(widths, 3, 4, 2, 2)) \\ a3 \leftarrow slope(submatrix(widths, 2, 3, 1, 1), submatrix(widths, 2, 3, 2, 2)) \\ b3 \leftarrow intercept(submatrix(widths, 2, 3, 1, 1), submatrix(widths, 2, 3, 2, 2)) \\ out \leftarrow \left|\begin{array}{ll} widths_{7,2} & \text{if } 0 \le y_{bot} \le 6 \\ (a1 \cdot y_{bot} + b1) & \text{if } 6 < y_{bot} \le 10.5 \\ widths_{4,2} & \text{if } 10.5 < y_{bot} \le (height - 7.5) \\ (a2 \cdot y_{bot} + b2) & \text{if } (height - 7.5) < y_{bot} \le (height - 5.5) \\ (a3 \cdot y_{bot} + b3) & \text{if } (height - 5.5) < y_{bot} \le (height - 3.5) \\ 42 & \text{if } (height - 3.5) < y_{bot} \le height \end{array}\right. \\ out \end{array}\right]$$

Function to generate piecewise exact width in integration notation:

$$\text{width}(y, \text{height}, c_{bot}) := \left[\begin{array}{l}
\text{widths} \leftarrow \begin{pmatrix} c_{bot} - \text{height} & 42 \\ c_{bot} - \text{height} + 3.5 & 42 \\ c_{bot} - \text{height} + 5.5 & 10 \\ c_{bot} - \text{height} + 7.5 & 6 \\ c_{bot} - 10.5 & 6 \\ c_{bot} - 6 & 26 \\ c_{bot} & 26 \end{pmatrix} \\
a1 \leftarrow \text{slope}(\text{submatrix}(\text{widths}, 5, 6, 1, 1), \text{submatrix}(\text{widths}, 5, 6, 2, 2)) \\
b1 \leftarrow \text{intercept}(\text{submatrix}(\text{widths}, 5, 6, 1, 1), \text{submatrix}(\text{widths}, 5, 6, 2, 2)) \\
a2 \leftarrow \text{slope}(\text{submatrix}(\text{widths}, 3, 4, 1, 1), \text{submatrix}(\text{widths}, 3, 4, 2, 2)) \\
b2 \leftarrow \text{intercept}(\text{submatrix}(\text{widths}, 3, 4, 1, 1), \text{submatrix}(\text{widths}, 3, 4, 2, 2)) \\
a3 \leftarrow \text{slope}(\text{submatrix}(\text{widths}, 2, 3, 1, 1), \text{submatrix}(\text{widths}, 2, 3, 2, 2)) \\
b3 \leftarrow \text{intercept}(\text{submatrix}(\text{widths}, 2, 3, 1, 1), \text{submatrix}(\text{widths}, 2, 3, 2, 2)) \\
\text{widths}_{7,2} \text{ if } (c_{bot}) \geq y \geq (c_{bot} - 6) \\
(a1 \cdot y + b1) \text{ if } (c_{bot} - 6) > y \geq (c_{bot} - 10.5) \\
\text{widths}_{4,2} \text{ if } (c_{bot} - 10.5) > y \geq (c_{bot} - \text{height}) + 7.5 \\
(a2 \cdot y + b2) \text{ if } (c_{bot} - \text{height}) + 7.5 > y \geq (c_{bot} - \text{height}) + 5.5 \\
(a3 \cdot y + b3) \text{ if } (c_{bot} - \text{height}) + 5.5 > y \geq (c_{bot} - \text{height}) + 3.5 \\
42 \text{ if } c_{bot} - \text{height} + 3.5 > y \geq (c_{bot} - \text{height}) \\
0 \text{ otherwise}
\end{array}\right]$$

Function to generate piecewise temperature profile interpolated from 13 locations:

$$\text{tempprofile}(y, \text{temp0}, \text{temp1}, \text{temp}_{ref}, c_{bot}, \text{height}_{temp}) :=$$

deltatemp0 $\leftarrow \overrightarrow{(\text{temp0} - \text{temp}_{ref})}$

deltatemp1 $\leftarrow \overrightarrow{(\text{temp1} - \text{temp}_{ref})}$

deltatemp $\leftarrow$ deltatemp1 $-$ deltatemp0

tempheight $\leftarrow -\overrightarrow{(\text{height}_{temp} - c_{bot})}$

a $\leftarrow$ for $i \in 1..12$

$a_i \leftarrow \text{slope}(\text{submatrix}(\text{tempheight}, i, i+1, 1, 1), \text{submatrix}(\text{deltatemp}, i, i+1, 1, 1))$

a

b $\leftarrow$ for $i \in 1..12$

$b_i \leftarrow \text{intercept}(\text{submatrix}(\text{tempheight}, i, i+1, 1, 1), \text{submatrix}(\text{deltatemp}, i, i+1, 1, 1))$

b

output $\leftarrow$

$a_1 \cdot y + b_1$ if $c_{bot} - \text{height} \le y \le \text{tempheight}_2$

$a_2 \cdot y + b_2$ if $\text{tempheight}_2 < y \le \text{tempheight}_3$

$a_3 \cdot y + b_3$ if $\text{tempheight}_3 < y \le \text{tempheight}_4$

$a_4 \cdot y + b_4$ if $\text{tempheight}_4 < y \le \text{tempheight}_5$

$a_5 \cdot y + b_5$ if $\text{tempheight}_5 < y \le \text{tempheight}_6$

$a_6 \cdot y + b_6$ if $\text{tempheight}_6 < y \le \text{tempheight}_7$

$a_7 \cdot y + b_7$ if $\text{tempheight}_7 < y \le \text{tempheight}_8$

$a_8 \cdot y + b_8$ if $\text{tempheight}_8 < y \le \text{tempheight}_9$

$a_9 \cdot y + b_9$ if $\text{tempheight}_9 < y \le \text{tempheight}_{10}$

$a_{10} \cdot y + b_{10}$ if $\text{tempheight}_{10} < y \le \text{tempheight}_{11}$

$a_{11} \cdot y + b_{11}$ if $\text{tempheight}_{11} < y \le \text{tempheight}_{12}$

$a_{12} \cdot y + b_{12}$ if $\text{tempheight}_{12} < y \le c_{bot}$

0 otherwise

output

Assemble above functions into single function to generate raw output #1:

Note: The term raw output is used to refer to the solution of Equation 8-17, however with the CTE term removed to allow for easier manipulation of results in MS EXCEL.

$$\text{centroidalstrainraw}(\text{height}, \text{temp}_{ref}, \text{height}_{temp}, \text{temp0}, \text{temp1}) := \left| \begin{array}{l} A \leftarrow \text{Area}(\text{height}) \\ Q \leftarrow Q(\text{height}) \\ c_{bot} \leftarrow \frac{Q}{A} \\ I \leftarrow \int_0^{\text{height}} (y_{bot} - c_{bot})^2 \cdot w(y_{bot}, \text{height})\, dy_{bot} \\ \text{centroidalstrainraw} \leftarrow \frac{1}{A} \cdot \int_{c_{bot}-\text{height}}^{c_{bot}} (\text{tempprofile}(y, \text{temp0}, \text{temp1}, \text{temp}_{ref}, c_{bot}, \text{height}_{temp}) \cdot \text{width}(y, \text{height}, c_{bot}))\, dy \\ \text{centroidalstrainraw} \end{array} \right.$$

Function to solve for change in curvature from measured data:

$$\text{deltacurvature}(\text{rawstrain0}, \text{rawstrain1}, \text{height}_{strain}, c_{bot}) := \left[\begin{array}{l} \text{strain} \leftarrow \text{rawstrain1} - \text{rawstrain0} \\ \text{strainheight} \leftarrow -\overrightarrow{(\text{height}_{strain} - c_{bot})} \\ \text{slope} \leftarrow \text{slope}(\text{strainheight}, \text{strain}) \\ \text{intercept} \leftarrow \text{intercept}(\text{strainheight}, \text{strain}) \\ \text{output} \leftarrow \text{slope} \end{array} \right]$$

Assemble above functions into single function to generate raw output #2:

Note: The term raw output is used to refer to the solution of Equation 8-25, however with the CTE term removed to allow for easier manipulation of results in MS EXCEL.

$$\text{curvatureraw}(\text{height}, \text{temp}_{ref}, \text{height}_{temp}, \text{temp0}, \text{temp1}) := \left| \begin{array}{l} A \leftarrow \text{Area}(\text{height}) \\ Q \leftarrow Q(\text{height}) \\ c_{bot} \leftarrow \frac{Q}{A} \\ I \leftarrow \int_0^{\text{height}} (y_{bot} - c_{bot})^2 \cdot w(y_{bot}, \text{height})\, dy_{bot} \\ \text{curvatureraw} \leftarrow \frac{1}{I} \cdot \int_{c_{bot}-\text{height}}^{c_{bot}} (\text{tempprofile}(y, \text{temp0}, \text{temp1}, \text{temp}_{ref}, c_{bot}, \text{height}_{temp}) \cdot \text{width}(y, \text{height}, c_{bot}) \cdot y)\, dy \\ \text{curvatureraw} \end{array} \right.$$

Adapt above function for centroidal strain to iterate through experimental data sets:

$$\begin{aligned}
&\text{midspan}_{\text{centroid}} := \text{for } aubie \in 1..\text{rows}(temps) - 1 \\
&\quad temp0backwards \leftarrow \text{submatrix}(temps, 1, 1, 1, 13)^{T} \\
&\quad temp0 \leftarrow \text{reverse}(temp0backwards) \\
&\quad temp1backwards \leftarrow \text{submatrix}(temps, aubie + 1, aubie + 1, 1, 13)^{T} \\
&\quad temp1 \leftarrow \text{reverse}(temp1backwards) \\
&\quad rawstrain0backwards \leftarrow \text{submatrix}(strains, 1, 1, 1, 4)^{T} \cdot 10^{-6} \\
&\quad rawstrain0 \leftarrow \text{reverse}(rawstrain0backwards) \\
&\quad rawstrain1backwards \leftarrow \text{submatrix}(strains, aubie + 1, aubie + 1, 1, 4)^{T} \cdot 10^{-6} \\
&\quad rawstrain1 \leftarrow \text{reverse}(rawstrain1backwards) \\
&\quad output_{aubie,1} \leftarrow \text{centroidalstrainraw}\left(height, temp_{ref}, height_{temp}, temp0, temp1\right) \\
&\quad output_{aubie,2} \leftarrow \text{centroidalstraindiff}\left(rawstrain0, rawstrain1, height_{strain}, c_{bot}\right) \\
&output
\end{aligned}$$

Adapt above function for curvature to iterate through experimental data sets:

$$\begin{aligned}
&\text{midspan}_{\text{curvature}} := \text{for } aubie \in 1..\text{rows}(time) - 1 \\
&\quad temp0backwards \leftarrow \text{submatrix}(temps, 1, 1, 1, 13)^{T} \\
&\quad temp0 \leftarrow \text{reverse}(temp0backwards) \\
&\quad temp1backwards \leftarrow \text{submatrix}(temps, aubie + 1, aubie + 1, 1, 13)^{T} \\
&\quad temp1 \leftarrow \text{reverse}(temp1backwards) \\
&\quad rawstrain0backwards \leftarrow \text{submatrix}(strains, 1, 1, 1, 4)^{T} \cdot 10^{-6} \\
&\quad rawstrain0 \leftarrow \text{reverse}(rawstrain0backwards) \\
&\quad rawstrain1backwards \leftarrow \text{submatrix}(strains, aubie + 1, aubie + 1, 1, 4)^{T} \cdot 10^{-6} \\
&\quad rawstrain1 \leftarrow \text{reverse}(rawstrain1backwards) \\
&\quad output_{aubie,1} \leftarrow \text{curvatureraw}\left(height, temp_{ref}, height_{temp}, temp0, temp1\right) \\
&\quad output_{aubie,2} \leftarrow \text{deltacurvature}\left(rawstrain0, rawstrain1, height_{strain}, c_{bot}\right) \\
&output
\end{aligned}$$

Appendix K: Raw Temperature Data from Field Tests #1-9

This appendix contains raw temperature measurements used in the temperature-corrections performed in Chapter 10 of this dissertation.

Field Test	Girder #	Time After Release (days)	VW1 Temperature (°C)	VW2 Temperature (°C)	VW3 Temperature (°C	VW4 Temperature (°C)
1	1	Pre-Release	34.3	34.2	35.6	38.8
		0.0	34.2	35.6	36.4	42.0
		0.1	34.5	37.0	37.9	44.4
	2	Pre-Release	34.4	34.2	35.6	38.7
		0.0	34.1	35.5	36.4	41.7
		0.1	34.6	37.0	37.9	44.5
	3	Pre-Release	34.7	34.2	35.7	38.0
		0.0	34.1	35.5	36.3	41.6
		0.1	34.5	37.0	37.9	44.4
2	1	Pre-Release	43.9	38.2	39.5	40.5
		0.0	42.9	37.4	38.5	39.6
		0.1	Data Collection System Malfunction			
		74.0	18.5	18.2	17.8	15.5
		231.2	9.4	12.9	7.7	8.7
	2	Pre-Release	44.4	38.6	39.9	41.0
		0.0	43.0	37.5	38.6	39.7
		0.1	Data Collection System Malfunction			
		74.0	18.5	18.2	17.8	15.4
		145.2	7.6	16.7	16.3	11.6
		231.2	9.3	12.8	7.6	8.5
3	1	Pre-Release	46.2	42.5	47.7	48.4
		0.0	45.1	40.5	45.3	46.2
		0.1	41.6	36.8	40.3	41.9
		73.2	19.3	18.5	18.7	16.9
		230.3	7.6	7.3	7.2	11.5
	2	Pre-Release	45.9	41.9	47.0	47.7
		0.0	44.8	40.1	44.8	45.7
		0.1	41.5	36.7	40.1	41.9
		73.2	19.2	18.5	18.7	17.0
		230.3	7.6	7.3	7.2	11.6

Field Test	Girder #	Time After Release (days)	VW1 Temperature (°C)	VW2 Temperature (°C)	VW3 Temperature (°C	VW4 Temperature (°C)
4	1	Pre-Release	57.6	52.9	55.6	55.1
		0.0	56.0	49.6	52.2	51.9
		0.1	51.9	45.3	47.3	47.1
		156.3	7.8	8.1	8.2	14.3
	2	Pre-Release	57.3	52.2	54.8	54.4
		0.0	55.7	49.2	51.8	51.5
		0.1	51.7	45.2	47.1	46.9
		156.3	7.8	8.1	8.1	14.1
5	1	Pre-Release	61.5	57.7	60.4	58.0
		0.0	60.2	54.6	57.4	55.2
		0.1	57.9	50.7	53.1	51.9
		67.1	0.6	3.0	3.2	0.1
		154.2	7.8	8.1	8.1	12.4
	2	Pre-Release	60.9	56.1	58.9	56.5
		0.0	60.0	54.1	56.8	54.7
		0.1	57.5	50.3	52.7	51.6
		154.2	7.7	8.0	8.0	12.8
6	1	Pre-Release	61.1	55.4	59.3	57.5
		0.0	60.1	52.8	56.7	55.2
		0.1	57.3	48.3	51.8	50.7
		153.3	10.6	8.1	8.0	11.7
	2	Pre-Release	61.5	56.7	60.6	58.5
		0.0	60.4	53.5	57.3	55.8
		0.1	57.3	48.3	51.8	50.7
		153.3	10.6	8.0	7.9	11.5
7	1	Pre-Release	50.2	49.3	51.7	49.6
		0.0	47.9	44.2	46.4	45.1
		0.1	44.0	39.5	40.9	41.0
		43.0	15.3	15.6	16.7	15.8
		82.1	6.3	6.4	6.4	5.5
	2	Pre-Release	49.8	48.2	50.6	48.5
		0.0	47.5	43.6	45.8	44.6
		0.1	43.6	39.1	40.5	40.7
		43.0	15.3	15.6	16.7	15.8
		82.2	6.3	6.5	6.5	6.4
	3	Pre-Release	49.1	46.4	48.8	47.0
		0.0	47.5	43.6	45.8	44.6
		0.1	43.4	39.0	40.3	40.6
		43.0	15.3	15.6	16.7	15.8
		82.2	6.4	6.5	6.6	6.9

Field Test	Girder #	Time After Release (days)	VW1 Temperature (°C)	VW2 Temperature (°C)	VW3 Temperature (°C	VW4 Temperature (°C)
8	1	Pre-Release	53.2	51.9	56.1	54.4
		0.0	51.1	46.9	50.7	50.4
		0.1	48.7	43.5	46.7	46.9
		41.1	15.4	15.5	15.7	16.1
		80.2	10.9	17.7	16.8	11.3
	2	Pre-Release	52.8	50.7	54.9	53.6
		0.0	50.8	46.5	50.2	50.0
		0.1	48.4	43.3	46.5	46.6
		41.1	15.4	15.5	15.8	16.1
		80.2	11.1	18.0	17.1	11.6
	3	Pre-Release	52.3	49.4	53.5	52.6
		0.0	50.6	46.0	49.7	49.6
		0.1	48.2	43.1	46.3	46.5
		41.1	15.4	15.5	15.8	16.1
		80.2	11.3	18.3	17.3	11.9
9	1	Pre-Release	51.1	50.5	52.7	49.7
		0.0	48.9	45.5	47.4	45.5
		0.1	46.0	41.9	42.8	42.1
		36.1	16.5	17.8	17.4	17.8
		75.3	13.0	17.2	15.3	14.7
	2	Pre-Release	50.6	49.0	51.1	48.4
		0.0	48.0	44.1	45.8	44.1
		0.1	45.8	41.9	42.6	42.0
		36.1	16.6	18.2	17.6	18.2
		75.3	13.1	17.1	15.3	14.7
	3	Pre-Release	50.0	47.4	49.4	47.2
		0.0	48.3	44.6	46.3	44.6
		0.1	45.7	41.8	42.5	42.0
		36.1	16.7	18.3	17.7	18.3

Appendix L: Raw Strain Gage Readings from Field Tests #1-9

This appendix contains raw strain gage readings (unzeroed) used in the analyses performed in Chapter 10 of this dissertation. For reference, the useful range of the gage is approximately 2,500 με +- 1,500 με.

Field Test	Girder #	Time After Release (days)	VW1 Raw Reading (με)	VW2 Raw Reading (με)	VW3 Raw Reading (με)	VW4 Raw Reading (με)
1	1	Pre-Release	2730.1	2695.1	2710.0	2621.1
		0.0	2185.4	2270.0	2492.1	2509.9
		0.1	2129.3	2228.9	2484.5	2514.5
	2	Pre-Release	2729.4	2694.8	2709.2	2621.8
		0.0	2193.8	2275.6	2493.6	2511.4
		0.1	2127.8	2228.3	2485.0	2514.8
	3	Pre-Release	2723.8	2702.3	2725.9	2653.1
		0.0	2196.0	2277.1	2494.1	2511.6
		0.1	2129.3	2228.9	2484.5	2514.5
2	1	Pre-Release	2639.2	2722.8	2797.4	2593.6
		0.0	2164.9	2394.0	2619.9	2494.3
		0.1	Data Collection System Malfunction			
		74.0	1717.1	2037.4	2402.9	2368.5
		231.2	1702.3	2025.4	2442.7	2399.4
	2	Pre-Release	2637.8	2722.3	2796.8	2594.0
		0.0	2171.1	2398.4	2622.1	2495.6
		0.1	Data Collection System Malfunction			
		74.0	1717.2	2036.9	2402.1	2366.9
		145.2	1760.1	2015.3	2407.1	2413.2
		231.2	1702.6	2026.1	2442.4	2398.7
3	1	Pre-Release	2597.4	2828.3	2737.3	2683.6
		0.0	2109.0	2424.6	2432.3	2474.8
		0.1	2011.4	2362.7	2434.9	2496.0
		73.2	1695.9	2019.0	2175.0	2341.1
		230.3	1682.3	2026.3	2221.1	2354.6
	2	Pre-Release	2596.8	2830.3	2740.5	2685.9
		0.0	2100.2	2418.3	2428.1	2471.9
		0.1	2010.2	2361.7	2435.9	2496.2
		73.2	1695.8	2019.3	2176.0	2340.5
		230.3	1682.1	2026.6	2222.1	2355.0

Field Test	Girder #	Time After Release (days)	VW1 Raw Reading (με)	VW2 Raw Reading (με)	VW3 Raw Reading (με)	VW4 Raw Reading (με)
4	1	Pre-Release	2537.18	2744.17	2507.06	2387.15
		0.0	2115.86	2378.45	2214.05	2236.77
		0.1	2031.53	2326.98	2225.57	2272.76
		156.3	1846.46	2113.04	2146.89	2222.16
	2	Pre-Release	2537.29	2746.79	2505.59	2384.43
		0.0	2107.30	2372.54	2210.44	2235.68
		0.1	2031.76	2326.18	2226.08	2273.29
		156.3	1846.45	2112.90	2146.61	2222.99
5	1	Pre-Release	2589.50	2672.57	2504.53	2720.91
		0.0	2173.58	2349.91	2259.89	2522.98
		0.1	2078.41	2306.27	2267.83	2552.10
		67.1	2009.54	2168.34	2242.15	2553.92
		154.2	1931.90	2144.51	2258.86	2513.90
	2	Pre-Release	2584.10	2584.10	2506.90	2720.00
		0.0	2158.50	2340.00	2253.50	2517.30
		0.1	2077.00	2306.00	2268.90	2552.40
		154.2	1932.00	2144.40	2258.50	2511.30
6	1	Pre-Release	2488.30	2676.90	2529.70	2581.40
		0.0	2002.60	2288.60	2267.10	2382.60
		0.1	1922.00	2253.70	2276.00	2410.40
		153.3	1761.40	2040.80	2231.10	2354.50
	2	Pre-Release	2491.10	2671.60	2527.00	2583.60
		0.0	2019.00	2298.50	2272.20	2386.80
		0.1	1922.00	2253.70	2276.00	2410.40
		153.3	1761.00	2040.40	2230.80	2355.80
7	1	Pre-Release	2453.90	2605.00	2595.40	2609.20
		0.0	1803.70	2116.40	2289.70	2449.10
		0.1	1711.60	2067.30	2299.30	2472.70
		43.0	1471.20	1833.40	2180.80	2408.80
		82.1	1445.10	1821.10	2187.70	2419.50
	2	Pre-Release	2451.00	2609.22	2597.58	2609.95
		0.0	1782.80	2103.61	2285.44	2448.42
		0.1	1710.91	2066.80	2300.81	2473.55
		43.0	1471.19	1833.47	2180.93	2408.86
		82.2	1444.90	1821.91	2190.22	2417.91
	3	Pre-Release	2449.14	2618.35	2604.66	2610.97
		0.0	1782.80	2103.61	2285.44	2448.42
		0.1	1710.63	2066.54	2301.38	2473.77
		43.0	1471.13	1833.56	2181.29	2409.13
		82.2	1444.73	1822.33	2191.52	2416.95

Field Test	Girder #	Time After Release (days)	VW1 Raw Reading (με)	VW2 Raw Reading (με)	VW3 Raw Reading (με)	VW4 Raw Reading (με)
8	1	Pre-Release	2517.7	2689.0	2599.2	2583.0
		0.0	1880.2	2192.6	2293.5	2412.0
		0.1	1815.2	2159.1	2299.7	2431.4
		41.1	1591.1	1919.6	2206.9	2381.1
		80.2	1606.3	1863.7	2178.2	2411.6
	2	Pre-Release	2517.1	2695.4	2602.7	2580.2
		0.0	1868.7	2185.4	2290.8	2410.3
		0.1	1814.3	2158.3	2300.2	2431.8
		41.1	1591.3	1919.7	2206.7	2380.5
		80.2	1605.6	1861.3	2176.4	2410.5
	3	Pre-Release	2517.2	2701.9	2608.3	2579.1
		0.0	1859.4	2180.5	2290.2	2411.0
		0.1	1813.8	2157.8	2300.5	2432.1
		41.1	1591.0	1919.5	2206.9	2380.8
		80.2	1604.5	1859.4	2175.4	2409.5
9	1	Pre-Release	2657.8	2748.8	2681.4	2698.3
		0.0	2457.2	2601.5	2575.1	2607.2
		0.1	1915.7	2195.8	2366.7	2500.8
		36.1	1645.7	1919.4	2230.1	2432.2
		75.3	1595.1	1865.7	2200.2	2431.9
	2	Pre-Release	2655.0	2756.1	2687.3	2699.1
		0.0	1982.5	2230.4	2347.6	2465.6
		0.1	1915.5	2194.4	2367.8	2501.3
		36.1	1647.2	1917.9	2230.5	2432.0
		75.3	1594.3	1866.3	2200.2	2431.6
	3	Pre-Release	2654.4	2764.8	2695.0	2701.0
		0.0	1991.7	2235.9	2349.0	2466.8
		0.1	1915.4	2193.4	2368.4	2501.2
		36.1	1647.6	1917.2	2230.5	2431.5